



BENZOYL ISOTHIOCYANATES DERIVED LIGANDS AS POTENTIAL HIV-1
PROTEASE INHIBITORS AND THEIR REACTIONS WITH GOLD IONS

by

Felix Odame

Submitted in fulfilment of the requirements for the degree of

DOCTOR OF PHILOSOPHY: CHEMISTRY

to be awarded at the

Nelson Mandela Metropolitan University

December 2016

Promoter: Prof. Z.R. Tshentu

Co-Promoters: Prof. C.L. Frost and Dr K.A. Lobb

Declaration

I, Felix Odame (213510251), hereby declare that the thesis for student qualification to be awarded is my own work and that it has not previously been submitted for assessment or completion of any postgraduate qualification at another University or for another qualification.

Felix Odame

ABSTRACT

The synthesis and evaluation of benzoyl isothiocyanate derivatives as potential HIV-1 protease inhibitors is presented. The ligands were first designed to fit the protease active site using Autodock 4.2. The design was based on the deNOVO method of drug design in which the active site coordinates from the crystal structure of protease bound to ritonavir was used. An attempt to access the scaffolds designed initially led to the formation of 2,2,4-trimethyl 2,3-dihydro-1*H*-1,5-benzodiazepin-5-ium isophthalate and 2-2-(3-methylphenyl-1*H*-benzimidazole which could not be converted to the desired intermediate. A further attempt led to formation of amino acid and amino acid ester derivatives of benzoyl isothiocyanates which have been fully characterized and the reasons why the desired intermediates were not readily accessible explained. Scaffolds based on the benzoyl isothiocyanate derivatives of structurally diverse diamines were then screened. Sixty compounds have been synthesized and fully characterized using elemental analysis, spectroscopy, GC-MS and twenty-six crystal structures have been discussed. The DFT transition state studies of 11-phenyl-1,8,10,12-tetraazatricyclo[7.4.0.0^{2,7}]trideca-2(7),3,5,9,11-pentaene-13-thione (**20**), *N*-(1*H*-benzimidazol-2-yl)benzamide (**21**), 3-(1,3-benzothiazol-2-yl)-1-(benzoyl)thiourea (**23**), and *N*-[(9*E*)-8,10,17-triazatetracyclo[8.7.0.0^{2,7}.0^{11,16}]heptadeca-1(17),2,4,6,11(16),12,14-heptaen-9-ylidene] benzamide (**39**), have been carried out and their detailed density functional theory reaction mechanism have been computed. The Bernly algorithm was used in the determination of saddle points (transition states), and the intrinsic reaction coordinates leading to the determination of intermediates were traced and optimized to a global minimum or in some cases a local minimum was obtained.

The cell viability tests of diamine derivatives which was done by exposing white blood cells to the compounds (inhibitors) at 37 °C and a pH of 7.4 showed that 1-(4-bromobenzoyl)-3-[2-(((4-bromophenyl)formamido)methanethiyl)amino)phenyl]thiourea (**46**), 1-(3-chlorobenzoyl)-3-[2-(((3-chlorophenyl)formamido)methanethiyl)amino)phenyl]thiourea (**48**), 1-(3-bromobenzoyl)-3-[2-(((3-bromophenyl)formamido)methanethiyl)amino)phenyl]thiourea (**49**) and 3-benzoyl-1-(4-(((phenylformamido)methanethiyl)amino)butyl)thiourea (**54**), in that group of compounds were cytotoxic with EC₅₀ values of 17.04 ± 9.75 μM, 69.20 ± 38.16 μM, 35.90 ± 20.55 μM and 68.37 ± 26.45 μM, respectively. 4-Bromo-*N*-[(9*E*)-8,10,17-triazatetracyclo[8.7.0.0^{2,7}.0^{11,16}]heptadeca-1(17),2,4,6,11(16),12,14-heptaen-9-ylidene] benzamide (**32**), 4-methoxy-*N*-[(9*E*)-8,10,17-triazatetracyclo[8.7.0.0^{2,7}.0^{11,16}]

heptadeca-1(17),2,4,6,11(16),12,14-heptaen-9-ylidene]benzamide (**33**) and 3-chloro-*N*-[(9E)-8,10,17-triazatetracyclo[8.7.0.0^{2,7}.0^{11,16}]heptadeca-1(17),2,4,6,11(16),12,14-heptaen-9-ylidene] benzamide (**37**) were also cytotoxic giving EC₅₀ values of 45.47 ± 21.92, 45.09 ± 13.79 and 74.94 ± 13.17 μM, respectively. 3-(1,3-Benzothiazol-2-yl)-1-(3-bromobenzoyl)thiourea (**31**) and 3-(1,3-benzothiazoyl-2-yl)-1-(4-nitrobenzoyl)thiourea (**30**) derivatives were also found to be cytotoxic with EC₅₀ values of 1.207 ± 0.58 and 24.08 ± 13.14 nM, respectively. 11-(4-Chlorophenyl)-1,8,10, 12-tetraazatricyclo[7.4.0.0^{2,7}]trideca-2(7),3,5,9,11-pentaene-13-thione (**12**), 11-(4-methoxyphenyl)-1,8,10,12-tetraazatricyclo[7.4.0.0^{2,7}]trideca-2(7),3,9,1-pentaene-13-thione (**14**), and 11-phenyl-1,8,10,12-tetraazatricyclo[7.4.0.0^{2,7}]trideca-2(7),3,5,9,11-pentaene-13-thione (**20**), were found to be cytotoxic giving EC₅₀ values of 0.152 ± 0.051, 37.96 ± 21.87 and 5.28 ± 2.95 μM, respectively. In the enzyme inhibition studies compound **49** gave a percentage inhibition of 97.03 ± 10.61% at 100 μM, but the fact that it is cytotoxic might make it less useful, whilst compounds **19** and **16** had a percentage inhibition of 59.57 ± 13.59% (4-nitro derivative) and 79.97 ± 11.97% (3-nitro derivative) respectively at 100 μM of inhibitor and 20 μM of enzyme (HIV-1 protease). The results suggests that the presence of the nitro group at position 3 (**16**) and 4 (**19**) leads to an increase in activity against HIV-1 protease.

Keywords: benzoyl isothiocyanate derivatives, transition states, global minimum, cell viability test, HIV-1 protease assay, enzyme inhibition.

ACKNOWLEDGEMENTS

Firstly, I would like to thank God for His grace, protection and guidance throughout my study and also for the mental fortitude to complete my doctoral thesis.

I would also like to thank Prof. Z.R. Tshentu, my promoter, for guiding me throughout the project. For his useful suggestions on alternative approaches to tackling problems, for constantly pushing me to do more. For helping to shape my thinking, refining my ideas and concretising them into actionable goals. Thank you very much.

I would like to thank Dr K.A. Lobb, my co-promoter, for introducing me to molecular modeling and helping me to learn the various techniques used in the different types of modeling.

I would also like to thank Prof. C.L. Frost, my co-promoter, for guiding me in the planning and execution of the biochemistry aspects of my project.

To Dr Jason Krause, I would like to thank him for assisting me with completing the cell viability tests and the HIV-1 protease assays.

I would like to thank Prof. Yasien Sayed and Allison Williams for providing us with the HIV-1 protease enzyme and for introducing me to the techniques involved in carrying out the protease assay.

Special thanks to Drs Eric Hosten and Richard Betz for the crystal structure solutions and some important structural discussions.

I would also like to acknowledge Medical Research Council (MRC), Faculty of Science, Nelson Mandela Metropolitan University Postgraduate Research Scholarship (NMMU PGRS) and National Research Foundation (NRF) for funding me.

Thanks to my group members; Dr Sunday Ogunlaja, Songeziwe Ntsimango, Cyprian Moyo, Puleng Moleko, Mohammed Abdulquadir, Sendibitiyosi Gandidzanwa, Masande Ndamase, Tendai Dembaremba and Darren Gelderbloem for the useful interactions.

Special thanks to my family for their unconditional love, support and sacrifices.

Thanks to my wife (Dorcas Larbi) for her support and patience throughout my studies.

TABLE OF CONTENTS

DECLARATION	ii
ABSTRACT	iii
ACKNOWLEDGEMENTS	v
TABLE OF CONTENTS	vii
LIST OF TABLES	xvi
LIST OF FIGURES	xix
APPENDICES	xxix
LIST OF SCHEMES	xxxix
LIST OF ABBREVIATIONS	xlii
Chapter One: Introduction	1
1.1 Overview of HIV	1
1.1.1 Morphology of the mature virion	2
1.1.2 The HIV-1 replication cycle	4
1.1.2.1 Early phase	5
1.1.2.2 Late phase	6
1.1.3 HIV Integrase enzyme	7
1.1.4 HIV Reverse transcriptase enzyme	9
1.2 Structure of HIV-1 protease enzyme	13
1.2.1 Structural features	13
1.2.2 HIV-1 protease active site	13
1.2.3 HIV protease and structure guided design of PIs	16
1.2.4 Evolution of drug resistance to PIs	17
1.3 Benzimidazole-based compounds	18
1.4 Benzoyl isothiocyanates derived compounds	30
1.5 Synthesis and biological activity of gold compounds	34
1.6 Gold catalyzed reactions	39
1.7 Activity of gold compounds against HIV	40
1.8 Dual action of gold	41
1.9 Scope of the thesis	45
Chapter Two: Experimental	46
2.1 Materials	46
2.2 Spectroscopic techniques	48
2.2.1 NMR Spectrometry	48

2.2.2	Infrared Spectroscopy	48
2.2.3	Microtitre plate	48
2.2.4	Fluorogenic microplate reader	48
2.3	Analytical methods	48
2.3.1	Elemental Analysis	48
2.3.2	Gas Chromatography–Mass Spectrometry	49
2.4	Single crystal X-ray	49
2.5	Autodock	49
2.6	Gaussian	50
2.7	Melting points	50
2.8	Centrifuge	50
2.9	Preparative work	51
2.9.1	Methyl- <i>N</i> -[2-(3-methylbenzamido)phenyl]benzamide (1)	51
2.9.2	2-(3-Methylphenyl)-1 <i>H</i> -benzimidazole (2)	52
2.9.3	2,2,4-Trimethyl-2,3-dihydro-1 <i>H</i> -1,5-benzodiazepin-5-ium isophthalate (3)	53
2.9.4	2,4-Trimethyl-2,3-dihydro-1 <i>H</i> -1,5-benzodiazepine (4)	53
2.9.5	2-[(Benzoylcarbamothioyl)amino]-3-hydroxypropanoic acid (5)	54
2.9.6	1-(Benzoylcarbamothioyl)pyrrolidine-2-carboxylic acid (6)	54
2.9.7	2-[(Benzoylcarbamothioyl)amino]-4-(methylsulfanyl)butanoic acid (7)	55
2.9.8	2-[(Benzoylcarbamothioyl)amino]propanoic acid (8)	56
2.9.9	2-Phenyl-1 <i>H</i> -benzimidazole (9)	56
2.9.10	Methyl-2-{[(phenylformamido)methanethioyl]amino}propanoate (10)	56
2.9.11	1,4-Dimethyl -2-{[(phenylformamido)methanethioyl]butanedioate (11)	57
2.9.12	11-Phenyl-1,8,10,12-tetraazatricyclo[7.4.0.0 ^{2,7}]trideca-2(7),3,5,9,11-pentaene-13-thione (12)	58
2.9.13	11-(4-Bromophenyl)-,8,10,2-tetraazatricyclo[7.4.0.0 ^{2,7}]trideca-2(7),3,5,9,11-pentaene-13-thione (13)	58
2.9.14	11-(4-Methoxyphenyl)-1,8,0,12-tetraazatricyclo[7.4.0.0 ^{2,7}]trideca-2(7),3,9,1-pentaene-13-thione (14)	59
2.9.15	11-(3-Methoxyphenyl)-1,8,0,12-tetraazatricyclo[7.4.0.0 ^{2,7}]trideca-2(7),3,5,9,11-pentaene-13-thione (15)	59
2.9.16	11-(3-Nitrophenyl)-1,8,10,12-tetraazatricyclo[7.4.0.0 ^{2,7}]trideca(7),3,5,9,11-pentaene-13-thione (16)	60

2.9.17	11-(3-Chlorophenyl)-1,8,10,12-tetraazatricyclo[7.4.0.0 ^{2,7}]trideca-2(7),3,5,9,11-pentaene-13-thione (17)	61
2.9.18	11-(3-Bromophenyl)-1,8,10,12-tetraazatricyclo[7.4.0.0 ^{2,7}]trideca-2(7),3,5,9,11-pentaene-13-thione (18)	61
2.9.19	11-(4-Nitrophenyl)-1,8,10,12-tetraazatricyclic[7.4.0.0 ^{2,7}]trideca-2(7),3,5,9,11-pentaene-13-thione(19)	62
2.9.20	11-Phenyl-1,8,10,12-tetraazatricyclo[7.4.0.0 ^{2,7}]trideca-2(7),3,5,9,11-pentaene-13-thione (20)	63
2.9.21	<i>N</i> -(1 <i>H</i> -Benzimidazol-2-yl)benzamide (21)	63
2.9.22	3-Benzoyl-1-(2-hydroxyphenyl) urea hydrate (22)	64
2.9.23	3-(1,3-Benzothiazol-2-yl)-1-(benzoyl)thiourea (23)	64
2.9.24	3-(1,3-Benzothiazol-2-yl)-1-(4-chlorobenzoyl)thiourea (24)	65
2.9.25	3-(1,3-Benzothiazol-2-yl)-1-(4-bromobenzoyl)thiourea (25)	65
2.9.26	3-(1,3-Benzothiazol-2-yl)-1-(4-methoxybenzoyl)thiourea (26)	66
2.9.27	3-(1,3-Benzothiazol-2-yl)-1-(methoxybenzoyl)thiourea (27)	66
2.9.28	3-(1,3-Benzothiazol-2-yl)-1-(3-nitrobenzoyl)thiourea (28)	67
2.9.29	3-(1,3-Benzothiazol-2-yl)-1-(3-chlorobenzoyl)thiourea (29)	67
2.9.30	3-(1,3-Benzothiazoyl-2-yl)-1-(4-nitrobenzoyl)thiourea (30)	68
2.9.31	3-(1,3-Benzothiazol-2-yl)-1-(3-bromobenzoyl)thiourea (31)	68
2.9.32	4-Bromo- <i>N</i> -[(9 <i>E</i>)-8,10,17-triazatetracyclo[8.7.0.0 ^{2,7} .0 ^{11,16}]heptadeca-1(17),2,4,6,11(16),12,14-heptaen-9-ylidene]benzamide (32)	69
2.9.33	4-Methoxy- <i>N</i> -[(9 <i>E</i>)-8,10,17-triazatetracyclo[8.7.0.0 ^{2,7} .0 ^{11,16}]heptadeca-(17),2,4,6,11(16),12,14-heptaen-9-ylidene]benzamide (33)	70
2.9.34	3-Methoxy- <i>N</i> -[(9 <i>E</i>)-8,10,17-triazatetracyclo[8.7.0.0 ^{2,7} .0 ^{11,16}]heptadeca-(17),2,4,6,11(16),12,14-heptaen-9-ylidene]benzamide (34)	70
2.9.35	4-Chloro- <i>N</i> -[(9 <i>E</i>)-8,10,17-triazatetracyclo[8.7.0.0 ^{2,7} .0 ^{11,16}]heptadeca-1(17),2,4,6,11(16),12,14-heptaen-9-ylidene]benzamide (35)	71
2.9.36	3-Nitro- <i>N</i> -[(9 <i>E</i>)-8,10,17-triazatetracyclo[8.7.0.0 ^{2,7} .0 ^{11,16}]heptadeca-1(17),2,4,6,11(16),12,14-heptaen-9-ylidene]benzamide (36)	72
2.9.37	3-Chloro- <i>N</i> -[(9 <i>E</i>)-8,10,17-triazatetracyclo[8.7.0.0 ^{2,7} .0 ^{11,16}]heptadeca1(17),2,4,6,11(16),12,14-heptaen-9-ylidene]benzamide (37)	72
2.9.38	4-Nitro- <i>N</i> -[(9 <i>E</i>)-8,10,17-triazatetracyclo[8.7.0.0 ^{2,7} .0 ^{11,16}]heptadeca-1(17),2,4,6,11(16),12,14-heptaen-9-ylidene]benzamide (38)	73
2.9.39	<i>N</i> -[(9 <i>E</i>)-8,10,17-triazatetracyclo[8.7.0.0 ^{2,7} .0 ^{11,16}]heptadeca-1(17),2,4,6,11(16),12,14-	

heptaen-9-ylidene]benzamide (39)	73
2.9.40 1-Benzoyl-3-(5-methyl-2-[[phenylformamido)methanethioyl]amino}phenyl)thiourea (40)	74
2.9.41 1-Benzoyl-3-(2-[[phenylformamido)methanethioyl]amino}phenyl)thiourea (41)	75
2.9.42 1-(4-Nitrobenzoyl)-3-[2-([[4-nitrophenyl]formamido]methanthioyl]amino}phenyl)thiourea (42)	75
2.9.43 1-(4-Chlorobenzoyl)-3-[2-([[4-chlorophenyl]formamido]methanethioyl}amino)phenylthiourea (43)	76
2.9.44 1-(3-Nitrobenzoyl)-3-[2-([[3-nitrophenyl]formamido]methane}amino)phenyl]thiourea (44)	76
2.9.45 1-(3-Methoxybenzoyl)-3-[2-([[3-methoxyphenyl]formamido]methanethioyl}amino)phenyl]thiourea (45)	77
2.9.46 1-(4-Bromobenzoyl)-3-[2-([[4-bromophenyl]formamido]methanethioyl}amino)phenyl]thiourea (46)	78
2.9.47 1-(4-Methoxybenzoyl)-3-[2-([[4-methoxyphenyl]formamido]methanethioyl}amino)phenyl]thiourea (47)	78
2.9.48 1-(3-Chlorobenzoyl)-3-[2-([[3-chlorophenyl]formamido]methanethioyl}amino)phenyl]thiourea (48)	79
2.9.49 1-(3-Bromobenzoyl)-3-[2-([[3-bromophenyl]formamido]methanethioyl}amino)phenyl]thiourea (49)	79
2.9.50 3-Benzoyl-1-(2-[[phenylformamido]methanethioyl]amino)ethylthiourea (50)	80
2.9.51 3-Benzoyl-1-[[phenylformido]methanethioyl]amino}thiourea (51)	80
2.9.52 3-Benzoyl-1-(phenylamino)thiourea (52)	81
2.9.53 1-((Benzamido)sulfanylenemethyl)urea (53)	82
2.9.54 3-Benzoyl-1-(4-[[phenylformamido]methanethioyl]amino)butylthiourea (54)	82
2.9.55 <i>N</i> -(Benzothiazol-2-yl)-4-nitrobenzamide (55)	83
2.9.56 <i>N</i> -(Benzothiazol-2-yl)-3-bromobenzamide (56)	83
2.9.57 <i>N</i> -(Benzothiazol-2-yl)-3-methoxybenzamide (57)	84
2.9.58 <i>N</i> -(Benzothiazol-2-yl)benzamide (58)	84
2.9.59 1-((Benzamido)formyl)urea (59)	85
2.9.60 <i>N</i> -(2,3-Dihydro-1 <i>H</i> -benzimidazol-2-yl)-3-nitrobenzamide (60)	85
2.10 Cytotoxicity protocol	86
2.10.1 Determination of EC ₅₀ values	87
2.11 HIV-1 Protease assay	87

2.11.1	Optimization of HIV-1 protease concentration screen of structurally diverse diamine derivatives of benzoyl isothiocyanate	88
Chapter Three: Design and synthesis of benzoyl isothiocyanate derivatives		90
3.1	Design and synthesis of benzoyl isothiocyanate derivatives: preliminary studies	90
3.2	Synthesis and crystal structures of 3-methyl- <i>N</i> -[2-(3-methylbenzamido)phenyl]benzamide (1) and 2-(3-methylphenyl)-1 <i>H</i> -benzimidazole (2)	96
3.2.1	HOMO-LUMO analysis	104
3.3	Synthesis and characterization of benzodiazepines	107
3.3.1	Proposed reaction mechanism for compounds 2,2,4-trimethyl-2,3-dihydro-1 <i>H</i> -benzodiazepin-5-ium isophthalate (3) and 2,2,4-trimethyl-2,3-dihydro-1 <i>H</i> -1,5-benzodiazopine (4)	114
3.3.2	X-ray crystallography of 2,2,4-trimethyl-2,3-dihydro-1 <i>H</i> -benzodiazepin-5-ium isophthalate (3) and 2,2,4-trimethyl-2,3-dihydro-1 <i>H</i> -1,5-benzodiazopine (4)	116
3.4	Synthesis and characterization of amino acid derivatives	121
3.4.1	Crystal structures of amino acid derivatives	132
3.4.2	HOMO-LUMO analysis	137
3.5	Synthesis of the amino acid ester derivatives	144
3.5.1	Methyl-2-[[phenylformamido)methanethiyl]amino}propanoate (10)	148
3.5.2	1,4-Dimethyl-2-[[phenylformamido)methanethiyl]butanedioate (11)	150
3.5.3	Crystal structures of amino acid esters derivatives	152
3.6	Design and synthesis of derivatives of benzoyl isothiocyanate with structurally diverse diamines	155
3.7	Conclusions	157
Chapter Four: Tetraazatricyclic derivatives		160
4.1	Synthesis of tetraazatricyclic derivatives	160
4.2	11-(4-Chlorophenyl)-1,8,10,12-tetraazatricyclo[7.4.0.0 ^{2,7}]trideca-2(7),3,5,9,11-pentaene-13-thione (12)	161
4.3	11-(4-Bromophenyl)-1,8,10,12-tetraazatricyclo[7.4.0.0 ^{2,7}]trideca-2(7),3,5,9,11-pentaene-13-thione (13)	161
4.4	11-(4-Methoxyphenyl)-1,8,10,12-tetraazatricyclo[7.4.0.0 ^{2,7}]trideca-2(7),3,5,9,11-pentaene-13-thione (14)	162
4.5	11-(3-Methoxyphenyl)-1,8,10,12-tetraazatricyclo[7.4.0.0 ^{2,7}]trideca-2(7),3,5,9,11-pentaene-13-thione (15)	162

4.6	11-(3-Nitrophenyl)-1,8,10,12-tetraazatricyclo[7.4.0.0 ^{2,7}]trideca-2(7),3,5,9,11-pentaene-13-thione (16)	- 162
4.7	11-(3-Chlorophenyl)-1,8,10,12-tetraazatricyclo[7.4.0.0 ^{2,7}]trideca-2(7),3,5,9,11-pentaene-13-thione (17)	- 165
4.8	11-(3-Bromophenyl)-1,8,10,12-tetraazatricyclo[7.4.0.0 ^{2,7}]trideca-2(7),3,5,9,11-pentaene-13-thione (18)	165
4.9	11-(4-Nitrophenyl)-1,8,10,12-tetraazatricyclic[7.4.0.0 ^{2,7}]trideca-2(7),3,5,9,11-pentaene-13-thione (19)	165
4.10	11-Phenyl-1,8,10,12-tetraazatricyclo[7.4.0.0 ^{2,7}]trideca-2(7),3,5,9,11-pentaene-13-thione (20)	166
4.11	Transition state studies on tetraazatricyclic derivatives	166
4.12	<i>N</i> -(1 <i>H</i> -Benzimidazol-2-yl)benzamide (21)	169
4.13	Transition state studies on <i>N</i> -(1 <i>H</i> -Benzimidazol-2-yl)benzamide (21)	172
4.14	3-Benzoyl-1-(2-hydroxyphenyl) urea (22)	175
4.15	Crystal structures of compounds 20 , 21 and 22	178
4.2	Biochemical studies	182
4.2.1	Cell viability and cytotoxicity tests	182
4.2.2	HIV-1 protease screen for tetraazatricyclics	184
4.3	Conclusions	188
	Chapter Five: 3-(1,3-Benzothiazol-2-yl)-1-(benzoyl)thiourea derivatives	190
5.1	Synthesis of 3-(1,3-benzothiazol-2-yl)-1-(benzoyl)thiourea derivatives	190
5.2	3-(1,3-Benzothiazol-2-yl)-1-(benzoyl)thiourea (23)	190
5.3	3-(1,3-Benzothiazol-2-yl)-1-(4-chlorobenzoyl)thiourea (24)	191
5.4	3-(1,3-Benzothiazol-2-yl)-1-(4-bromobenzoyl)thiourea (25)	191
5.5	3-(1,3-Benzothiazol-2-yl)-1-(4-methoxybenzoyl)thiourea (26)	191
5.6	3-(1,3-Benzothiazol-2-yl)-1-(3-methoxybenzoyl)thiourea (27)	192
5.7	3-(1,3-Benzothiazol-2-yl)-1-(3-nitrobenzoyl)thiourea (28)	194
5.8	3-(1,3-Benzothiazol-2-yl)-1-(3-chlorobenzoyl)thiourea (29)	194
5.9	3-(1,3-Benzothiazoyl-2-yl)-1-(4-nitrobenzoyl)thiourea (30)	195
5.10	3-(1,3-Benzothiazol-2-yl)-1-(3-bromobenzoyl)thiourea (31)	195
5.11	Transition state studies on 3-(1,3-Benzothiazol-2-yl)-1-(3-nitrobenzoyl)thiourea derivatives	197

5.12	Crystal structure of some 3-(1,3-benzothiazol-2-yl)-1-(benzoyl)thiourea derivatives	201
5.2	Biochemical studies	203
5.2.1	Cell viability and cytotoxicity tests	203
5.2.2	The HIV-1 protease screening of 3-(1, 3-benzothiazol-2-yl)-1-(benzoyl)thiourea derivatives	205
5.3	Conclusions	208
Chapters Six: Triazatetracyclic derivatives		209
6.1	Synthesis of triazatetracyclics	209
6.2	Problems with solubility	210
6.3	4-Bromo- <i>N</i> -[(9 <i>E</i>)-8,10,17-triazatetracyclo[8.7.0.0 ^{2,7} .0 ^{11,16}]heptadeca-1(17),2,4,6,11(16),12,14-heptaen-9-ylidene]benzamide (32)	210
6.4	4-Methoxy- <i>N</i> -[(9 <i>E</i>)-8,10,17-triazatetracyclo[8.7.0.0 ^{2,7} .0 ^{11,16}]heptadeca-1(17),2,4,6,11(16),12,14-heptaen-9-ylidene]benzamide (33)	211
6.5	3-Methoxy- <i>N</i> -[(9 <i>E</i>)-8,10,17-triazatetracyclo[8.7.0.0 ^{2,7} .0 ^{11,16}]heptadeca-1(17),2,4,6,11(16),12,14-heptaen-9-ylidene]benzamide (34)	211
6.6	4-Chloro- <i>N</i> -[(9 <i>E</i>)-8,10,17-triazatetracyclo[8.7.0.0 ^{2,7} .0 ^{11,16}]heptadeca-1(17),2,4,6,11(16),12,14-heptaen-9-ylidene]benzamide (35)	214
6.7	3-Nitro- <i>N</i> -[(9 <i>E</i>)-8,10,17-triazatetracyclo[8.7.0.0 ^{2,7} .0 ^{11,16}]heptadeca-1(17),2,4,6,11(16),12,14-heptaen-9-ylidene]benzamide (36)	214
6.8	3-Chloro- <i>N</i> -[(9 <i>E</i>)-8,10,17-triazatetracyclo[8.7.0.0 ^{2,7} .0 ^{11,16}]heptadeca-1(17),2,4,6,11(16),12,14-heptaen-9-ylidene]benzamide (37)	215
6.9	4-Nitro- <i>N</i> -[(9 <i>E</i>)-8,10,17-triazatetracyclo[8.7.0.0 ^{2,7} .0 ^{11,16}]heptadeca-1(17),2,4,6,11(16),12,14-heptaen-9-ylidene]benzamide (38)	215
6.10	<i>N</i> -[(9 <i>E</i>)-8,10,17-triazatetracyclo[8.7.0.0 ^{2,7} .0 ^{11,16}]heptadeca-1(17),2,4,6,11(16),12,14-heptaen-9-ylidene]benzamide (39)	216
6.11	Crystal structure of compound 39	216
6.12	Transition state studies on the formation of triazatetracyclics derivatives	218
6.2	Biochemical studies	221
6.2.1	Cell viability and cytotoxicity tests	221
6.2.2	HIV-1 protease screen of triazatetracyclic derivatives	223
6.3	Conclusions	226
Chapter Seven: Phenyl thiourea compounds and other diamine derivatives		228
7.1	Synthesis of phenyl thiourea compounds and other diamine derivatives	228

7.1.1	1-Benzoyl-3-(5-methyl-2-{{(phenylformamido)methanethioyl}amino}phenyl)thiourea (40)	229
7.1.2	1-Benzoyl-3-(2-{{(phenylformamido)methanethioyl}amino}phenyl)thiourea (41)	229
7.1.3	1-(4-Nitrobenzoyl)-3-[2-({[(4-nitrophenyl)formamido]methanthioylamino)phenyl]thiourea} (42)	230
7.1.4	1-(4-Chlorobenzoyl)-3-[2-({[(4-hlorophenyl)formamido]methanethioyl}amino)phenyl]thiourea (43)	230
7.1.5	1-(3-Nitrobenzoyl)-3-[2-({[(3-nitrophenyl)formamido]methane}amino)phenyl]thiourea(44)	230
7.1.6	1-(3-Methoxybenzoyl)-3-[2-({[(3-methoxyphenyl)formamido]methanethioyl}amino)phenyl]thiourea (45)	232
7.1.7	1-(4-Bromobenzoyl)-3-[2-({[(4-bromophenyl)formamido]methanethioyl}amino)phenyl]thiourea (46)	232
7.1.8	1-(4-Methoxybenzoyl)-3-[2-({[(4-methoxylphenyl)formamido]methanethioyl}amino)phenyl]thiourea (47)	233
7.1.9	1-(3-Chlorobenzoyl)-3-[2-({[(3-chlorophenyl)formamido]methanethioyl}amino)phenyl]thiourea (48)	233
7.1.10	1-(3-Bromobenzoyl)-3-[2-({[(3-bromophenyl)formamido]methanethioyl}amino)phenyl]thiourea (49)	234
7.1.11	3-Benzoyl-1-(2-{{(phenylformamido)methanethioyl}amino}ethyl)thiourea (50)	234
7.1.12	3-Benzoyl-1{{(phenylformido)methanethioyl}amino}thiourea (51)	235
7.1.13	Crystal structures of compounds 39 , 40 , 50 and 51	236
7.1.14	3-Benzoyl-1-(phenylamino)thiourea (52)	240
7.1.15	1-((Benzamido)sulfanylenemethyl)urea (53)	240
7.1.16	3-Benzoyl-1-(4-{{(phenylformamido)methanethioyl}amino}butyl)thiourea (54)	241
7.1.17	Crystal structures of compounds 53 and 54	243
7.2	Biochemical studies	247
7.2.1	Cell viability and cytotoxicity tests	247
7.2.2	HIV-1 protease screen of structurally diverse diamine derivatives of benzoyl isothiocyanate	248
7.3	Conclusions	255
Chapter Eight: Gold and silver catalysed reactions of benzoyl isothiocyanate derivatives		257
8.1	Attempted synthesis of gold compounds	257

8.1.1	<i>N</i> -(Benzothiazol-2-yl)-4-nitrobenzamide (55)	259
8.1.2	<i>N</i> -(Benzothiazol-2-yl)-3-bromobenzamide (56)	260
8.1.3	<i>N</i> -(Benzothiazol-2-yl)-3-methoxybenzamide (57)	260
8.1.4	<i>N</i> -(Benzothiazol-2-yl)benzamide (58)	260
8.1.5	Crystal structures of compounds 55 , 56 , 58 and triphenylphospine	262
8.2	Silver catalyzed transformations	266
8.2.1	1-((Benzamido)formyl)urea (59)	268
8.2.2	<i>N</i> -(2,3-Dihydro-1 <i>H</i> -benzo[d]imidazol-2-yl)-3-nitrobenzamide (60)	269
8.2.3	Crystal structures of compounds 59 and 60	270
8.3	Conclusions	273
	Chapter Nine: Conclusions and future work	275
9.1	Conclusions	275
9.2	Future work	277
	REFERENCES	279

LIST OF TABLES

Table 1.1	Chemical structures of some potential HIV-1 inhibitors under development	29
Table 2.1	List of chemicals used	46
Table 2.2	Determination of optimal HIV-1 protease concentration for use in inhibitor studies	88
Table 3.1	Pre-screening result for the potential HIV-1 inhibitors (Scheme 3.1)	91
Table 3.2	Pre-screening result for the potential HIV-1 inhibitors (Scheme 3.2)	92
Table 3.3	Crystallographic data and structure refinement summary for 3-methyl- <i>N</i> -[2-(3-methylbenzamido)phenyl]benzamide (1) and 2-(3-methylphenyl)-1 <i>H</i> -benzimidazole (2)	101
Table 3.4	Selected bond lengths (Å) and bond angles (°) of 3-methyl- <i>N</i> -[2-(3-methylbenzamido)phenyl]benzamide (1) and 2-(3-methylphenyl)-1 <i>H</i> -benzimidazole (2)	102
Table 3.5	Summary of the HOMO–LUMO energies for <i>o</i> -phenylenediamine, <i>m</i> -toluolyl chloride, <i>m</i> -toluic acid, and for 3-methyl- <i>N</i> -[2-(3-methylbenzamido)phenyl]benzamide (1) and 2-(3-methylphenyl)-1 <i>H</i> -benzimidazole (2)	104
Table 3.6	Crystallographic data and structure refinement for 2,2,4-trimethyl-2,3-dihydro-1 <i>H</i> -benzodiazepin-5-ium isophthalate (3) and 2,2,4-trimethyl-2,3-dihydro-1 <i>H</i> -1,5-benzodiazopine (4)	117
Table 3.7	Selected bond lengths (Å) and bond angles (°) for 2,2,4-trimethyl-2,3-dihydro-1 <i>H</i> -benzodiazepin-5-ium isophthalate (3) and 2,2,4-trimethyl-2,3-dihydro-1 <i>H</i> -1,5-benzodiazopine (4)	118
Table 3.8	Pre-screening results of benzimidazoles of the amino acid derivatives of benzoyl isothiocyanate (Scheme 3.7)	120
Table 3.9	Crystallographic data and structure refinement summary for compounds 5–8	133
Table 3.10	Selected bond length (Å) and bond angles (°) for compounds 5–8	134
Table 3.11	Summary of the HOMO-LUMO energies for compounds 5–8 and the starting materials	139
Table 3.12	Autodock pre-screening of alternative amino acid derivatives	144
Table 3.13	Crystallographic data and structure refinement summary for compounds 10 and 11	152

Table 3.14	Selected bond lengths (Å) and bond angles (°) for compounds 10 and 11	153
Table 3.15	Summary of compounds screened and their predicted inhibition constants of diamine derivatives of benzoyl isothiocyanates	156
Table 3.16	Summary of other diamines screened and their predicted inhibition constants	156
Table 4.1	Summary of compounds screened and their predicted inhibition constants of diamine derivatives of benzoyl isothiocyanates	179
Table 4.2	Summary of other diamines screened and their predicted inhibition constant	180
Table 4.3	Crystallographic data and structure refinement summary for compounds 20 , 21 and 22	184
Table 4.4	Selected bond lengths (Å), and bond angles (°) for compounds 20 , 21 and 22	185
Table 5.1	Crystallographic data and structure refinement summary for compounds 23 , 27 and 31	198
Table 5.2	Selected bond lengths (Å) and bond angles (°) for compounds 23 , 27 and 31	199
Table 5.3	Cell viability results for benzoyl isothiocyanate derivatives.	204
Table 5.4	HIV-1 protease screening results for 3-(1,3-benzothiazol-2-yl)-1-(benzoyl)thiourea derivatives.	206
Table 6.1	Crystallographic data and structure refinement summary for compounds 39	217
Table 6.2	Selected bond lengths (Å) and bond angles (°) for compounds 39	218
Table 6.3	Cell viability results for benzoyl isothiocyanate derivatives	221
Table 6.4	HIV-1 protease screening results for triazatetracyclics	223
Table 7.1	Crystallographic data and structure refinement summary for compounds 40 , 50 and 51	237
Table 7.2	Selected bond lengths (Å) and bond angles (°) for compounds 40 , 50 and 51	238
Table 7.3	Crystallographic data and structure refinement summary for compounds 53 and 54	244
Table 7.4	Selected bond lengths (Å), and bond angles (°) for compounds 53 and 54	245

Table 7.5	Cell viability results for diamine derivatives of benzoyl isothiocyanate derivatives	247
Table 7.6	HIV-1 protease screening results of some diamines derivatives of benzoyl isothiocyanate	250
Table 8.1	Crystallographic data and structure refinement summary for compounds 55 , 56 , 58 and chorotriphenylphosphinegold(I)	263
Table 8.2	Selected bond lengths (Å) and bond angles (°) for compounds 55 , 56 , 58 and chorotriphenylphosphinegold(I)	264
Table 8.3	Crystallographic data and structure refinement summary for compounds 59 and 60	271
Table 8.4	Selected bond lengths (Å) and bond angles (°) compounds for compounds 59 and 60	272

LIST OF FIGURES

Figure 1.1	Drawing of the mature HIV virion surrounded by ribbon representations of the structurally characterized viral proteins and protein fragments	3
Figure 1.2	General features of the HIV-1 replication cycle	5
Figure 1.3	Current HIV-1 protease inhibitors approved by the FDA	14
Figure 1.4	General Structure for topoisomerase 1 blockers	39
Figure 2.1	Progress curves for the hydrolysis of [Abz-Thr-Ile-pNO ₂ Phe Gln-Arg-NH ₂] by HIV-1 Protease. Ex/Em: 337/425 nm at 25 °C and a pH of 5.0.	89
Figure 3.1	The scaffold obtained from the initial pre-screening Scheme 3.1 .	90
Figure 3.2	The scaffold obtained from the initial pre-screening Scheme 3.2 .	90
Figure 3.3	Ligand binding interaction in protease active site for the alanine derivative.	91
Figure 3.4	IR spectrum of 3-methyl- <i>N</i> -[2-(3-methylbenzamido)phenyl]benzamide (1).	97
Figure 3.5	IR spectrum of 2-(3-methylphenyl)-1 <i>H</i> -benzimidazole (2).	98
Figure 3.6	¹ H NMR spectrum of 3-methyl- <i>N</i> -[2-(3-methylbenzamido)phenyl]benzamide (1).	99
Figure 3.7	¹³ C NMR spectrum of 3-methyl- <i>N</i> -[2-(3-methylbenzamido)phenyl]benzamide (1).	99
Figure 3.8	¹ H NMR spectrum of 2-(3-methylphenyl)-1 <i>H</i> -benzimidazole (2).	100
Figure 3.9	¹³ C NMR spectrum of 2-(3-methylphenyl)-1 <i>H</i> -benzimidazole (2).	100
Figure 3.10	An ORTEP view of compound 3-methyl- <i>N</i> -[2-(3-methylbenzamido)phenyl]benzamide (1) showing 50% probability displacement ellipsoids and the atom labelling.	103
Figures 3.11	An ORTEP view of 2-(3-methylphenyl)-1 <i>H</i> -benzimidazole (2) showing 50% probability displacement ellipsoids and the atom labelling.	103
Figure 3.12	The atomic orbitals composition of the frontier molecular orbital for <i>m</i> -toluic acid.	105
Figure 3.13	The atomic orbitals compositions of the frontier molecular orbitals for <i>m</i> -toluolyl chloride.	106
Figure 3.14	The atomic orbitals compositions of the frontier molecular orbital for <i>o</i> -phenylenediamine.	106
Figure 3.15	The atomic orbitals compositions of the frontier molecular orbital for 3-methyl- <i>N</i> -[2-(3-methylbenzamido)phenyl]benzamide (1).	107

Figure 3.16	The atomic orbitals compositions of the frontier molecular orbital for 2-(3-methylphenyl)-1 <i>H</i> -benzimidazole (2).	107
Figure 3.17	IR spectrum of 2,2,4-trimethyl-2,3-dihydro-1 <i>H</i> -benzodiazepin-5-ium isophthalate (3).	110
Figure 3.18	IR spectrum of 2,2,4-trimethyl-2,3-dihydro-1 <i>H</i> -1,5-benzodiazopine (4).	110
Figure 3.19	¹ H NMR spectra of 2,2,4-trimethyl-2,3-dihydro-1 <i>H</i> -1,5-benzodiazepin-5-ium isophthalate (3).	111
Figure 3.20	¹³ C NMR spectra of 2,2,4-trimethyl-2,3-dihydro-1 <i>H</i> -1,5-benzodiazepin-5-ium isophthalate (3).	111
Figure 3.21	DEPT spectrum of 2,2,4-trimethyl-2,3-dihydro-1 <i>H</i> -benzodiazepin-5-ium isophthalate (3).	112
Figure 3.22	¹ H NMR spectrum of 2,2,4-trimethyl-2,3-dihydro-1 <i>H</i> -1,5-benzodiazopine (4).	112
Figure 3.23	¹³ C NMR spectrum of 2,2,4-trimethyl-2,3-dihydro-1 <i>H</i> -1,5-benzodiazopine (4).	113
Figure 3.24	DEPT spectrum of 2,2,4-trimethyl-2,3-dihydro-1 <i>H</i> -1,5-benzodiazopine (4).	113
Figure 3.25	An ORTEP view of 2,2,4-trimethyl-2,3-dihydro-1 <i>H</i> -benzodiazepin-5-ium isophthalate (3) showing 50% probability displacement ellipsoids and the atom labelling.	118
Figure 3.26	An ORTEP view of 2,2,4-trimethyl-2,3-dihydro-1 <i>H</i> -1,5-benzodiazopine (4) showing 50% probability displacement ellipsoids and the atom labelling.	119
Figure 3.27	¹ H NMR spectrum of 2-[(benzoylcarbamothioyl)amino]-3-hydroxypropanoic acid (5).	124
Figure 3.28	¹ H- ¹ H COSY spectrum of 2-[(benzoylcarbamothioyl)amino]-3-hydroxypropanoic acid (5).	124
Figure 3.29	¹³ C NMR spectrum of 2-[(benzoylcarbamothioyl)amino]-3-hydroxypropanoic acid (5).	125
Figure 3.30	IR spectrum of 2-[(benzoylcarbamothioyl)amino]-3-hydroxypropanoic acid (5).	126
Figure 3.31	¹ H NMR spectrum of 1-(benzoylcarbamothioyl)pyrrolidine-2-carboxylic acid (6).	126
Figure 3.32	¹ H- ¹ H COSY spectrum of 1-(benzoylcarbamothioyl)pyrrolidine-2-carboxylic acid (6).	127

Figure 3.33	^{13}C NMR spectrum of 1-(benzoylcarbamoethyl)pyrrolidine-2-carboxylic acid (6).	127
Figure 3.34	IR spectrum of 1-(benzoylcarbamoethyl)pyrrolidine-2-carboxylic acid (6).	128
Figure 3.35	DEPT 135 spectrum of 1-(benzoylcarbamoethyl)pyrrolidine-2-carboxylic acid (6).	128
Figure 3.36	^1D NOESY spectrum of 1-(benzoylcarbamoethyl)pyrrolidine-2-carboxylic acid (6).	129
Figure 3.37	2D NOESY spectrum of 1-(benzoylcarbamoethyl)pyrrolidine-2-carboxylic acid (6).	129
Figure 3.38	HSQC spectrum of 1-(benzoylcarbamoethyl)pyrrolidine-2-carboxylic acid (6).	130
Figure 3.39	HMBC spectrum of 1-(benzoylcarbamoethyl)pyrrolidine-2-carboxylic acid (6).	130
Figure 3.40	An ORTEP view of 2-[(benzoylcarbamoethyl)amino]-3-hydroxypropanoic acid (5) showing 50% probability displacement ellipsoids and the atom labelling.	135
Figure 3.41	An ORTEP view of 1-(benzoylcarbamoethyl)pyrrolidine-2-carboxylic acid (6) showing 50% probability displacement ellipsoids and the atom labelling.	136
Figure 3.42	An ORTEP view of 2-[(benzoylcarbamoethyl)amino]-4-(methylsulfanyl)butanoic acid (7) showing 50% probability displacement ellipsoids and the atom labelling.	136
Figure 3.43	An ORTEP view of 2-[(benzoylcarbamoethyl)amino]propanoic acid (8) showing 50% probability displacement ellipsoids and the atom labelling.	137
Figure 3.44	The atomic orbitals compositions of the frontier molecular orbitals for benzoyl isothiocyanate.	139
Figure 3.45	The atomic orbitals compositions of the frontier molecular orbital for 2-[(benzoylcarbamoethyl)amino]-3-hydroxypropanoic acid (5).	140
Figure 3.46	The atomic orbitals compositions of the frontier molecular orbital for serine.	140

Figure 3.47	The atomic orbitals compositions of the frontier molecular orbitals for 1-(benzoylcarbamothioyl)pyrrolidine-2-carboxylic acid (6).	141
Figure 3.48	The atomic orbitals compositions of the frontier molecular orbitals for proline.	141
Figure 3.49	The atomic orbitals compositions of the frontier molecular orbitals for 2-[(benzoylcarbamothioyl)amino]-4-(methylsulfanyl)butanoic acid (7).	142
Figure 3.50	The atomic orbitals compositions of the frontier molecular orbitals for methionine.	142
Figure 3.51	The atomic orbitals compositions of the frontier molecular orbitals for 2-[(benzoylcarbamothioyl)amino]propanoic acid (8).	143
Figure 3.52	The atomic orbitals compositions of the frontier molecular orbitals for alanine.	143
Figure 3.53	IR spectrum of methyl-2-[[phenylformamido)methanethioyl]amino} propanoate (10).	148
Figure 3.54	¹ H NMR spectrum of methyl-2-[[phenylformamido)methanethioyl]amino} propanoate (10).	149
Figure 3.55	¹³ C NMR spectrum of methyl-2-[[phenylformamido)methanethioyl]amino} propanoate (10).	149
Figure 3.56	IR spectrum of 1,4-dimethyl-2-[[phenylformamido)methanethioyl] butanedioate (11).	150
Figure 3.57	¹ H NMR spectrum of 1,4-dimethyl-2-[[phenylformamido)methanethioyl] butanedioate (11).	151
Figure 3.58	¹³ C NMR spectrum of 1,4-dimethyl-2-[[phenylformamido)methanethioyl] butanedioate (11).	151
Figure 3.59	An ORTEP view of methyl-2-[[phenylformamido)methanethioyl]amino} propanoate (10).	154
Figure 3.60	An ORTEP view of 1,4-dimethyl-2-[[phenylformamido)methanethioyl] butanedioate (11).	154
Figure 4.1	IR spectrum of 11-(3-nitrophenyl)-1,8,10,12-tetraazatricyclo[7.4.0.0 ^{2,7}] trideca-2(7),3,5,9,11-pentaene-13-thione (16).	163
Figure 4.2	¹ H NMR spectrum of 11-(3-nitrophenyl)-1,8,10,12-tetraazatricyclo [7.4.0.0 ^{2,7}]trideca-2(7),3,5,9,11-pentaene-13-thione (16).	163

Figure 4.3	^1H ^1H COSY spectrum of 11-(3-nitrophenyl)-1,8,10,12-tetraazatricyclo[7.4.0.0 ^{2,7}]trideca-2(7),3,5,9,11-pentaene-13-thione (16).	164
Figure 4.4	^{13}C NMR spectrum of 11-(3-nitrophenyl)-1,8,10,12-tetraazatricyclo[7.4.0.0 ^{2,7}] trideca-2(7),3,5,9,11-pentaene-13-thione (16).	164
Figure 4.5	Potential energy surface for the formation of the tetraazatricyclic derivatives.	169
Figure 4.6	IR spectrum of <i>N</i> -(1 <i>H</i> -benzimidazol-2-yl)benzamide (21).	170
Figure 4.7	^1H NMR spectrum of <i>N</i> -(1 <i>H</i> -benzimidazol-2-yl)benzamide (21).	171
Figure 4.8	^1H - ^1H COSY spectrum of <i>N</i> -(1 <i>H</i> -benzimidazol-2-yl)benzamide (21).	171
Figure 4.9	^{13}C NMR spectrum of <i>N</i> -(1 <i>H</i> -benzimidazol-2-yl)benzamide (21).	172
Figure 4.10	Potential energy surface, derived from transition states and intrinsic reaction coordinate calculations illustrating the pathway for the formation of <i>N</i> -(1 <i>H</i> -benzimidazol-2-yl)benzamide (21).	175
Figure 4.11	IR spectrum of 3-benzoyl-1-(2-hydroxyphenyl) urea (22).	177
Figure 4.12	^1H NMR spectrum of 3-benzoyl-1-(2-hydroxyphenyl) urea (22).	177
Figure 4.13	^1H - ^1H COSY spectrum of 3-benzoyl-1-(2-hydroxyphenyl) urea (22).	178
Figure 4.14	^{13}C NMR spectrum of 3-benzoyl-1-(2-hydroxyphenyl) urea (22).	178
Figure 4.15	An ORTEP view of 11-phenyl-1,8,10,12-tetraazatricyclo[7.4.0.0 ^{2,7}]trideca-2(7),3,5,9,11-pentaene-13-thione (20) showing 50% probability displacement ellipsoids and the atom labelling.	181
Figure 4.16	An ORTEP view of <i>N</i> -(1 <i>H</i> -benzimidazol-2-yl)benzamide (21) showing 50% probability displacement ellipsoids and the atom labelling.	181
Figure 4.17	An ORTEP view of 3-benzoyl-1-(2-hydroxyphenyl) urea (22) showing 50% probability displacement ellipsoids and the atom labelling.	182
Figure 4.18	EC ₅₀ values for the tetraazatricyclics (μM). Error bars represent the SEM for n = 3.	182
Figure 4.19	EC ₅₀ values for compounds 18 and 19 (μM). Error bars represent the SEM for n = 3.	184
Figure 4.20	HIV-1 protease screening results illustrating % inhibition of tetraazatricyclics (100 μM) and ritonavir (10 μM) compared to untreated control. Error bars represent SEM for n = 3.	185
Figure 4.21	2D represent of 11-(3-nitrophenyl)-1,8,10,12-tetraazatricyclo[7.4.0.0 ^{2,7}] trideca-2(7),3,5,9,11-pentaene-13-thione (16) in protease active site.	186

Figure 4.22	2D represent of 11-(4-nitrophenyl)-1,8,10,12-tetraazatricyclic[7.4.0.0 ^{2,7}]trideca-2(7),3,5,9,11-pentaene-13-thione (19) in protease active site.	187
Figure 4.23	2D represent of compound 11-(3-bromophenyl)-1,8,10,12-tetraazatricyclic[7.4.0.0 ^{2,7}]trideca-2(7),3,5,9,11-pentaene-13-thione (18) in protease active site.	188
Figure 5.1	IR spectrum of 3-(1,3-benzothiazol-2-yl)-1-(3-methoxybenzoyl)thiourea (27).	192
Figure 5.2	¹ H NMR spectrum of 3-(1,3-benzothiazol-2-yl)-1-(3-methoxybenzoyl)thiourea (27).	193
Figure 5.3	¹ H– ¹ H COSY spectrum of 3-(1,3-benzothiazol-2-yl)-1-(3-)thiourea (27).	193
Figure 5.4	¹³ C NMR spectrum of 3-(1,3-benzothiazol-2-yl)-1-(3-methoxybenzoyl)thiourea (27).	194
Figure 5.5	IR spectrum of 3-(1,3-benzothiazol-2-yl)-1-(3-bromobenzoyl)thiourea (31).	195
Figure 5.6	¹ H NMR spectrum of 3-(1,3-benzothiazol-2-yl)-1-(3-bromobenzoyl)thiourea (31)	196
Figure 5.7	¹ H– ¹ H COSY spectrum of 3-(1,3-benzothiazol-2-yl)-1-(3-bromobenzoyl)thiourea (31).	196
Figure 5.8	¹³ C NMR spectrum of 3-(1,3-benzothiazol-2-yl)-1-(3-bromobenzoyl)thiourea (31).	197
Figure 5.9	An ORTEP view of compound 3-(1,3-benzothiazol-2-yl)-1-(benzoyl)thiourea (23) showing 50% probability displacement ellipsoids and the atom labelling.	199
Figure 5.10	An ORTEP view of compound 3-(1,3-benzothiazol-2-yl)-1-(3-methoxybenzoyl)thiourea (27) showing 50% probability displacement ellipsoids and the atom labelling.	200
Figure 5.11	An ORTEP view of compound 3-(1,3-benzothiazol-2-yl)-1-(3-bromobenzoyl)thiourea (31) showing 50% probability displacement ellipsoids and the atom labelling.	200
Figure 5.12	Potential energy surface for 3-(1,3-benzothiazol-2-yl)-1-(benzoyl)thiourea derivatives.	203
Figure 5.13	EC ₅₀ values for the benzothiazole derivatives (μM). Error bars represent the SEM for n = 3.	204

- Figure 5.14 EC_{50} values for compounds **28** and **31** (μM). Error bars represent the SEM for $n = 3$. 205
- Figure 5.15 HIV-1 protease screening results illustrating % inhibition of benzothiazole (100 μM) and ritonavir (10 μM) derivatives compared to untreated control. Error bars represent SEM for $n = 3$. 206
- Figure 5.16 2D representation of 3-(1,3-benzothiazol-2-yl)-1-(4-chlorobenzoyl)thiourea (**24**) in the HIV-1 protease binding site. 207
- Figure 6.1 IR spectrum of 3-methoxy-*N*-[(9*E*)-8,10,17-triazatetracyclo [8.7.0.0^{2,7}.0^{11,16}]heptadeca-1(17),2,4,6,11(16),12,14-heptaen-9-ylidene] benzamide (**34**). 212
- Figure 6.2 ¹H NMR spectrum of 3-methoxy-*N*-[(9*E*)-8,10,17-triazatetracyclo [8.7.0.0^{2,7}.0^{11,16}]heptadeca-1(17),2,4,6,11(16),12,14-heptaen-9-ylidene] benzamide (**34**). 212
- Figure 6.3 ¹H ¹H COSY spectrum of 3-methoxy-*N*-[(9*E*)-8,10,17-triazatetracyclo [8.7.0.0^{2,7}.0^{11,16}]heptadeca-1(17),2,4,6,11(16),12,14-heptaen-9-ylidene] benzamide (**34**). 213
- Figure 6.4 ¹³C NMR spectrum of 3-methoxy-*N*-[(9*E*)-8,10,17-triazatetracyclo [8.7.0.0^{2,7}.0^{11,16}]heptadeca-1(17),2,4,6,11(16),12,14-heptaen-9-ylidene] benzamide (**34**). 213
- Figure 6.5 An ORTEP view of *N*-[(9*E*)-8,10,17-triazatetracyclo[8.7.0.0^{2,7}.0^{11,16}]heptadeca-1(17),2,4,6,11(16),12,14-heptaen-9-ylidene]benzamide (**39**) showing 50% probability displacement ellipsoids and the atom labelling. 219
- Figure 6.6 Potential energy surface for the formation of triazatetracyclics. 221
- Figure 6.7 EC_{50} values for the triazatetracyclics (μM). Error bars represent the SEM for $n = 3$. 222
- Figure 6.8 EC_{50} values for compounds **35** and **33** (μM). Error bars represent the SEM for $n = 3$. 223
- Figure 6.9 HIV-1 protease screening results illustrating % inhibition of triazatetracyclics (100 μM) and ritonavir (10 μM) relative to untreated control. Error bars represent SEM for $n = 3$. 224
- Figure 6.10 2D representation of 4-nitro-*N*-[(9*E*)-8,10,17-triazatetracyclo [8.7.0.0^{2,7}.0^{11,16}]heptadeca-1(17),2,4,6,11(16),12,14-heptaen-9-ylidene] benzamide (**38**). in the HIV-1 protease binding site. 225

- Figure 6.11 2D representation of 4-chloro-*N*-[(9*E*)-8,10,17-triazatetracyclo[8.7.0.0^{2,7}.0^{11,16}]heptadeca-1(17),2,4,6,11(16),12,14-heptaen-9-ylidene]benzamide (**35**) in the HIV-1 protease binding site. 226
- Figure 7.1 IR spectrum of 1-(3-nitrobenzoyl)-3-[2-({[(3-nitrophenyl)formamido]methane}amino)phenyl]thiourea (**44**). 231
- Figure 7.2 ¹H NMR spectrum of 1-(3-nitrobenzoyl)-3-[2-({[(3-nitrophenyl)formamido]methane}amino)phenyl]thiourea (**44**). 231
- Figure 7.3 ¹³C NMR spectrum of 1-(3-nitrobenzoyl)-3-[2-({[(3-nitrophenyl)formamido]methane}amino)phenyl]thiourea (**44**). 232
- Figure 7.4 IR spectrum of 3-benzoyl-1-(2-{{(phenylformamido)methanethioyl}amino}ethyl)thiourea (**50**). 234
- Figure 7.5 ¹H NMR spectrum of 3-benzoyl-1-(2-{{(phenylformamido)methanethioyl}amino}ethyl)thiourea (**50**). 235
- Figure 7.6 ¹³C NMR spectrum of 1 3-benzoyl-1-(2-{{(phenylformamido)methanethioyl}amino}ethyl)thiourea (**50**). 235
- Figure 7.7 An ORTEP view of 1-benzoyl-3-(5-methyl-2-{{(phenylformamido)methanethioyl}amino}phenyl)thiourea (**40**) showing 50% probability displacement ellipsoids and the atom labelling. 239
- Figure 7.8 An ORTEP view of 3-benzoyl-1-(2-{{(phenylformamido)methanethioyl}amino}ethyl)thiourea (**50**) showing 50% probability displacement ellipsoids and the atom labelling. 239
- Figure 7.9 An ORTEP view of 3-benzoyl-1-{{(phenylformido)methanethioyl}amino}thiourea dimethyl sulfoxide (**51**) showing 50% probability displacement ellipsoids and the atom labelling. 240
- Figure 7.10 IR spectrum of 3-benzoyl-1-(4-{{(phenylformamido)methanethioyl}amino}butyl)thiourea (**54**). 242
- Figure 7.11 ¹H NMR spectrum of 3-benzoyl-1-(4-{{(phenylformamido)methanethioyl}amino}butyl)thiourea (**54**). 242
- Figure 7.12 ¹³C NMR spectrum of 3-benzoyl-1-(4-{{(phenylformamido)methanethioyl}amino}butyl)thiourea (**54**). 243
- Figure 7.13 An ORTEP view of 3-benzoyl-1-{{(phenylformido)methanethioyl}amino}thiourea (**53**) showing 50% probability displacement ellipsoids and the atom labelling. 245

- Figure 7.14 An ORTEP view of 3-benzoyl-1-(4-[(phenylformamido) methanethioyl] amino)butyl)thiourea (**54**) showing 50% probability displacement ellipsoids and the atom labelling. 246
- Figure 7.15 EC₅₀ values for the diamine derivatives of benzoyl isothiocyanate (μM). Error bars represent the SEM for n = 3. 248
- Figure 7.16 EC₅₀ values for compounds **46** and **40** (μM). Error bars represent the SEM for n = 3. 248
- Figure 7.17 HIV-1 protease screening results illustrating % inhibition of selected diamine derivatives of benzoyl isothiocyanate (100 μM) and ritonavir (10 μM) relative to untreated control. Error bars represent SEM of n = 3. 251
- Figure 7.18 2D representation of 1-(4-methoxybenzoyl)-3-[2-([(4-methoxyphenyl) formamido]methanethioyl] amino)phenyl]thiourea (**47**) in the HIV-1 protease binding site. 252
- Figure 7.19 2D representation of 3-benzoyl-1-(4-[(phenylformamido) methanethioyl] amino)butyl)thiourea (**54**) in the HIV-1 protease binding site. 253
- Figure 7.20 2D representation of 1-(4-bromobenzoyl)-3-[2-([(4-bromophenyl) formamido]methanethioyl] amino)phenyl]thiourea (**46**) in the HIV-1 protease binding site. 254
- Figure 7.21 2D representation of 1-(3-bromobenzoyl)-3-[2-([(3-bromophenyl) formamido]methanethioyl] amino)phenyl]thiourea (**49**) in the HIV-1 protease binding site. 255
- Figure 8.1 IR spectrum of *N*-(benzothiazol-2-yl)-benzamide (**58**). 261
- Figure 8.2 ¹H NMR spectrum of *N*-(benzothiazol-2-yl)-benzamide (**58**). 261
- Figure 8.3 ¹³C NMR spectrum of *N*-(benzothiazol-2-yl)-benzamide (**58**). 262
- Figure 8.4 An ORTEP view of *N*-(benzothiazol-2-yl)-4-nitrobenzamide (**55**) showing 50% probability displacement ellipsoids and the atom labelling. 264
- Figure 8.5 An ORTEP view of *N*-(benzothiazol-2-yl)-3-bromobenzamide (**56**) showing 50% probability displacement ellipsoids and the atom labelling. 265
- Figure 8.6 An ORTEP view of *N*-(benzothiazol-2-yl)benzamide (**58**) showing 50% probability displacement ellipsoids and the atom labelling. 265
- Figure 8.7 An ORTEP view of chlorotriphenylphosphinegold(I). 266
- Figure 8.8 An ORTEP view of 1-((benzamido)formyl)urea (**59**). 272

Figure 8.9 An ORTEP view of *N*-(2,3-dihydro-1*H*-benzo[d]imidazol-2-yl)-3-nitrobenzamide (**60**). 273

APPENDICES

APPENDIX A

CHARACTERIZATION DATA FOR SOME AMINO ACID DERIVATIVES OF BENZOYL ISOTHIOCYANATE

- Figure A3.1 ^1H NMR spectrum of 2-[(benzoylcarbamothioyl)amino]-4-(methylsulfanyl)butanoic acid (**7**).
- Figure A3.2 ^{13}C NMR spectrum of 2-[(benzoylcarbamothioyl)amino]-4-(methylsulfanyl)butanoic acid (**7**).
- Figure A3.3 DEPT spectrum of 2-[(benzoylcarbamothioyl)amino]-4-(methylsulfanyl)butanoic acid (**7**).
- Figure A3.4 IR spectrum of 2-[(benzoylcarbamothioyl)amino]-4-(methylsulfanyl)butanoic acid (**7**).
- Figure A3.5 ^1H NMR spectrum of 2-[(benzoylcarbamothioyl)amino]propanoic acid (**8**).
- Figure A3.6 ^{13}C NMR spectrum of 2-[(benzoylcarbamothioyl)amino]propanoic acid (**8**).
- Figure A3.7 IR spectrum of 2-[(benzoylcarbamothioyl)amino]propanoic acid (**8**).
- Figure A3.8 ^1H NMR spectrum of 2-phenyl-1*H*-benzimidazole (**9**).
- Figure A3.9 ^{13}C NMR spectrum of 2-phenyl-1*H*-benzimidazole (**9**).
- Figure A3.10 IR spectrum of 2-phenyl-1*H*-benzimidazole (**9**).

APPENDIX B

CHARACTERIZATION DATA FOR SOME TETRAAZATRICYCLIC DERIVATIVES

- Figure A4.1 IR spectrum of 11-(4-chlorophenyl)-1,8,10,12-tetraazatricyclo[7.4.0.0^{2,7}]trideca-2(7),3,5,9,11-pentaene-13-thione (**12**).
- Figure A4.2 ^1H NMR spectrum of 11-(4-chlorophenyl)-1,8,10,12-tetraazatricyclo[7.4.0.0^{2,7}]trideca-2(7),3,5,9,11-pentaene-13-thione (**12**).
- Figure A4.3 ^1H - ^1H COSY spectrum of 11-(4-chlorophenyl)-1,8,10,12-tetraazatricyclo[7.4.0.0^{2,7}]trideca-2(7),3,5,9,11-pentaene-13-thione (**12**).
- Figure A4.4 ^{13}C NMR spectrum of 11-(4-chlorophenyl)-1,8,10,12-tetraazatricyclo[7.4.0.0^{2,7}]trideca-2(7),3,5,9,11-pentaene-13-thione (**12**).
- Figure A4.5 IR spectrum of 11-(4-bromophenyl)-,8,10,2-tetraazatricyclo[7.4.0.0^{2,7}]trideca-2(7),3,5,9,11-pentaene-13-thione (**13**).

- Figure A4.6 ^1H NMR spectrum of 11-(4-bromophenyl)-,8,10,2-tetraazatricyclo [7.4.0.0^{2,7}] trideca-2(7),3,5,9,11-pentaene-13-thione (**13**).
- Figure A4.7 ^1H ^1H COSY spectrum of 11-(4-bromophenyl)-,8,10,2-tetraazatricyclo [7.4.0.0^{2,7}]trideca-2(7),3,5,9,11-pentaene-13-thione (**13**).
- Figure A4.8 ^{13}C NMR spectrum of 11-(4-bromophenyl)-,8,10,2-tetraazatricyclo [7.4.0.0^{2,7}]trideca-2(7),3,5,9,11-pentaene-13-thione (**13**).
- Figure A4.9 IR spectrum of 11-(4-methoxyphenyl)-1,8,10,12-tetraazatricyclo[7.4.0.0^{2,7}] trideca-2(7),3,9,1-pentaene-13-thione (**14**).
- Figure A4.10 ^1H NMR spectrum of 11-(4-methoxyphenyl)-1,8,10,12-tetraazatricyclo [7.4.0.0^{2,7}] trideca-2(7),3,9,1-pentaene-13-thione (**14**).
- Figure A4.11 ^1H ^1H COSY spectrum of 11-(4-methoxyphenyl)-1,8,10,12-tetraazatricyclo [7.4.0.0^{2,7}] trideca-2(7),3,9,1-pentaene-13-thione (**14**).
- Figure A4.12 ^{13}C NMR spectrum of 11-(4-methoxyphenyl)-1,8,10,12-tetraazatricyclo [7.4.0.0^{2,7}]trideca-2(7),3,9,1-pentaene-13-thione (**14**).
- Figure A4.13 IR spectrum of 11-(3-methoxyphenyl)-1,8,10,12-tetraazatricyclo [7.4.0.0^{2,7}] trideca-2(7),3,5,9,11-pentaene-13-thione (**15**).
- Figure A4.14 ^1H NMR spectrum of 11-(3-methoxyphenyl)-1,8,10,12-tetraazatricyclo [7.4.0.0^{2,7}]trideca-2(7),3,5,9,11-pentaene-13-thione (**15**).
- Figure A4.15 ^1H ^1H COSY spectrum of 11-(3-methoxyphenyl)-1,8,10,12-tetraazatricyclo [7.4.0.0^{2,7}]trideca-2(7),3,5,9,11-pentaene-13-thione (**15**).
- Figure A4.16 ^{13}C NMR spectrum of 11-(3-methoxyphenyl)-1,8,10,12-tetraazatricyclo [7.4.0.0^{2,7}] trideca-2(7),3,5,9,11-pentaene-13-thione (**15**).
- Figure A4.17 IR spectrum of 11-(3-chlorophenyl)-1,8,10,12-tetraazatricyclo[7.4.0.0^{2,7}] trideca-2(7),3,5,9,11-pentaene-13-thione (**17**).
- Figure A4.18 ^1H NMR spectrum of 11-(3-chlorophenyl)-1,8,10,12-tetraazatricyclo [7.4.0.0^{2,7}] trideca-2(7),3,5,9,11-pentaene-13-thione (**17**).
- Figure A4.19 ^1H ^1H COSY spectrum of 11-(3-chlorophenyl)-1,8,10,12-tetraazatricyclo 7.4.0.0^{2,7}] trideca-2(7),3,5,9,11-pentaene-13-thione (**17**).
- Figure A4.20 ^{13}C NMR spectrum of 11-(3-chlorophenyl)-1,8,10,12-tetraazatricyclo [7.4.0.0^{2,7}]trideca-2(7),3,5,9,11-pentaene-13-thione (**17**).
- Figure A4.21 ^{13}C NMR spectrum of 11-(3-bromophenyl)-1,8,10,12-tetraazatricyclo [7.4.0.0^{2,7}]trideca-2(7),3,5,9,11-pentaene-13-thione (**18**).
- Figure A4.22 ^1H NMR spectrum of 11-(3-bromophenyl)-1,8,10,12-tetraazatricyclo [7.4.0.0^{2,7}]trideca-2(7),3,5,9,11-pentaene-13-thione (**18**).

- Figure A4.23 ^1H ^1H COSY spectrum of 11-(3-bromophenyl)-1,8,10,12-tetraazatricyclo [7.4.0.0^{2,7}]trideca-2(7),3,5,9,11-pentaene-13-thione (**18**).
- Figure A4.24 ^{13}C NMR spectrum of 11-(3-bromophenyl)-1,8,10,12-tetraazatricyclo [7.4.0.0^{2,7}]trideca-2(7),3,5,9,11-pentaene-13-thione (**18**).
- Figure A4.25 IR spectrum of 11-(4-nitrophenyl)-1,8,10,12-tetraazatricyclic [7.4.0.0^{2,7}] trideca-2(7),3,5,9,11-pentaene-13-thione (**19**).
- Figure A4.26 ^1H NMR spectrum of 11-(4-nitrophenyl)-1,8,10,12-tetraazatricyclic [7.4.0.0^{2,7}] trideca-2(7),3,5,9,11-pentaene-13-thione (**19**).
- Figure A4.27 ^1H ^1H COSY spectrum of 11-(4-nitrophenyl)-1,8,10,12-tetraazatricyclic [7.4.0.0^{2,7}] trideca-2(7),3,5,9,11-pentaene-13-thione (**19**).
- Figure A4.28 ^{13}C NMR spectrum of 11-(4-nitrophenyl)-1,8,10,12-tetraazatricyclic [7.4.0.0^{2,7}] trideca-2(7),3,5,9,11-pentaene-13-thione (**19**).
- Figure A4.29 IR spectrum of 11-phenyl-1,8,10,12-tetraazatricyclo[7.4.0.0^{2,7}]trideca-2(7),3,5,9,11-pentaene-13-thione (**20**).
- Figure A4.30 ^1H NMR spectrum of 11-phenyl-1,8,10,12-tetraazatricyclo[7.4.0.0^{2,7}]trideca-2(7),3,5,9,11-pentaene-13-thione (**20**).
- Figure A4.31 ^1H - ^1H COSY spectrum of 11-phenyl-1,8,10,12-tetraazatricyclo[7.4.0.0^{2,7}] trideca-2(7),3,5,9,11-pentaene-13-thione (**20**).
- Figure A4.32 ^{13}C NMR spectrum of 11-phenyl-1,8,10,12-tetraazatricyclo[7.4.0.0^{2,7}]trideca-2(7),3,5,9,11-pentaene-13-thione (**20**).

APPENDIX C

CHARACTERIZATION DATA FOR SOME 3-(1,3-BENZOTHAZOL-2-YL)-1-(BENZOYL) THIOUREA DERIVATIVES

- Figure A5.1 IR spectrum 3-(1,3-benzothiazol-2-yl)-1-(benzoyl)thiourea (**23**).
- Figure A5.2 ^1H NMR spectrum 3-(1,3-benzothiazol-2-yl)-1-(benzoyl)thiourea (**23**).
- Figure A5.3 ^1H - ^1H COSY spectrum 3-(1,3-benzothiazol-2-yl)-1-(benzoyl)thiourea (**23**).
- Figure A5.4 ^{13}C NMR spectrum 3-(1,3-benzothiazol-2-yl)-1-(benzoyl)thiourea (**23**).
- Figure A5.5 IR spectrum of 3-(1,3-benzothiazol-2-yl)-1-(4-chlorobenzoyl)thiourea (**24**).
- Figure A5.6 ^1H NMR spectrum of 3-(1,3-benzothiazol-2-yl)-1-(4-chlorobenzoyl)thiourea (**24**).
- Figure A5.7 ^1H - ^1H COSY spectrum of 3-(1,3-benzothiazol-2-yl)-1-(4-chlorobenzoyl)thiourea (**24**).

- Figure A5.8 ^{13}C NMR spectrum of 3-(1,3-benzothiazol-2-yl)-1-(4-chlorobenzoyl)thiourea (**24**).
- Figure A5.9 IR spectrum of 3-(1,3-benzothiazol-2-yl)-1-(4-bromobenzoyl)thiourea (**25**).
- Figure A5.10 ^1H NMR spectrum of 3-(1,3-benzothiazol-2-yl)-1-(4-bromobenzoyl)thiourea (**25**).
- Figure A5.11 ^1H ^1H COSY spectrum of 3-(1,3-benzothiazol-2-yl)-1-(4-bromobenzoyl)thiourea (**25**).
- Figure A5.12 ^{13}C NMR spectrum of 3-(1,3-benzothiazol-2-yl)-1-(4-bromobenzoyl)thiourea (**25**).
- Figure A5.13 IR spectrum of 3-(1,3-benzothiazol-2-yl)-1-(4-methoxybenzoyl)thiourea (**26**).
- Figure A5.14 ^1H NMR spectrum of 3-(1,3-benzothiazol-2-yl)-1-(4-methoxybenzoyl)thiourea (**26**).
- Figure A5.15 ^1H ^1H COSY spectrum of 3-(1,3-benzothiazol-2-yl)-1-(4-methoxybenzoyl)thiourea (**26**).
- Figure A5.16 ^{13}C NMR spectrum of 3-(1,3-benzothiazol-2-yl)-1-(4-methoxybenzoyl)thiourea (**26**).
- Figure A5.17 IR spectrum of 3-(1,3-benzothiazol-2-yl)-1-(3-nitrobenzoyl)thiourea (**28**).
- Figure A5.18 ^1H NMR spectrum of 3-(1,3-benzothiazol-2-yl)-1-(3-nitrobenzoyl)thiourea (**28**).
- Figure A5.19 ^1H - ^1H COSY spectrum of 3-(1,3-benzothiazol-2-yl)-1-(3-nitrobenzoyl)thiourea (**28**).
- Figure A5.20 ^{13}C NMR spectrum of 3-(1,3-benzothiazol-2-yl)-1-(3-nitrobenzoyl)thiourea (**28**).
- Figure A5.21 IR spectrum of 3-(1,3-benzothiazol-2-yl)-1-(3-chlorobenzoyl)thiourea (**29**).
- Figure A5.22 ^1H NMR spectrum of 3-(1,3-benzothiazol-2-yl)-1-(3-chlorobenzoyl)thiourea (**29**).
- Figure A5.23 ^1H - ^1H COSY spectrum of 3-(1,3-benzothiazol-2-yl)-1-(3-chlorobenzoyl)thiourea (**29**).
- Figure A5.24 ^{13}C NMR spectrum of 3-(1,3-benzothiazol-2-yl)-1-(3-chlorobenzoyl)thiourea (**29**).
- Figure A5.25 IR spectrum of 3-(1,3-benzothiazoyl-2-yl)-1-(4-nitrobenzoyl)thiourea (**30**).
- Figure A5.26 ^1H NMR spectrum of 3-(1,3-benzothiazoyl-2-yl)-1-(4-nitrobenzoyl)thiourea (**30**).

Figure A5.27 ^1H - ^1H COSY spectrum of 3-(1,3-benzothiazoyl-2-yl)-1-(4-nitrobenzoyl)thiourea (**30**).

Figure A5.28 ^{13}C NMR spectrum of 3-(1,3-benzothiazoyl-2-yl)-1-(4-nitrobenzoyl)thiourea (**30**).

APPENDIX D

CHARACTERIZATION DATA FOR SOME TRIAZATETRACYCLIC DERIVATIVES

Figure A6.1 IR spectrum of 4-bromo-*N*-[(9*E*)-8,10,17-triazatetracyclo [8.7.0.0^{2,7}.0^{11,16}]heptadeca-1(17),2,4,6,11(16),12,14-heptaen-9-ylidene]benzamide (**32**).

Figure A6.2 ^1H NMR spectrum of 4-bromo-*N*-[(9*E*)-8,10,17-triazatetracyclo [8.7.0.0^{2,7}.0^{11,16}]heptadeca-1(17),2,4,6,11(16),12,14-heptaen-9-ylidene]benzamide (**32**).

Figure A6.3 ^1H - ^1H COSY spectrum of 4-bromo-*N*-[(9*E*)-8,10,17-triazatetracyclo 8.7.0.0^{2,7}.0^{11,16}]heptadeca-1(17),2,4,6,11(16),12,14-heptaen-9-ylidene]benzamide (**32**).

Figure A6.4 ^{13}C NMR spectrum of 4-bromo-*N*-[(9*E*)-8,10,17-triazatetracyclo [8.7.0.0^{2,7}.0^{11,16}]heptadeca-1(17),2,4,6,11(16),12,14-heptaen-9-ylidene]benzamide (**32**).

Figure A6.5 IR spectrum of 4-methoxy-*N*-[(9*E*)-8,10,17-triazatetracyclo[8.7.0.0^{2,7}.0^{11,16}]heptadeca-1(17),2,4,6,11(16),12,14-heptaen-9-ylidene]benzamide (**33**).

Figure A6.6 ^1H NMR spectrum of 4-methoxy-*N*-[(9*E*)-8,10,17-triazatetracyclo [8.7.0.0^{2,7}.0^{11,16}] heptadeca-1(17),2,4,6,11(16),12,14-heptaen-9-ylidene]benzamide (**33**).

Figure A6.7 ^1H - ^1H COSY spectrum of 4-methoxy-*N*-[(9*E*)-8,10,17-triazatetracyclo [8.7.0.0^{2,7}.0^{11,16}]heptadeca-1(17),2,4,6,11(16),12,14-heptaen-9-ylidene]benzamide (**33**).

Figure A6.8 ^{13}C NMR spectrum of 4-methoxy-*N*-[(9*E*)-8,10,17-triazatetracyclo [8.7.0.0^{2,7}.0^{11,16}]heptadeca-1(17),2,4,6,11(16),12,14-heptaen-9-ylidene]benzamide (**33**).

Figure A6.9 IR spectrum of 4-chloro-*N*-[(9*E*)-8,10,17-triazatetracyclo [8.7.0.0^{2,7}.0^{11,16}]heptadeca-1(17),2,4,6,11(16),12,14-heptaen-9-ylidene] benzamide (**35**).

- Figure A6.10 ^1H NMR spectrum of 4-chloro-*N*-[(9*E*)-8,10,17-triazatetracyclo [8.7.0.0^{2,7}.0^{11,16}]heptadeca-1(17),2,4,6,11(16),12,14-heptaen-9-ylidene] benzamide (**35**).
- Figure A6.11 ^1H H COSY spectrum of 4-chloro-*N*-[(9*E*)-8,10,17-triazatetracyclo [8.7.0.0^{2,7}.0^{11,16}]heptadeca-1(17),2,4,6,11(16),12,14-heptaen-9-ylidene] benzamide (**35**).
- Figure A6.12 ^{13}C NMR spectrum of 4-chloro-*N*-[(9*E*)-8,10,17-triazatetracyclo [8.7.0.0^{2,7}.0^{11,16}]heptadeca-1(17),2,4,6,11(16),12,14-heptaen-9-ylidene] benzamide (**35**).
- Figure A6.13 IR spectrum of 3-nitro-*N*-[(9*E*)-8,10,17-triazatetracyclo [8.7.0.0^{2,7}.0^{11,16}]heptadeca-1(17),2,4,6,11(16), 12,14-heptaen-9-ylidene] benzamide (**36**).
- Figure A6.14 ^1H NMR spectrum of 3-nitro-*N*-[(9*E*)-8,10,17-triazatetracyclo [8.7.0.0^{2,7}.0^{11,16}]heptadeca-1(17),2,4,6,11(16),12,14-heptaen-9-ylidene] benzamide (**36**).
- Figure A6.15 ^1H H COSY spectrum of 3-nitro-*N*-[(9*E*)-8,10,17-triazatetracyclo [8.7.0.0^{2,7}.0^{11,16}]heptadeca-1(17),2,4,6,11(16),12,14-heptaen-9-ylidene] benzamide (**36**).
- Figure A6.16 ^{13}C NMR spectrum of 3-nitro-*N*-[(9*E*)-8,10,17-triazatetracyclo [8.7.0.0^{2,7}.0^{11,16}]heptadeca-1(17),2,4,6,11(16),12,14-heptaen-9-ylidene] benzamide (**36**).
- Figure A6.17 IR spectrum of 3-chloro-*N*-[(9*E*)-8,10,17-triazatetracyclo [8.7.0.0^{2,7}.0^{11,16}]heptadeca-1(17),2,4,6,11(16),12,14-heptaen-9-ylidene] benzamide (**37**).
- Figure A6.18 ^1H NMR spectrum of, 3-chloro-*N*-[(9*E*)-8,10,17-triazatetracyclo [8.7.0.0^{2,7}.0^{11,16}]heptadeca-1(17),2,4,6,11(16),12,14-heptaen-9-ylidene] benzamide (**37**).
- Figure A6.19 ^{13}C NMR spectrum of 3-chloro-*N*-[(9*E*)-8,10,17-triazatetracyclo [8.7.0.0^{2,7}.0^{11,16}]heptadeca-1(17),2,4,6,11(16),12,14-heptaen-9-ylidene] benzamide (**37**).
- Figure A6.20 IR spectrum of 4-nitro-*N*-[(9*E*)-8,10,17-triazatetracyclo [8.7.0.0^{2,7}.0^{11,16}]heptadeca-1(17),2,4,6,11(16),12,14-heptaen-9-ylidene] benzamide (**38**).
- Figure A6.21 ^1H NMR spectrum of 4-nitro-*N*-[(9*E*)-8,10,17-triazatetracyclo [8.7.0.0^{2,7}.0^{11,16}]heptadeca-1(17),2,4,6,11(16),12,14-heptaen-9-ylidene] benzamide (**38**).

Figure A6.22 IR spectrum of *N*-[(9*E*)-8,10,17-triazatetracyclo[8.7.0.0^{2,7}.0^{11,16}]heptadeca-1(17),2,4,6,11(16),12,14-heptaen-9-ylidene]benzamide (**39**).

Figure A6.23 ¹H NMR spectrum of 3-bromo-*N*-[(9*E*)-8,10,17-triazatetracyclo[8.7.0.0^{2,7}.0^{11,16}]heptadeca-1(17),2,4,6,11(16),12,14-heptaen-9-ylidene]benzamide (**39**).

Figure A6.24 ¹H ¹H COSY spectrum of 3-bromo-*N*-[(9*E*)-8,10,17-triazatetracyclo[8.7.0.0^{2,7}.0^{11,16}]heptadeca-1(17),2,4,6,11(16),12,14-heptaen-9-ylidene]benzamide (**39**).

Figure A6.25 ¹³C NMR spectrum of 3-bromo-*N*-[(9*E*)-8,10,17-triazatetracyclo[8.7.0.0^{2,7}.0^{11,16}]heptadeca-1(17),2,4,6,11(16),12,14-heptaen-9-ylidene]benzamide (**39**).

APPENDIX E

CHARACTERIZATION DATA FOR SOME PHENYL THIOUREA COMPOUNDS AND OTHER DIAMINE DERIVATIVES

Figure A7.1 IR spectrum of 1-benzoyl-3-(5-methyl-2-[[phenylformamido)methanethiyl]amino}phenyl)thiourea (**40**).

Figure A7.2 ¹H NMR spectrum of 1-benzoyl-3-(5-methyl-2-[[phenylformamido)methanethiyl]amino}phenyl)thiourea (**40**).

Figure A7.3 ¹³C NMR spectrum of 1-benzoyl-3-(5-methyl-2-[[phenylformamido)methanethiyl]amino}phenyl)thiourea (**40**).

Figure A7.4 IR spectrum of 1-benzoyl-3-(2-[[phenylformamido)methanethiyl]amino}phenyl)thiourea (**41**).

Figure A7.5 ¹H NMR spectrum of 1-benzoyl-3-(2-[[phenylformamido)methanethiyl]amino}phenyl)thiourea (**41**).

Figure A7.6 ¹³C NMR spectrum of 1-benzoyl-3-(2-[[phenylformamido)methanethiyl]amino}phenyl)thiourea (**41**).

Figure A7.7 IR spectrum of 1-(4-nitrobenzoyl)-3-[2-([[4-nitrophenyl]formamido)methanethiylphenyl]thiourea}amino) (**42**).

Figure A7.8 ¹H NMR spectrum of 1-(4-nitrobenzoyl)-3-[2-([[4-nitrophenyl]formamido)methanethiylphenyl]thiourea}amino) (**42**).

- Figure A7.9 ^{13}C NMR spectrum of 1-(4-nitrobenzoyl)-3-[2-({[(4-nitrophenyl)formamido]methanthioyl phenyl}thiourea) amino) (**42**).
- Figure A7.10 IR spectrum of 1-(4-chlorobenzoyl)-3-[2-({[(4-chlorophenyl)formamido]methanethioyl} amino)phenylthiourea (**43**).
- Figure A7.11 ^1H NMR spectrum of 1-(4-chlorobenzoyl)-3-[2-({[(4-chlorophenyl)formamido]methanethioyl} amino)phenylthiourea (**43**).
- Figure A7.12 ^{13}C NMR spectrum of 1-(4-chlorobenzoyl)-3-[2-({[(4-chlorophenyl)formamido]methanethioyl} amino)phenylthiourea (**43**).
- Figure A7.13 IR spectrum of 1-(3-methoxybenzoyl)-3-[2-({[(3-methoxyphenyl)formamido]methanethioyl} amino)phenyl]thiourea (**45**).
- Figure A7.14 ^1H NMR spectrum of 1-(3-methoxybenzoyl)-3-[2-({[(3-methoxyphenyl)formamido]methanethioyl} amino)phenyl]thiourea (**45**).
- Figure A7.15 ^{13}C NMR spectrum of 1-(3-methoxybenzoyl)-3-[2-({[(3-methoxyphenyl)formamido]methanethioyl} amino)phenyl]thiourea (**45**).
- Figure A7.16 IR spectrum of 1-(4-bromobenzoyl)-3-[2-({[(4-bromophenyl)formamido]methanethioyl} amino)phenyl]thiourea (**46**).
- Figure A7.17 ^1H NMR spectrum 1-(4-bromobenzoyl)-3-[2-({[(4-bromophenyl)formamido]methanethioyl} amino)phenyl]thiourea (**46**).
- Figure A7.18 ^{13}C NMR spectrum of 1-(4-bromobenzoyl)-3-[2-({[(4-bromophenyl)formamido]methanethioyl} amino)phenyl]thiourea (**46**).
- Figure A7.19 IR spectrum of 1-(4-methoxybenzoyl)-3-[2-({[(4-methoxyphenyl)formamido]methanethioyl} amino)phenyl]thiourea (**47**).
- Figure A7.20 ^1H NMR spectrum of 1-(4-methoxybenzoyl)-3-[2-({[(4-methoxyphenyl)formamido]methanethioyl} amino)phenyl]thiourea (**47**).
- Figure A7.21 ^{13}C NMR spectrum of 1-(4-methoxybenzoyl)-3-[2-({[(4-methoxyphenyl)formamido]methanethioyl} amino)phenyl]thiourea (**47**).
- Figure A7.22 IR spectrum of 1-(3-chlorobenzoyl)-3-[2-({[(3-chlorophenyl)formamido]methanethioyl} amino)phenyl]thiourea (**48**).
- Figure A7.23 ^1H NMR spectrum of 1-(3-chlorobenzoyl)-3-[2-({[(3-chlorophenyl)formamido]methanethioyl} amino)phenyl]thiourea (**48**).
- Figure A7.24 ^{13}C NMR spectrum of 1-(3-chlorobenzoyl)-3-[2-({[(3-chlorophenyl)formamido]methanethioyl} amino)phenyl]thiourea (**48**).
- Figure A7.25 IR spectrum of 1-(3-bromobenzoyl)-3-[2-({[(3-bromophenyl)formamido]methanethioyl} amino)phenyl]thiourea (**49**).

Figure A7.26 ^1H NMR spectrum of 1-(3-bromobenzoyl)-3-[2-(((3-bromophenyl)formamido)methanethioyl)amino]phenyl]thiourea (**49**).

Figure A7.27 ^{13}C NMR spectrum of 1-(3-bromobenzoyl)-3-[2-(((3-bromophenyl)formamido)methanethioyl)amino]phenyl]thiourea (**49**).

Figure A7.28 IR spectrum of 3-benzoyl-1-(((phenylformido)methanethioyl)amino)thiourea (**51**).

Figure A7.29 ^1H NMR spectrum of 3-benzoyl-1-(((phenylformido)methanethioyl)amino)thiourea (**51**).

Figure A7.30 ^{13}C NMR spectrum of 3-benzoyl-1-(((phenylformido)methanethioyl)amino)thiourea (**51**).

Figure A7.31 IR spectrum of 3-benzoyl-1-(phenylamino)thiourea (**52**).

Figure A7.32 ^1H NMR spectrum of 3-benzoyl-1-(phenylamino)thiourea (**52**).

Figure A7.33 ^{13}C NMR 3-benzoyl-1-(phenylamino)thiourea (**52**).

Figure A7.34 IR spectrum of 1-((benzamido)sulfanylenemethyl)urea (**53**).

Figure A7.35 ^1H NMR spectrum of 1-((benzamido)sulfanylenemethyl)urea (**53**).

Figure A7.36 ^{13}C NMR spectrum of 1-((benzamido)sulfanylenemethyl)urea (**53**).

APPENDIX F

CHARACTERIZATION DATA FOR SOME BENZAMIDE DERIVATIVES

Figure A8.1 IR spectrum of *N*-(benzothiazol-2-yl)-4-nitrobenzamide (**55**).

Figure A8.2 ^1H NMR spectrum of *N*-(benzothiazol-2-yl)-4-nitrobenzamide (**55**).

Figure A8.3 ^{13}C NMR spectrum of *N*-(benzothiazol-2-yl)-4-nitrobenzamide (**55**).

Figure A8.4 IR spectrum of *N*-(benzothiazol-2-yl)-3-bromobenzamide (**56**).

Figure A8.5 ^1H NMR spectrum of *N*-(benzothiazol-2-yl)-3-bromobenzamide (**56**).

Figure A8.6 ^{13}C NMR spectrum of *N*-(benzothiazol-2-yl)-3-bromobenzamide (**56**).

Figure A8.7 IR spectrum of *N*-(benzothiazol-2-yl)-3-methoxybenzamide (**57**).

Figure A8.8 ^1H NMR spectrum of *N*-(benzothiazol-2-yl)-3-methoxybenzamide (**57**).

Figure A8.9 ^{13}C NMR spectrum of *N*-(benzothiazol-2-yl)-3-methoxybenzamide (**57**).

Figure A8.10 IR spectrum of 1-((benzamido)formyl)urea (**59**).

Figure A8.11 ^{13}C NMR spectrum of 1-((benzamido)formyl)urea (**59**).

Figure A8.12 ^{13}C NMR spectrum of 1-((benzamido)formyl)urea (**59**).

Figure A8.13 IR spectrum of *N*-(2,3-dihydro-1*H*-benzimidazol-2-yl)-3-nitrobenzamide

(60).

Figure A8.14 ^1H NMR spectrum of *N*-(2,3-dihydro-1*H*-benzimidazol-2-yl)-3-nitrobenzamide (60).

Figure A8.15 ^{13}C NMR spectrum of *N*-(2,3-dihydro-1*H*-benzimidazol-2-yl)-3-nitrobenzamide (60).

LIST OF SCHEMES

Scheme 1.1	Synthesis of benzimidazoles using dioxane dibromide	18
Scheme 1.2	Synthesis of benzimidazole using solid heteropoly supported on silica gel	18
Scheme 1.3	Synthesis of benzimidazoles from acid chloride in the presence of anhydrous acetone	19
Scheme 1.4	Synthesis of benzimidazoles using ytterbium perfluorooctanesulfonates	19
Scheme 1.5	Indium catalyzed synthesis of benzimidazoles	20
Scheme 1.6	Synthesis of benzimidazoles using air as catalyst	21
Scheme 1.7	AIKIT-5 catalyzed synthesis of benzimidazoles	21
Scheme 1.8	CAN and hydrogen peroxide catalyzed synthesis of benzimidazoles	22
Scheme 1.9	Dowex 50 W catalyzed synthesis of benzimidazoles in water	23
Scheme 1.10	Synthesis of benzimidazoles from carboxylic acids in SOCl ₂ -DMF	24
Scheme 1.11	1,3-Diaza Claisen rearrangement reactions of thiourea derivatives	30
Scheme 1.12	Double insertion reactions of benzoyl isothiocyanates	30
Scheme 1.13	Substitution reactions of thiones	31
Scheme 1.14	Triphenylphosphine catalyzed cyclizations of benzoyl isothiocyanate derivatives	31
Scheme 1.15	Double insertion reactions of benzoyl isothiocyanates	32
Scheme 1.16	Synthesis of thiosemicarbazones <i>via</i> a reaction of phenyl or <i>p</i> -chlorophenyl isothiocyanate, hydrazine, and aldehydes or ketones.	32
Scheme 1.17	Synthesis of 2-aminothiazoles from bromocarbonyl compounds and amines	33
Scheme 1.18	Synthesis of 2-aminothiazoles from isothiocyanates, amidines/guanidines and various halomethylenes	33
Scheme 1.19	Photocyclization of substituted 1,2,4-triazole-3-thiones, under base-mediated conditions	34
Scheme 1.20	Equilibrium for gold ligand scrambling reactions	42
Scheme 3.1	Proposed synthetic path to access some of the docked compounds (set 1)	92
Scheme 3.2	Proposed synthetic path to access some of the docked compounds (set 2)	93
Scheme 3.3	Proposed mechanism for the synthesis of compound 2 from an aldehyde	96
Scheme 3.4	A synthesis scheme of 3-methyl- <i>N</i> -[2-(3-methylbenzamido)phenyl]benzamide (1) and 2-(3-methylphenyl)-1 <i>H</i> -benzimidazole (2)	97

Scheme 3.5	Synthesis of 2,2,4-trimethyl-2,3-dihydro-1 <i>H</i> -benzodiazepin-5-ium isophthalate (3)	110
Scheme 3.6	A proposed mechanism for the formation of 2,2,4-trimethyl-2,3-dihydro-1 <i>H</i> -benzodiazepin-5-ium isophthalate (3) and 2,2,4-trimethyl-2,3-dihydro-1 <i>H</i> -1,5-benzodiazopine (4)	115
Scheme 3.7	Synthesis of benzimidazoles of amino acid derivatives of benzoyl isothiocyanate	121
Scheme 3.8	Synthesis scheme for compounds 5 and 7–9	122
Scheme 3.9	Synthesis scheme for compounds 6 and 9	122
Scheme 3.10	Synthesis of amide of amino acid derivatives of benzoyl isothiocyanate	145
Scheme 3.11	Synthesis of amides of amino acid derivatives of benzoyl isothiocyanate <i>via</i> chlorination of the acid	146
Scheme 3.12	Synthesis of amide of <i>via</i> chlorination of amino acid	147
Scheme 3.13	Synthesis of benzoyl isothiocyanate derivatives with structurally diverse diamines	155
Scheme 3.14	Synthesis of benzoyl isothiocyanate derivatives of other diamine	157
Scheme 4.1	Synthesis of tetraazatricyclic derivatives	160
Scheme 4.2	Synthesis of tetraazatricyclic derivatives from thiourea	160
Scheme 4.3	Synthesis of tetraazatricyclic derivatives from carbon disulphide	161
Scheme 4.4	DFT reaction mechanism of tetraazatricyclic derivatives	168
Scheme 4.5	Degradative synthesis of <i>N</i> -(1 <i>H</i> -benzimidazol-2-yl)benzamide (21)	170
Scheme 4.6	DFT reaction mechanism of <i>N</i> -(1 <i>H</i> -benzimidazol-2-yl)benzamide (21)	174
Scheme 4.7	Synthesis of 3-benzoyl-1-(2-hydroxyphenyl) urea (22)	175
Scheme 4.8	Proposed reaction mechanism for the formation of 3-benzoyl-1-(2-hydroxyphenyl) urea (22)	177
Scheme 5.1	Synthesis of 3-(1,3-benzothiazol-2-yl)-1-(benzoyl)thiourea derivatives	190
Scheme 5.2	DFT reaction mechanism of 3-(1,3-benzothiazol-2-yl)-1-(benzoyl)thiourea	203
Scheme 6.1	Synthesis of triazatetracyclics derivatives	210
Scheme 6.2	Proposed reaction mechanism for the formation of triazatetracyclics from ketones and aldehydes	216
Scheme 6.3	DFT reaction mechanism of triazatetracyclics	220
Scheme 7.1	Synthesis of 1-benzoyl-3-(2-[(phenylformamido)methanethioyl]amino)phenyl)thiourea derivatives	229

Scheme 8.1	Attempted synthesis of gold complex of benzothiazole derivatives	258
Scheme 8.2	Attempted synthesis of gold complexes of 3-(1,3-benzothiazol-2-yl)-1-(4-benzoyl)thiourea derivatives	259
Scheme 8.3	Synthesis of gold compounds <i>via</i> silver complexes	267
Scheme 8.4	Synthesis of 1-((benzamido)formyl)urea (59)	268
Scheme 8.5	Synthesis of <i>N</i> -(2,3-dihydro-1 <i>H</i> -benzo[d]imidazol-2-yl)-3-nitrobenzamide (60)	269
Scheme 8.6	Proposed pathway for the Synthesis of <i>N</i> -(2,3-dihydro-1 <i>H</i> -benzo[d]imidazol-2-yl)-3-nitrobenzamide (60)	270

LIST OF ABBREVIATIONS

AIDS	Acquired immune deficiency syndrome
ARV	Antiretroviral drugs
DFT	Density functional theory
DMSO	Dimethyl sulfoxide
DNA	Deoxyribonucleic aci
FDA	Food and drugs administration
GDP	Guanosine Diphosphate
GTP	Guanosine triphosphate
HAART	Highly active antiretroviral therapy
HIV	Human immune-deficiency Virus
IN	Integrase
NLS	Nuclear Localization signal
Nrna	Messenger ribonucleic acid
PI	Protease Inhibitors
PMBC	Perpheral blood mononuclear cells
PR	Protease
RBC	Red blood cells
RRE	Rev Response element
RSV	Rous Sarcoma Virus
RT	Reverse transcriptase
SIV	Simian Immunodeficiency Virus
THF	Tetrahydrofuran
M.p	Melting point
Hours	h
XRD	X-ray diffractometry
DIDS	4,4'- diisothiocyanatostilbene-2,2'-D,L-sulfonic acid

CHAPTER 1

INTRODUCTION

1.1 Overview of HIV

The Human Immuno-deficiency Virus (HIV) is one of the most challenging epidemics of the 21st century.¹ Its devastating consequences have been evident over decades. The disease was first reported in young homosexual men in whom a rare disease, *Pneumocystis carinii*, and other unusual infections had developed. They had abnormal ratios of lymphocyte subgroups which was actively shedding cytomegalovirus.² The major cause of acquired immune deficiency syndrome (AIDS) is the human immunodeficiency virus type 1 (HIV-1). Evolutionary comparisons have been used to trace the origin(s) of HIV-1 and AIDS. The closest relatives of HIV-1 are simian immunodeficiency viruses (SIVs) infecting wild-living chimpanzees (*Pan troglodytes troglodytes*) and gorillas (*Gorilla gorilla gorilla*) in west central Africa. Phylogenetic analyses have revealed that, chimpanzees were the original hosts of this clade of viruses; four lineages of HIV-1 have arisen by independent cross-species transmissions to humans and one or two of those transmissions may have been *via* gorillas.

However, SIVs are primarily monkey viruses and more than 40 species of African monkeys are infected with their own species-specific SIV and in some host species, the infection seems non-pathogenic. Chimpanzees have acquired, from monkeys, two distinct forms of SIVs that recombined to produce a virus with a unique genome structure. SIV infection has been found to cause CD4⁺ T-cell depletion and increased mortality in wild chimpanzees. Tracing the genetic changes that occurred as monkey viruses adapted to infect first chimpanzees and then humans may provide insights into the causes of the pathogenicity of these viruses.³ Cross-species transmissions of simian immunodeficiency virus (SIVcpzPtt) gave rise to pandemic (group M) and non-pandemic (groups N and O) clades of HIV-1. To identify host-specific adaptations in HIV-1, the inferred ancestral sequences of HIV-1 groups M, N and O to 12 full length genome sequences of SIVcpzPtt have been compared with four of the outlying but closely related SIVcpzPtt (from *P. t. schweinfurthii*).⁴

Low-to-middle income countries bear the overwhelming burden of the (HIV-1) epidemic in terms of the numbers of their citizens living with HIV/AIDS, the high degrees of viral

diversity often involving multiple HIV-1 clades circulating within their populations, and the social and economic factors that compromise current control measures. Distinct epidemics have emerged in different geographical areas. These epidemics differ in their severity, the population groups they affect, their associated risk behaviors, and the viral strains that drive them. In addition to inflicting great human cost, the high burden of HIV infection has a major impact on the social and economic development of many low- to middle-income countries. Furthermore, the high degrees of viral diversity associated with multiclade HIV epidemics impacts viral diagnosis and pathogenicity and treatment which poses daunting challenges for effective vaccine development.⁵

The human immunodeficiency virus 1 (HIV-1) synthesizes its genomic DNA in the cytoplasm as soon as it enters the cell. The newly synthesized DNA remains associated with viral/cellular proteins as a high molecular weight pre-integration complex (PIC) which precludes passive diffusion across the intact nuclear membrane. However, HIV-1 successfully overcomes the nuclear membrane barrier by actively delivering its DNA into the nucleus with the help of host nuclear import machinery. Such ability allows HIV-1 to productively infect non-dividing cells as well as dividing cells at interphase. HIV-1 nuclear import is also found to be important for the proper integration of viral DNA. Thus, nuclear import plays a crucial role in the establishment of infection and disease progression. While several viral components, including matrix, viral protein R, integrase, capsid, and central DNA flap are implicated in HIV-1 nuclear import and their molecular mechanism remains poorly understood.⁶

1.1.1 Morphology of the mature virion

HIV is a member of the lentivirus genus, which includes retroviruses that possess complex genomes and exhibit cone-shaped capsid core particles. HIV's genome is encoded by RNA, which is reverse-transcribed to viral DNA by the viral reverse transcriptase (RT) upon entering a new host cell. The general features of the mature HIV virion and ribbon drawings of the structurally characterized viral proteins are shown in **Figure 1.1**. All lentiviruses are enveloped by a lipid bilayer (yellow) that is derived from the membrane of the host cell. Exposed surface glycoproteins (SU, gp120; cyan) are anchored to the virus *via* interactions with the transmembrane protein (TM, gp41; violet).⁷ The lipid bilayer also contains several

cellular membrane proteins derived from the host cell, including major histocompatibility antigens, actin and ubiquitin.⁸

A matrix shell comprising approximately 2000 copies of the matrix protein (MA, p17; green) lines the inner surface of the viral membrane, and a conical capsid core particle comprising ca. 2000 copies of the capsid protein (CA, p24; red) is located in the center of the virus. The capsid particle encapsidates two copies of the unspliced viral genome, which is stabilized as a ribonucleoprotein complex with ca 2000 copies of the nucleocapsid protein (NC, p7; blue), and also contains three essential virally encoded enzymes: protease (PR; pink), reverse transcriptase (RT; purple) and integrase (IN; olive). Virus particles also package the accessory proteins, Nef (orange), Vif and Vpr (not shown). Three additional accessory proteins that function in the host cell, Rev, Tat and Vpu, do not appear to be packaged.⁹

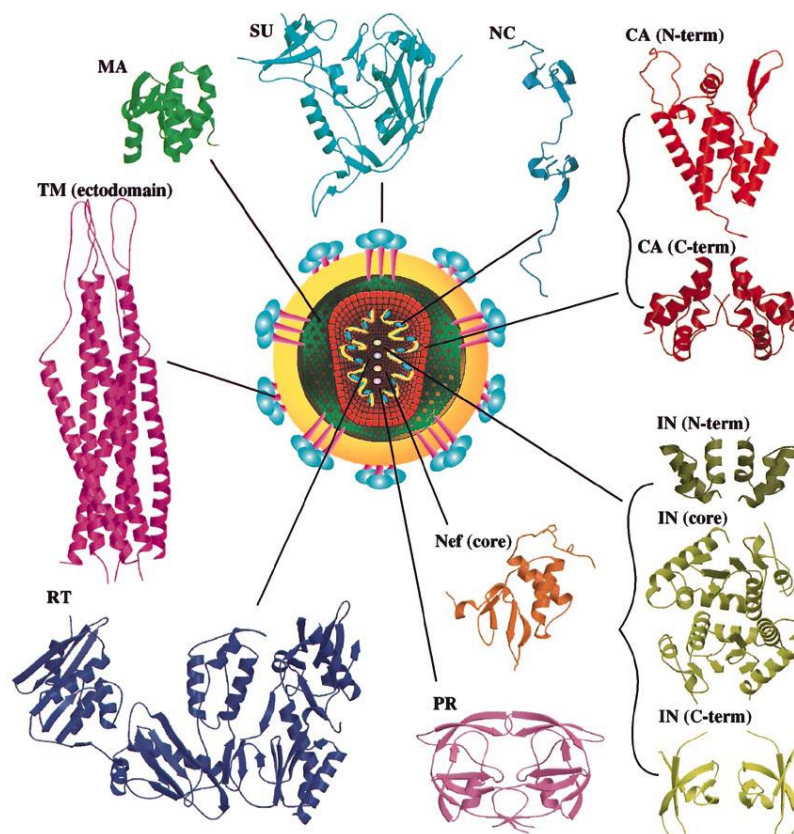


Figure 1.1 Drawing of the mature HIV virion surrounded by ribbon representations of the structurally characterized viral proteins and protein fragments. Reproduced with the permission of publisher (Elsevier).⁷ License number 3746560471809.

1.1.2 The HIV-1 replication cycle

Figure 1.2 gives the general features of the HIV replication cycle. The early phase starts with the recognition of the target cell by the mature virion and involves all processes leading to and including integration of the genomic DNA into the chromosome of the host cell. The late phase begins with the regulated expression of the integrated proviral genome, and involves all processes up to and including virus budding and maturation.

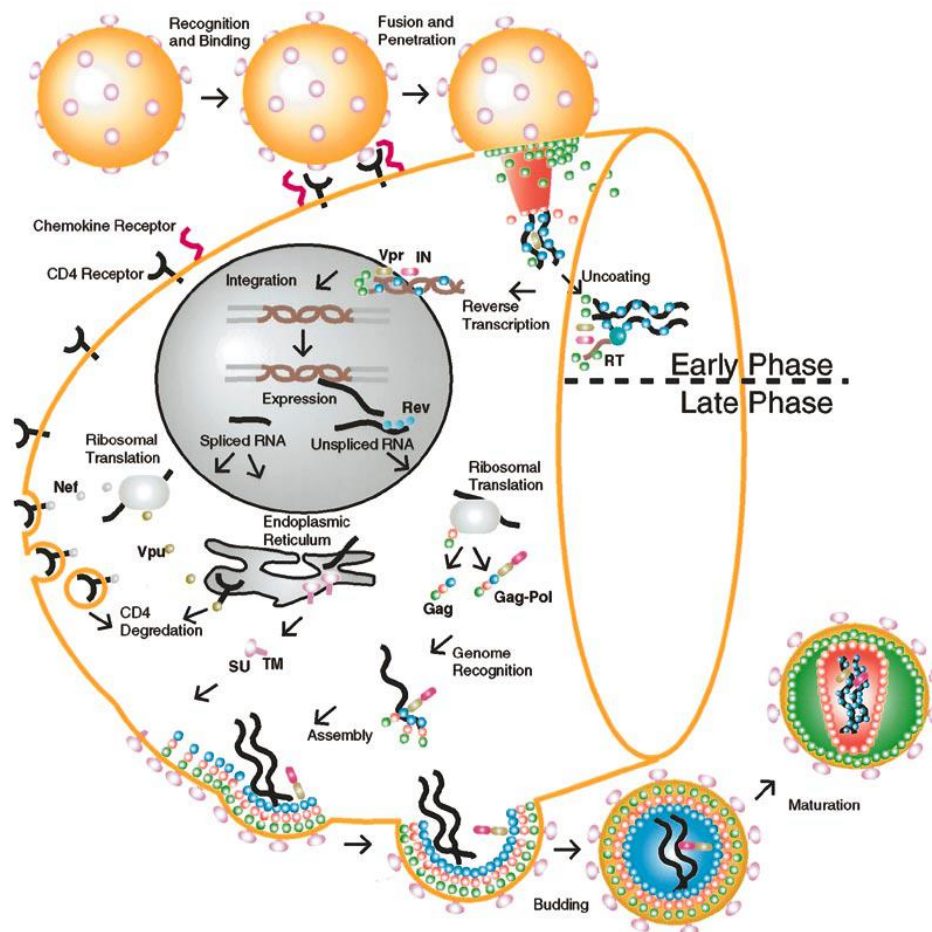


Figure 1.2 General features of the HIV-1 replication cycle Reproduced with the permission of publisher (Elsevier).⁷ License number 3746560471809.

1.1.2.1 Early phase

HIV-1 particles bind specifically to cells bearing CD4 (**Figure 1.2**), which is a protein that normally functions in immune recognition. Binding occurs by specific interactions between the viral envelope glycoprotein SU (gp120) and the amino-terminal immunoglobulin domain of CD4. These interactions are sufficient for binding but not for infection. Unlike other retroviruses, the primate lentiviruses require additional cell-surface proteins to promote fusion of the viral and cellular membranes. For HIV-1, membrane fusion can be triggered by one of several chemokine receptors, including CXCR4 and CCR5.¹⁰⁻¹² Membrane fusion is followed by a poorly understood uncoating event that affords an intracellular reverse transcription complex. Reverse transcription is catalyzed in the cytosol by reverse transcriptase (RT). The accessory protein Vif appears to be important during one or more of these early events, perhaps by facilitating the initial stages of reverse transcription. RT-dependent DNA synthesis is also dependent on the viral NC proteins, and is initiated by the binding of a cellular tRNA^{Lys} primer. Although the process of reverse transcription is complex, the mechanism of RT dependent DNA synthesis has emerged from extensive *in vitro* and *in vivo* studies.¹³⁻¹⁶

Once synthesized, the viral DNA is transported to the nucleus as part of a pre-integration complex that appears to include the IN, MA, RT, and Vpr proteins, as well as the cellular host protein HMG-I(Y).¹⁷ The HIV CA proteins do not appear to be part of the pre-integration complex, although they contribute to the structure of other retroviral pre-integration complexes.¹⁸ Nuclear localization of the pre-integration complex is directed by the accessory protein Vpr,¹⁹⁻²¹ which does not contain a nuclear localization signal but appears to function by connecting the pre-integration complex to the cellular nuclear import machinery, including importin- α and the nucleoporins.²²⁻²⁴ Vpr also interferes with normal cell cycle control by arresting the growth of infected cells in the G2 phase.²⁵⁻²⁷ Nuclear localization may be facilitated by the MA proteins.²⁸⁻²⁹ After active transport to the nucleus, the viral DNA is covalently integrated into the host genome by the catalytic activity of integrase.

1.1.2.2 Late phase

The late phase of the virus life cycle begins with the synthesis of unspliced and spliced mRNA transcripts, which are transported out of the nucleus for translation. Short spliced RNA species that encode the regulatory proteins Tat, Rev and Nef are initially synthesized. Tat is an essential transcriptional activator that binds to a stem loop element of the nascent RNA transcript (TAR, for trans-activating response element) and recruits the cellular proteins cyclin T and cyclin-dependent protein kinase-9. Recent studies indicate that cyclin T binds directly to Tat, enhancing its affinity and altering its specificity for the TAR RNA³⁰. Cdk9 then phosphorylates the RNA polymerase II transcription complex, stimulating transcription elongation³¹⁻³². Unspliced cellular mRNAs are mostly retained in the nucleus where they can be further processed or degraded.

However, full length and singly spliced HIV mRNA transcripts that contain functional introns are needed in the cytoplasm for Gag and Gag-Pol synthesis and packaging and their export is mediated by the essential HIV accessory protein Rev. Rev binds as an oligomer to the rev response element (RRE) of nascent unspliced mRNAs and recruits the cellular nuclear shuttling protein exportin-1,³³ and the nuclear export factor Ran guanosine triphosphatase (in its GTP-bound form). This complex is then transported through the nuclear pore to the cytosol where GTP is hydrolyzed to GDP, the complex dissociates, and the amino-terminal nuclear localization signal (NLS) of Rev directs its import back into the nucleus.³⁴ In this manner, Rev functions as a switch between the early synthesis of highly spliced mRNAs (encoding Tat, Rev and Nef) and the later synthesis of unspliced (encoding the Gag and Gag-Pol proteins) and singly spliced (encoding Env, Vpu, Vif and Vpr) mRNAs. The Env precursor polyprotein (gp160) is synthesized in the endoplasmic reticulum (ER) using the spliced env mRNA gene as the message. The protein appears to oligomerize to a trimeric structure in the ER, and is heavily glycosylated.³⁵⁻³⁸ Env is post translationally modified in the ER and Golgi apparatus and is cleaved to produce the non-covalently associated (TM-SU)₃ trimeric glycoprotein complex. The heterogeneously glycosylated TM-SU trimer is then transported to the cell membrane for virus assembly. Env and CD4 molecules are both synthesized in the ER, and the premature binding of CD4 to Env in the ER can inhibit translocation of Env to the cell membrane or the formation of a fully functional TM-SU complex.³⁹ Thus, CD4 is targeted for removal from the ER by the viral accessory protein

Vpu, which binds CD4 molecules and signals their degradation *via* the ubiquitin-proteasome pathway.⁴⁰⁻⁴² Similarly, cell-surface CD4 molecules are targeted for endosomal degradation by the binding of the accessory protein Nef, which also binds to the AP-2 adapter complex and stimulates the formation of clathrin-coated pits.⁴³

1.1.3 HIV integrase enzyme

HIV-1 integrase represents a protein with the molecular mass of 32 kDa, which is built of 288 amino acid residues. It is assigned to the family of polynucleotide transferases, which includes retroviral integrases, transposases, recombination proteins RuvC and RuvX and some other proteins⁴⁴. Enzymes of this family catalyse the processes that lead to the transfer of DNA or its fragments within a genome or between genomes. These processes occur without invoking any additional energy sources and ultimately, entail no changes in the number of phosphodiester bonds. Enzymes of this family are characterised by the formation of stable complexes with the DNA-substrate, however the reactions that they catalyse do not involve the formation of a covalent protein DNA bond.⁴⁵ To mediate integration, integrase should bind two DNA molecules at once, namely, a viral DNA (designated DNA-substrate) and a host cell DNA (DNA-target). The binding of the viral DNA is sequence-specific. Integrase recognises the end sequences of U5 and U3 segments in long terminal repeats (LTR) in the viral DNA, whereas the binding of the host cell DNA is independent of its nucleotide sequence. Integration includes several steps and begins in the cytoplasm of HIV-infected cells.⁴⁶⁻⁴⁷ The integrase protein of the HIV mediates a key step in the life cycle of the virus, namely the integration of a DNA copy of the viral genome into a host chromosome.⁴⁸ HIV-1 integrase is composed of three functional domains,⁴⁹⁻⁵² a small N-terminal domain that contains a His₂Cys₂ zinc binding motif, a central catalytic domain whose crystal structure has recently been solved and a C-terminal DNA binding domain. While the catalytic core domain can carry out a simple polynucleotidyl transfer termed disintegration,⁵³ all three domains are required for the 3' processing and DNA strand transfer activities that accomplish integration of the viral genome.⁵¹⁻⁵⁵ Consequently, the N- and C-terminal domains provide additional potentially useful targets for rational drug design aimed at inhibiting HIV integration into the host genome. The function of the N-terminal domain is at present unknown, and in the case of the related Rous Sarcoma virus integrase at least, its integrity appears not to be essential

for *in vitro* integration activity as it can be replaced by unrelated fusion peptides comprising polyhistidine sequences.⁵⁶

The C-terminal domain, on the other hand, displays the same DNA binding characteristics and affinity for both viral and nonspecific double stranded DNA as the intact integrase,⁵⁷ The minimal DNA binding domain has recently been shown to comprise residues 220–270.⁵⁸ Retroviruses integrate a DNA copy of the viral genome into host DNA as an obligatory step in their replication cycle. DNA integration occurs by a specialized recombination reaction mediated by the viral integrase protein.^{59–62} In the first step 3'-end processing, two nucleotides are cleaved from each of the viral DNA to form the DNA substrate for integration. In the next step, DNA strand transfer, the 3' hydroxyls at the ends of the viral DNA attack a pair phosphodiester bonds in the target DNA. The sites of attack on the two target DNA strands are separated by five nucleotides in the case of human immunodeficiency virus type-1 (HIV-1) integrase. To complete the integration process, the two unpaired nucleotides at the 5'ends of the viral and target DNA are filled and the 3' 3ends of the viral DNA are ligated to the 5'ends of the target DNA. These latter steps are likely to be accomplished by cellular enzymes. Integrase is sufficient to carry out both 3' processing and DNA strand transfer *in vitro* in the presence of a divalent metal ion that can be either Mg²⁺ or Mn²⁺. Stereochemical experiments have established that both of these reactions occur by a one-step trans-esterification mechanism.⁶³ Integrase is composed of three domains based on partial proteolysis and functional and structural studies.

The central core domain contains a triad of acidic residues, the D,D-35-E motif, that is conserved in integrase proteins encoded by retroviruses and retrotransposons and transposase proteins of many DNA transposons. Mutation of any of these residues abolishes or severely diminishes all catalytic activities of the protein, demonstrating their key role in catalysis.⁶⁴ By analogy with DNA polymerases, these acidic residues were proposed to coordinate a divalent metal ion.⁶⁵ The role of these acidic residues in binding a divalent metal ion has been demonstrated directly in the structures of the catalytic domain of HIV-1, simian immunodeficiency virus (SIV) and Rous sarcoma virus (RSV) integrases, which have been determined by X-ray crystallography either as a single domain^{66–68} or together with the C-terminal domain.^{69–71} The arrangement of the C-terminal domain relative to the catalytic core, however, differs among these structures, indicating considerable flexibility in the linkage between the catalytic and C-terminal domains. For instance, the C-terminal domain, as in the

case of RSV integrase, or as an independent monomeric domain, as in the case of HIV-1 integrase. These variations make definitive modelling of the complete integrase structure from three separated domains difficult. To process and integrate the two viral DNA ends into the host genome, two active sites theoretically are required. In the domain structures of HIV-1, SIV and RSV integrase, each catalytic core resembles a hemisphere that dimerizes *via* the extended flat surface to form a nearly spherical structure. The active sites are located on the opposite faces of the sphere and are separated by $>50 \text{ \AA}$, an arrangement that is incompatible with the 5 bp spacing between the sites of integration on the two target DNA strands. Rearrangement of this catalytic core dimer is unlikely because the dimer interface is very hydrophobic and conserved in all five independently determined retroviral integrase structures. Studies of the Mu transposase, which is functionally and structurally homologous to HIV-1 integrase,⁷² have revealed that only two of the four active sites present in a Mu transposase tetramer actually participate in the chemical reactions. It is thus proposed that a tetramer of integrase (dimer-of-dimers) is required for the integration reaction and within this tetramer, only one of the two active sites in each dimer is actually involved in the chemical reactions.⁷³⁻⁷⁶

1.1.4 HIV reverse transcriptase enzyme

HIV-1 RT is a heterodimer composed of two subunits known as p66 (560 amino acids) and p51 (440 amino acids). The DNA polymerase active site residues (Asp110, Asp185 and Asp186) are located in the palm subdomain of p66. In p66, the palm and connection subdomains consist of five stranded β sheets with two α helices on one side, while the thumb subdomain is composed of a bundle of four helices.⁷⁷ The fingers subdomain contains a mixed β sheet and three α helices. The RNase H domain consists of five β sheets flanked by four α helices. The p66 and p51 subunits have similar folds but p51 is more tightly packaged. Fingers, palm, thumb and connection subdomains fold similarly in both subunits, but their spatial organization changes due to the different positioning of the fingers, thumb and palm subdomains. Both HIV-1 RT subunits form a large cleft, where the thumb subdomain of p51 and the connection subdomains of p66 and p51 form the “floor”, and fingers, palm and thumb subdomains of p66 provide lateral and apical interactions with the nucleic acid substrate. Active site residues in p66 are exposed to the cleft, but they are buried in the 51-kDa subunit. The structure of the binary complex of HIV-1 RT and double-stranded DNA showed that the

nucleic acid binding cleft can accommodate 17 nucleotides between the active sites of the DNA polymerase and the RNase H.⁷⁸ The comparison of crystal structures of binary complexes with those obtained with unliganded RTs showed conformational changes involving the movement of the p66 thumb subdomain away from the fingers subdomain.

In addition, the bound DNA adopts an A-type conformation in the vicinity of the DNA polymerase active site, but a B-like conformation near the RNase H domain. These changes in orientation involve a 40° bend of the DNA/DNA complex, near α -helix H in the thumb subdomain of p66. The crystal structure of a binary complex of HIV-1 RT and an RNA/DNA hybrid revealed only small differences in comparison with the HIV-1 RT/double-stranded DNA complex.⁷⁹ Thus, the distance between the DNA polymerase and RNase H active sites is slightly larger (18 nucleotides) in the RNA/DNA complex, with most of the contacts between RT and template-primer being maintained. However, the RNA/DNA hybrid makes more contacts with the p66 subunit of the RT at α -helix I (thumb subdomain), β -sheet 5 (palm subdomain) and with residues of the RNase H domain.⁸⁰⁻⁸¹ Also, a number of contacts between the p51 subunit and the RNA template were not detected in the structure having the DNA/DNA substrate. Nucleic acids have similar A-like/B-like conformations in complexes containing DNA/DNA or RNA/DNA. However, the transition from the A- to the B-forms generates a wider minor groove in the RNA/DNA complex, which together with additional contacts between the RNase H primer grip and the RNA template seem to be determinant for the RNase H catalytic activity.

An important milestone towards understanding the mechanisms and nucleotide specificity in DNA polymerization by retroviral RTs was the determination of the crystal structure of a ternary complex of HIV-1 RT bound to double-stranded DNA and an incoming dNTP⁸². Nucleotide binding facilitates transition from an “open” conformation of the fingers subdomain in p66 (as observed in the structure of RT/DNA binary complexes) to a “closed” conformation where the β 3- β 4 hairpin loop in the fingers subdomain moves towards the p66 palm subdomain. This movement in the fingers subdomain is known to be the rate-limiting step in the polymerization reaction, and brings amino acid residues Lys65 and Arg72 into close proximity with the incoming nucleotide. Apart from these two residues, other important interactions in the nucleotide binding site are those established between the incoming dNTP and RT residues Asp113-Ala114-Tyr115-Phe116 and Gln151, as well as with the two divalent cations (probably Mg^{2+}); and between RT residues Tyr183 and Met184 and the DNA primer terminus. Binding of the incoming dNTP also produces a movement of the YMDD

motif (including catalytic residues Asp185 and Asp186) that allows proper coordination of the catalytic aspartates with the metal cofactors, and triggers the nucleophilic attack of the 3'OH of the primer terminus on the α phosphorous of the incoming kdNTP. This polymerization event renders an elongated DNA primer and a pyrophosphate molecule that is released in the reaction. Structural data suggest that the YMDD motif acts as a “springboard” supplying some of the energy required for translocation.⁸³

The rapid replication of HIV-1 and the errors made during viral replication, cause the virus to evolve rapidly in patients, making the problems of vaccine development and drug therapy particularly challenging. In the absence of an effective vaccine, drugs are the only useful treatment. Anti-HIV drugs work; so far drug therapy has saved more than three million years of life. Unfortunately, HIV-1 develops resistance to all of the available drugs. Although a number of useful anti-HIV drugs have been approved for use in patients, the problems associated with drug toxicity and the development of resistance means that the search for new drugs is an ongoing process. The three viral enzymes, reverse transcriptase (RT), integrase (IN), and protease (PR) are all good drug targets. Two distinct types of RT inhibitors, both of which block the polymerase activity of RT, have been approved to treat HIV-1 infections, nucleoside analogs (NRTIs) and non-nucleosides (NNRTIs), and there are promising leads for compounds that either block the RNase H activity or block the polymerase in other ways. A better understanding of the structure and function(s) of RT and of the mechanism(s) of inhibition can be used to generate better drugs; in particular drugs that are effective against the current drug-resistant strains of HIV-1.⁸⁴

Alanine-scanning mutants of the primer grip region of human immunodeficiency virus type 1 reverse transcriptase were tested for their ability to extend RNA and DNA versions of the polypurine tract primer, and an oligonucleotide representing the 18-nucleotide sequence at the 3' end of tRNA^{Lys3}. A majority of the mutant enzymes were either completely or severely deficient in RNA priming activity, but with only one exception, were able to efficiently extend DNA versions of the same primers. The mutant enzymes were able to bind to RNA primers, indicating that the defect in RNA priming was not simply a loss of binding activity. Mutations at positions 229, 233, and 235 dramatically reduced the amount of specific RNase H cleavage at the 3' terminus of the polypurine tract, which is required for primer removal. An alanine substitution at position 232 led to loss of cleavage specificity, although total activity was close to the wild-type level. Taken together, these results

demonstrate for the first time that there are residues in human immunodeficiency virus type 1 reverse transcriptase which are specifically involved in protein nucleic acid interactions with RNA primers.⁸⁵ Reverse transcriptase (RT)-associated ribonuclease H (RNase H) can cleave both the RNA template of DNA/ RNA hybrids as well as double-stranded (ds) RNA. This report shows that HIV-RT can also cleave the template strand of ds DNA when Mg^{2+} is replaced by Fe^{2+} in the RNase H active site of HIV-RT. The cleavage mechanisms as well as the positions of the cut vary depending on whether RNA or DNA is used. While DNA is cleaved at 17 base positions upstream of the primer 3*-end, RNA is cleaved 18 base positions upstream. Competition experiments show that Fe^{2+} replaces the catalytically active Mg^{2+} of RT-associated RNase H. The bound Fe^{2+} is the source of locally generated OH-radicals that cleave the most proximate base in the DNA. Electrophoretic mobility studies of the cleaved fragments suggest that DNA is cleaved by an oxidative mechanism, while RNA is cleaved by an enzymatic mechanism which is indistinguishable from the Mg^{2+} -dependent cleavage.

The Fe^{2+} -dependent cuts can be used to trace the active site of RT-associated RNase H on dsDNA as well as on dsRNA and DNA/RNA hybrids. The observed 1 base difference in the cleavage positions on DNA and RNA templates can be attributed to conformational differences of the bound nucleic acids. We suggest that the lower pitch of dsRNA and DNA/RNA hybrids compared with dsDNA permits accommodation of an additional base pair in the region between the primer 3*-end and the Fe^{2+} -dependent cleavage position at the RNase H active site.⁸⁶ HIV-1 drug resistance mutations are often inversely correlated with viral fitness, which remains poorly described at the molecular level. Some resistance mutations can also suppress resistance caused by other resistance mutations. Deval and co-worker reported the molecular mechanisms by which a virus resistant to lamivudine with the M184V reverse transcriptase mutation shows increased susceptibility to tenofovir and can suppress the effects of the tenofovir resistance mutation K65R. Additionally, how the decreased viral replication capacity of resistant viruses has been reported to be directly linked to their decreased ability to use natural nucleotide substrates and that combination of the K65R and M184V resistance mutations leads to greater decreases in viral replication capacity. All together, these results define at the molecular level how nucleoside-resistant viruses can be driven to reduced viral fitness.⁸⁷

1.2 Structure of HIV-1 protease enzyme

HIV-1 protease (HIV PR) is an aspartic protease that is essential for the life cycle of HIV, the retrovirus that causes AIDS.⁸⁸⁻⁸⁹ HIV PR cleaves newly synthesized polyproteins to be taken up by the immature HIV virion. Without effective HIV PR, HIV virions remain uninfectious.⁹⁰ Mutation of HIV PR's active site or inhibition of its activity disrupts HIV's ability to replicate and infect additional cells. This has made HIV PR inhibition the subject of much pharmaceutical research.⁹¹

1.2.1 Structural features

HIV-1 Protease is a homodimer (chain A, chain B). Each monomer contains 99 amino acids and is identical in conformation. The position of each monomer in the active protease forms an axis of symmetry. The secondary structure of each monomer includes, one alpha –helix and two anti-parallel beta sheets. The two Asp25 residues (one from each chain) act as the catalytic residues. A mechanism for the cleavage of HIV PR in which, water acts as a nucleophile, in concert with a well-placed aspartic acid to hydrolyze the scissile peptide bond has been proposed. Additionally, HIV PR has two molecular “flaps” which move a distance of up to 7 Å when the enzyme becomes associated with a substrate.⁹²

1.2.2 HIV-1 protease active site

HIV-1 protease consists of two protein chains. The chains are identical to one another, and each contains 99 amino acids. When the two chains assemble, a long tunnel is formed. Protein “flaps” cover the tunnel and open up to allow the enzyme to attach to a protein chain. After attachment, the flaps then close around the protein chain, thereby holding it in the tunnel and allowing the chain to be degraded.⁹³

The structures and activities of HIV protease and its drug-resistant variants and their interactions with inhibitors have been studied for nearly 20 years in order to combat the challenges of AIDS antiviral therapy and the evolution of HIV drug resistance.⁹⁴ About 25 different antiretroviral drugs (ARV) are currently used in the combat against HIV and AIDS. ARVs are divided into five different classes depending on their viral target. Currently

recommended AIDS therapy employs a mixture of drugs from different classes in HAART. Nine of these drugs target HIV protease and belong to the class of protease inhibitors (PIs). In most ARV formulations protease inhibitors are used together with reverse transcriptase inhibitors. The inclusion of PIs in antiviral therapy has resulted in major clinical benefits including prolonged viral suppression, control, reduced morbidity and mortality for HIV infected people.⁹⁵⁻⁹⁶ Encouraged by the potency and efficacy of the antiviral PIs, more efforts are underway to come up with the next generation of inhibitors.⁹⁷⁻⁹⁸

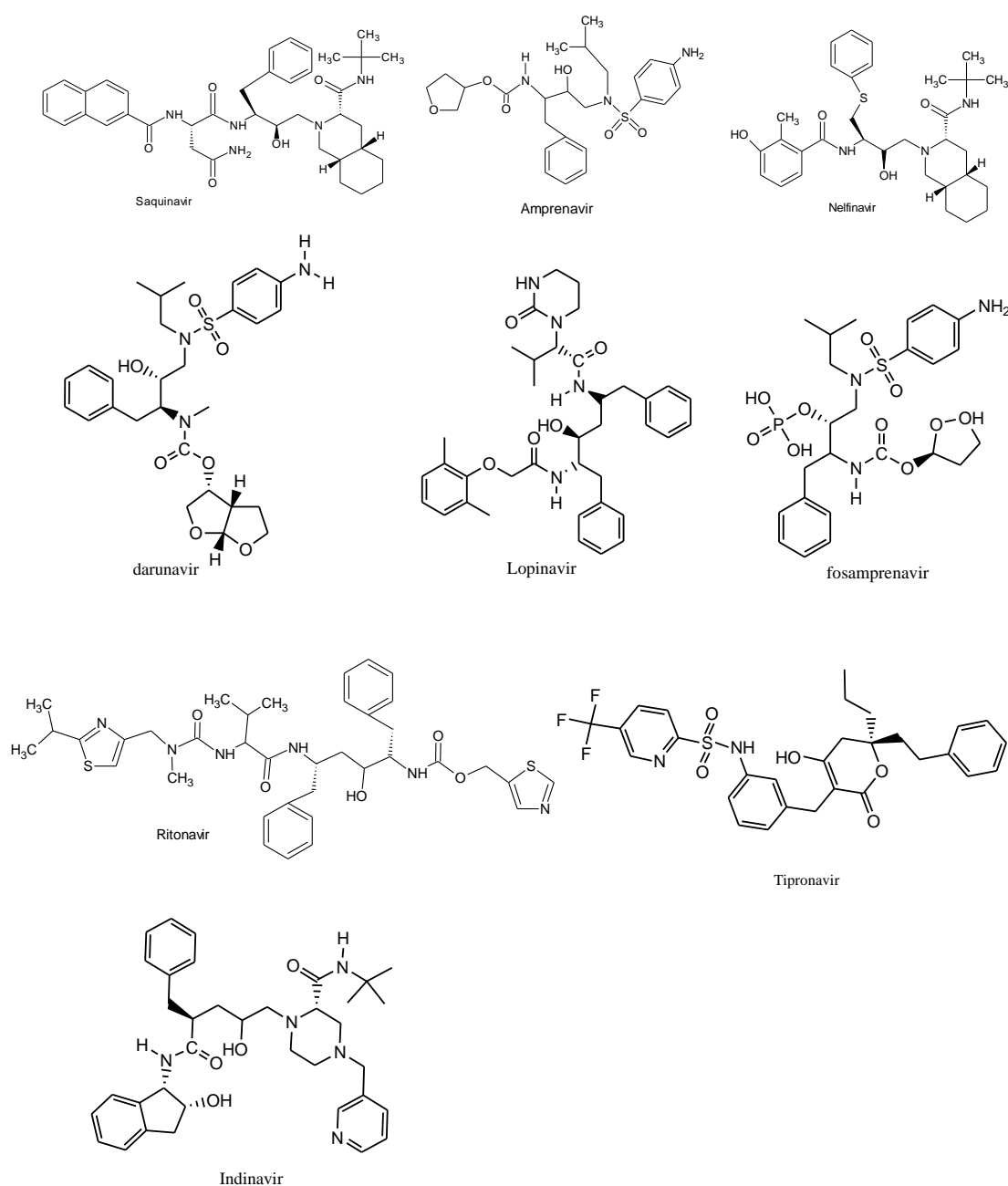


Figure 1.3 Current HIV-1 protease inhibitors approved by the FDA.

However, the emergence of drug resistance to PIs has compromised the effectiveness of treatment of HIV infections.^{99–101} Newer HIV infections that transmit drug resistant virus into drug naive patients limit antiviral options and thus complicate the management of HIV infection.^{102–104} More mutations are selected by PIs than any other class of ARV, partly due to their use for over a decade. The drug resistance to a particular PI also leads to cross resistance to other drugs within the PI class. The degree of cross-resistance depends on the number of mutations and the type of mutation selected by a PI.¹⁰⁵ With the availability of 9 PI drugs it is still possible to salvage a response from a different PI following failure of treatment with the first PI. Ritonavir is now solely used as a pharmacokinetic booster and ritonavir-boosted lopinavir, atazanavir, fosamprenavir and saquinavir are used as first line therapy against HIV infection.^{106–107}

1.2.3 HIV protease and structure guided design of PIs

HIV protease plays a critical role in viral maturation for producing infectious virus particles. The protease cleaves the precursor Gag and Gag-Pol polyproteins at a minimum of 9 distinct sites. The cleavages release the structural proteins matrix, capsid, and nucleocapsid, spacer peptides p1, p2, and p6, and functional enzymes reverse transcriptase, protease and integrase. Alteration of protease activity leads to defective viral particles and reduced infectivity.^{108–109} Inactivation of HIV protease resulting in the lack of infectious virus has made protease an attractive drug target for HIV and AIDS.^{110–111} Structure-guided inhibitor design has proved to be a powerful technique for discovering drug candidates with successful development of HIV protease inhibitors for AIDS therapy,¹¹² protein kinase inhibitors for cancer therapy¹¹³, and neuraminidase inhibitors for treatment of influenza virus infection¹¹⁴. Proteases are valuable targets for structure-based drug designs with therapeutic success for inhibiting aspartic proteases like renin as well as HIV protease.¹¹⁵

Knowledge of the crystal structure of HIV-1 protease and its recognition of substrate analog inhibitors was critical for the design of antiviral PIs. The HIV protease is an aspartic protease and the catalytic site has the characteristic Asp-Thr-Gly sequence common to all aspartic proteases. It functions as a symmetric homodimer consisting of 99 amino acids per monomer. The structure of protease is predominantly a sheet with the two aspartic acids Asp-25 from the two monomers forming the central active site. The three important regions in the protease

structure are the active site cavity, the flexible flaps, and the dimer interface. PIs are competitive inhibitors that bind at the active site of the protease with the flaps folded into a closed conformation over the active site. The dynamics of the flap region is important for the activity of the enzyme. The flaps were observed in closed and open conformation in the crystal structures of inhibitor bound and free protease.^{116–120} The protease active site cavity comprises residues Arg8, Leu23, Asp25, Gly27, Ala28, Asp29, Asp30, Val32, Lys45, Ile47, Met46, Gly48, Gly49, Ile50, Phe53, Leu76, Thr80, Pro81, Val82, Ile84. The majority of the residues forming the substrate binding site are hydrophobic; the exceptions are the catalytic Asp25 and Asp29, which form hydrogen bonds with peptide main chain groups, and Arg8, Asp30 and Lys45 which can interact with polar side chains or distal main chain groups in longer peptides.^{121–122} Knowledge of substrate recognition has benefited greatly from comparative analysis of other retroviral proteases.¹²³

Information on protease recognition of substrates has been incorporated into the design of antiviral inhibitors, which contain polar groups that form hydrogen bonds with the protease main chain and large hydrophobic groups replacing the P1 and P1' peptide side chains. The clinical PIs incorporate the common features deduced from the crystal structures of HIV protease with peptidic inhibitors. Saquinavir was the first drug approved for HIV protease; indinavir and ritonavir were introduced soon afterward. The PIs were designed to bind tightly to the wild type enzyme by mimicking the transition state of substrates.¹²⁴ The binding affinity of the PIs varies from nanomolar to picomolar. In the current stage, as exemplified by the recently developed drugs tipranavir and darunavir, the strategy was to target drug resistant variants of the HIV-1 protease. The PIs are generally shorter than the peptide substrates and contain hydrophobic groups that bind within the hydrophobic pockets at the S2–S2' subsites of protease. The early PIs were designed with polar groups resembling those of the substrate peptide main chain, and include a central hydroxyl that interacts with the catalytic aspartates and mimics the hydroxyl of a tetrahedral reaction intermediate. The later inhibitors amprenavir, tipranavir and darunavir were designed with less peptidic backbone features but retaining the central hydroxyl group.^{125–126}

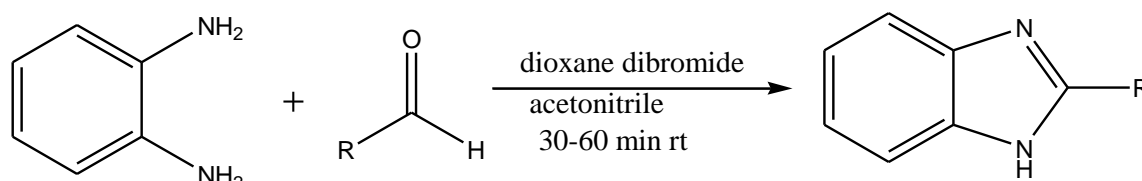
1.2.4 Evolution of drug resistance to PIs

Introduction of the first PI, saquinavir, in 1995 marked an important advance in the treatment of HIV infection. Then, it was possible for more effective therapy using a cocktail of drugs to target the protease as well as the reverse transcriptase. However, resistance to the PI quickly emerged.¹²⁷ Resistance is seen for all the drugs currently used in HAART, however, PIs appear to select more mutations than other classes of drugs. Drug resistant mutations of the protease have emerged against all the clinically available PIs. Though HAART is successful in suppressing the viral replication it cannot completely eliminate the integrated viral DNA. Thus, long term use of drugs is essential. Adherence to therapy greatly influences emergence of drug resistance.¹²⁸⁻¹³⁰ Drug side effects and toxicity are major reasons for loss of patient compliance and viral failure.¹³¹⁻¹³² Also, rapid mutation due to high rate of viral replication and lack of nucleoside proof reading in HIV assists emergence of drug resistance. Also, the number of primary infections involving transmission of PI drug resistant strains is on the rise further hindering the treatment process.¹³³ Although PIs select for specific mutations, the resistant mutation pattern for each PI is complex and difficult to predict¹³⁴⁻¹³⁵. Almost 50 different residues are mutated even in the absence of an inhibitor forming a large background of neutral mutations in the relatively small protease.¹³⁶

According to the International Aids Society-US panel for ARV resistance, mutations in 37 of 99 residues in HIV protease have clinical relevance to drug resistance among the current PIs.¹³⁷ These mutations are classified into major and minor mutations depending on their effect in antiviral therapy. Seventeen mutation sites are considered major mutations that render high levels of drug resistance to one or more PIs. Major resistance mutations are selected early and are much more inhibitor specific. Most of the minor mutations are considered to act as accessory mutations and compensate for the replication impairment due to the major drug resistance mutations. Furthermore, resistance mutations in protease can be accompanied by mutations in the viral polyprotein cleavage sites. Mutations in the Gag precursor cleavage sites, NC/p1 and p1/p6, are strongly associated with resistance to protease inhibitors.¹³⁸ Also protease drug resistance can emerge due to mutations in the Gag substrate alone, rather than in the enzyme.¹³⁹ In addition, recent reports indicate a role for amino acid insertions in the drug resistance of HIV protease.¹⁴⁰⁻¹⁴¹

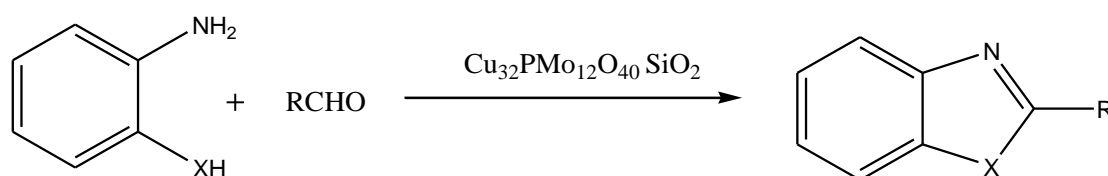
1.3 Benzimidazole-based compounds

The benzimidazole ring is a useful scaffold in medicinal chemistry and is a part of many biologically active compounds. A mild and efficient approach for the synthesis of the benzimidazole ring through oxidative cyclization of *o*-phenylenediamine and different aldehydes using dioxane dibromide has been reported (**Scheme 1.1**).¹⁴²



Scheme 1.1 Synthesis of benzimidazoles using dioxane dibromide.¹⁴²

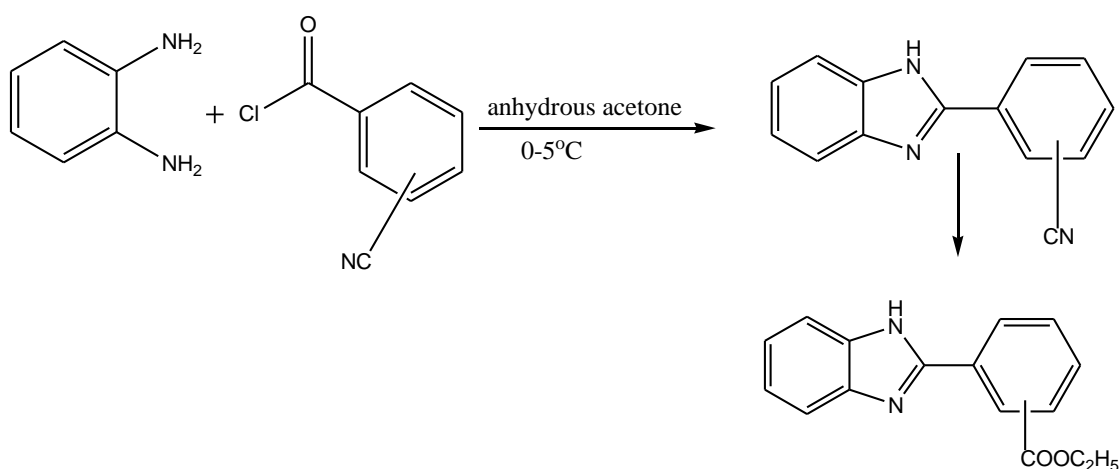
Solid heteropoly acid supported on silica gel ($\text{Cu}_{3/2}\text{PMo}_{12}\text{O}_{40}/\text{SiO}_2$) has been used as a heterogenous, reusable and efficient catalyst for synthesis of 2-arylbenzimidazoles and 2-arylbenzothiazoles by reaction of *o*-phenylenediamine and *o*-aminothiophenol with different aldehydes under various conditions (in solvent, under solvent-free conditions, microwave and ultrasonic wave irradiation). The catalyst can be reused several times but it will be less active (**Scheme 1.2**).¹⁴³



Scheme 1.2 Synthesis of benzimidazole using solid heteropoly supported on silica gel.¹⁴³

A series of benzimidazol-2-yl or benzimidazol-2-ylthiomethyl benzoylguanidines which have been found to inhibit NHE1-mediated platelet swelling in a concentration-dependent manner and to have significant cardioprotective effect against myocardial ischemic-reperfusion injury in *in vivo* and *in vitro* tests have been designed and synthesized as Na⁺/H⁺-exchanger inhibitors. Cyanobenzoic acids obtained by oxidation of corresponding cyanotoluene, were treated with SOCl_2 to offer benzoylchlorides which were then cyclocondensed with 4- or 1N-substituted

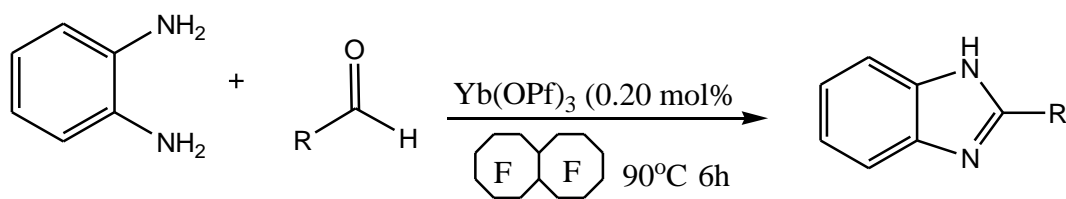
1,2-diaminobenzene to give benzimidazolyl phenylnitriles. This is a rare result as an amide would have been the expected product (**Scheme 1.3**).¹⁴⁴



Scheme 1.3 Synthesis of benzimidazoles from acid chloride in the presence of anhydrous acetone.¹⁴⁴

A library of benzimidazoles, benzoxazoles and benzothiazoles have been efficiently synthesized by condensation of *o*-phenylenediamine, *o*-aminophenol and *o*-aminothiophenol respectively with aromatic aldehydes in the presence of catalytic amounts of Animal Bone Meal (ABM) and Lewis acids doped ABMs. The products were attained by reflux of the reactants in air. This method has a high yield, short reaction times, and cleaner reaction profiles, straight forward procedure and reduced catalyst toxicity.¹⁴⁵

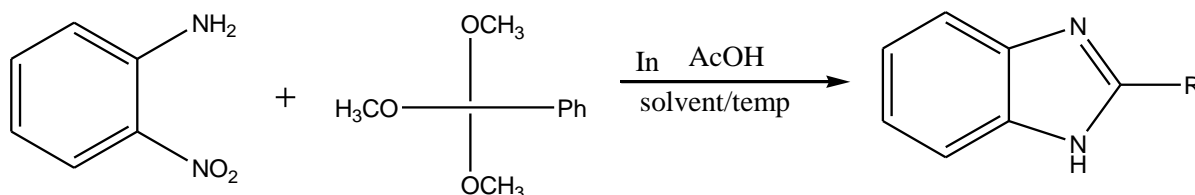
Catalytic condensation of *o*-phenylenediamine and aldehydes has been accomplished using rare earth(III)perfluorooctane sulfonates (RE(OPf)₃), RE = Sc, Y, La, Lu) as catalysts in fluoruous solvents. Ytterbium perfluorooctanesulfonates (Yb(OPf)₃) catalyzes the high-efficient synthesis of benzimidazole derivatives in fluoruous solvents. The fluoruous phase containing only catalyst can be reused after simple separation (**Scheme 1.4**).¹⁴⁶



Scheme 1.4 Synthesis of benzimidazoles using Ytterbium perfluorooctanesulfonates.¹⁴⁶

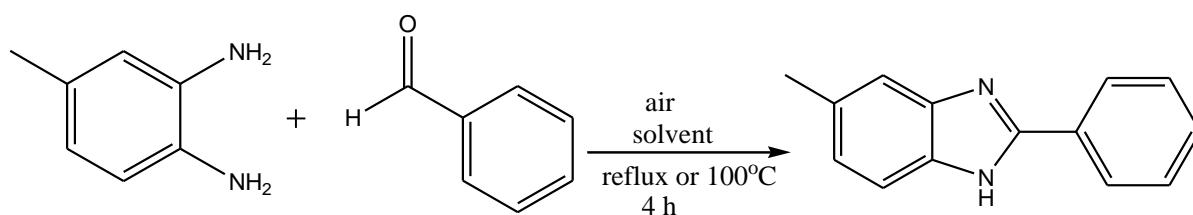
Methyl cis-deisopropyldehydroabietate has been selectively nitrated at the 12-position by reaction with 'claycop', a montmorillonite clay impregnated with copper(II) nitrate. The 12-nitro compound was reduced to the corresponding amine and subjected to a combined acylation and ortho nitration. The compounds so produced were further converted into octahydro-1*H*-phenanthro [2,3-*d*]imidazoles by reductive cyclization. The same acylation-ortho nitration methodology was shown to provide a short synthesis of 2-substituted benzimidazoles from aniline.¹⁴⁷

One-pot reduction-triggered heterocyclizations from 2-nitroanilines or 1,2-dinitroarenes to benzimidazoles has been reported. In the presence of indium/AcOH in ethyl acetate at reflux, reaction of 2-nitroanilines or 1,2-dinitroarenes with RC(OMe)₃ (R=Me, Ph) produced excellent yields of the corresponding benzimidazoles within 30 min to 6 h depending on the substituents of the starting materials. Indium-mediated heterocyclization of 2-nitroanilines to benzimidazole was faster and had better yields than 1,2-dinitroarenes to benzimidazole under similar reaction conditions (**Scheme 1.5**).¹⁴⁸



Scheme 1.5 Indium catalyzed synthesis of benzimidazoles¹⁴⁸

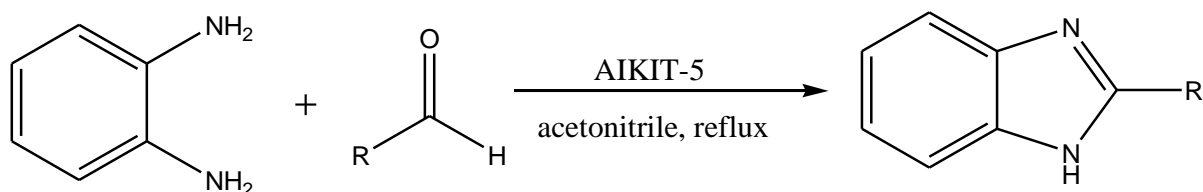
Direct one-step synthesis of various benzimidazoles from *o*-phenylenediamines and aldehydes has been reported using air as the oxidant. The salient features of this method include a simple procedure, mild conditions, no coupling agents or commercial oxidants/additives used, no waste produced (only by-product being water), easy purification, and high generality (**Scheme 1.6**).¹⁴⁹



Scheme 1.6 Synthesis of benzimidazoles using air as catalyst.¹⁴⁹

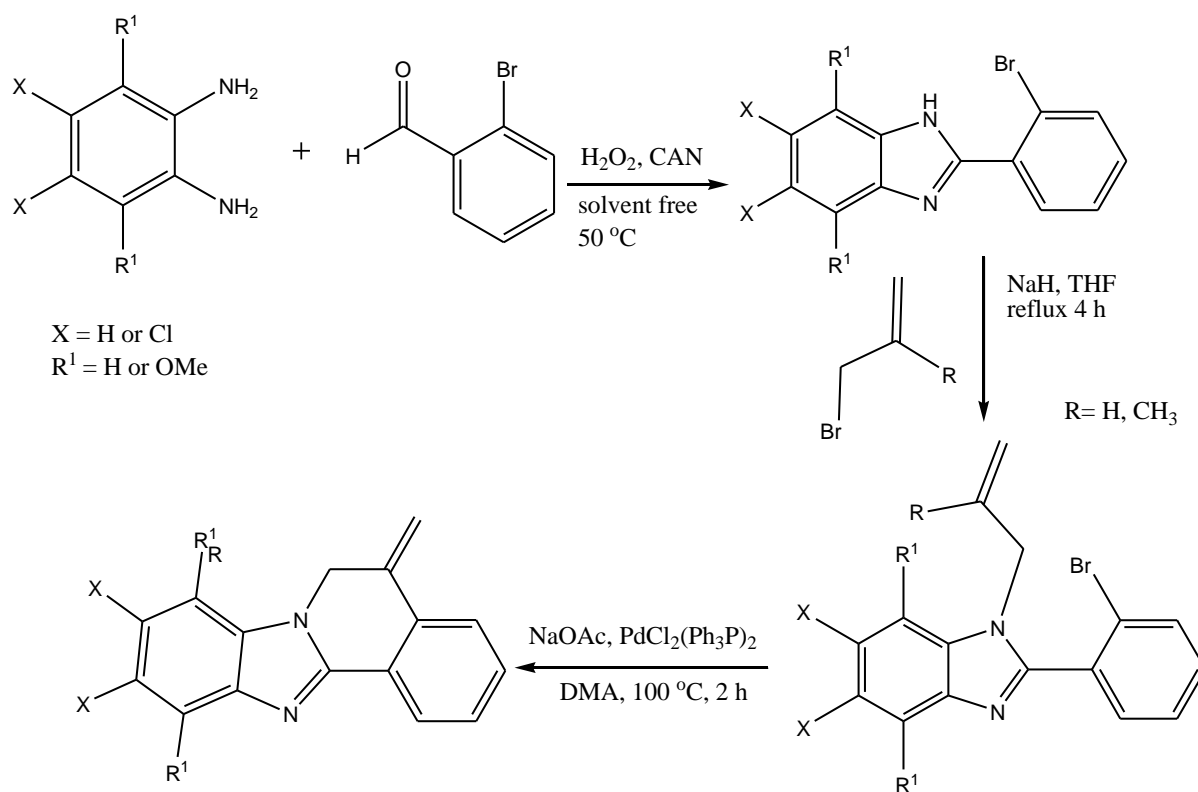
A wide variety of 2-substituted benzimidazoles and bis-benzimidazoles have been synthesized in high yields by PEG-mediated catalyst-free synthesis under solvent-free conditions.¹⁵⁰

The synthesis of benzimidazoles through the coupling of aldehydes with *o*-phenylenediamine by using highly acidic nanoporous aluminosilicate with 3D structure and cage-type pores as the catalyst has been achieved. The catalyst resulted in excellent yields in short reaction times presumably due to its high acidity, large pore diameter, high surface area, and cage-type 3D porous structure (**Scheme 1.7**).¹⁵¹



Scheme 1.7 AIKIT-5 catalyzed synthesis of benzimidazoles.¹⁵¹

An efficient route for the synthesis of benzimidazo [2,1-*a*]isoquinolines and its condensed analogues has been developed *via* the palladium-catalyzed cyclization/C–H activation of *N*-allyl and *N*-methallyl derivatives of benzimidazoles (**Scheme 1.8**).¹⁵²



Scheme 1.8 CAN and hydrogen peroxide catalyzed synthesis of benzimidazoles.¹⁵²

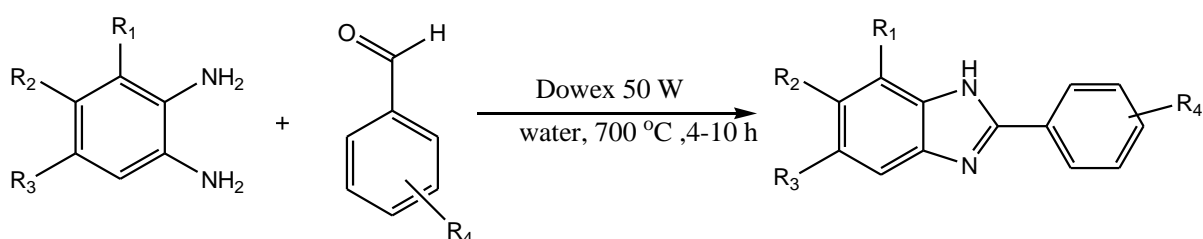
Zinc chloride-exchanged K10- montmorillonite (claytic) has been employed as a Lewis acid catalyst in aqueous media at room temperature for the synthesis of various benzimidazoles and quinoxalines from carbonyl compounds and *o*-phenylenediamine.¹⁵³ The laccase-catalyzed diamino reaction of *o*-phenylenediamine and benzaldehydes with aerial oxygen as the oxidant exclusively yields 2-aryl-1*H*-benzimidazoles in good yields.¹⁵⁴ The regiospecific synthesis of a range of anti-tumour 2-arylbenzothiazoles substituted in the benzothiazole ring has been achieved. A bromine atom situated *ortho* to the anilido nitrogen is used to direct a regiospecific cyclisation.¹⁵⁵

A series of benzimidazole derivatives have been synthesized expeditiously in good yields by condensation of 1,2-diaminobenzene and aromatic aldehydes in the presence of modified scolecite catalyst.¹⁵⁶ Benzimidazole-naphthalimide derivatives have been synthesized and its photophysical properties have been determined. The compounds showed highly selective and sensitive colorimetric and ratiometric sensing ability for fluoride anion.¹⁵⁷

Ammonium metavanadate (10 mol%) has been used as a catalyst for the synthesis of 2-substituted aryl benzimidazoles from *o*-phenylenediamine and different substituted aryl

aldehydes at room temperature in ethanol.¹⁵⁸ Various 2-arylbenzimidazoles have been obtained from *o*-phenylenediamine and aldehydes *via* one-step process with DMP (Dess–Martin-periodinane) reagent as an oxidant.¹⁵⁹ Vanadyl acetylacetonate, VO(acac)₂, has been found to be very a effective catalyst for the synthesis of a variety of benzimidazoles under solvent-free condition. *o*-Phenylenediamine and selected aromatic carboxylic acids/aldehydes have been irradiated by microwave radiation to access the products.¹⁶⁰

One-pot condensation of *o*-aminothiophenol or *o*-phenylenediamine with different aldehydes have been catalyzed by hexamethylenetetramine–bromine (HMTA-Bromine).¹⁶¹ Regioselective one-pot synthesis of 2-aryl benzimidazoles, benzoxazoles and benzothiazoles have been achieved in excellent isolated yields under ambient conditions using the ionic liquids, 1-butylimidazolium tetraflouroborate ([Hbim]BF₄) and 1,3-di-*n*-butylimidazolium tetrafluoroborate ([bbim]BF₄) as reaction media and promoters.¹⁶² 2-Substituted benzimidazoles have been synthesized in excellent yields in a single pot under solvent-free conditions from *o*-phenylenediamine and aldehydes in the presence of a catalytic amount of In(OTf)₃ at room temperature.¹⁶³ Synthesis of benzimidazoles from the condensation of *o*-phenylenediamine and acyl chlorides in the presence of a catalytic amount of various heteropolyacids (HPAs) have been reported.¹⁶⁴ 10 mol% of Dowex 50W in water has been used as an efficient catalyst for the synthesis of a wide variety of 2-substituted benzimidazoles (**Scheme 1.9**).¹⁶⁵



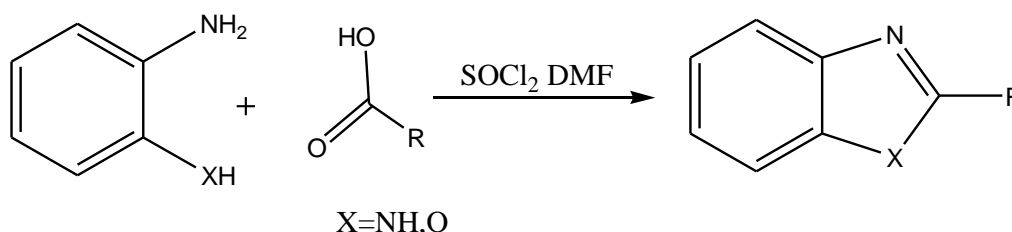
Scheme 1.9 Dowex 50 W catalyzed synthesis of benzimidazoles in water.¹⁶⁵

The synthesis of 2-arylbenzimidazoles through a one-pot condensation of *o*-phenylenediamines with aryl aldehydes in water have been reported.¹⁶⁶

2-Substituted benzimidazoles have been synthesized from benzo[*c*][1,2,5]thiadiazole-4,5-diamine and aromatic aldehydes in the presence of catalytic amount of CuPy_2Cl_2 , at room temperature.¹⁶⁷

Benzimidazole derivatives have been synthesized using catalytic amount of $\text{Fe}(\text{ClO}_4)_3/\text{SiO}_2$ at room temperature under solvent-free conditions.¹⁶⁸ The reaction of *o*-phenylenediamine derivatives and substituted benzaldehydes have been carried out in 1M glucose solution as reaction medium and catalyst at 60 °C.¹⁶⁹ A set of benzothiazoles and benzimidazoles have been prepared from aromatic ortho-diamines or ortho-aminothiophenol and aldehydes by ultrasonic irradiation using chlorotrimethylsilane in dimethylformamide as promoter and water scavenger.¹⁷⁰ A mild and efficient procedure for synthesis of benzimidazole derivatives in the presence of a catalytic amount of mechanochemically synthesized zinc oxide nanoparticles under solvent-free condition has been achieved.¹⁷¹ An efficient method for the synthesis of 1,2-disubstitued benzimidazoles and 2-substitued benzothiazoles under solvent-free and ultrasonic irradiation conditions, employing rare-earth metal chlorides as catalysts have been reported.¹⁷² The synthesis of 2,4,6-triphenyl-1*H*-imidazoles using benzil, aromatic aldehyde and NH_4OAc have been carried out with ZnO as catalyst at room temperature.¹⁷³ The cyclization of 2,3-diaminobenzoic acid and aromatic aldehydes to give 2-aryl-1*H*-benzimidazole-4-carboxylic acids have been reported.¹⁷⁴

N,N-Dimethylchlorosulfitemethaniminium chloride ($\text{SOCl}_2\text{-DMF}$) has been used to access benzimidazoles and benzoxazoles by condensation of carboxylic acids with *o*-phenylenediamine or *o*-aminophenol (**Scheme 1.10**).¹⁷⁵



Scheme 1.10 Synthesis of benzimidazoles from carboxylic acids in $\text{SOCl}_2\text{-DMF}$.¹⁷⁵

Benzimidazoles have been readily prepared from *o*-phenylenediamine and aldehydes using air and catalytic amount of *N*-hydroxyphthalimide/ $\text{Co}(\text{OAc})_2$.¹⁷⁶ *o*-Phenylenediamines have

been reacted with carbonyl compounds, β -ketoesters, and 1,2-diketones in presence of ammonium salts to give benzimidazoles and quinoxalines.¹⁷⁷ A simple and efficient method for the convenient synthesis of 2-arylbenzimidazole has been achieved by reacting *o*-phenylenediamine and various aromatic aldehydes using cobalt(II) chloride hexahydrate as a catalyst.¹⁷⁸ KI has been used as catalyst to synthesize benzimidazoles from aromatic aldehydes and *o*-phenylenediamine in air by microwave irradiation.¹⁷⁹ FeCl₃-doped polyaniline nanoparticles has been used to catalyze the synthesis of 2-substituted benzimidazoles by the reaction of aldehydes with *o*-phenylenediamine.¹⁸⁰ Benzimidazole derivatives have been synthesized using a catalytic amount of lead peroxide (PbO₂) at room temperature.¹⁸¹

One-pot synthesis of benzimidazole compounds from *o*-phenylenediamine and a variety of aldehydes has been achieved in the presence of samarium triflate (10 mol%) in acetonitrile at room temperature.¹⁸² A library of benzimidazole derivatives have been prepared through the reaction of *o*-phenylenediamine and aldehydes in the presence of catalytic amount of silica supported sodium hydrogen sulfate (NaHSO₄-SiO₂) by refluxing in ethanol.¹⁸³ A microwave-assisted method for the synthesis of 2-substituted benzimidazoles in the presence of alumina-methanesulfonic acid (AMA) has been reported.¹⁸⁴

Silica functionalized Mn(acac)₃ has been prepared and employed for the one-pot synthesis of 2-arylbenzimidazoles, 2-arylbenzothiazoles; and oxidation of benzoin to benzil under air and in water.¹⁸⁵ A series of 2-(hetero)arylbenzimidazoles has been synthesized by the catalytic condensation of (hetero)aryl aldehydes with *o*-phenylenediamine derivatives at room temperature in air with copper nanoparticles on charcoal as catalyst.¹⁸⁶ Libraries of 2-substituted-benzimidazoles, benzoxazoles, benzothiazoles as well as quinazolin-4 (3*H*)-ones have been synthesized *via* potassium persulfate-CuSO₄-mediated oxidative coupling of aldehydes with *o*-phenylenediamines, *o*-aminophenols, *o*-aminothiophenols, and anthranilamide, respectively, in aqueous micelles.¹⁸⁷ The FeCl₃-catalyzed aerobic oxidation process for the synthesis of benzoxazoles, benzothiazole and benzimidazole has been reported.¹⁸⁸

Ceric ammonium nitrate (CAN) has been reported to efficiently catalyze the synthesis of benzimidazole derivatives from *o*-phenylene diamine and aldehydes in PEG.¹⁸⁹ The synthesis of *o*-phenylbenzimidazole from *o*-phenylene diamine and benzoic acid have been achieved in

water at high temperatures.¹⁹⁰ A new enzymatic synthesis has been reported for the synthesis of 2-alkyl-benzimidazoles which involved a supported enzyme (Lipozymes), the reaction has been carried out in very mild conditions in hydrocarbon solvents.¹⁹¹ A solid phase strategy for the synthesis of substituted 2-arylbenzimidazoles over silica gel have been achieved using *o*-phenylene diamines and aromatic aldehydes.¹⁹²

A practical and convenient synthetic method has been developed for the facile synthesis of 1,2-disubstituted benzimidazoles, 2-substituted benzimidazoles and 2-substituted benzothiazoles with high chemoselectivity.¹⁹³ Diversity oriented synthesis of benzimidazole and benzoxa/(thia)zole libraries have been achieved through polymer-supported hypervalent iodine reagent by a reaction between, *o*-phenylene diamine, *o*-aminophenol and *o*-aminothiophenol and aldehydes.¹⁹⁴ Benzimidazole has been synthesized by a reaction between anthranilic acid and *o*-phenylene diamine. The acetylated product of benzimidazole undergoes Claisen-Schmidt condensation with aryl aldehyde to produce corresponding chalcones.¹⁹⁵

A series of 4'-(6-methoxy-2-substituted-benzimidazole-1-ylmethyl)-biphenyl-2-carboxylic acid has been synthesized expeditiously in 4-methoxy-1, *o*-phenylenediamine and different substituted carboxylic acids in the presence of $\text{BF}_3 \cdot \text{OEt}_2$ as a catalyst.¹⁹⁶ A series of benzimidazole derivatives have been synthesized by the reaction of *o*-phenylenediamine and different aromatic aldehydes in the presence of sodium hexafluoroaluminate, Na_3AlF_6 , as an efficient catalyst at 50 °C.¹⁹⁷ Solid silica supported ferric chloride ($\text{SiO}_2\text{-FeCl}_3$) catalyzed one-step synthesis of various benzimidazoles from *o*-phenylenediamine and aldehydes using H_2O_2 has been reported.¹⁹⁸ The synthesis of substituted benzimidazoles, 2-aminobenzimidazoles, 2-aminobenzothiazoles, and benzoxazoles have been achieved *via* intramolecular cyclization of *o*-bromoaryl derivatives using copper(II) oxide nanoparticles in DMSO under.¹⁹⁹ Benzimidazoles synthesized by the copper-catalyzed, one-pot, three-component reaction of 2-haloanilines, aldehydes, and NaN_3 have been reported.²⁰⁰

A new convenient method for the syntheses of 2-substituted benzimidazole and benzothiazole have been reported.²⁰¹ Synthesis of 5-benzoxadiazepines from the condensation of *o*-phenylenediamine and acyl chlorides has been achieved in the presence of a catalytic amount of various heteropolyacids (HPAs).²⁰² A one-pot synthesis of 2-arylbenzothiazoles *via* the reaction of 2-aminothiophenols and aromatic aldehydes in glycerol at ambient temperature

have been reported.²⁰³ Synthesis of N-1- and C-2-substituted benzimidazole *via* reductive cyclization of *o*-nitroarylamine using Na₂S₂O₄ has been reported.²⁰⁴ *o*-Phenylene diamine derivatives have been reported to react with benzoyl chloride derivatives in the presence of MCM-41 as catalyst to yield 2-substituted benzimidazoles.²⁰⁵ Synthesis of 2-substituted benzimidazoles using polyphosphoric acid (PPA) as a catalyst from organic acid and *o*-phenylene diamine *via* microwave irradiation has been achieved.²⁰⁶ Microwave irradiated synthesis of 2-substituted benzimidazoles *via* the Na₂S₂O₄ reduction of *o*-nitroanilines in the presence of aldehydes have been reported.²⁰⁷

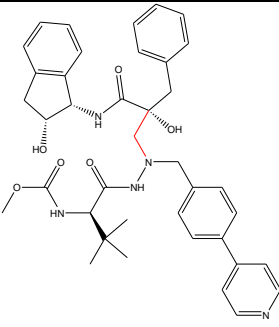
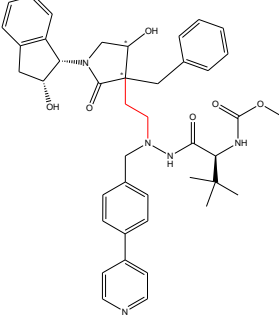
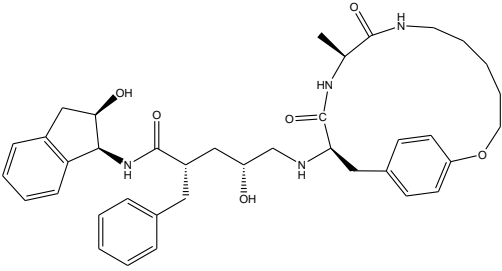
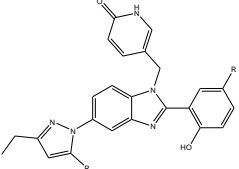
The antiviral activity of a series of benzimidazole derivatives and substituted benzimidazole have been reported.²⁰⁸ 2-Phenylbenzimidazole derivatives have been synthesized and evaluated in cell-based assays for cytotoxicity and antiviral activity against a panel of 10 RNA and DNA viruses, poxviruses, pestiviruses and even HCV, which are important human and veterinary pathogens.²⁰⁹ In an effort to identify a new class of HIV-1 protease inhibitors, four different stereopure β -hydroxy γ -lactam containing inhibitors have been synthesized, biologically evaluated, and cocrystallized. The impact of the tether length of the central spacer (two or three carbons) was also investigated. A compound with a shorter tether and (3R,4S) absolute configuration exhibited high activity with a K_i of 2.1 nM and an EC₅₀ of 0.64 μ M. Further optimization by decoration of the P1' side chain furnished an even more potent HIV-1 protease inhibitor (K_i = 0.8 nM, EC₅₀ = 0.04 μ M). According to X-ray analysis, the new class of inhibitors did not fully succeed in forming two symmetric hydrogen bonds to the catalytic aspartates. The crystal structures of the complexes further explain the difference in potency between the shorter inhibitors (two carbon spacer) and the longer inhibitors (three-carbon spacer).²¹⁰

Three new peptidomimetics have been developed with highly stable and conformationally constrained macrocyclic components that replace tripeptide segments of protease substrates. Each compound inhibits both HIV-1 protease and viral replication (HIV-1, HIV-2) at nanomolar concentrations without cytotoxicity to uninfected cells below 10 μ M. Their activities against HIV-1 protease (K_i 1.7 nM (**1**), 0.6 nM (**2**), 0.3 nM (**3**)) are 1-2 orders of magnitude greater than their antiviral potencies against HIV-1-infected primary peripheral blood mononuclear cells (IC₅₀ 45 nM (**1**), 56 nM (**2**), 95 nM (**3**)) or HIV-1-infected MT2 cells (IC₅₀ 90 nM (**1**), 60 nM (**2**)), suggesting suboptimal cellular uptake.²¹¹

The emergence of resistance to existing classes of antiretroviral drugs necessitates finding new HIV-1 targets for drug discovery. The viral capsid (CA) protein represents one such potential new target. CA is sufficient to form mature HIV-1 capsids *in vitro*, and extensive structure-function and mutational analyses of CA have shown that the proper assembly, morphology, and stability of the mature capsid core are essential for the infectivity of HIV-1 virions. The development of an *in vitro* capsid assembly assay based on the association of CA-NC subunits on immobilized oligonucleotides. This assay has been used to screen a compound library, yielding several different families of compounds that inhibited capsid assembly. Optimization of two chemical series, the benzodiazepines (BD) and the benzimidazoles (BM), resulted in compounds with potent antiviral activity against wild-type and drug-resistant HIV-1. Nuclear magnetic resonance (NMR) spectroscopic and X-ray crystallographic analyses showed that both series of inhibitors bound to the N-terminal domain of CA. These inhibitors induced the formation of a pocket that overlaps with the binding site for the previously reported CAP inhibitors but is expanded significantly by these new, more potent CA inhibitors. Virus release and electron microscopic (EM) studies showed that the BD compounds prevented virion release, whereas the BM compounds inhibited the formation of the mature capsid. Passage of virus in the presence of the inhibitors selected for resistance mutations that mapped to highly conserved residues surrounding the inhibitor binding pocket, but also to the C-terminal domain of CA.

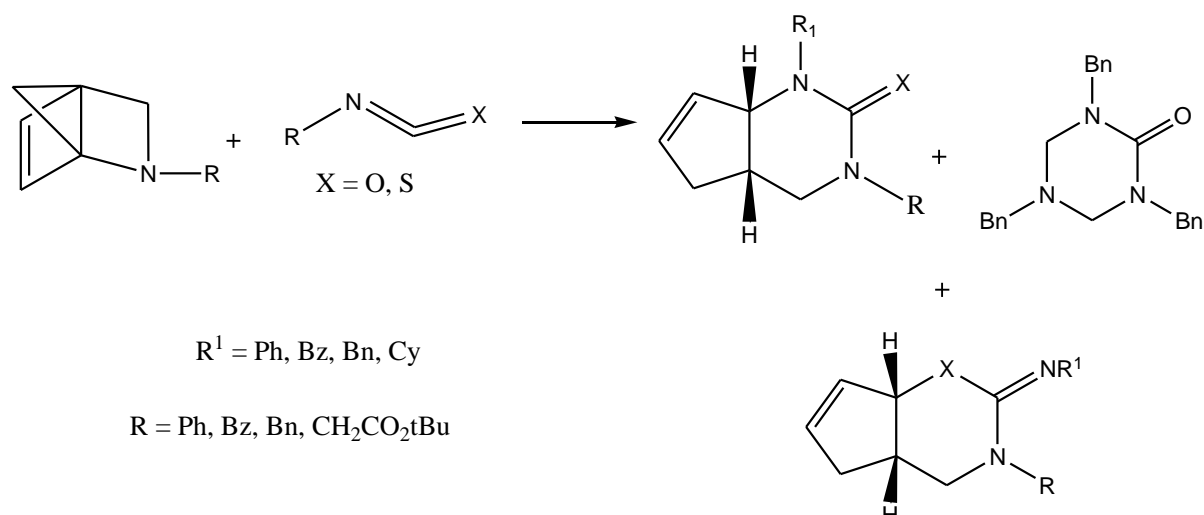
The resistance mutations selected by the two series differed, consistent with differences in their interactions within the pocket, and most also impaired virus replicative capacity. Resistance mutations had two modes of action, either directly impacting inhibitor binding affinity or apparently increasing the overall stability of the viral capsid without affecting inhibitor binding. These studies demonstrate that CA is a viable antiviral target and demonstrate that inhibitors that bind within the same site on CA can have distinct binding modes and mechanisms of action.²¹² **Table 1.1** gives the chemical structures of some potential HIV-1 protease inhibitors.

Table 1.1 Chemical structures of some potential HIV-1 inhibitors under development

Structure	Enzyme inhibited
	Protease inhibitors ²¹⁰
	Protease inhibitors ²¹⁰
	Protease inhibitors ²¹¹
	HIV-1CA inhibitors ²¹²

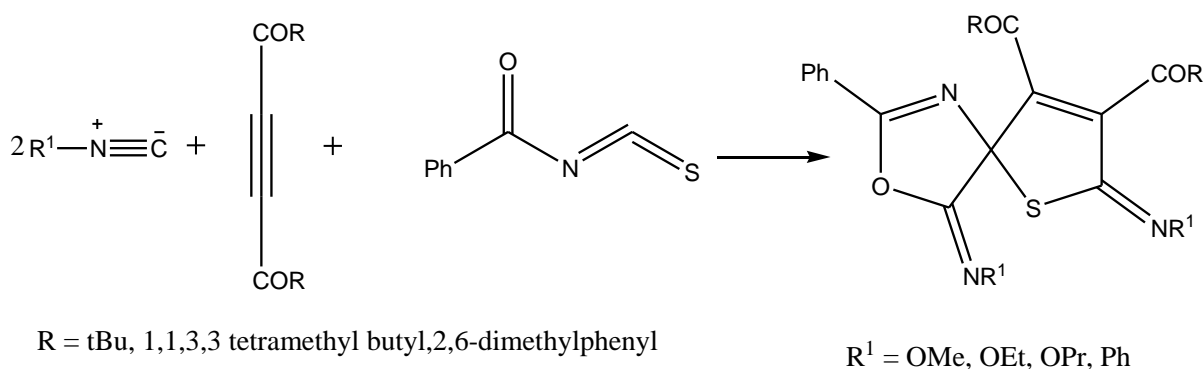
1.4 Benzoyl isothiocyanates based compounds

The regiospecific synthesis of 5-bromothiophenethyl thioureas has been accomplished in four steps with an overall yield of 40 – 60%. The requisite regioselectivity for bromination of the thiophene ring was achieved using bromine in acetic acid at low temperatures.²¹³ Isoyanates and isothiocyanates that are not activated by an electron withdrawing group react with azanorbornenes in benzene at reflux to afford ureas and thioureas through the corresponding 1,3-diaza-Claisen rearrangements (**Scheme 1.11**).²¹⁴



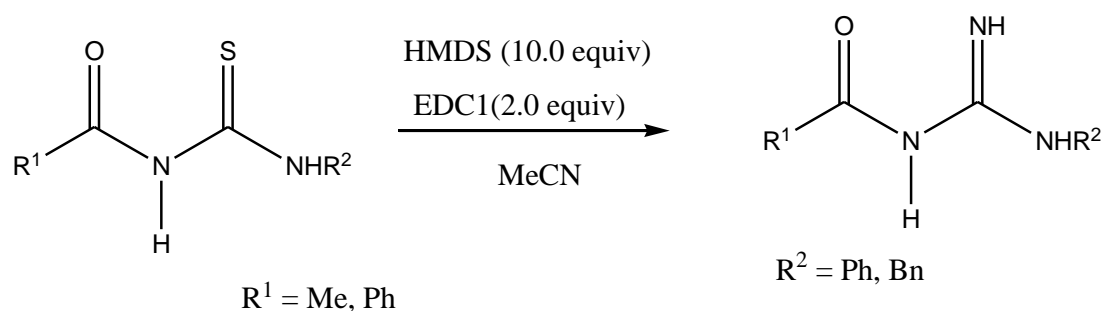
Scheme 1.11 1,3-Diaza Claisen rearrangement reactions of thiourea derivatives.²¹⁴

The enantioselective *N*-heterocyclic carbene-catalyzed formal [2 + 2] and [2 + 2 + 2] cycloaddition of ketenes and isothiocyanates have been reported.²¹⁵ Alkyl-(aryl) isocyanides have been reported to react with benzoyl isothiocyanate in the presence of dialkylacetylenedicarboxylates or dibenzoylacetylene in one-pot to afford highly substituted 4,7-bis[alkyl(aryl)imino]-2-phenyl-3-oxa-6-thia-1-azaspiro[4.4]nona-1,8-dienes, with double insertion of the isocyanide (**Scheme 1.12**).²¹⁶



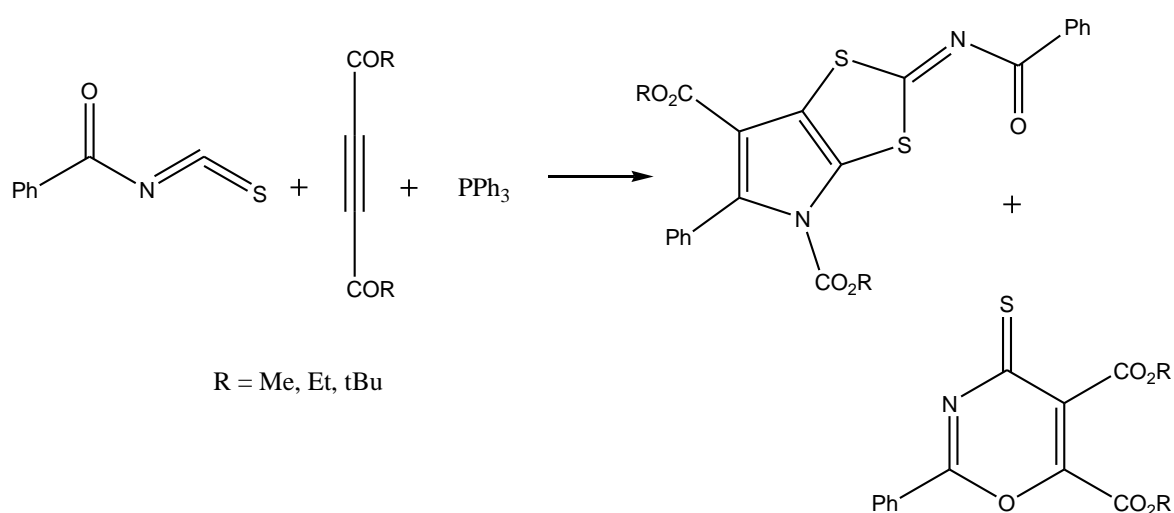
Scheme 1.12 Double insertion reactions of benzoyl isothiocyanates.²¹⁶

An efficient synthesis of *N*-acyl-*N'*-substituted guanidines by condensation reaction of thiourea and $(\text{Me}_3\text{Si})_2\text{NH}$ in the presence of EDCI have been achieved (**Scheme 1.13**).²¹⁷



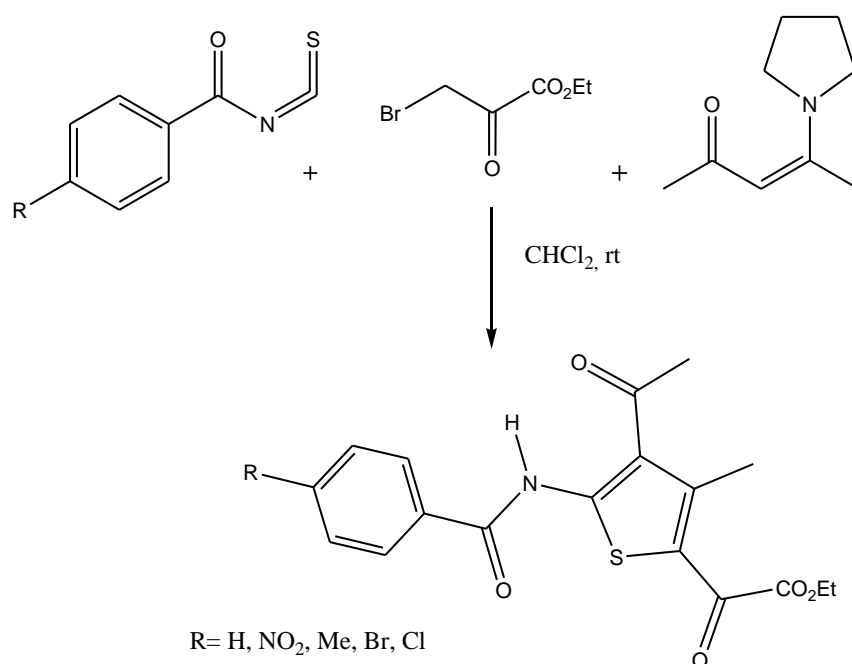
Scheme 1.13 Substitution reactions of thiones.²¹⁷

Benzoyl isothiocyanate has been reported to react with dialkyl acetylenedicarboxylates in the presence of triphenylphosphine in a mechanistically novel reaction to afford highly substituted dialkyl 2-(benzoylimino)-5-phenyl-4*H*-[1,3]dithiolo[4,5-*b*]pyrrole-4,6-dicarboxylates (**Scheme 1.14**).²¹⁸



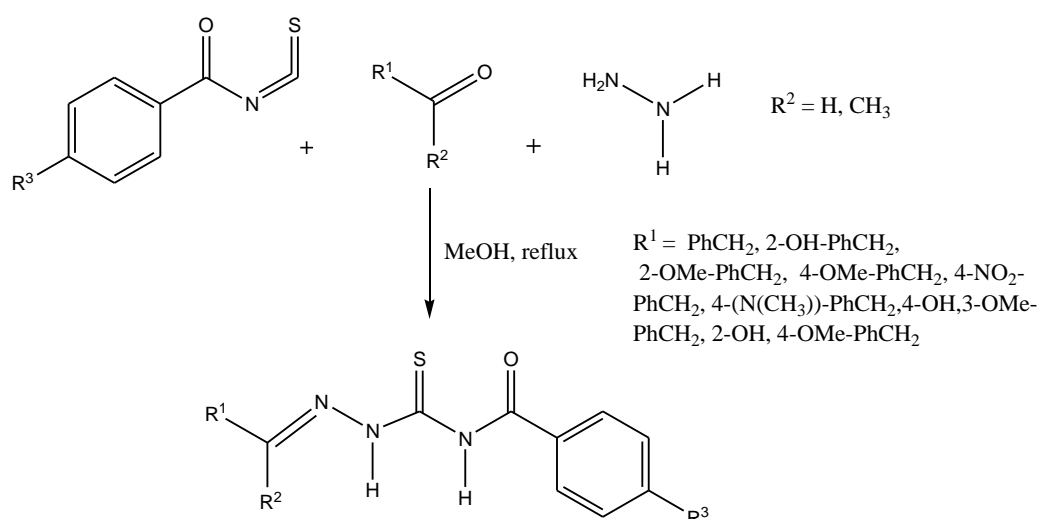
Scheme 1.14 Triphenylphosphine catalyzed cyclizations of benzoyl isothiocyanate derivatives.²¹⁸

An efficient synthesis of ethyl 2-(4-acetyl-5-benzoylamino-3-methyl-2-thienyl)-2-oxoacetates have been achieved *via* a reaction between benzoyl isothiocyanates and ethyl bromopyruvate in the presence of enamines (**Scheme 1.15**).²¹⁹



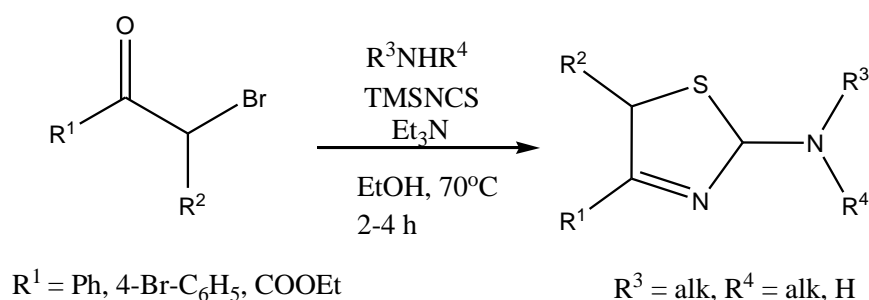
Scheme 1.15 Double insertion reactions of benzoyl isothiocyanates.²¹⁹

Sodium bis(trimethylsilyl)amide has been used as a desulfurizing agent for the conversion of isothiocyanates to cyanamides.²²⁰ A novel and efficient procedure for the synthesis of thiosemicarbazones has been achieved *via* a reaction of phenyl or *p*-chlorophenyl isothiocyanate, hydrazine, and aldehydes or ketones (**Scheme 1.16**).²²¹



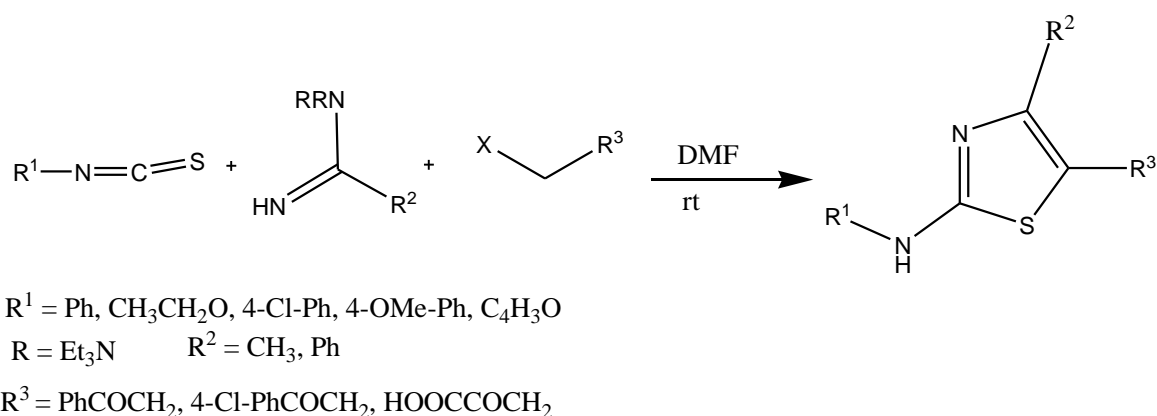
Scheme 1.16 Synthesis of thiosemicarbazones *via* a reaction of phenyl or *p*-chlorophenyl isothiocyanate, hydrazine, and aldehydes or ketones.²²¹

2-Aminothiazoles from bromocarbonyl compounds and amines (aromatic and aliphatic) using trimethylsilyl isothiocyanate have been reported (**Scheme 1.17**).²²²



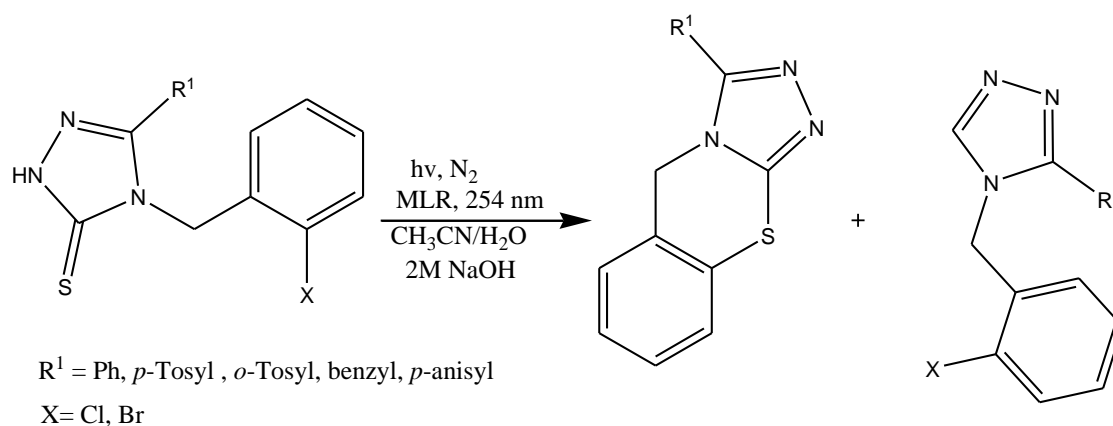
Scheme 1.17 Synthesis of 2-aminothiazoles from bromocarbonyl compounds and amines.²²²

The synthesis of 2-aminothiazoles from isothiocyanates, amidines/guanidines and various halomethylenes has been achieved.²²³



Scheme 1.18 Synthesis of 2-aminothiazoles from isothiocyanates, amidines/guanidines and various halomethylenes.²²³

The photocyclization of substituted 1,2,4-triazole-3-thiones, under base-mediated conditions, afforded 1,2,4-triazolo[3,4-*b*]-1,3-(4*H*)-benzothiazines along with the desulfurization product has been reported.²²⁴



Scheme 1.19 Photocyclization of substituted 1,2,4-triazole-3-thiones, under base-mediated conditions.²²⁴

One pot synthesis of *N,N*-disubstituted acylguanidines have been accessed from primary amides.²²⁵ The synthesis of di- and tri-substituted *N*-acyl ureas on solid support has been reported. Addition of carboxylic acids to a resin-bound carbimidoyl chloride gave an *O*-acyl isourea which subsequently rearranged to the corresponding *N*-acyl urea.²²⁶

A polymer-supported carbodiimide has been used for the synthesis of 2-aminobenzimidazoles and related heterocycles.²²⁷ The use of a thiobenzophenone as a self-indicating linker in the polymer-supported synthesis of isothiocyanates has been reported. Isothiocyanates were furnished *via* 1,3-dipolar cycloaddition of nitrile oxides with the polymer-supported thiobenzophenone linker, followed by Lewis acid-assisted fragmentation of the resulting polymer-supported oxathiazole.²²⁸ Two novel glycocluster ligands with cyclam core bearing thiourea-linked D-glucose and 2-acetamido-2-deoxy-D-glucose at the periphery have been synthesized.²²⁹ While facile one-pot sequential three-component route to 2,4-diaminothiazoles has been achieved.²³⁰

1.5 Synthesis and biological activity of gold compounds

A series of gold(1) coordination complexes including analogues of the antiarthritic agent auranofin have been evaluated for *in vitro* cytotoxic potency against both B16 melanoma cells and P388 leukemia cells and *in vivo* antitumor activity against P388 leukemia in mice. A number of the complexes showed potent cytotoxic activity *in vitro* and antitumor activity in

vivo, with the phosphine-coordinated gold(I) thiosugar complexes demonstrating the greatest *in vitro* and *in vivo* activity.²³¹ Gold(III) compounds are emerging as a new class of metal complexes with outstanding cytotoxic properties and are presently being evaluated as potential antitumor agents. The solution, electrochemical properties, and the biological behavior of some gold(III) dithiocarbamate derivatives which have been recently proved to be 1 to 4 orders of magnitude more cytotoxic *in vitro* than cisplatin and to be able to overcome to a large extent both intrinsic and acquired resistance to cisplatin itself. Their solution properties have been monitored in order to study their stability under physiological conditions. They have been shown to undergo complete hydrolysis within 1 h, the metal center remaining in the +3 oxidation state. Their DNA binding properties and ability in hemolyzing red blood cells have also been evaluated. These gold(III) complexes showed high reactivity toward some biologically important isolated macromolecules, resulting in a dramatic inhibition of both DNA and RNA synthesis and inducing DNA lesions with faster kinetics than cisplatin. Nevertheless, they also induce a strong and fast hemolytic effect (compared to cisplatin), suggesting that intracellular DNA might not represent their primary or exclusive biological target.²³²

A series of mono- and dimetallic Au(I) triphenylphosphine complexes derived from 1,2-, 1,4-, and 1,8-dialkynyloxyanthraquinone have been prepared. The photophysical and cytotoxic behavior of the ligands and complexes have been explored, with all of the complexes showing both appreciable cytotoxicity against the MCF-7 carcinoma cell line and room-temperature anthraquinone-based visible luminescence, which allowed their successful application as fluorophores in cell imaging microscopy.²³³ New Au(III) complexes of the type [(thione)₂Au(diamine)]Cl₃ have been reported, where thione = 1,3-imidazolidine-2-thione (Imt), 1,3-Diazinane-2-thione (Diaz) and diamine = diaminoethane (en), 1,3-diaminopropane (pn) or 1,4-diaminobutane (bn).²³⁴ A facile and efficient synthetic route leading to catalytically relevant *N*-heterocyclic carbene (NHC) gold complexes have been achieved. In this imidazolium salts and [AuCl(tht)] have been used in the presence of K₂CO₃.²³⁵

The synthesis and characterization of three propynyloxy coumarins have been reported, together with the formation of three different series of gold(I) complexes. Neutral complexes are constituted by water soluble phosphines (PTA and DAPTA) which confer water solubility to them. The X-ray crystal structure of 7-(prop-2-yn-1-yloxy)-1-benzopyran-2-one and its

corresponding dialkynyl complex. The formation of rectangular dimers for the gold derivative in the solid state can be observed. A detailed analysis of the absorption and emission spectra of both ligands and complexes showed that the luminescent behaviour was attributable to the coumarin organic ligand. Moreover, the presence of the gold(I) metal atom seems to be responsible for an increase of coumarin phosphorescence emission. The biological activity of the complexes showed that the anionic complexes triggered strong cytotoxic effects in two different cell lines whereas the neutral gold alkynyl complexes led to lower effects against tumor cell growth. Thioredoxin reductase (TrxR) inhibition was very strong in the case of the neutral complexes (IC_{50} values below $0.1 \mu\text{M}$) but moderate for the anionic complexes.²³⁶

A class of chiral gold amide complexes featuring amino acid derived ligands have been reported. They were all found to exhibit *in vitro* cytotoxicity against two slow growing breast cancer cell lines with limited toxicity towards normal epithelial cells.²³⁷ Gold and its complexes have long been known to display unique biological and medicinal properties. Extensive cell-based (*in vitro*) and animal (*in vivo*) studies have revealed the potent anti-cancer activities of diverse classes of gold(I) and gold(III) complexes. Most of the reported anti-cancer active gold complexes are highly cytotoxic and unstable under physiological conditions, which hamper their development to be launched clinically. Several clinical reports showed that lipophilic organic cations are promising anti-cancer drug candidates targeting the mitochondria. Through metal–ligand coordination, gold(I) and gold(III) ions can form stable lipophilic cations containing organic ligands having tunable lipophilicity and diverse functionalities.²³⁸

Auranofin, a linear tetraacetylthioglucose gold(I) phosphine complex, increased the life span of mice inoculated with P388 leukaemia, inhibited DNA polymerases and was preferentially cytotoxic to cells with altered mitochondria. Triethylphosphine gold(I) chloride inhibited tumor colony formation *in vitro*, reacted with DNA, and inhibited oxidative phosphorylation, ATP production and the viability of isolated rat hepatocytes. Bis[1,2-bis(diphenylphosphino)ethane]gold(I) chloride ($[\text{Au}(\text{dppe})_2]\text{Cl}$) had reproducible and significant antitumor activity in a number of murine tumor models *in vivo*. $[\text{Au}(\text{dppe})_2]\text{Cl}$ also inhibited tumor colony formation *in vitro*, formed DNA strand breaks, induced DNA-protein cross links and had antimitochondrial effects on P388 leukemia cells and isolated hepatocytes. Tetrahedral Au(I) complexes of bidentate pyridyl phosphines have shown

promising *in vitro* and *in vivo* antitumor properties that were determined by their drug lipophilicity. Although the exact intracellular targets responsible for their antitumor activity are unclear, gold(I) phosphines are directly cytotoxic and many appear to have antimitochondrial activity. Optimization of their hydrophilic/lipophilic balance may be key to improving their selectivity for tumor mitochondria versus oxidative phosphorylation pathways of normal cells.²³⁹

A series of both mono- and dinuclear gold(I) phosphine complexes containing monoanionic seleno and thiosemicarbazones as ligands have been prepared and fully characterized by spectroscopic methods and in some cases, by single crystal X-ray diffraction. The *in vitro* anti-malaria activity of some of these compounds was investigated in chloroquine sensitive strains of *Plasmodium falciparum*. The IC₅₀ results showed that the sulfur containing compounds exhibit activity similar to that of chloroquine, whilst the selenium derivatives display only moderate anti-malaria activity.²⁴⁰ Binuclear gold compounds, [Au(R₂PC(S)NR')]₂, were characterized from the reactions of HAuCl₄ or Ph~PAuCl with R₂PC(S)N(H)R'. The complexes had bidentate bridging ligands that link two gold centres leading to eight-membered metallacycles and linear S-Au-P coordination geometries. In the case of [Au(Ph₂PC(S)NPh)]₂, crystal structure analysis showed the presence of two conformations in the one lattice, i.e. an extended chair and a twisted conformation.²⁴¹

Gold is emerging as a potential therapeutic agent in the treatment of arthritis, cancer and AIDS. The therapeutic mechanism of arthritic gold drugs and their modification in the presence of stomach hydrochloric acid, in the joints, and in the presence of mild and strong oxidizing agents is still unclear. It is believed that gold affects the entire immune response and reduces its potency and limits its oxidizing nature. DNA apparently is not the main target of gold in cancer treatment. Rheumatoid arthritis, cancer, heart diseases and HIV have all been targeted with gold nanoparticles therapy. The era of gold nanoparticles started with cancer imaging and treatment studies. Gold nanoparticles have emerged as smart drug vehicles.²⁴² ([3,5-Me₂bpzaH₂][AuCl₄]Cl, **A**) (Me₂bpza = bis(3,5-dimethylpyrazolyl)acetic acid), has been prepared by reacting H[AuCl₄] with 3,5-Me₂bpza; and spectroscopically and structurally characterized. In the solid state structure of **A**, the pyrazolyl ligand was doubly protonated to form two strong charge assisted hydrogen bonds with the single chloride anion whilst the [AuCl₄] anion remains discrete. The anti-HIV-1 activity of **A** was determined by a colorimetric direct enzyme reverse transcriptase (RT) assay and a fluorogenic protease (PR)

assay. Compound **A** significantly ($p < 0.05$) inhibited RT over a concentration range of 5–250 μM and inhibited HIV-1 protease at 100 μM . Compound **A** inhibited two very important HIV-1 enzymes (RT and PR) in direct enzyme assays and therefore warrants further evaluation.²⁴³ The reaction of thiosemicarbazones (TSCs) with $[\text{Au}(\text{THT})\text{Cl}]$, THT = tetrahydrothiophene, has been investigated. The resulting gold(I) complexes were characterized by a range of spectroscopic techniques: NMR spectroscopy, mass spectrometry, microanalysis and infrared spectroscopy. The *in vitro* antimalarial data for gold(I) TSC complexes suggested that coordination of gold(I) to TSCs enhanced their efficacy against the malaria parasite *Plasmodium falciparum* and their inhibition of the parasite cysteine protease.²⁴⁴ The synthesis and structure of rare acyclic alkoxy- and aminocarbene complexes of gold(I) are reported, including a novel ferrocenophane dinuclear biscarbene complex. X-Ray diffraction analyses and DFT calculations reveal that these complexes are stabilized by genuine aurophilic interactions.²⁴⁵

Topoisomerase IB (Top1) is a key eukaryotic nuclear enzyme that regulates the topology of DNA during replication and gene transcription. Anticancer drugs that block Top1 are either well-characterized interfacial poisons or lesser known catalytic inhibitor compounds. A new class of cytotoxic redox-stable cationic Au^{3+} macrocycles has been accessed which through hierarchical cluster analysis of cytotoxicity data for the lead compound, **3**, were identified as either poisons or inhibitors of Top1 (**Figure 1.4**, **Table 1.2**). Two pivotal enzyme inhibition assays proved that the compounds were true catalytic inhibitors of Top1. Inhibition of human topoisomerase II α (Top2 α) by **3** was 2 orders of magnitude weaker than its inhibition of Top1, confirming that **3** is a type I-specific catalytic inhibitor. Importantly, Au^{3+} is essential for both DNA intercalation and enzyme inhibition. Macromolecular simulations show that **3** intercalates directly at the 5'-TA-3' dinucleotide sequence targeted by Top1 *via* crucial electrostatic interactions, which include π - π stacking and an $\text{Au}\cdots\text{O}$ contact involving a thymine carbonyl group, resolving the ambiguity of conventional (drug binds protein) vs unconventional (drug binds substrate) catalytic inhibition of the enzyme. Surface plasmon resonance studies confirm the molecular mechanism of action elucidated by the simulations (**Figure 1.4**).²⁴⁶

	M	X	R	Y	Z
1	Au	CH ₂ CH ₂ CH ₂	H	+	PF ₆ ⁻
2a	Au	CH ₂ C(CH ₃) ₂ CH ₂	H	+	PF ₆ ⁻
2b	Au	CH ₂ C(CH ₃) ₂ CH ₂	H	+	CF ₃ SO ₃ ⁻
3a	Au	CH ₂ (CH ₂) ₂ CH ₂	H	+	PF ₆ ⁻
4	Au	CH ₂ CHClCH ₂	H	+	PF ₆ ⁻
5	Au	CH ₂ (CH ₂) ₂ CH ₂	H	+	PF ₆ ⁻
6	2H	CH ₂ CH ₂ CH ₂	CH ₃	+	O
7	Ni	CHCH ₂ CH ₂	H	O	O

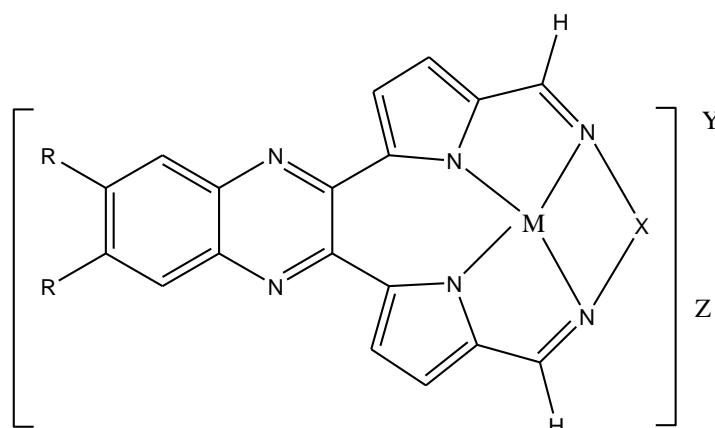


Figure 1.4 General Structure for topoisomerase 1 blockers²⁴⁶

1.6 Gold catalysed reactions

The unique versatility and efficiency of gold complexes have been obtained including carbene ligated gold complexes. Due to the special linear coordination mode of gold(I) complex, Au catalyzed asymmetric reactions have become a huge challenge. Chiral carbene–gold complexes also have been applied in asymmetric reactions.²⁴⁷ Methyl esters can be produced in high yields by oxidizing methanolic solutions of primary alcohols with dioxygen over a heterogeneous gold catalyst. The versatility of this new methodology is demonstrated

by the fact that alkylic, benzylic and allylic alcohols, as well as alcohols containing an amine functionality are oxidized in good to excellent yields.²⁴⁸

Reactions of 1,6-enynes catalyzed by gold(I) complexes usually proceed stereospecifically through highly distorted cyclopropyl gold carbenes. Substrates with an alkoxy substituent at the propargylic position undergo stereoselective transformations through intermediates in which the OR group and the gold carbene are anti-oriented. Intramolecular attack of carbonyl groups to the cyclopropyl gold carbene is faster than the 1,5-migration of the OR groups, which itself is faster than the intramolecular cyclopropanation by a pendant alkenyl group. The intramolecular attack of carbonyl groups is the key transformation in the [2+2+2] gold-catalyzed cycloaddition, which has been applied in the total synthesis of (+)-orientalol F²⁴⁹.

1.7 Activity of gold compounds against HIV

The synthesis and characterization of some imidazole-based gold-selenolates have been carried out which indicated that the selenolate plays an important role in ligand exchange reactions in gold(I) selenolates. Furthermore, the reactivity of imidazole-based gold(I) selenolates toward nucleophiles such as selenols and phosphines is strikingly different from that of the *N,N*-dimethylaminobenzylamine-based gold(I) complexes. The presence of Se-N non-bonded interactions in *N,N*-dimethylaminobenzylamine-based gold(I) complexes is known to modulate the reactivity of Au(I) centre towards incoming nucleophiles.²⁵⁰

Rheumatoid arthritis is currently treated with gold-based drugs and there is increasing interest in the application of gold complexes as potential anticancer agents. Gold based compounds have been developed as anti-parasitic agents and used in the treatment of major tropical diseases such as malaria, leishmaniasis, trypanosomiasis and schistosomiasis.²⁵¹

Four analogues of the gold(III) complex [AuCl₂(damp)] (**1**) (damp)₂-[(dimethylamino)methyl]-phenyl) have been evaluated for antitumor activity. The compounds have structural features in common with cisplatin which was included as a comparison in the study. *In vitro*, against a panel of cell lines established from tumors of different tissue types, the gold complexes showed broadly similar growth inhibitory properties with some selectivity to the HT1376 bladder cell line. In a panel of human ovarian carcinoma cell lines, non-cross-

resistance to cisplatin was observed, for the complexes, in an acquired cisplatin-resistant line. *In vivo*, using subcutaneously implanted xenografts derived from the HT1376 bladder and CH1 ovarian cell lines, [Au-(acetato)₂(damp)] (**3**) and [Au(malonato)(damp)] (**5**) (administered intraperitoneally) gave significant tumor inhibition. Mechanistic studies performed with compound **3** showed marked differences to cisplatin.²⁵²

Intermittent infusions of interleukin-2 a cytokine that regulates the proliferation and differentiation of lymphocytes led to increases in CD4 counts in patients with HIV infection and more than 200 CD4 cells per cubic millimeter. A controlled study to evaluate the long-term effects of such therapy on both CD4 counts and the viral burden has been carried out. In patients with HIV infection and base-line CD4 counts above 200 cells per cubic millimeter, intermittent infusions of interleukin-2 produced substantial and sustained increases in CD4 counts with no associated increase in plasma HIV RNA levels.²⁵³

1.8 Dual action of gold

The use of HAART has resulted in decreased mortality and morbidity from AIDS caused by HIV. Drug resistance and toxicity of HAART has led to the search for novel inhibitors of HIV infection. Gold-based compounds have shown promising activity against a wide range of clinical conditions and microorganism infections including HIV-1. A typical example is auranofin which resulted in an elevated CD4⁺ T-cell count in an HIV patient being treated for psoriatic arthritis.²⁵⁴

The increasing incidence of HIV infection and the associated AIDS mortality rates as well as the sometimes severe side effects of HAART warrants the continuous search for new, less toxic drug candidates. The anti-HIV activity (inhibition of reverse transcriptase-RT and protease-PR in direct enzyme assays) of eleven gold(I) phosphine compounds have been reported. Uptake of the compounds by peripheral blood mononuclear cells (PBMCs) has been demonstrated by inductively coupled plasma atomic emission spectroscopy (ICP-AES) while the effect of the compounds on cell viability was assessed using flow cytometry with annexin V and propidium iodide (PI). Of the 11 gold compounds tested, 7 significantly ($p < 0.05$) inhibited RT activity at concentrations of 25 and 250 mM while 3 compounds significantly inhibited its activity at 6.25 mM. In the anti-protease assay, 4 of the compounds significantly

inhibited the enzyme ($p < 0.05$) at 100 mM. All of the compounds were taken up by PBMCs (demonstrated by ICP-AES) and were non toxic to these cells at clinically tolerable concentrations. The potential of these novel gold(I) phosphine compounds as anti-HIV agents is therefore promising and worthy of further investigation.²⁵⁵

Gold(I) complexes, containing cyanide and some other ligand (L), {LAuCN} though stable in the solid state dissociate to form ionic species. The X-ray and IR studies showed that some cyanogold(I) complexes exist as non-ionic complexes (LAuCN) and some as the ionic species $\{[\text{Au}(\text{L}_2)]^+[\text{Au}(\text{CN})_2]^- \}$ in the solid state. In solution, the LAuCN complexes undergo ligand scrambling reactions exhibiting the equilibrium (**Scheme 1.20**).



Scheme 1.20 Equilibrium for gold ligand scrambling reactions.

Equilibrium constants (K_{eq}) for the scrambling equilibria were determined by integration of the ^{13}C and ^{31}P NMR spectra. The equilibrium constant was found to be dependent on factors such as the initial concentration of the complex, ionic strength of the solution, temperature and polarity of the solvent, with polarity of the solvent showing major influence on K_{eq} . The order of ability of different L–Au–CN complexes undergoing disproportionation was: $[(\text{C}=\text{Se})\text{Au}(\text{CN})] > [(\text{R}_3\text{PSe})\text{Au}(\text{CN})] > [(\text{C}=\text{S})\text{Au}(\text{CN})] > [(\text{R}_3\text{P})\text{Au}(\text{CN})] \geq [(\text{R}_3\text{PS})\text{Au}(\text{CN})]$. The reactions of gold drugs and their metabolites, with cyanide led to the formation of intermediates, $[(\text{RS})\text{Au}(\text{CN})]^-$ and $[(\text{Et}_3\text{P})\text{Au}(\text{CN})]$, which undergo disproportionation generating $[\text{Au}(\text{CN})_2]^-$ which is readily taken up by red blood cells. The formation of aurocyanide is dependent on thiocyanate and occurs both by the peroxidase dependent oxidation of thiocyanate and by a secondary reaction of hypochlorous acid with thiocyanate. $[\text{Au}(\text{CN})_2]^-$ is a common metabolite of the gold drugs in the blood and urine of chrysotherapy patients. The oxidation of $[\text{Au}(\text{CN})_2]^-$ by OCl^- could lead to the formation of gold(III) metabolites.²⁵⁶

Aurothioglucose and aurothiomalate have anti-HIV-1 *in vitro* and antiviral activity requires the formation of reactive intermediate with a molar equivalent amount of a thiol ligand. This activates gold(I) ligand exchange between the reactive species bis(thiolato)gold(I) and acidic

thiols groups exposed on the surface of proteins. Bis(thiogluco)gold(I) (bisAuTG) which is formed by the reaction of molar equivalent amounts of aurothiogluco and 1-thio- β -D-glucose completely protected MT-4 and CEM cells against HIV-1_{NL4-3} induced cytopathogenicity. Although bisAuTG is an inhibitor of HIV-1 reverse transcriptase in a cell free assay, its antiviral effect is due to modification of surface component of the virion. The HIV-1 strain NL4-3 is 200-fold more sensitive to inhibition of infectivity by bisAuTG than are the strains MN, RF and SF-2. HIV-1_{NL4-3} has a unique cysteine residue close to the amino terminus of its gp41 envelope glycoprotein (residue 532 of gp160) which has been hypothesized as the target of bisAuTG binding. Mutation of that residue alters HIV-1_{NL4-3} infectivity and dominantly suppresses virus assembly when coexpressed with the wild-type NL4-3 genome. It has been shown that bisAuTG treatment releases gp 120 from the surface of cells expressing wild-type HIV-1_{NL4-3} envelope glycoprotein, but it does not release gp120 if Cys⁵³² is mutationally altered to Ala. Thus, the antiviral effect of bisAuTG on HIV-1_{NL4-3} is due to an effect on the association of gp41.²⁵⁷

Gold(I) has a much higher affinity for thiolate S compared to thioether S, and a much lower affinity for N and O ligands. Therefore, Au(I) binds to DNA very weakly and is not usually carcinogenic or mutagenic. Thiolate exchange reactions on Au(I) are facile and therefore the administered drugs are probably not the pharmacologically-active species.²⁵⁸ Auranofin [2,3,4,6-tetra-O-acetyl-1-thio- β -D-glucopyranosato-S)-(triethylphosphine)gold], a new gold compound for treating rheumatoid arthritis (RA), is unique in that it produces its therapeutic benefit when administered by the oral route. Currently used gold preparations (sodium aurothiomalate, aurothiogluco) must be given by injection to be effective. Auranofin has been used in the treatment of rheumatoid arthritis (RA) patients in clinical trials, and is comparable in efficacy to presently used injectable agents. Side effects with auranofin are mild in nature and result in fewer withdrawals from therapy than do injectable gold preparations.²⁵⁹ It has been reported that dicyanogold(I), [Au(CN)₂] is a common metabolite found in blood and urine samples of patients treated with different gold based drugs. Some patients have high levels of gold within their red blood cells (RBCs). Size exclusion and reversed phase chromatography show that the majority of the gold in RBC lysates is bound to protein, but small molecules such as dicyanogold(I) and gold-glutathione complexes are also present. Dicyanogold incubation with red blood cells *in vitro* leads to a rapid and complete uptake of gold. This uptake is unaffected by DIDS, an inhibitor of the anion channel, but is blocked by the addition of external cyanide. Dicyanogold is also readily taken up by H9 cells,

a continuous CD4 cell line. This uptake is significantly inhibited by *N*-ethylmaleimide, suggesting a requirement for sulfhydryl groups. Dicyanogold inhibits the replication of the AIDS virus, HIV, in a cell culture model.²⁶⁰

The reactions of serum albumin, a blood carrier of gold(I), with the auranofin analogue triisopropylphosphine-(2,3,4,6-tetra-*Q*-acetyl-1-thio-glucopyranosato-*S*)gold(I)(*i*-Pr₃P AuSATg) and free triisopropylphosphine have been studied in buffered aqueous solution using (¹H)³¹P NMR and chromatographic methods. Triisopropylphosphine (*i*-Pr₃P) is oxidized to *i*-Pr₃PS *via* an albumin-thiolato-triisopropylphosphonium ion, *i*-Pr₃P+SCHZ(HSCHZ)Alb, which is formed by attack on a protein disulfide bond. This species is the key intermediate in the albumin-driven conversion of a phosphine ligand (e.g., from auranofin or an analogue) into phosphine oxide or phosphine sulfide. *i*-Pr₃PSCHZ- (HSCHZ)Alb, which is characterized by a ³¹P(¹H) NMR chemical shift of 75.4 ppm, forms quickly and then reacts slowly to form *i*-Pr₃PS and a small quantity of *i*-Pr₃PO. The auranofin analogues *i*-Pr₃PAuSATg and *i*-Pr₃PAuC1, react with serum albumin and cysteine-34 to form AlbSAuPi-Pr₃ *via* displacement of the anions. *i*-Pr₃PAuC1 reacts further at weak binding sites analogous to the histidine binding sites of auranofin. In contrast to the displacement of Et₃P from AlbSAuPEt, by thiols, cyanide is required to displace *i*-Pr₃P from AlbSAuPi-Pr₃. The liberated *i*-Pr₃P also reacts *via* the albuminphosphonium intermediate to form *i*-PpPS and traces of *i*-PoPO. In order to interpret the protein studies, a variety of potential reaction products (*i*-Pr₃PAuX, X = CN, ATgS, C1; *i*-Pr₃PY, Y = O, S) have been prepared and characterized by ³¹P NMR spectroscopy. Model reactions of *i*-Pr₃PAuX (X = C1, ATgS) with cyanide have also been reported.²⁶¹

Gold distribution and binding sites in blood and red blood cells (RBCs) have been determined. RBCs were separated from plasma and lysed. The cytosol was separated from membranes which were then solubilized *via* detergents. Total gold in each fraction was measured *via* flow injection analysis (FIA) with (ICP-MS) detection. Various high-performance liquid chromatography (HPLC) techniques such as ion-pairing, reversed-phase and size exclusion chromatography have been applied to RBC samples prepared by incubation with specific compounds and to RBCs from rheumatoid arthritis (RA) patients. Preliminary studies of RA patients' samples indicate very different gold uptake into RBCs depending on the particular patient. Size-exclusion chromatography indicates that gold in the lysate is not bound principally to haemoglobin, but rather to a significantly higher molecular

weight species (about 330 000 Da). Low molecular weight species in the ultrafiltered RBC lysate include the dicyanogold(I) anion and possibly the bis(glutathione)gold(I) complex. Incubation experiments have been designed to measure dicyanogold(I) and gold drug uptake by RBCs. Experiments with DIDS, an anion channel blocker, indicate that dicyanogold(I) enters the cell by some path other than the anion channel. The inhibition of gold uptake on addition of free cyanide suggests that the loss of cyanide from dicyanogold(I) is important in dicyanogold(I) uptake by RBCs. Given the rapid uptake of dicyanogold(I) and its apparently high tolerance in humans, this material is suggested as a possible therapy in the treatment of AIDS²⁶².

1.9 Scope of the thesis

The principal aim of this study was to pre-screen sulfur containing ligands for their fit and activity in the HIV-1 protease active site using Autdock 4.2, to synthesize and fully characterize the compounds and their gold complexes and to carry out cell viability tests and HIV-1 protease assays of resulting compounds. The research objectives are as follows:

- Pre-screening of sulfur containing ligands (benzoyl-isothiocyanate derivatives) to establish their fit and predicted activity at the HIV-1 protease active site.
- Synthesize the compounds that give good predicted inhibition constants and fully characterize them using IR, NMR, microanalysis, GC-MS and single crystal XRD for some of the ligands.
- Synthesis and characterization of the corresponding gold complexes of these compounds, which were largely unsuccessful but led to the dethiocyanation of the ligands and subsequent C-N coupling to form benzamides.
- DFT transition state studies of the reaction mechanism of the compounds.
- Cell viability and cytotoxicity studies to ascertain the effects of the compounds on peripheral blood mononuclear cells.
- HIV-1 protease assay and enzyme inhibition studies of the promising compounds.

CHAPTER 2

EXPERIMENTAL

This chapter focuses on chemicals and the suppliers of the reagents that were used in the preparation of the compounds, as well as synthesis and some characterization data reported in this thesis. Details concerning the instrumentation and softwares used are also provided.

2.1 Materials

Analytical grade reagents and solvents for synthesis were obtained from the suppliers indicated in the table below (**Table 2.1**). The chemicals were used as received (i.e. without further purification).

Table 2.1. List of chemicals used.

Chemical	% Purity	Supplier
<i>o</i> -Phenylenediamine	99.5	Sigma Aldrich
Isophthalic acid	99.0	Sigma Aldrich
4-Methyl- <i>o</i> -phenylenediamine	98.0	Sigma Aldrich
2-Aminobenzimidazole	97.0	Sigma Aldrich
<i>m</i> -Toluic acid	99.0	Sigma Aldrich
2-Aminobenzothiazole	97.0	Sigma Aldrich
2-Aminobenzoxazole	97.0	Sigma Aldrich
2-(2-Aminophenyl)- <i>1H</i> -benzimidazole	97.0	Sigma Aldrich
Benzoyl chloride	98.5	Fluka
4-Methoxybenzoyl chloride	99.0	Sigma Aldrich
4-Chlorobenzoyl chloride	99.0	Sigma Aldrich
4-Nitrobenzoyl chloride	98.0	Sigma Aldrich
4-Bromo benzoyl chloride	98.0	Sigma Aldrich
Ammonium thiocyanate	98.5	Merck Chemicals
3-Methoxybenzoyl chloride	99.0	Sigma Aldrich
3-Chlorobenzoyl chloride	99.0	Sigma Aldrich
3-Nitrobenzoyl chloride	98.0	Sigma-Aldrich
3-Bromobenzoyl chloride	98.0	Sigma Aldrich
Poly phosphoric acid	115.0	Sigma Aldrich
H ₂ SO ₄	95.0	Merck Chemicals
HCl	32.0	SMM Instruments
L-Serine	99.0	Sigma Aldrich

Table 2.1 continued

L-Proline	99.0	Sigma Aldrich
L-Alanine	98.0	Sigma Aldrich
D-Methionine	98.0	Sigma Aldrich
Chloro(triphenyl phosphine)gold(I)	99.9	Sigma Aldrich
Triphenyl phosphine	99.0	Aldrich
Gold(III) chloride	99.0	Sigma Aldrich
Chloro(dimethylsulfide)gold (I)	95.0	Sigma Aldrich
Silver Oxide	94.0	Merck Chemicals
Silver Nitrate	99.0	Sigma Aldrich
Alanine methyl ester Hydrochloride	99.0	Sigma Aldrich
Aspartic acid dimethyl ester hydrochloride	97.0	Sigma Aldrich
Ethyl acetate	98.8	Sigma Aldrich
Triethylamine	99.0	Merck Chemicals
Pyridine	99.8	Merck Chemicals
Acetone	99.0	SMM Instruments
Diethylether	99.0	Merck Chemicals
DMSO	99.0	Merck Chemicals
THF	99.0	Merck Chemicals
Toluene	99.0	Associated Chemicals
Methanol	99.0	Merck Chemicals
Ethanol	99.8	Sigma Aldrich
Dichloromethane	98.0	SMM Instruments
Acetonitrile	99.9	Merck Chemicals
Hexane	98.5	Merck Chemicals
Thionyl Chloride	98.0	Sigma Aldrich
FBS	--	BioWest, France
HyClone RPMI	-	GE Healthcare Life Sciences, USA
PenStrep	-	Sigma, USA
MTT	98	Melford Biolaboratories, UK
EDTA	99	Merck, USA
Camptothecin	95	Sigma, USA
Protease Assay Kit		
Trypan blue		Lonza, Belgium
KHCO ₃	99	Minema, South Africa
NH ₄ Cl	99	Minema, South Africa
Ritonavir	95	Enamine

2.2 Spectroscopic techniques

2.2.1 NMR Spectrometry

The purity and identification of compounds were determined using ^1H and ^{13}C NMR spectra which were recorded on a Bruker Avance AV 400 MHz spectrometer operating at 400 MHz for ^1H and 100 MHz for ^{13}C using DMSO-d_6 as solvent and tetramethylsilane as internal standard. Chemical shifts are expressed in ppm.

2.2.2 Infrared Spectroscopy

FT-IR spectra of the compounds were recorded on a Bruker Platinum ATR Spectrophotometer Tensor 27 and the machine is controlled by Bruker's OPUS software.

2.2.3 Microtitre plate reader

The microtitre plate was used to measure the absorbance of cell cultures or any other biological matrix. The absorbance was measured at 540 nm using a BioTek Epoch 2 microtitre plate reader.

2.2.4 Fluorogenic microplate reader

The fluorogenic microplate reader was used to measure the absorbance or fluorescence of cell cultures or any other biological matrix. The fluorescence was measured using a BioTek SynergyMx microtitre plate reader. Excitation/Emission: 340 nm/490 nm.

2.3 Analytical methods

2.3.1 Elemental Analysis

Elemental analysis was carried out with a Vario Elementary ELIII Microcube CHNS elemental analyser.²⁶³ Calibration of the instrument was done with the use of the following standards in a linear curve adjustment within the total working range.

Standard 1: Sulfanilamide – C; 41.81, H; 4.65, N; 16.25, S; 18.62%

Standard 2: Acetanilide – C; 71.09, H; 0.67, N; 10.36, O; 12.0%

The basic principle of quantitative CHNOS analysis is high temperature combustion of organic and many inorganic solid or liquid samples. The gaseous combustion products are purified, separated into their various components and analysed with a suitable detector such as thermal conductivity detector (TCD), optional infrared detector (IR) for sulfur, etc.²⁶⁴

2.3.2 Gas Chromatography–Mass Spectrometry

The masses were determined using an Agilent 7890A GC System connected to a 5975C VL–MSC with electron impact as the ionization mode and detection by a triple-Axis detector. The GC was fitted with a 30 m x 0.25 mm x 0.25 μm DB-5 capillary column. Helium was used as carrier gas at a flow rate of 1.6 mL.min⁻¹ with an average velocity of 30.2 cm s⁻¹ and a pressure of 63.7 kPa.

2.4 Single crystal X-ray

X-ray diffraction studies were performed at 200 K using a Bruker Kappa Apex II diffractometer with graphite monochromated Mo K α radiation ($\lambda = 0.71073 \text{ \AA}$). The crystal structures were solved by direct methods using SHELXTL.²⁶⁵ All non-hydrogen atoms were refined anisotropically. Carbon-bound hydrogens were placed in calculated positions and refined as riding atoms with bond lengths 0.95 (aromatic CH), 0.99 (CH₂), and 0.98 (CH₃) \AA and with Uiso(H) = 1.2 (1.5 for methyl) Ueq (C). Hydrogens bonded to nitrogen were located on a Fourier map and allowed to refine freely. Hydrogens on water were restrained to an O–H bond length of 0.84 \AA and H–O–H angle of 110°. Diagrams and publication material were generated using SHELXTL, PLATON,²⁶⁶ and ORTEP-3.²⁶⁷

2.5 Autodock

Autodock is a suite of C programs used to predict the bound conformations of a small, flexible ligand to a macromolecular target of known structure. The technique combines simulated annealing for conformation searching with a rapid grid-based method of energy evaluation.²⁶⁸⁻²⁶⁹ In this work AutoDock 4.2 was used in the pre-screening of the scaffolds.

The crystal structure of protease (1hxw) was obtained from the protein database and the coordinates of ritonavir in the binding pocket noted. Discovery studio was then used to create a library of scaffolds which were then minimised using VEGAZZ or Gaussian. The minimized structures were then docked in the defined binding pocket and the scaffold with the lowest inhibition constants taken forward.

2.6 Gaussian

The calculations were carried out using Gaussian 09 program.²⁷⁰ Molecular geometries of the singlet ground state of all the compounds were fully optimised in the gas phase at the density functional theory (DFT) level of theory using B3LYP or BWP391 with different functions, depending on the specific compound in question but a single function was used per reaction mechanism. The corresponding vibrational frequencies were calculated at the same level to take account of the zero-point vibrational energy (ZPVE). We confirmed that all the reactants, intermediates and products have no imaginary frequencies, and each transition state has one and only one, imaginary frequency. The intrinsic reaction coordinate (IRC) calculations were performed at the same level of theory to ensure that the transition states led to the expected reactants and products.²⁷¹⁻²⁷³

2.7 Melting point determination

The melting points of the compounds were determined using a Stuart Lasec SMP30 melting point apparatus.

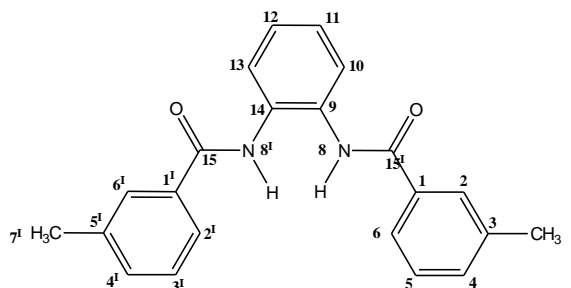
2.8 Centrifuge

Centrifuging of whole blood and buffy coat was done with an Eppendorf Centrifuge 5702

2.9 Preparative work

2.9.1 Methyl-*N*-[2-(3-methylbenzamido)phenyl]benzamide (1) ²⁷⁹

m-Toluic acid (0.01 mol, 1.36 g) was heated under reflux in thionyl chloride for 3 h. The thionyl chloride was distilled off and the product (*m*-toluoyl chloride) dried under vacuum for 16 h. *o*-Phenylenediamine (0.01 mol, 1.08 g) was reacted with *m*-toluoyl

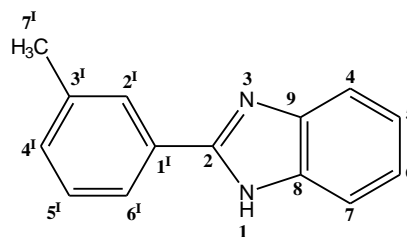


chloride under reflux in pyridine for 12 h. The pyridine was distilled off and the crude product was dissolved in a small quantity of methanol and placed on a column. It was then eluted with hexane:ethyl acetate by gradient elution starting from 0% ethyl acetate up to 100%. The elution was started with 50 mL of hexane (100%), followed by 250 mL hexane:ethylacetate (1:20) and then 250 mL of hexane:ethylacetate (1:10). The column was further eluted with 250 L of hexane:ethyl acetate (3:20) which gave the product. The elution was continued with 500 mL of hexane:ethyl acetate (1:5). and then with 250 mL of hexane:ethyl acetate (3:10) followed by 250 mL of hexane ethyl acetate (1:1), and it was further eluted with 200 mL of ethyl acetate (100%). The column was then washed with 250 mL methanol (100%). Melting point = 148–150 °C. Yield = 32.0%. ¹H NMR (ppm): 10.02 (s, 2H, N–H), 7.76 (s, 2H, (**2**^I, **2**)), 7.75 (d, 2H, *J* = 4.4 Hz, (**6**, **6**^I)), 7.68 (d, 2H, *J* = 4 Hz (**10**, **13**)), 7.66 (d, 2H, *J* = 4.0 Hz, (**4**, **4**^I)), 7.42 (m, 2H, *J* = 4.0 Hz, (**11**, **12**)), 7.30 (m, 2H, (**5**, **5**^I)), 2.36 (s, 6H, (**7**, **7**^I)). ¹³C NMR (ppm): 20.9 (CH₃, **7**, **7**^I), 124.6 (**10**, **13**), 125.6 (**6**, **6**^I), 125.7 (**10**, **13**), 128.0 (**2**, **2**^I), 128.5 (**9**, **14**), 131.3 (**5**, **5**^I), 132.4 (**4**, **4**^I), 134.1 (**1**, **1**^I), 137.9 (**3**, **3**^I), 165.8 (C=O, (**15**, **15**^I)). IR (*v*_{max}, cm⁻¹): 3272 (N–H), 2916 (C–H), 1644 (C=O), 1596 (C=C), 1513 (C–N), 1276 (C–O). Anal. Calcd for C₂₂H₂₀N₂O₂: C, 76.72; H, 5.85; N, 8.13. Found: C, 77.15; H, 6.30; N, 8.15. LRMS (*m/z*, M⁺): Found for C₂₂H₂₀N₂O₂ = 344.41, Expected mass = 344.90.

2.9.2 2-(3-Methylphenyl)-1*H*-benzimidazole (2) ²⁹¹

Method A

Polyphosphoric acid (52 g), in 10 mL of toluene, was heated at 120 °C for 30 min, *m*-Toluic acid (0.1 mol, 13.6 g) and *o*-phenylenediamine (0.1 mol, 10.8 g) were added and the mixture was heated at 165 °C for 6 h. 20 mL of water was added with stirring and then sodium hydrogen



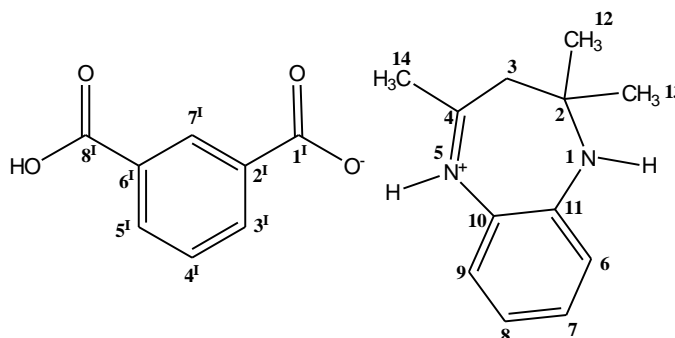
carbonate was added until effervescence ceased. The product was recrystallized from methanol:THF (1:1) and obtained as a white solid. Melting point = 213–215 °C, Yield = 89%.

Method B:

o-Phenylenediamine (0.03 mol, 3.24 g) was mixed with *m*-methylbenzaldehyde (0.03 mol, 3.60 g) in 20 mL of triethylamine and heated at 120 °C for 12 h. The reaction was followed by TLC to completion. The solvent was removed under high vacuum to obtain brown solid, which was washed with ethanol and purified on a column using ethyl acetate:methanol (1:1). The product was recrystallized from methanol:THF (1:1) and obtained as a white solid. Melting point = 213–215 °C, Yield = 78.0%. ¹H NMR (ppm): 8.04 (s, 1H, (2^I)), 7.98 (d, 1H, *J* = 8.0 Hz, (6^I)), 7.59 (dd, 2H, *J* = 4.0 Hz, (5, 6)), 7.43 (t, 1H, *J* = 8.0 Hz, (5^I)), 7.30 (d, 1H, *J* = 8 Hz, (4^I)), 7.19 (q, 2H, (4, 7)), 2.41 (s, 3H, (7^I)). ¹³C NMR (ppm): 151.5 (C=N, (2)), 138.1 (8, 9), 130.4 (3^I), 130.2 (1^I, 2^I), 128.8 (4^I, 5^I), 127.0 (6^I), 123.6 (5, 6), 121.9 (4, 7), 21.0 (CH₃, (7^I)). IR (ν_{\max} , cm⁻¹): 3052 (N–H), 2986 (C–H), 2879 (C–H), 1661 (C=N), 1590 (C=C), 1487 (C–N). Anal. Calcd for C₂₃H₂₄N₂O₃: C, 74.97; H, 6.71; N, 11.66. Found: C, 74.67; H, 6.42; N, 11.95. LRMS (*m/z*, M⁺): Found for C₁₄H₁₂N₂ = 208.20, Expected mass = 208.36.

2.9.3 2,2,4-Trimethyl-2,3-dihydro-1*H*-1,5-benzodiazepin-5-ium isophthalate (3) ²⁹⁶

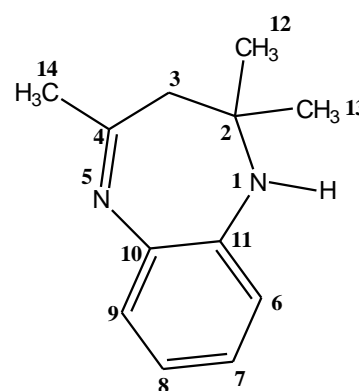
o-Phenylenediamine (0.01 mol, 1.08 g) and isophthalic acid (0.01 mol, 1.66 g) were subjected to microwave irradiation at 180 W (50 °C) for 15 min, after which 2 mL of an ethanol:acetone mixture (3:1) was added to dissolve the solidified



reaction mixture. The reaction mixture was allowed to stand for 12 h during which a solid product was formed. Finally, the solid was filtered and the product (84%) obtained as a yellow solid after recrystallization from ethanol. M.p. 168–172 °C (DSC melting range: 166.3–181.3 °C). ¹H NMR (ppm): 8.48 (s, 1H, (7^I)), 8.16 (d, 2H, *J* = 7.7 Hz, (3^I, 5^I)) 7.64 (t, 1H, *J* = 7.8 Hz, (4^I)), 6.84–6.95 (m, 2H, *J* = 7.6 (8, 9)), 6.79 (d, 2H, *J* = 7.5 Hz, (6, 7)), 3.50–4.50 (br, 2H, N–H), 2.51 (s, 3H, (14)), 2.16 (s, 2H, (3)), 1.23 (s, 6H, (12, 13)). ¹³C NMR (ppm): 171.0 (C=N(4)), 166.7 (C=O(1)), 139.5, (11), 139.1 (10), 133.5 (3^I, 5^I), 131.4 (2^I, 6^I), 130.1 (7^I), 129.3 (4^I), 126.9 (8), 125.3, (9), 121.2, (7), 120.1 (6), 66.5 (2), 45.2 (3), 30.0 (12, 13), 29.3 (8). IR (ν_{\max} , cm⁻¹): 1710 (C=O), 1607 (C=N), 1208 (C–N), 1552 (COO⁻), 3309 (N–H). Anal. calcd. for C₁₂H₂₂N₂O₄: C, 67.79; H, 6.21; N, 7.90. Found: C, 67.80; H, 6.24 N, 7.49. HRMS: *m/z* 189.1392 [*M*_A⁺ = 189], *m/z* 165.0195⁻ [*M*_B⁻ = 165].

2.9.4 2,2,4-Trimethyl-2,3-dihydro-1*H*-1,5-benzodiazepine (4) ²⁹⁴

o-Phenylenediamine (0.02 mol, 2.16 g) was heated under reflux with ethanol (10 mL) and acetone (5 mL) at 80 °C for 8 h. The solvent was removed under vacuum to give a light brown oily residue which was then redissolved in ethanol and placed in the refrigerator for 48 h. The product (62%) was obtained as a yellow solid after recrystallization from ethanol. M.p. 124–125 °C. ¹H NMR (ppm): 6.89–6.93 (m, 2H, (8, 9)), 6.79–6.87 (m, 2H, (6, 7)), 4.71 (s, N–H), 2.22 (s, 3H, (3)), 2.16 (s, 2H, (14)),

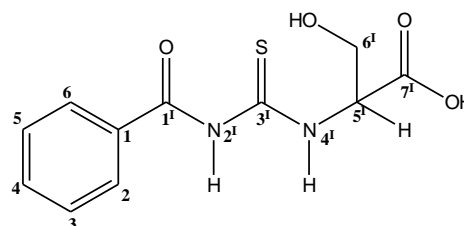


1.24 (s, 6H, (12, 13)). ¹³C NMR (ppm): 170.7 (C=N(4)), 139.3 (11), 139.1 (10), 126.8 (8), 125.0 (9), 121.0 (7) 119.9 (6), 66.5 (2), 45.2 (3), 30.0 (12, 13), 29.4 (14). IR: (ν_{\max} , cm⁻¹)

3294 (N–H), 2964 (C–H), 1633 (C=N), 1430 (C–N). Anal calcd. for C₁₂H₂₂N₂: C, 76.60; H, 8.51; N, 14.89. Found: C, 76.17; H, 8.47; N, 14.76. LRMS (*m/z*, M⁺): Found for C₁₁H₁₂N₂O₃S = 268.00, Expected mass = 268.29.

2.9.5 2-[(Benzoylcarbamothioyl)amino]-3-hydroxypropanoic acid (**5**)³¹⁵⁻³¹⁶

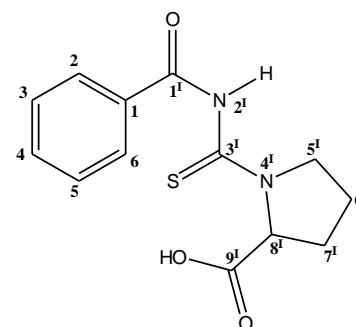
Ammonium thiocyanate (0.10 mol, 7.60 g) was dissolved in 100 mL of acetone. Benzoyl chloride (0.10 mol, 14.57 g) was added followed by heating under reflux at 100–120 °C for 2 h. The product was filtered and serine (0.10 mol) was added to the filtrate



and heated under reflux at 100–120 °C for 6 h. 20 mL of water was then added and the mixture was heated for a further 2 h. The reaction mixture was extracted with diethyl ether, and the solvent removed *via* rotary evaporation. The followed by drying the compound was dried under high vacuum and the product recrystallized as a colourless solid from acetone:water (4:1). Yield = 71.0%, Mp = 163–165 °C. ¹H NMR (ppm): 11.49 (s, 1H, O(**7**^I)-H), 11.43 (d, 1H, *J* = 8 Hz, N–H(**4**^I)), 7.96 (d, 2H, *J* = 8.0 Hz, (**1**, **6**)), 7.65 (t, 1H, *J* = 7.6 Hz, (**4**)), 7.53 (t, 2H, *J* = 7.6 Hz, (**3**, **5**)), 5.34 (br, 1H, N–H, (**2**^I)), 4.94 (t, 1H, *J* = 4.0 Hz, (**5**^I)), 3.88 (dd, 2H, *J* = 4.0 Hz, (**5**)). ¹³C NMR (ppm): 180.3 (C=S(**3**^I)), 170.7 (C=O(**1**^I)), 168.3 (C=O(**7**^I)), 128.4 (**3**, **5**), 128.5 (**2**, **6**), 132.1 (**4**), 133.0 (**1**), 60.5 (**6**^I), 60.3 (**5**^I). IR (*v*_{max}, cm⁻¹): 3229 (N–H), 2980 (C–H), 1725 (C=S), 1654 (C=O), 1509 (C=C), 1164 (C–N). Anal. calcd. for C₁₁H₁₂N₂O₄S.H₂O: C, 46.15; H, 4.93; S, 11.20; N, 9.78. Found: C, 46.92; H, 4.87; S, 10.67; N, 9.76. LRMS (*m/z*, M⁺): Found for C₁₁H₁₂N₂O₃S = 268.00, Expected mass = 268.29.

2.9.6 1-(Benzoylcarbamothioyl)pyrrolidine-2-carboxylic acid (**6**)³¹⁵⁻³¹⁶

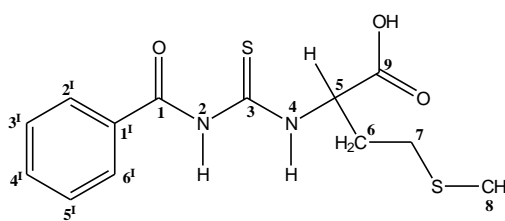
Compound **6** was synthesized in a similar manner as compound **5**. The product recrystallized as a white solid from acetone:water (4:1). Yield = 75.0%, M.p = 114–117 °C. ¹H NMR (ppm): 10.90 (s, 1H, O(**9**^I)-H), 7.94 (d, 1H, *J* = 7.6 Hz, (**2**)), 7.85 (d, 1H, *J* = 7.6 Hz, (**6**)), 7.58 (dd, 1H, *J* = 7.2, 7.6 Hz (**4**)), 7.50 (m, 2H, (**3**, **5**)), 4.68 (t, 1H, *J* = 9.6 Hz, (**8**^I)), 3.68 (m, 2H, (**5**^I)), 2.02 (m,



2H, (**6^I**), 1.99 (dd, 2H, $J = 8.8, 6.4$ Hz, (**7^I**)). ^{13}C NMR (ppm): 179.1 (C=S(**3^I**)), 171.9 (**9^{II}**), 171.2 (**9^I**), 164.0 (**1^I**), 132.9 (**1**), 132.2 (**4**), 128.4 (**2**, **6**), 128.2 (**3**, **5**), 65.4 (**8^I**), 62.7 (**5^I**), 61.7 (**5^{II}**), 31.0 (**6^I**), 29.4 (**6^{II}**), 24.19 (**7^I**), 22.94 (**7^{II}**). IR (ν_{max} , cm^{-1}): 3270 (N–H), 2987 (C–H), 1730 (C=S), 1659 (C=O), 1491 (C–N). Anal.calcd. for $\text{C}_{13}\text{H}_{14}\text{N}_2\text{O}_3\text{S}\cdot\text{H}_2\text{O}$: C, 52.69; H, 5.44; S, 10.83; N, 9.45. Found: C, 52.55; H, 5.64; S, 9.80; N, 9.11. LRMS (m/z , M^+): Found for $\text{C}_{13}\text{H}_{14}\text{N}_2\text{O}_3\text{S} = 278.40$, Expected mass = 278.33.

2.9.7 2-[(Benzoylcarbamothioyl)amino]-4-(methylsulfanyl)butanoic acid (**7**)³¹⁵⁻³¹⁶

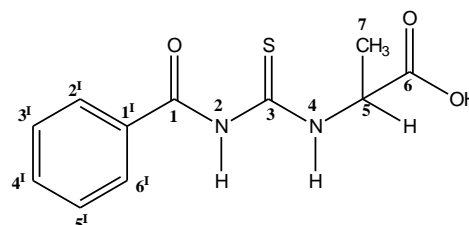
Compound **7** was synthesized in a similar manner as compound **5**. The product recrystallized as a white solid from acetone:water (4:1). Yield = 77%, Mp = 123–125 °C. ^1H NMR (ppm): 11.54 (s, 1H, O(**9**)–H), 11.28 (d, 1H, $J = 7.6$ Hz, N(**2**)–H), 7.96



(d, 2H, $J = 7.6$ Hz, (**2^I**, **6^I**)), 7.65 (t, 1H, $J = 7.6$ Hz, (**4^I**)), 7.52 (t, 2H, $J = 7.6$ Hz, (**3^I**, **5^I**)), 5.03 (q, 1H, $J = 6.8$ Hz, (**5**)), 2.26 (m, 2H, (**6**)), 2.17 (m, 2H, (**7**)), 2.09 (s, 3H, (**8**)). ^{13}C NMR (ppm): 180.5 (C=S(**3**)), 171.8 (9), 168.4 (**1**), 133.1 (**1^I**), 132.1 (**4^I**), 128.6 (**2^I**, **6^I**), 128.2 (**3^I**, **5^I**), 66.6 (**5**), 30.5 (**8**), 29.2 (**6**), 14.6 (**7**). IR (ν_{max} , cm^{-1}): 3282 (N–H), 3202 (N–H), 2914 (C–H), 1715 (C=S), 1664 (C=O), 1519 (C=C), 1193 (C–N). Anal.calcd. for $\text{C}_{13}\text{H}_{16}\text{N}_2\text{O}_3\text{S}_2$: C, 49.98; H, 5.16; S, 20.53; N, 8.97. Found: C, 50.40; H, 5.52; S, 20.03; N, 8.97. LRMS (m/z , M^+): Found for $\text{C}_{13}\text{H}_{16}\text{N}_2\text{O}_3\text{S}_2 = 312.90$, Expected mass = 312.41.

2.9.8 2-[(Benzoylcarbamothioyl)amino]propanoic acid (**8**)³¹⁵⁻³¹⁶

Compound **8** was synthesized in a similar manner as compound **5**. The product recrystallized as a yellow solid from acetone:water (4:1). Yield = 65%, Mp = 161–163 °C ^1H NMR (ppm): 11.51 (s, 1H, O(**2**)–H), 11.30 (d, 1H, $J = 6.8$ Hz, N(**4**)–H), 7.93 (d, 2H, $J =$

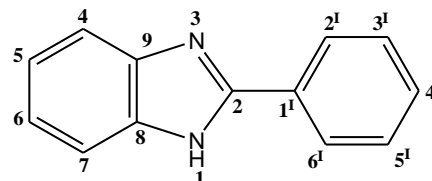


7.6 Hz, (**2^I**, **6^I**), 7.64 (t, 1H, $J = 7.6$ Hz, (**4^I**)), 7.52 (t, 2H, $J = 7.6$ Hz, (**3^I**, **5^I**)), 4.85 (q, 1H, $J = 7.2$ Hz, (**5**)), 1.49 (d, 3H, $J = 7.2$ Hz (**7**)). ^{13}C NMR (ppm): 179.9 (C=S(**3**)), 172.9 (**6**), 168.5 (**1**), 133.0 (**1^I**), 132.1 (**4^I**), 128.7 (**2^I**, **6^I**), 128.4 (**3^I**, **5^I**), 63.1 (**5**), 17.2 (**7**). IR (ν_{max} , cm^{-1}):

3384 (N–H), 2992 (C–H), 1726 (C=S), 1678 (C=O), 1489 (C=C), 1196 (C–N). Anal. calcd. for $C_{11}H_{12}N_2O_3S$: C, 52.37; H 4.79; S 12.71; N 11.10. Found: C, 52.59; H 5.11; S 12.56; N 11.07. LRMS (m/z , M^+): Found for $C_{11}H_{12}N_2O_3S$ = 252.00, Expected mass = 252.29.

2.9.9 2-Phenyl-1*H*-benzimidazole (9)²⁹¹

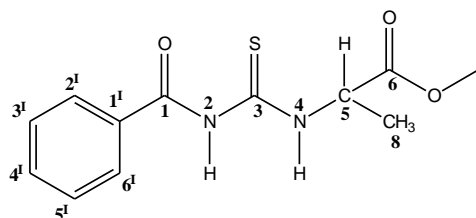
Polyphosphoric acid (15 g), in 5 mL of toluene, was heated at 120 °C for 30 minutes. Compounds **5**, **6**, **7** or **8** (0.20 mol) was each added to *o*-phenylenediamine (0.2 mol) and the mixture was heated at 165 °C for 6 h. After cooling, 20



mL of water was added with stirring and then sodium hydrogen carbonate was added until effervescence ceased. The dark brown precipitate obtained was re-dissolved in little methanol and placed on the silica gel column and eluted with methanol:ethyl acetate (1:1). The product was recrystallized from ethanol:toluene (1:1) and obtained as a brown solid. Yield = 55–68%, Mp = 240–242 °C. ¹H NMR (ppm): 8.20 (d, 2H, J = 7.2 Hz (**4**, **7**)), 7.61 (m, 2H, J = 2.8, 3.2 Hz, (**5**, **6**)), 7.56 (t, 2H, J = 7.6 Hz, (**2**¹, **6**¹)), 7.50 (t, 1H, J = 7.6, 6.8 Hz, (**4**¹)), 7.21 (m, 2H, J = 7.6 Hz, (**3**¹, **5**¹)), ¹³C NMR (ppm): 151.2 (C=N) (**2**), 130.0 (**1**¹), 129.9 (**8**, **9**), 128.9 (**3**¹, **4**¹, **5**¹), 126.4 (**2**¹, **6**¹), 122.1 (**4**, **7**). IR (ν_{max} , cm^{-1}): 3048 (N–H), 2961 (C–H), 2850 (C–H), 1539 (C=N), 1461 (C=C), 1443 (C–N). Anal. Calcd for $C_{13}H_{10}N_2$: C, 80.39; H, 5.19; N, 14.42. Found: C, 80.29; H, 5.32; N, 14.64. Found for $C_{13}H_{10}N_2$ = 194.10, Expected mass = 194.23.

2.9.10 Methyl-2-[[**(phenylformamido) methanethioly**amino}propanoate (**10**)³¹⁷

Ammonium thiocyanate (0.03 mol, 2.28 g) was dissolved in 60 mL of acetone. Benzoyl chloride (0.03 mol, 4.22 g) was added followed by heating under reflux at 100–120 °C for 2 h. The product was filtered and alanine methyl ester hydrochloride was

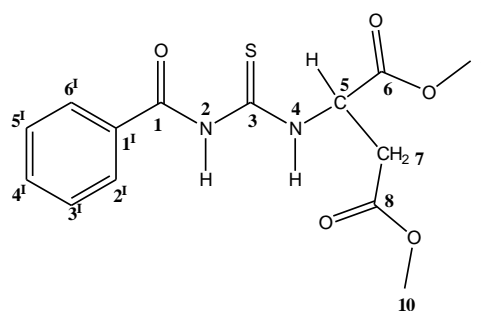


added (0.03, 4.19 g) and refluxed at 100–120 °C for 6 h. The solvent was removed and the residue redissolved in THF:ethyl acetate(1:1). The product was recrystallized from methanol:THF (1:1) and obtained as a white solid. Melting point = 213–215 °C, Yield = 76.0%. The ¹H NMR (ppm) :11.43 (t, 1H, J = 8.0, 7.2 Hz, N(**4**)–H), 7.93 (d, 2H, J = 7.6 Hz

(**2^I**, **6^I**), 7.65 (t, 1H, $J = 7.2, 6.8$ Hz, (**4^I**)), 7.52 (t, 2H, $J = 7.6, 7.2$ Hz, (**3^I**, **5^I**), 4.91 (d, 1H (**5**)), 2.5 (s, 3H (**7**)), ¹³C NMR (ppm): 180.3 (C=S), 170.8 (**4**), 168.3 (**1**), 133.1 (**1^I**), 132.1 (**2^I**, **6^I**) 128.7 (**3^I**, **4^I**, **5^I**), 60.5 (**8**), 59.9 (**5**). IR (ν_{\max} , cm^{-1}): 3229 (N–H), 2929 (C–H), 1724 (C=S), 1652 (C=O), 1540 (C=C), 1445 (C–N). Anal. Calcd for $\text{C}_{12}\text{H}_{14}\text{N}_2\text{O}_3\text{S}$: C, 54.12; H, 5.30; N, 10.52; S, 12.04; Found: C, 54.27; H, 5.42; N, 10.48, S, 12.10. LRMS (m/z , M^+): Found for $\text{C}_{14}\text{H}_{12}\text{N}_2 = 266.07$, Expected mass = 266.32.

2.9.11 1,4-Dimethyl -2-[(phenylformamido)methanethioly]butanedioate (**11**)³¹⁶

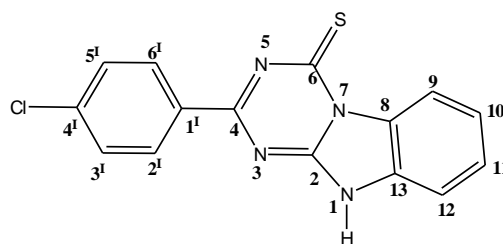
Ammonium thiocyanate (0.03 mol, 2.28 g) was dissolved in 60 mL of acetone. Benzoyl chloride (0.03 mol, 4.22 g) was added and heated under reflux at 100–120 °C for 2 h. The product was filtered and aspartic acid dimethyl ester hydrochloride (0.03 mol, 5.93 g) added and refluxed at 100–120 °C for 6 h. The product was recrystallized from methanol:THF



(1:1) and obtained as a white solid. Melting point = 213–215 °C, Yield = 81.0%. The ¹H NMR (ppm): 11.56 (s, 1H, N(**1**)–H, 11.50 (d, 1H, $J = 7.6$ Hz, N(**2**)–H)), 7.92 (d, 2H, $J = 7.6$ Hz, (**2^I**, **6^I**)), 7.65 (t, 1H, $J = 7.6$ Hz, (**4^I**)), 7.52 (t, 2H, $J = 7.60$ Hz, (**3^I**, **5^I**), 5.41 (d, 1H, $J = 6$ Hz, (**5**)), 3.70 (s, 3H, (**9**)) 3.09 (d, 2H, $J = 4.4$ Hz, (**6**)). ¹³C NMR (ppm): 180.4 (C=S), 170.7 (**4**), 170.1 (**8**), 168.4 (**1**), 133.0 (**1^I**), 131.9 (**3^I**, **4^I**, **5^I**), 128.4 (**2^I**, **6^I**), 53.8 (**5**), 52.7 (**7**), 51.8 (**9**), 34.8 (**10**). IR (ν_{\max} , cm^{-1}): 3326 (N–H), 3230 (N–H), 2999 (C–H), 2947 (C–H), 1745 (C=S), 1722 (C=O), 1666 (C=O), 1578 (C=C), 1437 (C–N). Anal. Calcd for $\text{C}_{14}\text{H}_{16}\text{N}_2\text{O}_5\text{S}$: C, 51.84; H, 4.97; N, 8.64; S, 9.89. Found: C, 51.73; H, 4.82; N, 8.53; S, 9.92. LRMS (m/z , M^+): Found for $\text{C}_{14}\text{H}_{12}\text{N}_2 = 324.35$, Expected mass = 324.14.

2.9.12 11-(4-Chlorophenyl)-1,8,10,12-tetraazatricyclo[7.4.0.0^{2,7}]trideca-2(7),3,5,9,11-pentaene-13-thione (**12**) (New)

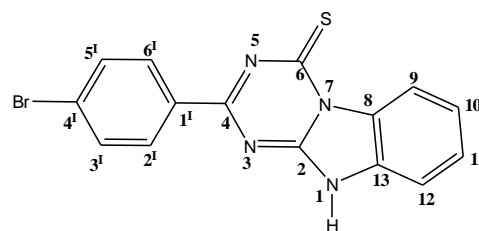
Ammonium thiocyanate (0.04 mol, 3.05 g) was dissolved in 80 mL of acetone. 4-Chlorobenzoyl chloride (0.04 mol, 7.00 g) was added followed by heating under reflux at 100–120 °C for 2 h. The 4-chlorobenzoyl isothiocyanate (0.04 mol)



obtained was filtered and 2-aminobenzimidazole (0.04 mol, 5.33 g) added to the filtrate and refluxed at 100–120 °C for 6 h. The mother liquor was allowed to stand in the fumehood overnight. The product obtained was filtered and recrystallized from DMSO:Toluene (1:1) as a light yellow solid. Melting point = 322–324 °C. Yield = 76.3%. ¹H NMR (ppm): 9.48 (d, 1H, N–H), 8.45 (d, 1H, *J* = 8.4 Hz (**9**)), 8.16 (d, 1H, *J* = 8.4 Hz, (**12**)), 7.95 (d, 1H, *J* = 8.4 Hz, (**11**)), 7.66 (d, 1H, *J* = 8 Hz, (**10**)), 7.56 (m, 2H, (**2'**, **6'**)), 7.46 (m, 1H, (**5'**)), 7.18 (m, 1H, (**3'**)). ¹³C NMR (ppm): 166.5 (C=S), 137.7 (**4'**), 136.6 (**1'**), 131.2 (**8**, **13**), 130.4 (**4**), 128.7 (**3'**, **5'**), 121.7 (**9**, **12**), 117.4 (**10**, **11**), 113.1 (**2'**, **6'**). IR (ν_{\max} , cm⁻¹): 3387 (N–H), 3051 (N–H), 2967 (C–H), 1622 (C=N), 1589 (C=C), 1453 (C–N), 1431(C–N). Anal. Calcd for C₁₅H₉ClN₄S: C, 57.60; H, 2.90; N, 17.91; S, 10.10. Found: C, 57.49; H, 2.95; N, 17.86; S, 10.25. LRMS (*m/z*, M⁺): Found for C₁₅H₉ClN₄S = 312.90, Expected mass = 312.78.

2.9.13 11-(4-Bromophenyl)-,8,10,2-tetraazatricyclo[7.4.0.0^{2,7}]trideca-2(7),3,5,9,11-pentaene-13-thione (**13**) (New)

Ammonium thiocyanate (0.04 mol, 3.05 g) was dissolved in 80 mL of acetone. 4-Bromobenzoyl chloride (0.04 mol, 8.78 g) was added followed by heating under reflux at 100–120 °C for 2 h. The 4-bromobenzoyl chloride (0.04 mol) obtained was

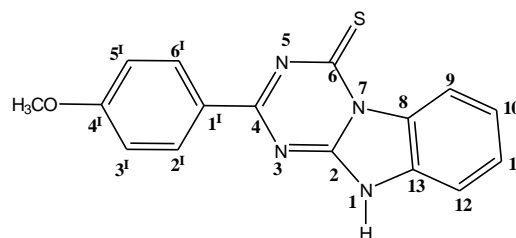


filtered, 2-aminobenzimidazole (0.04 mol, 5.33 g) added to the filtrate and refluxed at 100–120 °C for 6 h. The mother liquor was allowed to stand in the fumehood overnight. The product obtained was filtered and recrystallized from DMSO:Toluene (1:1) as a light yellow solid. Melting point = 242–243 °C. Yield = 72.7%. ¹H NMR (ppm): 9.49 (d, 1H, *J* = 8.4 Hz, N–H), 8.34 (d, 1H, *J* = 7.6 Hz, (**9**)), 8.09 (d, 1H, *J* = 7.6 Hz, (**11**)), 7.85 (d, 1H, *J* = 7.6 Hz,

(**2^I**), 7.78 (d, 1H, $J = 7.2$ Hz, (**25**)), 7.72 (m, 2H, (**3^I**,**12**)), 7.45 (m, 1H, (**5^I**)), 7.16 (m, 1H, (**6^I**)). ¹³C NMR (ppm): 166.7 (C=S), 131.6 (**1^I**, **4^I**), 131.2 (**8**, **13**), 130.4 (**4**), 128.7 (**3^I**, **5^I**), 121.9 (**9**, **12**), 117.2 (**10**, **11**), 112.7 (**2^I**, **6^I**). IR (ν_{\max} , cm^{-1}): 3372 (N–H), 1669(C=S), 1585 (C=C), 1544 (C=C), 1464 (C=N). Anal. Calcd for $\text{C}_{15}\text{H}_9\text{BrN}_4\text{S}$: C, 50.43; H, 2.54; N, 15.68; S, 8.98. Found: C, 50.21; H, 2.67; N, 15.51; S, 9.12. LRMS (m/z , M^+): Found for $\text{C}_{15}\text{H}_9\text{BrN}_4\text{S} = 357.80$, Expected mass = 357.97.

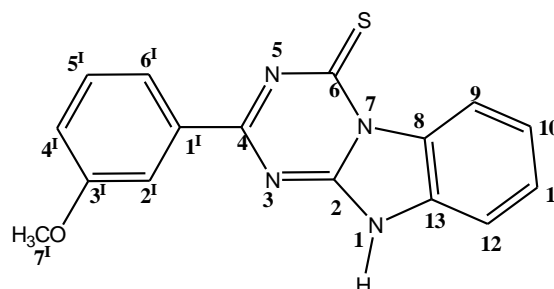
2.9.14 11-(4-Methoxyphenyl)-1,8,0,12-tetraazatricyclo[7.4.0.0^{2,7}]trideca-2(7),3,9,1-pentaene-13-thione (**14**) (New)

Ammonium thiocyanate (0.04 mol, 3.05 g) was dissolved in 80 mL of acetone. 4-Methoxybenzoyl chloride (0.04 mol, 6.82 g) was added followed by heating under reflux at 100–120 °C for 2 h. The 4-methoxybenzoyl isothiocyanate (0.04 mol) obtained was filtered, 2-aminobenzimidazole (0.04 mol, 5.33 g) added to the filtrate and refluxed at 100–120 °C for 6 h. The mother liquor was allowed to stand in the fumehood overnight, the product obtained was filtered and recrystallized from DMSO:Toluene (1:1) as a yellow solid. Melting point = 207–208 °C. Yield = 77.1%. ¹H NMR (ppm): 9.47 (d, 1H, $J = 8.0$ Hz (**12**)), 8.40 (d, 2H, $J = 8.4$ Hz, (**5^I**, **6^I**)), 7.64 (m, 2H, (**9**, **10**)), 7.48 (t, 1H, $J = 7.6$ Hz, (**11**)), 7.13 (d, 2H, $J = 8.4$ Hz, (**2^I**, **3^I**)), 3.98 (s, 3H, (**7^I**)). ¹³C NMR (ppm): 162.6 (C=S), 130.9 (**4**), 127.4 (**3^I**, **5^I**), 122.6 (**9**, **12**), 117.1 (**10**, **11**), 113.8 (**2^I**, **6^I**), 55.6 (**7^I**), IR (ν_{\max} , cm^{-1}): 3387 (N–H), 3009 (N–H), 2987 (C–H), 1691 (C=S), 1593 (C=C), 1434 (C=N). Anal. Calcd for $\text{C}_{16}\text{H}_{12}\text{N}_4\text{OS}$: C, 62.32; H, 3.92; N, 18.17; S, 10.40. Found: C, 62.51; H, 4.04; N, 18.30; S, 10.34. LRMS (m/z , M^+): Found for $\text{C}_{16}\text{H}_{12}\text{N}_4\text{OS} = 308.20$, Expected mass = 308.36.



2.9.15 11-(3-Methoxyphenyl)-1,8,0,12-tetraazatricyclo[7.4.0.0^{2,7}]trideca-2(7),3,5,9,11-pentaene-13-thione (**15**) (New)

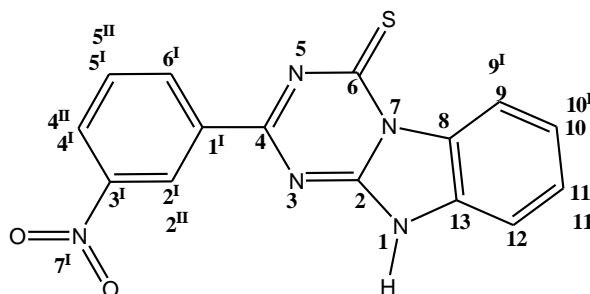
Ammonium thiocyanate (0.04 mol, 3.05 g) was dissolved in 80 mL of acetone. 3-



Methoxybenzoyl chloride (0.04 mol, 6.82 g) was added followed by heating under reflux at 100–120 °C for 2 h. The 4-methoxybenzoyl isothiocyanate (0.04 mol) obtained was filtered, 2-aminobenzimidazole (0.04 mol, 5.33 g) added to the filtrate and refluxed at 100–120 °C for 6 h. The mother liquor was allowed to stand in the fumehood overnight, the product obtained was filtered and recrystallized from DMSO:Toluene (1:1) as a yellow solid. Melting point = 268–269 °C. Yield = 81.8 %. ¹H NMR (ppm): 9.47 (d, 1H, *J* = 8.0 Hz, (**12**)), 8.03 (d, 1H, *J* = 7.2 Hz, (**9**)), 7.95 (s, 1H, (**2^I**)), 7.65 (m, 2H, (**4^I**, **6^I**)), 7.49 (t, 2H, *J* = 7.2, 8.0 Hz, (**5^I**, **11**)), 7.19 (d, 1H, *J* = 8.0 Hz (**10**)), 3.87 (s, 3H, (**7^I**)). ¹³C NMR (ppm): 159.5 (**4**), 150.8, 129.8, 127.6, 122.4, 121.4, 118.6, 117.4, 113.4, 55.3 (**7^I**), IR (ν_{\max} , cm^{-1}): 3196 (N–H), 3068 (N–H), 2941 (C–H), 2835 (C–H), 1628 (C=O), 1560 (C=C), 1494 (C–N), 1451 (C–N). Anal. Calcd for C₁₆H₁₂N₄OS: C, 62.32; H, 3.92; N, 18.17; S, 10.40. Found: C, 62.22; H, 3.76; N, 18.08; S, 10.56. LRMS (*m/z*, M⁺): Found for C₁₆H₁₂N₄OS = 308.10, Expected mass = 308.36.

2.9.16 11-(3-Nitrophenyl)-1,8,10,12-tetraazatricyclo[7.4.0.0^{2,7}]trideca-2(7),3,5,9,11-pentaene-13-thione (**16**) (New)

Ammonium thiocyanate (0.04 mol, 3.05 g) was dissolved in 80 mL of acetone. 3-Nitrobenzoyl chloride (0.04 mol, 7.42 g) was heated under reflux at 100–120 °C for 2 h. The 3-nitrobenzoyl isothiocyanate (0.04 mol) obtained filtered was filtered, 2-

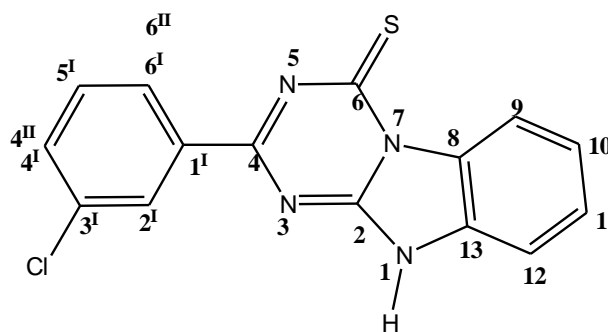


aminobenzimidazole (0.04 mol, 5.33 g) added to the filtrate and refluxed at 100–120 °C for 6 h. The mother liquor was allowed to stand in the fumehood overnight, the product obtained was filtered and recrystallized from DMSO:Toluene (1:1) as a light yellow solid. Melting point = 332–333 °C. Yield = 73.41%. ¹H NMR (ppm): 9.48 (d, 1H, *J* = 8.0 Hz, (**23**)), 9.22 (s, 1H, (**2^I**)), 8.97 (s, 1H, (**2^{II}**)), 8.85 (d, 1H, *J* = 7.6 Hz, (**5^I**)), 8.54 (d, 1H, *J* = 7.6 Hz, (**6^I**)), 8.40 (t, 2H, *J* = 7.2, 9.2 Hz, (**4^I**, **11**)), 7.64 (m, 2H, *J* = 8.0 Hz, (**9**, **10**)), 7.54 (m, 1H, *J* = 7.6 Hz, (**11^I**)), 7.47 (m, 2H, (**6^{II}**, **12^I**)), 7.31 (m, 2H, (**4^{II}**, **9^I**)), 7.21 (m, 2H, (**5^{II}**, **10^I**)). ¹³C NMR (ppm): 158.0 (**4**), 152.5 (**3^I**), 150.6 (**3**), 148.1 (**1**), 138.8 (**13**), 134.4 (**1^I**), other aromatic resonances (130.5, 128.5, 125.5, 120.1, 117.2, 115.8). IR (ν_{\max} , cm^{-1}): 3334 (N–H), 3096 (N–H), 1684 (C=O), 1524 (C=C), 1470 (C–N), 1422 (C–N). Anal. Calcd for C₁₅H₉N₅O₂S: C,

55.72; H, 2.81; N, 21.10; S, 9.92. Found: C, 55.59; H, 2.73; N, 21.22; S, 9.86. LRMS (m/z , M^+): Found for $C_{15}H_9N_5O_2S = 323.30$, Expected mass = 323.33.

2.9.17 11-(3-Chlorophenyl)-1,8,10,12-tetraazatricyclo[7.4.0.0^{2,7}]trideca-2(7),3,5,9,11-pentaene-13-thione (17) (New)

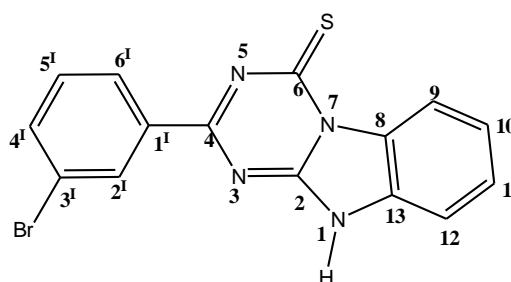
Ammonium thiocyanate (0.04 mol, 3.05 g) was dissolved in 80 mL of acetone. 3-Chlorobenzoyl chloride (0.04 mol, 7.00 g) was added followed by heating under reflux at 100–120 °C for 2 h. The 3-chlorobenzoyl isothiocyanate (0.04 mol) obtained was



filtered, 2-aminobenzimidazole (0.04 mol, 5.33 g) added to the filtrate and refluxed at 100–120 °C for 6 h. The mother liquor was allowed to stand in the fumehood overnight, the product obtained was filtered and recrystallized from DMSO:Toluene (1:1) as a light yellow solid. Melting point= 324–325 °C. Yield = 74.4%. ¹H NMR (ppm): 12.72 (br, 1H, (N–H)), 8.17 (s, 1H, (**2^I**)), 8.09 (d, 1H, $J = 7.6$ Hz, (**4^I**)), 7.90 (m, 2H, (**4^{II}**, **6^{II}**)), 7.71 (d, 1H, $J = 8.0$ Hz, (**6^I**)), 7.62 (d, 1H, $J = 8.0$ Hz, (**12**)), 7.53 (t, 2H, $J = 7.6$ Hz, (**5^I**, **9**)), 7.45 (m, 2H, (**10**, **10^I**)), 7.18 (m, 2H, (**11**, **11^I**)). ¹³C NMR (ppm): 168.03 (**6**) 150.61 (**4**). Aromatic carbon resonances (138.10, 132.87, 132.67, 131.22, 130.17, 128.78, 126.94, 122.02, 112.54). IR (ν_{max} , cm^{-1}): 3102 (N–H), 2974 (C–H), 2898 (C–H), 1625, 1480, 1353, 1302, 1282, 1272, 1233, 1172, 1155, 1103, 1068, 1035, 1008, 947. Anal. Calcd for $C_{15}H_9ClN_4S$: C, 57.60; H, 2.90; N, 17.91; S, 10.25. Found: C, 57.52; H, 2.95; N, 17.82; S, 10.36. LRMS (m/z , M^+): Found for $C_{15}H_9ClN_4S = 312.57$, Expected mass = 312.78.

2.9.18 11-(3-Bromophenyl)-1,8,10,12-tetraazatricyclo[7.4.0.0^{2,7}]trideca-2(7),3,5,9,11-pentaene-13-thione (18) (New)

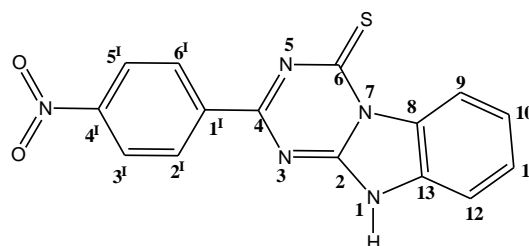
Ammonium thiocyanate (0.04 mol, 3.05 g) was dissolved in 80 mL of acetone. 3-Bromobenzoyl chloride (0.04 mol, 8.78 g) was added followed by heating under reflux at 100–120 °C for 2 h. The 3-



chlorobenzoyl isothiocyanate (0.04 mol) obtained was filtered, 2-aminobenzimidazole (0.04 mol, 5.33 g) added to the filtrate and refluxed at 100–120 °C for 6 h. The mother liquor was allowed to stand in the fumehood overnight, the product obtained was filtered and recrystallized from DMSO:Toluene (1:1) as a light yellow solid. Melting point= 258–260 °C. Yield = 75.6%. ¹H NMR (ppm): 12.48 (br, 1H, (N–H)), 8.32 (s, 1H, (**2^I**)), 8.12 (d, 1H, *J* = 8.4 Hz, (**6^I**)), 7.72 (d, 1H, *J* = 8.0 Hz, (**4^I**)), 7.46 (m, 3H, (**5^I**, **9**, **12**)), 7.16 (m, 2H, (**10**, **11**)) ¹³C NMR (ppm): Aromatic carbon resonances (134.0, 131.1, 130.5, 127.5, 122.1, 121.5, 112.5). R (*v*_{max}, cm⁻¹): 3306 (N–H), 1622 (C=O), 1600 (C=C), 1550 (C=C), 1501 (C=C), 1473 (C–N). Anal. Calcd for C₁₅H₉BrN₄S: C, 50.43; H, 2.54; N, 15.68; S, 8.98. Found: C, 50.32; H, 2.49; N, 15.52; S, 9.06. LRMS (*m/z*, M⁺): Found for C₁₅H₉BrN₄S = 357.12, Expected mass = 357.23.

2.9.19 11-(4-Nitrophenyl)-1,8,10,12-tetraazatricyclic[7.4.0.0^{2,7}]trideca-2(7),3,5,9,11-pentaene-13-thione (**19**) (New)

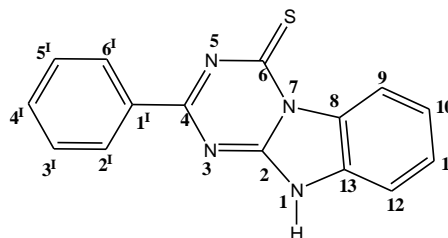
Ammonium thiocyanate (0.04 mol, 3.05 g) was dissolved in 80 mL of acetone. 4-Nitrobenzoyl chloride (0.04 mol, 7.42 g) was added followed by heating under reflux at 100–120 °C for 2 h. The 4-nitrobenzoyl isothiocyanate (0.04 mol)



obtained was filtered, 2-aminobenzimidazole (0.04 mol, 5.33 g) added to the filtrate and refluxed at 100–120 °C for 6 h. The mother liquor was allowed to stand in the fumehood overnight. The product obtained was filtered and recrystallized from DMSO:Toluene (1:1) as a light yellow solid. Melting point= 286–288 °C. Yield = 79.3%. ¹H NMR (ppm): 12.88 (br, 1H, (N–H)), 9.50 (d, 1H, *J* = 8.4 Hz, (**9**)), 8.34 (m, 2H, (**10**, **11**)), 8.21 (d, 1H, *J* = (**12**)), 7.46 (m, 2H, (**2^I**, **3^I**)), 7.21 (m, 2H, (**5^I**, **6^I**)). ¹³C NMR (ppm): 165.6 (**2**), 150.1 (**4**), 149.2 (**3**), Aromatic carbon resonances (136.6, 130.9, 129.7, 123.5, 122.5, 112.1). IR (*v*_{max}, cm⁻¹): 3140 (N–H), 1682 (C=O), 1591 (C=C), 1537 (C=C), 1516 (C=C), 1466 (C–N). Anal. Calcd for C₁₅H₉N₅O₂S: C, 55.72; H, 2.81; N, 21.66; S, 9.92. Found: C, 55.61; H, 2.90; N, 21.52; S, 9.86. LRMS (*m/z*, M⁺): Found for C₁₅H₉N₅O₂S = 323.15, Expected mass = 323.33.

2.9.20 11-Phenyl-1,8,10,12-tetraazatricyclo[7.4.0.0^{2,7}]trideca-2(7),3,5,9,11-pentaene-13-thione (20) (New)

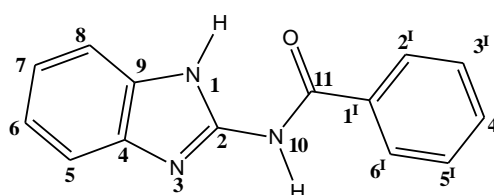
Ammonium thiocyanate (0.04 mol, 3.05 g) was dissolved in 80 mL of acetone, benzoyl chloride (0.04 mol, 4.65 mL) was added followed by heating under reflux at 100–120 °C for 2 h. The benzoyl isothiocyanate (0.04 mol) obtained was filtered, 2-



aminobenzimidazole (0.04 mol, 5.33 g) added to the filtrate and refluxed at 100–120 °C for 6 h. The solvent was removed at the pump, the product obtained was filtered and recrystallized from DMSO:Toluene (1:1) as a light yellow solid. Melting point = 185–187 °C. Yield = 74.3%. ¹H NMR (ppm): 9.49 (d, 1H, *J* = 8.4 Hz, (12)), 8.44 (d, 2H, *J* = 7.6 Hz, (2¹, 6¹)), 7.67 (m, 3H, (4¹, 9, 11)), 7.60 (m, 2H, (3¹, 5¹)), 7.50 (t, 1H, *J* = 8.0 Hz, (10)). ¹³C NMR (ppm): Aromatic carbon resonances (132.5, 128.9, 128.7, 127.6, 122.6, 117.4). IR (ν_{\max} , cm⁻¹): 3309 (N–H), 3069 (N–H), 1664 (C=O), 1573 (C=C), 1521 (C=C), 1459 (C–N), 1447 (C–N). Anal. Calcd for C₁₅H₁₀N₄S: C, 64.73; H, 3.62; N, 20.13; S, 11.52. Found: C, 64.81; H, 3.53; N, 20.20; S, 11.46. LRMS (*m/z*, M⁺): Found for C₁₅H₁₀N₄S = 278.21, Expected mass = 278.33.

2.9.21 *N*-(1*H*-Benzimidazol-2-yl)benzamide (21) (New)

N-(1*H*-Benzimidazol-2-yl)benzamide (21) was accessed by refluxing 11-phenyl-1,8,10,12-tetraazatricyclo[7.4.0.0^{2,7}]trideca-2(7),3,5,9,11-pentaene-13-thione (0.02 mol, 5.56 g) in 20 mL of

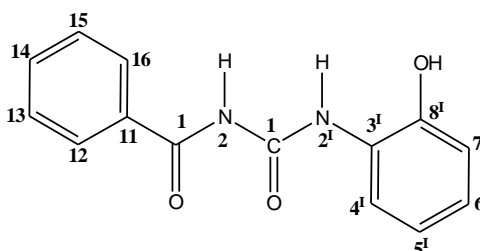


methanol:water and 5 mL of triethylamine. The solvent was removed and the residue redissolved in methanol. The product obtained was filtered and recrystallized from DMSO:Toluene (1:1) as a light yellow solid. Melting point = 228–229 °C. Yield = 76.6%. ¹H NMR (ppm): 8.17 (d, 2H, *J* = 7.2 Hz, (2¹, 6¹)), 7.59 (d, 1H, *J* = 7.2 Hz, (4¹)), 7.52 (d, 2H, *J* = 7.2 Hz, (5, 8)), 7.48 (m, 2H, (3¹, 5¹)), 7.14 (m, 2H, (6, 7)). ¹³C NMR (ppm): 168.4 (C=O), 149.1 (2), 134.5 (4, 9), 131.9 (1¹), 128.3 (2¹, 3¹, 5¹, 6¹), 121.7 (5, 6, 7, 8), 113.1 (4¹). IR (ν_{\max} , cm⁻¹): 3314 (N–H), 3062 (N–H), 1661 (C=O), 1629 (C=O), 1558 (C=C), 1519 (C=C), 1475 (C–N), 1455 (C–N). Anal. Calcd for C₁₄H₁₁N₃O: C, 70.87; H, 4.67; N, 17.71. Found: C,

70.62; H, 4.79; N, 17.82; S, 13.86. LRMS (m/z , M^+): Found for $C_{14}H_{11}N_3S$ = 237.06, Expected mass = 237.26.

2.9.22 3-benzoyl-1-(2-hydroxyphenyl) urea (22) (New)

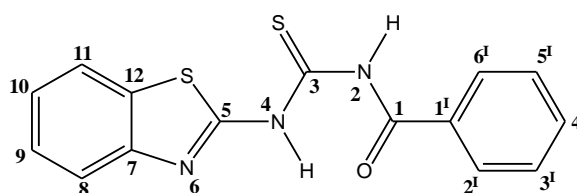
2-Aminobenzoxazole (0.04 mol, 5.37 g) was added to benzoyl isothiocyanate (0.04 mol, 7.91 g) and refluxed for 6 h. The solvent was removed and redissolved in ethanol. The product obtained was filtered and recrystallized from DMSO:Toluene



(1:1) as a white solid. Melting point = 202–204 °C Yield = 74.8%. 1H NMR (ppm): 11.22 (s, 1H, N–H, **2**), 11.13 (s, 1H, N–H, **2'**), 10.97 (s, 1H, 8–OH), 8.15 (d, 1H, J = 7.6 Hz, (**7'**)). 8.05 (d, 2H, J = 8.0 Hz, (**5**, **9**)), 7.94 (d, 1H, J = 8.0 Hz, (**4'**)), 7.64 (dd, 1H, J = 6.8, 7.2 Hz, (**7**)), 7.50 (m, 2H, (**6**, **8**)), 6.93 (d, 1H, J = 4.0 Hz, (**6'**)), 6.82 (m, 1H, (**5'**)). ^{13}C NMR (ppm): 182.2 (C=O, (**3**)), 168.7 (C=O, (**1**)), 167.9 (C=O, (**1'**)), 150.8 (**4**), 146.2 (**3'**), 132.6 (**7**), 128.4 (**6**, **8**), 126.24 (**5**, **9**), 123.6 (**6'**), 119.4 (**4'**), 119.1 (**5'**), 114.5 (**7'**). IR (ν_{max} , cm^{-1}): 3233 (N–H), 3155 (N–H), 1694 (C=O), 1655 (C=O), 1599 (C=O), 1559 (C=O), 1475 (C–N), 1456 (C–N). Anal. Calcd for $C_{14}H_{12}N_2O_3$: C, 65.62; H, 4.72; N, 10.93. Found: C, 65.55; H, 4.65; N, 11.01. LRMS (m/z , M^+): Found for $C_{14}H_{12}N_2O_3$ = 256.26, Expected mass = 256.16.

2.9.23 (3-(1,3-Benzothiazol-2-yl)-1-(benzoyl)thiourea (23) (New)

2-Aminobenzothiazole (0.04 mol, 6.00 g) was added to benzoyl isothiocyanate (0.04 mol, 6.53 g) and refluxed for 6 h. The mother liquor was allowed to stand overnight in a

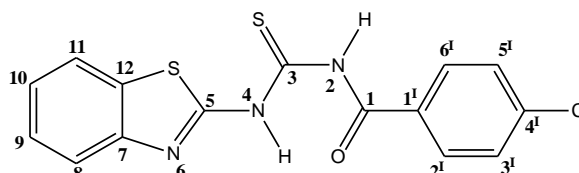


fume hood. The product obtained was filtered and recrystallized from DMSO:Toluene (1:1) as a yellow solid. Melting point = 161–163 °C. Yield = 75.0% 1H NMR (ppm): 8.14 (d, 2H, J = 7.6 Hz, (**2'**, **6'**)), 8.0 (d, 1H, J = 7.6 Hz, (**8**)), 7.8 (d, 1H, J = 8.0 Hz, (**11**)), 7.66 (t, 1H, J = 7.6 Hz, (**4'**)), 7.56 (t, 2H, (**3'**, **5'**)), 7.47 (m, 1H, (**10**)), 7.34 (m, 1H, (**9**)). ^{13}C NMR (ppm): 169.0 (C=S), 166.0 (C=O), 159.1 (**5**), 133.0 (**1'**), 128.9 (**4'**), 128.6 (**2'**, **6'**), 128.3 (**3'**, **5'**), 127.3 (**8**), 126.1 (**11**), 123.7 (**9**), 121.8 (**10**), 120.3 (**12**). IR (ν_{max} , cm^{-1}): 3327 (N–H), 3055

(N–H), 1673 (C=O), 1595 (C=C), 1436 (C–N). Anal. Calcd for $C_{15}H_{11}N_3OS_2$: C, 57.49; H, 3.54; N, 13.41; S, 20.46. Found: C, 57.38; H, 3.457; N, 13.55; S, 20.33. LRMS (m/z , M^+): Found for $C_{15}H_{11}N_3OS_2$ = 313.25, Expected mass = 313.40.

2.9.24 3-(1,3-Benzothiazol-2-yl)-1-(4-chlorobenzoyl)thiourea (24) (New)

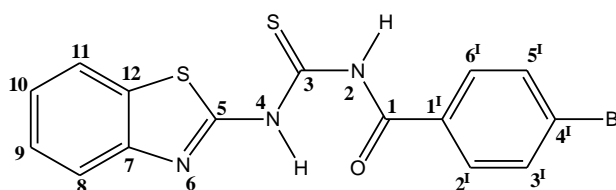
2-Aminobenzothiazole (0.04 mol, 5.33 g) was added to of 4-chlorobenzoyl isothiocyanate (0.04 mol, 7.91 g) and refluxed for 6 h. The mother liquor was allowed to



stand overnight in a fume hood. The product obtained was filtered and recrystallized from DMSO:Toluene (1:1) as a yellow solid. Melting point = 206–207 °C. Yield = 85.9%. 1H NMR (ppm): 14.17 (br, 1H, N–H), 12.31 (br, 1H, N–H), 8.03 (m, 3H, (**3^I**, **6^I**, **11**)), 7.81 (m, 1H, (**8**)), 7.62 (m, 2H, (**2^I**, **6^I**)), 7.51 (m, 1H, (**9**)), 7.39 (m, 1H, (**10**)). ^{13}C NMR (ppm): 131.7 (**3^I**, **6^I**), 131.0 (**2^I**, **5^I**), 126.60 (**9**, **10**), 124.5 (**8**, **11**). IR (ν_{max} , cm^{-1}): 3379 (N–H), 3229 (N–H), 1676 (C=O), 1595 (C=C), 1538 (C=C), 1486 (C–N), 1475 (C–N). Anal. Calcd for $C_{15}H_{10}ClN_3OS_2$: C, 51.79; H, 2.90; Cl, 10.19; N, 12.08, S, 18.44. Found: C, 51.65; H, 3.01; Cl, 10.25, N, 12.16; S, 18.52. LRMS (m/z , M^+): Found for $C_{15}H_{10}ClN_3OS_2$ = 347.95, Expected mass = 347.84.

2.9.25 3-(1,3-Benzothiazol-2-yl)-1-(4-bromobenzoyl)thiourea (25) (New)

2-Aminobenzothiazole (0.04 mol, 6.00 g) was added to a 4-bromo benzoyl isothiocyanate (0.04 mol, 9.68 g) and refluxed for 6 h. The mother liquor was

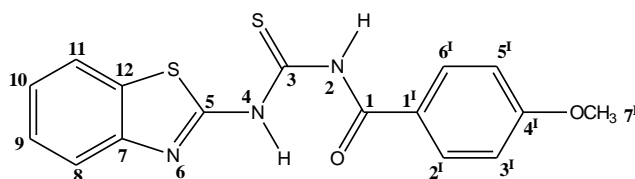


allowed to stand overnight in a fume hood. The product obtained was filtered and recrystallized from DMSO:Toluene (1:1) as a yellow solid. Melting point = 230–232 °C. Yield = 75.0%. 1H NMR (ppm): 14.17 (br, 1H, N–H), 12.31 (br, 1H, N–H), 8.06 (d, 1H, J = 8.0 Hz, (**8**)), 7.93 (d, 2H, J = 8.0 Hz, (**3^I**, **5^I**)), 7.78 (m, 3H, J = 8.0 Hz, (**2^I**, **6^I**, **23**)), 7.50 (t, 1H, J = 8.0 Hz, (**10**)), 7.39 (t, 1H, J = 7.6 Hz, (**9**)). ^{13}C NMR (ppm): 131.5 (**3^I**, **5^I**), 130.9 (**2^I**, **6^I**), 126.6 (**1^I**), 124.5 (**4^I**), 122.0 (**12**). IR (ν_{max} , cm^{-1}): 3060 (N–H), 3018 (N–H), 1676 (C=O),

1561 (C=C), 1499 (C–N), 1475 (C–N). Anal. Calcd for $C_{15}H_{10}BrN_3OS_2$: C, 45.92; H, 2.57; N, 10.71; S, 16.35. Found: C, 46.03; H, 2.65; N, 10.68; S, 16.42. LRMS (m/z , M^+): Found for $C_{15}H_{10}BrN_3OS_2$ = 392.10, Expected mass = 392.29.

2.9.26 3-(1,3-Benzothiazol-2-yl)-1-(4-methoxybenzoyl)thiourea (26) (New)

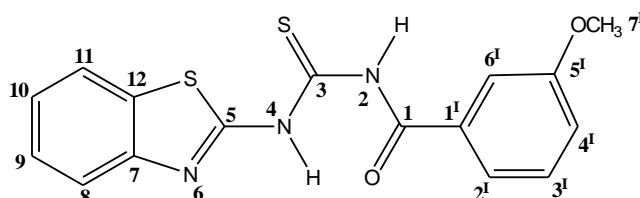
2-Aminobenzothiazole (0.04 mol, 6.00 g) was added to a slight excess of 4-methoxybenzoyl isothiocyanate (0.04 mol, 7.73 g) and refluxed for 6 h. The



mother liquor was allowed to stand overnight in a fume hood. The product obtained was filtered and recrystallized from DMSO:Toluene (1:1) as a yellow solid. Melting point = 192–193 °C. Yield = 73.0%. 1H NMR (ppm): 12.06 (s, 1H, N–H), 8.06 (m, 3H, (**2^I**, **6^I**, **11**)), 7.83 (d, 1H, J = 8.0 Hz, (**8**)), 7.51 (t, 1H, J = 7.2 Hz, (**9**)), 7.40 (t, 2H, J = 7.2, 7.6 Hz, (**10**)), 7.11 (d, 2H, J = 8.0 Hz, (**3^I**, **5^I**)), 3.87 (s, 3H, (**7^I**)). ^{13}C NMR (ppm) : 163.6 (C=O), 131.3 (**2^I**, **6^I**), 126.6 (**1^I**), 124.2 (**10**), 121.9 (**9**), 113.9 (**2^I**, **5^I**), 55.5 (**7^I**). IR (ν_{max} , cm^{-1}): 3303 (N–H), 3054 (N–H), 2961 (C–H), 2928 (C–H), 1675 (N–H), 1594 (C=C), 1533 (C=C), 1499 (C–N), 1476 (C–N), 1437 (C–N). Anal. Calcd for $C_{16}H_{13}N_3O_2S_2$: C, 55.96; H, 3.82; N, 12.24; S, 18.67. Found: C, 56.02; H, 3.86; N, 12.31; S, 18.74. LRMS (m/z , M^+): Found for $C_{16}H_{13}N_3O_2S_2$ = 343.30, Expected mass = 343.42.

2.9.27 3-(1,3-Benzothiazol-2-yl)-1-(3-methoxybenzoyl)thiourea (27) (New)

2-Aminobenzothiazole (0.04 mol, 6.00 g) was added to 3-methoxybenzoyl isothiocyanate (0.04 mol, 7.73 g) and refluxed for 6 h. The mother liquor was allowed to stand overnight in a fume

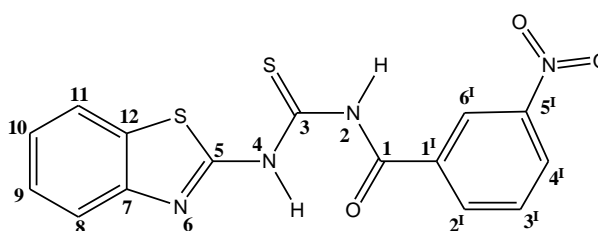


hood. The product obtained was filtered and recrystallized from DMSO:Toluene (1:1) as a yellow solid. Melting point = 117–119 °C. Yield = 78.5%. 1H NMR (ppm): 12.89 (br, 1H, N–H), 12.21 (br, 1H, N–H), 8.04 (dd, 1H, J = 8.0 Hz, (**8**)), 7.80 (t, 1H, J = 8.0 Hz, (**11**)), 7.73 (s, 1H, (**6^I**)), 7.57 (m, 1H, (**10**)), 7.48 (t, 2H, J = 8.0 Hz, (**2^I**, **4^I**)), 7.36 (m, 1H, (**9**)), 7.23 (t, 1H, J

= 8.0 Hz, (**3^I**), 3.86 (s, 3H, (**7^I**)). ¹³C NMR (ppm): 159.50 (C=O), 159.0 (**7**), 129.8 (**5^I**), 129.7 (**1^I**), 126.6 (**3**), 126.2 (**10**), 124.5 (**9**), 123.7 (**12**), 121.5 (**11**), 120.7 (**8**), 119.4 (**2^I**), 113.4 (**4^I**), 112.9 (**6^I**), 55.4 (**7^I**). IR (ν_{\max} , cm^{-1}): 3313 (N–H), 3070 (N–H), 2075 (C–H), 1650 (C=O), 1596 (C=C), 1582 (C=C), 1515 (C=C), 1464 (C–N), 1429 (C–N). Anal. Calcd for $\text{C}_{16}\text{H}_{13}\text{N}_3\text{O}_2\text{S}_2$: C, 55.96; H, 3.82; N, 12.24; S, 18.67. Found: C, 55.91; H, 3.88; N, 12.30; S, 18.75. LRMS (m/z , M^+): Found for $\text{C}_{16}\text{H}_{13}\text{N}_3\text{O}_2\text{S}_2 = 343.36$, Expected mass = 343.42.

2.9.28 3-(1,3-Benzothiazol-2-yl)-1-(3-nitrobenzoyl)thiourea (**28**) (New)

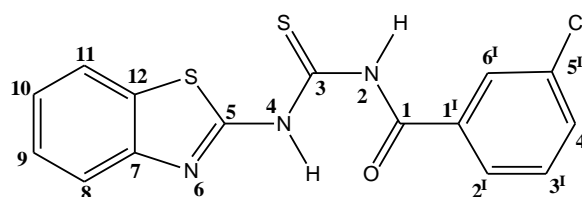
2-Aminobenzothiazole (0.04 mol, 6.00 g) was added to 3-nitrobenzoyl isothiocyanate (0.04 mol, 8.33 g) and refluxed for 6 h. The mother liquor was allowed to stand overnight in a fume hood. The product



obtained was filtered and recrystallized from DMSO:Toluene (1:1) as a yellow solid. Melting point = 215–216 °C. Yield = 77.3%. ¹H NMR (ppm): 14.03 (br, 1H, N–H), 12.60 (br, 1H, N–H), 8.81 (s, 1H, (**6^I**)), 8.50 (d, 1H, $J = 8.0$ Hz, (**4^I**)), 8.39 (d, 1H, $J = 7.6$ Hz, (**2^I**)), 8.06 (d, 1H, $J = 7.6$ Hz, (**8**)), 7.86 (dd, 2H, $J = 8$ Hz, (**13^I**, **11**)), 7.52 (t, 1H, $J = 7.6$ Hz, (**9**)), 7.41 (t, 1H, $J = 7.6$ Hz, (**10**)). ¹³C NMR (ppm): aromatic carbon signals (147.4, 135.2, 130.3, 124.7, 123.7). IR (ν_{\max} , cm^{-1}): 3460 (N–H), 3088 (N–H), 1692 (C=S), 1670 (C=O), 1567 (C=C), 1516 (C=C), 1482 (C–N), 1410 (C–N). Anal. Calcd for $\text{C}_{15}\text{H}_{10}\text{N}_4\text{O}_3\text{S}_2$: C, 50.27; H, 2.81; N, 15.63; S, 17.89. Found: C, 50.35; H, 2.74; N, 15.69; S, 17.94. LRMS (m/z , M^+): Found for $\text{C}_{15}\text{H}_{10}\text{N}_4\text{O}_3\text{S}_2 = 358.80$, Expected mass = 358.39.

2.9.29 3-(1,3-Benzothiazol-2-yl)-1-(3-chlorobenzoyl)thiourea (**29**)³³⁵

2-Aminobenzothiazole (0.04 mol, 6.00 g) was added to 3-chlorobenzoyl isothiocyanate (0.04 mol, 7.91 g) and refluxed for 6 h. The mother liquor was allowed to stand overnight in a fume hood. The product obtained was

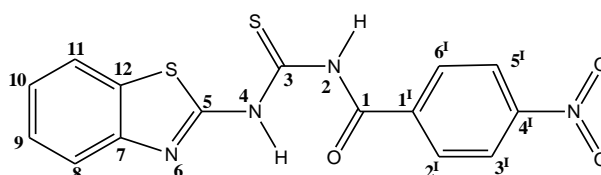


filtered and recrystallized from DMSO:Toluene (1:1) as a yellow solid. Melting point = 140–

142 °C. Yield = 76.4%. ^1H NMR (ppm): 12.29 (br, 1H, N–H), 8.20 (s, 1H, (**6^I**)), 8.06 (m, 2H, (**8**, **11**)), 7.93 (d, 1H, $J = 8$ Hz, (**2^I**)), 7.80 (t, 1H, $J = 8.4, 8.8$ Hz, (**14**)), 7.73 (t, 1H, $J = 8.0, 8.4$ Hz, (**13**)), 7.59 (m, 1H, (**9**)), 7.51 (m, 1H, (**10**)). ^{13}C NMR (ppm): Aromatic carbon signals (133.4, 133.1, 133.0, 130.5, 128.6, 128.1, 127.6, 127, 126.6, 124.2, 124.5, 123.8, 122.0, 121.8). IR (ν_{max} , cm^{-1}): 3296 (N–H), 3058 (N–H), 1670 (C=O), 1596 (C=C), 1544 (C=C), 1457 (C–N), 1432 (C–N). Anal. Calcd for $\text{C}_{15}\text{H}_{10}\text{ClN}_3\text{OS}_2$: C, 51.79; H, 2.90; N, 12.08; S, 18.44. Found: C, 51.73; H, 2.84; N, 12.12; S, 18.49. LRMS (m/z , M^+): Found for $\text{C}_{15}\text{H}_{10}\text{ClN}_3\text{OS}_2 = 347.70$ Expected mass = 347.84.

2.9.30 3-(1,3-Benzothiazoyl-2-yl)-1-(4-nitrobenzoyl)thiourea (**30**) (New)

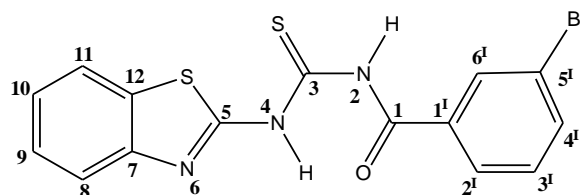
2-Aminobenzothiazole (0.04 mol, 6.00 g) was added to 4-nitrobenzoyl isothiocyanate (0.04 mol, 8.33 g) and refluxed for 6 h. The mother liquor was allowed to stand



overnight in a fume hood. The product obtained was filtered and recrystallized from DMSO:Toluene (1:1) as a yellow solid. Melting point = 226–228 °C. Yield = 75.6% ^1H NMR (ppm): 12.44 (br, 1H, N–H), 9.14 (br, 1H, 0 N–H), 8.36 (d, 2H, $J = 8.0$ Hz, (**2^I**, **6^I**)), 8.29 (d, 2H, $J = 8.0$ Hz, (**3^I**, **5^I**)), 8.20 (d, 1H, $J = 8.0$ Hz (**8**)), 8.10 (m, 2H, (**9^I**, **10^I**)), 7.79 (m, 1H, (**11**)), 7.71 (m, 1H, (**8^I**)), 7.52 (m, 1H, (**11^I**)), 7.41 (m, 1H, (**10**)), 7.25 (m, 1H, (**9**)). ^{13}C NMR (ppm): 166.5, 148.8, 140.0, 129.9, 128.7, 114.9. IR (ν_{max} , cm^{-1}): 3351 (N–H), 3075 (N–H), 2073, 1679 (C=O), 1595 (C=C), 1510 (C=C), 1462 (C–N). Anal. Calcd for $\text{C}_{15}\text{H}_{10}\text{N}_4\text{O}_3\text{S}_2$: C, 50.27; H, 2.81; N, 15.63; S, 17.89. Found: C, 50.31; H, 2.84; N, 15.57; S, 17.86. LRMS (m/z , M^+): Found for $\text{C}_{15}\text{H}_{10}\text{N}_4\text{O}_3\text{S}_2 = 358.28$, Expected mass = 358.39.

2.9.31 3-(1,3-Benzothiazol-2-yl)-1-(3-bromobenzoyl)thiourea (**31**) (New)

2-Aminobenzothiazole (0.04 mol, 6.00 g) was added to 3-bromobenzoyl isothiocyanate (0.04 mol, 9.68 g) and refluxed for 6 h. The mother liquor was allowed to stand overnight

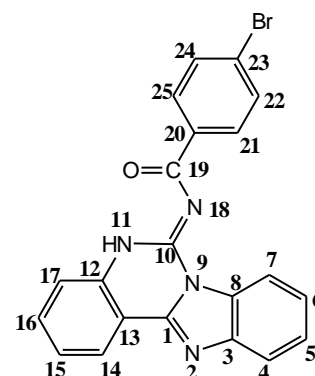


in a fume hood. The product obtained was filtered and recrystallized from DMSO:Toluene

(1:1) as a yellow solid. Melting point = 152–153 °C. Yield = 80.0% ^1H NMR (ppm): 8.34 (s, 1H, (**6^I**)), 8.13 (d, 1H, $J = 8.0$ Hz, (**8**)), 8.01 (m, 1H, (**11**)), 7.87 (d, 1H, $J = 8.0$ Hz, (**2^I**)), 7.80 (d, 1H, $J = 7.6$ Hz, (**4^I**)), 7.54 (t, 1H, $J = 7.6, 8.0$ Hz (**3^I**)), 7.48 (t, 1H, $J = 8.0$ Hz, (**10**)), 7.37 (t, 1H, $J = 8.0$ Hz, (**9**)) ^{13}C NMR (ppm): aromatic resonances (135.6, 130.9, 127.5, 126.6, 123.64, 121.8). IR (ν_{max} , cm^{-1}): 3232 (N–H), 3155 (N–H), 1694 (C=S), 1665 (C=O), 1599 (C=C), 1509 (C=C), 1475 (C–N), 1456 (C–N). Anal. Calcd for $\text{C}_{15}\text{H}_{10}\text{BrN}_3\text{OS}_2$: C, 45.92; H, 2.57; N, 10.71; S, 16.35. Found: C, 45.88; H, 2.57; N, 10.65; S, 16.43. LRMS (m/z , M^+): Found for $\text{C}_{15}\text{H}_{10}\text{BrN}_3\text{OS}_2 = 392.40$, Expected mass = 392.29.

2.9.32 4-Bromo-*N*-[(9*E*)-8,10,17-triazatetracyclo[8.7.0.0^{2,7}.0^{11,16}]heptadeca-1(17),2,4,6,11(16),12,14-heptaen-9-ylidene]benzamide (32**) (New)**

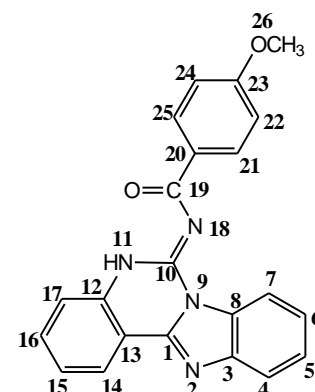
Ammonium thiocyanate (0.02 mol, 1.52 g) was dissolved in 80 mL of acetone, 4-bromobenzoyl chloride (0.02 mol, 4.84 g) was added followed by heating under reflux at 100–120 °C for 2 h. The 4-bromobenzoyl isothiocyanate (0.02 mol) obtained was filtered, 2(2-aminophenyl)-*1H*-benzimidazole (0.02 mol, 4.19 g) added to the filtrate and refluxed at 100–120 °C for 6 h. The product obtained was filtered, dried and recrystallized from DMSO:Toluene (1:1) as a cream flaky solid. Melting point =



296–297 °C. Yield = 83.3%. ^1H NMR (ppm): 13.26 (br, 1H, N–H), 8.36 (m, 6H, (**21**, **22**, **24**, **25**)), 8.01 (d, 1H, $J = 8.0$ Hz, (**14**)), 7.77 (d, 1H, $J = 8.0$ Hz, (**17**)), 7.50 (t, 1H, $J = 8.0$ Hz, (**15**)), 7.35 (t, 1H, $J = 7.2, 7.6$ Hz, (**16**)). ^{13}C NMR (ppm): 149.7 (**12**), 129.8 (**21**, **22**, **24**, **25**), 126.4 (**14**), 124.0 (**15**, **16**), 123.6 (**4**, **5**, **6**, **7**), 121.9 (**17**). IR (ν_{max} , cm^{-1}): 3026 (N–H), 1637 (C=O), 1574 (C=C), 1548 (C=C), 1478 (C–N). Anal. Calcd for $\text{C}_{21}\text{H}_{13}\text{BrN}_4\text{O}$: C, 60.45; H, 3.14; N, 13.43. Found: C, 60.31; H, 3.19; N, 13.48; LRMS (m/z , M^+): Found for $\text{C}_{21}\text{H}_{13}\text{BrN}_4\text{O} = 417.18$, Expected mass = 417.26.

2.9.33 4-Methoxy-*N*-[(9*E*)-8,10,17-triazatetracyclo[8.7.0.0^{2,7}.0^{11,16}]heptadeca-1(17),2,4,6,11(16),12,14-heptaen-9-ylidene]benzamide (33) (New)

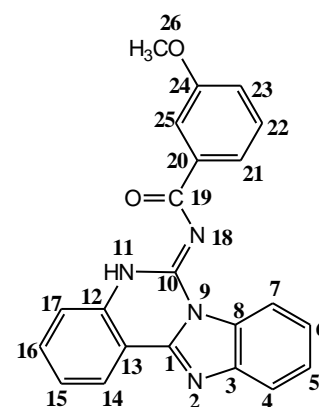
Ammonium thiocyanate (0.02 mol, 1.52 g) was dissolved in 40 mL of acetone, 4-methoxybenzoyl chloride (0.02 mol, 4.39 g) was added followed by heating under reflux at 100–120 °C for 2 h. The 4-methoxybenzoyl isothiocyanate (0.02 mol) obtained was filtered and 2-(2-aminophenyl)-1*H*-benzimidazole (0.02 mol, 4.19 g) added to the filtrate and refluxed at 100–120 °C for 4 h. The product obtained was filtered and recrystallized from DMSO:Toluene (1:1) as a yellow solid. Melting point = 180–181



°C. Yield = 75.5%. ¹H NMR (ppm): 13.74 (s, 1H, N–H), 8.84 (br, 1H, (7)), 8.36 (d, 1H, *J* = 7.6 Hz, (17)), 8.23 (d, 2H, *J* = 8.0 Hz, (21, 25)), 7.89 (m, 1H, (15)), 7.84 (d, 1H, *J* = 8.4 Hz, (14)), 7.70 (t, 1H, *J* = 7.6 Hz, (5)), 7.54 (m, 2H, *J* = 2.8, 3.2 Hz, (4, 6, 16)), 7.08 (d, 2H, *J* = 8.0 Hz, (22, 24)), 3.86 (s, 3H, 26). ¹³C NMR (ppm): 162.8 (19, 23), 148.7 (10), 146.4 (12), 143.9 (1, 3), 134.0 (8), 132.4 (21, 25), 131.0 (14, 16, 20), 129.1 (5, 6), 124.2 (15), 123.9 (17), 119.3 (4, 7), 117.7 (13), 113.8 (22, 24), 55.4 (17), IR (ν_{\max} , cm⁻¹): 3043 (N–H), 2950 (C–H), 2913 (C–H), 1635 (C=O), 1567 (C=C), 1507 (C=C), 1478 (C–N), 1445 (C–N), 1415 (C–N). Anal. Calcd for C₂₂H₁₆N₄O₂: C 71.73; H, 4.38; N, 15.21. LRMS (*m/z*, M⁺): Found for C₂₂H₁₆N₄O₂ C 71.62; H, 4.46; N, 15.26; LRMS (*m/z*, M⁺): Found for C₂₂H₁₆N₄O₂ = 368.28, Expected mass = 368.39.

2.9.34 3-Methoxy-*N*-[(9*E*)-8,10,17-triazatetracyclo[8.7.0.0^{2,7}.0^{11,16}]heptadeca-1(17),2,4,6,11(16),12,14-heptaen-9-ylidene]benzamide (34)(New)

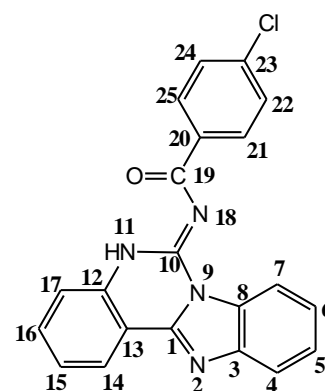
Ammonium thiocyanate (0.02 mol, 1.52 g) was dissolved in 40 mL of acetone 3-methoxybenzoyl chloride (0.02 mol, 3.41 g) was added followed by heating under reflux at 100–120 °C for 2 h. The 3-methoxybenzoyl isothiocyanate (0.02 mol) obtained was filtered and 2-(2-aminophenyl)-1*H*-benzimidazole (0.02 mol, 4.19 g) added to the filtrate and refluxed at 100–120 °C for 4 h. The product obtained was filtered and recrystallized from DMSO:Toluene (1:1) as a yellow solid. Melting point = 163–164



°C. Yield = 85.5%. ^1H NMR (ppm): 13.56 (s, 1H, N–H), 8.66 (br, 1H, (7)), 8.25 (d, 1H, $J = 7.6$ Hz, (5)), 7.72 (d, 3H, $J = 7.6$ Hz, (21, 23, 25)), 7.64 (m, 2H, (15, 16)), 7.40 (m, 4H, (4, 6, 14, 22)), 7.11 (d, 1H, $J = 8.0$ Hz, (17)), 3.79 (s, 3H, (26)), ^{13}C NMR (ppm): 177.2 (C=O), 159.0 (12, 24), 146.1 (1), 143.8 (3, 12), 132.3 (8, 20), 130.0 (22), 129.4 (14, 16), 125.3 (5, 6), 124.1 (21, 23), 123.6 (4, 7), 121.1 (17), 119.1 (15), 118.4 (13), 113.4 (25), 54.9 (26). IR (ν_{max} , cm^{-1}): 3110 (N–H), 2991 (C–H), 2836 (C–H), 1634 (C=O), 1568 (C=C), 1446 (C–N). Anal. Calcd for $\text{C}_{22}\text{H}_{16}\text{N}_4\text{O}_2$: C 71.73; H, 4.38; N, 15.21. LRMS (m/z , M^+): Found for $\text{C}_{22}\text{H}_{16}\text{N}_4\text{O}_2$ C 71.64; H, 4.49; N, 15.16; LRMS (m/z , M^+): Found for $\text{C}_{22}\text{H}_{16}\text{N}_4\text{O}_2 = 368.30$, Expected mass = 368.39.

2.9.35 4-Chloro-*N*-[(9*E*)-8,10,17-triazatetracyclo[8.7.0.0^{2,7}.0^{11,16}]heptadeca-1(17),2,4,6,11(16),12,14-heptaen-9-ylidene]benzamide (35) (New)

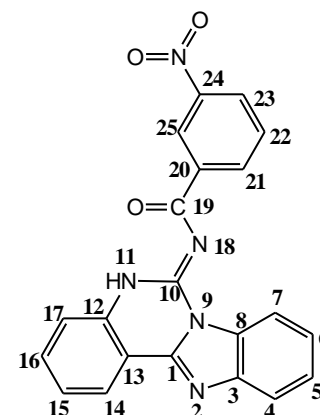
Ammonium thiocyanate (0.02 mol, 1.52 g) was dissolved in 40 mL of acetone 4-chlorobenzoyl chloride (0.02 mol, 3.50 g) was added followed by heating under reflux at 100–120 °C for 2 h. The 4-chlorobenzoyl isothiocyanate (0.02 mol) obtained was filtered and 2-(2-aminophenyl)-1*H*-benzimidazole (0.02 mol, 4.19 g) added to the filtrate and refluxed at 100–120 °C for 4 h. The product obtained was filtered and recrystallized from DMSO:Toluene (1:1) as a yellow solid. Melting point = 245–



247 °C. Yield = 79.3%. NMR (ppm): 10.94 (s, 1H, N–H), 8.40 (d, 1H, $J = 8.4$ Hz (14)), 8.05 (d, 1H, $J = 8.0$ Hz, (7)), 7.90 (m, 3H, (17, 21, 25)), 7.74 (m, 1H, (5)), 7.50 (m, 2H, (4, 6)), 7.46 (m, 3H, (15, 22, 24)), 6.87 (m, 1H, (16)) ^{13}C NMR (ppm): 180.2 (C=O), 167.7 (1), 132.9–128.4 (aromatic carbon signals). IR (ν_{max} , cm^{-1}): 3400 (N–H), 3217 (N–H), 2929 (C–H), 1666 (C=O), 1511 (C=C), 1432 (C–N). Anal. Calcd for $\text{C}_{21}\text{H}_{13}\text{ClN}_4\text{O}$: C, 67.66; H, 3.51; N, 15.03. LRMS (m/z , M^+): Found for $\text{C}_{21}\text{H}_{13}\text{ClN}_4\text{O}$: C, 67.73; H, 3.59; N, 15.10; S, 13.86 LRMS (m/z , M^+): Found for $\text{C}_{21}\text{H}_{13}\text{ClN}_4\text{O} = 372.70$, Expected mass = 372.81.

2.9.36 3-Nitro-*N*-[(9*E*)-8,10,17-triazatetracyclo[8.7.0.0^{2,7}.0^{11,16}]heptadeca-1(17),2,4,6,11(16),12,14-heptaen-9-ylidene]benzamide (36) (New)

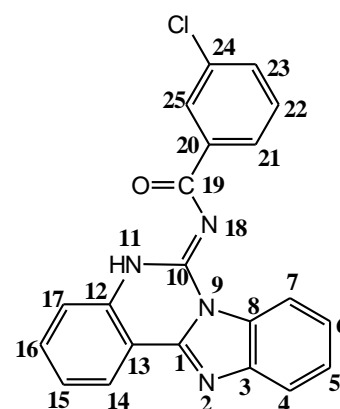
Ammonium thiocyanate (0.02 mol, 1.52 g) was dissolved in 40 mL of acetone 3-nitrobenzoyl chloride (0.02 mol, 3.714 g) was added followed by heating under reflux at 100–120 °C for 2 h. The 3-nitrobenzoyl isothiocyanate (0.02 mol) obtained was filtered and 2-(2-aminophenyl)-1*H*-benzimidazole (0.02 mol, 4.19 g) added to the filtrate and refluxed at 100–120 °C for 4 h. The product obtained was filtered and recrystallized from DMSO:Toluene (1:1) as a yellow solid. Melting point = 250–252 °C. Yield = 73.5%. ¹H NMR (ppm): 8.69 (s, 1H, (25)), 8.35 (m,



3H, (4, 7, 23)), 7.92 (m, 1H, (14)), 7.74 (m, 3H, (5, 6, 22)), 7.48 (m, 1H, (15)), 7.34 (m, 1H, (16)), 6.86 (d, 1H, *J* = 8.0 Hz, (17)). ¹³C NMR (ppm): 167.3, 166.4, 144.2, Aromatic carbon resonances (131.8, 130.7, 129.4, 129.2, 128.8, 128.5, 128.1, 127.4, 124.4, 122.3, 113.5). IR (ν_{\max} , cm^{-1}): 3327 (N–H), 3134 (N–H), 1673 (C=O), 1596 (C=C), 1514 (C=C), 1486 (C–N). Anal. Calcd for $\text{C}_{21}\text{H}_{13}\text{N}_3\text{O}_3$: C, 65.79; H, 3.42; N, 18.27. LRMS (*m/z*, M^+): Found for $\text{C}_{21}\text{H}_{13}\text{N}_5\text{O}_3$ C, 65.57; H, 3.53; N, 18.35. LRMS (*m/z*, M^+): Found for $\text{C}_{21}\text{H}_{13}\text{N}_5\text{O}_3$ = 383.20, Expected mass = 383.36.

2.9.37 3-Chloro-*N*-[(9*E*)-8,10,17-triazatetracyclo[8.7.0.0^{2,7}.0^{11,16}]heptadeca-1(17),2,4,6,11(16),12,14-heptaen-9-ylidene]benzamide (37) (New)

Ammonium thiocyanate (0.02 mol, 1.52 g) was dissolved in 40 mL of acetone 3-bromobenzoyl chloride (0.02 mol, 3.50 g) was added followed by heating under reflux at 100–120 °C for 2 h. The 3-bromobenzoyl isothiocyanate (0.02 mol) obtained was filtered and 2-(2-aminophenyl)-1*H*-benzimidazole (0.02 mol, 4.19 g) added to the filtrate and refluxed at 100–120 °C for 4 h. The product obtained was filtered and recrystallized from DMSO:Toluene (1:1) as a light yellow solid. Melting point =

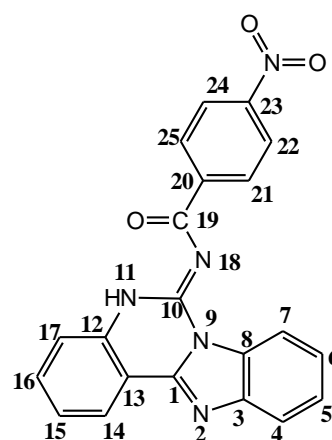


216–217 °C. Yield = 74.9%. ¹H NMR (ppm): 12.30 (s, 1H, N–H, 11), 12.13 (s, 1H, 25), 836 (d, 2H, *J* = 8.0 Hz, 14, 17), 8.09 (m, 1H, 5, 6), 7.92 (m, 3H, 21, 22, 23), 7.84 (m, 2H, 4, 7),

7.53 (m, 2H, **15**, **16**) ^{13}C NMR (ppm): 180.1, 166.8, 149.8, 137.9, 133.3, 129.7, 127.3, 126.7, 123.7. IR (ν_{max} , cm^{-1}): 1638 (C=O), 1595 (C=C), 1575 (C=C), 1446 (C-N), 1432 (C-N). Anal. Calcd for $\text{C}_{21}\text{H}_{13}\text{ClN}_4\text{O}$: C, 67.66; H, 3.51; N, 15.03. LRMS (m/z , M^+): Found for $\text{C}_{17}\text{H}_{12}\text{N}_4\text{OS}$ C, 67.74; H, 3.59; N, 15.10. LRMS (m/z , M^+): Found for $\text{C}_{21}\text{H}_{13}\text{ClN}_4\text{O}$ = 372.90, Expected mass = 372.81.

2.9.38 4-Nitro-*N*-[(9*E*)-8,10,17-triazatetracyclo[8.7.0.0^{2,7}.0^{11,16}]heptadeca-1(17),2,4,6,11(16),12,14-heptaen-9-ylidene]benzamide (38) (New)

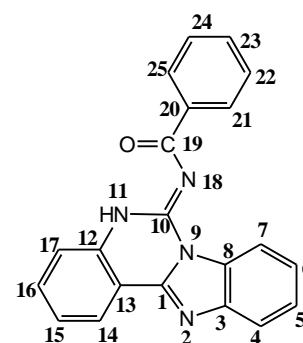
Ammonium thiocyanate (0.02 mol, 1.52 g) was dissolved in 40 mL of acetone 4-nitrobenzoyl chloride (0.02 mol, 3.71 g) was added to the acetone solution followed by heating under reflux at 100–120 °C for 2 h. The 4-nitrobenzoyl isothiocyanate (0.02 mol) obtained was filtered and 2-(2-aminophenyl)-1*H*-benzimidazole (0.02 mol, 4.19 g) added to the filtrate and refluxed at 100–120 °C for 4 h. The product obtained was filtered and recrystallized from DMSO:Toluene (1:1) as a yellow solid. Melting point = 311–313 °C. Yield = 75.60%.



^1H NMR (ppm): 14.38 (s, 1H, N-H), 8.94 (d, 1H, J = 10.4 Hz, (**14**)), 8.61 (d, 1H, J = 8.4 Hz, (**17**)), 8.47 (d, 2H, J = 9.6 Hz, (**25**, **21**)), 8.22 (m, 2H, (**5**)), 7.95 (m, 1H, (**7**)), 7.62 (m, 2H, (**15**, **16**)), 7.38 (m, 2H, (**22**, **24**)). IR (ν_{max} , cm^{-1}): 3052 (N-H), 1634 (C=O), 1574 (C=C), 1549 (C=C), 1520 (C=C), 1485 (C-N), 1406 (C-N). Anal. Calcd for $\text{C}_{21}\text{H}_{13}\text{N}_5\text{O}_3$: C, 65.79; H, 3.42; N, 18.27. LRMS (m/z , M^+): Found for $\text{C}_{21}\text{H}_{13}\text{N}_5\text{O}_3$: C, 65.83; H, 3.47; N, 18.25. LRMS (m/z , M^+): Found for $\text{C}_{21}\text{H}_{13}\text{N}_5\text{O}_3$: = 383.45, Expected mass = 383.36.

2.9.39 *N*-[(9*E*)-8,10,17-Triazatetracyclo[8.7.0.0^{2,7}.0^{11,16}]heptadeca-1(17),2,4,6,11(16),12,14-heptaen-9-ylidene]benzamide (39) (New)

Ammonium thiocyanate (0.02 mol, 1.52 g) was dissolved in 40 mL of acetone, benzoyl chloride (0.02 mol, 5.62 mL) was added followed by heating under reflux at 100–120 °C for 2 h. The benzoyl isothiocyanate (0.02 mol) obtained was filtered and 2-(2-

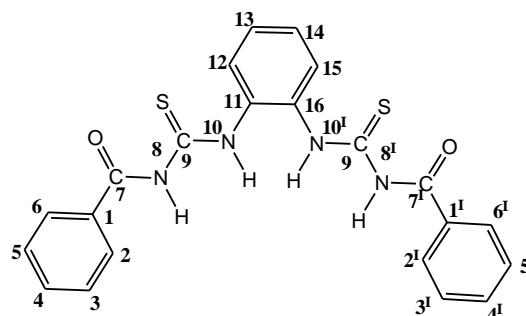


General method for the synthesis of compounds 41 to 49

The compounds were accessed by dissolving ammonium thiocyanate (0.04 mol) in 80 mL of acetone, the relevant benzoyl chloride (0.04 mol) derivative was then added and heated under reflux at 100–120 °C for 2 h. The benzoyl isothiocyanate (0.04 mol) derivative obtained was filtered, *o*-phenylenediamine (0.04 mol) added to the filtrate and refluxed at 100–120 °C for 3 h. The mother liquor was allowed to stand overnight in a fume hood.

2.9.41 1-Benzoyl-3-(2-[[phenylformamido]methanethiyl]amino)phenylthiourea (41)

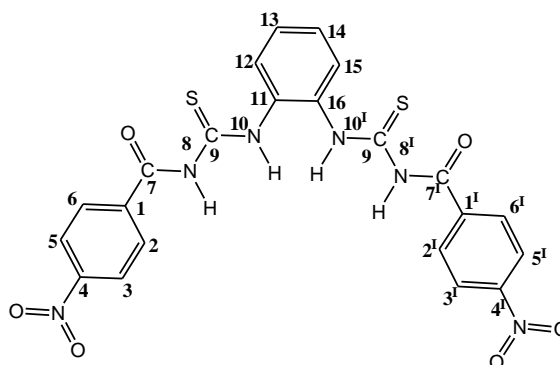
The product obtained was filtered and recrystallized from DMSO:Toluene (1:1) as a light brown solid. Melting point = 174–176 °C. Yield = 78.0%. ¹H NMR (ppm): 12.52 (s, 1H, N–H), 8.10 (d, 2H, *J* = 7.2 Hz, (2, 2^I)), 7.94 (d, 2H, *J* = 7.2 Hz, (11, 16)), 7.71 (m, 2H, (4, 4^I)), 7.65 (t, 2H, (3, 3^I)), 7.59 (d, 2H, (12, 15)), 7.48



(t, 2H, (5, 5^I)), 7.42 (m, 2H, (13, 14)). ¹³C NMR (ppm): 167.3 (C=O), 166.4 (C=O), 144.2 (11, 16), 131.8 (1, 1^I), 130.7 (4, 4^I), 129.2 (3, 5, 3^I, 5^I), 128.8 (12, 15), 128.5 (2, 6, 2^I, 6^I), 124.4, 113.5 (13, 14). IR (ν_{\max} , cm⁻¹): 3327 (N–H), 3262 (N–H), 3134 (N–H), 1673 (C=S), 1643 (C=O), 1596 (C=C), 1514 (C=C), 1486 (C–N). Anal. Calcd for C₂₂H₁₈N₂O₂S₂: C, 60.81; H, 4.18; N, 12.89; S, 14.76. Found: C, 60.56; H, 4.28; N, 12.78; S, 14.52. LRMS (m/z, M⁺): Found for C₂₂H₁₈N₄O₂S₂ = 434.45, Expected mass = 434.53.

2.9.42 1-(4-Nitrobenzoyl)-3-[2-[[4-nitrophenyl]formamido]methanthiyl]amino]phenylthiourea (42)

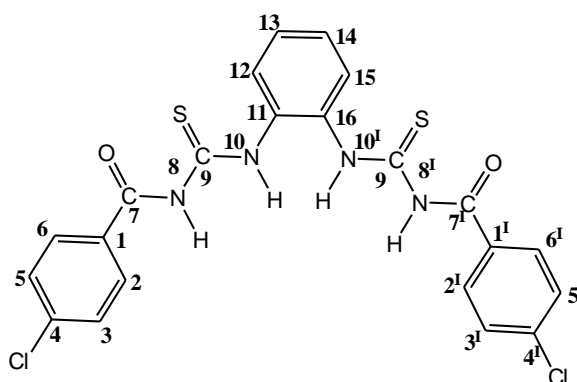
The mother liquor was allowed to stand overnight in a fume hood. The product obtained was filtered and recrystallized from DMSO:Toluene (1:1) as a yellow solid. Melting point = 202–204 °C Yield = 74.7%.



^1H NMR (ppm): 12.30 (s, 2H, N–H), 12.13 (s, 2H, N–H), 833 (d, 4H, $J = 8.0$ Hz, (**2**, **6**, **2^I**, **6^I**)), 8.09 (d, 4H, $J = 8.0$ Hz, (**3**, **5**, **3^I**, **5^I**)), 7.93 (m, 2H, (**13**, **14**)), 7.42 (m, 2H, (**12**, **15**)). ^{13}C NMR (ppm): 180.1 (C=S), 161.0 (C=O), 149.7 (**4**, **4^I**), 138.1 (**1**, **1^I**), 133.3 (**11**, **16**), 130.20 (**2**, **6**, **2^I**, **6^I**), 127.3 (**12**, **15**), 126.8 (**13**, **14**), 123.2 (**3**, **5**, **3^I**, **5^I**). IR (ν_{max} , cm^{-1}): 3200 (N–H), 3071 (N–H), 1683 (C=S), 1662 (C=O), 1508 (C=C), 1484 (C–N). Anal. Calcd for $\text{C}_{22}\text{H}_{16}\text{N}_6\text{O}_6\text{S}_2$: C, 50.38; H, 3.07; N, 16.02; S, 12.23. Found: C, 50.49; H, 3.11; N, 16.17; S, 12.36. LRMS (m/z , M^+): Found for $\text{C}_{22}\text{H}_{16}\text{N}_6\text{O}_6\text{S}_2 = 524.20$, Expected mass = 524.53.

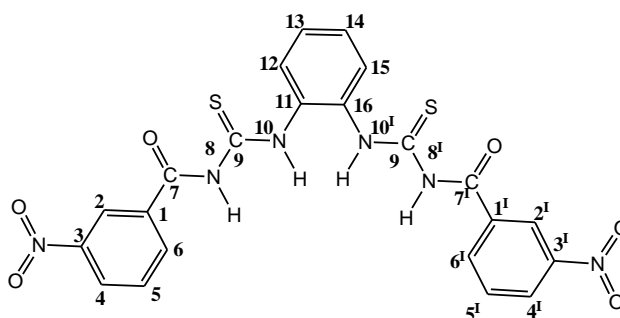
2.9.43 1-(4-Chlorobenzoyl)-3-[2-({[(4-chlorophenyl)formamido]methanethioyl}amino)phenylthiourea (43)

The product obtained was filtered and recrystallized from DMSO:Toluene (1:1) as a yellow solid. Melting point = 173–175 °C. Yield = 70.7% ^1H NMR (ppm): 8.52 (m, 2H), 7.93 (d, 2H, $J = 7.6$ Hz, (**3**, **5**)), 7.89 (d, 2H, $J = 7.6$ Hz, (**2**, **6**)), 7.81 (br, 2H, , (**2^I**, **6^I**)), 7.65 (br, 2H, (**3^I**, **6^I**)), 7.55 (t, 2H, $J = 8.0$ Hz, (**13**, **14**)), 7.50 (t, 2H, $J = 8.0$ Hz, (**12**, **15**)). ^{13}C NMR (ppm): 143.8 (**1**, **1^I**), 132.1 (**6**, **6^I**), 125.9 (**12**, **15**), 124.0 (**13**, **14**), 119.6 (**2**, **2^I**). IR (ν_{max} , cm^{-1}): 3038 (N–H), 1640 (C=O), 1578 (C=C), 1555 (C=C), 1476 (C–N), 1447 (C–N). Anal. Calcd for $\text{C}_{22}\text{H}_{16}\text{Cl}_2\text{N}_4\text{O}_2\text{S}_2$: C, 52.49; H, 3.20; N, 11.13; S, 12.74. Found: C, 52.56; H, 3.26; N, 11.22; S, 12.85. LRMS (m/z , M^+): Found for $\text{C}_{22}\text{H}_{16}\text{Cl}_2\text{N}_4\text{O}_2\text{S}_2 = 503.20$, Expected mass = 503.42.



2.9.44 1-(3-Nitrobenzoyl)-3-[2-({[(3-nitrophenyl)formamido]methane}amino)phenyl]thiourea (44)

The product obtained was filtered and recrystallized from DMSO:Toluene (1:1) as a yellow solid. Melting point = 201–203 °C. Yield = 73.0 % ^1H NMR

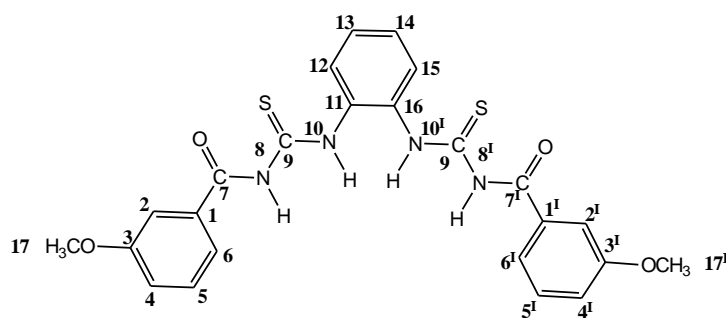


(ppm): 12.34 (s, 2H, (N–H)), 12.18 (s, 2H, (N–H)), 8.65 (s, 2H, (**2**, **2^I**)), 8.48 (d, 2H, $J = 8.0$ Hz (**4**, **4^I**)), 8.31 (d, 2H, $J = 8.0$ Hz, (**6**, **6^I**)), 7.96 (m, 2H, (**5**, **5^I**)), 7.78 (dd, 2H, $J = 8$ Hz, (**12**, **15**)), 7.44 (t, 2H, $J = 4.0, 5.2$ Hz (**13**, **14**)). ^{13}C NMR (ppm): 180.2 (C=S), 166.4 (C=O), 147.3 (**3**, **3^I**), 135.1 (**1**, **1^I**), 133.7 (**11**, **16**), 133.3 (**6**, **6^I**), 130.1 (**4**, **4^I**), 127.4 (**5**, **5^I**), 127.2 (**12**, **15**), 126.6 (**13**, **14**), 123.5 (**2**, **2^I**). IR (ν_{max} , cm^{-1}): 3351 (N–H), 3204 (N–H), 1687 (C=O), 1515 (C=C). Anal. Calcd for $\text{C}_{22}\text{H}_{16}\text{N}_6\text{O}_6\text{S}$: C, 50.38; H, 3.07; N, 16.02; S, 12.23. Found: C, 50.24; H, 3.20; N, 16.18; S, 12.19. LRMS (m/z , M^+): Found for $\text{C}_{22}\text{H}_{16}\text{N}_6\text{O}_6\text{S} = 524.60$, Expected mass = 524.53.

2.9.45 1-(3-Methoxybenzoyl)-3-[2-((3-methoxyphenyl)formamido)methanethioyl]amino)phenyl]thiourea (**45**)

The product obtained was filtered and recrystallized from DMSO:Toluene (1:1) as a white solid. Melting point = 164–166 °C.

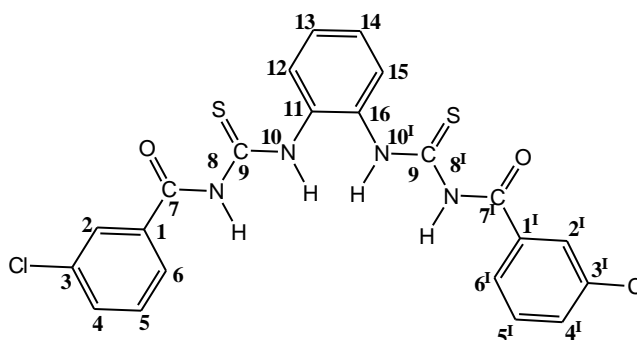
Yield = 76.4% ^1H NMR (ppm): 12.50 (s, 2H), 11.69 (s, 2H), 7.92 (m, 2H, (**13**, **14**), 7.50 (d, 2H, $J =$



7.6 Hz, (**4**, **4^I**)), 7.45 (s, 2H, (**2**, **2^I**)), 7.41 (t, 4H, $J = 8$ Hz, (**5**, **6**, **5^I**, **6^I**)), 7.21 (d, 2H, $J = 8.8$ Hz (**12**, **15**)), 3.77 (s, 6H, (**17**, **17^I**)). ^{13}C NMR (ppm): 180.4 (C=S), 168.1 (C=O), 159.0 (**3**, **3^I**), 133.4 (**1**, **1^I**), 129.8 (**11**, **16**), 127.1 (**5**, **5^I**), 126.6 (**12**, **15**), 120.8 (**13**, **14**), 119.3 (**6**, **6^I**), 113.3 (**2**, **4**, **2^I**, **4^I**), 55.5 (**17**, **17^I**)). IR (ν_{max} , cm^{-1}): 3326 (N–H), 3184 (N–H), 3003 (N–H), 1663 (C=O), 1597 (C=C), 1506 (C=C), 1464 (C–N). Anal. Calcd for $\text{C}_{24}\text{H}_{22}\text{N}_4\text{O}_4\text{S}_2$: C, 58.28; H, 4.48; N, 11.33; S, 12.97. Found: C, 58.12; H, 4.29; N, 11.42; S, 12.86. LRMS (m/z , M^+): Found for $\text{C}_{24}\text{H}_{22}\text{N}_4\text{O}_4\text{S}_2 = 494.35$, Expected mass = 494.59.

2.9.48 1-(3-Chlorobenzoyl)-3-[2-((3-chlorophenyl)formamido)methanethioyl]amino phenyl]thiourea (48)

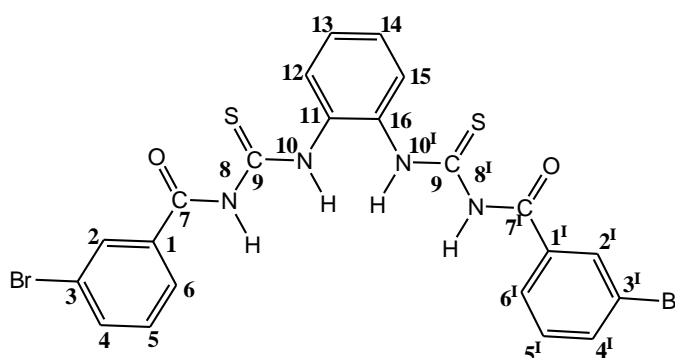
The product obtained was filtered and recrystallized from DMSO:Toluene (1:1) as a light brown solid. Melting point = 143–145 °C. Yield = 75.3% ¹H NMR (ppm): 12.40 (br, 2H), 11.88 (s, 2H, N–H), 8.04 (m, 1H, (6^I)), 7.91 (d, 3H (6, 13, 14)), 7.83 (d, 2H, J = 7.6 Hz



(12, 15)), 7.70 (d, 2H, J = 8.0 Hz, (4, 4^I)), 7.52 (m, 2H, J = 8.0, 7.2 Hz, (5, 5^I)), 7.41 (s, 2H, (2, 2^I)). ¹³C NMR (ppm): 180.4 (C=S, (9, 9^I)), 167.0 (C=O, (7, 7^I)), 134.3 (1, 1^I), 133.2 (3, 3^I), 132.8 (4, 4^I), 130.5 (5, 5^I), 128.5 (2, 2^I), 127.3 (12, 15), 127.1 (6, 6^I), 126.7 (13, 14). IR (ν_{\max} , cm⁻¹): 3440 (N–H), 3166 (N–H), 2971 (C–H), 1668 (C=O), 1593 (C=C), 1510 (C=C), 1471 (C–N). 1459 (C–N). Anal. Calcd for C₂₂H₁₆Cl₂N₄O₂S₂: C, 52.49; H, 3.20; N, 11.13; S, 12.74. Found: C, 52.31; H, 3.29; N, 11.22; S, 12.86. LRMS (m/z, M⁺): Found for C₂₂H₁₆Cl₂N₄O₂S₂ = 503.35, Expected mass = 503.42.

2.9.49 1-(3-Bromobenzoyl)-3-[2-((3-bromophenyl)formamido)methanethioyl]amino phenyl]thiourea (49)

The mother liquor was allowed to stand overnight in a fume hood. The product obtained was filtered and recrystallized from DMSO:Toluene (1:1) as a light yellow solid. Melting point = 191–193 °C. Yield = 80.0% ¹H NMR (ppm) : 12.29 (s, 2H), 11.75 (s, 2H), 7.93 (s, 2H, (2, 2^I)), 7.89 (m,

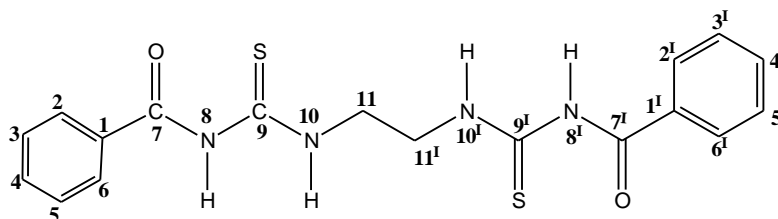


2H, (13, 14)), 7.79 (d, 4H, (4, 6, 4^I, 6^I)), 7.44 (d, 2H, J = 8 Hz, (12, 15)), 7.41 (m, 2H, (5, 5^I)). ¹³C NMR (ppm) : 180.65 (C=S), 167.74 (C=O), 136.3 (1, 1^I), 134.5 (4, 4^I), 133.8 (11, 16), 131.5 (5, 5^I), 131.2 (2, 2^I), 127.9 (12, 15), 126.9 (6, 6^I), 122.1 (13, 14). IR (ν_{\max} , cm⁻¹): 3389 (N–H), 3176 (N–H), 3016 (N–H), 1662 (C=O), 1595 (C=C), 1563 (C=C), 1456 (C–N).

Anal. Calcd for $C_{22}H_{16}Br_2N_4O_2S_2$: C, 44.61; H, 2.72; N, 9.46; S, 10.83. Found: C, 44.75; H, 2.68; N, 9.39; S, 10.70. LRMS (m/z , M^+): Found for $C_{22}H_{16}Br_2N_4O_2S_2 = 592.10$, Expected mass = 592.33.

2.9.50 3-Benzoyl-1-(2-[[[(phenylformamido)methanethioyl]amino]ethyl]thiourea (50)

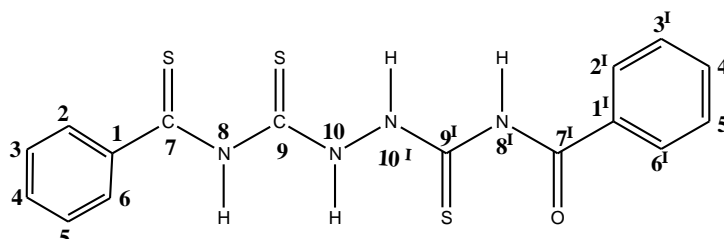
Compound **50** was accessed by dissolving ammonium thiocyanate (0.04 mol, 3.05 g) in 80 mL of acetone, benzoyl chloride (0.04 mol, 5.63 g)



was then added and heated under reflux at 100–120 °C for 2 h. The benzoyl isothiocyanate (0.04 mol) obtained was filtered; ethylene diamine (0.04 mol, 2.40 g) was added to benzoyl isothiocyanate and refluxed for 6 h. The mother liquor was allowed to stand overnight in a fume hood. The product obtained was filtered and recrystallized from DMSO:Toluene (1:1) as a light brown solid. Melting point = 220–222 °C. Yield = 70.85%. 1H NMR (ppm): 10.98 (s, 2H, **10**, **10^I**), 7.91 (d, 4H, $J = 7.6$ Hz, (**2**, **6**, **2^I**, **6^I**)), 7.61 (t, 2H, $J = 7.2$ Hz, (**4**, **4^I**)), 7.51 (t, 4H, $J = 7.6$ Hz, (**3**, **5**, **3^I**, **5^I**)), 3.09 (s, 4H, (**11**, **11^I**)). ^{13}C NMR (ppm): 180.8 (C=S), 167.3 (C=O), 132.9 (**1**, **1^I**), 132.2 (**4**, **4^I**), 128.5 (**2**, **3**, **5**, **6**, **2^I**, **3^I**, **5^I**, **6^I**), 43.4 (**11**, **11^I**), IR (ν_{max} , cm^{-1}): 3420 (N–H), 3229 (N–H), 3047 (N–H), 1664 (C=O), 1579 (C=C), 1507 (C=C), 1448 (C–N). Anal. Calcd for $C_{18}H_{18}N_4O_2S_2$: C, 55.94; H, 4.69; N, 14.50; S, 16.59. Found: C, 56.03; H, 4.74; N, 14.42; S, 16.63. LRMS (m/z , M^+): Found for $C_{18}H_{18}N_4O_2S_2 = 386.30$, Expected mass = 386.49.

2.9.51 3-Benzoyl-1-[[[(phenylformido)methanethioyl]amino]thiourea (51)

Compound **51** was accessed by dissolving ammonium thiocyanate (0.04 mol, 3.05 g) in 80 mL of acetone, benzoyl chloride (0.04 mol, 5.62 g) was then added and

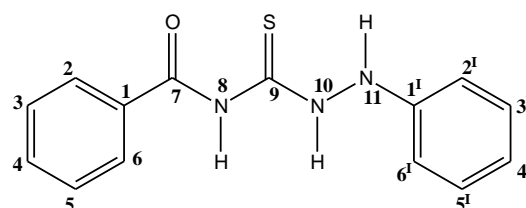


heated under reflux at 100–120 °C for 2 h. The benzoyl isothiocyanate (0.04 mol) obtained

was filtered hydrazine mono hydrate (0.04 mol, 2.00 g) was added to benzoyl isothiocyanate and refluxed for 6 h. The mother liquor was allowed to stand overnight in a fume hood. The product obtained was filtered and recrystallized from DMSO:Toluene (1:1) as a white solid. Melting point = 345–346 °C. Yield = 71.8%. ¹H NMR (ppm): 14.24 (s, 1H, N–H), 12.12 (s, 1H, N–H), 8.13 (d, 2H, *J* = 8.0 Hz, (**2**, **6**)), 8.01 (d, 2H, *J* = 8.0 Hz, (**2^I**, **6^I**)), 7.94 (d, 1H, *J* = 8.0 Hz, (**3**)), 7.65 (m, 1H, (**4^I**)), 7.55 (t, 3H, *J* = 8.0 Hz, (**3^I**, **5^I**, **5**)), 7.50 (m, 1H, (**4**)) ¹³C NMR (ppm): 171.5 (C=O), 168.3 (C=S), 167.3 (C=O), 165.0 (C=O), 156.0 (**1**), 150.2 (**1^I**), 134.2 (**4**), 132.8 (**4^I**), 131.6 (**2**), 131.2 (**2^I**), 130.7 (**3**), 128.8 (**3^I**), 128.4 (**5**), 128.3 (**5^I**), 128.2 (**6**), 125.4 (**6^I**). IR (ν_{\max} , cm^{-1}): 2988 (C–H), 2911 (C–H), 1670 (C=O), 1658 (C=O), 1536 (C=C), 1489 (C–N), 1424 (C–N). Anal. Calcd for C₁₆H₁₄N₄O₂S₂: C, 53.61; H, 3.94; N, 15.63; S, 17.89. Found: C, 53.73; H, 4.02; N, 15.60; S, 17.78. LRMS (*m/z*, M⁺): Found for C₁₆H₁₄N₄O₂S₂ = 358.36, Expected mass = 358.44.

2.9.52 3-Benzoyl-1-(phenylamino)thiourea (**52**)

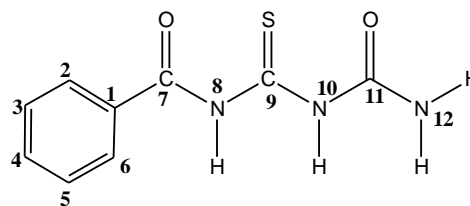
Compound **52** was accessed by dissolving ammonium thiocyanate (0.04 mol, 3.05 g) in 80 mL of acetone, benzoyl chloride (0.04 mol, 5.62 g) was then added and heated under reflux at 100–120 °C for 2 h. The product was filtered;



phenylhydrazine (0.04 mol, 4.33 g) was added to benzoyl isothiocyanate and refluxed for 6 hours. The solvent was removed at the pump to an oily liquid which was redissolved in tetrahydrofuran and allowed to stand for three days. The product recrystallized from DMSO:Toluene (1:1) as a white solid. Melting point = 242–244 °C. Yield = 71.6%. ¹H NMR (ppm): 8.03 (m, 2H (**3**, **5**)), 7.44 (m, 2H, (**3^I**, **5^I**)), 7.37 (d, 5H, (**2**, **6**, **2^I**, **6^I**)), 7.34 (s, 1H, (**5**)), 7.19 (s, 1H, (**4^I**)) ¹³C NMR (ppm): 162.9 (C=O), 149.6 (**1^I**), 136.8 (**1**), 129.9 (**2^I**), 129.4 (**4^I**), 129.3 (**3^I**, **5^I**), 128.7 (**3**, **5**), 126.6 (**2**, **6**), 125.1 (**3^I**, **5^I**). IR (ν_{\max} , cm^{-1}): 3070 (N–H), 3018 (N–H), 2727 (C–H), 1591 (C=O), 1561 (C=O), 1499 (C–N), 1475 (C–N). Anal. Calcd for C₁₄H₁₃N₃OS: C, 62.31; H, 5.19; N, 14.42; S, 13.86. Found: C, 62.31; H, 5.19; N, 14.42; S, 13.86. LRMS (*m/z*, M⁺): Found for C₁₄H₁₃N₃OS = 271.80, Expected mass = 271.97.

2.9.53 1-((Benzamido)sulfanylenemethyl)urea (53)

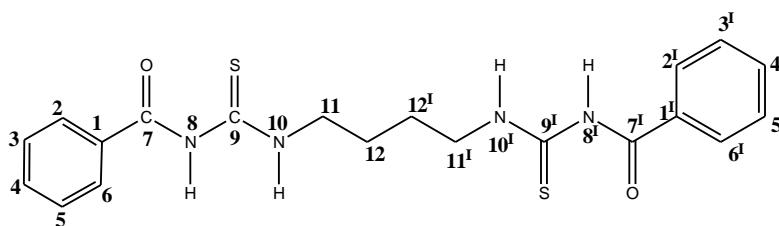
Compound **53** was accessed by dissolving ammonium thiocyanate (0.04 mol, 3.05 g) in 80 mL of acetone, benzoyl chloride (0.04 mol, 5.62 g) was then added and heated under reflux at 100–120 °C for 2 h. The benzoyl isothiocyanate (0.04 mol)



obtained was filtered, urea (0.04 mol, 2.40 g) was added to resulting benzoyl isothiocyanate solution and refluxed for 6 h. The mother liquor was allowed to stand overnight in a fume hood. The product obtained was filtered and recrystallized from DMSO:Toluene (1:1) as a yellow solid. Melting point = 124–126 °C. Yield = 88.2%. ¹H NMR (ppm): 13.23 (br, 1H, N–H), 11.29 (br, 1H, N–H), 7.84 (d, 2H, *J* = 7.2 Hz, (**2**, **6**)), 7.64 (t, 1H, *J* = 7.6 Hz, (**4**)), 7.56 (t, 2H, *J* = 7.6 Hz, (**3**, **5**), ¹³C NMR (ppm): 179.8 (C=S), 154.8 (C=O), 134.1, (**4**), 129.5, (**3**, **5**), 128.6 (**2**, **6**),. IR (ν_{\max} , cm⁻¹): 3343 (N–H), 3197 (N–H), 1651 (C=O), 1615 (C=O), 1577 (C=C), 1528 (C–N), 1489 (C–N), 1449 (C–N). Anal. Calcd for C₉H₉N₃O₂S: C, 48.42; H, 4.06; N, 18.82; S, 14.36. Found: C, 48.53; H, 4.01; N, 18.34; S, 14.45. LRMS (*m/z*, M⁺): Found for C₉H₉N₃O₂S = 223.10, Expected mass = 223.25.

2.9.54 3-Benzoyl-1-(4-[[[(phenylformamido)methanethioyl]amino]butyl]thiourea (54)

Compound **54** was accessed by dissolving ammonium thiocyanate (0.04 mol, 3.05 g) in 80 mL of acetone, benzoyl chloride (0.04 mol, 5.62 g)



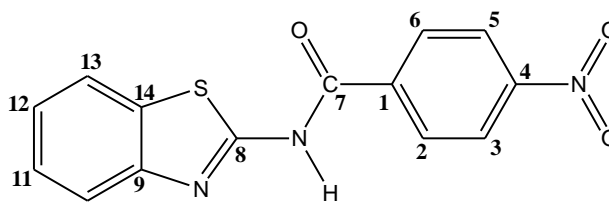
was then added and heated under reflux at 100–120 °C for 2 h. The benzoyl isothiocyanate (0.04 mol) obtained was filtered, 1,4-butanediamine (0.04 mol, 3.53 g) was added to the resulting benzoyl isothiocyanate solution and refluxed for 6 h. The solvent was reduced to a smaller volume and redissolved in methanol. The product was filtered and recrystallized from DMSO:Toluene (1:1) as a light brown solid. Melting point = 159–161 °C. Yield = 80.8%. ¹H NMR (ppm): 11.24 (s, 1H), 10.94 (br, 1H), 7.90 (d, 2H, *J* = 8.0 Hz, (**2**, **6**, **2'**, **6'**)), 7.62 (t, 1H, *J* = 7.2, 7.6 Hz, (**4**, **4'**)), 7.48 (t, 2H, *J* = 7.6 Hz, (**3**, **5**, **3'**, **5'**)), 3.76 (m, 4H, (**11**, **11'**)), 2.51, (br, 2H, N–H (**8**, **8'**)), 2.06 (t, 2H, N–H(**10**, **10'**)) ¹³C NMR (ppm): 180.2 (C=S), 167.7 (C=O),

132.9 (**1**, **1^I**), 132.2 (**4**, **4^I**), 128.4 (**3**, **5**, **3^I**, **5^I**), 128.3 (**2**, **6**, **2^I**, **6^I**), 42.6 (**11**, **11^I**), 26.7 (**12**, **12^I**). IR (ν_{\max} , cm^{-1}): 3405 (N–H), 3217 (N–H), 2929 (C–H), 1666 (C=O), 1511 (C=C), 1432 (C–N). Anal. Calcd for $\text{C}_{20}\text{H}_{22}\text{N}_4\text{O}_2\text{S}_2$: C, 57.95; H, 5.35; N, 13.32; S, 15.47. Found: C, 57.87; H, 5.42; N, 13.45; S, 15.36. LRMS (m/z , M^+): Found for $\text{C}_{20}\text{H}_{22}\text{N}_2\text{O}_2\text{S}_2 = 414.70$, Expected mass = 414.54.

2.9.55 *N*-(Benzothiazol-2-yl)-4-nitrobenzamide (**55**)

3-(1,3-Benzothiazol-2-yl)-1-(4-

nitrobenzoyl)thiourea (**30**) (0.08 mmol, 24 mg) was dissolved in 10 ml of THF, and then dimethylsulfoxide gold(I) chloride (0.08 mmol, 20 mg) or gold (III) chloride

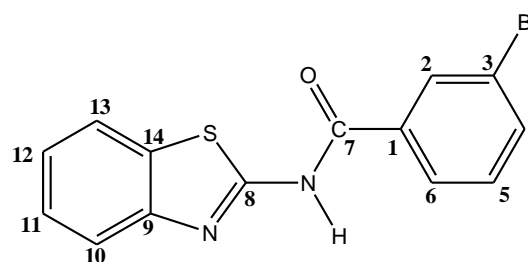


(0.08 mmol, 24 mg) was added in the absence of light and stirred under nitrogen at 60 °C for 4 h. The reaction mixture was filtered and allowed to stand overnight. The product that formed was recrystallized from methanol as a white solid of melting point = 295–296 °C. Yield = 42.0%. ^1H NMR (ppm): 8.39 (q, 4H, $J = 6.8, 8.8$ Hz, (**2**, **3**, **5**, **6**)), 8.05 (d, 1H, $J = 8.0$ Hz, (**10**)), 7.81 (d, 1H, $J = 8.0$ Hz, (**13**)), 7.50 (d, 1H, $J = 7.6, 8.0$ Hz, (**11**)), 7.37 (t, 1H, $J = 7.6$ Hz, (**12**)). IR (ν_{\max} , cm^{-1}): 3117 (N–H), 3038 (N–H), 1686 (C=O), 159 (C=C), 1522 (C=C), 1461 (C–N), 1441 (C–N). Anal. Calcd for $\text{C}_{14}\text{H}_9\text{N}_3\text{O}_3\text{S}$: C, 56.18; H, 3.03; N, 14.04; S, 10.71. Found: C, 56.05; H, 3.01; N, 13.96; S, 10.52. LRMS (m/z , M^+): Found for $\text{C}_{14}\text{H}_9\text{N}_3\text{O}_3\text{S} = 299.70$, Expected mass = 299.50.

2.9.56 *N*-(Benzothiazol-2-yl)-3-bromobenzamide (**56**)

3-(1,3-Benzothiazol-2-yl)-1-(3-bromobenzoyl)

thiourea (**31**) (0.08 mmol, 25 mg) was dissolved in 10 ml of THF, dimethylsulfoxide gold(I) chloride (0.08 mmol, 20 mg) or gold (III) chloride (0.08 mmol, 24 mg) was added in the absence of light and stirred under nitrogen at 60

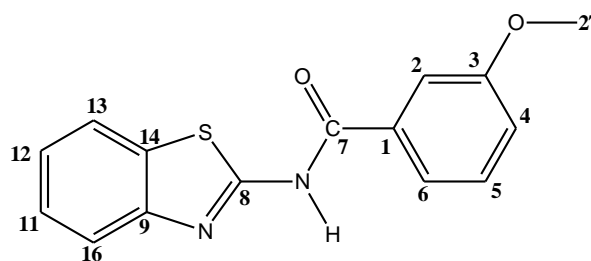


°C for 4 h. The reaction mixture was filtered and allowed to stand overnight. The product

recrystallized from methanol as a white solid of melting point = 194–196 °C Yield = 42.0%. ¹H NMR (ppm): 8.35 (s, 1H, (2,6)), 8.12 (d, 1H, *J* = 8.0 Hz, (10)), 8.02 (d, 1H, *J* = 8.4 Hz, (13)), 7.86 (d, 1H, *J* = 8.4 Hz, (6, 2)), 7.79 (d, 1H, *J* = 8.4 Hz, (4)), 7.55 (t, 1H, *J* = 7.6, 8.4 Hz, (5,3)), 7.49 (t, 1H, *J* = 7.6, 6.8 Hz, (11)), 7.36 (t, 1H, *J* = 7.6, 6.8 Hz, (12)). IR (ν_{\max} , cm^{-1}): 3066 (N–H), 2918 (C–H), 2850 (C–H), 1677 (C=O), 1654 (C=O), 1600 (C=C), 1555 (C=C), 1522 (C=C), 1453 (C–N), 1425 (C–N). Anal. Calcd for C₁₄H₉BrN₂OS: C, 50.46; H, 2.72; N, 8.41; S, 9.62. Found: C, 50.65; H, 2.63; N, 8.57; S, 9.73 LRMS (*m/z*, M⁺): Found for C₁₄H₉BrN₂OS = 333.10, Expected mass = 333.20.

2.9.57 *N*-(Benzothiazol-2-yl)-3-methoxybenzamide (57)

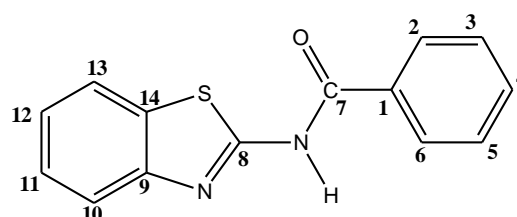
3-(1,3-Benzothiazol-2-yl)-1-(3-methoxybenzoyl) thiourea (27) (0.07 mmol, 23 mg) was dissolved in 10 ml of THF, dimethylsulfoxide gold(I) chloride (0.07 mmol, 23 mg) or gold (III) chloride (0.07 mmol, 21 mg) was added in the absence of



light and stirred under nitrogen at 60 °C for 4 h. The reaction mixture was filtered the solvent was removed and the product recrystallized from methanol as a yellow solid of melting point = 170–176 °C. Yield = 38.0%. ¹H NMR (ppm): ¹H NMR (ppm): 11.58 (s, 1H, N–H), 8.02 (t, 1H, *J* = 7.2 Hz, (10)), 7.77 (m, 1H, *J* = 6.8, 7.6 Hz, (13)), 7.73 (s, 1H, (2)), 7.54–7.47 (m, 3H, (6, 11, 12)), 7.37 (m, 1H, (5)), 7.21 (m, 1H, (4)). IR (ν_{\max} , cm^{-1}): 3458 (N–H), 3290 (N–H), 2922 (N–H), 2852 (C–H), 1686 (C=O), 1578 (C=C), 1538 (C=C), 1448 (C–N), 1426 (C–N). Anal. Calcd for C₁₅H₁₂N₂O₂S: C 63.36; H, 4.25; N, 9.85, S, 11.28. Found: C 63.41; H, 4.33; N, 9.93, S, 11.32. LRMS (*m/z*, M⁺): Found for C₁₅H₁₂N₂O₂S = 284.20, Expected mass = 284.33.

2.9.58 *N*-(Benzothiazol-2-yl)benzamide (58)

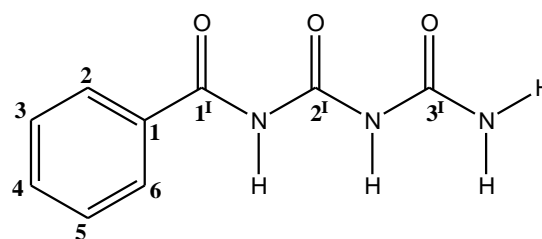
3-Benzothiazol-2-yl)-1-(benzoyl)thiourea (23) (0.09 mmol, 28 mg) was dissolved in 10 ml of THF, dimethylsulfoxide gold(I) chloride (0.09



mmol, 28 mg) or gold (III) chloride was added in the absence of light and stirred under nitrogen at 60 °C for 4 h. The reaction mixture was filtered the solvent was removed and the product recrystallized from methanol as a white solid of melting point = 115–117 °C. Yield = 47.0%. ¹H NMR (ppm): 8.35 (s, 1H, (**10**)), 8.14 (d, 1H, *J* = 7.6 Hz, (**13**)), 8.04 (d, 1H, *J* = 8.0 Hz, (**2**)), 7.88 (d, 1H, *J* = 7.6 Hz, (**6**)), 7.81 (d, 1H, *J* = 7.6 Hz, (**3**)), 7.69 (m, 1H, *J* = 8.0 Hz, (**6**)), 7.55 (t, 1H, *J* = 7.2, 7.6 Hz, (**11**)), 7.49 (t, 1H, *J* = 7.2, 8.0 Hz, (**12**)), 7.36 (t, 1H, *J* = 7.6 Hz, (**4**)). ¹³C NMR (ppm): 136.1 (**1**), 131.5 (**4**), 127.9 (**3**, **5**), 126.9 (**3**, **6**), 124.3 (**11**, **12**), 122.3 (**10**, **13**). IR (ν_{\max} , cm^{-1}): 3273 (N–H), 3059 (N–H), 2917 (C–H), 1693 (C=O), 1599 (C=C), 1549 (C=C), 1456 (C–N), 1442 (C–N). Anal. Calcd for C₁₄H₁₀N₂OS: C, 66.12; H, 3.96; N, 11.02; S, 12.61. Found: C, 65.98; H, 4.05; N, 11.10; S, 12.55. LRMS (*m/z*, M⁺): Found for C₁₄H₁₀N₂OS = 254.42, Expected mass = 254.31.

2.9.59 1-((Benzamido)formyl)urea (**59**)

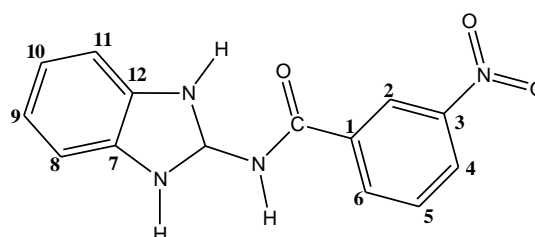
Compound **52** (0.009 mol, 2.03 g) was refluxed in THF (20 mL) for 8 h with silver nitrate (0.009 mol, 1.55 g). The reaction mixture was then extracted with diethyl ether:methanol(1:1) (100 mL) and filtered over celite. The solvent



was removed at the pump. The product recrystallized from DMSO:Toluene (1:1) as a the white fluffy solid of melting point 204–206 °C. Yield = 33.0%. ¹H NMR (ppm): 7.82 (d, 2H, *J* = 8.0 Hz, (**2**, **6**)), 7.53 (t, 1H, *J* = 8.0 Hz, (**3**, **5**)), 7.45 (t, 2H, *J* = 7.6 Hz (**4**)). ¹³C NMR (ppm): 169.6 (C=O), 133.9 (**1**), 132.1 (**4**), 128.8 (**2**, **6**), 127.8 (**3**, **5**). IR (ν_{\max} , cm^{-1}): 3345 (N–H), 3225 (N–H), 1710 (C=O), 1663 (C=O), 1598 (C=C), 1578 (C=C), 1466 (C–N). Anal. Calcd for C₉H₉N₃O₃: C 52.17; H, 4.38; N, 20.28. Found: C 52.37; H, 4.45; N, 20.40. LRMS (*m/z*, M⁺): Found for C₉H₉N₃O₃ = 207.06, Expected mass = 207.19.

2.9.60 *N*-(2,3-Dihydro-1*H*-benzimidazol-2-yl)-3-nitrobenzamide (**60**)

Compound **44** (0.0019 mol, 1.006 g) was refluxed in THF (20 mL) for 8 h with silver nitrate (0.0017 mol mol, 0.29 g) The reaction



mixture was then extracted with diethyl ether:methanol(1:1) (100 mL) and filtered over celite. The solvent was removed at the pump. The product recrystallized from DMSO:Toluene (1:1) as a light yellow solid of melting point 158–159 °C. Yield = 45.0%. ¹H NMR (ppm): 8.88 (s, 1H, **(2)**), 8.49 (d, 1H, *J* = 7.6 Hz, **(4)**), 8.42 (d, 1H, *J* = 7.6 Hz, **(6)**), 7.81 (t, *J* = 7.6, 8.0 Hz, **(5)**), 7.52 (m, 2H, **(8, 11)**), 7.29 (m, 2H, **(9, 10)**). ¹³C NMR (ppm): 148.1, **(3)**, 135.3 **(7, 12)**, 130.5 **(1)**, 130.4 **(6)**, 124.0 **(5)**, 123.6 **(9, 10)**, 113.1 **(8, 11)**. IR (ν_{\max} , cm^{-1}): 3321(N–H), 3100 (N–H), 1703 (C=O), 1634 (C=O), 1531 (C=C), 1471 (C–N), 1447 (C–N). Anal. Calcd for C₁₄H₁₂N₄O₃: C 59.15; H, 4.25; N, 19.71. Found: C 59.43; H, 4.32; N, 19.59 LRMS (*m/z*, M⁺): Found for C₁₄H₁₂N₄O₃ = 284.14, Expected mass = 284.27.

2.10 Cytotoxicity assay protocol

The acute cytotoxic effects of the compounds were determined by exposing them to isolated human white blood cells, for a 24 h period. The cell viability was assessed using the MTT reduction assay. Briefly, white blood cells were seeded at 25000 cells/well and exposed to varying concentrations (500, 50, 5, 0.5 and 0.05 μM) of the compounds. Following the 24 h exposure period, MTT was added to the wells and the plates were incubated at 37 °C for 3 h. The resulting formazan crystals formed were dissolved with DMSO and the absorbance at 405 nm was measured using a BioTek Epoch2 microtitre plate reader. The results of this study are presented in Table 4.3 which indicates the compound numbers (in bold) as well as the EC₅₀ values calculated for each compound tested.

Whole blood was collected from healthy volunteers (*n* = 3, 50 ml/person, ethical clearance number H15-SCI-BCM-002) in EDTA acid vacutainers and centrifuged at 500 x *g* (10 min). The supernatant (buffy coat) was retained. The blood samples were further centrifuged at 2000 x *g* (10 min) and the supernatant (buffy coat) aspirated. Lysis buffer (0.15 M NH₄Cl, 1 mM KHCO₃, 0.1 mM EDTA, pH 7.4) was then added with a blood:buffer ratio of 1:9. It was then vortexed for 10 seconds and incubated at room temperature for 3 min. Centrifuging was completed at 2000 x *g* (10 min.) and the pellets retained and washed with 3 ml of lysis buffer and centrifuged at 1000 x *g* for 5 min., this step was repeated thrice. The white blood cells were diluted in 10 mL RPMI media and supplemented with 5 % FBS and 50 $\mu\text{g}/\text{mL}$ PenStrep. The white blood cells were stained with 0.4% trypan blue and counted with a haemocytometer, the cells were then seeded at 100 $\mu\text{L}/\text{well}$, 250000 cells/well in 96-well

plates. The cells were exposed to 20 μ L of the compounds (500, 50, 5, 0.5 and 0.05 μ M) were added for a 24 h period, camptothecin was added as a positive control, whilst PBS:DMSO (990:10) was added as a vehicle control and RPMI media used as untreated control. 20 μ L of 3-(4,5-dimethylthiazol-2-yl)-2, 5-diphenyltetrazolium bromide (MTT)²⁷⁴ reagent (0.50 mg/mL final concentration in the well) was added and incubated for 3 h at 37 °C. 100 μ L DMSO was added, mixed gently and Incubated for 15 min at 37 °C it was then shaken for 5 min using the microplate reader and the absorbance measured at $A_{560\text{ nm}}$.

2.10.1 Determination of EC₅₀ values

The term half maximal effective concentration (EC₅₀) refers to the concentration of a drug, antibody or toxicant which induces a response halfway between the baseline and maximum after a specified exposure time.²⁷⁵ It is commonly used as a measure of drug's potency. The EC₅₀ of a graded dose response curve therefore represents the concentration of a compound where 50% of its maximal effect is observed. The EC₅₀ values were determined based on the dose response curve.²⁷⁶ Different concentrations gave different absorbance values. A small change in ligand concentration typically result in rapid changes in response in the biological system, following a sigmoidal function. The concentration of ligand at half maximum activity is the EC₅₀.²⁷⁷⁻²⁷⁸

2.11 HIV-1 Protease assay

The kinetic profile of HIV-1 protease was characterized at various inhibitor concentrations (100 nM to 0.0500 nM) by measuring the cleavage of the synthetic substrate (Abz-Thr-Ile-pNO₂Phe-Gln-Arg-NH₂) concentrations at an excitation/emission wavelength of 340 nm/490 nm using a BioTek SynergyMx fluorimeter. Positive controls used in the assay were pepstatin (14 nM to 0.080 mM) and ritonavir (100 nM to 0.05 nM). The fluorescence was measured using a BioTek SynergyMx microtitre plate reader. Excitation/Emission: 340 nm/490 nm. This assay is based on the ability of protease to cleave (Abz-Thr-Ile-pNO₂Phe-Gln-Arg-NH₂) It cleaves the Abz-Thr bond which causes Abz to fluoresce the rate of fluorescence is then measured over time. Buffer 1 (72.73 mM NaAc, pH 5.0) (55 μ L) was added to the followed inhibitor (20 μ L), 20 μ L of protease (20 nM) was added to the well and incubated at 25°C for

an hour. 120 μL of the substrate (Abz-Thr-Ile-pNO₂Phe-Gln-Arg-NH₂) dissolve in buffer 2 (60 mM NaAc, 2 M NaCl, 2.4% DMSO, pH 5.0) was added per well (50 μM). The substrate was prepared by dissolving the fluorogenic substrate (10 mg) in 50% acetonitrile (20 mL) and further diluting the the stock to 83.3 μM with buffer 2 (1.44 mL substrate + 7.2 mL buffer 2). The stock was covered with aluminium foil and stored at -80°C . The mixture was incubated for 30 seconds. The reaction rate was measured using relative fluroscence at Ex 337 nm/Em 425 nm using a BioTek SynergyMx microtitre plate reader, every second for 1 minute (Excitation bandwidth = 2.5 nm; Emission bandwidth = 5 nm)

2.11.1 Optimiszation of HIV-1 protease concentration screen of structurally diverse diamine derivatives of benzoyl isothiocyanate

HIV-1 protease activity was assayed at varying concentrations (2–20 nM) of the protease in order to ascertain the optimal concentration to employ in the assay. The concentrations tested in the assay are listed in **Table 2.2**. The rate is obtained from the gradient of the fluorescence plotted time. It gives the rate of change in fluorescence with time. A lower rate signify a smaller quantity of a fluorogenic species is product per unit time. Whilst a higher rate signify that a higher quantity of fluorogenic species is produced per unit time due cleavage by protease hence it can be linked directly to protease activity.

Table 2.2 Determination of optimal HIV-1 protease concentration for use in inhibitor studies.

Concentration (nM)	Rate
1	-9.3841
2	6.3757
5	46.814
10	503.58
20	896.66

Examples of the progress curves obtained for the hydrolysis of HIV-1 protease substrate by HIV-1 protease are shown in **Figure 2.1**. The rate is the gradient obtained from the progress curves for the different concentrations.

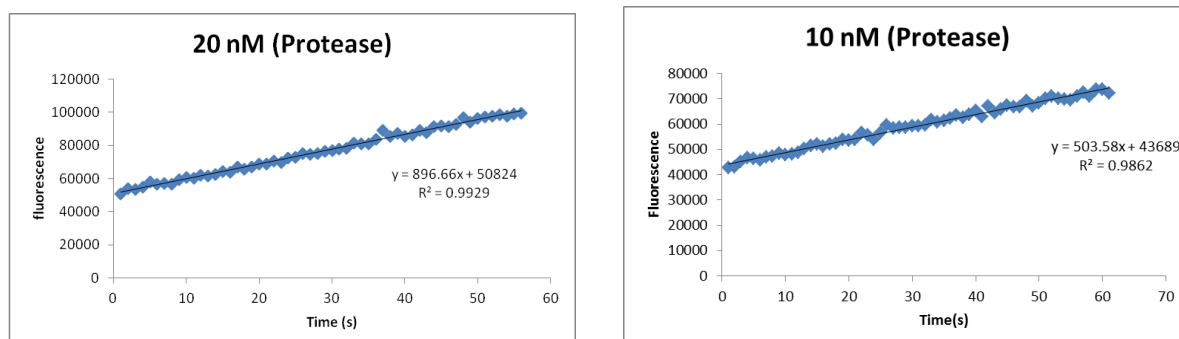


Figure 2.1 Progress curves for the hydrolysis of [Abz-Thr-Ile-pNO₂Phe Gln-Arg-NH₂] by HIV-1 Protease. Ex/Em: 337/425 nm at 25 °C and a pH of 5.0.

From the results above, it was decided that 20 nM of protease would be the best concentration for the assay because it had an optimal rate.

CHAPTER THREE

DESIGN AND SYNTHESIS OF BENZOYL ISOTHIOCYANATE DERIVATIVES

3.1 Design and synthesis of benzoyl isothiocyanate derivatives: preliminary studies

The premise of this work was to first screen potential compounds which are based on the benzimidazole moiety for HIV-1 protease activity using Autodock 4.2 and to synthesize the compounds that give good predicted inhibition constants. The initial pre-screening gave the predicted inhibition constants for the following scaffolds (**Figures 3.1** and **3.2**). **Table 3.1** gives the pre-screening results for some of the derivatives whilst **Figure 3.3** gives the ligand binding in the active site for the alanine derivative.

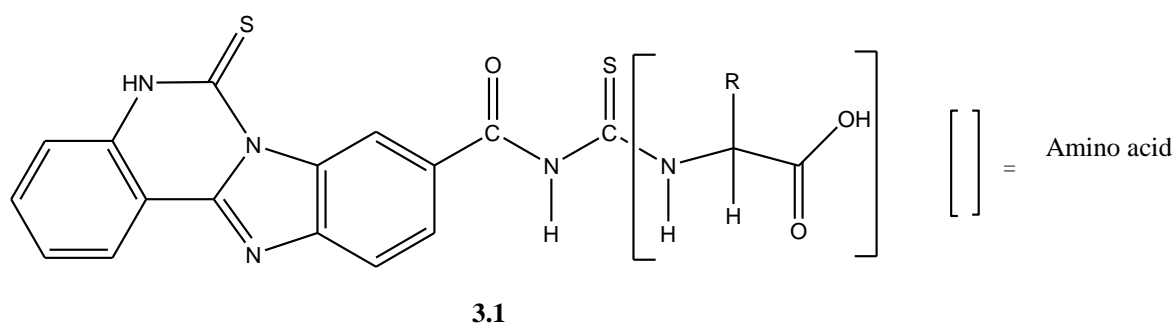


Figure 3.1 The scaffold obtained from the initial pre-screening **Scheme 3.1**

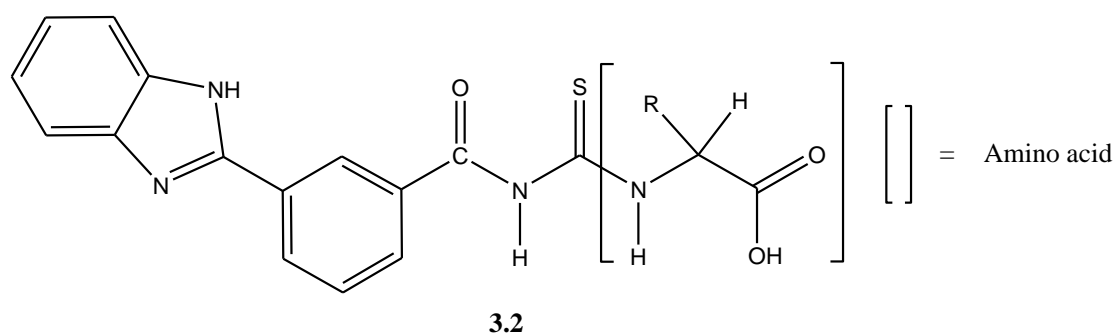
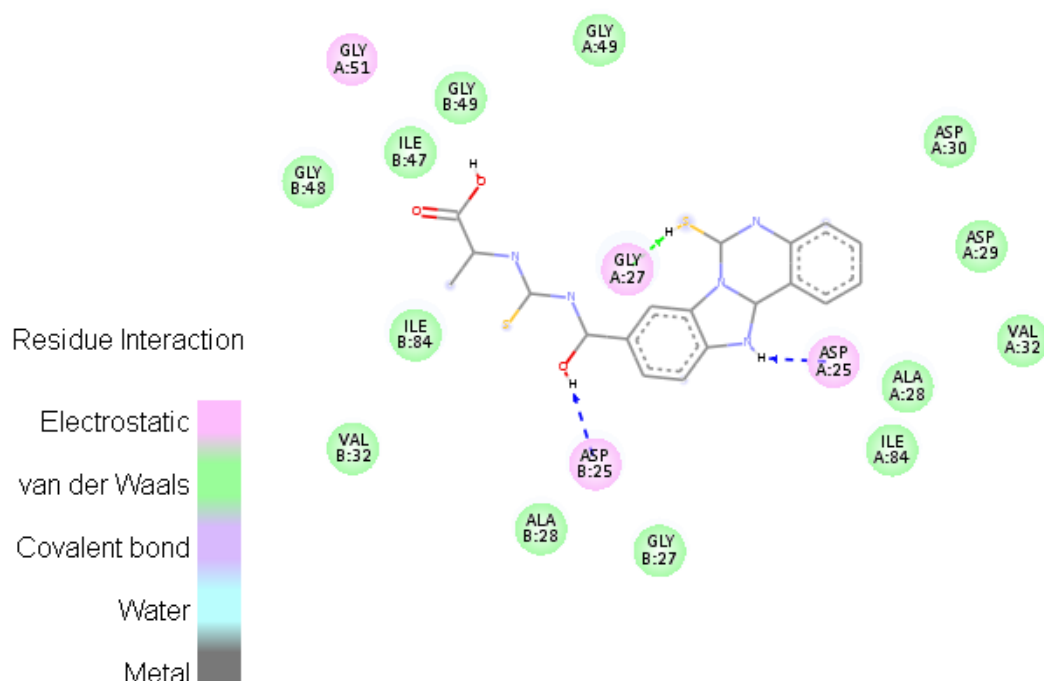


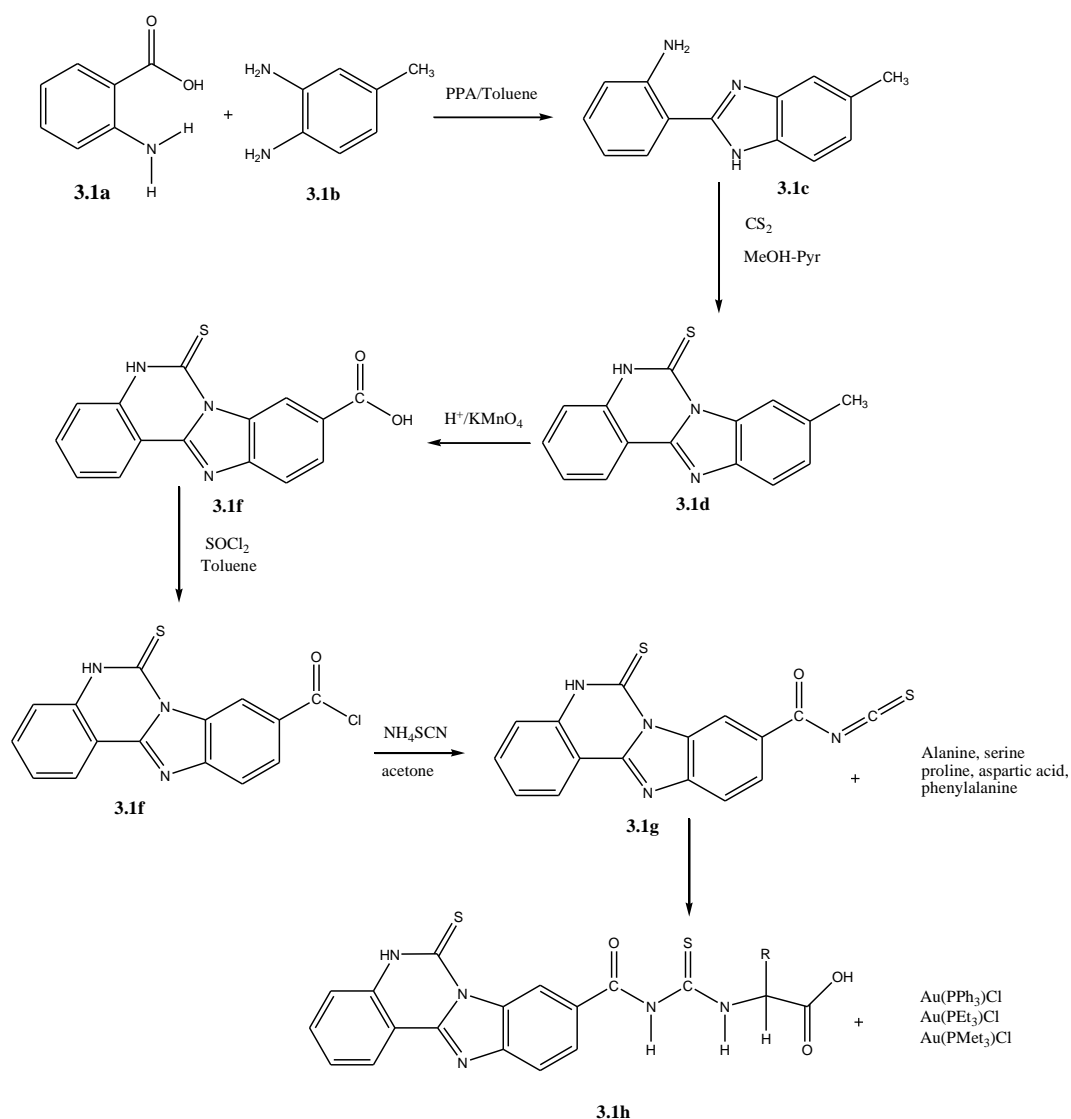
Figure 3.2 The scaffold obtained from the initial pre-screening **Scheme 3.2**

Table 3.1 Pre-screening result for the potential HIV-1 inhibitors (**Schemes 3.1**).

Description code	Free binding energy	Inhibition constants K_i (μM) (Scheme 3.1)
Alanine derivative	-7.25	4.85
Aspartic acid derivative	-7.59	2.72
Amprenavir	-4.28	728.93
Proline derivative	-7.72	2.19
Serine derivative	-8.33	0.79
Phenylalanine derivative	-6.85	9.59

**Figure 3.3** Ligand binding interaction in protease active site for the alanine derivative.

Based on the pre-screening results **schemes 3.1** and **3.2** were developed to access the docked compounds.



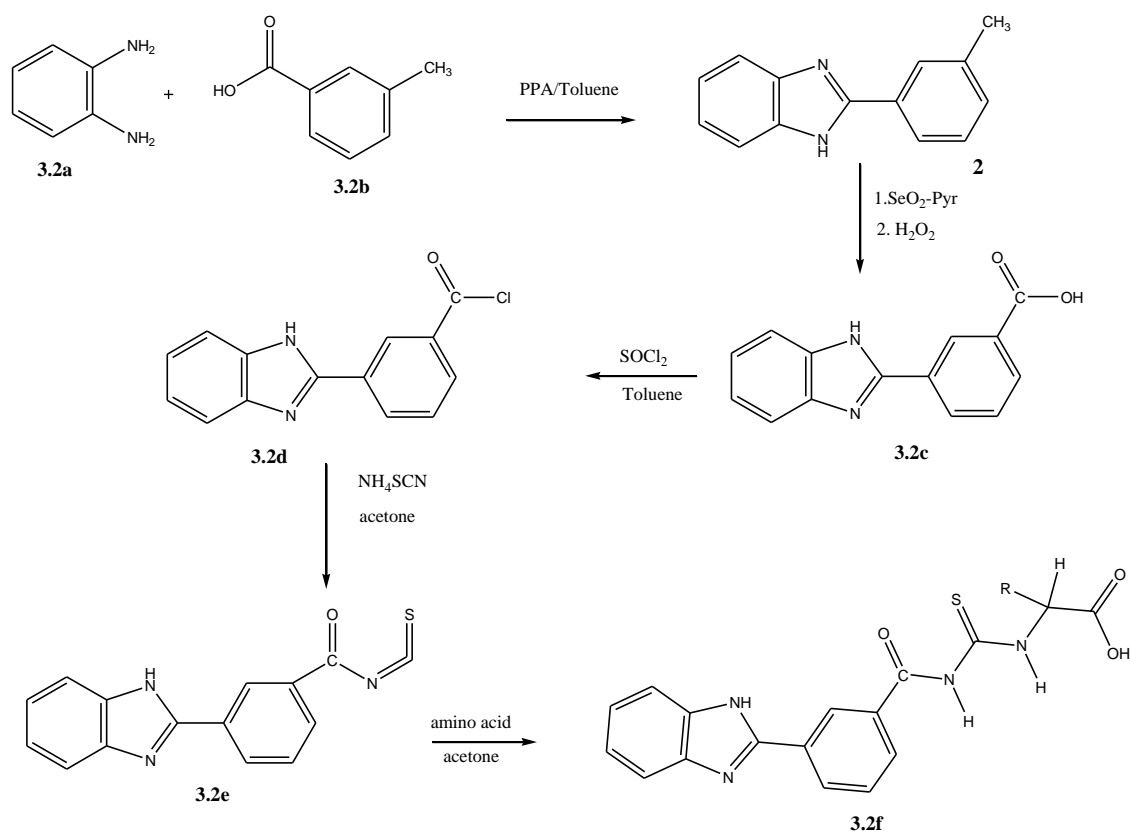
Scheme 3.1 Proposed synthetic path to access some of the docked compounds.

The first step of **Scheme 3.1** gave a de-aminated product which could not be taken further. The excess acid protonated the amine group which easily deaminated upon heating.

Table 3.2 Pre-screening result for the potential HIV-1 inhibitors (**Scheme 3.2**).

Description code	Free binding energy	Inhibition constants K_i (μM) (Scheme 3.2)
Tyrosine derivative	-9.58	5.88
Serine derivative	-5.92	45.97
Proline	-6.45	18.61
Methionine derivative	-5.86	50.65

The synthesis of the compounds in **Scheme 3.2** was then attempted.



Scheme 3.2 Proposed synthetic path to access some of the docked compounds (**Figure 3.2**).

3.2 Synthesis and crystal structures of 3-methyl-*N*-[2-(3-methylbenzamido)phenyl]benzamide (**1**) and 2-(3-methylphenyl)-1*H*-benzimidazole (**2**)

To access the compounds in **scheme 3.2** an attempt at synthesizing a benzimidazole by heating in 4 N HCl for 4 h was unsuccessful as the starting materials were recovered. Refluxing in 1 M sodium hydroxide and 1 M sulfuric acid were equally unsuccessful. 3-Methylbenzoic acid was converted to the acid chloride by heating it with thionyl chloride in toluene at 120 °C for 3 h. An attempt to convert the acid chloride into a benzimidazole by reacting it with *o*-phenylenediamine in pyridine gave 3-methyl-*N*-[2-(3-methylbenzamido)phenyl]benzamide (**1**) (**Scheme 3.4**). Critical to the success of this reaction is the anhydrous atmosphere and the lower temperature of the reaction ensuring that the activation energy for the formation of a diamide is not achieved. This allows a single attack by the lone pair of electrons on the amine leading to the formation of a benzimidazole, whilst in our case the

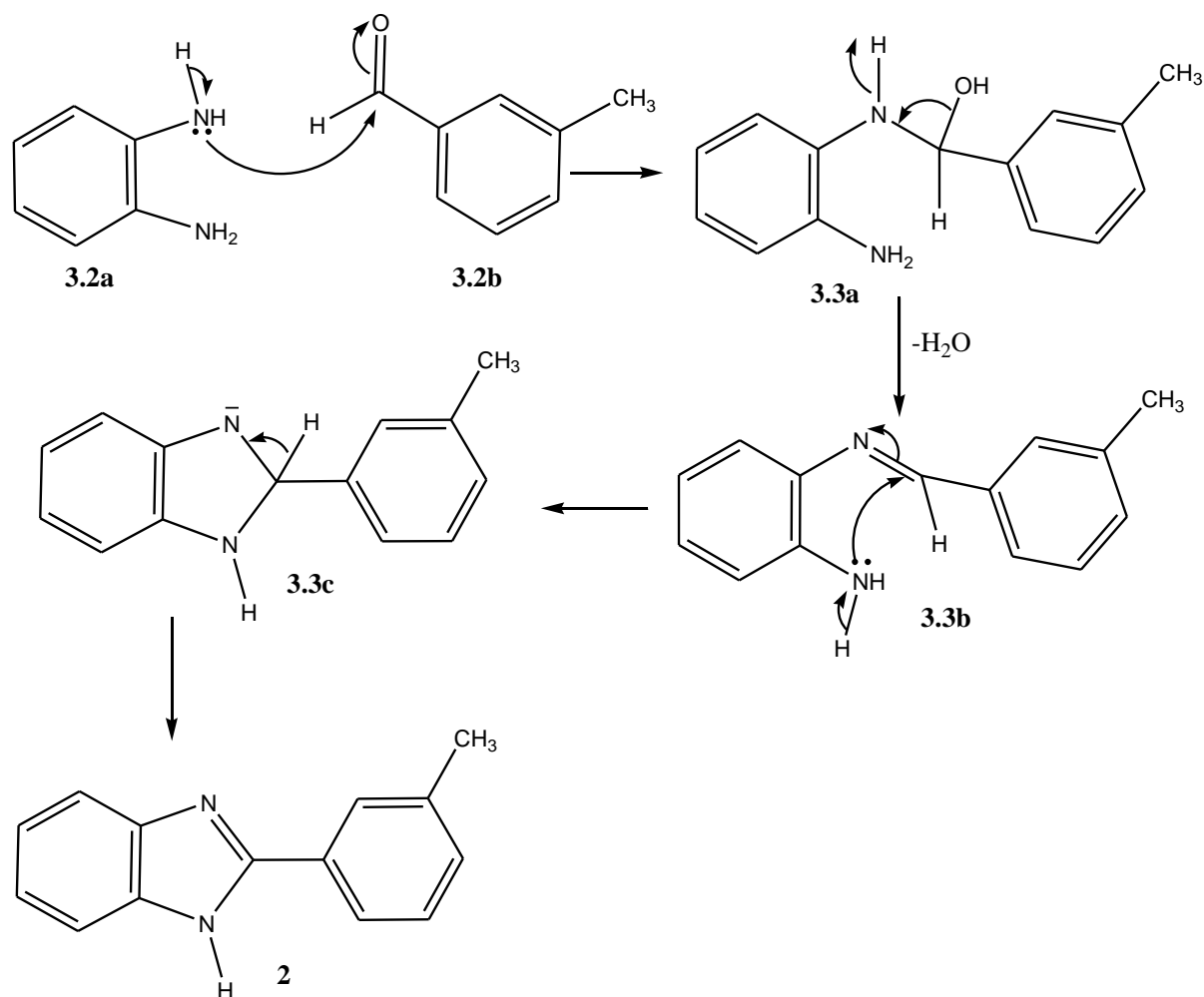
reaction was attempted at an elevated temperature making a single attack not achievable. The synthesis of the diamide was readily achieved by the nucleophilic attack of the carbonyl by the diamine with the subsequent loss of a hydrogen chloride gas and this process is aided by the presence of a base such as pyridine which takes up the protons from solution (**Scheme 3.3**). The ease of loss of the chloride makes it easy for the amide to be formed but the absence of a proton source to protonate the carbonyl makes the second attack of the carbonyl by the other amine impossible. This resulted in the formation of an amide on the second amine of the diamines (diamide formation) rather than the cyclization to form a benzimidazole.

Acyl halides enable facile access to amides and they are prepared using chlorinating agents such as thionyl chloride, oxalyl chloride, phosphorus trichloride and phosphorus pentachloride.^{279, 280} The acyl halide is not absolutely necessary, ZnO has been used as a catalyst in the formation of amides from formic acid and amines under solvent-free conditions at 70 °C,²⁸¹ with excellent yield in short reaction times with reusability of catalyst. Extension to other catalysts have been reported, with catalytic amounts of indium trioxide being used in the conversion of carboxylic acid esters to primary amides,²⁸² and Han *et al*,²⁸³ have reported a process for preparation of amides from esters and amines using a catalytic system comprised of Group IV metal alkoxides in conjunction with additives including 1-hydroxy-7-azabenzotriazole (HOAt). In this case, the ester-amide exchange proceeds using a variety of structurally diverse esters and amines without azeotropic reflux to remove the alcohol by-product. Hydrogen peroxide has been used in the catalytic oxidative amidation between aldehydes and amines using Pd-Cl₂-xantophos as a catalyst in methanol under acidic conditions.²⁸⁴ *N*-Heterocyclic carbene-based ruthenium complexes have been developed as highly active catalysts for direct amide synthesis from alcohols and amines.²⁸⁵

A reaction of *m*-toluic acid with *o*-phenylenediamine in the presence of polyphosphoric acid in toluene which gave 2-(3-methylphenyl)-1*H*-benzimidazole (**2**) was then carried out. The reaction is thought to proceed by the protonation of the hydroxyl group and the subsequent attack of the carbonyl carbon by one of the amines with the loss of water from the carboxylic acid. The subsequent protonation of the carbonyl enables it to be attacked by the other amine group leading to the loss of water. This reaction is driven by high temperature and excess of protons. The workup to remove the excess polyphosphoric acid can complicate the purification.

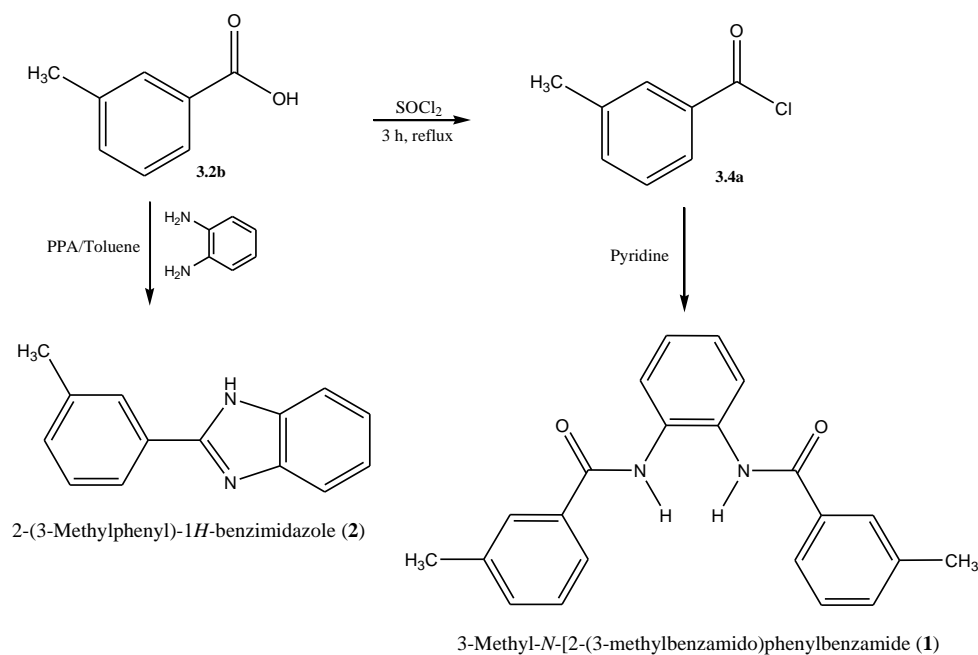
The common route for the synthesis of benzimidazoles from diamines is through a condensation reaction with carboxylic acids under acid catalysis at high temperatures.²⁸⁶ A series of benzimidazoles have also been synthesized by the reaction of phenylenediamine and carboxylic acids under solvent free conditions.²⁸⁷ The aldehyde route has also been explored to achieve benzimidazoles from diamines despite the fact that monoimines or diimines should be the expected products. 2-Substituted benzimidazoles have been synthesized in the presence of alumina–methanesulfonic acid (AMA) by microwave irradiation.²⁸⁸ Catalytic amounts of zinc acetate have been used to synthesize benzimidazoles from aldehydes and *o*-phenylenediamine at room temperature.²⁸⁹ Boron trifluoride dietherate has also been used to catalyze the synthesis of benzimidazoles from *o*-phenylenediamine and aldehydes under solvent free conditions.²⁹⁰

The synthesis of compound **2** has been achieved by reacting *m*-tolualdehyde with *o*-phenylenediamine in the presence of triethylamine. The reaction is proposed to proceed by the abstraction of a proton by triethylamine from an amine of the *o*-phenylenediamine **3.1a** this allows the attack of the carbonyl of the aldehyde **3.2b** by the amine forming a hydroxylamine **3.3a**, the loss of water from **3.3a** gives an imine **3.3b** which loses a proton to give **3.3c**, a further proton loss in the presence of molecular oxygen and rearrangement leads to the formation of **2**.



Scheme 3.3 Proposed mechanism for the synthesis of compound **2** from an aldehyde.

Compound **2** have been reported to be accessed by a one pot microwave promoted synthesis using sodium hydrogen sulfite in dimethylacetamide.²⁹¹ Shen *et al* have also reported the synthesis of compound **2** from aryl azides using Iron (III) bromide as catalyst.²⁹² An attempt to convert the methyl group in compound **2** to the carboxylic acid using acidified potassium dichromate was not successful. The use of selenium dioxide-pyridine in DMSO led to the recovery of the starting materials whilst the use of potassium permanganate in benzene and 3 mol % of 18 crown 6 was also not successful.



Scheme 3.4 A synthesis scheme of 3-methyl-*N*-[2-(3-methylbenzamido)phenyl]benzamide (1) and 2-(3-methylphenyl)-1*H*-benzimidazole (2).

The FTIR spectrum of compound 1 (Figure 3.4) gave a band at 3272 cm^{-1} for the N–H and a band at 2916 cm^{-1} for the aliphatic C–H. The C=O stretch of an amide occurred at 1644 cm^{-1} whilst the aromatic C=C stretch occurred at 1596 cm^{-1} . It gave the C–N stretch at 1513 cm^{-1} and the C–O stretch occurred at 1276 cm^{-1} .

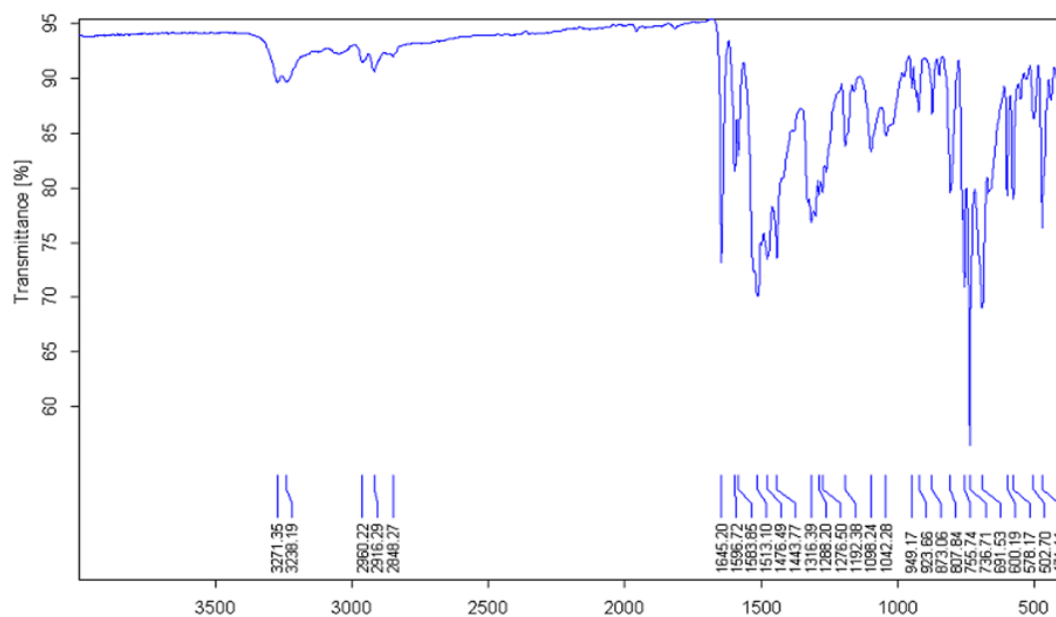


Figure 3.4 IR spectrum of 3-methyl-*N*-[2-(3-methylbenzamido)phenyl]benzamide (1).

The IR spectrum of **2** (**Figure 3.5**) gave a band at 3052 cm^{-1} for the N–H stretch, whilst the aliphatic C–H stretch occurred at 2986 cm^{-1} and 2879 cm^{-1} . The C=N stretch occurred at 1661 cm^{-1} whilst the C=C stretch of an aromatic ring occurred at 1590 cm^{-1} . The C–N stretch occurred at 1487 cm^{-1} .

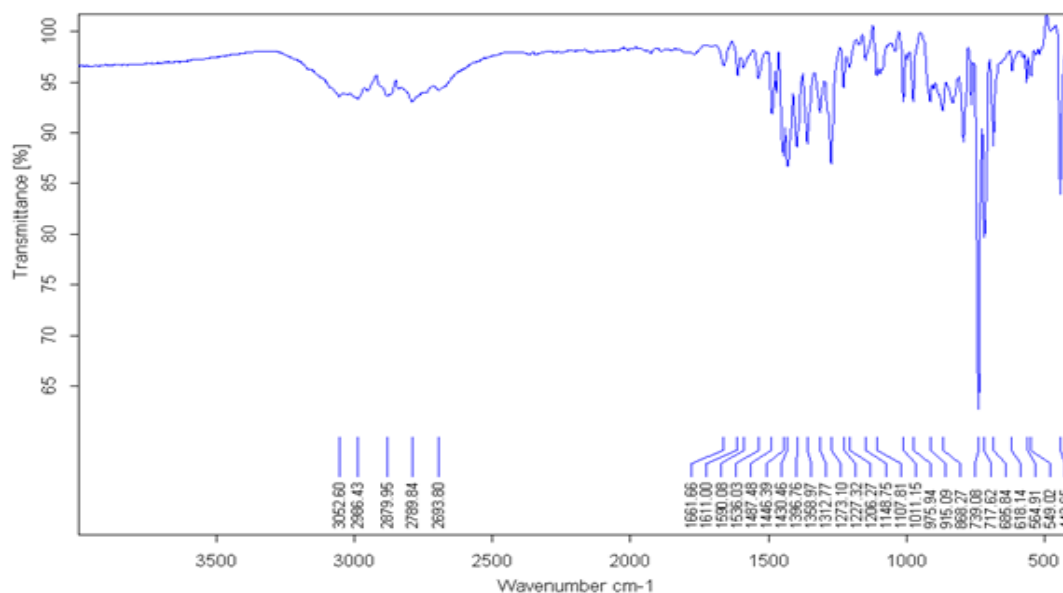


Figure 3.5 IR spectrum of 2-(3-methylphenyl)-1H-benzimidazole (**2**).

The ^1H NMR spectrum of compound **1** (**Figure 3.6**) showed a singlet signal at 10.02 ppm for the N–H of the amide. Signals for the aromatic ring occurred between 7.74 and 7.30 ppm, and the methyl protons occurred as a singlet signal at 2.36 ppm with integration for six protons. The ^{13}C NMR spectrum of compound **1** (**Figure 3.7**) also gave a signal at 20.9 ppm for the methyl groups.

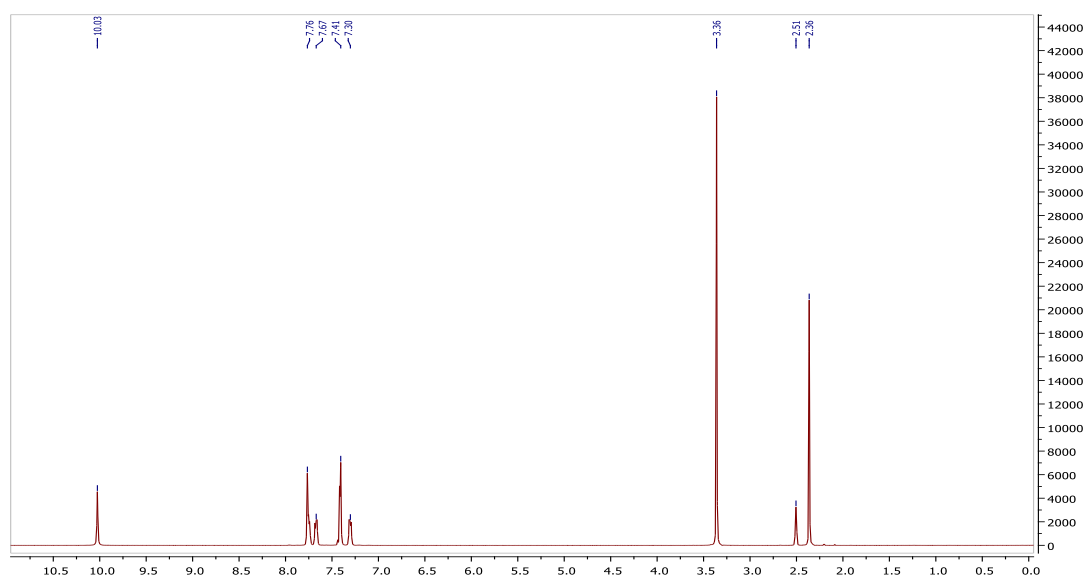


Figure 3.6 ^1H NMR spectrum of 3-methyl-*N*-[2-(3-methylbenzamido)phenyl]benzamide (1).

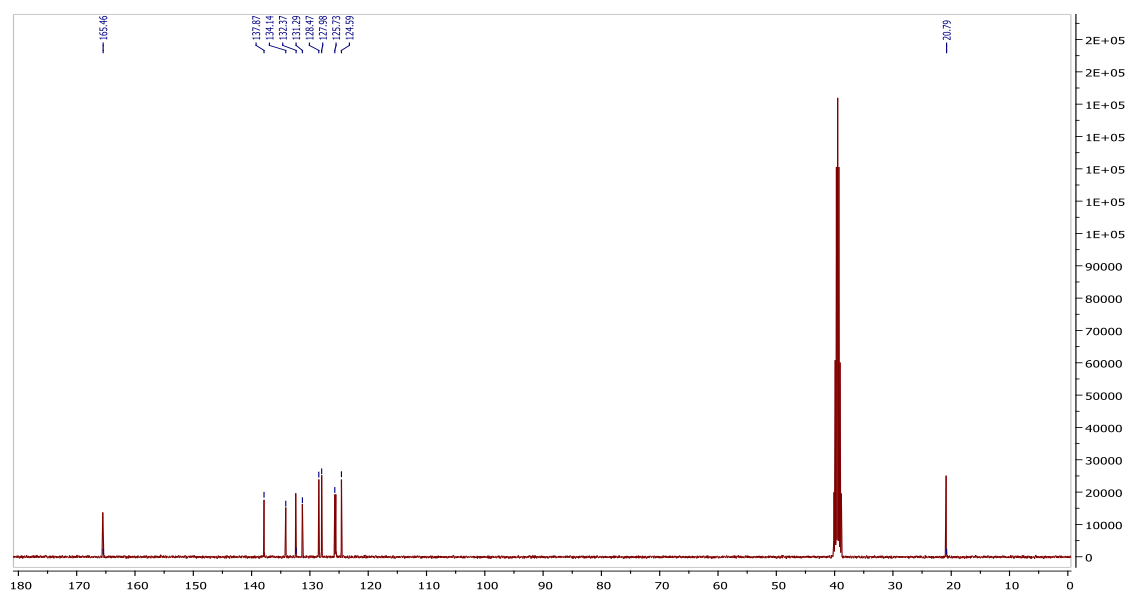


Figure 3.7 ^{13}C NMR spectrum of 3-methyl-*N*-[2-(3-methylbenzamido)phenyl]benzamide (1).

The ^1H NMR spectrum of **2** (Figure 3.8) showed signals for the aromatic ring between 8.04 and 7.20 ppm. The methyl group occurred as a singlet at 2.41 ppm which was also confirmed in the ^{13}C NMR spectrum of compound **2** (Figure 3.9) at 21.0 ppm.

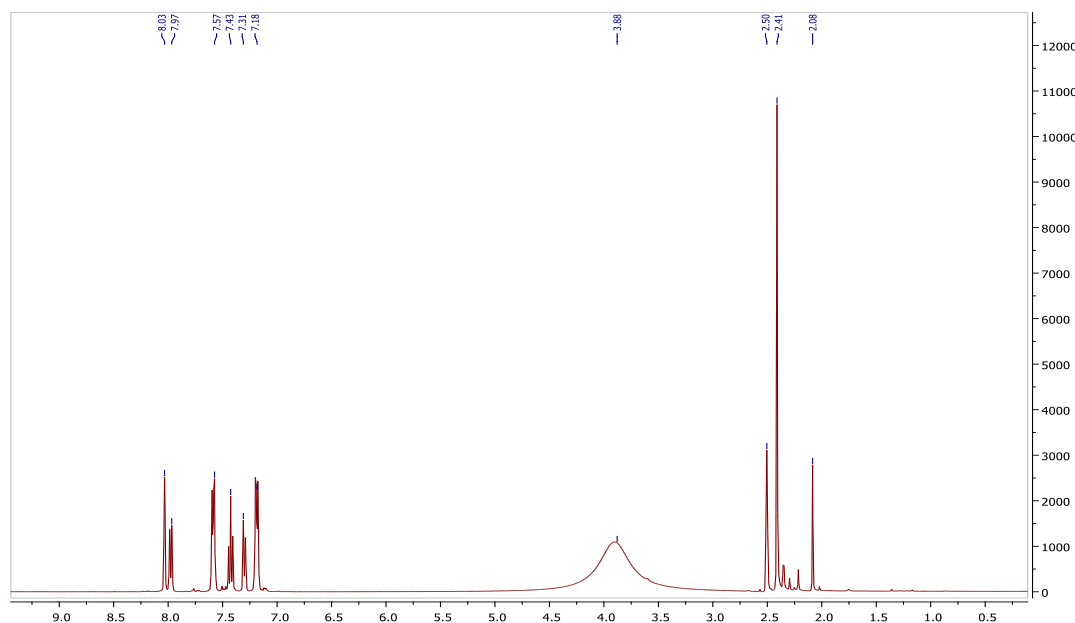


Figure 3.8 ^1H NMR spectrum of 2-(3-methylphenyl)-1*H*-benzimidazole (**2**).

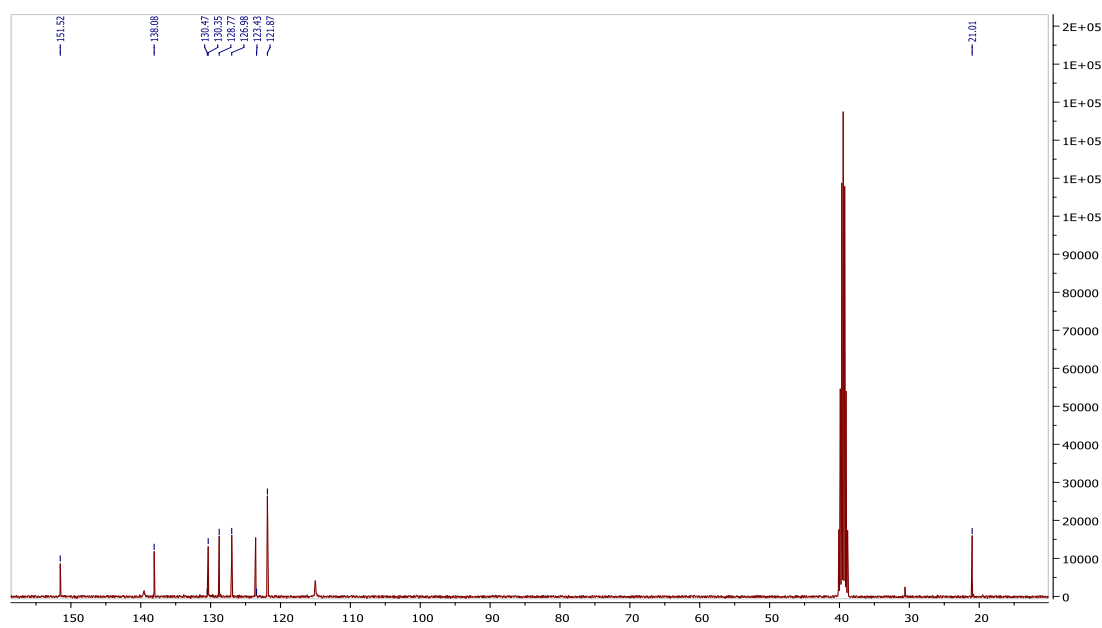


Figure 3.9 ^{13}C NMR spectrum of 2-(3-methylphenyl)-1*H*-benzimidazole (**2**).

Compound **1** was recrystallized from ethyl acetate:hexane (1:3) and obtained as colourless crystals, whilst compound **2** was recrystallized from DMSO:THF (1:2) and obtained as a white solid. The crystallographic data, selected bond lengths and bond angles for the crystal structures of compounds **1** and **2** are provided in **Tables 3.3** and **3.4**. The ORTEP diagrams

for compounds **1** and **2** are presented in **Figures 3.10** and **3.11**. Compound **1** crystallized in the trigonal space group $R\bar{3}$, while compound **2** crystallized in the monoclinic space group $P2_1/c$.

Table 3.3 Crystallographic data and structure refinement summary for 3-methyl-*N*-[2-(3-methylbenzamido)phenyl]benzamide (**1**) and 2-(3-methylphenyl)-1*H*-benzimidazole (**2**).

Property	1	2
Empirical formula	C ₂₂ H ₂₀ N ₂ O ₂	C ₁₄ H ₁₂ N ₂
Formula weight	344.40	208.26
Temperature	200	200
Crystal system	Trigonal	Monoclinic
Space group	$R\bar{3}$	$P2_1/c$
<i>a</i> (Å)	28.7614(9)	12.3990(6)
<i>b</i> (Å)	28.7614(9)	9.7826(5)
<i>c</i> (Å)	11.7819(4)	9.6028(4)
α (°)	90	90
β (°)	90	110.615(2)
γ (°)	120	90
Volume (Å ³)	8440.5(7)	1090.18(9)
<i>Z</i>	18	4
D (Calc) (g/cm ³)	1.220	1.269
<i>F</i> (000)	3276	440
Crystal size (mm ³)	0.21 x 0.28 x 0.54	0.08 x 0.23 x 0.56
μ (MoKa) (/mm)	0.079	0.076
Radiation (Å)	0.71073	0.71073
θ Min-Max (°)	2.4, 28.3	2.7, 28.3
Dataset	-38: 38 ; -32: 38 ; -15: 9	-16: 16 ; -12: 12 ; -12:
Tot., Uniq. Data, <i>R</i> _{int}	16186, 4646, 0.021	12429, 2692, 0.014
[<i>I</i> > 2.0 σ (<i>I</i>)]	2944	2217
<i>N</i> _{ref}	4646	2692
<i>N</i> _{par}	302	150
<i>R</i>	0.0511	0.0392
<i>wR</i> ₂	0.1554	0.1115
<i>S</i>	1.02	1.03
Max and Av. Shift/Error	0.00, 0.00	0.00, 0.00
Min Residual Density (e/Å ³)	-0.24	-0.19
Max, Residual Density (e/Å ³)	0.28	0.26

Table 3.4 Selected bond lengths (Å) and bond angles (°) of 3-methyl-*N*-[2-(3-methylbenzamido)phenyl]benzamide (**1**) and 2-(3-methylphenyl)-1*H*-benzimidazole (**2**).

Bond lengths (Å)			
1		2	
O1–C2	1.238(1)	N1–C21	1.387(2)
O2–C3	1.239(2)	N2–C2	1.362(1)
N1–C2	1.339(1)	N1–C2	1.322(2)
N1–C21	1.416(2)	N2–C22	1.377(2)
N2–C3	1.356(2)	C1–C13	1.507(2)
C2–C11	1.553(1)	C2–C11	1.464(2)
N2–C22	1.422(2)	C11–C12	1.393(2)
C2–C41	1.400(2)	C12–C13	1.389(2)
Bond angles (°)			
1		2	
O1–C2–N1	122.6(2)	C2–N2–C22	106.9(1)
N1–C21–C26	120.9(2)	C2–N1–C21	104.9(1)
O1–C2–C11	124.5(1)	N1–C2–N2	112.9(1)
O1–C2–C41	107.8(1)	N(2)–C(2)–C11	122.3(1)
O2–C3–N2	121.8(2)	N1–C2–C11	124.7(1)
N1–C2–C11	112.9(1)	N1–C21–C22	109.7(1)
O2–C3–C31	120.9(2)	N2–C22–C21	105.5(1)
C2–N1–C21	125.2(2)	N1–C21–C26	130.1(1)
C3–N2–C22	126.8(1)	C2–C11–C16	121.3(1)

The bond distances of N1–C2, and N2–C3, which were 1.339(2), and 1.356(2) Å respectively, were consistent with the C–N bond of the amide of compound **1** whilst N(2)–C22 and N1–C21 were 1.422(2) and 1.416(2) Å, showing the C–N with the carbon being part of the aromatic ring system. Compound **1** exhibits a disorder in one of its toluene rings with a disorder ratio of 0.675:0.325.

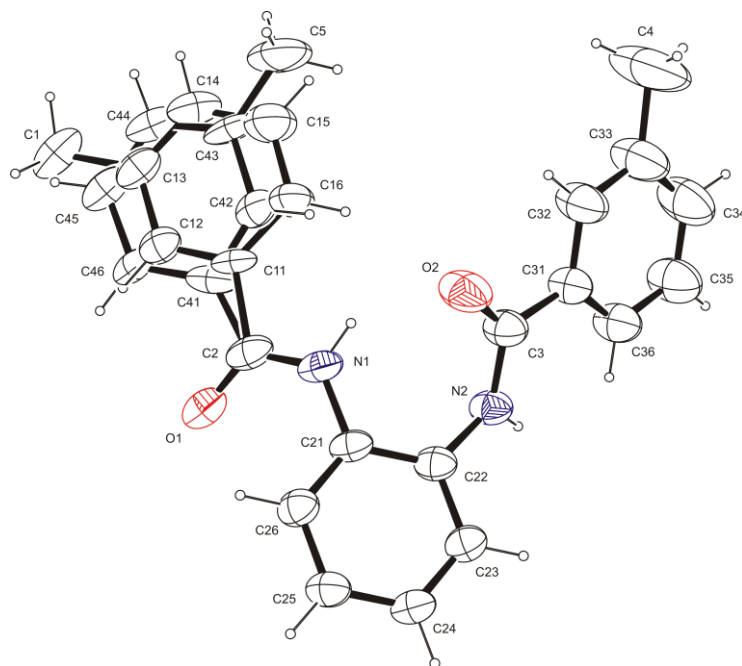
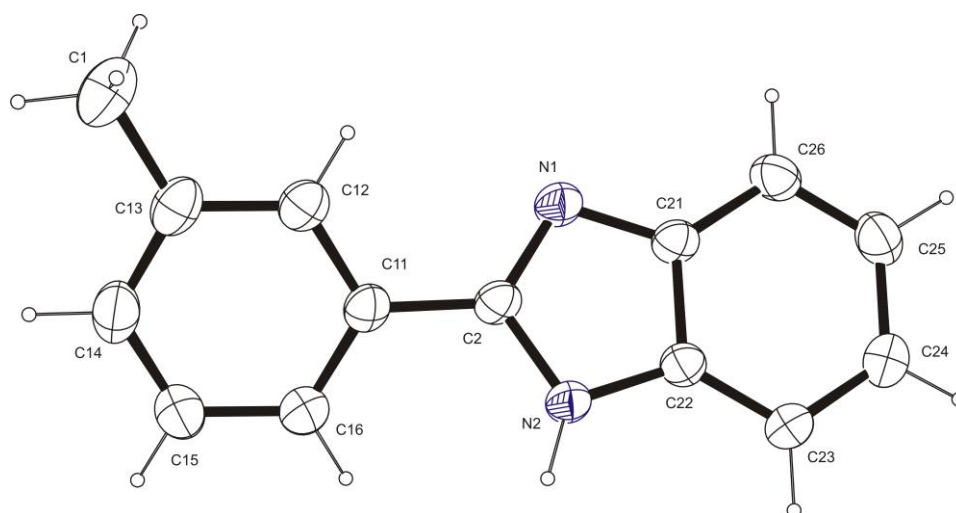


Figure 3.10 An ORTEP view of compound 3-methyl-*N*-[2-(3-methylbenzamido)phenyl]benzamide (**1**) showing 50% probability displacement ellipsoids and the atom labelling.



Figures 3.11 An ORTEP view of 2-(3-methylphenyl)-1*H*-benzimidazole (**2**) showing 50% probability displacement ellipsoids and the atom labelling.

The bond distances of O1–C2 and O2–C3 which were 1.238(3) and 1.239(2) Å, respectively, in compound **I** show usual C=O double bond character. The bond lengths are comparable with the average bond length of C=O bonds on the CCDC database which is 1.228 Å.²⁹³ The

O1–C2–N1, O1–C2–C11 and O1–C2–C41 bond angles which were 122.62 (2), 124.50 (4) and 107.80(7)°, respectively, were the angles around the sp² carbon atoms of the carbonyl in compound **1**. The disorder in the molecule was clearly shown by the two different angles around C(2) with one angle being narrower than the other. These are comparable to the average O–C–N bond angle on the CCDC database which is 122.30°. ²⁹⁴ The bond distances of N2–C2 and N1–C2 which were 1.362(1) and 1.322(2) Å respectively, were consistent with the C–N bond of the benzimidazole in compound **2** whilst the bond angles of N2–C2–C11 and N1–C2–C11 which were 122.3(1) and 124.7(1) Å, were consistent with sp² carbon in compound **2**.

3.2.1 HOMO-LUMO analysis

Table 3.5 gives the computed HOMO–LUMO energies for *o*-phenylenediamine, *m*-toluoyl chloride, *m*-toluic acid, compounds **1** and **2**. The frontier orbitals of *m*-toluic acid, which was used in the synthesis of compound **2**, are shown in **Figure 3.12**. The HOMO is delocalised over the entire molecule except the carbonyl group whilst the LUMO is largely delocalised over the entire molecule except the methyl group.

Table 3.5 Summary of the HOMO–LUMO energies for *o*-phenylenediamine, *m*-toluoyl chloride, *m*-toluic acid, and 3-methyl-*N*-[2-(3-methylbenzamido) phenylbenzamide (**1**) and 2-(3-methylphenyl)-1*H*-benzimidazole (**2**).

	HOMO (kJ/mol)	LUMO (kJ/mol)	HOMO-LUMO Gap (kJ/mol)
<i>o</i> -Phenylenediamine	-520.93	-37.70	483.23
<i>m</i> -Toluoyl chloride	-692.24	-197.04	495.20
<i>m</i> -Toluic acid	-684.65	-165.64	519.01
Compound 1	-620.93	-163.23	457.70
Compound 2	-573.91	-144.61	429.30

This indicates that during charge transfer in a reaction the molecule is stabilised by delocalization of electrons over the entire molecule and also confirming the susceptibility of the carbonyl to attack by the *o*-phenylenediamine.

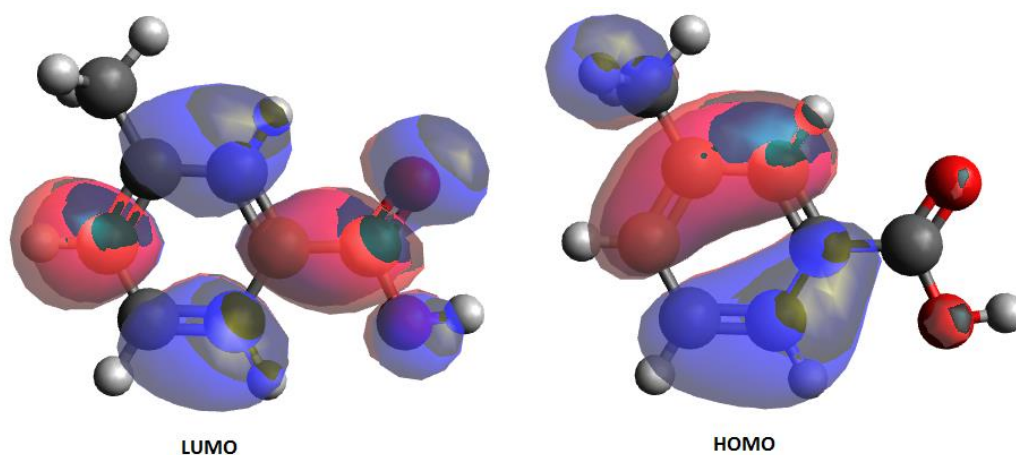


Figure 3.12 The atomic orbitals composition of the frontier molecular orbital for *m*-toluic acid.

The frontier orbitals of *m*-toluoyl chloride, which were used for the synthesis of compound **1**, are shown in **Figure 3.13**. The HOMO is delocalised over the entire molecule except the chloride, and the LUMO is also delocalised over the entire molecule except the methyl group. This confirms the susceptibility of the molecule to attack by *o*-phenylenediamine (a nucleophile). During charge transfer in this reaction the molecule is stabilised by delocalization of electrons over the entire molecule. The contribution of the carbonyl carbon atom and the chloride to the LUMO confirm the susceptibility of carbonyl attack by nucleophiles and subsequent loss of chloride.

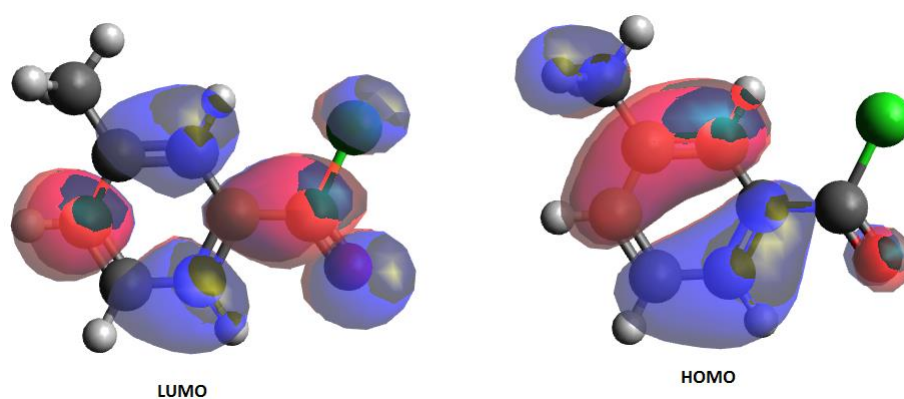


Figure 3.13 The atomic orbitals compositions of the frontier molecular orbitals for *m*-toluoyl chloride.

Figure 3.14. shows the frontier orbitals of *o*-phenylenediamine which was used in the syntheses of compounds **1** and **2**. The HOMO is delocalised over the entire molecule while the LUMO is largely delocalised over the nitrogen atoms and portions of the benzene ring. The high electron density on the nitrogen atom enables it to attack the carbonyl centre in the synthesis of a diamide. In the synthesis of benzimidazoles in an acidic medium there is no loss of a proton but the delocalization of the HOMO on the nitrogen allows the diamine to attack the highly susceptible protonated carbonyl of the carboxylic acid.

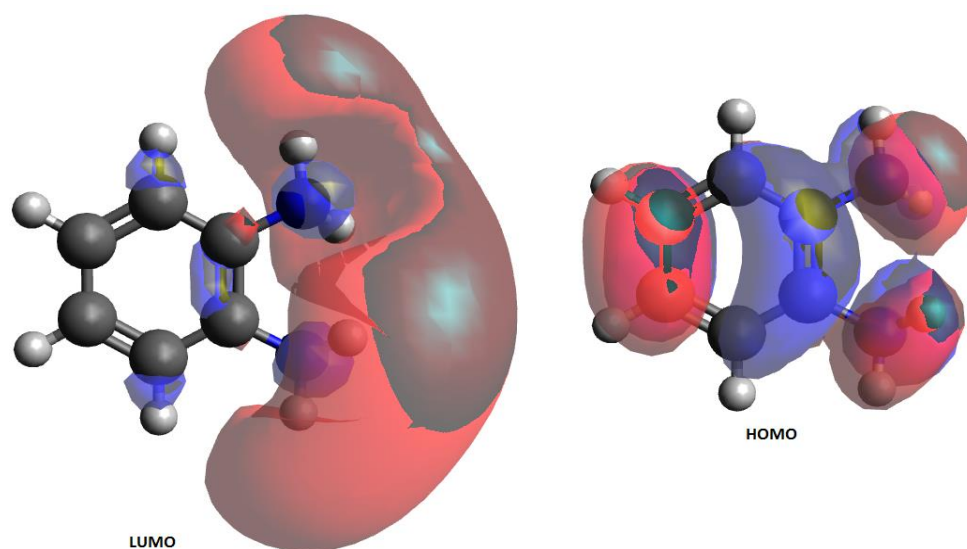


Figure 3.14 The atomic orbitals compositions of the frontier molecular orbital for *o*-phenylenediamine.

Figure 3.15 shows the frontier orbitals of 3-methyl-*N*-[2-(3-methylbenzamido) phenyl]benzamide (**1**). The HOMO is largely delocalised over the benzene ring contributed by *o*-phenylenediamine, the nitrogen and the carbonyl groups while the LUMO is delocalised over the benzene ring contributed by *o*-phenylenediamine and one of the benzene rings contributed by *m*-toluolyl chloride. The disorder in the molecule obtained from its crystal structure since the rings contributed by *m*-toluolyl chloride would have different reactivities.

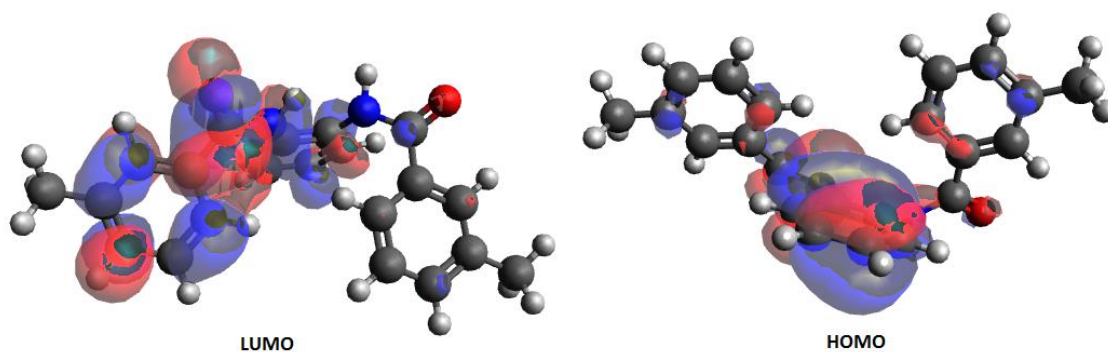


Figure 3.15 The atomic orbitals compositions of the frontier molecular orbital for 3-methyl-*N*-[2-(3-methylbenzamido)phenyl]benzamide (**1**).

Figure 3.16 shows the frontier orbitals of compound **2**. The HOMO and LUMO are largely delocalised over the entire molecule except the methyl group. This confirms the stability of the molecule to attack by an incoming group, possibly due to charge transfer *via* delocalization over the entire molecule. This also confirmed the inability to convert the methyl group on compound **2** to a carboxylic acid by a reaction with potassium permanganate or to an aldehyde by using selenium dioxide.

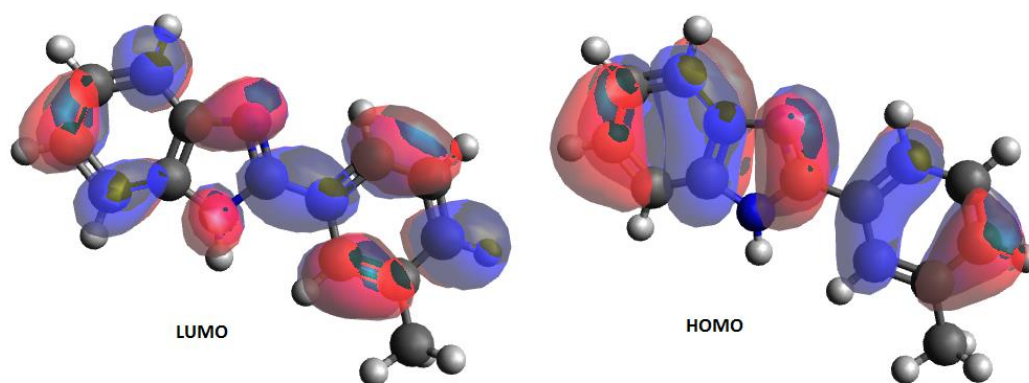


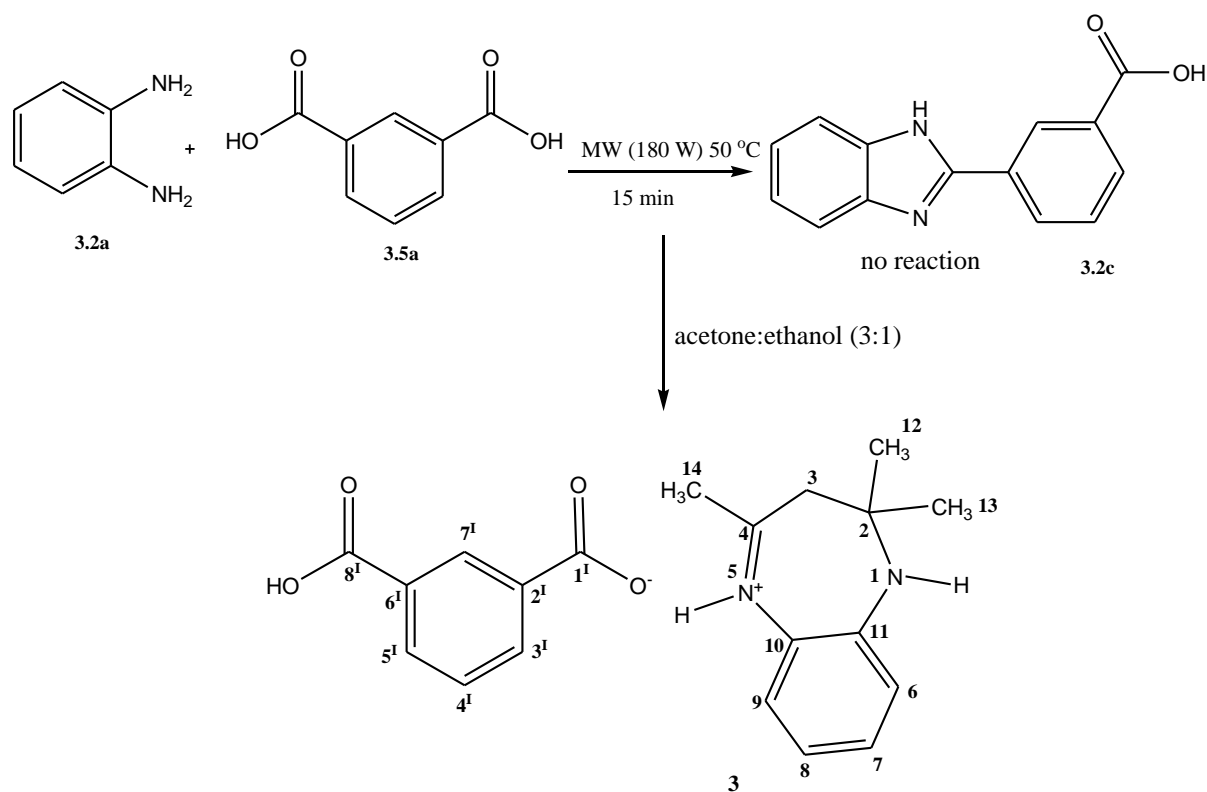
Figure 3.16 The atomic orbitals compositions of the frontier molecular orbital for 2-(3-methylphenyl)-1*H*-benzimidazole (**2**).

3.3 Synthesis and characterization of benzodiazepines

The next attempt was to form the benzimidazole with a free carboxylic acid retained on the product due to our inability to convert the methyl group on the benzimidazole to a carboxylic

acid. This was attempted through a reaction of *o*-phenylenediamine and isophthalic acid under microwave irradiation conditions. Equimolar quantities (0.01 mol) of the starting materials were irradiated at 180 W (50 °C) for 15 min. To dissolve the solidified reaction mixture, 2 mL of an ethanol:acetone mixture (3:1) were added while the reaction mixture was still hot. Finally, the reaction mixture was allowed to stand for 12 h. **Scheme 3.5** illustrates the reaction of *o*-phenylenediamine and isophthalic acid under microwave irradiation conditions. It was later observed that the benzimidazole formation *via* a condensation reaction did not take place. This was attributed to the fact that the activation energy required for the reaction of *o*-phenylenediamine and isophthalic acid was not achieved.

However, the energy acquired during the microwave irradiation was not immediately lost. This is because there was no other reagent, be it a solid support or solvent, to absorb the energy acquired by the reactants during the microwave irradiation. The introduction of an acetone:ethanol mixture into the reaction resulted in the reaction of acetone with *o*-phenylenediamine to yield the benzodiazepine, which was protonated by the isophthalic acid to form benzodiazepium salt (**3**), due to a lower activation energy required for this reaction (**Scheme 3.4**). Other researchers have reported similar benzodiazepine derivatives by the condensation of *o*-phenylenediamine and a ketone or an aldehyde in the presence of a catalyst (alumina and zirconia),²⁹⁴ and the formation of 7-membered ring (diazepine) systems by microwave irradiation of a mixture of an aldehyde, a ketone and ethylene diamine in the presence of potassium hydroxide has also been reported.²⁹⁵ The monocarboxylate anion formed from the dicarboxylic acid resulted in the formation of a salt with the benzodiazepinium cation. Interestingly, it appeared that the reaction occurred without the involvement of isophthalic acid, except in the salt formation.²⁹⁶ This phenomenon was further ascertained by performing the reaction of *o*-phenylenediamine and acetone under reflux condition in the absence of isophthalic acid to yield compound **4**. Compound **4** has been accessed *via* condensation of *o*-phenylenediamines (OPDA) and ketones in the presence of catalytic amount of H-MCM-22 using acetonitrile as a solvent at room temperature.²⁹⁷ Also 2,4,6-trichloro-1,3,5-triazine (TCT) has been used to catalyze the condensation of 1,2-diamines and various enolizable ketones to afford 1,5-benzodiazepines in good to excellent yields.²⁹⁸



Scheme 3.5 Synthesis of 2,2,4-trimethyl-2,3-dihydro-1*H*-benzodiazepin-5-ium isophthalate (**3**).

When *o*-phenylenediamine were heated under reflux with ethanol and acetone for 8 h, the product obtained was 2,2,4-trimethyl-2,3-dihydro-1*H*-1,5-benzodiazepine (**4**) which confirmed that the cyclization occurred without the involvement of isophthalic acid. The IR spectrum for 2,2,4-trimethyl-2,3-dihydro-1*H*-1,5-benzodiazepin-5-ium isophthalate (**3**) showed a band at 1710 cm^{-1} due to the presence of the carbonyl group (C=O) of the carboxylic acid (**Figure 3.17**). The band at 1607 cm^{-1} was attributed to the presence of the iminium group (C=NH⁺). The bands at 1208 and 1552 cm^{-1} indicated the presence of the C–N bond and the C–O bond of the carboxylate ion, respectively. The band at 3309 cm^{-1} confirmed the presence of the amine group (NH).

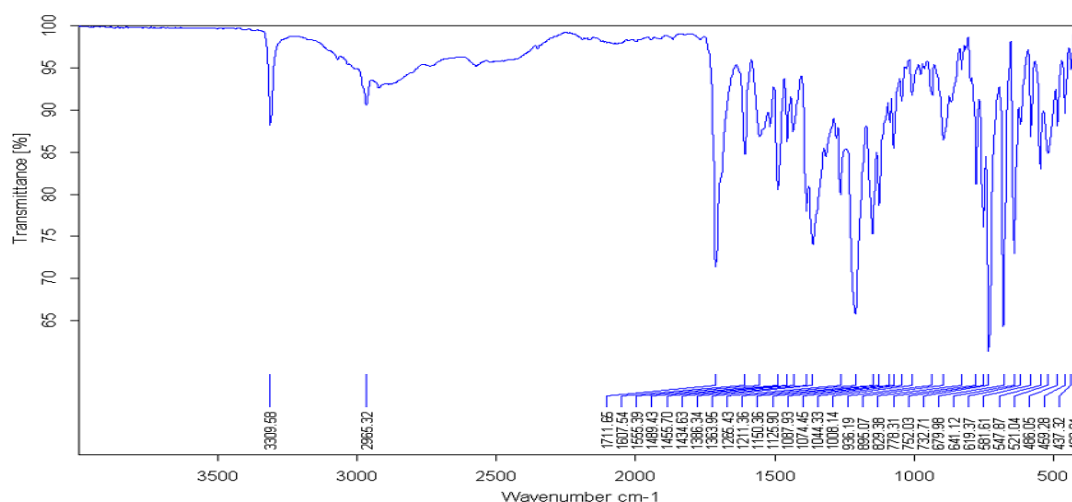


Figure 3.17 IR spectrum of 2,2,4-trimethyl-2,3-dihydro-1*H*-benzodiazepin-5-ium isophthalate (**3**).

Furthermore, the IR spectrum of 2,2,4-trimethyl-2,3-dihydro-1*H*-1,5-benzodiazepine (**4**) showed bands at 3294 cm^{-1} for the amine group (N–H) and a band at 2964 cm^{-1} for the methyl groups (**Figure 3.18**). The bands at 1633 and 1430 cm^{-1} were observed for the presence of an imine group (C=N) and a C–N group, respectively.

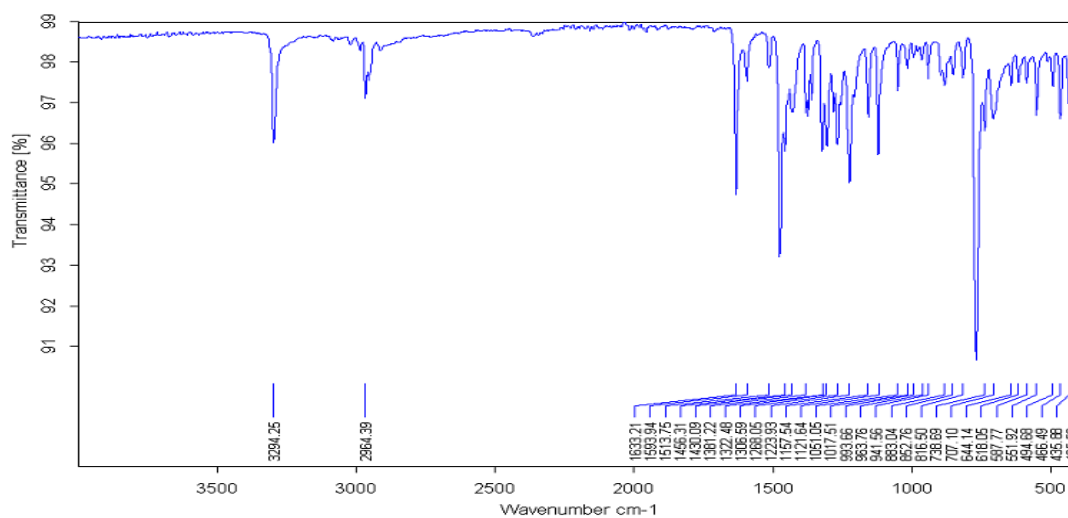


Figure 3.18 IR spectrum of 2,2,4-trimethyl-2,3-dihydro-1*H*-1,5-benzodiazepine (**4**).

The ^1H NMR spectrum of compound 2,2,4-trimethyl-2,3-dihydro-1*H*-benzodiazepin-5-ium isophthalate (**3**) displayed a singlet at $\delta = 2.16$ ppm indicating the presence of methylene

(CH₂) protons (**Figure 3.19**). The presence of the methylene group was also confirmed by both the ¹³C NMR spectroscopy ($\delta = 45.2$ ppm) (**Figure 3.20**) and DEPT-135 (**Figure 3.21**). The iminium proton appeared as a broad signal between $\delta = 3.50$ and 4.50 ppm. The carbon signal at $\delta = 30.0$ ppm was attributable to the two methyl groups attached to the sp³ carbon atom of the 7-membered ring. On the other hand, the singlet at $\delta = 29.3$ ppm was attributable to a methyl group attached to the sp² carbon of the 7-membered ring. The signals at $\delta = 171.0$ and 166.6 were attributable to the carbon atom of the iminium ion and carbonyl groups of the isophthalate anion, respectively.

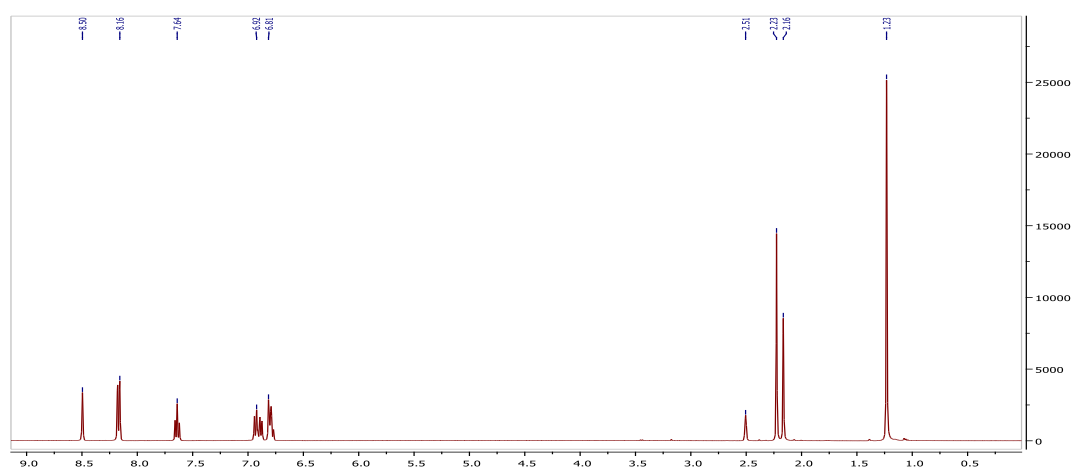


Figure 3.19 ¹H NMR spectra of 2,2,4-trimethyl-2,3-dihydro-1*H*-1,5-benzodiazepin-5-ium isophthalate (**3**).

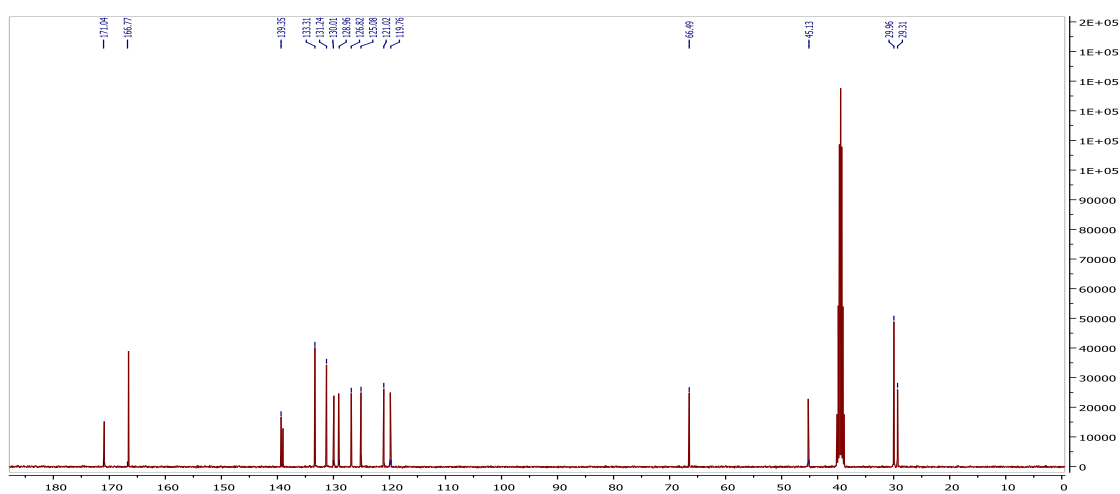


Figure 3.20 ¹³C NMR spectra of 2,2,4-trimethyl-2,3-dihydro-1*H*-1,5-benzodiazepin-5-ium isophthalate (**3**).

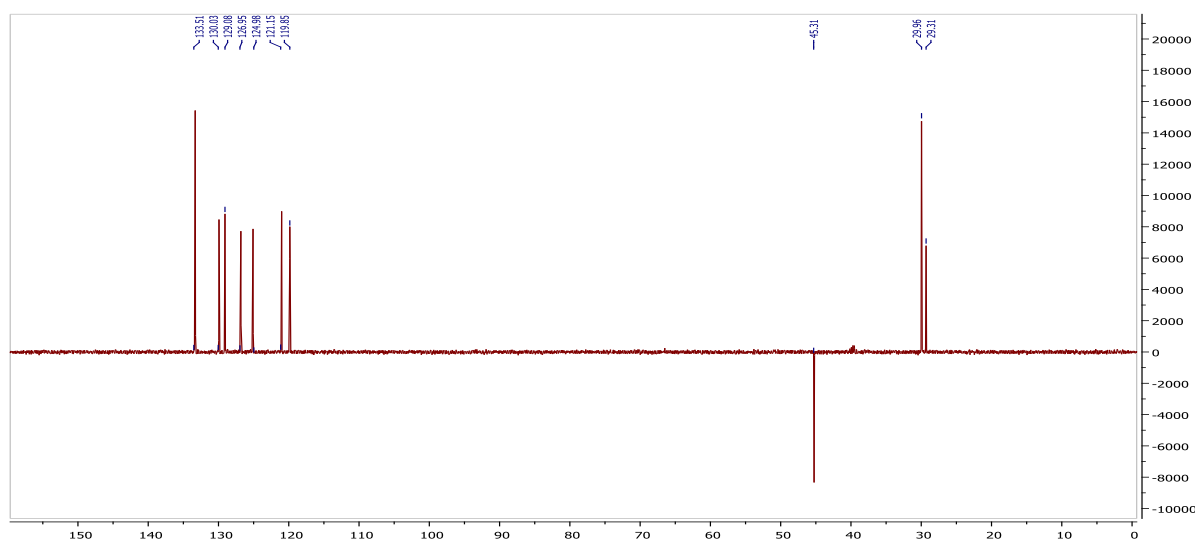


Figure 3.21 DEPT spectrum of 2,2,4-trimethyl-2,3-dihydro-1*H*-benzodiazepin-5-ium isophthalate (**3**).

^1H NMR spectrum of **4** (**Figure 3.22**) displayed a singlet at $\delta = 2.16$ ppm which integrated for two hydrogens indicating the presence of a CH_2 group. The presence of the CH_2 group in the ^{13}C NMR spectrum (**Figure 3.23**) was also confirmed by the inversion of the signal ($\delta = 45.2$ ppm) in the DEPT-135 spectrum (**Figure 3.24**). The N–H group appeared as a singlet at $\delta = 4.71$ ppm in the ^1H spectrum. The singlet at $\delta = 1.24$ ppm which integrated for six hydrogens was attributable to the methyl groups attached to the quaternary sp^3 carbon, whilst the singlet signal at $\delta = 2.22$ ppm with integration for three hydrogens was attributable to the methyl group at position 4 on the seven-membered ring.

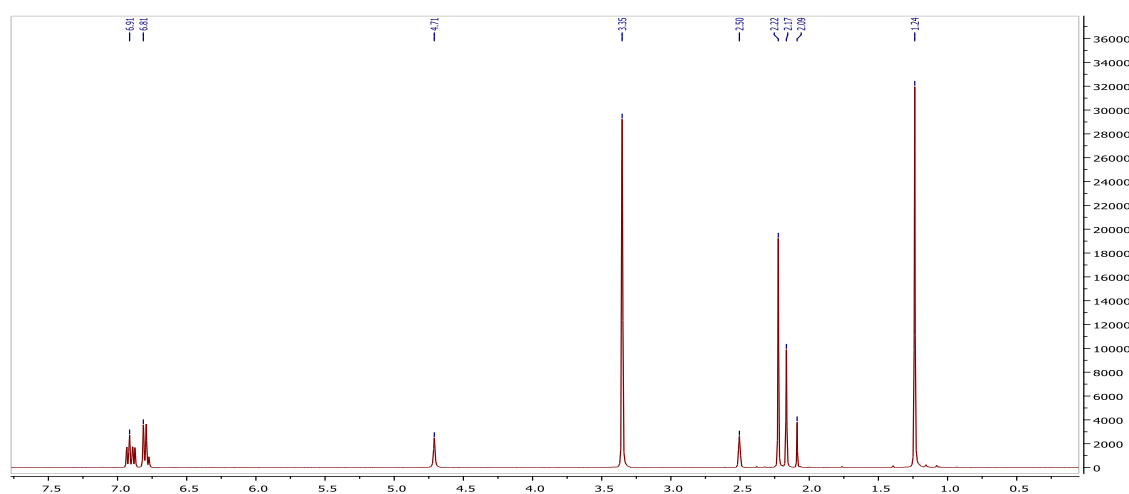


Figure 3.22 ^1H NMR spectrum of 2,2,4-trimethyl-2,3-dihydro-1*H*-1,5-benzodiazopine (**4**).

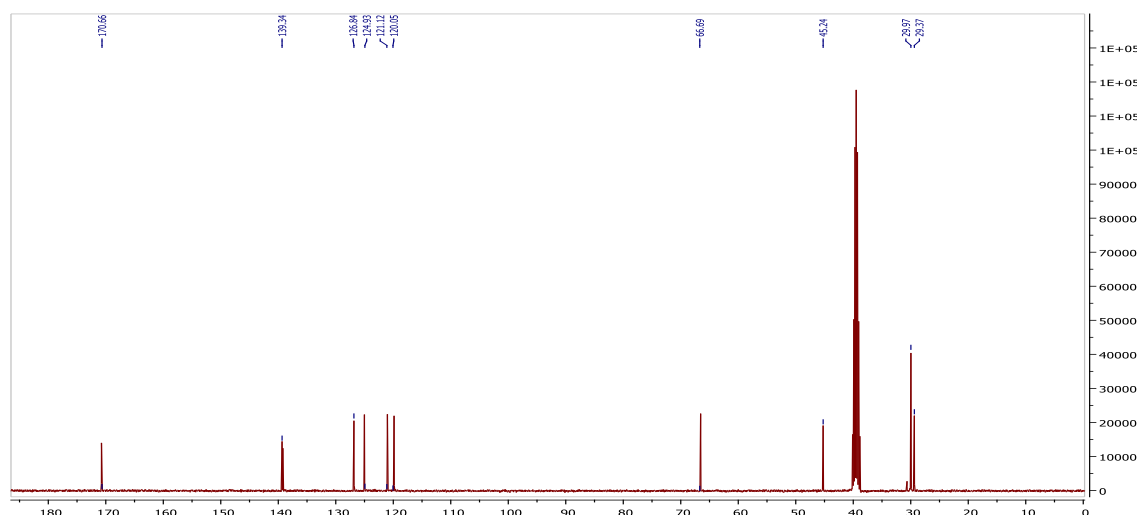


Figure 3.23 ^{13}C NMR spectrum of 2,2,4-trimethyl-2,3-dihydro-1*H*-1,5-benzodiazepine (**4**).

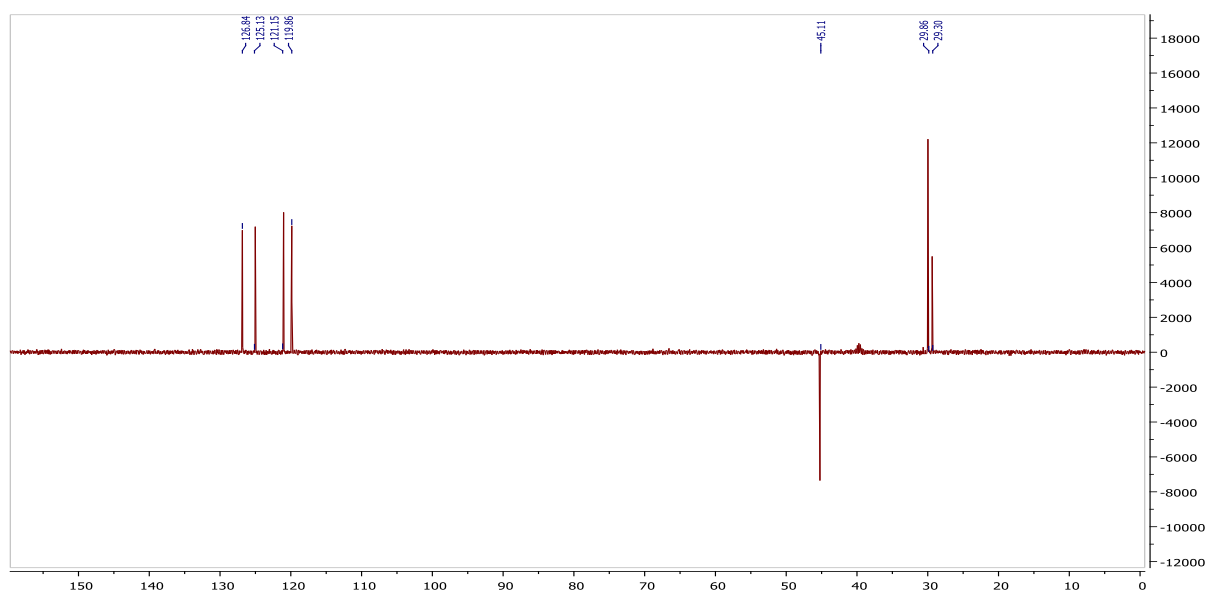
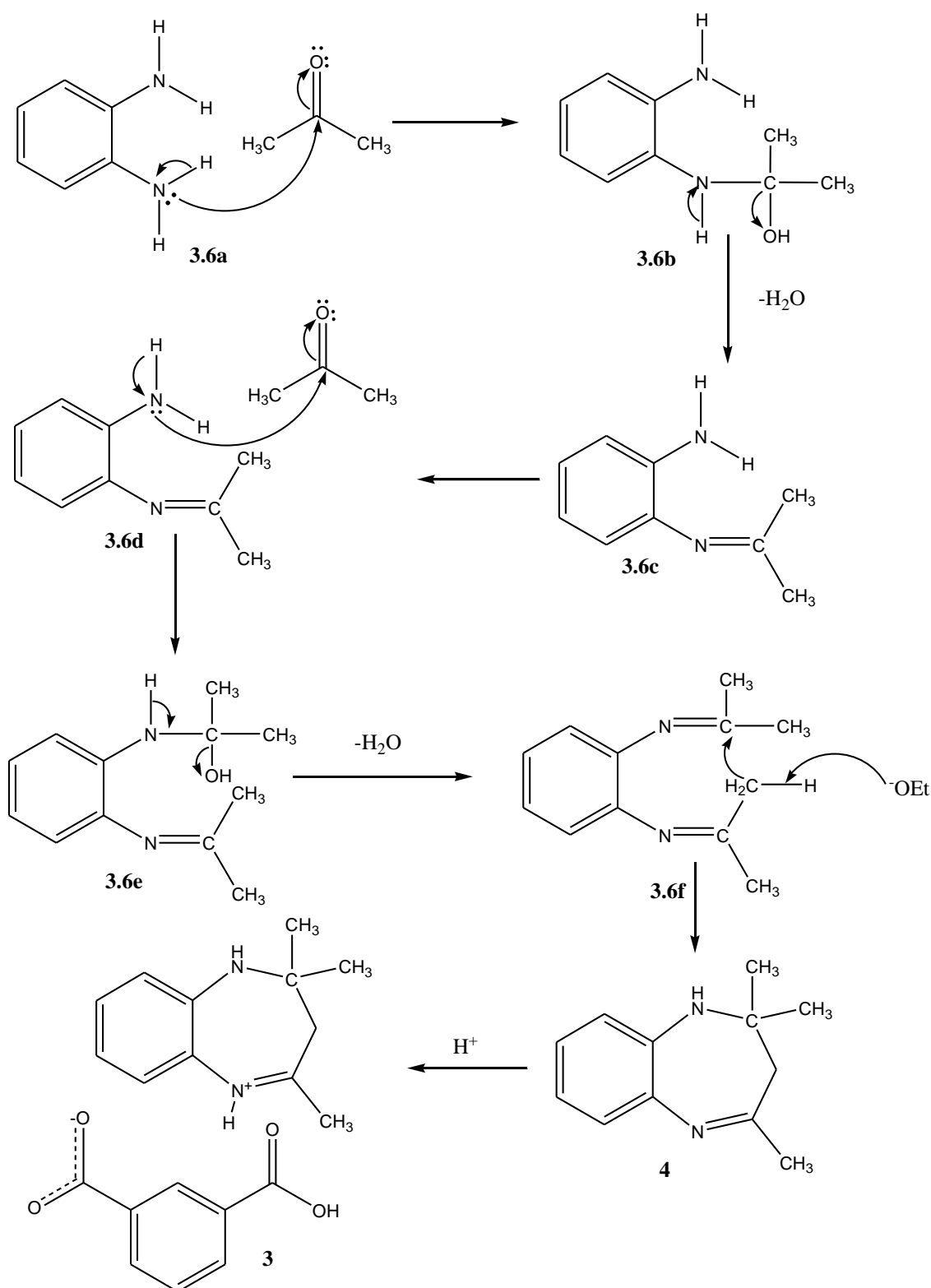


Figure 3.24 DEPT spectrum of 2,2,4-trimethyl-2,3-dihydro-1*H*-1,5-benzodiazepine (**4**).

The main fragments in the high resolution mass spectra (in negative and positive mode) were m/z 165.0195 for the isophthalate ion ($\text{C}_8\text{H}_5\text{O}_4^-$) and m/z 189.1392 for the benzodiazepinium ion ($\text{C}_{12}\text{H}_{17}\text{N}_2^+$) and these were also consistent with the assigned structures.

3.3.1 Proposed reaction mechanism for compounds 2,2,4-trimethyl-2,3-dihydro-1*H*-benzodiazepin-5-ium isophthalate (**3**) and 2,2,4-trimethyl-2,3-dihydro-1*H*-1,5-benzodiazopine (**4**)

Scheme 3.6 shows the proposed reaction mechanism for the formation of benzodiazepine. It is proposed that the initial step is the attack of the carbonyl carbon of acetone by the lone pair of electrons on the amino group. Due to the difference in electronegativity between the carbon atom and the oxygen atom of the carbonyl group, the electron density is shifted slightly more towards the oxygen than the carbon, rendering the oxygen to acquire a partial negative charge and the carbon atom a partial positive charge. Also, the tendency of the nitrogen to attract electrons towards itself allows the hydrogen (N–H) to be easily abstracted. The negatively charged the nitrogen which is a better nucleophile, attack the carbonyl in **I** (**Scheme 3.6**). Loss of a water molecule from **II** results in the formation of a C=N bond in **III**. The second amine group attacks the carbonyl of another acetone molecule in **IV** resulting in the formation of **V** and the subsequent loss of a water molecule leads to the formation of the C=N group in **VI**.²⁹⁹ The ethoxide ion, formed from the dissociation of ethanol, abstracts a proton from the methyl group, resulting in the formation of the enolate ion in **VI**. Since ethanol is a weak acid, it produces a strong conjugate base that can easily deprotonate a weakly acidic proton in this case from a methyl group which is made acidic by the presence of unsaturation and a heteroatom on the adjoining carbon.³⁰⁰ The loss of the proton by the methyl group makes it a good nucleophile which then attacks the carbon of the C=N bond because of the partial positive charge of the carbon as a result of the electron withdrawing effect of the nitrogen forming the benzodiazepine **VII**. In the case of compound **3** the benzodiazepine formed in **VII** is then protonated by the isophthalic acid to form an iminium ion which subsequently forms a salt with the isophthalate ion in **VIII**.



Scheme 3.6 A proposed mechanism for the formation of 2,2,4-trimethyl-2,3-dihydro-1*H*-benzodiazepin-5-ium isophthalate (**3**) and 2,2,4-trimethyl-2,3-dihydro-1*H*-1,5-benzodiazopine (**4**).

3.3.2 X-ray crystallography of 2,2,4-trimethyl-2,3-dihydro-1*H*-benzodiazepin-5-ium isophthalate (**3**) and 2,2,4-trimethyl-2,3-dihydro-1*H*-1,5-benzodiazopine (**4**)

X-ray crystal structures of the 2,2,4-trimethyl-2,3-dihydro-1*H*-benzodiazepin-5-ium isophthalate (**3**) and 2,2,4-trimethyl-2,3-dihydro-1*H*-1,5-benzodiazopine (**4**) were obtained using single crystals grown by crystallization from ethanol. **Table 3.6** shows the crystallographic and structure refinement data for the compounds **3** and **4**. The bond distances C27–O1 and C27–O2 of the carboxylate ion in **3** were 1.24(2) Å and 1.25(2) Å, respectively (**Table 3.7**). The bond distances indicated delocalisation of the electron density on the carboxylate group, with none of the two bonds being distinctly a single or double bond. The bond distance of C28–O3 was 1.20(2) Å and was attributable to the C=O double bond whilst the bond distance of C28–O4 was 1.32(2) Å indicating C–O single bond of the non-ionized carboxylic acid group. The bond length of N2–C5 was 1.28(2) Å which was indicative of the C=N double bond whilst the bond length of N1–C1 was 1.47(2) Å which confirmed the C–N single bond. The bond angle of C2–C1–C4 was 109.1(1)° confirming the tetrahedral geometry (sp³) of the carbon C(3). The bond angle of C6–C5–C4 was 121.2(1)° which was consistent with the trigonal planar geometry (sp²) of C5. Similarly, for compound **4**, the bond length of the N1–C1 single bond was 1.48(2) Å whilst that of the N(2)–C(5) double bond was 1.28(2) Å (**Table 3.7**). The bond angle of the sp² carbon was N(2)–C(5)–C(4) = 123.7(1)° confirming that the geometry of carbon C(5) is trigonal planar. The sp³ carbon C(1) had a bond angle of N(1)–C(1)–C(4) = 108.6(1)° which is consistent with its tetrahedral geometry.

Table 3.6 Crystallographic data and structure refinement for 2,2,4-trimethyl-2,3-dihydro-1*H*-benzodiazepin-5-ium isophthalate (**3**) and 2,2,4-trimethyl-2,3-dihydro-1*H*-1,5-benzodiazopine (**4**).

Property	3	4
Formula	C ₁₂ H ₁₇ N ₂ C ₈ H ₅ O ₂	C ₁₂ H ₁₆ N ₂
Formula Weight	354.40	188.27
Temperature (K)	200	200
Crystal System	Triclinic	Orthorhombic
Space group	<i>P</i> -1	<i>P</i> na 21
<i>a</i> (Å)	9.3608(4)	12.1454(3)
<i>b</i> (Å)	9.5706(3)	7.2730(2)
<i>c</i> (Å)	11.9881(4)	11.9222(3)
α (°)	101.128(1)	90
β (°)	102.728(1)	90
γ (°)	114.297(1)	90
<i>V</i> (Å ³)	904.91(6)	1053.13(5)
<i>Z</i>	2	4
<i>D</i> (calc) (g/cm ³)	1.301	1.187
μ (MoK α) (mm)	0.091	0.091
F(000)	376	408
Crystal Size (mm)	0.15 x 0.36 x 0.42	0.19 x 0.44 x 0.45
Radiation (Å)	Mo K α 0.71073	Mo K α 0.71073
θ Min–Max (°)	2.5–28.3	3.3–28.3
Data set	–12:12; –12:12,	–15:15; –15:16; –9:9; –10:15
Tot. Uniq. Data R(int)	16298, 4492 , 0.015	9541, 2371, 0.015
Observed data (<i>I</i> > 2.0 sigma (<i>I</i>))	3854	2285
<i>N</i> _{ref} , <i>N</i> _{par}	4492, 240	2371, 134
<i>R</i> , <i>W</i> <i>r</i> ² , <i>S</i>	0.0385, 0.1045, 1.04	0.0306, 0.0802, 1.03
Max and Av. Shift/Error	0.00, 0.00	0.00, 0.00
Min and Max, Resd Dens (e/Å ³)	0.20, 0.30	–0.20, 0.18

Table 3.7 Selected bond lengths (Å), and bond angles for 2,2,4-trimethyl-2,3-dihydro-1*H*-benzodiazepin-5-ium isophthalate (**3**) and 2,2,4-trimethyl-2,3-dihydro-1*H*-1,5-benzodiazopine (**4**).

Bond length		
	3	4
C27–O1	1.24(2)	
C27–O2	1.25(2)	
C28–O3	1.20(2)	
C28–O4	1.32(2)	1.28(2)
N2–C5	1.28(2)	1.28(2)
N1–C1	1.47(2)	1.48(2)
Bond angles		
C2–C1–C4	109.1(1)	108.6(1)
C4–C5–C6	121.2(2)	117.5(1)
C13–C12–N2	117.7(2)	116.9(1)
16–C11–N1	121.2(1)	119.7(1)

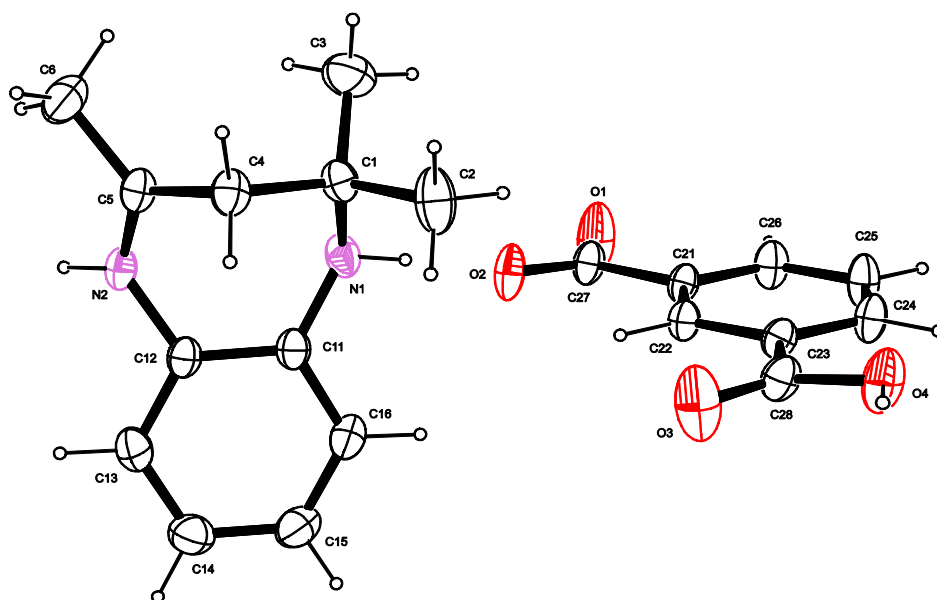


Figure 3.25 An ORTEP view of 2,2,4-trimethyl-2,3-dihydro-1*H*-benzodiazepin-5-ium isophthalate (**3**) showing 50% probability displacement ellipsoids and the atom labelling.

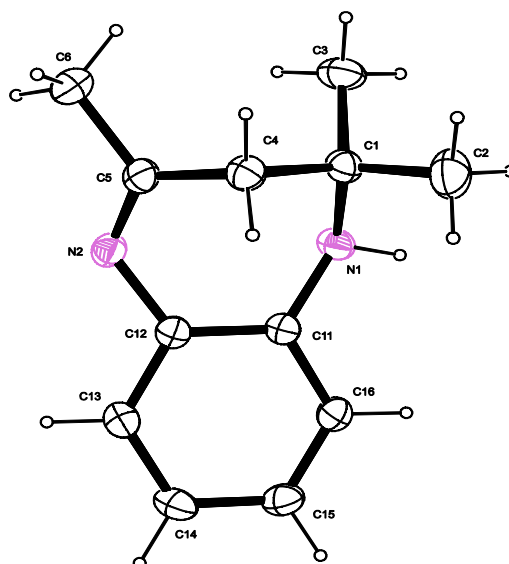


Figure 3.26 An ORTEP view of 2,2,4-trimethyl-2,3-dihydro-1H-1,5-benzodiazopine (**4**) showing 50% probability displacement ellipsoids and the atom labelling.

An alternative approach was to synthesize the benzimidazole directly on the amino acids derivatives of benzoyl isothiocyanate (**Scheme 3.7**). Pre-screening with Autodock gave good predicted inhibition constants. Hence an attempt was made to synthesize them. Amino acid derivatives of benzoyl isothiocyanate can be used as intermediates to construct other biologically active molecules with a thiourea backbone, and in this work it was envisaged to access benzimidazoles by reacting the amino acids derivatives with 1,2-diaminobenzene. However, some thiourea derivatives of various amines have also been synthesized in acetone and tested for their anti-amoebic properties.³⁰¹

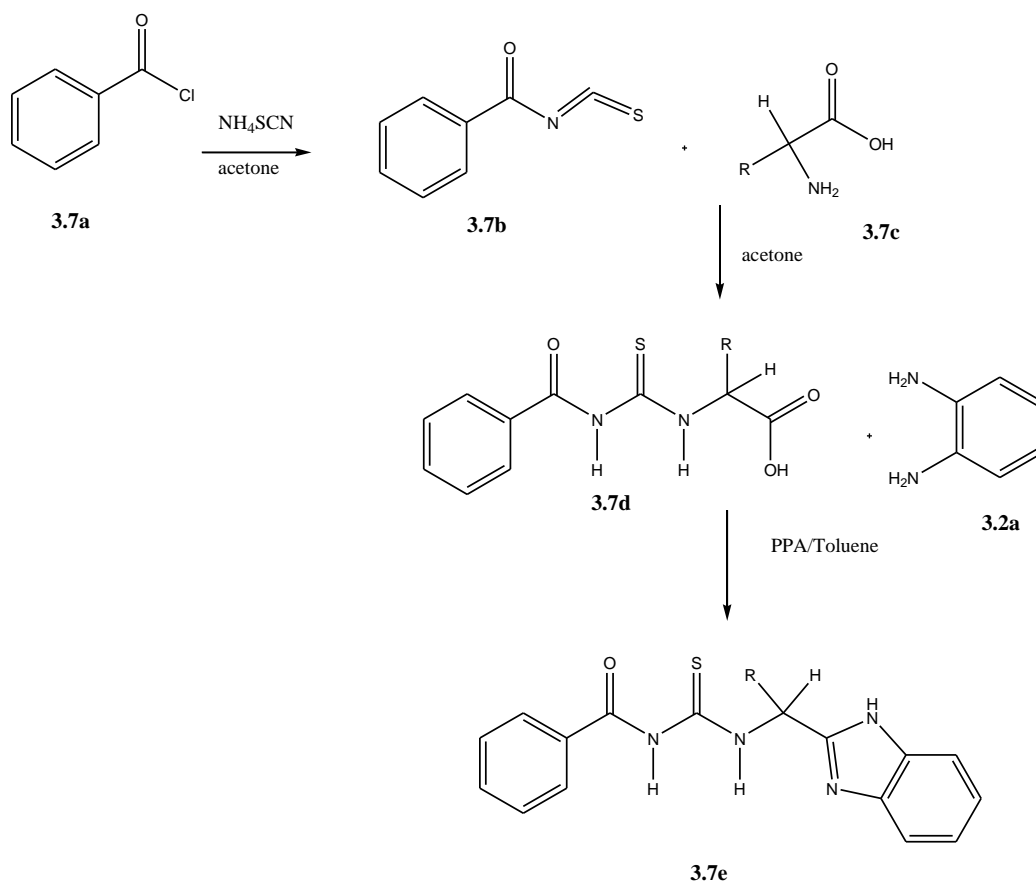
The isothiocyanates can be generated by a reaction of the acylated intermediates with ammonium thiocyanate in the presence of polyethylene glycol 400 (PEG 400),³⁰² and then reacted with amines to generate the thiourea derivatives. Thiourea derivatives have been synthesized through several ways. For example, ethyl isothiocyanates and aromatic amines were mixed and stirred at room temperature in acetone for 15 h to give the corresponding thioureas in high yields.³⁰³ A simple and efficient method for the synthesis of thiourea derivatives in high purity and high yield has been reported using tetrabutyl ammonium bromide (TBAB) as a phase transfer catalyst.³⁰⁴ A series of thiourea derivatives containing the quinazoline 4(3H) framework have been synthesized by Saeed *et al.*³⁰⁵ Pyrazole acyl thiourea derivatives have also been synthesized from monomethylhydrazine (or

phenylhydrazine) and ethyl acetoacetate.³⁰⁶ N-(5-Aryl-2-furyl) thiourea derivatives containing substituted pyrimidine rings have been synthesized in good yield using PEGe400 as a phase transfer catalyst under ultrasonic irradiation.³⁰⁷

Fluorinated pyrazoles, benzene sulfonylurea and thiourea derivatives as well as their cyclic sulfonylthioureas have been prepared by the reaction of brominated trifluoromethyl diketones with isocyanates and isothiocyanates.³⁰⁸ Benzimidazoles conjugated to thioureas have been synthesized by the refluxing of isothiocyanates and benzimidazoles in dimethyl formamide.³⁰⁹ Versatile and expeditious syntheses of taurine-derived thioureas, ureas, and guanidines using taurine isothiocyanate as the key intermediate have also been reported. The thioureas were obtained by a one-pot two-step procedure starting from taurine by the isothiocyanation reaction with thiophosgene in aqueous tetrahydrofuran, followed by coupling with aliphatic and aromatic amines. Desulfurization of the thiourea derivatives with mercury (II) oxide gave either taurine-containing ureas or guanidine.³¹⁰ Urea and thiourea derivatives of diphenylphosphoramidate may be aromatic isocyanates and isothiocyanates in tetrahydrofuran in the presence of triethylamine.³¹¹ Multifunctional thioureas bearing a variety of functional groups at a position remote from the thiourea moiety have been synthesized *via* ruthenium catalyzed Huisgen cycloaddition.³¹²

Table 3.8 Pre-screening results of benzimidazoles of the amino acid derivatives of benzoyl isothiocyanate.

CODE	Energy kcal/mol	Inhibition constant K_i (μM)
Cysteine derivative	-7.19	5.37
Glycine dervative	-7.31	4.38
Alanine derivative	-6.39	20.68
Leucine derivative	-7.52	3.08
Serine derivative	-7.69	2.30
Proline derivative	-8.29	0.84



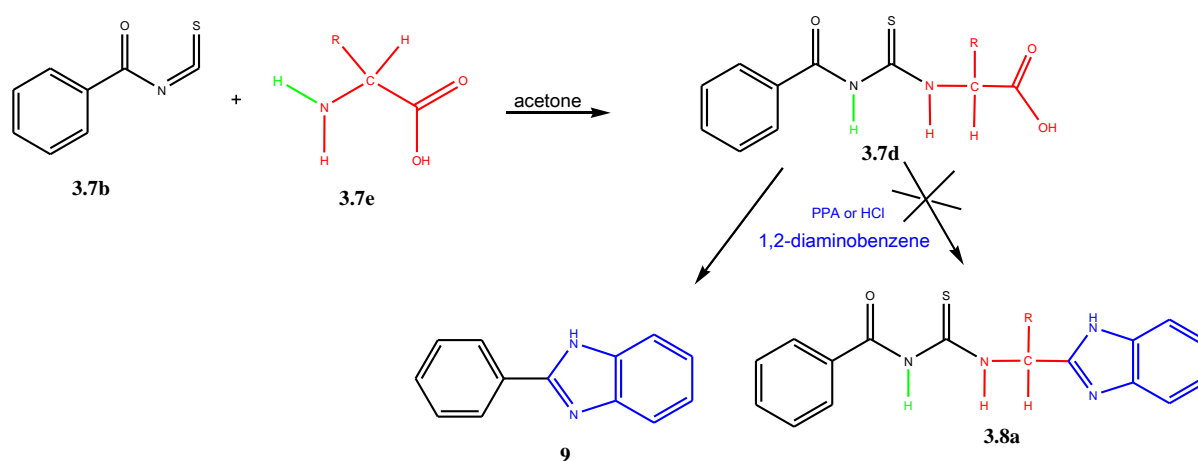
Scheme 3.7 Synthesis of benzimidazoles of amino acid derivatives of benzoyl isothiocyanate.

3.4 Synthesis and characterization of amino acid derivatives

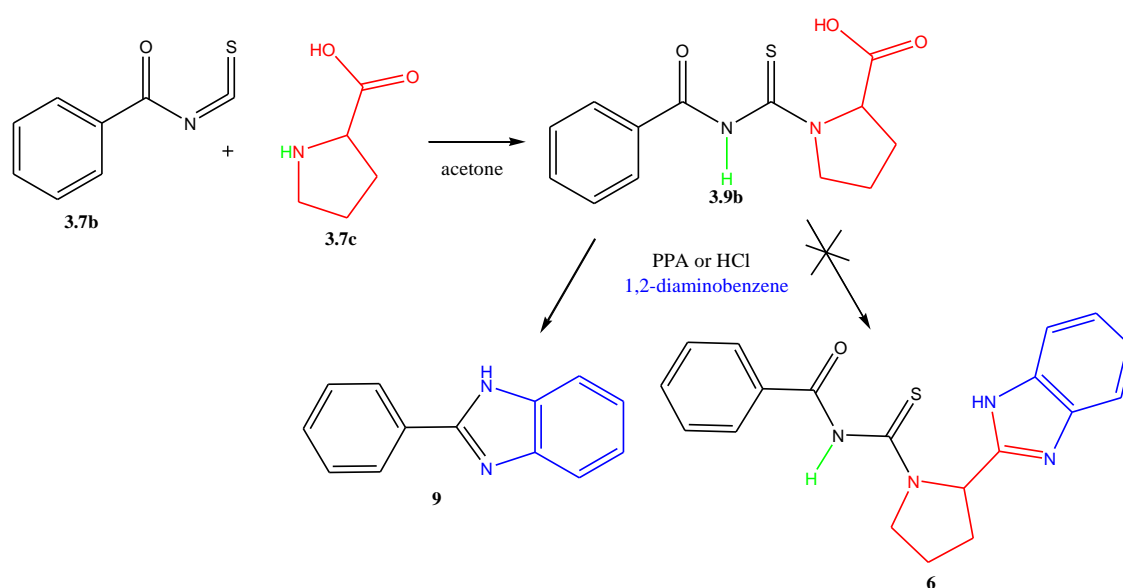
Cyclohexanecarbonyl isothiocyanate has been reacted with various amines in acetone, with a slightly different work-up procedure which involved the addition of 0.1 N hydrochloric acid to the mother liquor before filtration, and this was reported to give higher yields of between 86 and 93%.³¹³ Amino acid derivatives of benzoyl isothiocyanate have been accessed by treating potassium thiocyanate with benzoyl chloride in anhydrous acetone for 1 h and adding amino acids and few drops of pyridine to the product and further refluxing for 6 h.³¹⁴

The syntheses of 2-[(benzoylcarbamoithiyl)amino]-3-hydroxypropanoic acid (**5**), 2-[(benzoylcarbamoithiyl)amino]-4-(methylsulfanyl)butanoic acid (**7**) and 2-[(benzoylcarbamoithiyl)amino]propanoic acid (**8**) were readily achieved by the reaction of benzoyl isothiocyanate with the different amino acids (**Scheme 3.8**). **Scheme 3.9** gives the

reaction path for 1-(benzoylcarbamothioyl)pyrrolidine-2-carboxylic acid (**6**). The lone pair of electrons on the nitrogen atom of the amino acid attacks the carbon of the thione. This shifts the electron density onto the nitrogen of the isothiocyanate allowing it to abstract a proton from the amine of the amino acid. The FTIR, ^1H NMR and ^{13}C NMR confirmed the formation of the amino acid derivatives. 2-Phenyl-1*H*-benzimidazole (**9**) (Schemes 3.8 and 3.9) was accessed by the reaction of compounds **5–8** with *o*-phenylenediamine. The diamine attacks the carbonyl close to the benzene ring (benzoyl group) instead of the carboxylic acid to form the desired benzimidazole.



Scheme 3.8 Synthesis scheme for compounds **5** and **7–9**.



Scheme 3.9 Synthesis scheme for compounds **6** and **9**.

N-Benzoyl-*N'*-carboxyl substituted thiourea derivatives have been synthesized by the reaction of benzoyl isothiocyanate with amino acids. In this reaction potassium thiocyanate was used as the isothiocyanate source and few drops of pyridine was added after the addition of the amino acid.³¹⁵ *N*-[Benzoylamino]thioxomethyl]amino acid derivatives have been prepared by the reaction of benzoyl isothiocyanate with various amino acids in acetone, namely, histidine, alanine, phenylalanine, serine and cysteine, however only the alanine and serine derivatives were characterised by NMR.³¹⁵ The cadmium(II) and zinc(II) complexes of the phenylalanine derivatives have also been reported and characterized by IR, NMR, and microanalysis.³¹⁶ The cobalt(II), copper(II) and nickel(II) complexes of the aspartic acid, glutamic acid, methionine, leucine and tryptophan derivatives of benzoyl isothiocyanates have been synthesized and tested for their antibacterial activity.³¹⁷

The ¹H NMR spectrum (**Figure 3.27**) of **5** gave a singlet signal at 11.43 ppm for the N–H of an amide, another singlet signal attributable to the proton of a hydroxyl group occurred at 11.49 ppm. This was confirmed in the ¹H–¹H COSY spectrum (**Figure 3.28**). A broad signal for an N–H also occurred at 5.34 ppm. Aromatic protons occurred between 7.96–7.53 ppm, a triplet signal for one proton occurred at 4.94 ppm, a singlet signal for two –methylene protons occurred at 3.88 ppm. The ¹³C NMR spectrum (**Figure 3.29**) showed a signal at 180.3 ppm for the C=S of thione, and two signals at 170.7 and 168.3 for the carbonyl group. Aromatic carbons occurred between 133.0 and 128.4 ppm. Two signals at 60.5 and 60.3 ppm were observed for the C–H and methylene groups were also observed. The IR spectrum (**Figure 3.30**) showed a band at 3229 cm⁻¹ for the N–H of an amide. The aliphatic C–H stretch was observed at 2980 cm⁻¹ whilst the C=S stretch occurred at 1725 cm⁻¹. The C=O and the C=C bands were observed at 1654 and 1509 cm⁻¹, respectively. The C–N stretch occurred at 1164 cm⁻¹.

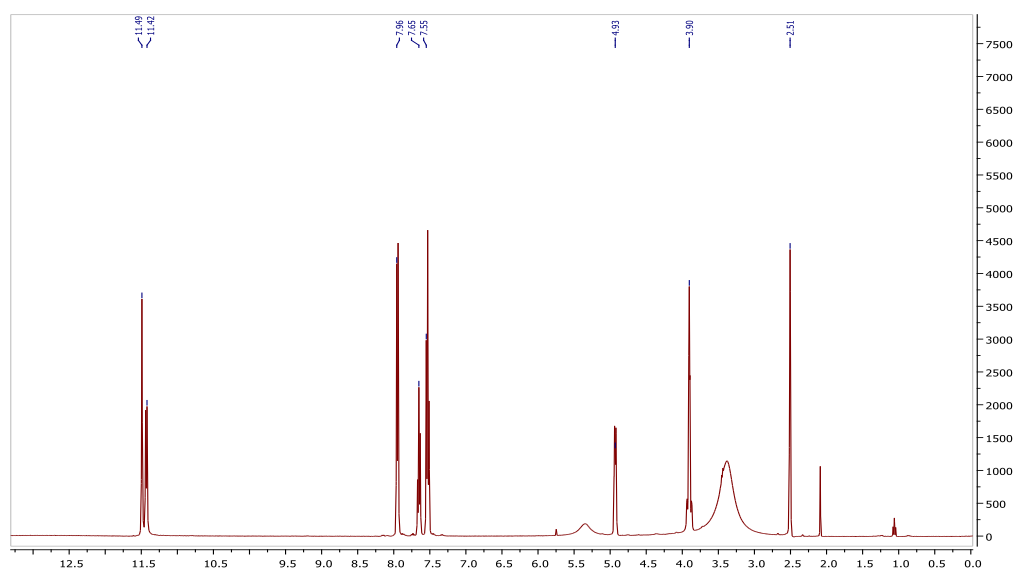


Figure 3.27 ^1H NMR spectrum of 2-[(benzoylcarbamothioyl)amino]-3-hydroxypropanoic acid (**5**).

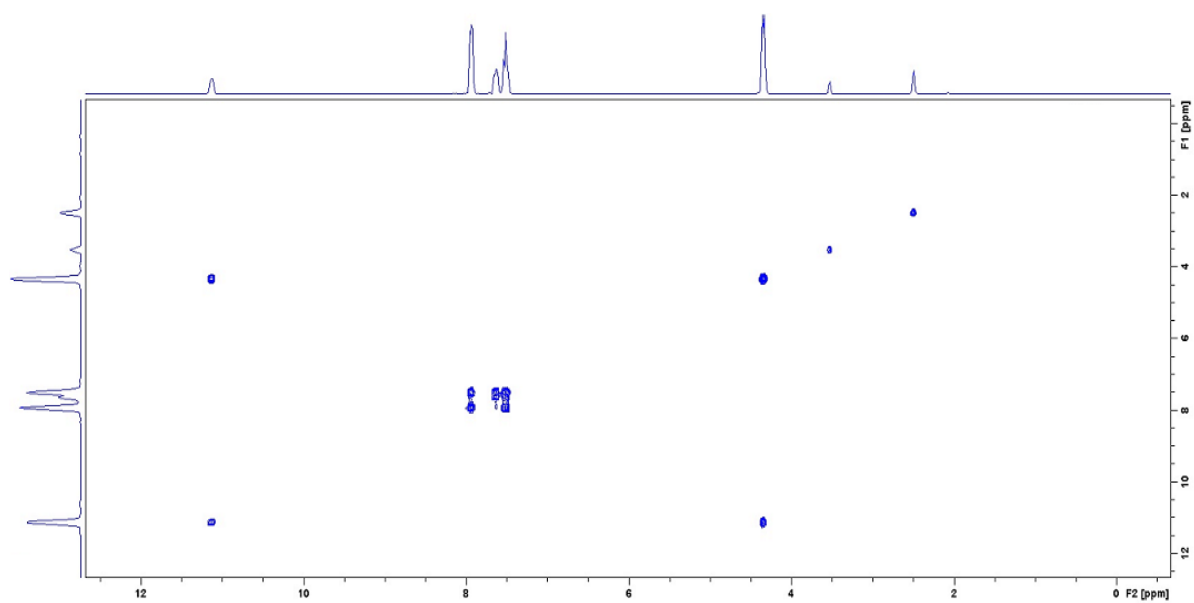


Figure 3.28 ^1H - ^1H COSY spectrum of 2-[(benzoylcarbamothioyl)amino]-3-hydroxypropanoic acid (**5**).

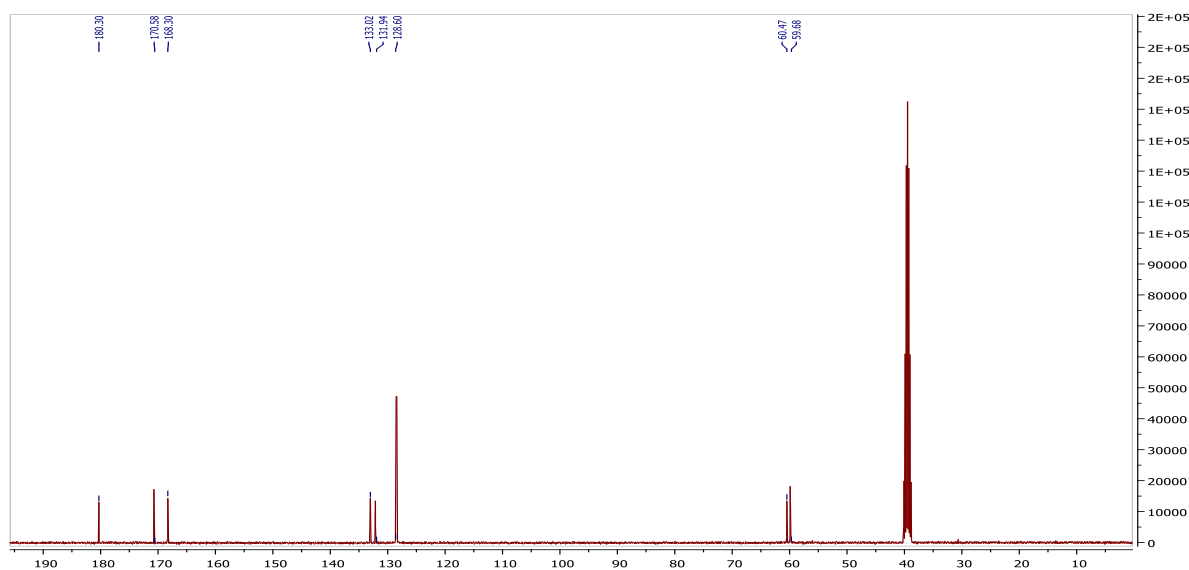


Figure 3.29 ^{13}C NMR spectrum of 2-[(benzoylcarbamothioyl)amino]-3-hydroxypropanoic acid (**5**).

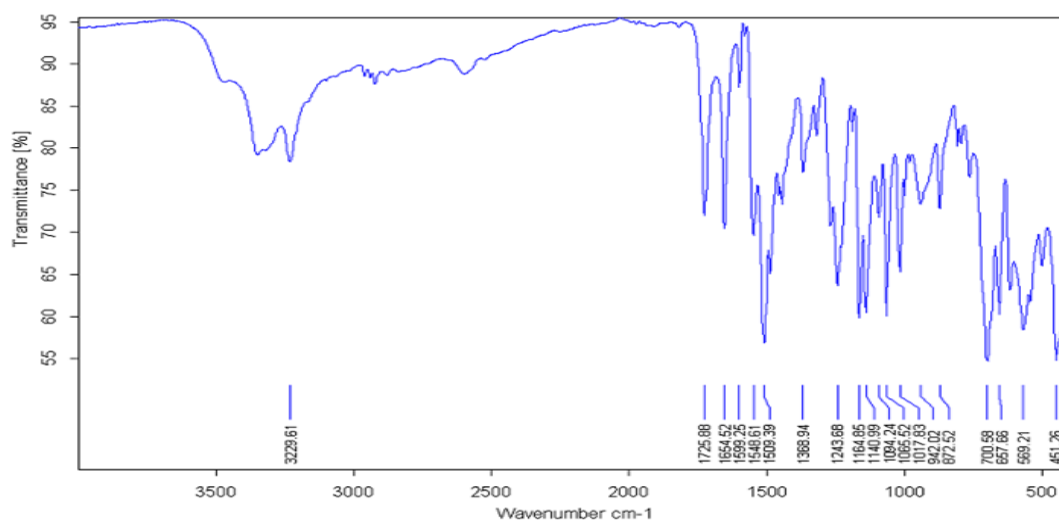


Figure 3.30 IR spectrum of 2-[(benzoylcarbamothioyl)amino]-3-hydroxypropanoic acid (**5**).

The nitrogen protons which do not appear in the ^1H NMR spectra of compounds **6**, **7** and **8** exchange with the residual water molecules in DMSO hence are undetectable. The ^1H NMR spectrum (**Figure 3.31**) of **6** gave a singlet signal at 10.90 ppm for the proton of a hydroxyl group which was consistent with the ^1H - ^1H COSY spectrum (**Figure 3.32**). Aromatic protons occurred between 7.94–7.50 ppm. A triplet signal for one proton was observed at 4.68 ppm.

Three sets of multiplet signals for methylene protons were observed at 3.68, 2.02 and 1.99 ppm. The ^{13}C NMR spectrum (**Figure 3.33**) showed a signal at 179.1 ppm for the C=S of thione, and two signals at 171.9 and 171.2 ppm were due to the carbonyl of two different rotamers of **6**. Whilst the carbonyl of the amide was observed at 164.0 ppm. Aromatic carbons occurred between 132.9 to 128.2 ppm. Six signals for methylene protons were observed between 65.4 to 22.94 ppm. The IR spectrum (**Figure 3.34**) showed a band at 3229 cm^{-1} for the N–H stretch. The aliphatic C–H stretch was observed at 2987 cm^{-1} , whilst the C=S stretch occurred at 1730 cm^{-1} . The C=O and the C=C bands were observed at 1659 and 1491 cm^{-1} , respectively. The C–N stretch occurred at 1182 cm^{-1} . The two rotamers in solution are formed by restricted rotation around the nitrogen of the proline, specifically around the N(2)–C(2) bond, making the carbon signals for all the four carbon atoms in the proline ring double but with reduced intensities. This also gave rise to two carbonyl signals for the proline part of compound **6** as evident in the ^{13}C NMR and DEPT–135 (**Figure 3.35**) spectra.

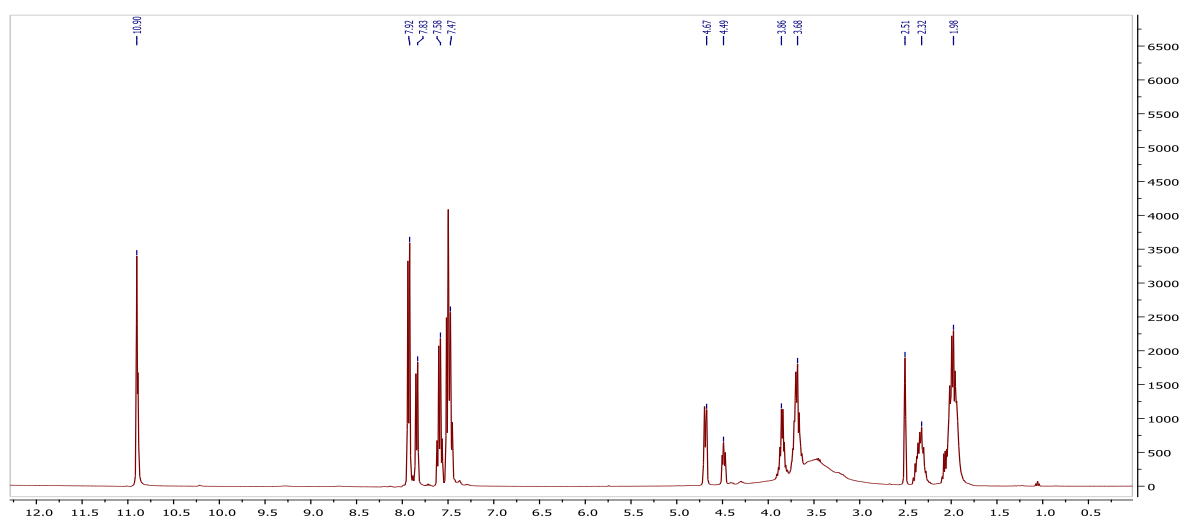


Figure 3.31 ^1H NMR spectrum of 1-(benzoylcarbamothioyl)pyrrolidine-2-carboxylic acid (**6**).

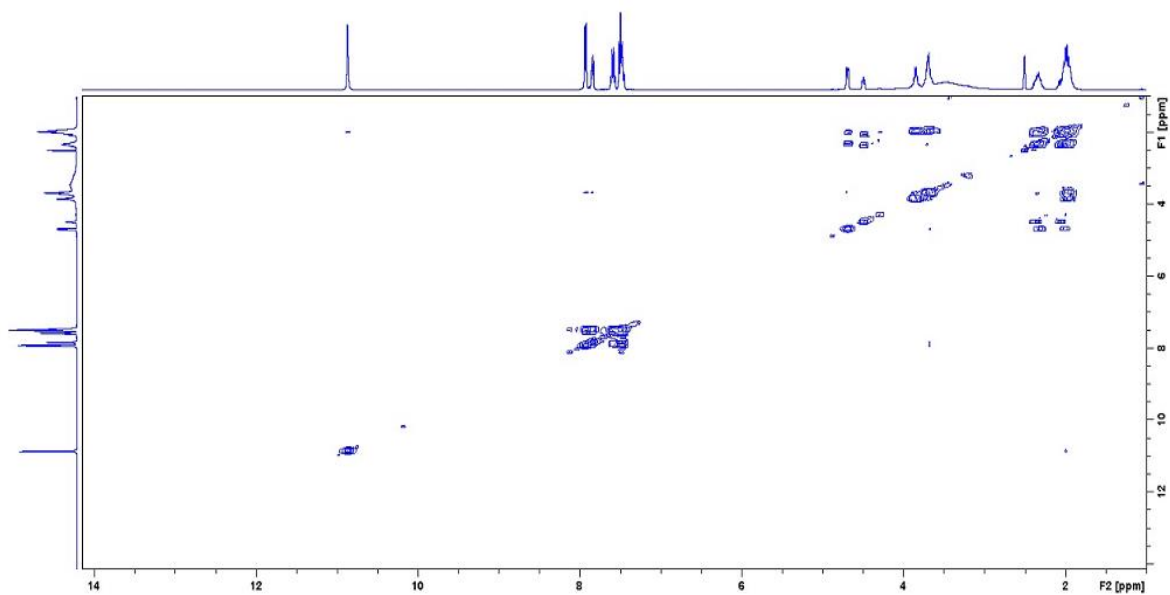


Figure 3.32 ^1H - ^1H COSY spectrum of 1-(benzoylcarbamothioyl)pyrrolidine-2-carboxylic acid (**6**).

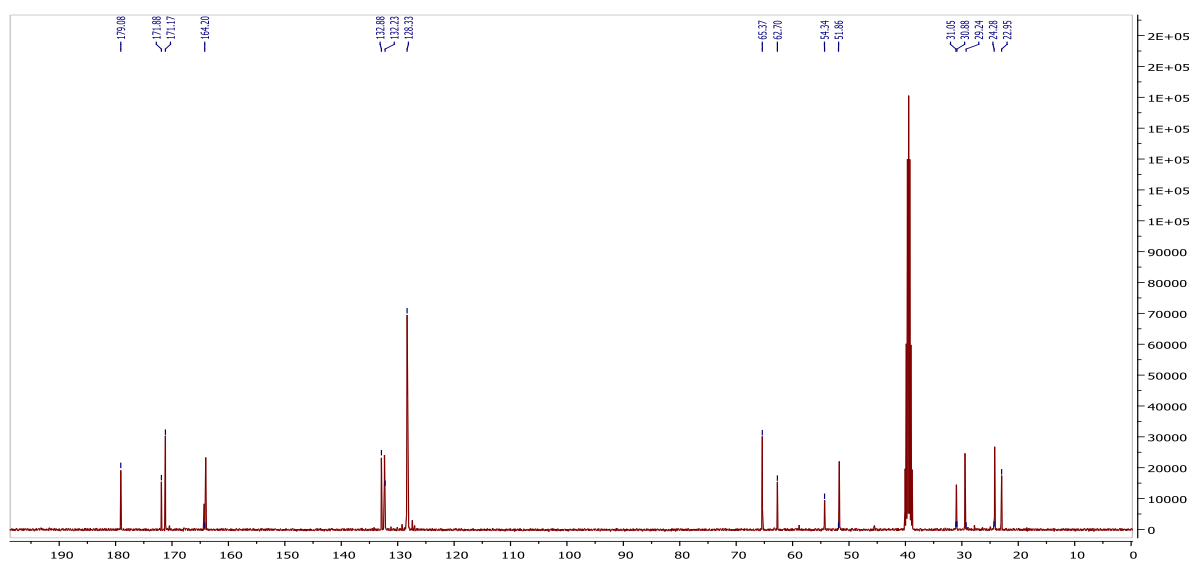


Figure 3.33 ^{13}C NMR spectrum of 1-(benzoylcarbamothioyl)pyrrolidine-2-carboxylic acid (**6**).

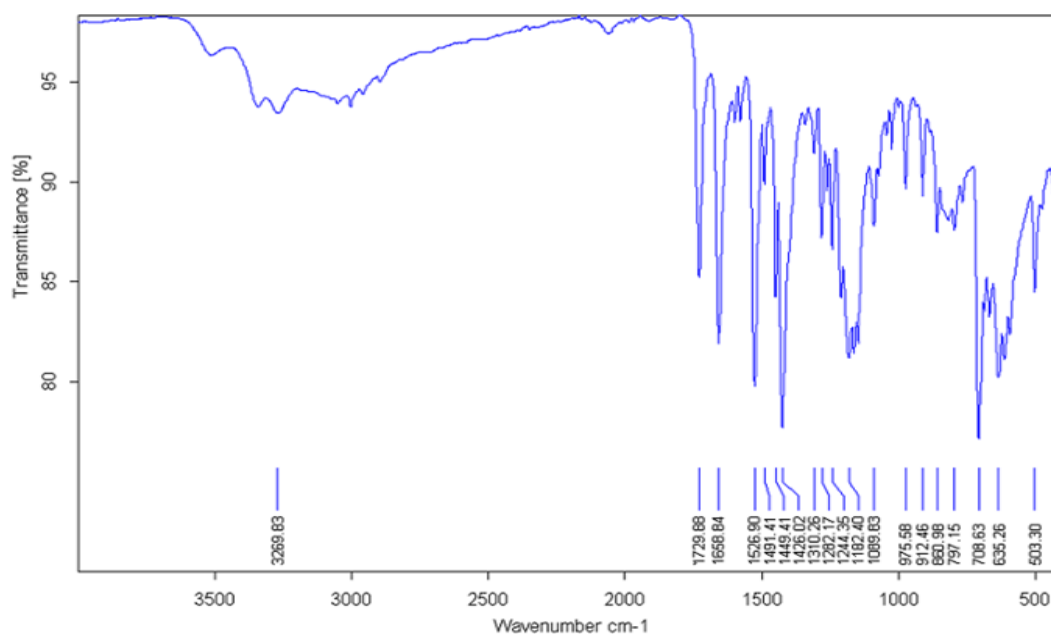


Figure 3.34 IR spectrum of 1-(benzoylcarbamothioyl)pyrrolidine-2-carboxylic acid (**6**).

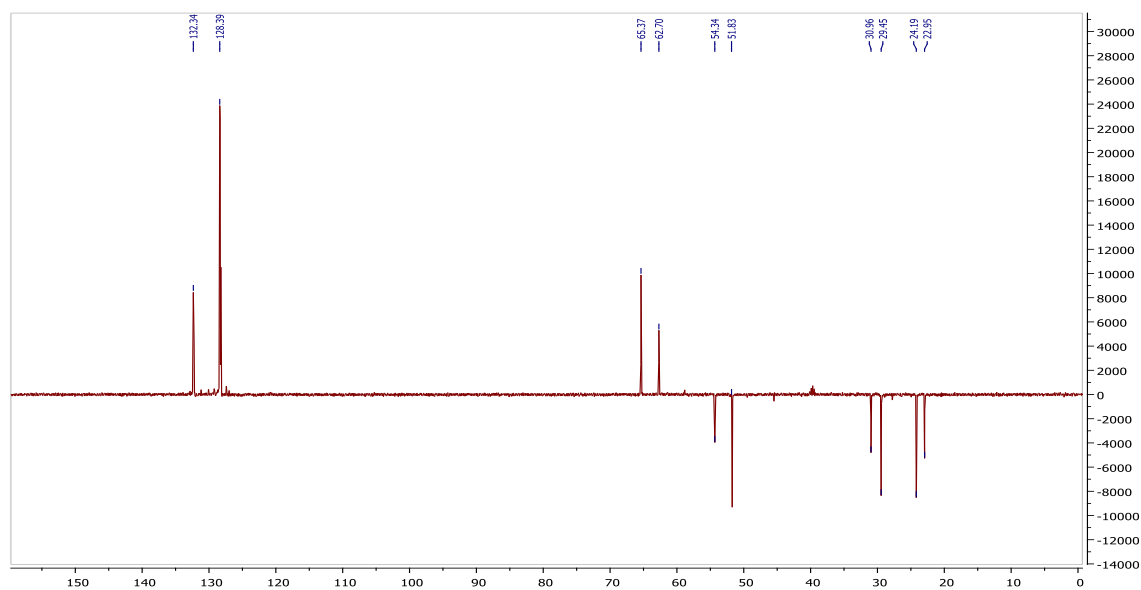


Figure 3.35 DEPT 135 spectrum of 1-(benzoylcarbamothioyl)pyrrolidine-2-carboxylic acid (**6**).

The 1D NOESY (**Figure 3.36** and 2D NOESY (**Figure 3.37**) spectra showed an exchange between the signals at 4.42 and 4.62 ppm, and both signals are attached to the same carbon

that changes position as indicated in the HSQC (Figure 3.38) and HMBC (Figure 3.39) spectra.

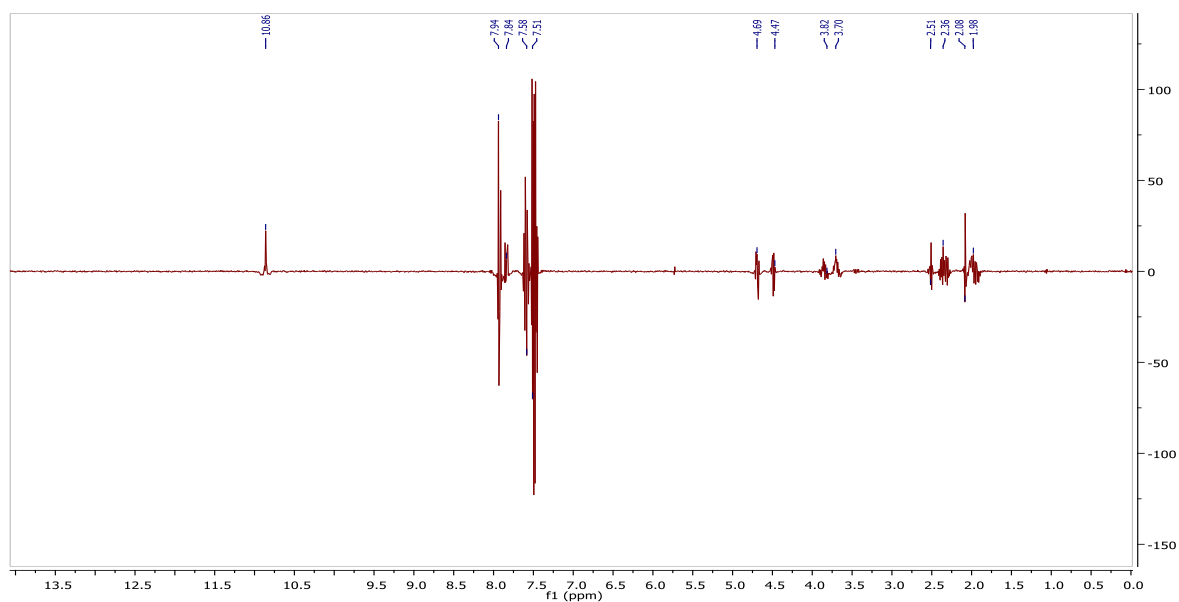


Figure 3.36 ^1D NOESY spectrum of 1-(benzoylcarbamothioyl)pyrrolidine-2-carboxylic acid (**6**).

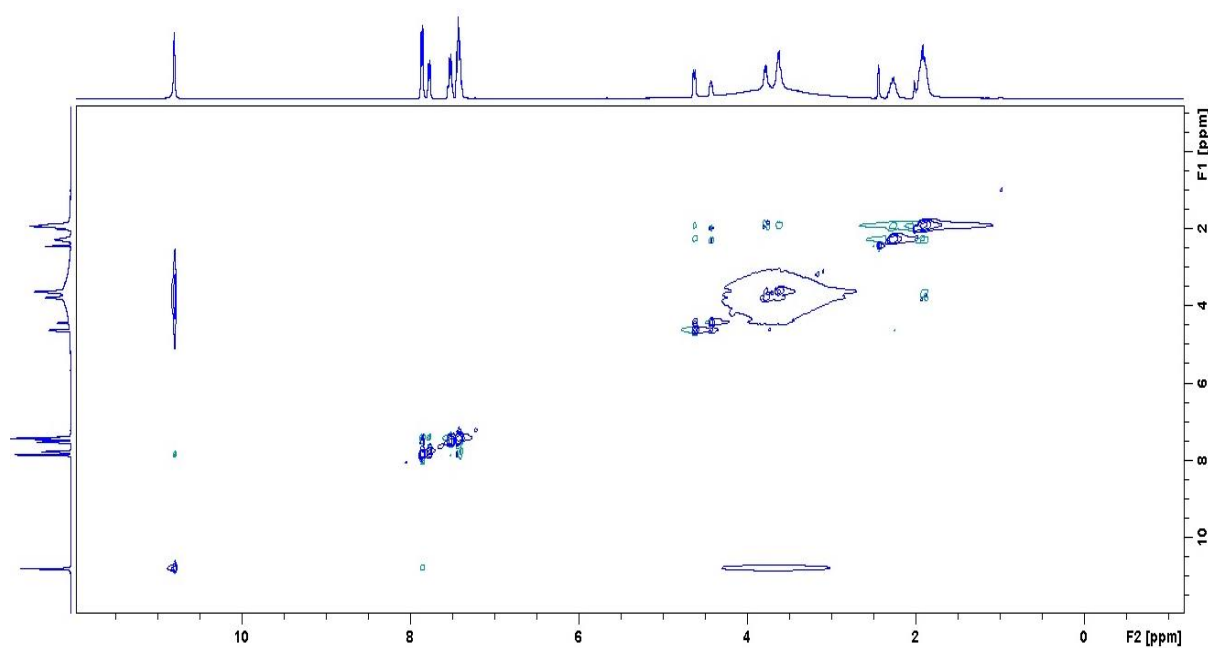


Figure 3.37 2D NOESY spectrum of 1-(benzoylcarbamothioyl)pyrrolidine-2-carboxylic acid (**6**).

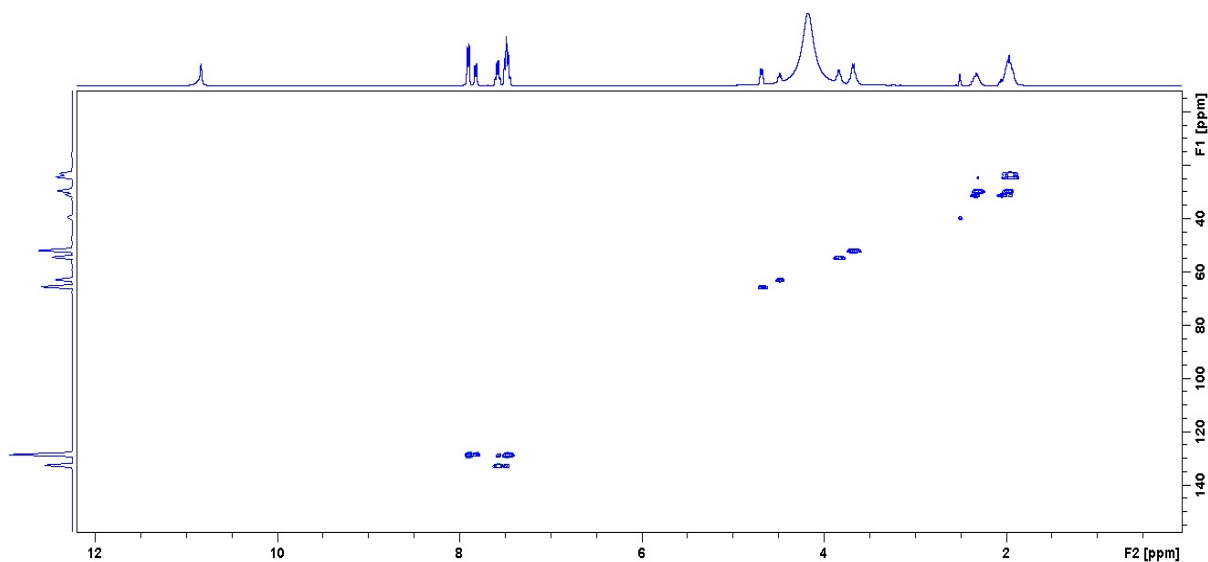


Figure 3.38 HSQC spectrum of 1-(benzoylcarbamothioyl)pyrrolidine-2-carboxylic acid (6).

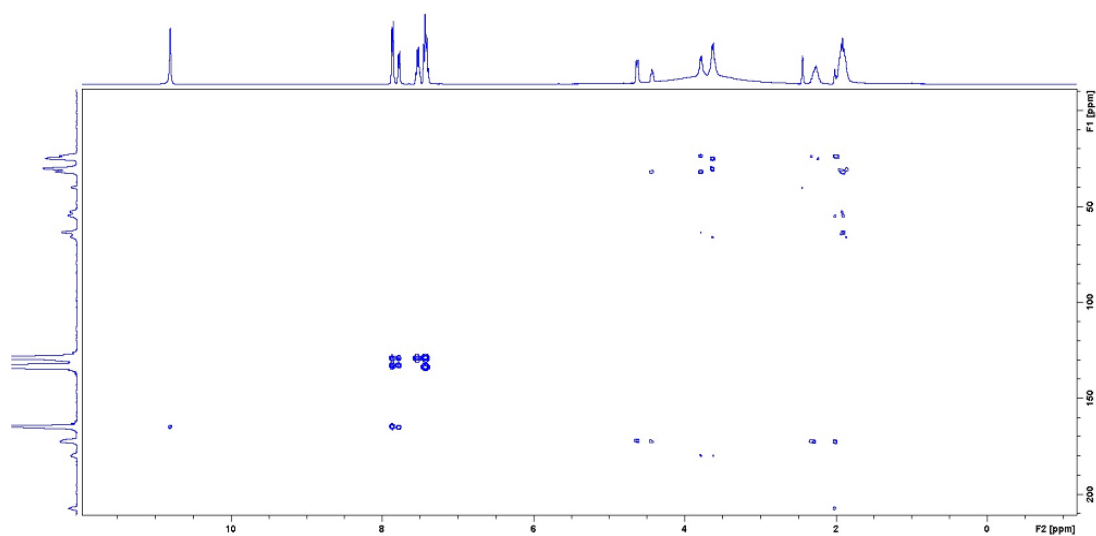


Figure 3.39 HMBC spectrum of 1-(benzoylcarbamothioyl)pyrrolidine-2-carboxylic acid (6).

The ^1H NMR spectrum (**Figure A3.1**) of **7** showed a singlet signal at 11.54 ppm and a doublet signal at 11.28 ppm for the hydroxyl and N–H group of the amide, respectively. Aromatic protons occurred between 7.96–7.52 ppm. A quartet signal at 5.03 ppm was observed for the chiral proton, two multiplet signals for two set of methylene protons

occurred at 2.26 and 2.17 ppm. A singlet signal for three methyl protons occurred at 2.09 ppm. The ^{13}C NMR spectrum (**Figure A3.2**) showed a signal at 180.50 ppm for the C=S of the thione. Two signals were observed at 171.8 and 168.4 ppm for the carbonyl. Aromatic carbons occurred between 133.1 and 128.2 ppm. A signal for a C–H was observed at 66.6 ppm. Two methylene groups were observed at 30.5 and 29.2 ppm which were confirmed by the inversion in the DEPT–135 spectrum (**Figure A3.3**). A signal for a methyl group occurred at 14.6 ppm. The IR spectrum (**Figure A3.4**) showed two signals at 3282 and 3202 cm^{-1} for N–H stretch. A signal at 2914 cm^{-1} was observed for the aliphatic C–H stretch. The C=S stretch of a thione was observed at 1715 cm^{-1} whilst the C=O and C=C signals were observed at 1664 and 1519 cm^{-1} . The C–N stretch occurred at 1193 cm^{-1} .

The ^1H NMR spectrum (**Figure A3.5**) of **8**, gave a singlet signal at 11.51 ppm due to hydroxyl group, and another signal at 11.30 ppm for the N–H of an amide. Aromatic protons were observed between 7.93 and 7.52 ppm. A quartet signal for one proton was observed at 4.85 ppm, whilst a doublet signal for three protons was observed 1.49 ppm. The ^{13}C NMR spectrum (**Figure A3.6**) showed a signal at 179.9 ppm for the C=S of thione, and two signals at 172.9 and 168.5 for the carbonyl group. Aromatic carbons occurred between 133.0 and 128.4 ppm. Two signals at 63.1 and 17.2 ppm were observed for the C–H and methyl groups. The IR spectrum (**Figure A3.7**) showed a band at 3384 cm^{-1} for the N–H of an amide. The aliphatic C–H stretch was observed at 2992 cm^{-1} whilst the C=S stretch occurred at 1726 cm^{-1} . The C=O and the C=C bands were observed at 1678 and 1489 cm^{-1} , respectively. The C–N stretch occurred at 1196 cm^{-1} .

The ^1H NMR spectrum (**Figure A3.8**) of compound 2-phenyl-1*H*-benzimidazole (**9**) gave signals between 8.20 and 7.21 ppm for aromatic protons. The ^{13}C NMR spectrum (**Figure A3.9**) showed a signal at 151.2 ppm for the C=N of the benzimidazole. Signals for aromatic carbons were observed between 130.0 and 122.1 ppm. The IR spectrum (**Figure A3.10**) showed a band at 3048 cm^{-1} for the N–H of an amide. The aliphatic C–H stretch was observed at 2961 and 2850 cm^{-1} whilst the C=N stretch occurred at 1539 cm^{-1} . The C=C and the C–N bands were observed at 1461 and 1443 cm^{-1} , respectively.

3.4.1 Crystal structures of amino acid derivatives

Compounds **5**, **6** and **7** were recrystallized from acetone:water (4:1) as colourless crystals, whilst compound **8** was recrystallized from acetone:water (4:1) as yellow crystals. The crystallographic data, selected bond lengths, bond angles and torsion angles for the structures of **5–8** are provided in tables **3.9** and **3.10**. Compounds **5** and **6** crystallized in orthorhombic space group $P2_12_12_1$, whilst compound **7** crystallized in monoclinic space group $P2_1$ and compound **8** in orthorhombic space group $C2_22_1$. The absence of rotamers in the solid state was confirmed during the refinement procedure by means of the Flack parameter in each case.

The crystal structure of compound **6** has been reported by Ngah *et al.* and the compound was accessed by refluxing proline with benzoyl isothiocyanate in acetone giving a yield of 76%.³¹⁶

Table 3.9 Crystallographic data and structure refinement summary for compounds 5–8.

Property	5	6	7	8
CCDC Number	1014079	1014083	1014284	1014322
Empirical Formula	C ₁₁ H ₁₂ N ₂ O ₄ S,H ₂ O	C ₁₃ H ₁₄ N ₂ O ₃ S,H ₂ O	C ₁₃ H ₁₆ N ₂ O ₃ S ₂	C ₁₁ H ₁₂ N ₂ O ₃ S
Formula Weight	286.31	296.35	312.42	252.30
Crystal System	orthorhombic	Orthorhombic	Monoclinic	Orthorhombic
Space group	<i>P</i> 2 ₁ 2 ₁ 2 ₁	<i>P</i> 2 ₁ 2 ₁ 2 ₁	<i>P</i> 2 ₁	<i>C</i> 2 ₂ 2 ₁
<i>a</i> (Å)	7.0613(3)	8.8347(5)	5.1663(2)	8.2584(3)
<i>b</i> (Å)	11.0752(4)	11.8182(7)	1.4170(5)	21.7331(8)
<i>c</i> (Å)	16.5713(7)	13.3896(8)	12.7108(5)	13.4905(6)
α (°)	90	90	90	90
β (°)	90	90	96.843(1)	90
γ (°)	90	90	90	90
V [Å ³]	1295.96(9)	1398.01(14)	744.39(5)	2421.28(17)
Z	4	4	2	8
D(calc) (g/cm ³)	1.467	1.408	1.394	1.384
μ (MoKa) (/mm)	0.268	0.246	0.365	0.265
<i>F</i> (000)	600	624	328	1056
Crystal Size (mm)	0.26 x 0.39 x 0.52	0.47 x 0.48 x 0.56	0.16 x 0.37 x 0.49	0.23 x 0.53 x 0.72
Temperature (K)	200	200	200	200
Radiation (Å)	0.71073	0.71073	0.71073	0.71073
θ Min–Max (°)	2.2–28.3	2.8–28.4	2.4–28.3	1.9–28.3
Dataset	–7:9;–14:9 ;–22:20	–1:8;–15:13;–17:17	–6:4;–14:15;–16:16	–11:9;–25:28;–15:17
Tot., Uniq. Data	6893, 3088	10872, 3334	6845, 3344	6792, 3009
R _{int}	0.01	0.014	0.017	0.014
[I > 2.0 sigma(I)]	2991	3224	3176	2879
Nref, Npar	3088,180	3334, 195	3344,185	3009, 164
R _w	0.0227	0.0240	0.0252	0.0238
R ₂	.0 43	0.0650	0.0654	0.0659
S	1.09	1.03	1.03	1.04
Max. and Av. Shift/Error	0.00, 0.00	0.00, 0.00	0.000 ,0.00	0.000 ,0.00
Min..Residual. Density. [e/Å ³]	–0.17	–0.17	–0.20	–0.14
Max.Residual. Density. [e/Å ³]	0 25	0.24	0.26	0.25
Flack parameter	0.020(13)	0.002(14)	0.00(2)	0.012(19)

Table 3.10 Selected bond lengths (Å) and bond angles (°) of compounds **5–8**.

Bond lengths	5	6	7	8
S1–C2	1.670(2)	1.661(2)	1.676(2)	1.677(1)
O1–C1	1.232(2)	1.229(2)	1.226(2)	1.222(2)
N1–C2	1.399(2)	1.420(2)	1.385(3)	1.323(2)
N1–C1	1.372(2)	1.367(2)	1.383(3)	1.386(2)
N2–C2	1.331(2)	1.326(2)	1.331(3)	1.487(2)
C1–C11	1.489(2)	1.488(2)	1.486(3)	1.487(2)
S2–C7	-	-	1.793(3)	-
S2–C6	-	-	1.801(2)	-
Bond angles	5	6	7	8
O1–C1–N1	121.8(1)	121.8(1)	121.5(2)	122.0(1)
O1–C1–C11	121.6(1)	120.9(1)	121.3(2)	121.8(1)
S1–C2–N1	118.3(1)	119.2(1)	120.9(2)	119.6(1)
S1–C2–N2	125.2(1)	124.4(1)	122.3(2)	123.5(1)
N1–C1–C11	116.6(1)	117.3(1)	117.2(2)	116.2(1)
N1–C2–N2	116.6(1)	116.3(1)	116.8(2)	116.8(1)
C1–N1–C2	127.8(1)	123.2(1)	126.9(2)	127.4(1)

The ORTEP diagram of **5** is presented in **Figure 3.40**. The experimental bond distance of S1–C2 = 1.670(2) Å in **5** is consistent with the C=S of the thione ³¹⁸, whilst the C1–O1 and C4–O3 bond distances of 1.233(2) Å and 1.202(2) Å show the presence of the carbonyl bond of the amide and the carbonyl of the carboxylic acid, respectively. The bond distance of C1–N1 = 1.372(2) Å is indicative of the C–N bond of the amide. The O2–C4–O3 bond angle of 124.8(2)° is consistent with the bond angle around the sp² carbon of the carboxylic acid whilst the S1–C2–N2 bond angle of 125.2(1)° indicated the presence of the sp² carbon of the thione. The O1–C1–N1 bond angle of 121.6(1)° also showed the presence of the sp² carbon of the amide.

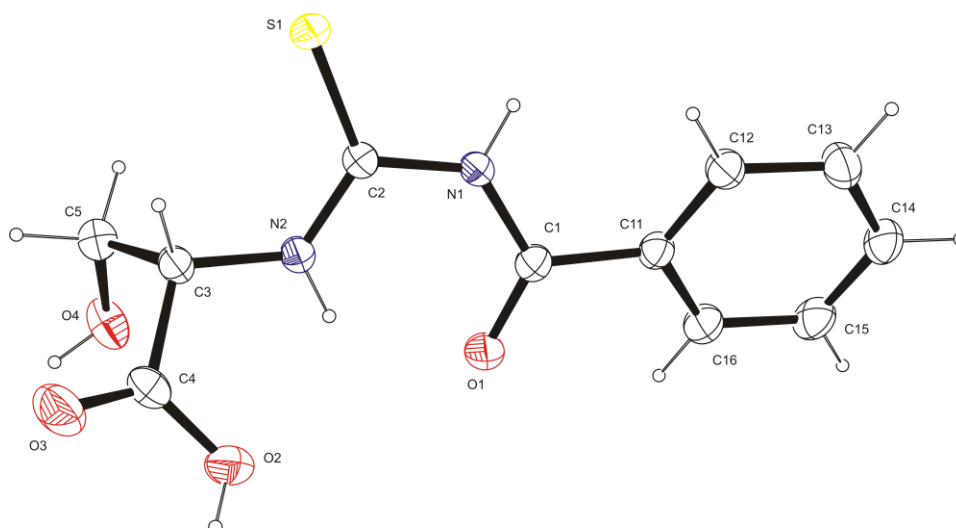


Figure 3.40 An ORTEP view of 2-[(benzoylcarbamothioyl)amino]-3-hydroxypropanoic acid (**5**) showing 50% probability displacement ellipsoids and the atom labelling.

The structure of **6** is presented in **Figure 3.41**. The bond distances of O2–C3 and C1–O1 which were 1.201(2) Å and 1.229(2) Å are consistent with the carbonyl of the carboxylic acid and the carbonyl of the amide, respectively. This also compared favourably with the carbonyl bond distances in **5**. The bond distance of C1–N1 = 1.367(2) Å indicated the C–N bond of the amide and it was comparable to the C–N bond distance in **5** which was 1.372(2) Å. The bond distance of S(1)–C(2) = 1.661(2) Å showed the presence of the C=S of the thione and was comparable to that of **5** (1.670(2) Å). The O3–C3–O2 bond angle of 125.0(1)° is indicative of the sp² carbon of the carbonyl of the carboxylic acid and the N1–C1–O1 bond angle of 121.8(1)° also confirmed the presence of the sp² carbon of the carbonyl and these were comparable to the bond angles observed in **5**. The S1–C2–N1 bond angle of 119.2(1)° also indicated the presence of the sp² carbon of the thione. The ORTEP diagrams of compounds **7** and **8** are presented in **Figures 3.42** and **3.43**. Their metrical parameters are similar to those of compounds **5** and **6**.

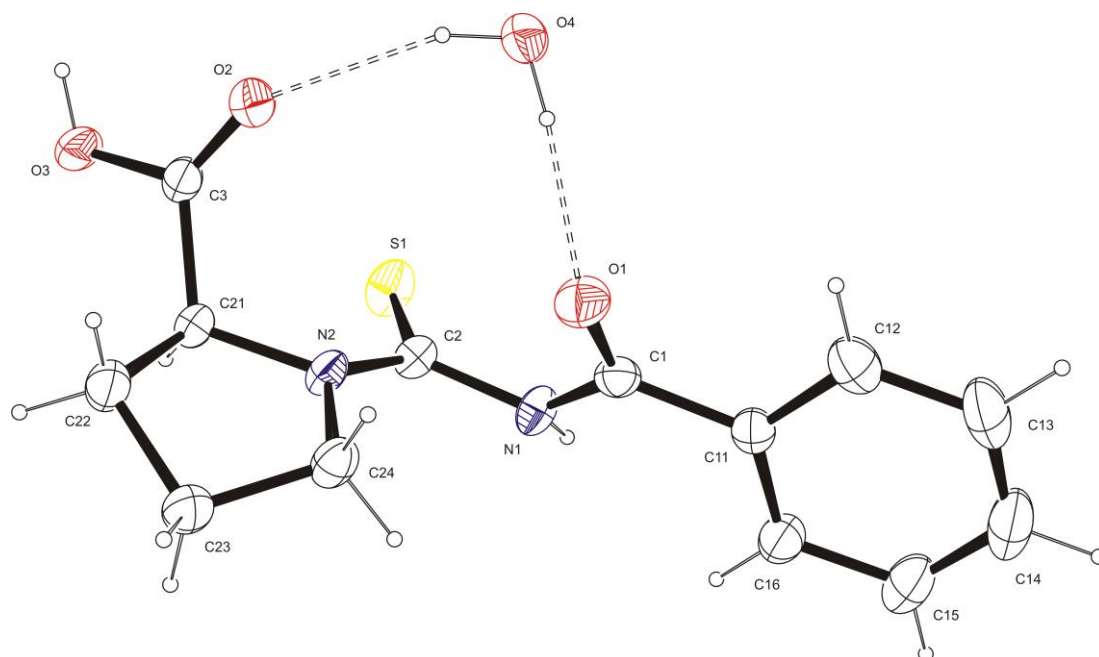


Figure 3.41 An ORTEP view of 1-(benzoylcarbamothioyl)pyrrolidine-2-carboxylic acid (**6**) showing 50% probability displacement ellipsoids and the atom labelling.

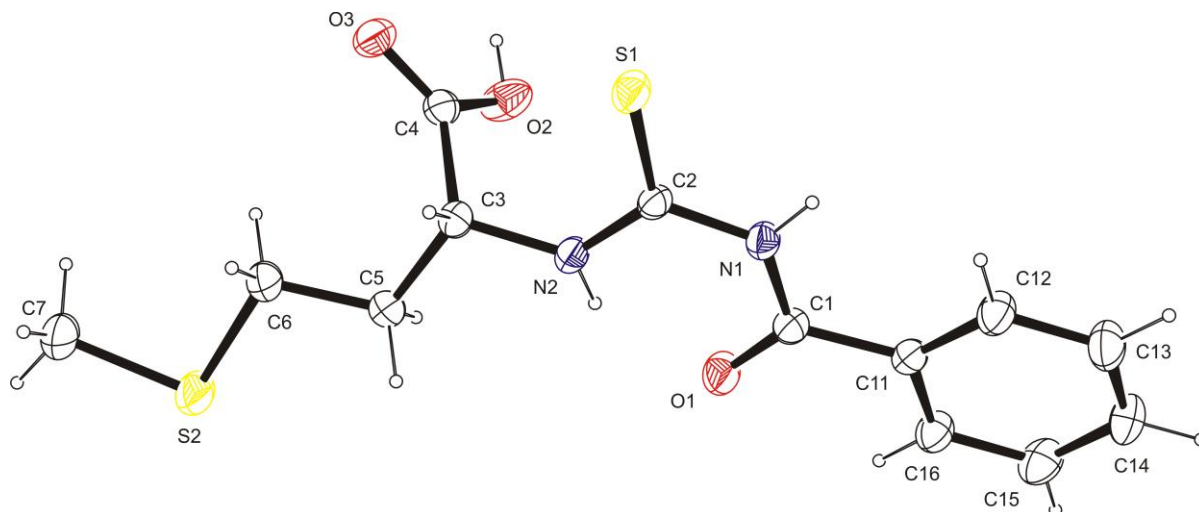


Figure 3.42 An ORTEP view of 2-[(benzoylcarbamothioyl)amino]-4-(methylsulfonyl)butanoic acid (**7**) showing 50% probability displacement ellipsoids and the atom labelling.

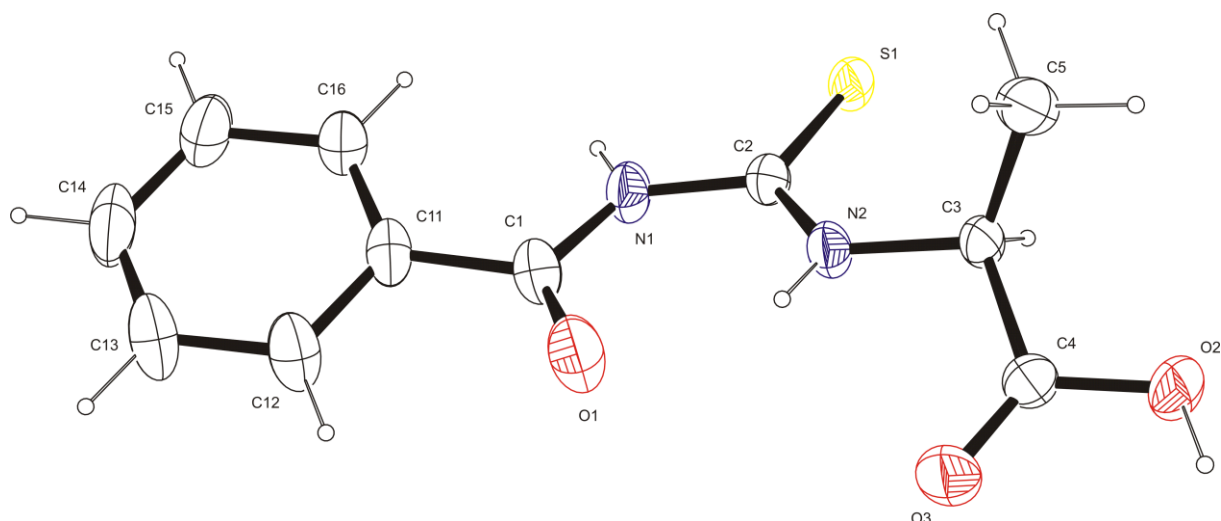


Figure 3.43 An ORTEP view of 2-[(benzoylcarbamothioyl)amino]propanoic acid (**8**) showing 50% probability displacement ellipsoids and the atom labelling.

3.4.2 HOMO-LUMO analysis

In view of the fact that compounds **5-8** are useful intermediates in accessing other complex molecules, it was important to carry out some theoretical studies to gain insight into the nature of these compounds in terms of their chemical reactivity. In fact, a chemical reaction that was attempted on compounds **5-8**, i.e. a cyclization reaction with 1,2-diaminobenzene at the carboxylic acid site to form benzimidazoles, has been unsuccessful yielding rather a benzimidazole through the diamine attacking the carbonyl of the benzoyl group (compound **9**) instead of the carboxylic acid site. This prompted us to carry out some computational studies in order to predict the reactivity of these compounds. The highest occupied molecular orbital and lowest unoccupied molecular orbital energy separations, HOMO–LUMO energy gaps, have been evaluated by DFT methods. The frontier orbitals are useful in predicting the most reactive position in π -electron systems³¹⁹ and to explain several types of reactions in a conjugated system like benzoyl isothiocyanate.

Benzoyl isothiocyanate is characterised by a small highest occupied molecular orbital–lowest unoccupied molecular orbital (HOMO–LUMO) separation, which is the result of a significant degree of intramolecular charge transfer from the end capping electron-donor groups through a π -conjugated path.³²⁰ The HOMO and LUMO are the main orbitals that determine chemical

stability of the species.³²¹ The HOMO, which represents the ability to donate an electron, is delocalised over the entire molecule except the carbonyl and carbon of the thione whilst the LUMO (which represent the ability to accept an electron) shows delocalization of its orbitals over both the carbon atoms of the carbonyl and the thione indicating that both are susceptible to attack by an incoming group but because the carbonyl is sterically hindered the carbon of the thione is the preferred site of attack and this attack is further stabilized by charge transfer through the benzene ring. The energy of the HOMO is directly related to the ionization potential whilst the energy of the LUMO is related to the electron affinity. The energy difference between HOMO and LUMO orbitals, known as the energy gap, determines the stability or reactivity of molecules.³²² A narrow energy gap for benzoyl isothiocyanate is consistent with its high reactivity. The energy gap is a critical parameter in determining molecular electrical transport properties because it is a measure of electron conductivity.³²³ The hardness of a molecule also corresponds to the gap between the HOMO–LUMO orbitals.³²⁴ Large HOMO–LUMO gap indicates high stability and resistance to charge transfer, therefore, hard molecules have a large HOMO–LUMO gap.

Table 3.11 gives the computed energy gap between the LUMO and HOMO of compounds **5–8** and benzoyl isothiocyanate as well as the amino acids. The computed energy gap between the LUMO and HOMO of benzoyl isothiocyanate is narrow which implies that it is a soft molecule.³²⁵ Compound **5** with a HOMO–LUMO gap of 432.18 kJ/mol is lower compared to that of serine which is 606.60 kJ/mol, confirming that L-serine is harder and less reactive than **5**, even though their sites of reactivity differ. L-Proline with a HOMO–LUMO gap of 564.14 kJ/mol is harder but less reactive than **6** which has a HOMO–LUMO gap of 410.45 kJ/mol, but the reactivity of these compounds are concentrated on different sites of the molecules. Compound **7** with a HOMO–LUMO gap of 349.67 kJ/mol is harder but less reactive than D-methionine which has a HOMO–LUMO gap of 508.09 kJ/mol, and alanine with a HOMO–LUMO gap of 592.37 kJ/mol is hard and less reactive than **8** which is 418.40 kJ/mol. From this information, it is not clear why the carboxylic acid site is less reactive in the benzoyl isothiocyanates derivatives compared with the amino acids since these molecules are softer than the parent amino acids. This prompted the study of the frontier orbitals.

Table 3.11 Summary of the HOMO-LUMO energies for compounds **5–8** and the starting materials.

	HOMO (kJ/mol)	LUMO (kJ/mol)	HOMO–LUMO gap (kJ/mol)
Benzoyl isothiocyanate	–715.16	–498.40	216.76
Compound 5	–675.93	–243.75	432.18
Serine	–692.24	–85.64	606.60
Compound 6	–616.00	–205.55	410.45
Proline	–638.97	–74.83	564.14
Compound 7	–564.17	–214.50	349.67
Methionine	–599.43	–91.34	508.09
Compound 8	–651.52	–233.12	418.40
Alanine	–678.72	–86.35	592.37

Figure 3.44 shows the HOMO and LUMO orbitals of benzoyl isothiocyanate. The HOMO is delocalised over the thione, nitrogen and the ring with the oxygen atom making no contribution whilst the LUMO is delocalised over nearly the entire molecule. This suggests that the entire molecule is involved in the acceptance of electrons which makes this species very reactive.

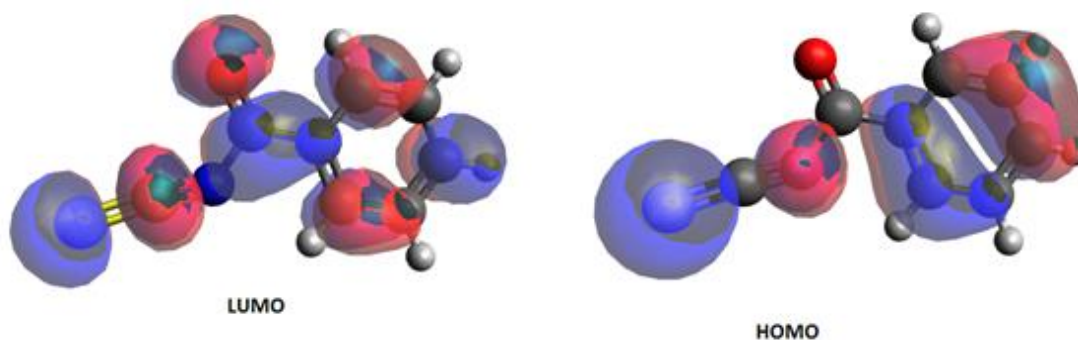


Figure 3.44 The atomic orbitals compositions of the frontier molecular orbitals for benzoyl isothiocyanate.

The frontier orbitals of **5** (**Figure 3.45**) shows that the HOMO is mostly concentrated on the sulfur of the thione, the nitrogen atoms and the phenyl ring, whilst the LUMO is largely delocalised over the thione, the nitrogen atoms, the carbonyl and over the benzene ring which

aids in stabilising the compound during charge transfer *via* delocalization over the benzene ring. The carboxylic acid has no contribution to the frontier orbitals (LUMO) hence is unreactive in the compound. This further confirmed the inability to convert it to a benzimidazole by reacting it with 1,2-diaminobenzene. The frontier orbitals of serine (**Figure 3.46**) are distributed over the entire molecule with most of the atoms making a contribution. The carboxylic acid makes a little contribution to the LUMO hence the cyclization should be possible on a free serine.

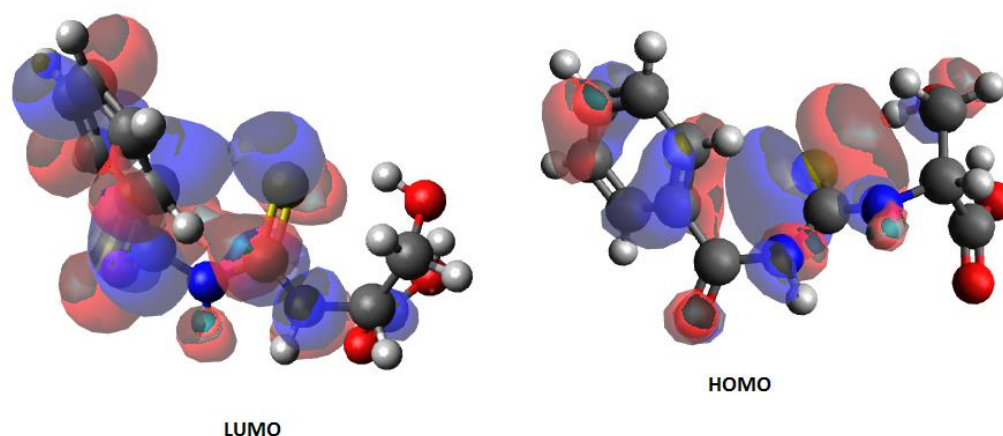


Figure 3.45 The atomic orbitals compositions of the frontier molecular orbital for 2-[(benzoylcarbamothioyl)amino]-3-hydroxypropanoic acid (**5**).

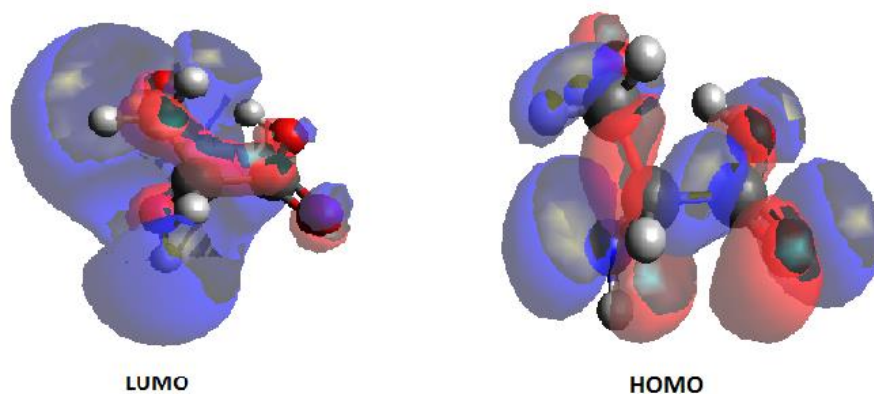


Figure 3.46 The atomic orbitals compositions of the frontier molecular orbital for serine.

The frontier orbitals of **6** are shown in **Figure 3.47**. The HOMO is mostly concentrated on the sulfur of the thione and is slightly delocalised on the nitrogen atoms whilst the LUMO is

largely delocalised over the entire molecule except the carboxylic acid and the methylene groups. Once again, the carboxylic acid was unreactive because it makes no contribution to the frontier orbitals which confirmed why it could not be converted to a benzimidazole. The frontier orbitals of proline are delocalized over nearly the entire molecule in LUMO confirming the possibility for benzimidazole formation whilst in the HOMO the orbital is delocalized over the nitrogen and the surrounding carbon atoms (**Figure 3.48**).

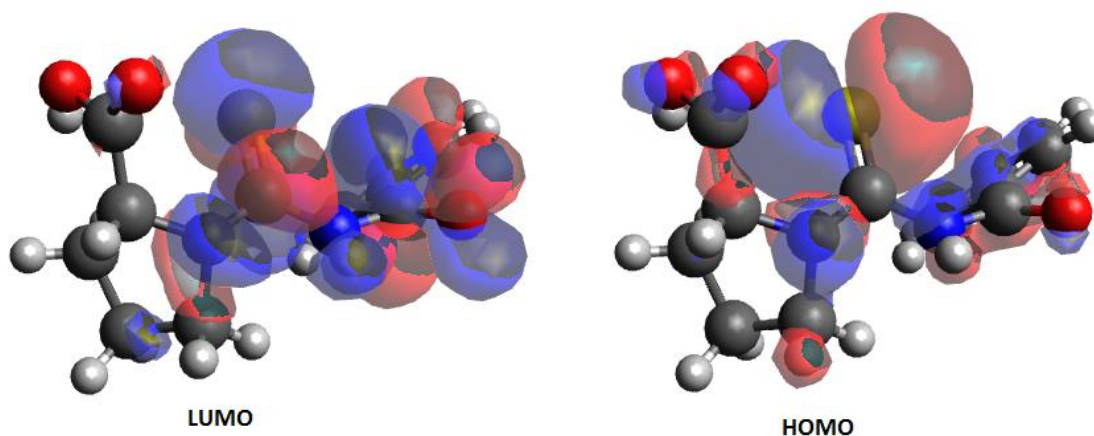


Figure 3.47 The atomic orbitals compositions of the frontier molecular orbitals for 1-(benzoylcarbamothioyl)pyrrolidine-2-carboxylic acid (**6**).

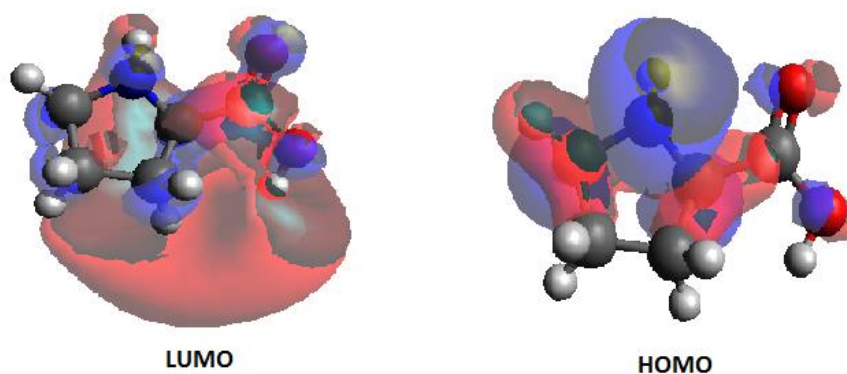


Figure 3.48 The atomic orbitals compositions of the frontier molecular orbitals for proline.

Figure 3.49 shows the frontier orbitals of **7**. The HOMO is mostly concentrated on the sulfur atoms and the methylene groups from the methionine whilst the LUMO is mostly delocalised over the benzene ring, the carbonyl, the nitrogen atoms and the thione. The delocalisation of the LUMO over the benzene ring aids in stabilising the compound during charge transfer.

The carboxylic acid makes no contribution to the frontier orbitals (LUMO) which again confirmed its unreactivity. In frontier orbitals of methionine (**Figure 3.50**) the LUMO is delocalised over the entire molecule except the sulfur and methyl group attached to it, whilst its HOMO is delocalized on the entire molecule except the carboxylic acid.

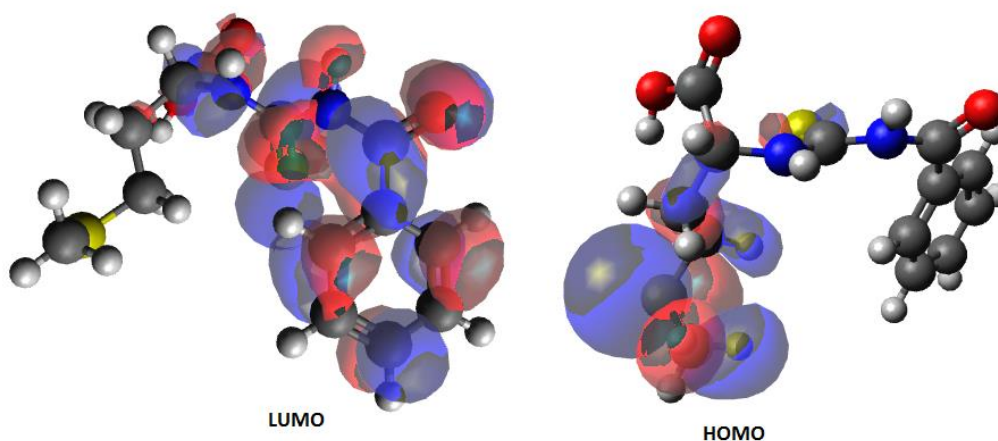


Figure 3.49 The atomic orbitals compositions of the frontier molecular orbitals for 2-[(benzoylcarbamothioyl)amino]-4-(methylsulfanyl)butanoic acid (**7**).

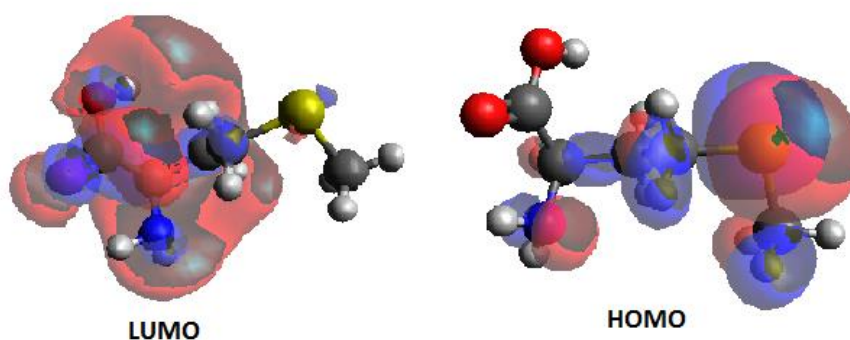


Figure 3.50 The atomic orbitals compositions of the frontier molecular orbitals for methionine.

The frontier orbitals of compound **8** are shown in **Figure 3.51**. The HOMO is mostly concentrated on the sulfur of the thione and is slightly delocalised on the nitrogen and the carboxylic acid whilst the LUMO is largely delocalised over the entire molecule except the carboxylic acid and the methyl group. The carboxylic acid could not be functionalized to a

benzimidazole by the attachment of 1,2-diaminobenzene due to the fact that the carboxylic acid has no contribution to the LUMO, which would receive the incoming electrons. The frontier orbitals of alanine in **Figure 3.52** shows delocalization over the entire molecule in the LUMO whilst the HOMO is also delocalized over the entire molecule with little contribution from the carboxylic acid.

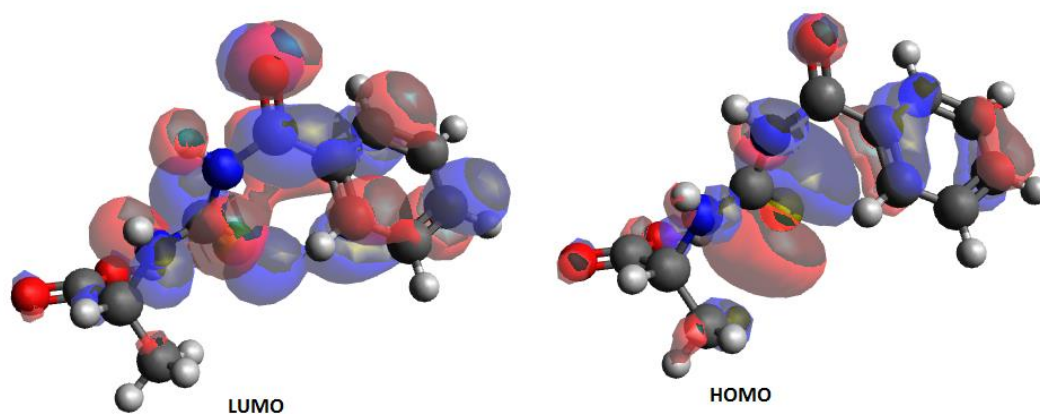


Figure 3.51 The atomic orbitals compositions of the frontier molecular orbitals for 2-[(benzoylcarbamoithioyl)amino]propanoic acid (**8**).

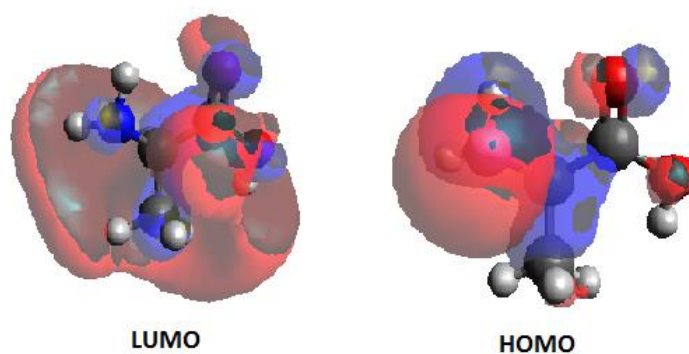


Figure 3.52 The atomic orbitals compositions of the frontier molecular orbitals for alanine.

The cyclization to form a benzimidazole using the alanine has been reported to be accessed by solvent free melting³²⁶ and also in the presence of a mixture of orthophosphoric acid and polyphosphoric acid *via* microwave irradiation.³²⁷ Hence, the compounds were not reproduced here. However, the theoretical calculations indicate that the amino acid derivatives of benzoyl

isothiocyanate are not reactive to the cyclization reaction with 1,2-diaminobenzene at the carboxylic acid site. The frontier orbitals are rather concentrated on the carbonyl attached to the phenyl ring and the thione making that carbonyl more susceptible to and attack by the lone pair of electrons of an amine.

3.5 Synthesis of the amino acid ester derivatives

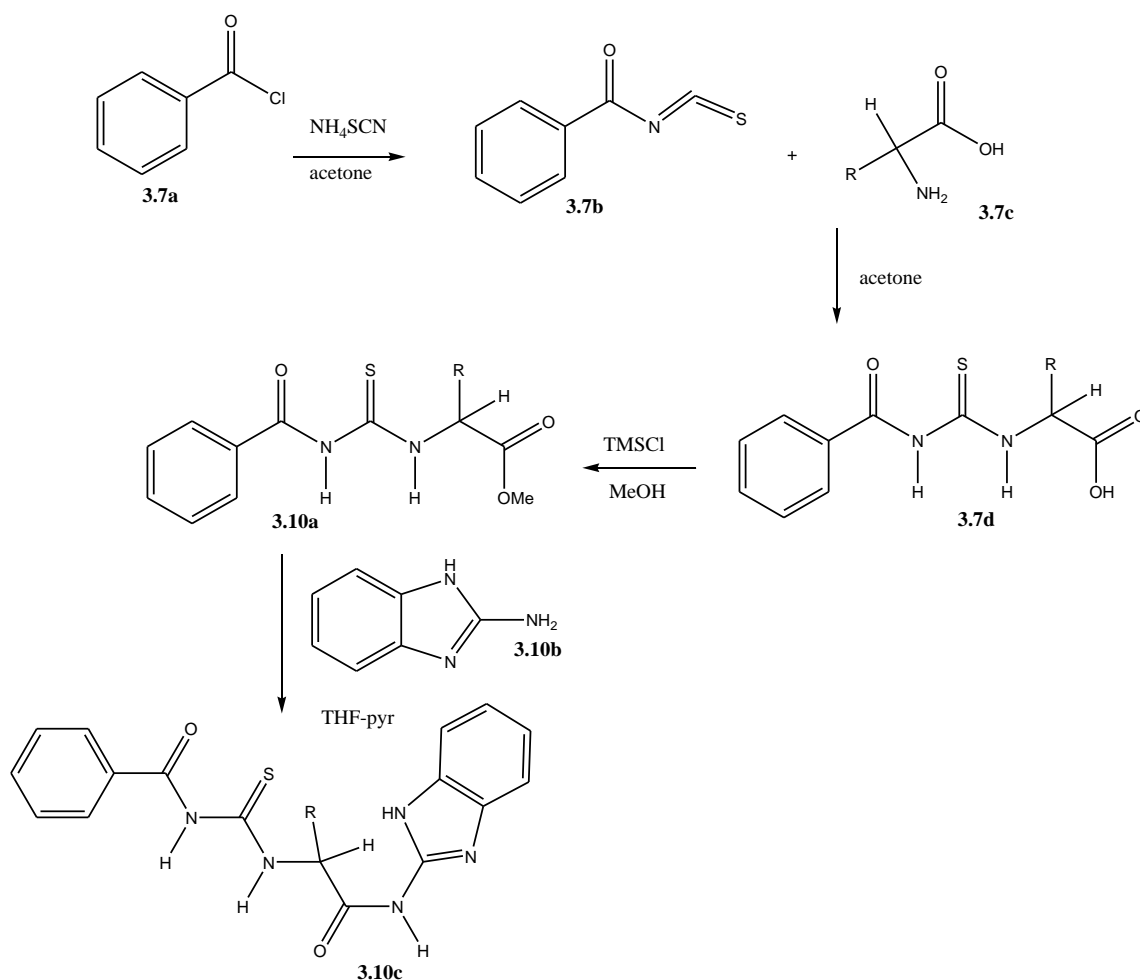
A new set of scaffolds were pre-screened (**Table 3.12**) and an attempt was made at synthesizing them.

Table 3.12 Autodock pre-screening of alternative benzimidazole linked amino acid derivatives (**Scheme 3.10**).

Descriptive Code	Free binding energy	Inhibition constant K_i (μM)
Alanine derivative	-6.56	15.57
Serine derivative	-7.23	5.00
Methionine derivative	-7.27	4.67
Glycine derivative	-7.74	2.10
Leucine derivative	-7.48	3.32
Cysteine derivative	-7.38	3.92

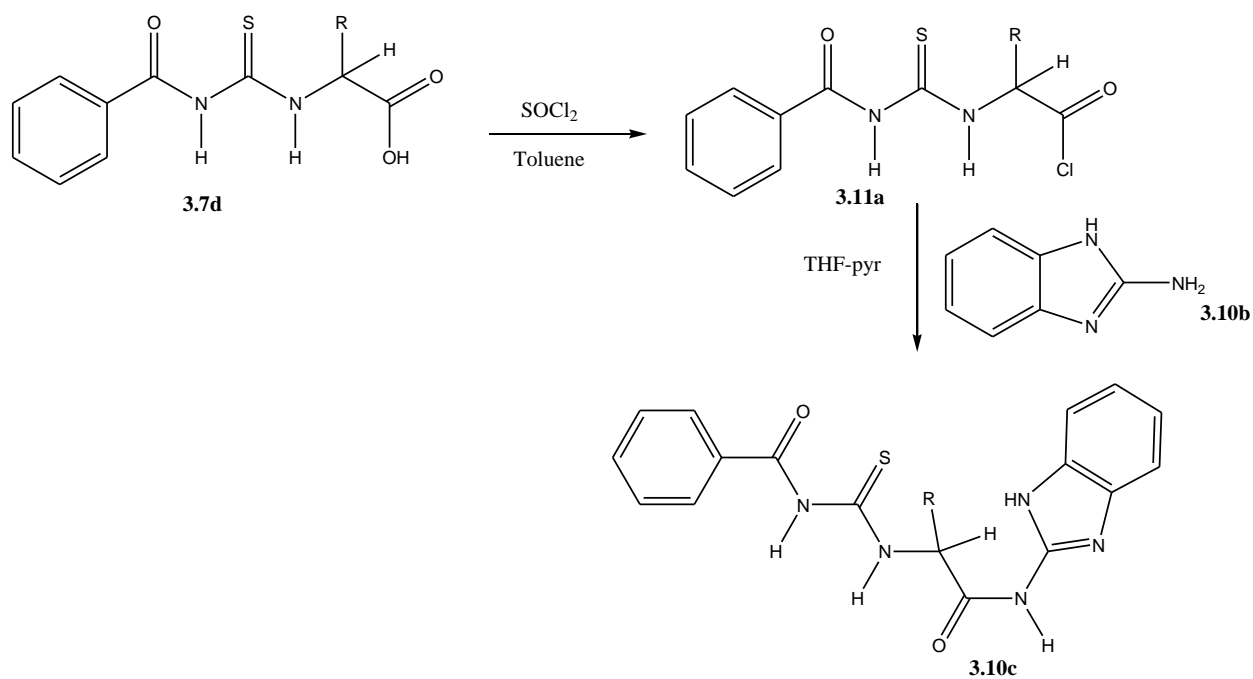
Synthesis of the amino acid ester derivatives of the compounds was then attempted based on the pre-screening results. The first approach was to make the amino acid derivatives of benzoyl isothiocyanate, convert it to the ester by heating it in trimethylsilyl chloride in methanol and reacting it with 2-aminobenzimidazole to form an amide as indicated in **Scheme 3.10** below. The products were oily and purification was not successful. TLC gave a continuous streak in ethyl acetate:hexane (4:1). Purification on column still gave oily products which were impure and could not be purified or separated by the techniques available.

Amino acid methyl esters were then used as starting materials instead of the acids. The workup to isolate a pure product was not successful in most cases and only yielded impure oils that never solidified or could not be purified.



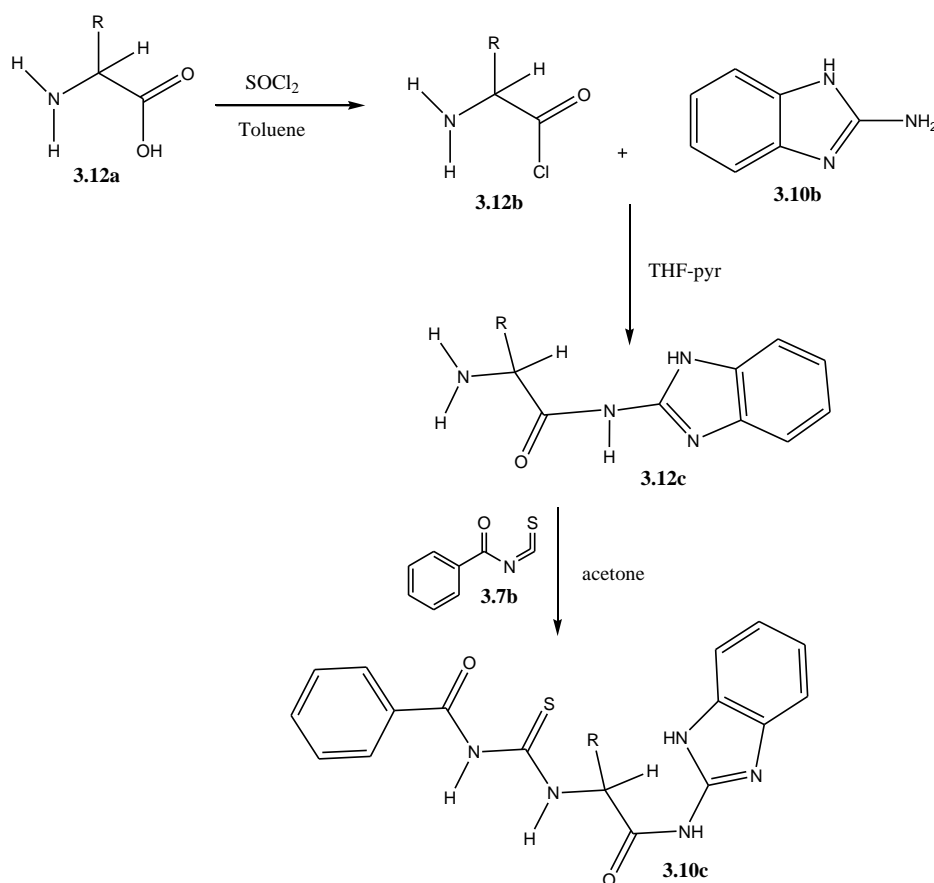
Scheme 3.10 Synthesis of amide of amino acid derivatives of benzoyl isothiocyanate.

Also chlorination of the amino acid derivatives was carried out (**Scheme 3.11**). Any attempt to purify the products led to their decomposition, possibly due to the presence of water in the solvents used.



Scheme 3.11 Synthesis of amides of amino acid derivatives of benzoyl isothiocyanate *via* chlorination of the acid.

Direct chlorination of the amino acid was also attempted (**Scheme 3.12**). In this the amine group also reacted with the thionyl chloride used. The product formed breaks down upon addition of a solvent.



Scheme 3.12 Synthesis of amide of *via* chlorination of amino acid.

Reaction of the alanine methyl ester hydrochloride and aspartic acid dimethyl ester with benzoyl isothiocyanate gave the desired products but an attempt to convert the alanine methyl ester derivative to the amide by reacting it with 2-aminobenzimidazole in THF and pyridine was not successful as starting materials were recovered. The aspartic acid dimethyl ester and alanine methyl ester derivatives of benzoyl isothiocyanate have also been synthesized in acetone from the corresponding thione.^{328, 329} A methoxy substituted derivative of benzoyl isothiocyanate has been accessed by boiling the thione directly in methanol.³³⁰ The amino acid methyl ester derivative of benzoyl isothiocyanate has been accessed by refluxing the amino acid and benzoyl isothiocyanate in alcohol in the presence of a base.³³¹

3.5.1 Methyl-2-[[[(phenylformamido)methanethioyl]amino]propanoate (10)

The alanine methyl ester hydrochloride reacted with benzoyl isothiocyanate *via* an attack of the thione carbon by the lone pair of electrons on the nitrogen which is separated from the

hydrochloride *in situ* to form compound **10**. The IR spectrum (**Figure 3.53**) showed a band at 3229 cm^{-1} for the N–H stretch, a band at 2929 cm^{-1} for the aliphatic C–H stretch, a band at 1652 cm^{-1} for the C=O stretch, a band at 1599 cm^{-1} for the C–N stretch and another band at 1540 cm^{-1} for the C=C stretch. The ^1H NMR (**Figure 3.54**) gave a triplet signal at 11.43 ppm for the N-H, signals for aromatic protons were observed between 7.93 and 7.51 ppm, a doublet signal was observed at 4.91 ppm for proton of the chiral carbon. Whilst a singlet signal for three protons was observed at 2.51 ppm for the methoxy group. The ^{13}C NMR (**Figure 3.55**), showed a signal at 180.28 ppm for the C=S, signals for the carbonyl were observed at 170.79 ppm and 168.30 ppm. Signals were observed between 133.1 and 128.7 ppm, for aromatic carbons, a signal was observed at 60.48 ppm for the methoxy group and another signal was observed at 59.55 ppm for the chiral carbon.

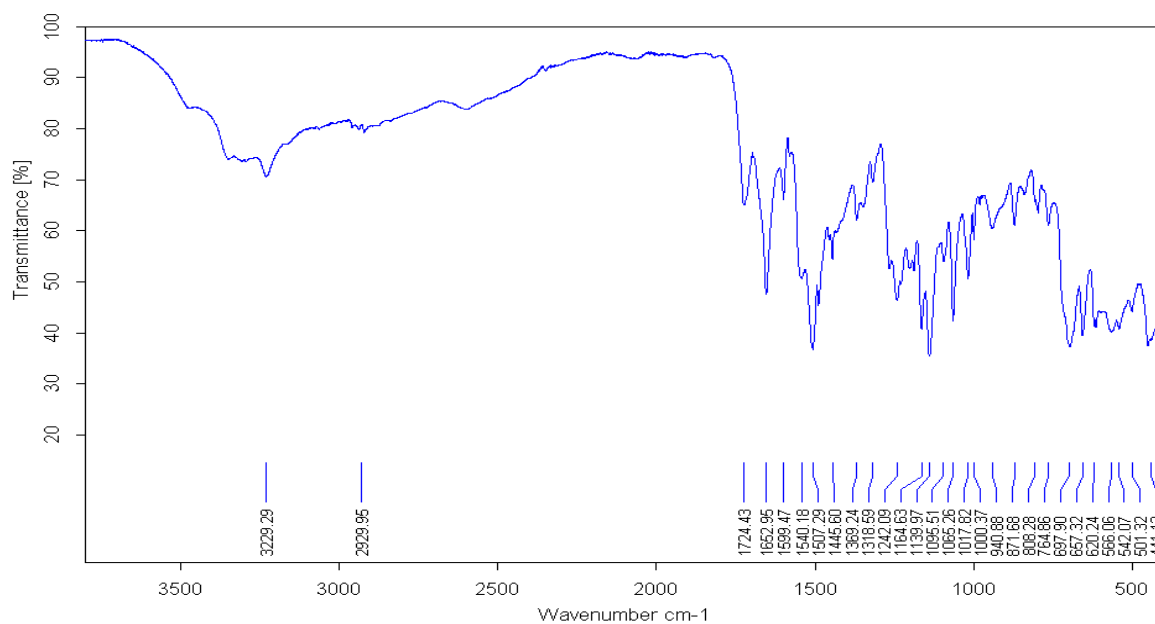


Figure 3.53 IR spectrum of methyl-2-[[[(phenylformamido)methanethioyl]amino]propanoate (**10**).

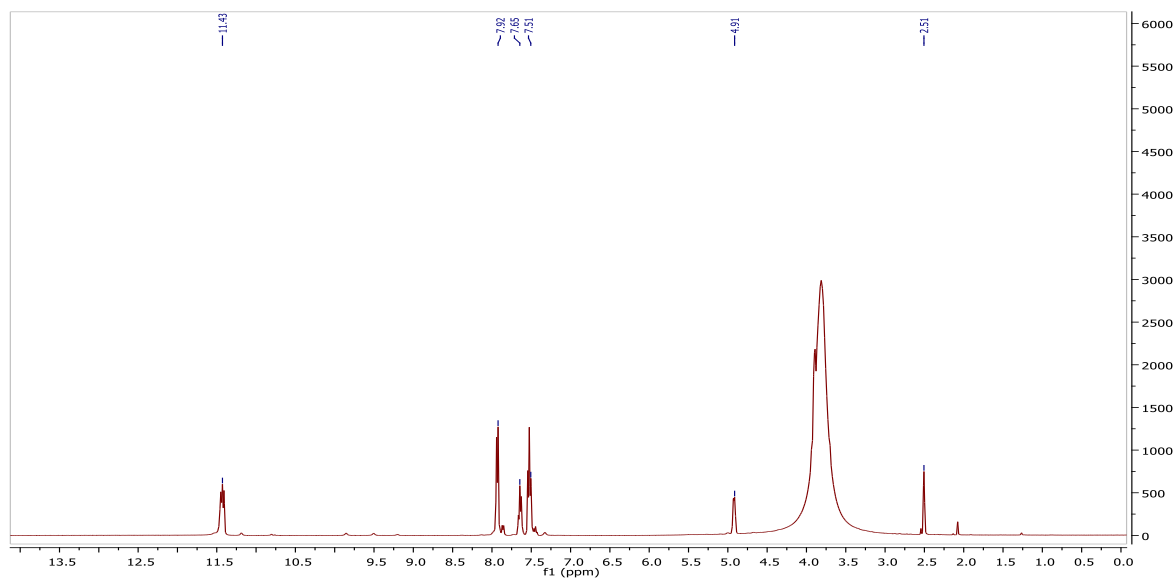


Figure 3.54 ¹H NMR spectrum of methyl-2-[[phenylformamido)methanethioyl]amino} propanoate (**10**).

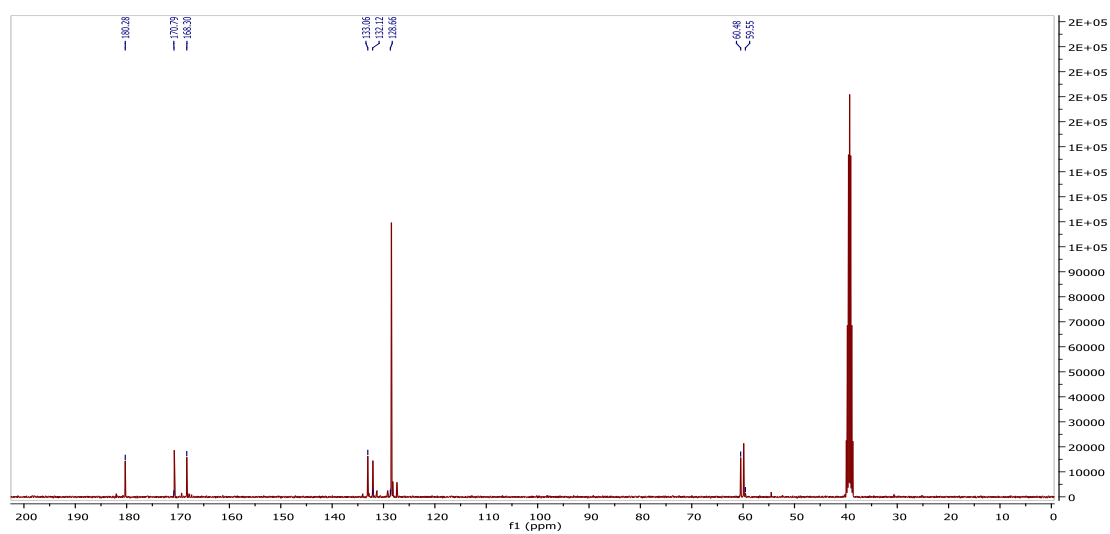


Figure 3.55 ¹³C NMR spectrum of methyl-2-[[phenylformamido)methanethioyl]amino} propanoate (**10**).

3.5.2 1,4-Dimethyl-2-[[phenylformamido)methanethiyl]butanedioate (11)

The aspartic acid dimethyl ester dihydrochloride reacted with benzoyl isothiocyanate *via* an attack of the thione carbon by the lone pair of electrons on the nitrogen which is separated from the hydrochloride *in situ* to form compound **11**.

The IR spectrum (**Figure 3.56**) showed a bands 3326 and 3230 cm^{-1} for the N–H stretch, bands at 2999 and 2947 cm^{-1} were observed for the aliphatic C–H stretch, a band was observed at 1745 cm^{-1} for the C=O stretch, a band was observed at 1578 cm^{-1} for the C=C stretch. The ^1H NMR (**Figure 3.57**) gave singlet signal at 11.56 ppm and a doublet signal at 11.50 ppm for N(1)–H and N(2)–H respectively. While signals for aromatic protons were observed between 7.92 and 7.52 ppm, a doublet signal for a proton was observed at 5.41 ppm, whilst doublet signal for two protons was observed at 3.09 ppm. The ^{13}C NMR (**Figure 3.58**), showed a signal at 180.4 ppm for C=S, signals at 170.7 and 168.4 ppm were observed for C=O, signals were observed between 133.0–128.4 ppm for aromatic carbons. Signals at 53.8 ppm and 52.7 ppm were observed for the methoxy group. Another signal was observed at 51.8 ppm for the chiral carbon and a signal was observed at 34.8 ppm for the methylene carbon.

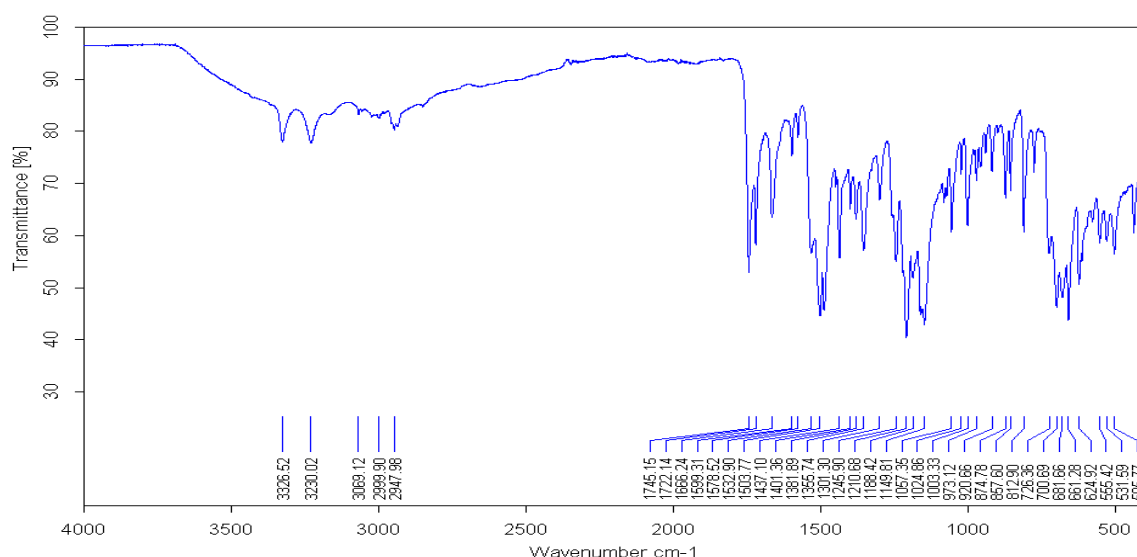


Figure 3.56 IR spectrum of 1,4-dimethyl-2-[[phenylformamido)methanethiyl]butanedioate (**11**).

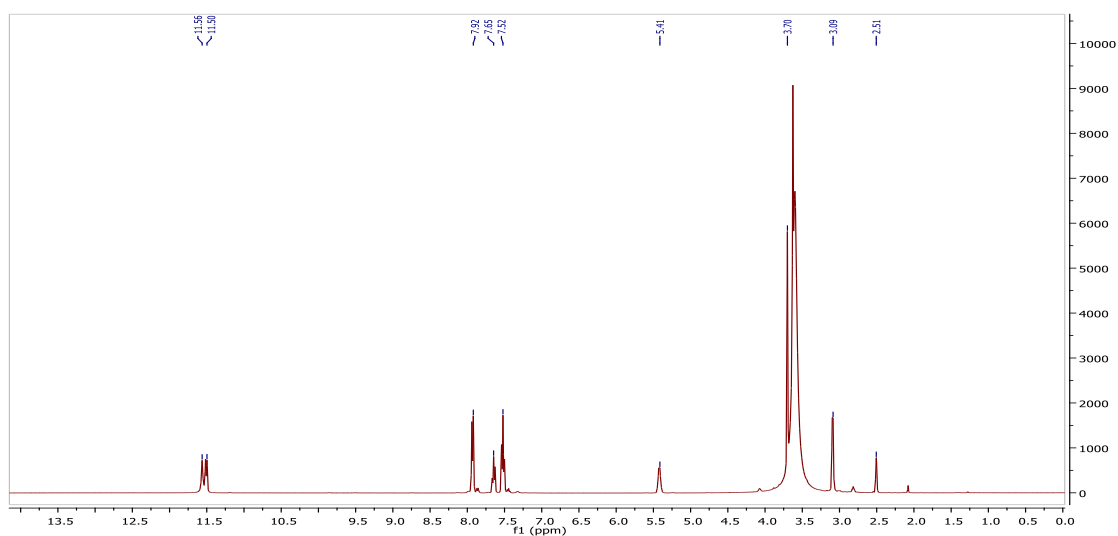


Figure 3.57 ^1H NMR spectrum of 1,4-dimethyl-2-[[phenylformamido)methanethioyl]butanedioate (**11**).

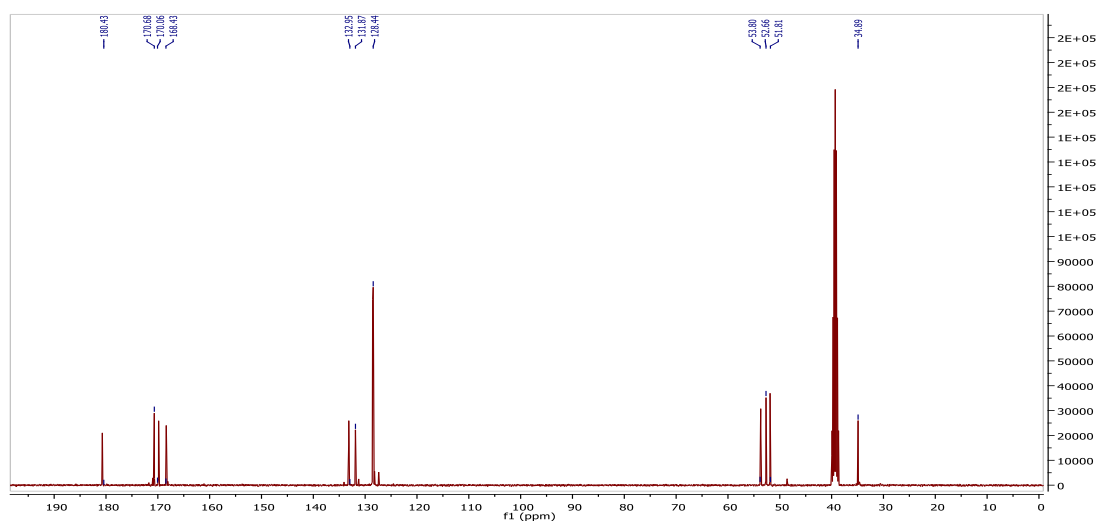


Figure 3.58 ^{13}C NMR spectrum of 1,4-dimethyl-2-[[phenylformamido)methanethioyl]butanedioate (**11**).

3.5.3 Crystal structures of amino acid ester derivatives

Compounds **10** and **11** were recrystallized from methanol:THF (1:1) as white crystals. The crystallographic data, selected bond lengths, bond angles and torsion angles for the structures

of **10** and **11** are provided in tables **3.14** and **3.15**. Compounds **10** and **11** crystallized in triclinic space group *P-1* whilst compound **10** crystallized in monoclinic space group *P2₁*.

Table 3.13 Crystallographic data and structure refinement summary for compounds **10** and **11**.

Property	10	11
Formula	C ₁₂ H ₁₄ N ₂ O ₃ S	C ₁₄ H ₁₆ N ₂ O ₅ S
Formula Weight	266.31	324.35
Crystal System	Triclinic	Monoclinic
Space group	<i>P-1</i>	<i>P2₁</i>
a [Å]	7.4237(4)	7.5089(3)
b [Å]	8.7173(5)	11.0379(5)
c [Å]	11.3227(6)	9.2036(5)
α [°]	73.411(2)	90
β [°]	72.173(3)	93.469(2)
γ [°]	68.967(3)	90
V [Å ³]	638.24(6)	761.42(6)
Z	2	2
D(calc) [g/cm ³]	1.386	1.415
Mu(MoKa) [/mm]	0.256	0.238
F(000)	280	340
Crystal Size [mm]	0.10 x 0.21 x 0.23	0.16 x 0.37 x 0.67
Temperature (K)	200	200
Radiation [Å]	MoKa 0.71073	MoKa 0.71073
Theta Min-Max [°]	1.9, 28.3	2.7, 28.3
Dataset	-9: 9 ; -11: 11 ; -14: 15	-9: 9 ; -14: 14 ; -7: 12
Tot., Uniq. Data, R(int)	11443, 3178, 0.018	5643, 3578, 0.009
Observed Data [I > 2.0 sigma(I)]	2539	3475
Nref, Npar	3178, 173	3578, 209
R, wR ₂ , S	0.0425, 0.1166, 1.02	0.0246, 0.0679, 1.04
Max. and Av. Shift/Error	0.00, 0.00	0.00, 0.00
Min. and Max. Resd. Dens. [e/Å ³]	-0.29, 0.93	-0.19, 0.23

Figures 3.59 and 3.60 gives the ORTEP diagrams for compounds **10** and **11**. The bond distances of S1-C2 in compound **10** was 1.676(2) which comparable to the bond distance of S1-C2 in compound **11** which was 1.671(2). The bond distance of N1-C1 in compound **10** was 1.380 whilst the bond distance for whilst the N1-C1 bond distance of compound **11** was 1.378(2). The bond distance of N2-C2 in compound **10** was 1.318(2) compared to the N2-C2 in compound **11** which 1.324(2). The bond angle of C1-N1-C2 in compound **10** was 127.2(1) whilst the bond angle of C1-N1-C2 in compound **11** was 127.1(1). In compound **10** the S1-C2-N2 bond angle was 124.3(1) which was comparable to the S1-C2-N2 bond angle in compound **11** which was 124.5(1). The bond angle of N2-C3-C6 was 110.4(2) in compound **10** whilst the bond angle of N2-C3-C6 in compound **11** was 113.6(1).

Table 3.14 Selected bond lengths (Å) and bond angles (°) for methyl-2-[[[(phenylformamido)methanethioly]amino]propanoate (**10**).

Bond lengths			
10		11	
S1-C2	1.676(2)	S1-C2	1.671(2)
O1-C1	1.219(2)	O3-C4	1.333(2)
O3-C4	1.194(1)	O1-C1	1.223(2)
N1-C2	1.392(2)	N2-C3	1.454(2)
N2-C3	1.455(2)	N1-C1	1.378(2)
N2-C2	1.318(2)	N2-C2	1.324(2)
N1-C1	1.380(2)	N1-C2	1.396(2)
Bond angles			
10		11	
C1-N1-C2	127.2(1)	S1-C2-N1	118.4(1)
O1-C1-N1	121.9(2)	C1-N1-C2	127.1(1)
N1-C1-C11	116.9(1)	O1-C1-N1	122.5(2)
S1-C2-N1	118.9(1)	N1-C1-C11	116.1(1)
N1-C2-N2	116.7(2)	N1-C2-N2	117.1(1)
N2-C-C6	110.4(2)	N2-C3-C6	113.6(1)
O3-C4-C3	126.2(2)	N2-C3-C4	108.7(1)
S1-C2-N2	124.3(1)	O2-C4-O3	124.8(2)
O1-C1-C11	121.2(2)	S1-C2-N2	124.5(1)

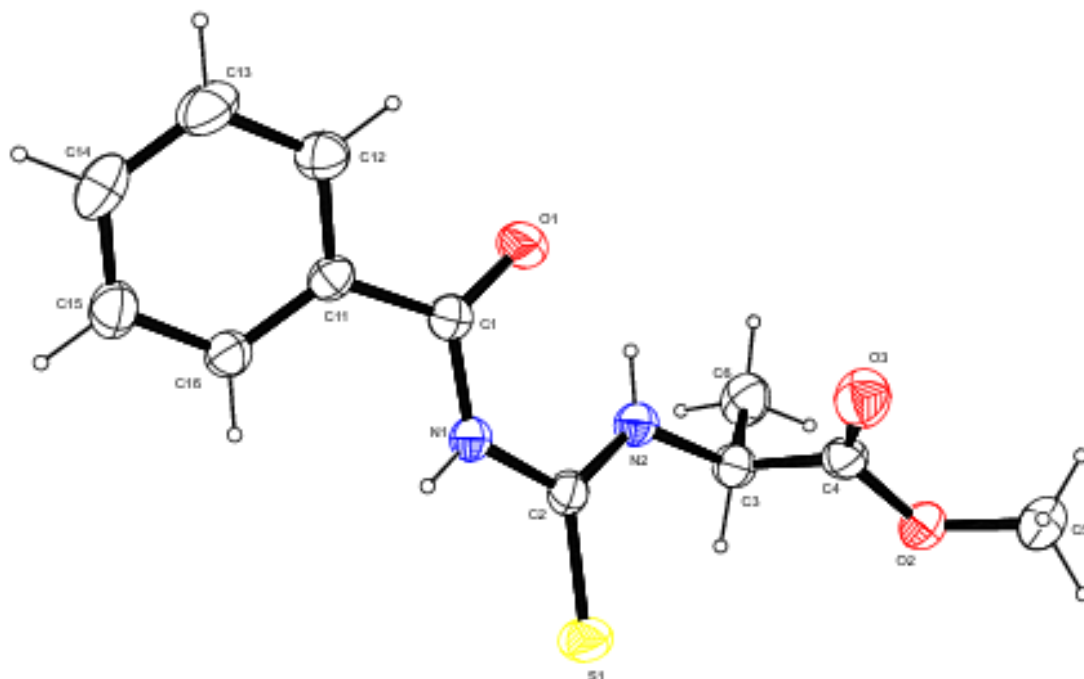


Figure 3.59 An ORTEP view of methyl-2-[[[(phenylformamido)methanethioly]amino]propanoate (**10**).

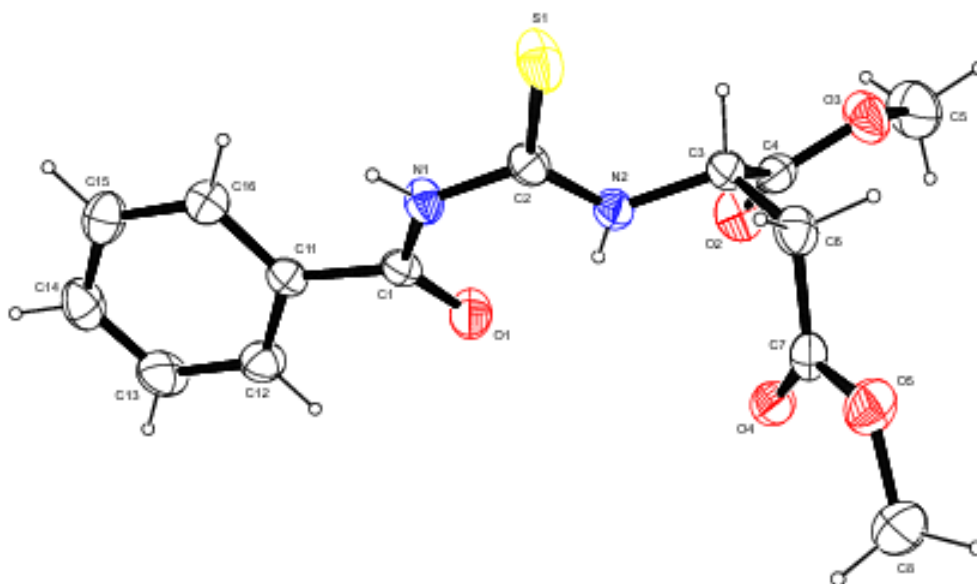
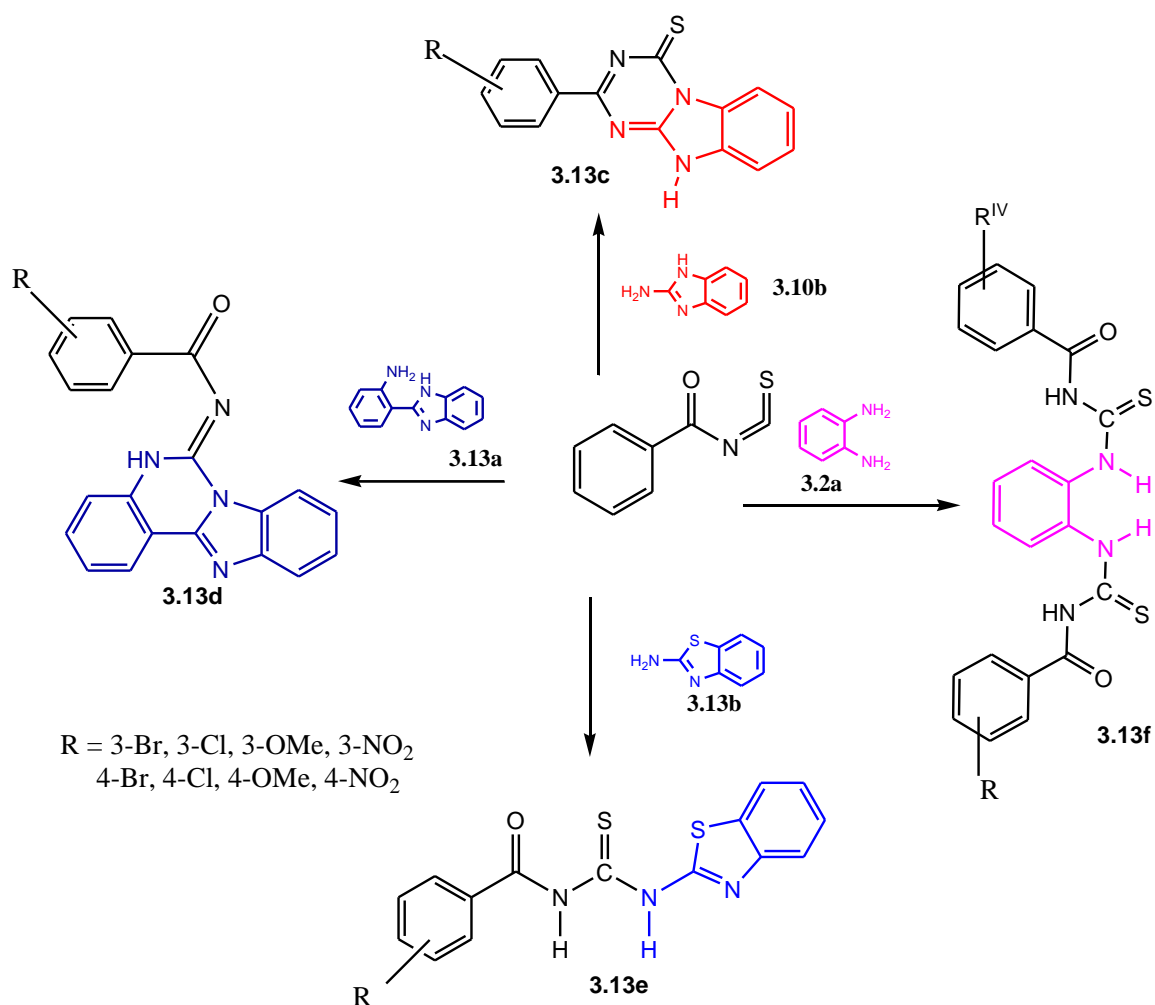


Figure 3.60 An ORTEP view of 1,4-dimethyl-2-[[[(phenylformamido)methanethioly]butanedioate (**11**).

3.6 Design and synthesis of benzoyl isothiocyanate derivatives with structurally diverse diamines

Due to the lack of success in the synthesis of the pre-screened scaffolds a new set of compounds (**Scheme 3.13**), were then screened for their anti-HIV-1 protease activity using **Autodock 4.2**. **Table 3.16** gives the summary of the compounds screened and their predicted inhibition constants.



Scheme 3.13 Synthesis of benzoyl isothiocyanate derivatives with structurally diverse diamines.

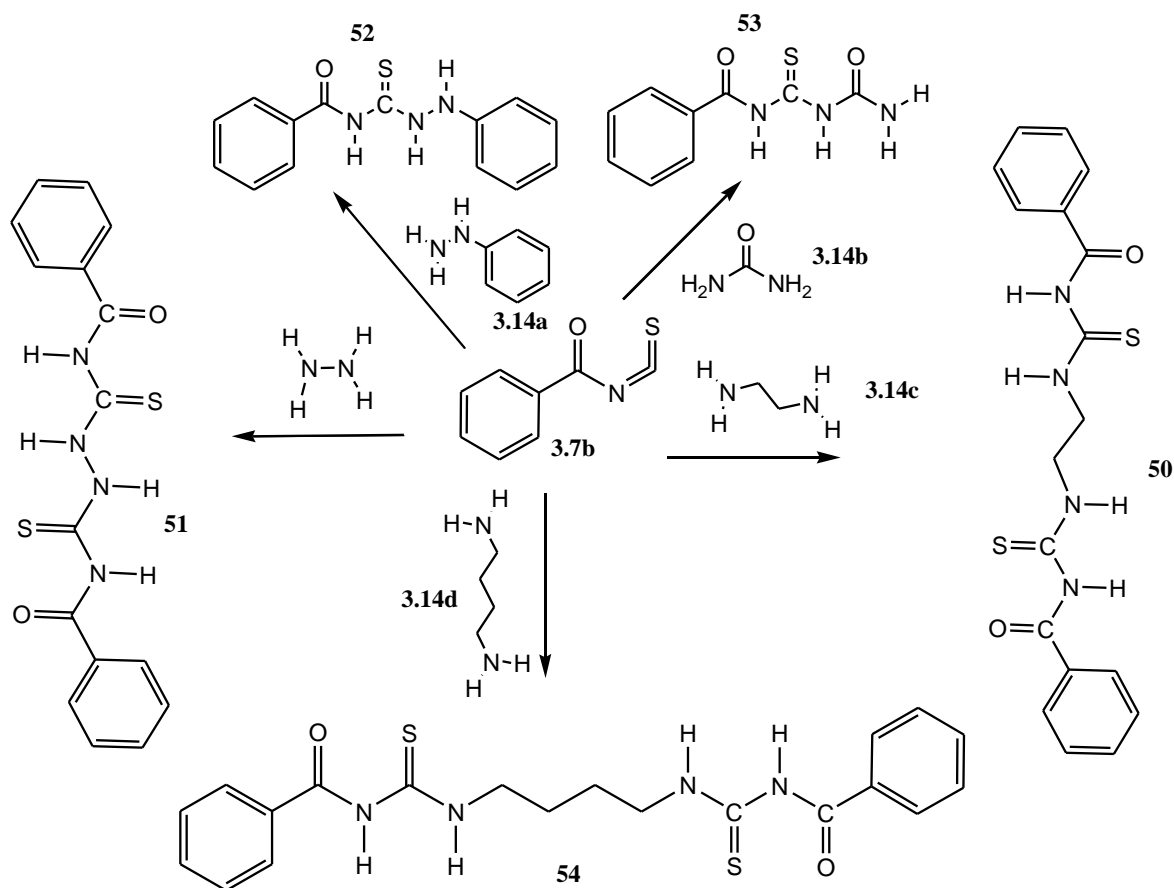
Table 3.15 Summary of compounds screened and their predicted inhibition constants of diamine derivatives of benzoyl isothiocyanates.

Group I (R ^I)	K _i μM	Group II (R ^{II})	K _i μM	Group III (R ^{III})	K _i μM	Group IV (R ^{IV})	K _i μM
4-Cl	6.88	H	5.87	4-Br	1.28	3-Br	0.095
4-Br	4.67	4-Cl	6.16	4-OMe	2.50	H	0.13
4-OMe	8.22	4-Br	5.30	3-OMe	1.07	4-NO ₂	0.47
3-OMe	4.66	4-OMe	11.09	4-Cl	1.65	4-Cl	0.21
3-NO ₂	3.37	3-OMe	7.55	3-NO ₂	0.98	3-NO ₂	0.11
3-Cl	3.72	3-NO ₂	9.71	3-Cl	0.796	3-OMe	1.90
3-Br	3.47	3-Cl	3.11	4-NO ₂	2.68	4-Br	0.12
4-NO ₂	7.74	4-NO ₂	11.31	H	3.02	4-OMe	0.81
H	6.33	3-Br	7.70			3-Cl	0.06
						H, 3-Me	0.106

Other diamines derivatives (**Scheme 3.14**) other than phenylenediamine based derivatives that were also pre-screened and synthesized are showed in **Scheme 3.14** and **Table 3.17**.

Table 3.16 Summary of other diamines screened and their predicted inhibition constants.

Other diamines Group IV	K _i μM
1,2-ethane diamine	0.45
Hydrazine	10.98
Phenylhydrazine	0.25
1,4-butane diamine	1.34



Scheme 3.14 Synthesis of benzoyl isothiocyanate derivatives of other diamines.

3.7 Conclusions

-The attempted synthesis of benzimidazole *via* an acid chloride led to the formation of 3-methyl-*N*-[2-(3-methylbenzamido)phenyl]benzamide (**1**). The single crystal XRD molecular structure of compound **1** showed a disorder in the molecule by a ratio 0.675:0.325.

-The synthesis of 2-(3-methylphenyl)-1*H*-benzimidazole (**2**) has been achieved by polyphosphoric acid catalyzed condensation of carboxylic acids and *o*-phenylenediamine. A novel triethylamine catalyzed condensation of *o*-phenylenediamine with 3-methylbenzaldehyde has been carried out and the product characterized. The single crystal XRD molecular structure of compound **2** has been discussed.

-A novel method for the synthesis of 2,2,4-trimethyl-2,3-dihydro-1*H*-benzodiazepin-5-ium isophthalate (**3**) *via* microwave irradiation of *o*-phenylenediamine and isophthalic acid in the presence of acetone has been presented and the compound was characterized by IR, NMR, microanalysis and GC-MS. The single crystal XRD molecular structure of compound has been discussed.

-The synthesis of 2-[(benzoylcarbamoithiyl)amino]-3-hydroxypropanoic acid (**5**), 1-(benzoylcarbamoithiyl)pyrrolidine-2-carboxylic acid (**6**), 2-[(benzoylcarbamoithiyl) amino]-4-(methylsulfanyl) butanoic acid (**7**) and 2-[(benzoylcarbamoithiyl)amino]propanoic acid (**8**) has been achieved from the reaction of benzoyl isothiocyanate with L-serine, L-proline, D-methionine and L-alanine respectively and characterized by IR, NMR, microanalysis and GC-MS. The existence of two rotamers of compound **6** in solution which has not been reported is first presented in this thesis. The single crystal XRD molecular structure of compounds **5**, **6**, **7** and **8** have been discussed.

-The reaction of the carboxylic acid on each of compounds **5**, **6**, **7** and **8** with a *o*-phenylenediamine led to the formation of 2-phenyl-1*H*-benzimidazole (**9**) in each case and the product have been characterized by IR, NMR, microanalysis and GC-MS. The unsuccessful conversion of the carboxylic acids in compounds **5**, **6**, **7** and **8** to the benzimidazole upon reaction with *o*-phenylenediamine confirms the low reactivity of the carboxylic acid in these compounds.

-DFT computational studies have been carried out to compute the HOMO and LUMO and the species that contribute to the frontier orbitals and also to attempt to explain the reasons why the attempted condensation of the carboxylic acids on comopounds **5**, **6**, **7** and **8** with *o*-phenylenediamine to form a benzimidazole was unsuccessful.

-The synthesis methyl-2-[[phenylformamido)methanethiyl]amino}propanoate (**10**) has been achieved by the reaction of alanine methyl ester hydrochloride with benzoyl isothiocyanate . The product has been characterized by IR, NMR, microanalysis and GC-MS. The single crystal XRD molecular structure of compound **10** has been discussed.

-The synthesis of 1,4-dimethyl-2-[[phenylformamido)methanethiyl]butanedioate (**11**) has been achieved by the reaction of aspartic acid dimethyl ester hydrochloride with benzoyl

isothiocyanate and characterized by IR, NMR, microanalysis and GC-MS. The single crystal XRD molecular structure of compound **11** is presented.

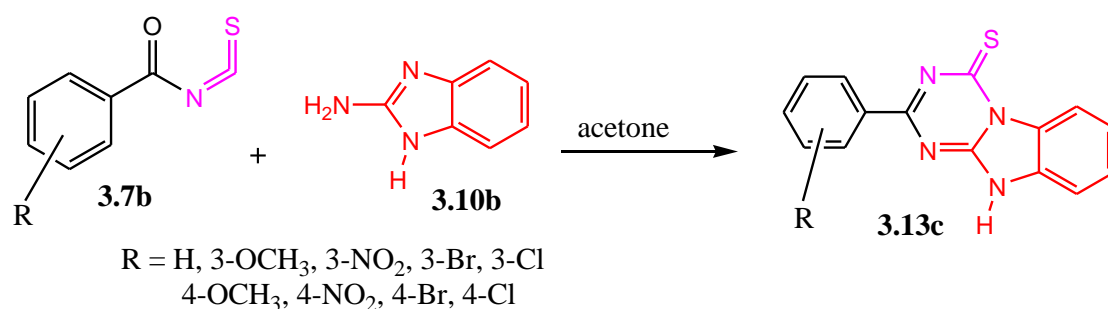
-The pre-screening of a large number of benzoyl isothiocyanate derivatives of structurally diverse diamines using Autodock 4.2 to ascertain their fit of the protease active site have been presented. The computed inhibition constants and binding energies have been used to inform the synthesis of the compounds.

CHAPTER FOUR

TETRAAZATRICYCLIC DERIVATIVES

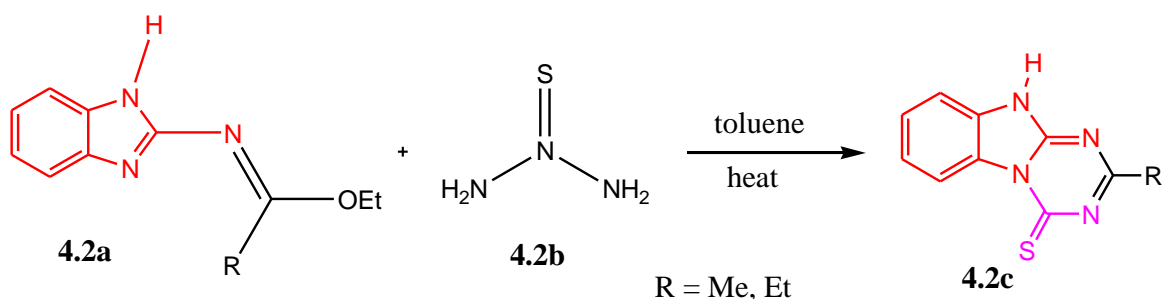
4.1 Synthesis and characterization of tetraazatricyclic derivatives

Based on the pre-screening the following set of compounds were synthesized (**Scheme 4.1**). The tetraazatricyclics are thought to proceed by the attack of the carbonyl of the benzoyl isothiocyanate derivative by the 2-substituted amino group of the benzimidazole. Water is formed in the process while the lone pair of the nitrogen in the benzimidazole ring attacks the carbon of the thione leading to the formation of a tetraazatricyclic ring. A detailed reaction mechanism for this reaction has been discussed in **Scheme 4.4** and **Figure 4.5**.



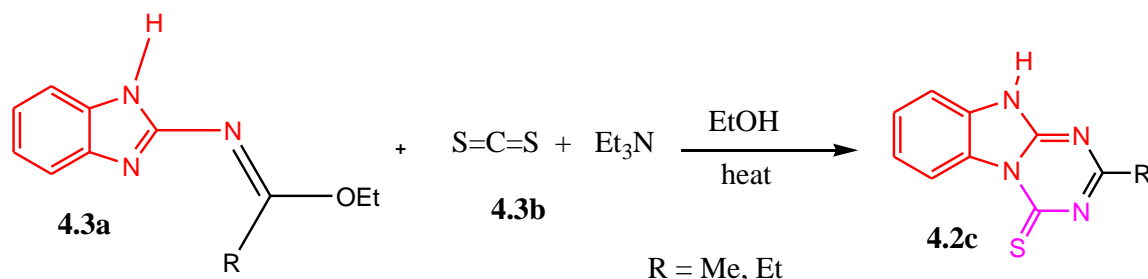
Scheme 4.1 Synthesis of tetraazatricyclic derivatives.

Tetraazatricyclics with aliphatic side chains have been synthesized before by different methods (**Schemes 4.2, 4.3**). *N*-benzimidazol-2-yl iminoester has been heated with thiourea in dry toluene under reflux for 48 h to afford 1,3,5-triazino [1,2-*a*]benzimidazolo-2-thione.³³²



Scheme 4.2 Synthesis of tetraazatricyclic derivatives from thiourea.

Reaction of *N*-benzimidazol-2-yl iminoester with carbon disulfide in the presence of triethylamine and under reflux in ethanol afforded thiadiazine thione [1,2-*a*] benzimidazolo-1,3,5-thiadiazin-2-thione.³³²



Scheme 4.3 Synthesis of tetraazatricyclic derivatives from carbon disulfide.

4.2 11-(4-Chlorophenyl)-1,8,10,12-tetraazatricyclo[7.4.0.0^{2,7}]trideca-2(7),3,5,9,11-pentaene-13-thione (12)

The IR spectrum (**Figure A4.1**) showed an N–H stretch at 3387 cm⁻¹ and a C–H stretch for an sp² carbon at 2967 cm⁻¹, a band for the C=N stretch was observed at 1622 cm⁻¹ and the aromatic C=C was observed at 1589 cm⁻¹. The ¹H NMR (**Figure A4.2**) and ¹H–¹H COSY (**Figure A4.3**) spectra showed a doublet resonance at 9.48 ppm for an aromatic deshielded by the electron pair from a heteroatoms whilst other protons appeared between 8.45 and 7.18 ppm. The ¹³C NMR spectrum (**Figure A4.4**) gave resonances between 166.5 and 113.1 ppm for aromatic carbons.

4.3 11-(4-Bromophenyl)-,8,10,2-tetraazatricyclo[7.4.0.0^{2,7}]trideca-2(7),3,5,9,11-pentaene-13-thione (13)

The IR spectrum (**Figure A4.5**) showed an N–H stretch at 3372 cm⁻¹, a band for the C=N stretch at 1669 cm⁻¹ and the aromatic C=C was observed at 1585 cm⁻¹. In the ¹H NMR (**Figure A4.6**) and ¹H–¹H COSY (**Figure A4.7**) spectra resonances for aromatic protons occurred between 9.49 and 7.17 ppm. In the ¹³C NMR spectrum (**Figure A4.8**) resonances between 177.8 and 112.7 ppm were observed for aromatic carbons.

4.4 11-(4-Methoxyphenyl)-1,8,0,12-tetraazatricyclo[7.4.0.0^{2,7}]trideca-2(7),3,9,1-pentaene-13-thione (14)

The IR spectrum (**Figure A4.9**) showed an N–H stretch at 3387 cm⁻¹, a band for the C=N stretch was observed at 1691 cm⁻¹ and the aromatic C=C was observed at 1593 cm⁻¹. The ¹H NMR (**Figure A4.10**) and ¹H–¹H COSY (**Figure A4.11**) spectra gave a signal at 9.47 ppm for an aromatic proton deshielded by the electron pair of a heteroatom. Whilst other resonances for aromatic protons occurred between 8.40 and 7.13 ppm. The protons of the methoxy group occurred at 3.98 ppm. The ¹³C NMR spectrum (**Figure A4.12**) gave signals between 177.8 and 112.7 ppm for aromatic carbons. The methoxy group occurred at 55.5 ppm.

4.5 11-(3-Methoxyphenyl)-1,8,0,12-tetraazatricyclo[7.4.0.0^{2,7}]trideca-2(7),3,5,9,11-pentaene-13-thione (15)

The IR spectrum (**Figure A4.13**) showed an N–H stretch at 3196 cm⁻¹, a band for aliphatic C–H stretch was observed at 2941 cm⁻¹, the C= stretch was observed at 1628 cm⁻¹ whilst a band for aromatic C=C was observed at 1560 cm⁻¹. The ¹H NMR (**Figure A4.14**) and ¹H–¹H COSY (**Figure A4.15**) spectra gave a signal at 9.47 ppm for an aromatic proton deshielded by the electron pair of a heteroatom. Other aromatic protons resonated between 8.03 and 7.19 ppm. The protons of the methoxy group appeared at 3.87 ppm. The ¹³C NMR spectrum (**Figure A4.16**) gave signals between 159.5 and 113.4 ppm for aromatic carbons whilst the methoxy group occurred at 55.4 ppm.

4.6 11-(3-Nitrophenyl)-1,8,10,12-tetraazatricyclo[7.4.0.0^{2,7}]trideca-2(7),3,5,9,11-pentaene-13-thione (16)

The IR spectrum (**Figure 4.1**) showed an N–H stretch at 3334 cm⁻¹, a band for the C=N stretch at 1684 cm⁻¹ and the aromatic C=C was observed at 1524 cm⁻¹. The ¹H NMR (**Figure 4.2**) and ¹H–¹H COSY (**Figure 4.3**) spectra gave signals between 9.48 ppm and 7.19 ppm for aromatic protons. The signals in both the ¹H NMR and ¹³C NMR spectra have been doubled possible due to the existence of two different species in solution that might have been triggered by the presence of the nitro group. This confirms tautomerism in the 3-nitro

derivative of tetraazatricyclics synthesized from thiones. In the ^{13}C NMR spectrum (Figure 4.4) aromatic carbons resonated between 179.0 and 111.4 ppm for aromatic carbons.

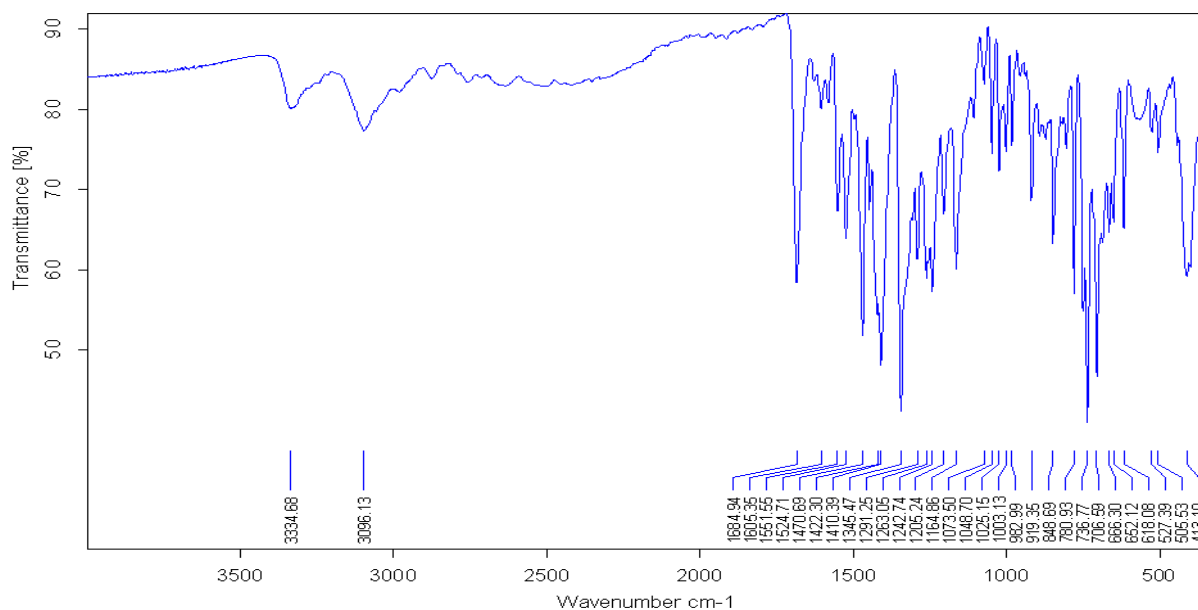


Figure 4.1 IR spectrum of 11-(3-nitrophenyl)-1,8,10,12-tetraazatricyclo[7.4.0.0^{2,7}]trideca-2(7),3,5,9,11-pentaene-13-thione (**16**).

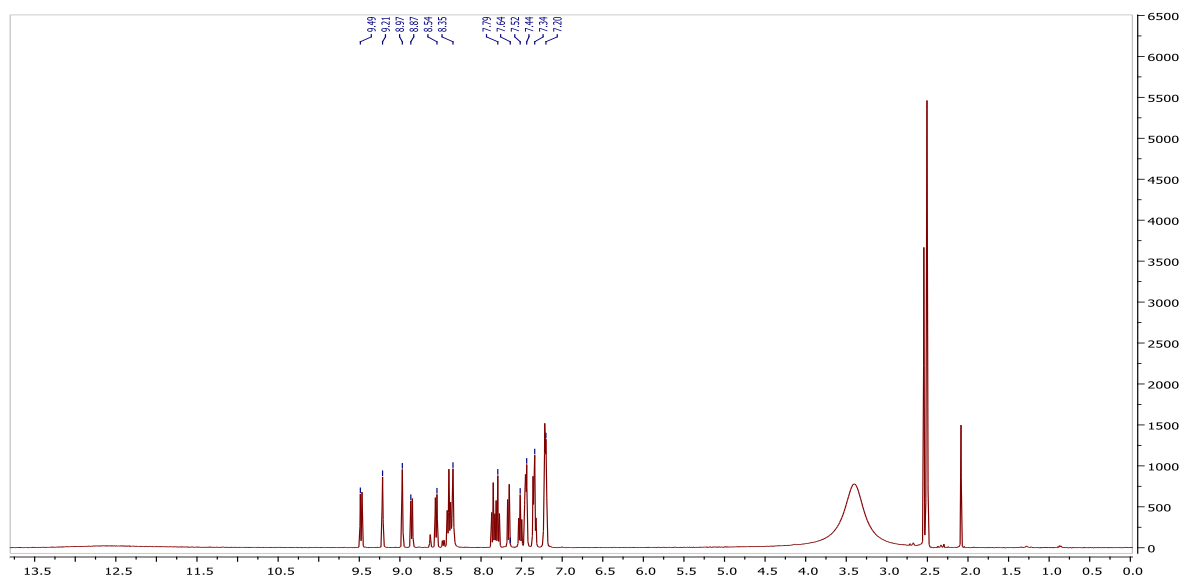


Figure 4.2 ^1H NMR spectrum of 11-(3-nitrophenyl)-1,8,10,12-tetraazatricyclo[7.4.0.0^{2,7}]trideca-2(7),3,5,9,11-pentaene-13-thione (**16**).

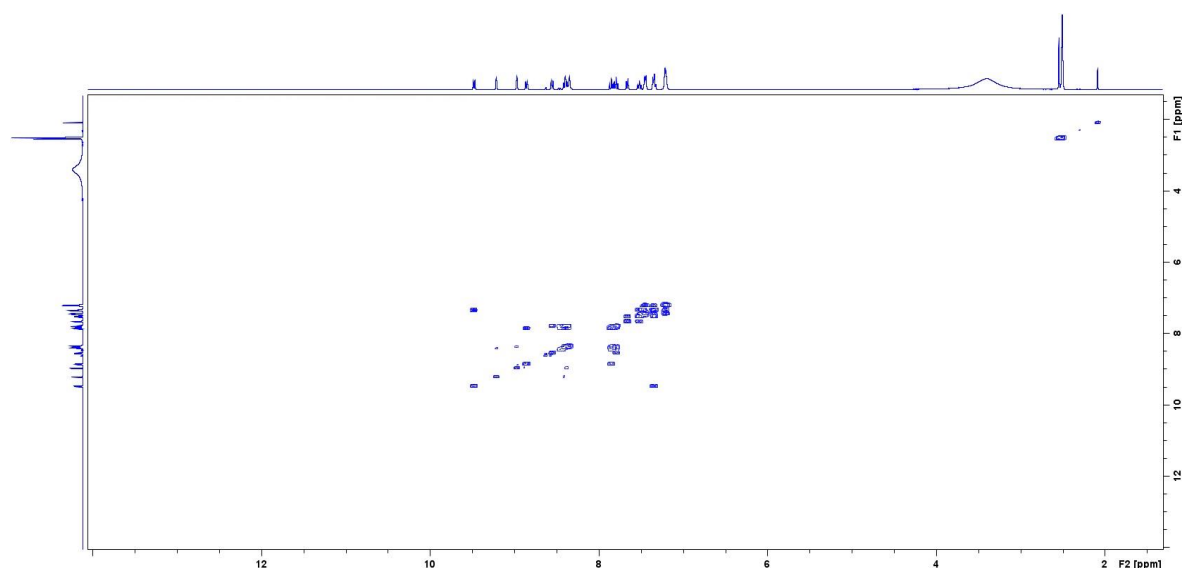


Figure 4.3 ^1H ^1H COSY spectrum of 11-(3-nitrophenyl)-1,8,10,12-tetraazatricyclo [7.4.0.0^{2,7}]trideca-2(7),3,5,9,11-pentaene-13-thione (**16**).

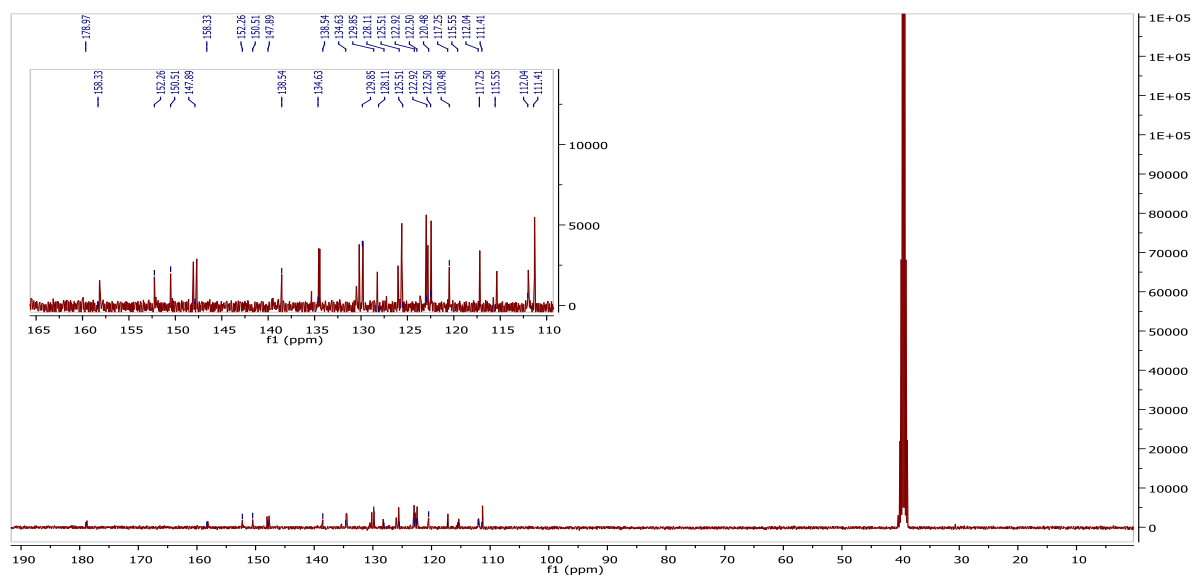


Figure 4.4 ^{13}C NMR spectrum of 11-(3-nitrophenyl)-1,8,10,12-tetraazatricyclo [7.4.0.0^{2,7}] trideca-2(7),3,5,9,11-pentaene-13-thione (**16**).

4.7 11-(3-Chlorophenyl)-1,8,10,12-tetraazatricyclo[7.4.0.0^{2,7}]trideca-2(7),3,5,9,11-pentaene-13-thione (17)

The IR spectrum (**Figure A4.17**) showed an N–H stretch at 3102 cm⁻¹, a band for the C=N stretch at 1625 cm⁻¹ and the aromatic C=C was observed at 1595 cm⁻¹. The ¹H NMR (**Figure A4.18**) and ¹H–¹H COSY (**Figure A4.19**) spectra gave a resonance at 12.77 ppm for a proton of a benzimidazol NH whilst other aromatic protons occurred between 8.17 and 7.18 ppm. In the ¹³C NMR spectrum (**Figure A4.20**) aromatic carbons resonated between 166.0 and 112.5 ppm.

4.8 11-(3-Bromophenyl)-1,8,10,12-tetraazatricyclo[7.4.0.0^{2,7}]trideca-2(7),3,5,9,11-pentaene-13-thione (18)

The IR spectrum (**Figure A4.21**) showed an N–H stretch at 3306 cm⁻¹ a band for the C=N stretch at 1622 cm⁻¹ and the aromatic C=C was observed at 1550 cm⁻¹. The ¹H NMR (**Figure A4.22**) and ¹H–¹H COSY (**Figure A4.23**) spectra gave signals at 12.48 ppm a proton of a benzimidazol NH whilst the aromatic protons appeared 8.32 and 7.16 ppm. In the ¹³C NMR spectrum (**Figure A4.24**) resonance between 134.0 and 112.5 ppm were observed for aromatic carbons.

4.9 11-(4-Nitrophenyl)-1,8,10,12-tetraazatricyclic[7.4.0.0^{2,7}]trideca-2(7),3,5,9,11-pentaene-13-thione (19)

The IR spectrum (**Figure A4.25**) showed an N–H stretch at 3140 cm⁻¹, a band for the C=N stretch at 1682 cm⁻¹ and the aromatic C=C was observed at 1591 cm⁻¹. In the ¹H NMR (**Figure A4.26**) and ¹H–¹H COSY (**Figure A4.27**) spectra the benzimidazol proton resonated at 12.88 ppm whilst the aromatic protons appeared between 9.50 and 7.21 ppm. The ¹³C NMR spectrum (**Figure A4.28**) gave signals between 165.6 and 112.5 ppm for aromatic carbons.

4.10 11-Phenyl-1,8,10,12-tetraazatricyclo[7.4.0.0^{2,7}]trideca-2(7),3,5,9,11-pentaene-13-thione (20)

The IR spectrum (**Figure A4.29**) showed an N–H stretch at 3309 cm⁻¹, a band for the C=N stretch at 1664 cm⁻¹ and the aromatic C=C was observed at 1573 cm⁻¹. The ¹H NMR (**Figure A4.30**) and ¹H–¹H COSY (**Figure A4.31**) spectra gave signals between 9.49 and 7.21 ppm for aromatic protons. The ¹³C NMR spectrum (**Figure A4.32**) gave signals between 165.6 and 117.4 ppm for aromatic carbons.

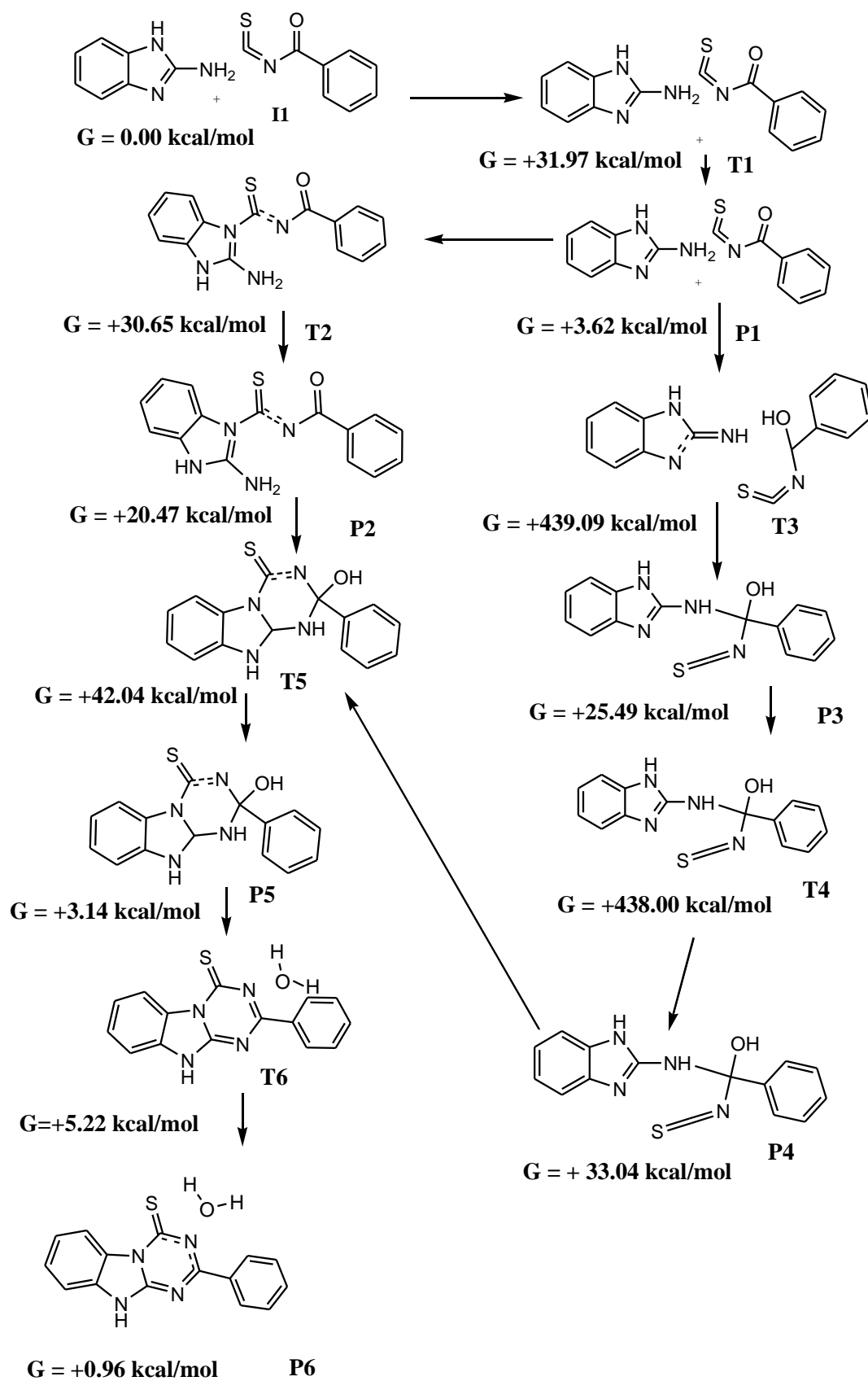
4.11 Transition state studies on tetraazatricyclic derivatives

The predicted reaction pathway computed proceeds by the coming together of benzoyl isothiocyanate and 2-aminobenzimidazole as indicated in **I1** (**Scheme 4.4**). With the distance between the 2-amino group and the carbon of the thione being 4.41 Å. **I1** is a singlet species of no charge with no imaginary frequency and a dipole moment of 9.10 Debye. **I1** is used as reference in the computation of the relative free energies. The functional used in the computation of **I1** is B3LYP with the basis set of 6-31G(d), it was obtained by optimising the starting material to a minimum and also tracing the reverse IRC path of the transition state **T1**. During the transition from **I1** to **T1** there is a reduction in the bond distance to 1.70 Å in **T1**, which is a singlet species of no charge with a single imaginary frequency and a dipole moment of 5.81 Debye. The relative free energy of **T1** compared to **I1** is +31.97 kcal/mol.

A forward displacement of **T1** along the IRC pathway and an optimization of the resultant species gives **P1** which is a singlet species of no charge, no imaginary frequency and with a dipole moment of 2.98 Debye. The relative free energy of **P1** is +3.62 kcal/mol. The transition from **T1** to **P1** involves a change in orientation of 2-aminobenzimidazole with the bond distance between the amine group and the thione carbon increasing to 4.01 Å in the process. **P1** proceeds *via* two distinct pathways through **T2** or **T3**. In **T2** the amine of the benzimidazole attacks the thione carbon whilst in **T3** the carbonyl is converted to a hydroxyl group by the abstraction of a proton from 2-aminobenzimidazole leading to the formation of a hydroxy group. **T2** is a singlet species of no charge with a single imaginary frequency and a dipole moment of 3.24 Å. The relative free energy of **T2** is +30.65 kcal/mol. **T3** is also a singlet species of charge 2 with a single imaginary frequency and a dipole moment of 9.03

Debye. The relative free energy of **T3** is +439.09 kcal/mol. The forward displacement of **T2** along the IRC pathway leads to **P2** a singlet species of no charge, no frequency and a dipole moment of 8.66 Debye. The relative energy of **P2** is +20.47 kcal/mol.

The intermediate obtained from **T3** is **P3** which is a singlet species of no charge and no imaginary frequency with a dipole moment of 2.85 Debye. **P3** leads to **T4**, which is a singlet species of no charge with a single imaginary frequency. The dipole moment of **T4** is 8.81 Debye. The relative energy of **T4** is +438.00 kcal/mol. Forward displacement of **T4** along the IRC pathway leads to **P4**, which is a singlet species of no charge, no imaginary frequency with a dipole moment 7.34 Debye. The relative energy of **P4** is +33.04 kcal/mol. **T5** which is a singlet species of no charge with a single imaginary of 1 and a dipole moment of **T5** is 12.25 Debye. The relative energy of **T5** is +42.04 kcal/mol. **P5** is a singlet species of no charge, no imaginary frequency with a dipole moment 10.40 Debye. The relative energy of **P5** is +3.14 kcal/mol. **T6** which is a singlet species of no charge with an imaginary frequency of 1. The dipole moment of **T5** is 5.78 Debye. The relative energy of **T6** is +5.22 kcal/mol. **P6** is a singlet species of no charge, no imaginary frequency with a dipole moment of 8.70 Debye. The relative energy of **P6** is +0.96 kcal/mol. The pathway through **T2** would be the preferred pathway because the energy required to go through the transition state is much lower than for **T3**.



Scheme 4.4 DFT reaction mechanism of tetraazatricyclic derivatives.

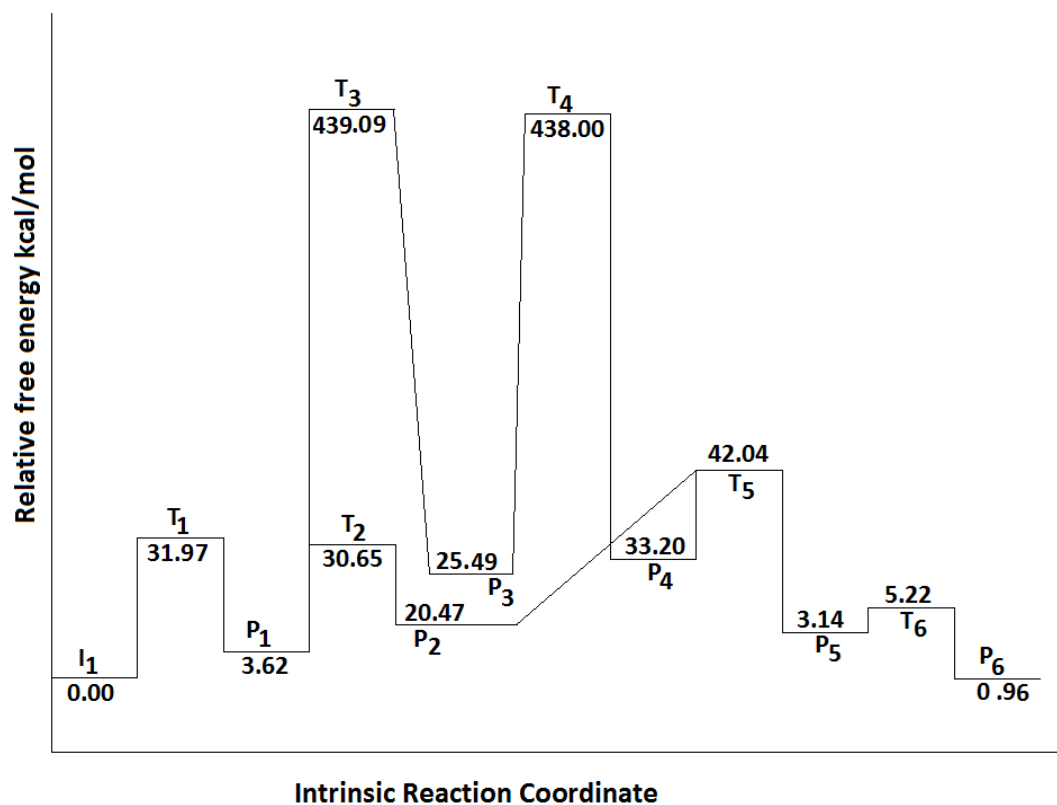
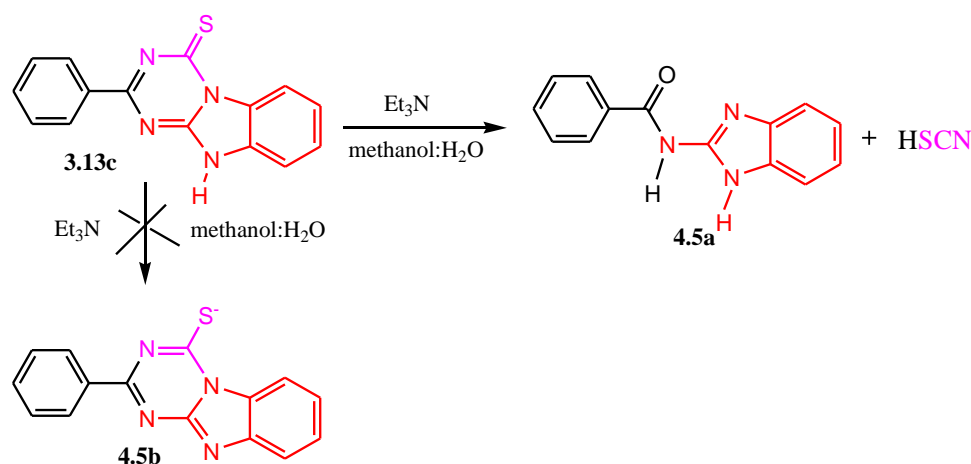


Figure 4.5 Potential energy surface for the formation of the tetraazatricyclic derivatives.

4.12 *N*-(1*H*-Benzimidazol-2-yl)benzamide (21)

Tautomerism is a phenomena associated to thiones and some thione tautomers have been reported to exist at very low temperatures.³³³ *Ab initio* calculations including continuum treatments of the solvent effect, leading to thione forms HC(dS)OH and CH₃C(dS)OH have been found to be less predominant, irrespective of the solvent polarity.³³⁴ An attempt at exploiting the tautomerism in tetraazatricyclics (**Scheme 4.5**) led to the a degradation of the tetraazatricyclic to form *N*-(1*H*-benzimidazol-2-yl)benzamide (**21**).



Scheme 4.5 Degradative synthesis of *N*-(1*H*-benzimidazol-2-yl)benzamide (21).

An attempt to convert the tetraazatricyclic to the tautomer of S by abstracting a proton led to its degradation through a base catalysed dethiocyanation. A full mechanism is described Section 4.13. The IR spectrum (Figure 4.6) showed bands at 3314 and 3062 cm^{-1} for N–H stretch, a band for the C=O stretch was observed at 1661 cm^{-1} , and the C=N and C=C bands were observed at 1558 and 1519 cm^{-1} , respectively. The ^1H NMR (Figure 4.7) and ^1H – ^1H COSY (Figure 4.8) spectra gave signals between 8.17 and 7.14 ppm for aromatic protons, amide proton signals exchanges with the water molecules hence are not observable. The ^{13}C NMR spectrum (Figure 4.9) gave signals between 168.6 and 111.4 ppm for aromatic carbons.

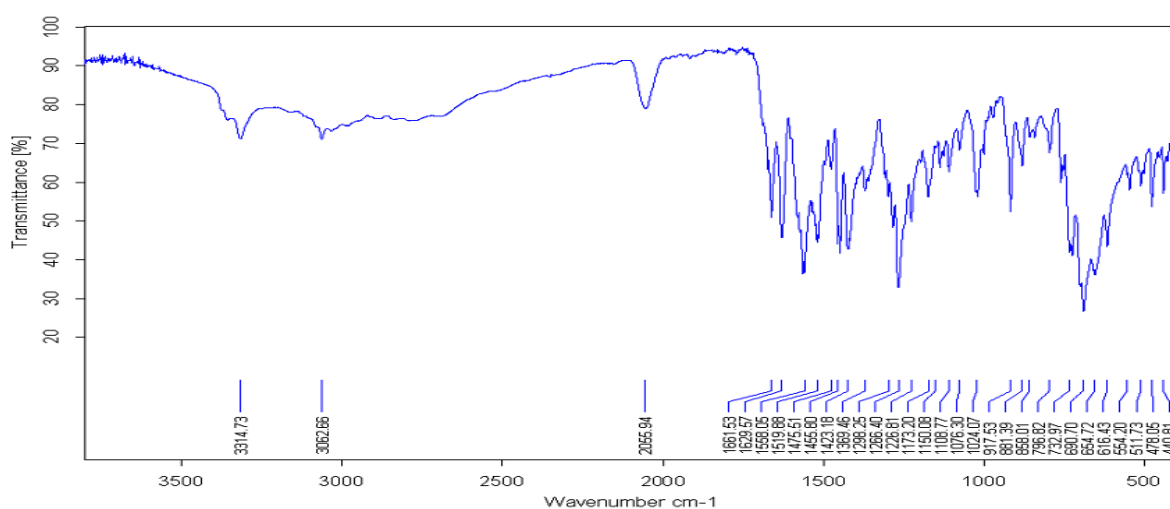


Figure 4.6 IR spectrum of *N*-(1*H*-benzimidazol-2-yl)benzamide (21).

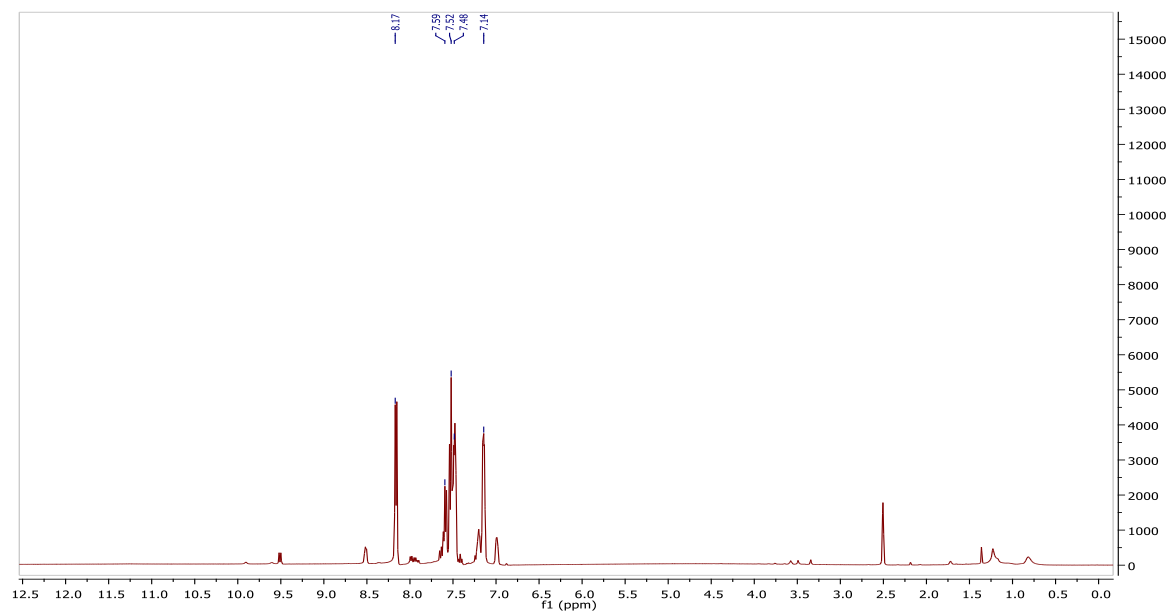


Figure 4.7 ^1H NMR spectrum of *N*-(1*H*-benzimidazol-2-yl)benzamide (**21**).

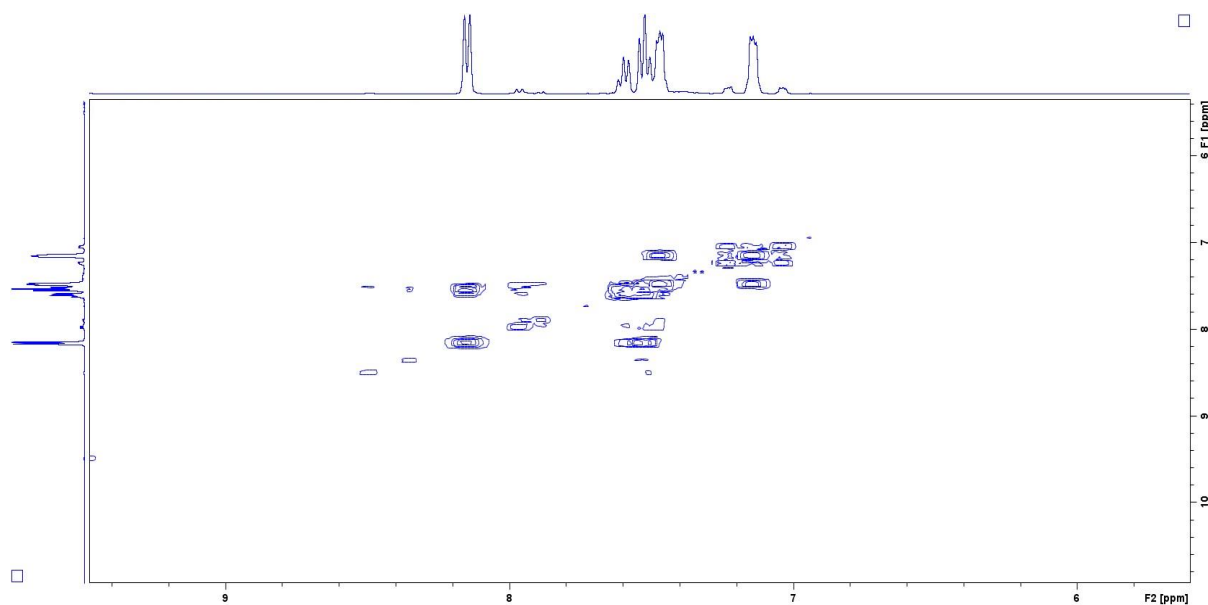


Figure 4.8 ^1H - ^1H COSY spectrum of *N*-(1*H*-benzimidazol-2-yl)benzamide (**21**).

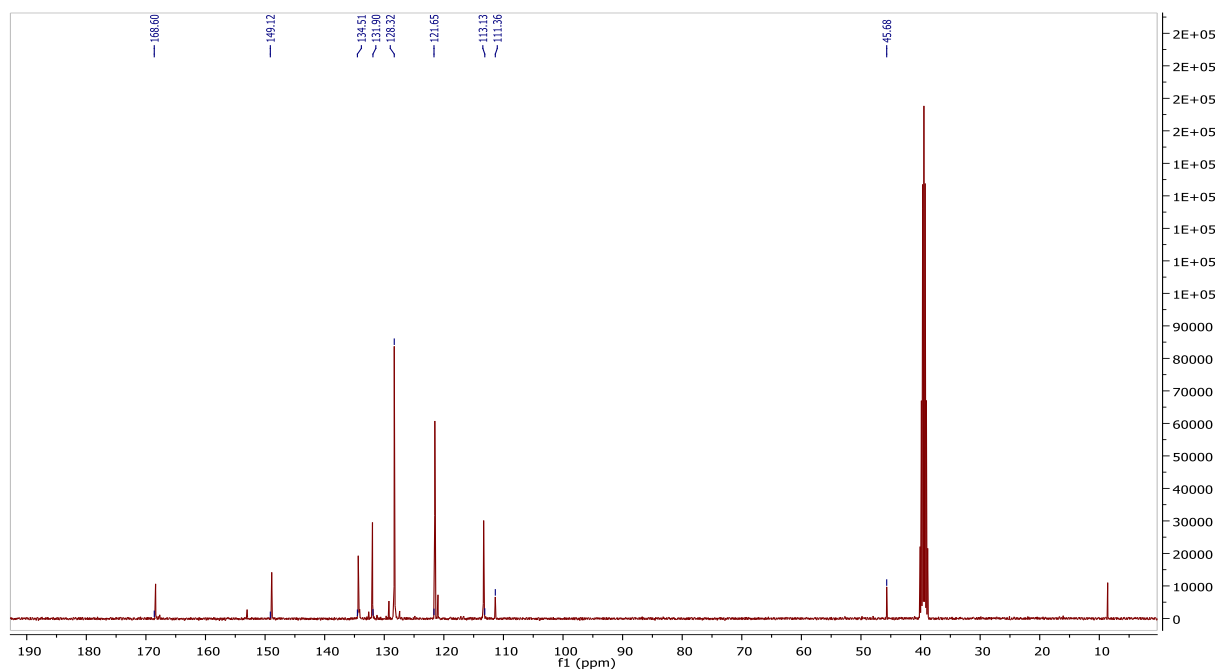


Figure 4.9 ^{13}C NMR spectrum of *N*-(1*H*-benzimidazol-2-yl)benzamide (**21**).

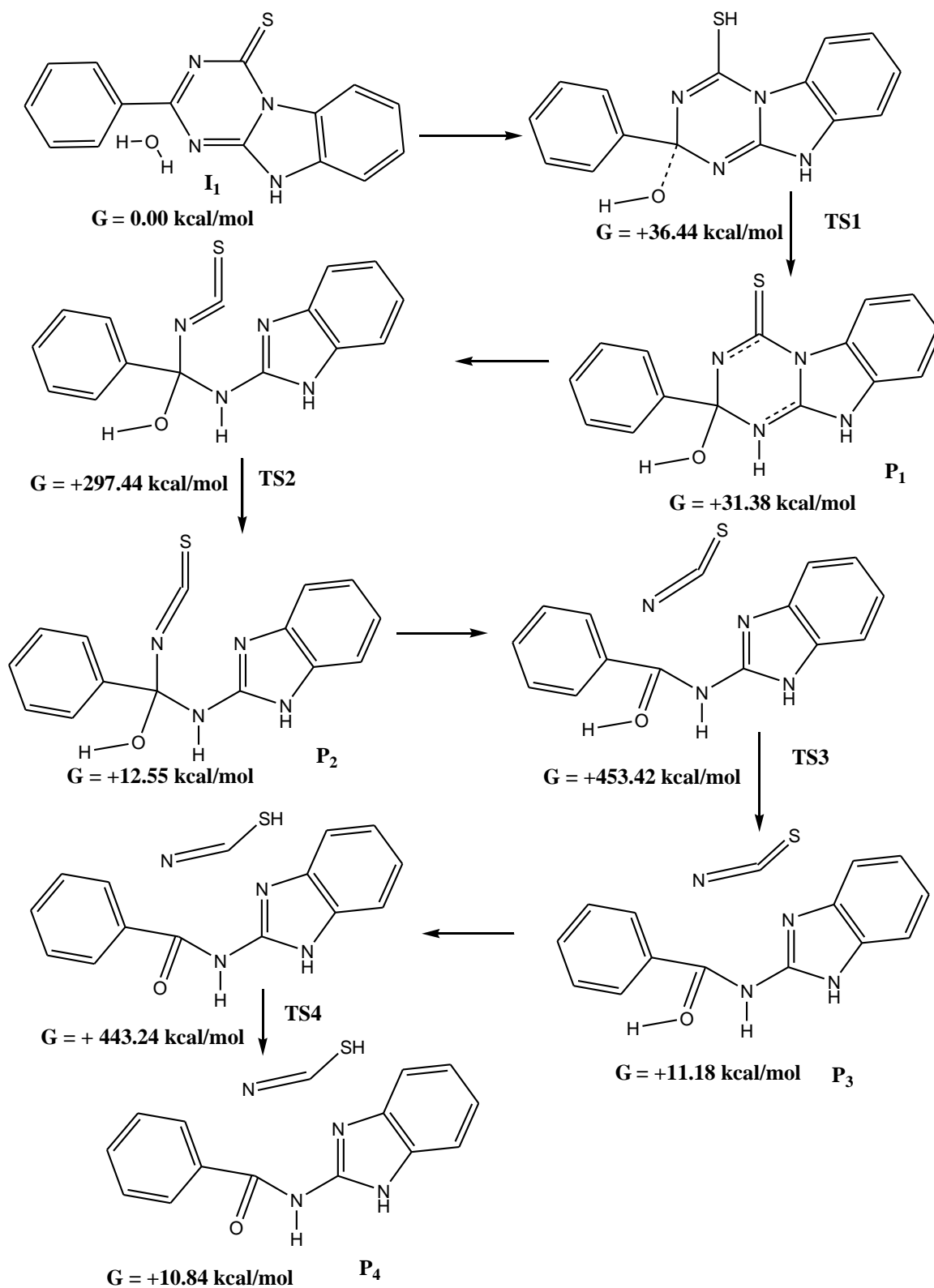
4.13 Transition state studies on *N*-(1*H*-benzimidazol-2-yl)benzamide (**21**)

The density functional theory based computation using Gaussian 09 at the B3PW91 with a basis set of 6-31G(d) level has been used to compute and predict a reaction pathway for the formation of compounds *N*-(1*H*-benzimidazol-2-yl)benzamide (**21**), **Scheme 4.6** gives the computed reaction mechanism for the formation of *N*-(1*H*-benzimidazol-2-yl)benzamide (**21**) in the gas phase. The predicted reaction pathway proceeds by the attack of the tetrazatetracyclic by a water molecule as indicated in **I1**, which is a singlet species of no charge and a dipole moment of 8.60 Debye. **I1** is used as reference in the computation of the relative free energies. The functional used in the computation of **I1** is B3PW91 with the basis set of 6-31G(d), it was obtained by optimising the starting material to a minimum and also tracing the reverse intrinsic reaction coordinate (IRC) path of the transition state **TS1**. **TS1** is singlet species of no charge with a dipole moment of 12.32 Debye. It is a saddle point with a single imaginary frequency, obtained according to the Berny algorithm and subsequent vibrational analysis. The relative free energy of **TS1** is 36.44 kcal/mol.

A forward IRC computation and optimization of the subsequent structure gave **P1** which is a singlet species of no charge with a dipole moment of 10.14 Debye. The relative free energy

of **P1** is 31.38 kcal/mol. The cleavage of a C–N bond in **P1** leads to the formation of **TS2** which is also a singlet species with a charge of 2 and a dipole moment of 16.23 Debye. **TS2** is a saddle point with a single imaginary frequency. The relative free energy of **TS2** is 297.44 kcal/mol. A forward IRC pathway from **TS2** gives **P2** which is a singlet species of no charge, and an imaginary frequency of zero. The dipole moment of **P2** is 5.80 Debye, with a relative free energy of 12.55 kcal/mol. The cleavage of the thiocyanate from the **P2** gives **TS3** which is a saddle point of charge 2 and a single imaginary frequency. It is a singlet species of dipole moment 3.04 Debye. The relative free energy of **TS3** is 453.42 kcal/mol. A forward displacement of **TS3** gives **P3** which is also a singlet of no charge and an imaginary frequency of zero. The relative free energy of **P3** is 11.18 kcal/mol.

A rearrangement of **P3** gives **TS4** which is also a saddle point with a charge of 2 and it is a singlet species with a single imaginary frequency and a dipole moment of 7.32 Debye and a relative free energy of 443.24 kcal/mol. The forward displacement of **TS4** along the IRC path and a subsequent minimization of the resulting intermediate gave **P4** which is a singlet species of no charge with a dipole moment of 1.48 Debye and a relative free energy of 10.85 kcal/mol. The computation of the various transition states that give compound **21** have been carried out. Several of the steps in this computational scheme have a plausible activation, and this scheme serves as proof of concept that a computational path exists with a continuous path from reactants to products. Further work will investigate alternative pathways from **P2** to **P3**, for example where the computed activation is an unphysical 441 kcal/mol. Other aspects that will be included in further work will be the use of modern functionals such as wB97-XD or M06.



Scheme 4.6 DFT reaction mechanism of *N*-(1*H*-benzimidazol-2-yl)benzamide (**21**).

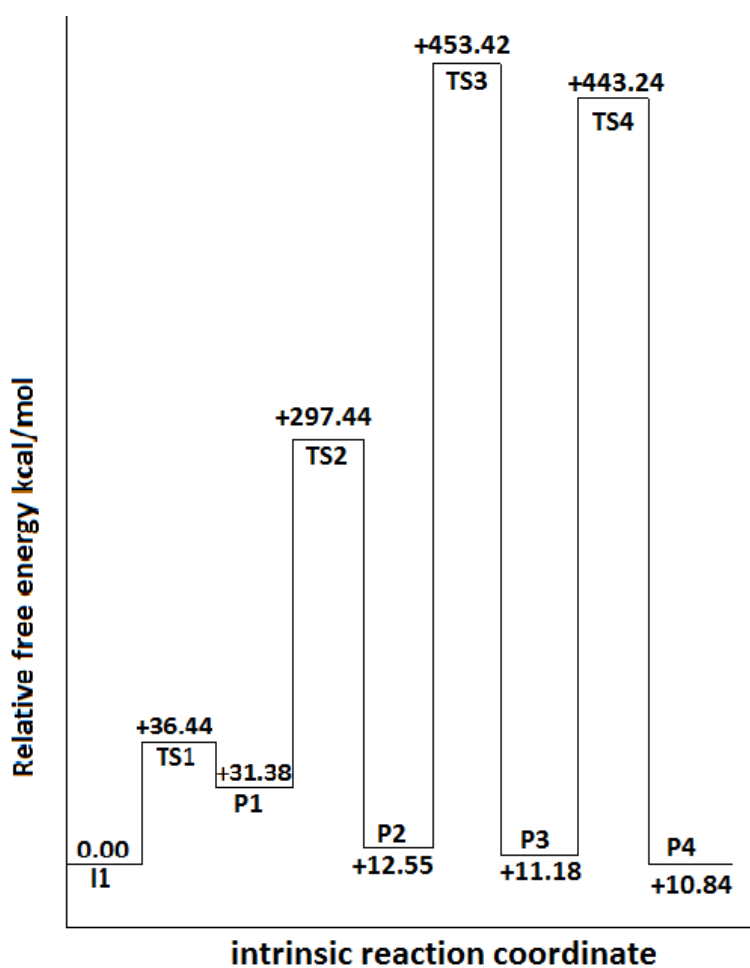
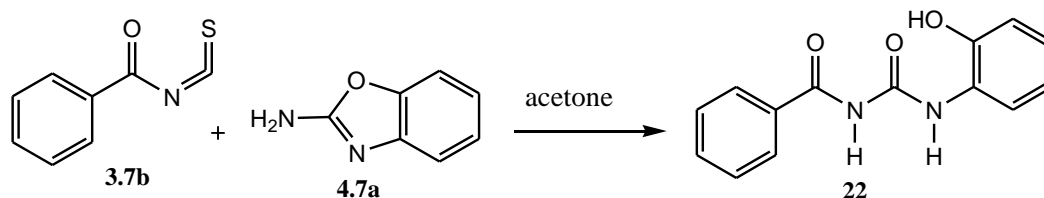


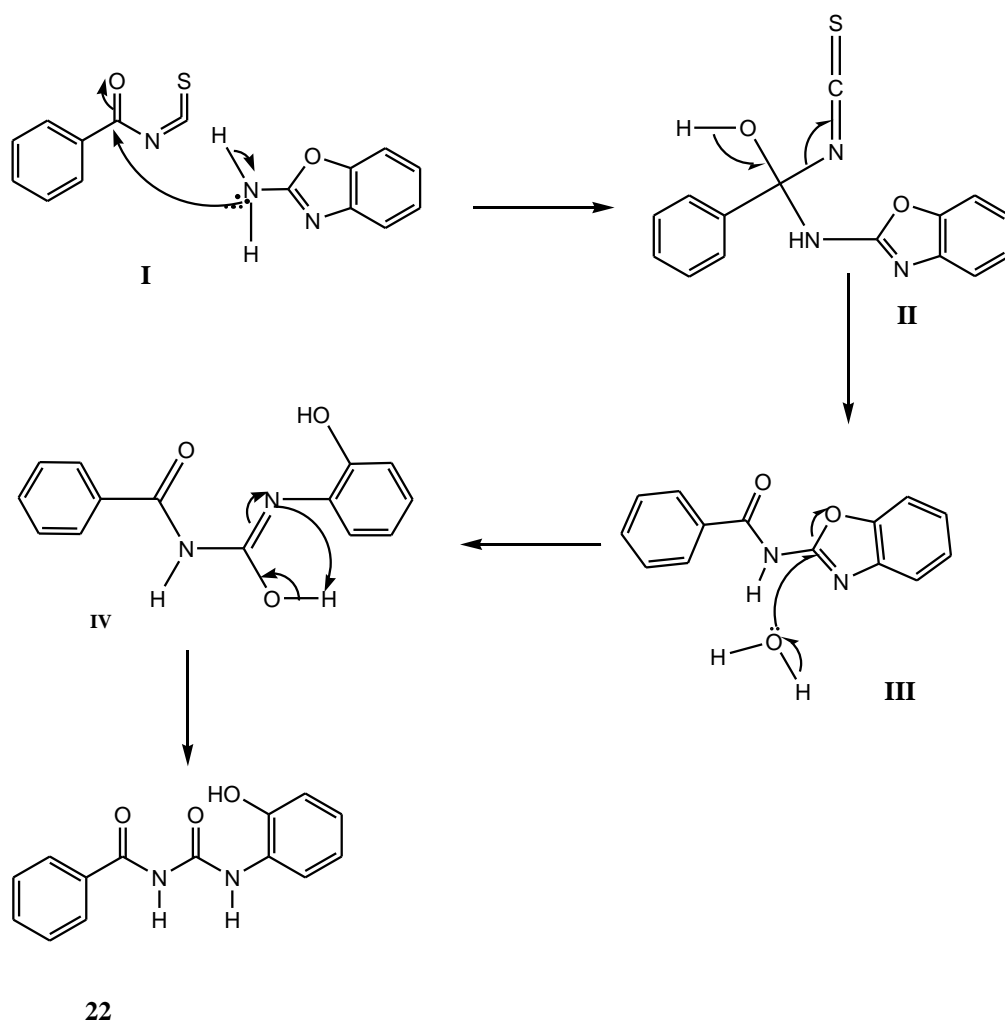
Figure 4.10 Potential energy surface, derived from transition states and intrinsic reaction coordinate calculations illustrating the pathway for the formation of *N*-(1*H*-benzimidazol-2-yl)benzamide (**21**)

4.14 3-Benzoyl-1-(2-hydroxyphenyl) urea (**22**)



Scheme 4.7 Synthesis of 3-benzoyl-1-(2-hydroxyphenyl) urea (**22**).

Compound **22** is thought to be formed by the attack of the carbonyl of the benzoyl isothiocyanate by the 2-amino group of the 2-aminobenzoxazole as shown in **I** with a subsequent picking up of a proton by the carbonyl to form a hydroxyl group in **II** (**Scheme 4.8**). The loss of the thiocyanate group and a proton led to the formation of **III**. Water attacks the carbon atom between the heteroatoms leading to a ring opening as shown in **IV** with a further loss of a proton leading to the formation of **22**.



Scheme 4.8 Proposed reaction mechanism for the formation of 3-benzoyl-1-(2-hydroxyphenyl) urea (**22**).

The IR spectrum (**Figure 4.11**) showed two bands for an N–H stretch at 3233 and 3155 cm^{-1} . Two bands for the C=O stretch were observed at 1694 and 1655 cm^{-1} , the C=N stretch was observed at 1599 cm^{-1} whilst the aromatic C=C was observed at 1559 cm^{-1} . The ^1H NMR (**Figure 4.12**) and ^1H – ^1H COSY (**Figure 4.13**) spectra gave singlet signals at 11.22 and 11.13

ppm for the proton of an amide. A signal was observed at 10.97 ppm for the hydroxyl proton, whilst three signals were observed at 10.11, 9.87 and 9.55 ppm possibly due to long range coupling amongst the protons. The aromatic protons occurred between 8.15 and 6.82 ppm. The ^{13}C NMR spectrum (**Figure 4.14**) gave a signal at 182.06 ppm. Signals for carbonyls were observed at 168.67 and 167.94 ppm, signals between 150.8 and 114.1 ppm for aromatic carbons.

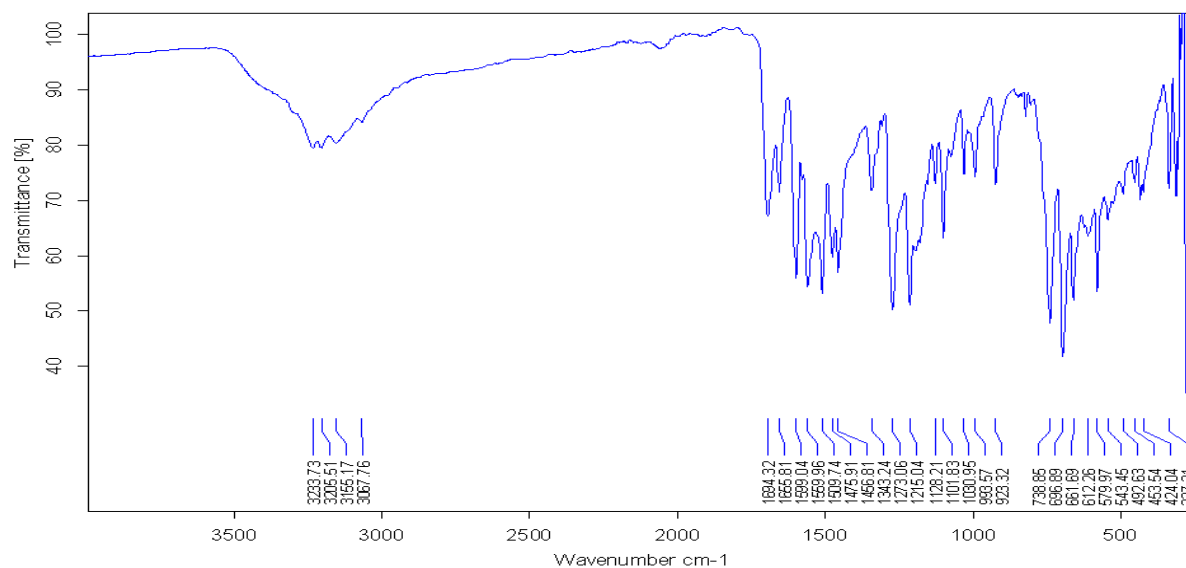


Figure 4.11 IR spectrum of 3-benzoyl-1-(2-hydroxyphenyl) urea (**22**).

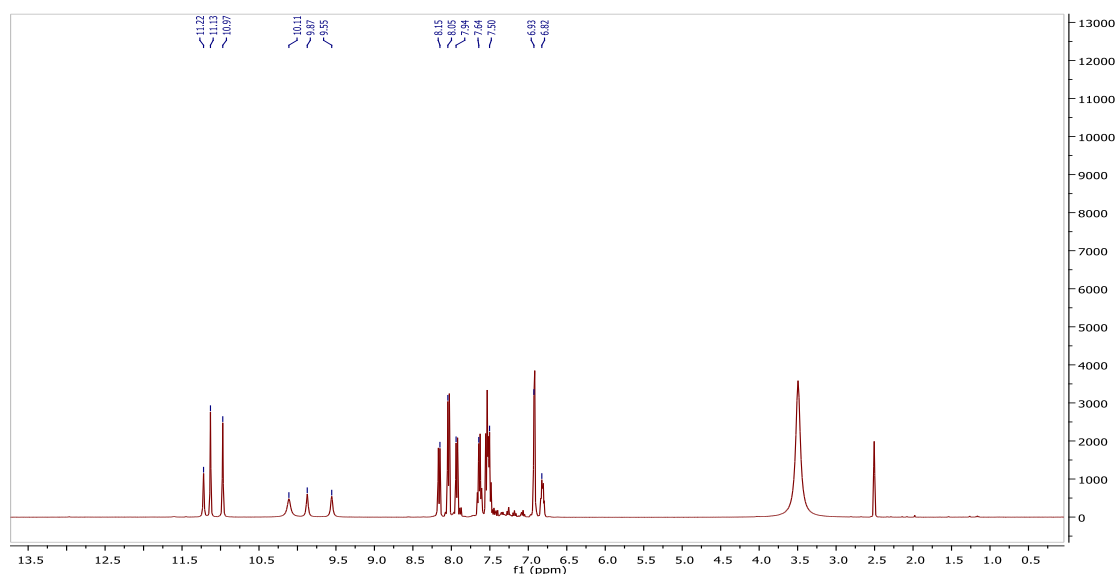


Figure 4.12 ^1H NMR spectrum of 3-benzoyl-1-(2-hydroxyphenyl) urea (**22**).

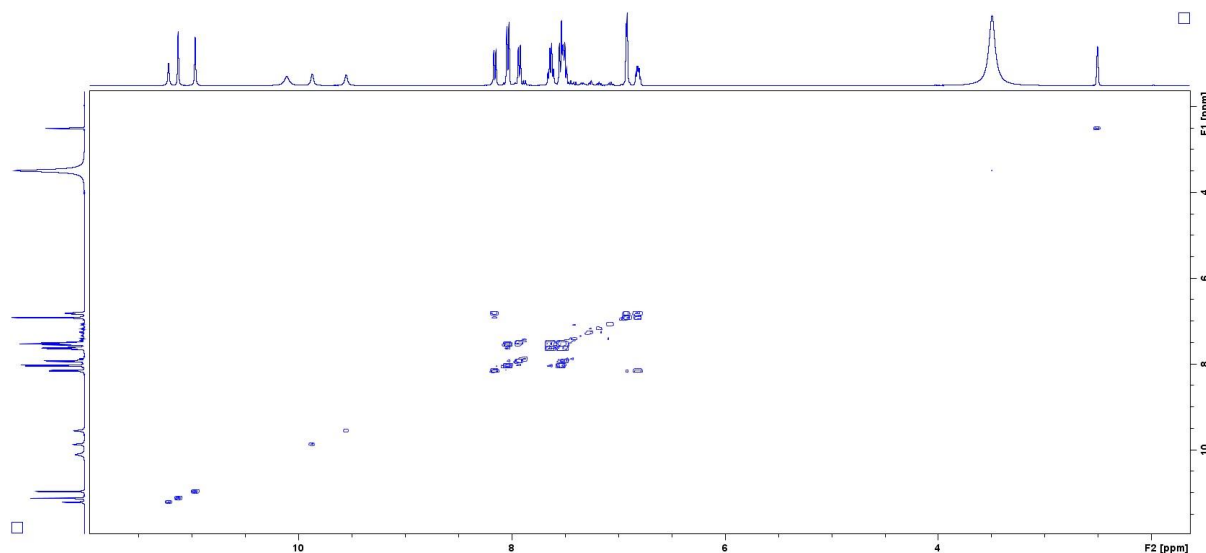


Figure 4.13 ^1H - ^1H COSY spectrum of 3-benzoyl-1-(2-hydroxyphenyl) urea (**22**).

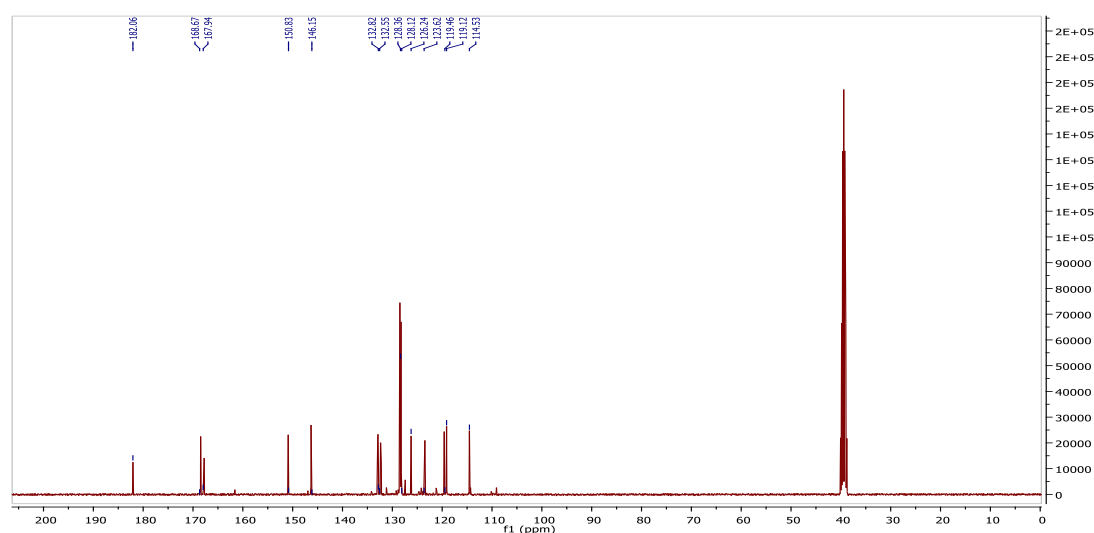


Figure 4.14 ^{13}C NMR spectrum of 3-benzoyl-1-(2-hydroxyphenyl) urea (**22**).

4.15 Crystal structures of compounds **20**, **21** and **22**

Compounds **20**, **21** and **22** were recrystallized from DMSO:toluene (1:1). Compound **20** was obtained as a yellow solid, whilst compounds **21** and **22** were obtained as white crystals. The crystallographic data, selected bond lengths, bond angles and torsion angles for the crystal structures of compounds **20**, **21** and **22** are provided in **Tables 4.1** and **4.2**. The ORTEP diagrams for compounds **20**, **21** and **22** are presented in **Figures 4.15**, **4.16** and **4.17**.

Compounds **20** and **22** crystallized in the monoclinic space group P21/c, whilst compound **21** crystallized in the monoclinic space group C2/c.

Table 4.1 Crystallographic data and structure refinement summary for compounds **20**, **21** and **22**.

Property	20	21	22
Formula	C ₁₅ H ₁₀ N ₄ S ₂ C ₂ H ₆ OS	C ₁₄ H ₁₁ N ₃ O	C ₁₄ H ₁₂ N ₂ O ₃
Formula Weight	356.48	237.26	256.26
Crystal System	Monoclinic	monoclinic	Monoclinic
Space group	P21/c	C2/c	P21/c
a [Å]	12.4761(4)	29.0638(13)	12.5355(16)
b [Å]	14.7020(4)	5.0660(2)	6.3401(9)
c [Å]	9.7388(2)	25.8395(10)	16.262(2)
α [°]	90	90	90
β [°]	104.209(1)	113.493(1)	110.324(5)
γ [°]	90	90	90
V [Å ³]	1731.68(8)	3489.2(2)	1212.0(3)
Z	4	12	4
D(calc) [g/cm ³]	1.367	1.355	1.404
Mu(MoKa) [/mm]	0.319	0.089	0.101
F(000)	744	1488	536
Crystal Size [mm]	0.10 x 0.27 x 0.31	0.12 x 0.42 x 0.63	0.18 x 0.19 x 0.32
Temperature (K)	200	200	200
Radiation [Å]	MoKa 0.71073	MoKa 0.71073	MoKa 0.71073
θ Min-Max [°]	2.2, 28.3	2.7, 28.4	1.7, 28.4
Dataset	-16: 16 ; -18: 19 ; -12: 9	-38: 32 ; -6: 6 ; -28: 34	-16: 16 ; -8: 7 ; -21: 20
Tot., Uniq. Data, R(int)	15730, 4306, 0.022	15397, 4347, 0.019	10913, 3016, 0.045
Observed data [I > 2.0 sigma(I)]	3443	2992	1807
Nref, Npar	4306, 223	4347, 325	3016, 181
R, wR ₂ , S	0.0345, 0.0966, 1.04	0.0518, 0.1336, 1.03	0.0478, 0.1223, 1.01
Max. and Av. Shift/Error	0.00, 0.00	0.00, 0.00	0.00, 0.00
Min. and Max. Resd. Dens. [e/Å ³]	-0.31, 0.29	-0.31, 0.33	-0.27, 0.19

The bond distance of S1–C2 in compound **20** is 1.664(1) Å, whilst the N3-C3 bond distance is 1.322(2), the bond distances of N1-C2, N2-C3, N2-C2 and N3-C1 which forms part of the six membered ring are 1.349(2), 1.336(2), 1.402(2) and 1.346 (2) Å, respectively. The bonds

are not distinctly single or double bonds suggesting that the nitrogen atoms are sp^2 hybridized. This ensures that an electron cloud is delocalized over the atoms in the six membered ring for stability. The bond angles of N1-C2-N2, S1-C2-N2 and C1-N1-C2 in compound **20** are 116.1(1), 121.1(1) and 120.2(1), respectively. The bond angles are consistent with the sp^2 hybridization of the carbon and nitrogen atoms. In compound **21** the six membered ring collapses through base-catalysed dethiocyanation leading to the formation of an amide. The bond distance of O11-C12 is 1.227(2) Å which is consistent with a carbonyl whilst the bond distances of N13-C12 and N11-C11 are 1.368(2) and 1.350(2) Å, respectively. The bond angles of N11-C11-N13, O11-C11-N13 and N12-C12-N13 are 123.6(2), 121.8(2) and 122.0(2) Å, respectively. The bond distances of O1-C1 and O2-C2 in compound **22** are 1.236(2) Å and 1.226(2) Å, respectively which is consistent with the bond length of a carbonyl whilst the O3-C22 bond distance is 1.366(2) Å. The N1-C1 and N1-C2 bond distances are 1.369(2) and 1.406(2) respectively. The bond angles of N11-C11-N13, O11-C12-N13 and N12-C11-N13 in compound **22** are 123.6(2), 121.8(2) and 122.0(2) respectively confirming that the carbon atoms involved are sp^2 hybridized.

Table 4.2 Selected bond lengths (Å) and bond angles (°) for compounds **20**, **21** and **22**.

Bond lengths					
20		21		22	
S1-C2	1.664(1)	O11-C12	1.227(2)	O1-C1	1.2364(19)
N3-C3	1.322(2)	N13-C12	1.368(2)	O2-C2	1.2262(19)
N1-C2	1.349(2)	N11-C11	1.350(2)	O3-C22	1.366(2)
N1-C1	1.336(2)	N13-C11	1.381(2)	N1-C1	1.369(2)
N2-C3	1.382(2)	N12-C112	1.397(2)	N1-C2	1.406(2)
N2-C2	1.402(2)	N12-C11	1.318(2)	N2-C2	1.339(2)
N3-C1	1.346(2)			N2-C21	1.402(2)
Bond angles					
20		21		22	
C1-N1-C2	120.2(1)	N11-C11-N12	114.4(2)	C1-N1-C2	128.8(1)
N1-C2-N2	116.1(1)	N11-C11-N13	123.6(2)	C2-N2-C21	128.0(1)
S1-C2-N2	121.1(1)	O11-C12-N13	121.8(2)	O1-C1-N1	120.9(2)
N1-C1-N2	113.3(1)	N12-C11-N13	122.0(2)	O2-C2-N1	118.3(2)
N3-C2-N4	126.2(1)			O2-C2-N2	125.5(2)
N2-C2-N3	115.4(1)			N1-C2-N2	116.2(1)

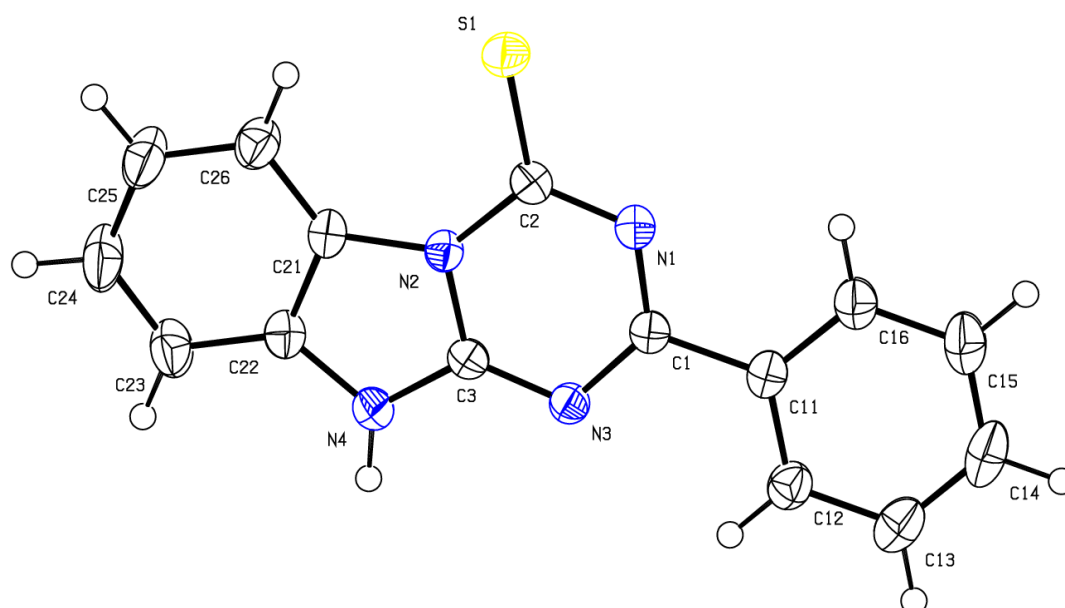


Figure 4.15 An ORTEP view of 11-phenyl-1,8,10,12-tetraazatricyclo[7.4.0.0^{2,7}]trideca-2(7),3,5,9,11-pentaene-13-thione (**20**) showing 50% probability displacement ellipsoids and the atom labelling.

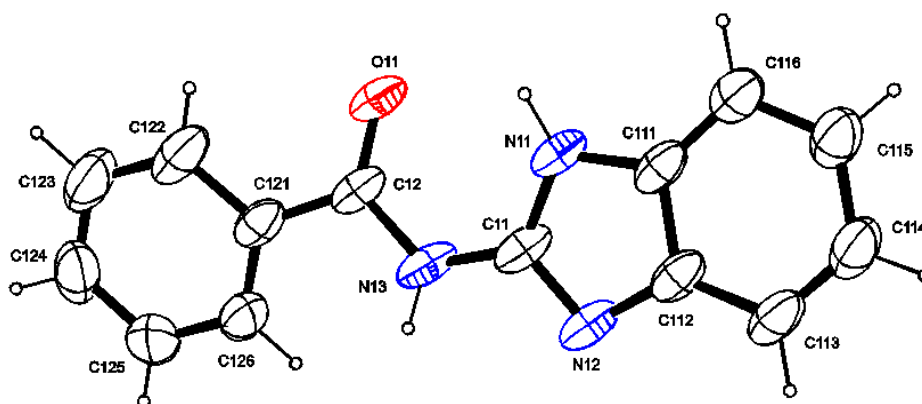


Figure 4.16 An ORTEP view of *N*-(1*H*-benzimidazol-2-yl)benzamide (**21**) showing 50% probability displacement ellipsoids and the atom labelling.

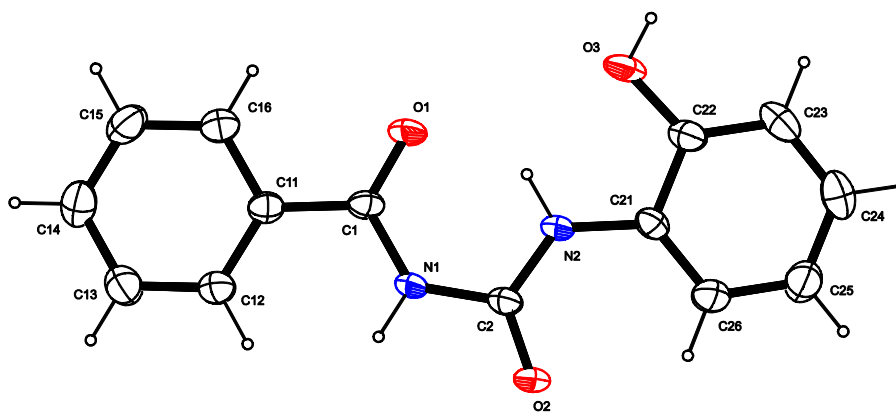


Figure 4.17 An ORTEP view of 3-benzoyl-1-(2-hydroxyphenyl) urea (**22**) showing 50% probability displacement ellipsoids and the atom labelling.

4.2 Biochemical studies

4.2.1 Cell viability and cytotoxicity tests

The acute cytotoxic effects of tetraazatriacyclic derivatives determined by exposing them to isolated human white blood cells, for a 24-hour period. The cell viability was assessed using the MTT reduction assay and the results are presented in **Table 4.3** which indicates the compound numbers (in bold) as well as the EC_{50} values calculated for each compound tested.

Table 4.3 Cell viability results for tetraazatriacyclics.

Tetraazatriacyclics	EC_{50} μM
12	38.0
13	179.2
14	5.3
15	86.0
16	126.5
17	126.3
18	0.2
19	350.0
20	175.0
21	175.5

The EC₅₀ values for the tetraazatriacyclics (**Figure 4.18**) showed varying effects on the cell viability of human white blood cells. Compound **18** (unsubstituted), **12** (4-chloro) and **14** (4-methoxy) derivatives were found to be cytotoxic, giving EC₅₀ values of 0.15 ± 0.051 , 37.96 ± 21.87 and 5.28 ± 2.95 μM , respectively. This suggested that substitution at position 4 on the phenyl ring of tetraazatriacyclics with a methoxy or a chloro group leads to increased cytotoxic effects.

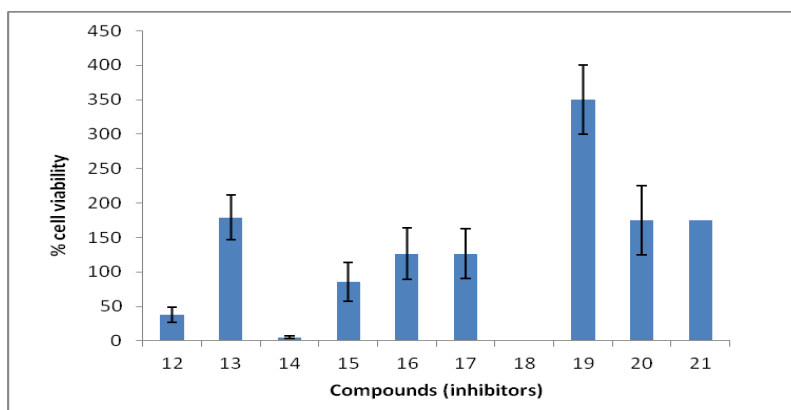


Figure 4.18 EC₅₀ values for the tetraazatriacyclics (μM). Error bars represent the SEM for $n = 3$.

A library of eleven compounds were tested and for the next section only typical examples are illustrated of how the EC₅₀ values were calculated. The cytotoxic effects of compounds **18** and **19**, which are the most cytotoxic and least cytotoxic compounds among the tetraazatriacyclic derivatives, respectively, are represented in **Figure 4.19**. The 3-bromo derivative (**18**) of the tetraazatriacyclics was the most cytotoxic suggesting that the presence of the bromo group at position 3 leads to an increase in cytotoxicity whilst the presence of the nitro group (**19**) at position 4 leads to a decrease in cytotoxicity.

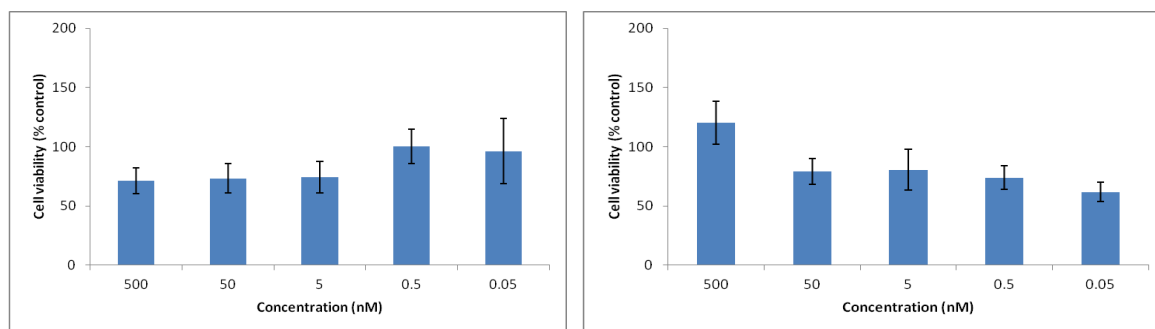


Figure 4.19 EC₅₀ values for compounds **18** and **19** (μM). Error bars represent the SEM for $n = 3$.

4.2.2 HIV-1 protease screen of tetraazatricyclics

Table 4.3 and **Figure 4.20** show the HIV-1 screening results for the tetraazatricyclics. The screening of the compounds was done at 100 μM of inhibitor and that for ritonavir was done at 10 μM . Most of the compounds gave a percentage inhibition of less than 40%, except compounds **19** (4-nitro derivative) and **16** (3-nitro derivative) with % inhibition of 59.57 ± 13.59 and 79.97 ± 11.97 , respectively. These compounds are not cytotoxic. Their activity might be due to the rigid scaffold of the tetraazatricyclic which enables it to fit the active site of HIV-1 protease to be able to interact with the bridging water molecules *via* hydrogen bonding or dipole-dipole interaction.

Table 4.3 HIV-1 protease screening results for tetraazatricyclics.

Compound	Fluorescence	Standard deviation	% Activity relative to untreated control	% Inhibition relative to untreated control
Ritonavir	36.24	1.88	9.34	90.66
12	423.28	2.28	109.12	0
13	394.04	4.61	101.58	0
14	416.40	0.72	107.35	0
15	148.69	4.61	65.80	34.20
16	45.26	11.97	20.03	79.97
17	346.13	10.82	89.23	10.77
18	448.35	6.19	115.58	0
19	156.83	13.59	40.43	59.57
20	351.26	7.94	90.55	9.45
21	320.73	1.71	82.68	17.32

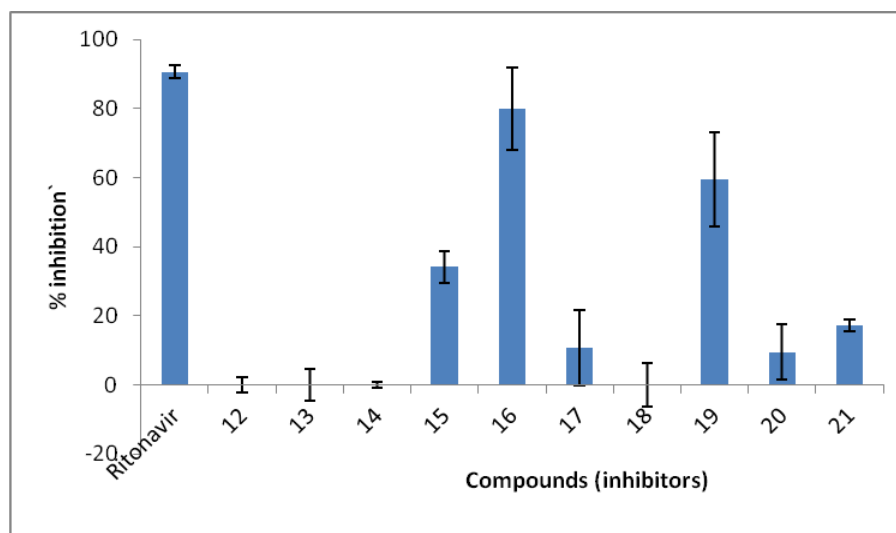


Figure 4.20 HIV-1 protease screening results illustrating % inhibition of tetraazatricyclics (100 μM) and ritonavir (10 μM) compared to untreated control. Error bars represent SEM for $n = 3$.

11-(3-Nitrophenyl)-1,8,10,12-tetraazatricyclo [7.4.0.0^{2,7}] trideca-2(7),3,5,9,11-pentaene-13-thione (**16**) gave the best inhibition of 79.97% at an inhibitor concentration of 100 μM and protease concentration of 20 μM among the tetraazatricyclics. It is consistent with the docking results which gave a predicted inhibition constant of 3.37 μM as the best docking result among the tetraazatricyclics. **Figure 4.21** gives the 2D representation of compound **16** in the protease active site. Compound **16** binds to the aspartate B25 residue in the protease active site via hydrogen bonding this allows the molecule to sit in the protease active site. Further binding to aspartate A29 and A30 residues *via* the oxygen atoms on the nitro group allows the molecule to effectively hinder access to the bridging water molecules by the natural substrate hence inhibiting protease activity to a larger extent.

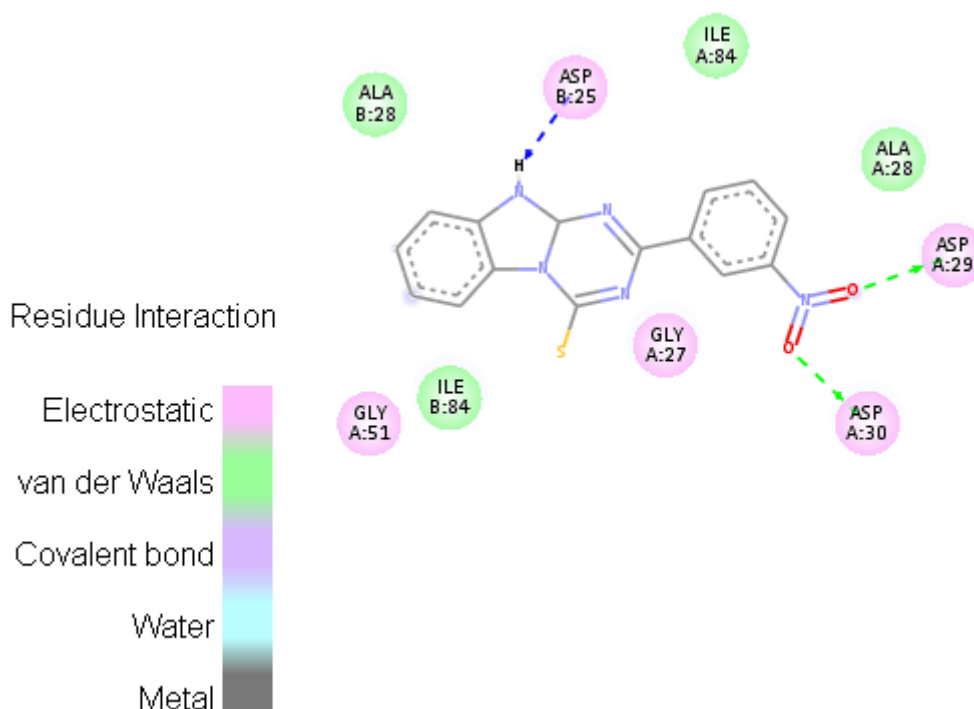


Figure 4.21 2D represent of 11-(3-nitrophenyl)-1,8,10,12-tetraazatricyclo[7.4.0.0^{2,7}]trideca-2(7),3,5,9,11-pentaene-13-thione (**16**) in protease active site.

11-(4-Nitrophenyl)-1,8,10,12-tetraazatricyclic [7.4.0.0^{2,7}]trideca-2(7),3,5,9,11-pentaene-13-thione (**19**) also gave very good inhibition in the bioassay with a percentage inhibition of 59.57% at an inhibitor concentration of 100 μM and a protease concentration of 20 μM gave a predicted inhibition constant of 3.37 μM in the docking studies. **Figure 4.22** gives the 2D representation of compound **19** in the protease active site. The activity of compound **19** against protease can be explained from the fact that it binds to the aspartate B25 residue at the protease active site through hydrogen bonding, and further binding to the aspartate B30 of protease ensures that it can inhibit the natural substrate by binding more strongly to amino acid groups at the active site denying it access to the bridging water molecule. The lower activity of compound **19** compared to compound **16** is due to the fact that it binds less strongly to the aspartate moiety hence its inhibition of the active site is lower. The predicted inhibition constant of 7.74 μM for compound **19** is lower than that of compound **16** (3.37 μM).

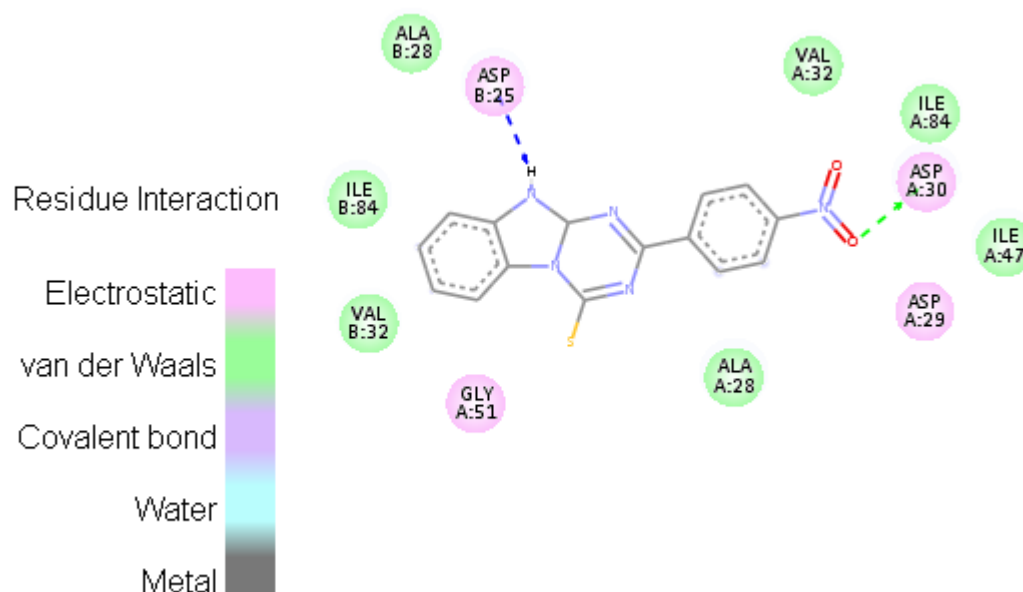


Figure 4.22 2D represent of 11-(4-nitrophenyl)-1,8,10,12-tetraazatricyclic[7.4.0.0^{2,7}]trideca-2(7),3,5,9,11-pentaene-13-thione (**19**) in protease active site.

Figure 4.23 give sthe 2D representation of compound **18** in the protease active site. The zero inhibition of 11-(3-bromophenyl)-1,8,10,12-tetraazatricyclo [7.4.0.0^{2,7}]trideca-2(7),3,5,9,11-pentaene-13-thione (**18**) in the bioassay is due to the fact the the bromide group is not able to effectively bind to groups in the active site. Even though the N-H group of compound **18** binds to the aspartate A25 unit, the orientation acquired upon binding to the aspartate A25 unit moves the bromide group away from the aspartate A29 and B29 greatly reducing it ability to effectively inhibit the natural substrate. In the docking studies due to the large size of bromide its presence in the active site ensures that most of the volume of the binding site is unavailable for occupancy by the natural substrate hence a fairly good inhibition constant of 3.47 μM is predicted for compound **18**.

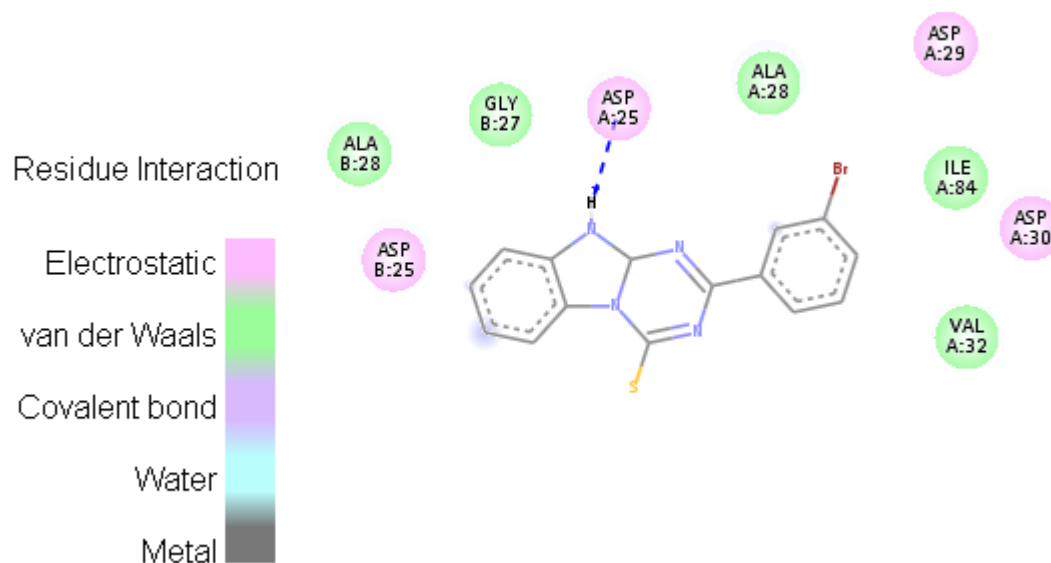


Figure 4.23 2D represent of compound 11-(3-bromophenyl)-1,8,10,12-tetraazatricyclo [7.4.0.0^{2,7}]trideca-2(7),3,5,9,11-pentaene-13-thione (**18**) in protease active site.

4.3 Conclusions

-The synthesis of novel tetraazatricyclic derivatives by the reaction of 2-aminobenzimidazole and benzoyl isothiocyanate derivatives has been carried out and the compounds have been characterized by IR, NMR, microanalysis and GC-MS. Tautomerism of the thione residue has been observed when a nitro group is substituted at position 3 in the aryl ring leading to the existence of two different species in solution.

-The transition state studies on the formation of tetraazatricyclic derivatives using the density functional theory in Gaussian is presented. The reaction pathway from reactants leading up to the products with the different intermediates and transition states have been computed and their feasibility discussed.

-The novel triethylamine catalyzed decomposition of tetraazatricyclics to give *N*-(1*H*-benzimidazol-2-yl)benzamide (**21**) have been carried out and characterized by IR, NMR, microanalysis and GC-MS.

-The transition state studies on the degradation of tetraazatricyclics to form *N*-(1*H*-benzimidazol-2-yl)benzamide (**21**) have been presented. The computation involved the density functional theory in Gaussian. The reaction pathway from reactants leading up to the products with the different intermediates and transition states have been carried out and their feasibility discussed.

-The novel synthesis of 3-benzoyl-1-(2-hydroxyphenyl) urea (**22**) from the reaction of benzoyl isothiocyanate and 2-aminobenzoxazole has been carried out and characterized by IR, NMR, microanalysis and GC-MS.

-Single crystal XRD molecular structure of 11-phenyl-1,8,10,12-tetraazatricyclo [7.4.0.0^{2,7}]trideca-2(7),3,5,9,11-pentaene-13-thione (**20**), *N*-(1*H*-benzimidazol-2-yl) benzamide (**21**) and 3-benzoyl-1-(2-hydroxyphenyl) urea (**22**) have been discussed.

-Cell viability tests of the tetraazatricyclics have been carried out. Compound **18** (unsubstituted), **12** (4-chloro) and **14** (4-methoxy) derivatives were found to be cytotoxic, with EC₅₀ values of 0.15 ± 0.051, 37.96 ± 21.87 and 5.28 ± 2.95 μM, respectively

-HIV-1 protease screen of the tetraazatricyclic derivatives have been presented. Compounds **19** (4-nitro derivative) and **16** (3-nitro derivative) showed good activity against HIV-1 protease with % inhibition of 59.57±13.59 and 79.97±11.97 μM respectively. The results were consistent with the docking studies, and the orientation adopted by compound **16** at the active site of protease ensures that it binds more strongly to amino acid residues than the other derivatives.

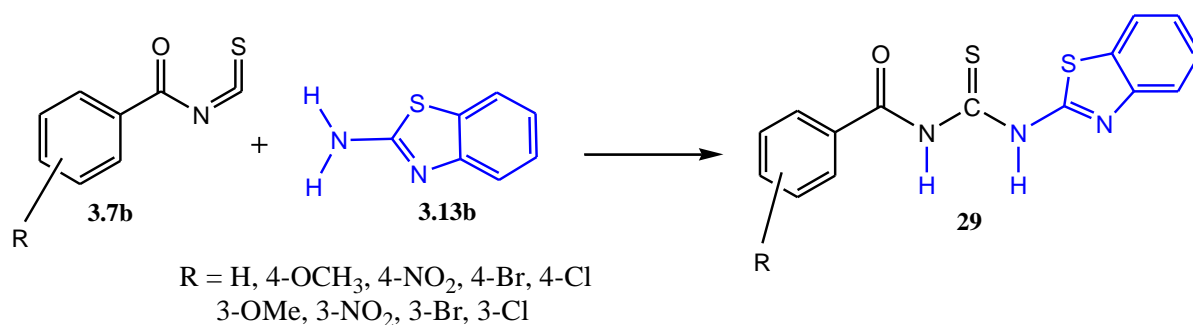
CHAPTER FIVE

3-(1,3-BENZOTHAZOL-2-YL)-1-(BENZOYL)THIOUREA DERIVATIVES

5.1 Synthesis of 3-(1,3-benzothiazol-2-yl)-1-(benzoyl)thiourea derivatives

A series of 1-(2/4-substituted-benzoyl)-3-benzothiazol-2-yl-thioureas has been synthesized from benzothiazol-2-ylamine and benzoyl isothiocyanates in satisfactory yields.³³⁵ The synthesized compounds were evaluated for analgesic activity by the hot plate method using aspirin (100 mg/kg). Some of the compounds showed analgesic activity.³³⁵

The benzothiazole derivatives were formed by the direct attack of the thione carbon by the 2-amino group of benzothiazole.



Scheme 5.1 Synthesis of 3-(1,3-benzothiazol-2-yl)-1-(benzoyl)thiourea derivatives.

5.2 3-(1,3-Benzothiazol-2-yl)-1-(benzoyl)thiourea (23)

The IR spectrum (**Figure A5.1**) showed bands at 3327 and 3055 cm⁻¹ for the N–H stretch, a band for the C=O stretch occurred at 1673 cm⁻¹ whilst a band for the C=N stretch was observed at 1595 cm⁻¹ and the aromatic C=C was observed at 1505 cm⁻¹. The ¹H NMR (**Figure A5.2**) and ¹H–¹H COSY (**Figure A5.3**) spectra gave signals at 12.22 and 11.23 ppm for a proton of an amide whilst the aromatic protons occurred between 8.14 and 7.34 ppm. The ¹³C NMR spectrum (**Figure A5.4**) gave a signal at 169.0 ppm, for the C=S while the C=O signal occurred at 166.0 ppm. Signals between 133.0 and 114.7 ppm were aromatic carbons.

5.3 3-(1,3-Benzothiazol-2-yl)-1-(4-chlorobenzoyl)thiourea (24)

The IR spectrum (**Figure A5.5**) showed an N–H stretch at 3302 and 3035 cm^{-1} , a band for the C=O stretch at 1668 cm^{-1} , a band for the C–N stretch at 1591 cm^{-1} and the aromatic C=C stretch was observed at 1549 cm^{-1} . The ^1H NMR (**Figure A5.6**) and ^1H – ^1H COSY (**Figure A5.7**) spectra gave signals at 14.16 and 12.29 ppm for a proton of an amide whilst the aromatic protons occurred between 8.03 and 7.39 ppm. The ^{13}C NMR spectrum (**Figure A5.8**) gave signals between 138.2 and 122.1 ppm for aromatic carbons.

5.4 3-(1,3-Benzothiazol-2-yl)-1-(4-bromobenzoyl)thiourea (25)

The IR spectrum (**Figure A5.9**) showed an N–H stretch at 3379 and 3229 cm^{-1} , a band for the C=N stretch at 1682 cm^{-1} and the aromatic C=C was observed at 1591 cm^{-1} . The ^1H NMR (**Figure A5.10**) and ^1H – ^1H COSY (**Figure A5.11**) spectra gave signals at 14.17 and 12.31 ppm for a proton of an amide whilst the aromatic protons occurred between 8.06 and 7.39 ppm. The ^{13}C NMR spectrum (**Figure A5.12**) gave signals between 131.7 and 122.0 ppm for aromatic carbons.

5.5 3-(1,3-Benzothiazol-2-yl)-1-(4-methoxybenzoyl)thiourea (26)

The IR spectrum (**Figure A5.13**) showed an N–H stretch at 3303 and 3054 cm^{-1} , bands for the aliphatic C–H stretch occurred at 2961 and 2928 cm^{-1} , a band for the C=O stretch at 1675 cm^{-1} , a band for the C=N stretch at 1594 cm^{-1} and the aromatic C=C was observed at 1533 cm^{-1} . The ^1H NMR (**Figure A5.14**) and ^1H – ^1H COSY (**Figure A5.15**) spectra gave signals at 12.08 ppm for a proton of an amide whilst the aromatic protons occurred between 8.06 and 7.40 ppm. The methoxy protons occurred as a singlet signal at 3.87 ppm. The ^{13}C NMR spectrum (**Figure A5.16**) gave a signal at 163.6 for the C=N whilst aromatic resonances were observed between 131.3 and 113.9 ppm for aromatic carbons. The methoxy carbon occurred at 55.4 ppm.

5.6 3-(1,3-Benzothiazol-2-yl)-1-(3-methoxybenzoyl)thiourea (27)

The IR spectrum (**Figure 5.1**) showed an N–H stretch at 3313 and 3070 cm^{-1} , a band for the C=O stretch at 1650 cm^{-1} , a band for the C=N stretch at 1596 cm^{-1} and the aromatic C=C was observed at 1582 cm^{-1} . Signals for protons of an amide resonates at 12.89 and 12.21 ppm in ^1H NMR (**Figure 5.2**) and ^1H – ^1H COSY (**Figure 5.3**) spectra whilst the aromatic protons occurred between 8.04 and 7.23 ppm. The methoxy protons occurred as a singlet signal at 3.86 ppm. The ^{13}C NMR spectrum (**Figure 5.4**) gave signals between 159.5 and 112.9 ppm for aromatic carbons. The methoxy carbon occurred at 55.4 ppm.

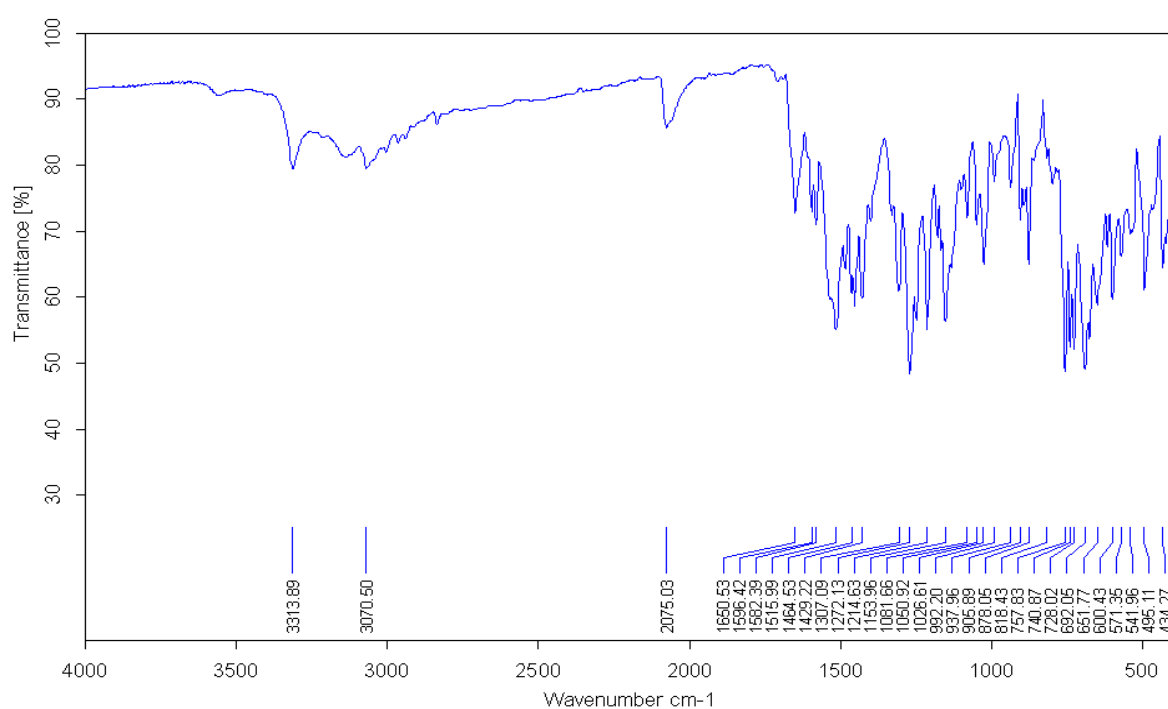


Figure 5.1 IR spectrum of 3-(1,3-benzothiazol-2-yl)-1-(3-methoxybenzoyl)thiourea (27).

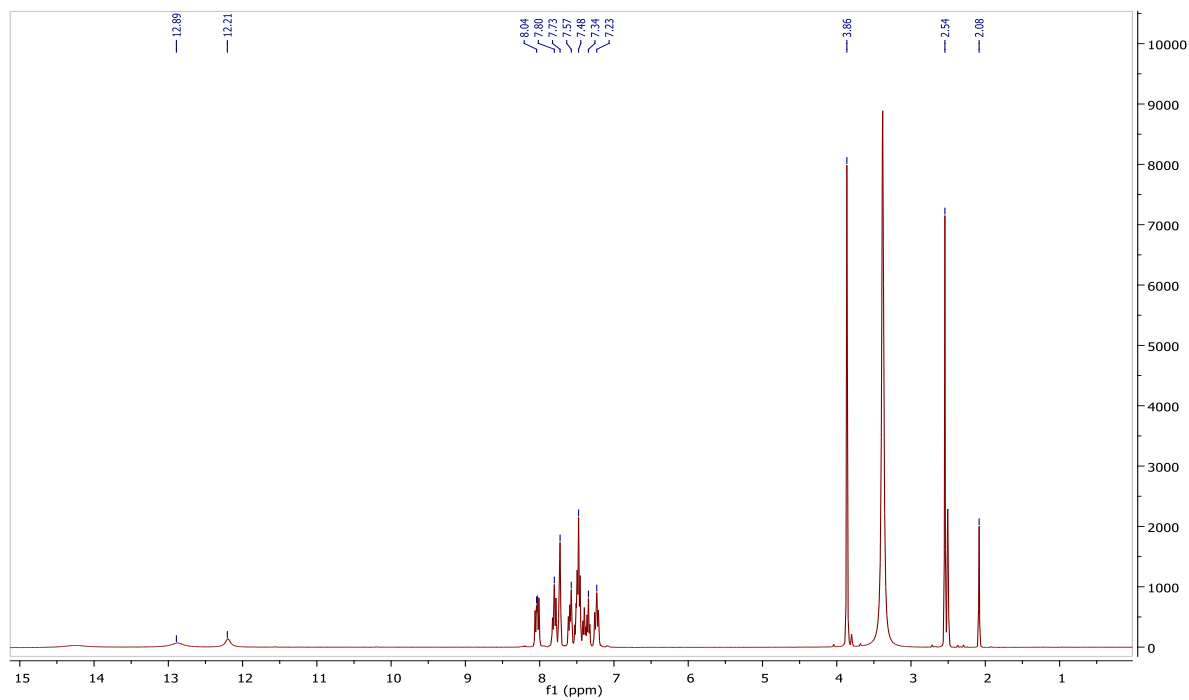


Figure 5.2 ^1H NMR spectrum of 3-(1,3-benzothiazol-2-yl)-1-(3-methoxybenzoyl)thiourea (**27**).

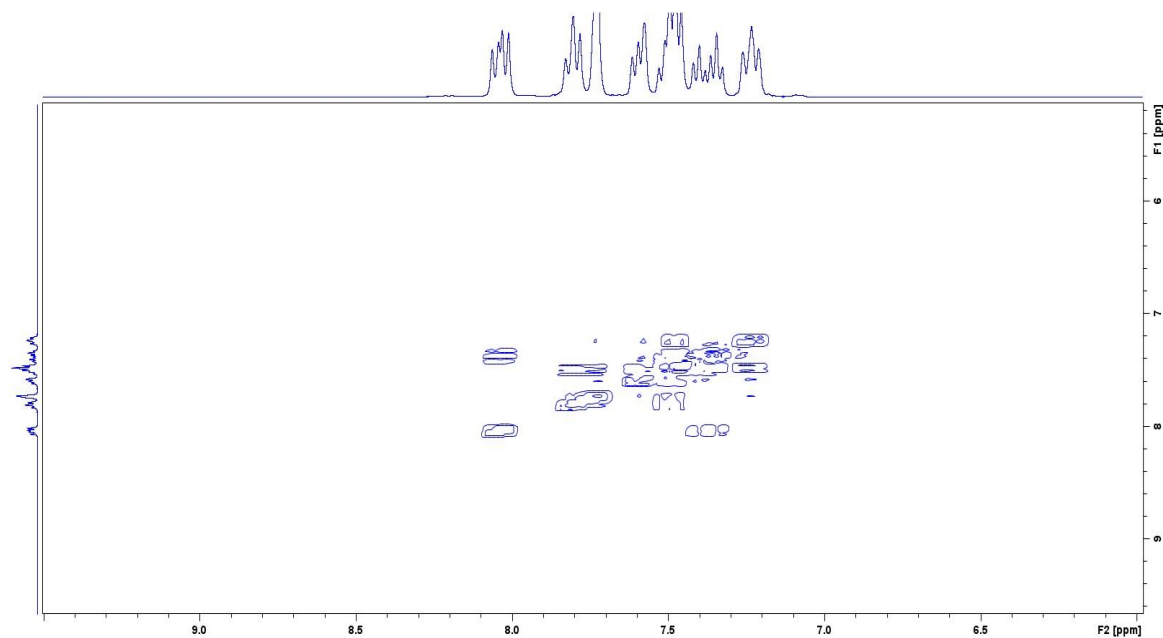


Figure 5.3 ^1H - ^1H COSY spectrum of 3-(1,3-benzothiazol-2-yl)-1-(3-methoxybenzoyl)thiourea (**27**).

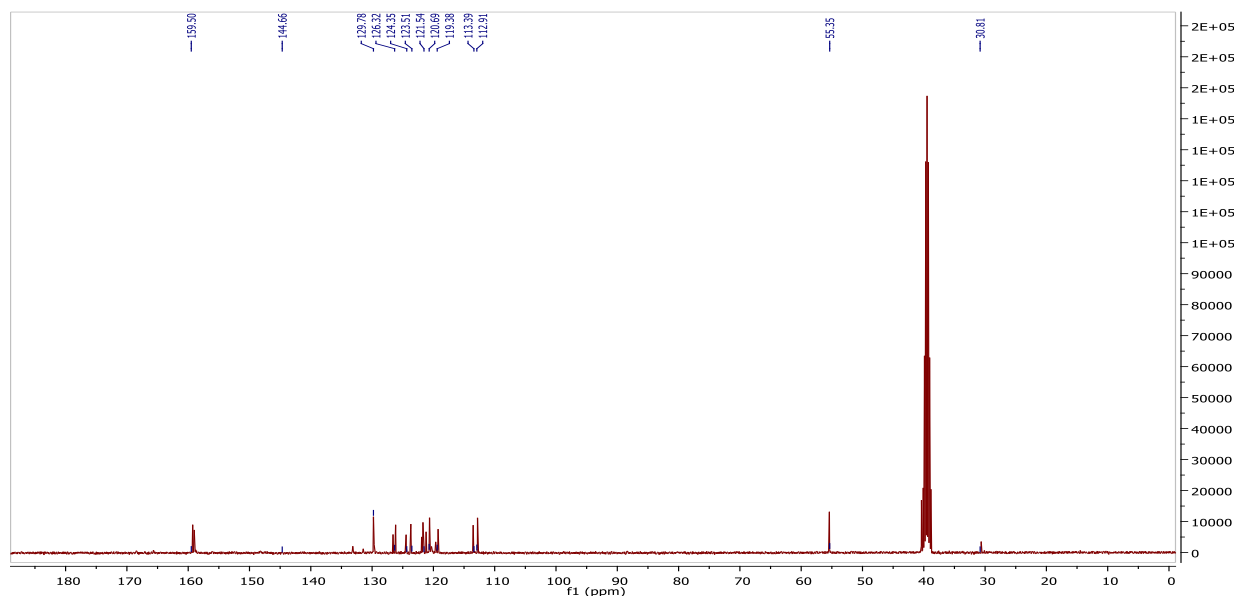


Figure 5.4 ^{13}C NMR spectrum of 3-(1,3-benzothiazol-2-yl)-1-(3-methoxybenzoyl)thiourea (**27**).

5.7 3-(1,3-Benzothiazol-2-yl)-1-(3-nitrobenzoyl)thiourea (**28**)

The IR spectrum (**Figure A5.17**) showed an N–H stretch bands at 3460 and 3088 cm^{-1} , a band for the C=O stretch at 1692 cm^{-1} , a band for the C=N stretch at 1670 cm^{-1} and the aromatic C=C was observed at 1615 cm^{-1} . The ^1H NMR (**Figure A5.18**) and ^1H - ^1H COSY (**Figure A5.19**) spectra gave signals at 14.03 and 12.60 ppm for a proton of an amide whilst the aromatic protons resonates between 8.81 and 7.41 ppm. The ^{13}C NMR spectrum (**Figure A3.20**) gave signals between 147.4 and 123.7 ppm for aromatic carbons.

5.8 3-(1,3-Benzothiazol-2-yl)-1-(3-chlorobenzoyl)thiourea (**29**)

The IR spectrum (**Figure A5.21**) showed an N–H stretch 3296 and 3058 $^{-1}$, a band for the C=C stretch at 1670 cm^{-1} , and a band for the C=N stretch at 1596 cm^{-1} . The aromatic C=C was observed at 1544 cm^{-1} . The ^1H NMR (**Figure A5.22**) and ^1H - ^1H COSY (**Figure A5.23**) spectra gave a broad signal at 12.29 ppm for a proton of an amide whilst the aromatic protons occurred between 8.20 and 7.38 ppm. The ^{13}C NMR spectrum (**Figure A5.24**) gave signals between 133.4 and 121.8 ppm for aromatic carbons.

5.9 3-(1,3-Benzothiazoyl-2-yl)-1-(4-nitrobenzoyl)thiourea (30)

The IR spectrum (**Figure A5.25**) showed an N–H stretch at 3351 and 3075 cm^{-1} , a band for the C=O stretch occurred at 1679 cm^{-1} whilst a band for the C=N stretch observed at 1595 cm^{-1} and the aromatic C=C was observed at 1510 cm^{-1} . The ^1H NMR (**Figure A5.26**) and ^1H – ^1H COSY (**Figure A5.27**) spectra gave a signal at 12.44 ppm for a proton of an amide whilst the aromatic protons occurred between 9.14 and 7.25 ppm. The ^{13}C NMR spectrum (**Figure A5.28**) gave signals between 165.6 and 112.5 ppm for aromatic carbons.

5.10 3-(1,3-Benzothiazol-2-yl)-1-(3-bromobenzoyl)thiourea (31)

The IR spectrum (**Figure 5.5**) showed an N–H stretch at 3232 and 3155 cm^{-1} , band for the C=O stretch at 1694 cm^{-1} , a band for the C=N stretch at 1682 cm^{-1} and the aromatic C=C was observed at 1599 cm^{-1} . The ^1H NMR (**Figure 5.6**) and ^1H – ^1H COSY (**Figure 5.7**) spectra gave signals at 8.34 ppm for a proton of an amide whilst the aromatic protons occurred between 8.12 and 7.37 ppm. In the ^{13}C NMR spectrum, (**Figure 5.8**) the signal at 206.6 ppm was due to the C=O of acetone. Signals between 135.6 and 121.8 ppm were observed for aromatic carbons. Whilst the signal at 30.0ppm was due to the methyl groups of acetone.

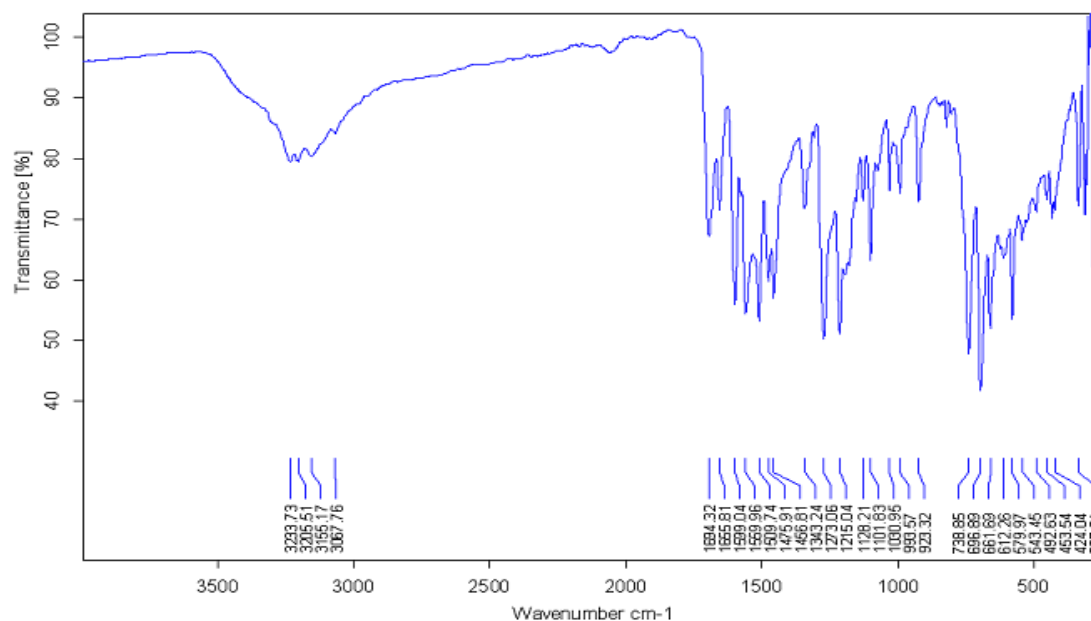


Figure 5.5 IR spectrum of 3-(1,3-benzothiazol-2-yl)-1-(3-bromobenzoyl)thiourea (31).

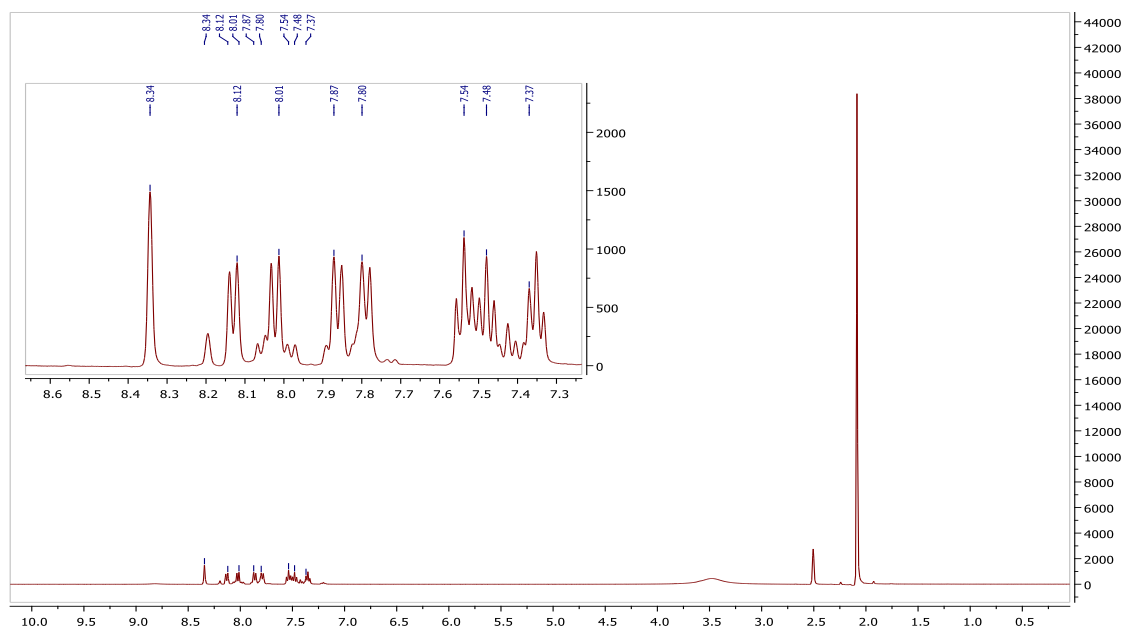


Figure 5.6 ^1H NMR spectrum of 3-(1,3-benzothiazol-2-yl)-1-(3-bromobenzoyl)thiourea (**31**).

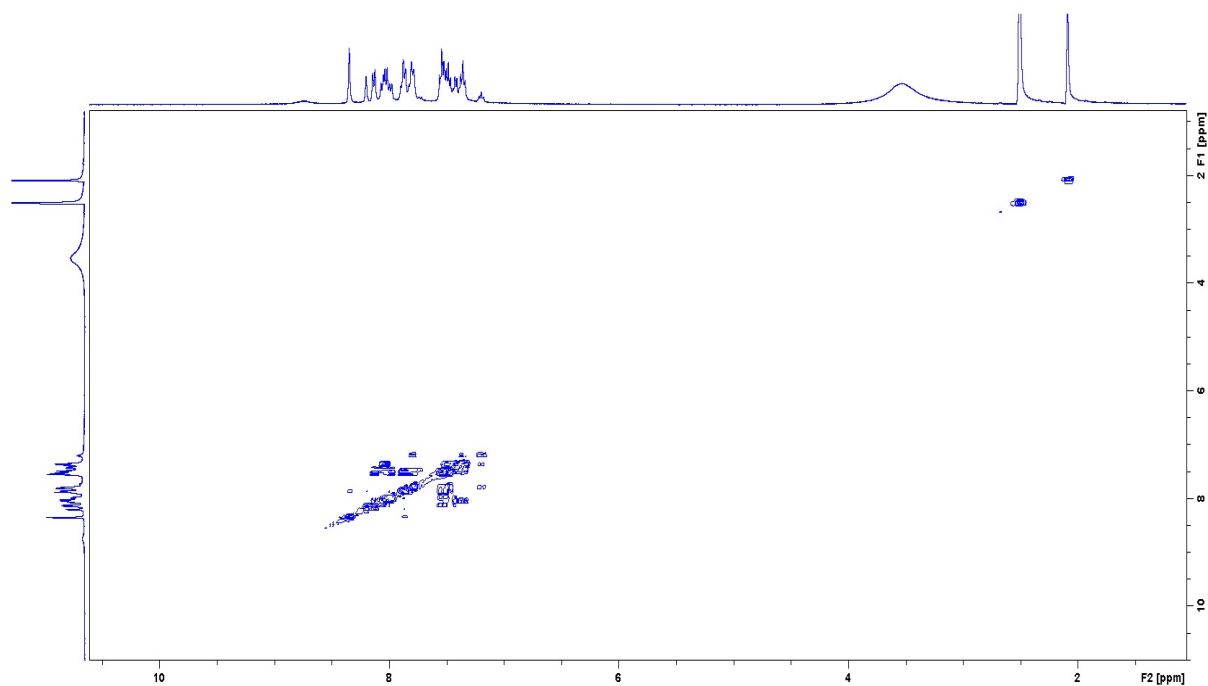


Figure 5.7 ^1H - ^1H COSY spectrum of 3-(1,3-benzothiazol-2-yl)-1-(3-bromobenzoyl)thiourea (**31**).

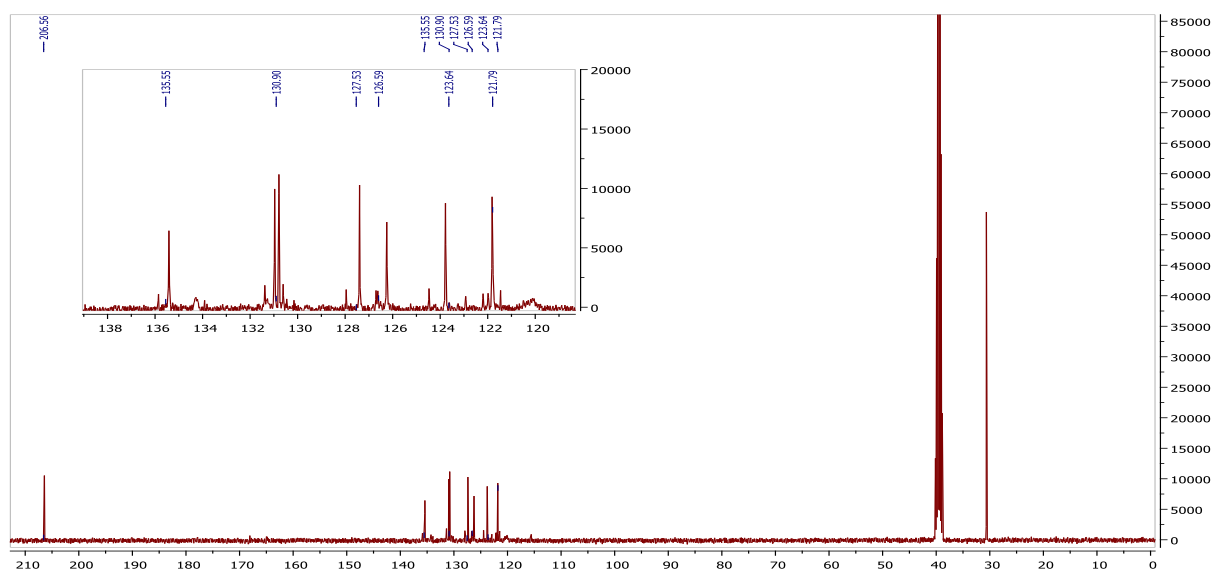


Figure 5.8 ^{13}C NMR spectrum of 3-(1,3-benzothiazol-2-yl)-1-(3-bromobenzoyl)thiourea (**31**).

5.11 Crystal structure of some 3-(1,3-benzothiazol-2-yl)-1-(benzoyl)thiourea derivatives

Compounds **23**, **27** and **31** were recrystallized from DMSO:Toluene (1:1) and obtained as yellow crystals. The crystallographic data, selected bond lengths and bond angles for the crystal structures of compounds **23**, **27** and **31** are provided in **Tables 5.1** and **5.2**. The ORTEP diagrams for compounds **23**, **27** and **31** are presented in **Figures 5.9**, **5.10** and **5.11**. Compound **23** crystallized in the monoclinic space group $P2_1/c$, while compound **27** crystallized in the triclinic space group $P\bar{1}$. Compound **31** crystallized in the orthorhombic space group $Pbca$. The bond distance of O1–C1 in compound **23** is 1.219(2) Å, which is consistent with a carbonyl whilst the O1–C1 bond distances in compound **27** and **31** are 1.418 (9) and 1.220 (2) respectively. The S2–C22 bond distances for compounds **23**, **27** and **31** are 1.744(1), 1.751(1) and 1.745(2) respectively confirms the the C=S bond of a thione whilst the N1–C2 bond distances in compounds **23**, **27** and **31** are 1.386(2), 1.389(8) and 1.391(2) respectively which are consistent with C–N single bond.

The bond angles of O1–C1–N1 in compounds **23** and **31** are 121.6(1) and 122.6(2) whilst the bond angle of O2–C2–O1 in compound **27** is 120.6(2), confirming that the carbon atom

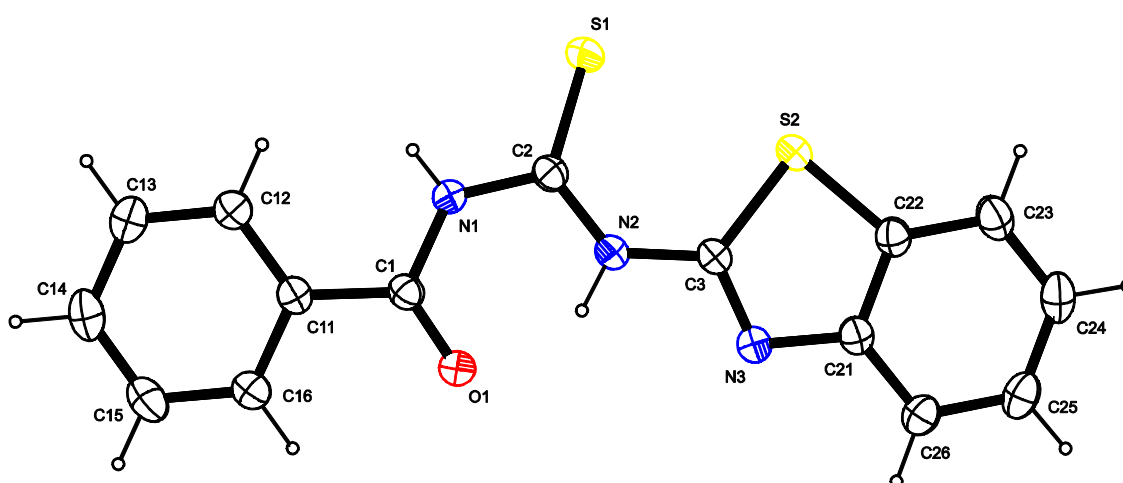
involved is sp^2 hybridized. The bond angles in C1-N1-C2 in compound **23** is 127.7(1) whilst the bond angle in C2-N1-C3 in compound **27** is 128.6(5). The bond angle of C1-N1-C2 is 127.8(2) in compound **31** confirming the sp^2 hybridization of the nitrogen atom.

Table 5.1 Crystallographic data and structure refinement summary for compounds **23**, **27** and **31**.

Property	24	27	31
Formula	C ₁₅ H ₁₁ N ₃ OS ₂	C ₁₆ H ₁₄ N ₃ O ₂ S ₂	C ₁₅ H ₁₀ BrN ₃ OS ₂
Formula Weight	313.41	344.42	392.28
Crystal System	Monoclinic	Triclinic	Orthorhombic
Space group	<i>P2/c</i>	<i>P-1</i>	<i>Pbca</i>
a [Å]	12.3658(3)	5.8481(5)	13.4779(7)
b [Å]	5.8347(1)	11.6099(11)	11.7371(5)
c [Å]	19.5189(4)	11.7178(10)	19.2452(10)
α [°]	90	90.784(4)	90
β [°]	90.154(1)	90.059(3)	90
γ [°]	90	101.936(3)	90
V [Å ³]	1408.30(5)	778.31(12)	3044.4(3)
Z	4	2	8
D(calc) [g/cm ³]	1.478	1.470	1.712
Mu(MoKa) [/mm]	0.379	0.355	2.978
F(000)	648	358	1568
Crystal Size [mm]	0.00 x 0.00 x 0.00	0.10 x 0.17 x 0.64	0.36 x 0.40 x 0.43
Temperature (K)	200	200	200
Radiation [Å]	MoKa 0.71073	MoKa 0.71073	MoKa 0.71073
θ Min-Max [°]	2.1, 28.4	1.7, 28.4	2.5, 28.4
Dataset	-16: 16 ; -6: 7 ; -26: 26	-7: 4 ; -15: 15 ; -15: 15	-17: 16 ; -15: 15 ; -25: 20
Tot., Uniq. Data, R(int)	12549, 3499, 0.017	12421, 3776, 0.024	22448, 3759, 0.024
Observed data [I > 2.0 sigma(I)]	3041	3526	3052
Nref, Npar	3499, 198	3776, 210	3759, 207
R, wR ₂ , S	0.0285, 0.0791, 1.08	0.1036, 0.2738, 1.12	0.0235, 0.0610, 1.04
Max. and Av. Shift/Error	0.00, 0.00	0.00, 0.00	0.00, 0.00
Min. and Max. Resd. Dens. [e/Å ³]	-0.20, 0.34	-0.60, 1.27	-0.40, 0.35

Table 5.2 Selected bond lengths (Å) and bond angles (°) for compounds **23**, **27** and **31**.

Bond lengths					
23		27		31	
O1-C1	1.219(2)	O1-C1	1.418(1)	O1-C1	1.220(2)
S2-C22	1.744(1)	S2-C22	1.751(1)	S2-C22	1.745(2)
N1-C2	1.386(2)	N1-C2	1.389(1)	N1-C2	1.391(2)
N2-C3	1.383(2)	N2-C3	1.331(1)	N2-C3	1.384(2)
N3-C21	1.385(2)	N3-C21	1.385(1)	N3-C21	1.382(2)
S1-C2	1.662(1)	S1-C3	1.671(1)	S1-C2	1.650(2)
S2-C3	1.748(1)	S2-C4	1.762(1)	S2-C3	1.746(2)
N1-C1	1.393(2)	O2-C2	1.231(1)	N1-C1	1.379(2)
N2-C2	1.337(2)	N1-C3	1.377(1)	N2-C2	1.340(2)
N3-C3	1.293(2)	O1-C14	1.346(1)	Br1-C13	1.896(2)
Bond angles					
23		27		31	
O1-C1-N1	121.6(1)	O2-C2-N1	120.6(6)	O1-C1-N1	122.6(2)
C1-N1-C2	127.7(1)	C2-N1-C3	128.6(5)	C1-N1-C2	127.8(2)
S1-C2-N1	119.8(1)	S1-C3-N1	119.5(1)	S1-C2-N1	120.0(1)
S1-C2-N2	125.5(1)	S1-C3-N2	125.0(1)	S1-C2-N2	125.2(1)
S2-C3-N2	125.12(9)	S2-C4-N2	124.5(1)	S2-C3-N2	125.4(1)
S2-C3-N3	117.54(9)	S2-C4-N3	117.1(1)	S2-C3-N3	117.4(1)
O1-C1-C11	122.2(1)	N2-C4-N3	118.4(1)	N2-C3-N3	117.3(2)
N3-C21-C22	115.0(1)	C1-O1-C14	118.8(1)	C3-N3-C21	109.9(1)
C3-S2-C22	87.7(1)	C4-S2-C22	87.5(1)	O1-C1-C11	121.3(2)

**Figure 5.9** An ORTEP view of compound 3-(1,3-benzothiazol-2-yl)-1-(benzoyl)thiourea (**23**) showing 50% probability displacement ellipsoids and the atom labelling.

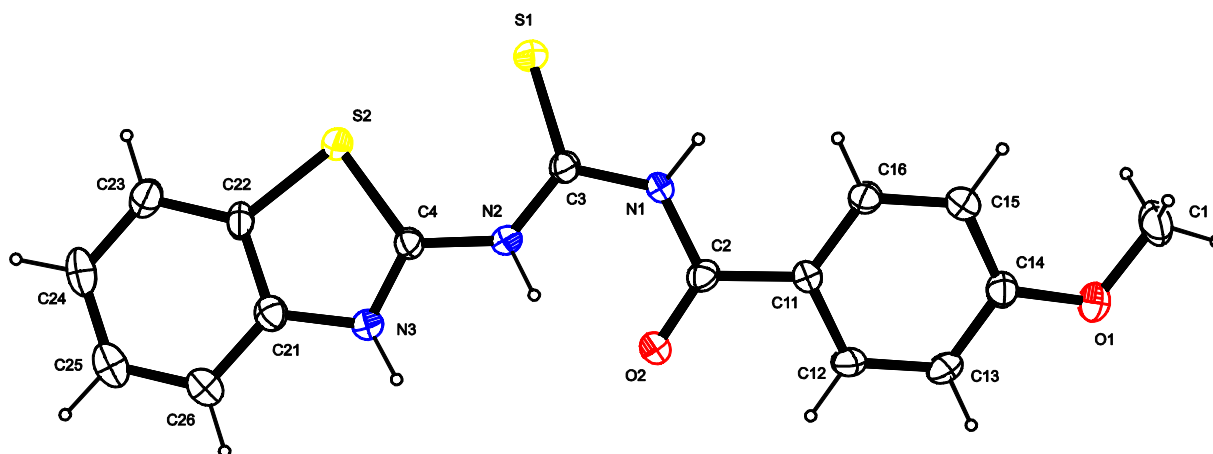


Figure 5.10 An ORTEP view of compound 3-(1,3-benzothiazol-2-yl)-1-(3-methoxybenzoyl)thiourea (**27**) showing 50% probability displacement ellipsoids and the atom labelling.

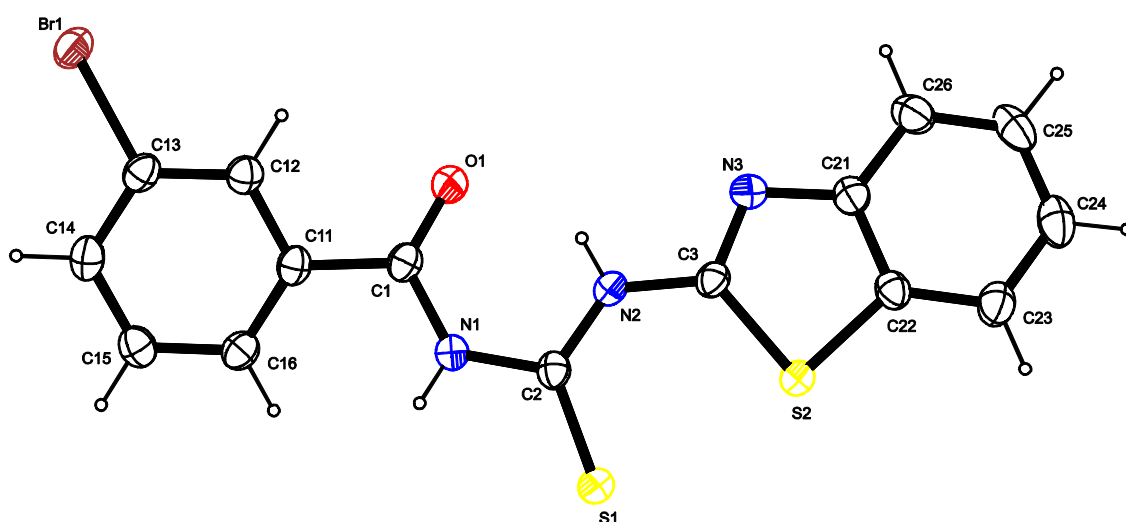
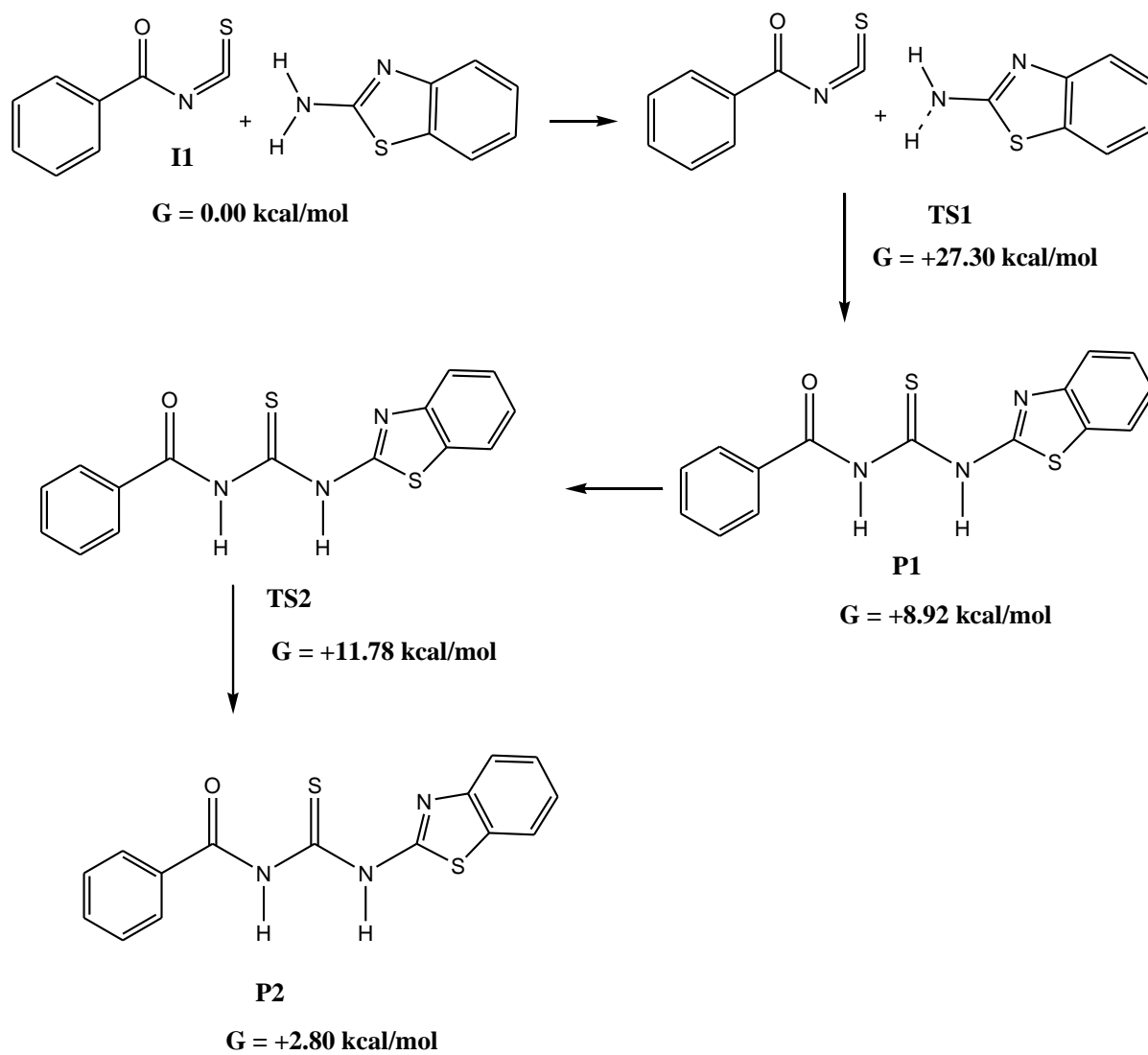


Figure 5.11 An ORTEP view of compound 3-(1,3-benzothiazol-2-yl)-1-(3-bromobenzoyl)thiourea (**31**) showing 50% probability displacement ellipsoids and the atom labelling.

5.12 Transition state studies on the formation of 3-(1,3-Benzothiazol-2-yl)-1-(3-nitrobenzoyl)thiourea derivatives

The predicted reaction pathway proceeds by the coming together of 2-aminobenzothiazole and benzoyl isothiocyanate (**I1**) (**Scheme 5.1**). The computation of all the transition states and intermediates was carried out using the B3LYP function and the basis set was 6-31g(d). **I1** is used as reference in the computation of the relative free energies, it is a singlet with no charge of zero and a dipole moment of 2.15 Debye and an imaginary frequency of zero. The distance between the carbon of the thione and the nitrogen of the 2-aminobenzothiazole for **I1** is 3.66 Å. **I1** is obtained from the backward displacement of **TS1** through the IRC pathway. **TS1** is singlet species of no charge and a single imaginary frequency. It has a dipole moment of 4.38 Debye.

The distance between the carbon of the thione and the nitrogen of the 2-aminobenzothiazole to 1.60 Å and a relative free energy of +27.30 kcal/mol. The C-N bond then forms in **P1** which is a singlet species of no charge with a frequency of zero. **P1** has a dipole moment of 6.47 Debye and a relative free energy of +8.92 kcal/mol. **TS2** is a singlet species of no charge with a single imaginary frequency and a dipole moment of 6.85 Debye as well as a relative free energy of +11.78 kcal/mol. **P2** is obtained from the forward displacement of **TS1**. It is a singlet species of no charge with an imaginary frequency of zero. **P2** has a dipole moment of 5.57 Debye and a relative free energy of +2.80 kcal/mol. A detailed reaction mechanism has been successfully carried out. The computation of two transition states has been carried out based on an intermediate **P1** and a product **P2** has been obtained.



Scheme 5.2 DFT reaction mechanism of 3-(1,3-benzothiazol-2-yl)-1-(benzoyl)thiourea.

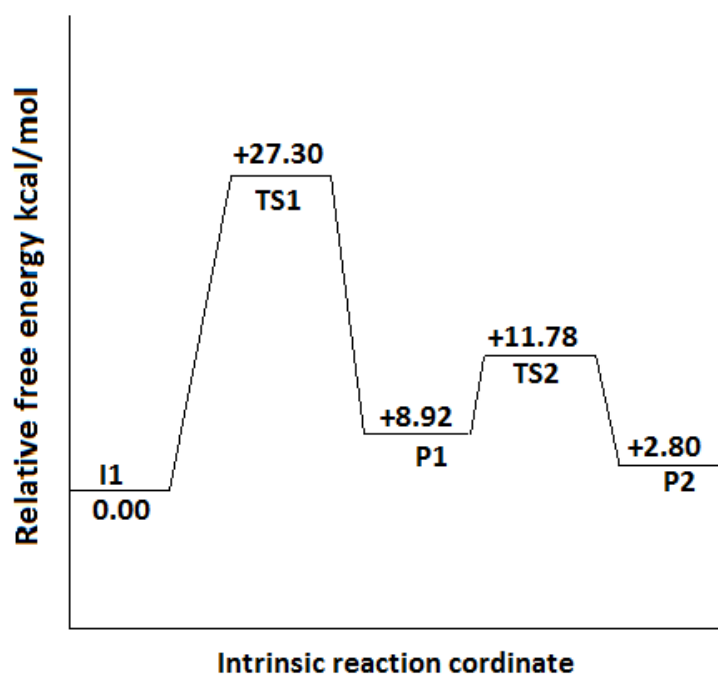


Figure 5.12 Potential energy surface for 3-(1,3-benzothiazol-2-yl)-1-(benzoyl)thiourea derivatives.

5.2 Biochemical studies

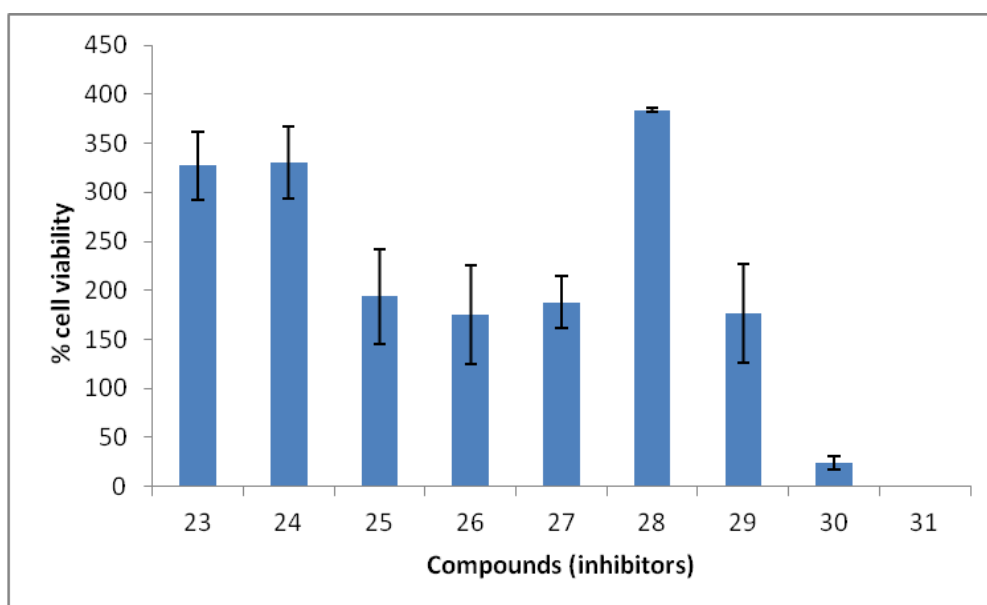
5.2.1 Cell viability and cytotoxicity tests

The acute cytotoxic effects of benzoyl isothiocyanate derivatives of 3-(1,3-benzothiazol-2-yl)-1-(benzoyl)thiourea derivatives were determined by exposing them to isolated human white blood cells, for a 24-hour period. The results of cytotoxicity test are presented in **Table 5.3** which indicates the compound numbers (in bold) as well as the EC_{50} values calculated for each compound tested.

Table 5.3 Cell viability results for benzoyl isothiocyanate derivatives.

Benzothiazoles	EC ₅₀ μM
23	327.3
24	330.2
25	193.6
26	175.2
27	188.0
28	383.9
29	176.3
30	24.1
31	1.2

The EC₅₀ values for the benzothiazole derivatives (**Figure 5.13**) gave varying effects on the cell viability of human white blood cells. Compounds **31** (3-bromo) and **30** (4-nitro) derivatives were found to be cytotoxic with EC₅₀ values of 1.207 ± 0.58 and 24.08 ± 13.14 μM , respectively. This suggest that substitution at position three with a bromo group and substitution at position four with a nitro group leads to an increase in cytotoxic effects among the benzothiazole derivatives.

**Figure 5.13** EC₅₀ values for the benzothiazole derivatives (μM). Error bars represent the SEM for $n = 3$.

The cytotoxicity of compounds **31** and **28**, which are the most and least cytotoxic compounds, respectively, among the benzothiazole derivatives are shown in **Figure 5.14**. The presence of the bromo group (**31**) at position 3 among the benzothiazole derivatives leads to an increase in cytotoxicity whilst the presence of the nitro group (**28**) leads to a decrease in cytotoxicity.

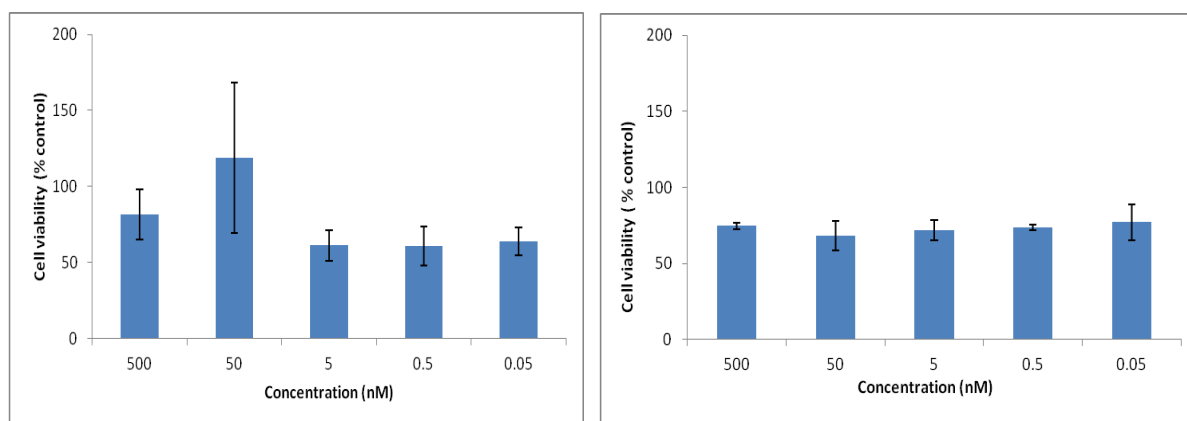


Figure 5.14 EC_{50} values for compounds **28** and **31** (μM). Error bars represent the SEM for $n = 3$.

5.2.2 The HIV-1 protease screening of 3-(1,3-benzothiazol-2-yl)-1-(benzoyl)thiourea derivatives

The HIV-1 screening of the 3-(1,3-benzothiazol-2-yl)-1-(benzoyl)thiourea derivatives was done at $100 \mu\text{M}$ of inhibitor and that for ritonavir was done at $10 \mu\text{M}$. All the compounds gave a percentage inhibition of less than 40%. Their lack of activity might be due to their the presence of polar groups making them more reactive to the constituents of the matrix used for their introduction to protease. In the modeling of these scaffolds of the 3-(1,3-benzothiazol-2-yl)-1-(benzoyl)thiourea derivatives, there was some interaction between the atoms in the protease active site and the substituents *via* hydrogen bonding or dipole dipole interaction but does not seem to occur in the HIV-1 screens, hence the lack of activity among these compounds.

Table 5.4 HIV-1 protease screening results for 3-(1,3-benzothiazol-2-yl)-1-(benzoyl)thiourea derivatives.

Compound	Fluorescence	Standard deviation	% Activity relative to untreated control	% Inhibition relative to untreated control
Ritonavir	36.24	1.88	9.34	90.66
23	304.19	3.42	78.42	21.58
24	296.57	11.7	76.46	23.54
25	350.75	25.84	90.42	9.58
26	335.22	6.93	86.42	13.58
27	438.39	6.12	113.02	0
28	403.1	10.75	103.92	0
29	418.44	16.41	107.87	0
30	222.43	0.65	98.43	1.57
31	151.6	6.27	67.09	32.91

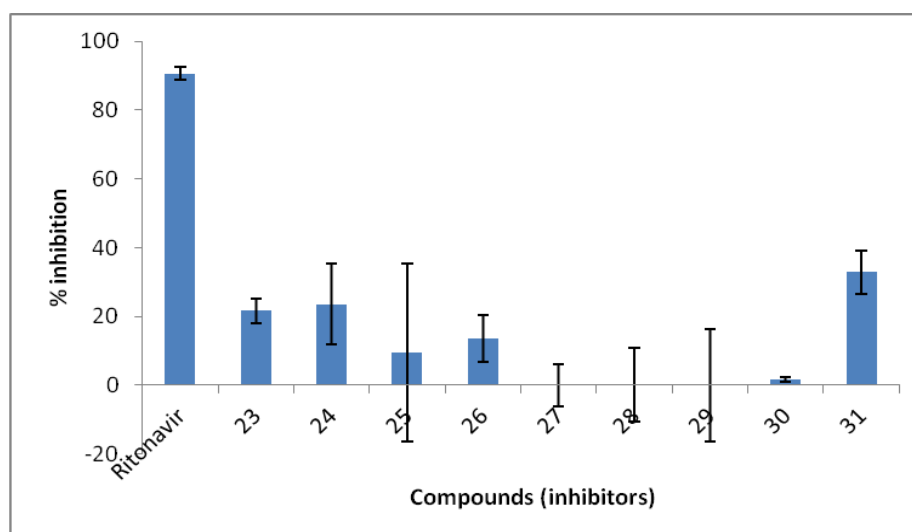


Figure 5.15 HIV-1 protease screening results illustrating % inhibition of benzothiazole (100 μ M) and ritonavir (10 μ M) derivatives compared to untreated control. Error bars represent SEM for $n = 3$.

The presence of polar groups on 3-(1,3-benzothiazol-2-yl)-1-(benzoyl)thiourea derivatives makes these compounds more reactive in the complex matrix of the acetate buffer used. The

5.3 Conclusions

-2-Aminobenzothiazole derivatives of benzoyl isothiocyanates have been synthesized and characterized by IR, NMR, GC-MS, and microanalysis.

-The single crystal XRD molecular structures of compounds 3-(1,3-benzothiazol-2-yl)-1-(benzoyl)thiourea (**23**), 3-(1,3-benzothiazol-2-yl)-1-(3-methoxybenzoyl)thiourea (**27**) and 3-(1,3-benzothiazol-2-yl)-1-(3-bromobenzoyl)thiourea (**31**) have been discussed.

-DFT transition state studies of the formation of 3-(1,3-benzothiazol-2-yl)-1-(benzoyl)thiourea (**23**) have been carried out and the factors that drive the reaction discussed.

-Cell viability test on the benzothiazole derivatives have been computed and EC₅₀ values obtain. Compounds **31** (3-bromo) and **30** (4-nitro) derivatives were found to be cytotoxic with EC₅₀ values of 1.207 ± 0.58 and 24.08 ± 13.14 μM , respectively.

-HIV-1 protease screen for the benzothiazole derivatives have been carried out. All the compounds in this set gave percentage inhibition lower than 40% at a concentration of 100 μM of inhibitor and 20 μM of protease.

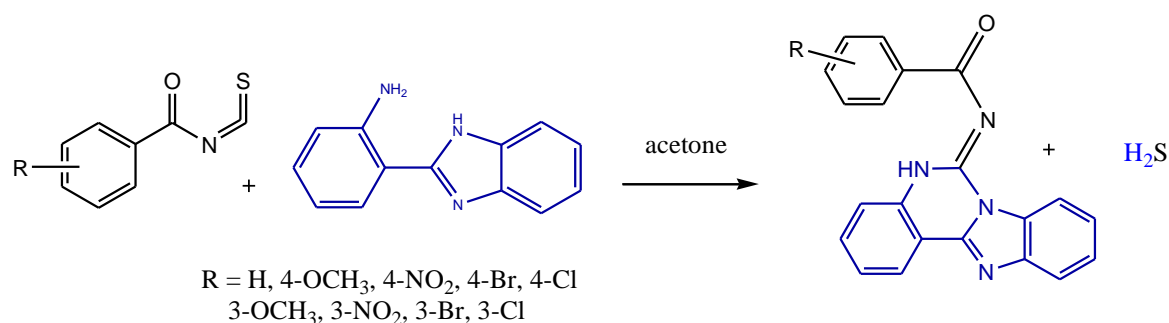
CHAPTER SIX

TRIAZATETRACYCLIC DERIVATIVES

6.1 Synthesis of triazatetracyclics

Triazatetracyclics have been made by other methods.³³⁶⁻³⁴⁰ Twelve *N*-glycosyl amines have been synthesised using 4,6-*O*-benzylidene-*D*-glucopyranose and different substituted aromatic amines, including some diamines that resulted in *bis*-glycosyl amines. Another set of six *N*-glycosyl amines were synthesised using different hexoses and pentoses with 2-(*o*-aminophenyl)benzimidazole. In these reactions only the 2-amino group reacted with the hydroxyl groups of 2-(*o*-aminophenyl)benzimidazole.³³⁶ Reactions of substituted aldehydes with 2-(*o*-aminophenyl)benzimidazole have been reported to yield Schiff bases.³³⁷ The syntheses of 2-(2-nitrophenyl)-1-benzoyl-1*H*-benzimidazole derivatives and their reduction to the corresponding 2-benzimidazolylbenzamides have been reported. The compounds were cleanly and efficiently converted to the corresponding 6-arylbenzimidazo[1,2-*c*]quinazolines by microwave activation using SiO₂-MnO₂ as solid inorganic support.³³⁸ Triazatetracyclics have also been synthesized by heating 2-(2-aminophenyl) benzimidazole and aryl aldehyde under reflux in ethanol for 5 h.³³⁹ Also some triazatetracyclic compounds with substitution on the aryl ring have been synthesized from aminophenylbenzimidazole and substituted aryl aldehydes at room temperature in ethanol- acetic acid mixtures.³⁴⁰

Triazatetracyclics have been accessed by the reaction of benzoyl isothiocyanate derivatives with 2-(2-aminophenyl)-1*H*-benzimidazole in this work. The reaction is thought to proceed by the attack of the thione carbon by the lone pair on the nitrogen of the 2-aminophenyl group without the presence of a base leading to the formation of thiol. Protonation of the thiol leads to the evolution of hydrogen sulfide, during which the nitrogen of the benzimidazole also attacks the carbon. The loss of the hydrogen sulfide is what drives the reaction. A reaction scheme is presented in **Scheme 6.1**.



Scheme 6.1 Synthesis of triazatetracyclics derivatives.

6.2 Problems with solubility

Most of the triazatetracyclics are partially soluble in DMSO and insoluble in D₂O and deuterated chloroform. It was impossible to conclusively assign signals in the ¹H NMR and ¹³C NMR spectra in DMSO because signal suppression. Hence conclusive characterization of these compounds were achieved using GC-MS, microanalysis, IR and single crystal XRD.

6.3 4-Bromo-*N*-[(9*E*)-8,10,17-triazatetracyclo[8.7.0.0^{2,7}.0^{11,16}]heptadeca-1(17),2,4,6,11(16),12,14-heptaen-9-ylidene]benzamide (32)

The IR spectrum (**Figure A6.1**) showed a band at 3026 cm⁻¹ for and N–H stretch. A band at 1637 cm⁻¹ was observed for the C=O stretch. The C–N stretch was observed at 1574cm⁻¹, whilst the C=C band was observed at 1548 cm⁻¹. The ¹H NMR (**Figure A6.2**) and ¹H–¹H COSY (**Figure A6.3**) spectra of compound **32** showed a signal at 13.27 ppm for the NH proton. Aromatic protons resonating between 8.36 and 7.37 ppm were observed. The ¹³C NMR spectrum (**Figure A6.4**) showed signals between 149.7 and 121.9 ppm for aromatic protons.

6.4 4-Methoxy-*N*-[(9*E*)-8,10,17-triazatetracyclo[8.7.0.0^{2,7}.0^{11,16}]heptadeca-1(17),2,4,6,11(16),12,14-heptaen-9-ylidene]benzamide (33)

The IR spectrum (**Figure A6.5**) showed a band at 3043 cm⁻¹ for and N–H stretch. Bands for the aliphatic C–H stretch were observed at 2950 and 2913 cm⁻¹. A band at 1635 cm⁻¹ was observed for the C=O stretch. The C–N stretch was observed at 1567, whilst the C=C band were observed 1478 cm⁻¹. In the ¹H NMR (**Figure A6.6**) and ¹H–¹H COSY (**Figure A6.7**) spectra a singlet signal for the proton of the NH resonated at 13.74 ppm. Aromatic protons were observed between 8.84 and 7.08 ppm. A singlet signal for three protons occurred at 3.86 ppm for the methoxy protons. The ¹³C NMR spectrum (**Figure A6.8**) showed signals between 170.2 and 113.8 ppm for aromatic carbons. The methoxy group was observed at 55.41 ppm.

6.5 3-Methoxy-*N*-[(9*E*)-8,10,17-triazatetracyclo[8.7.0.0^{2,7}.0^{11,16}]heptadeca-1(17),2,4,6,11(16),12,14-heptaen-9-ylidene]benzamide (34)

The IR spectrum (**Figure 6.1**) showed a band at 3110 cm⁻¹ for and N–H stretch. Bands for the aliphatic C–H stretch were observed at 2991 and 2836 cm⁻¹. A band at 1634 cm⁻¹ was observed for the C=O stretch. The C–N stretch was observed at 15680 cm⁻¹. The ¹H NMR (**Figure 6.2**) and ¹H–¹H COSY (**Figure 6.3**) spectra of compound **33** gave a singlet resonance at 13.56 ppm for the NH proton. Aromatic protons resonating 8.66 and 7.11 ppm were observed. A singlet signal for three protons was observed at 3.79 ppm for the methoxy protons. The ¹³C NMR spectrum (**Figure 6.4**) showed signals between 177.20 and 113.4 ppm for aromatic protons. The methoxy group was observed at 54.94 ppm.

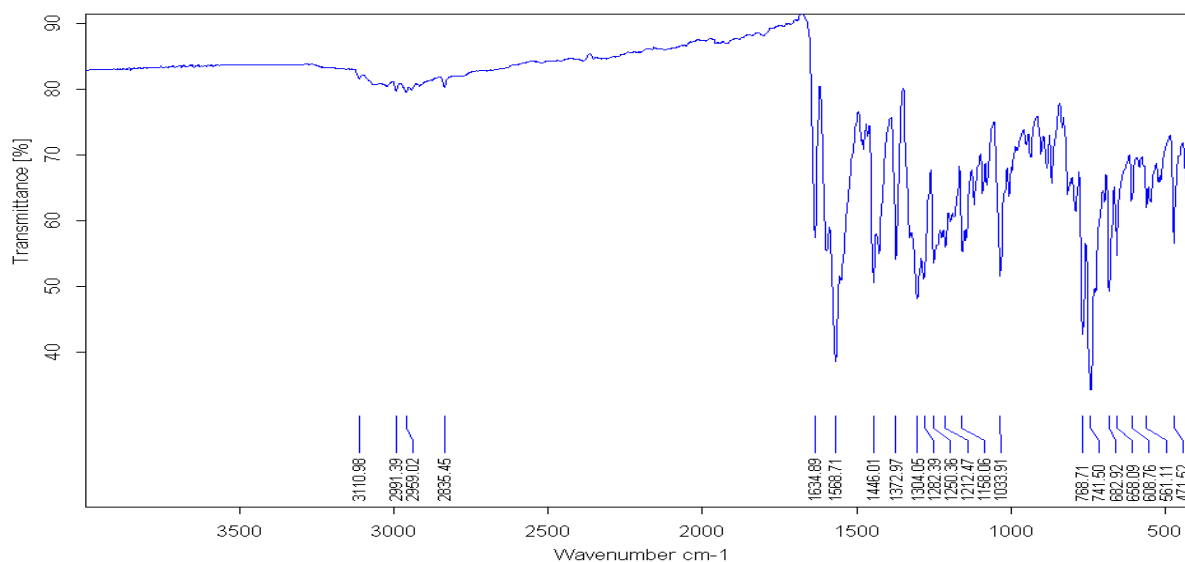


Figure 6.1 IR spectrum of 3-methoxy-*N*-[(*E*)-8,10,17-triazatetracyclo [8.7.0.0^{2,7}.0^{11,16}]heptadeca-1(17),2,4,6,11(16),12,14-heptaen-9-ylidene] benzamide (**34**).

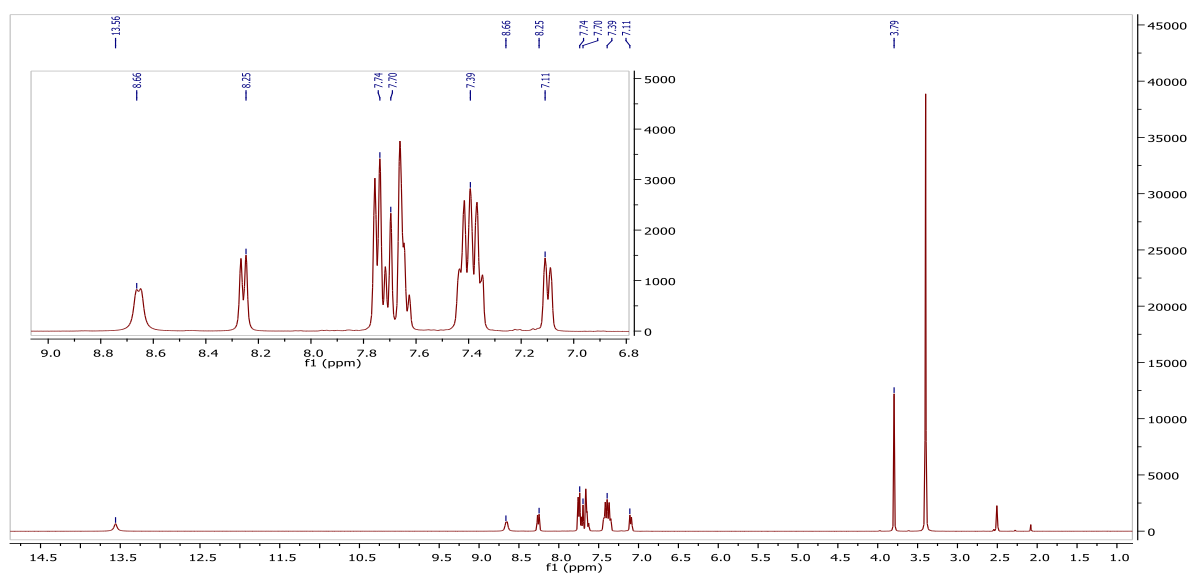


Figure 6.2 ¹H NMR spectrum of 3-methoxy-*N*-[(*E*)-8,10,17-triazatetracyclo [8.7.0.0^{2,7}.0^{11,16}]heptadeca-1(17),2,4,6,11(16),12,14-heptaen-9-ylidene] benzamide (**34**).

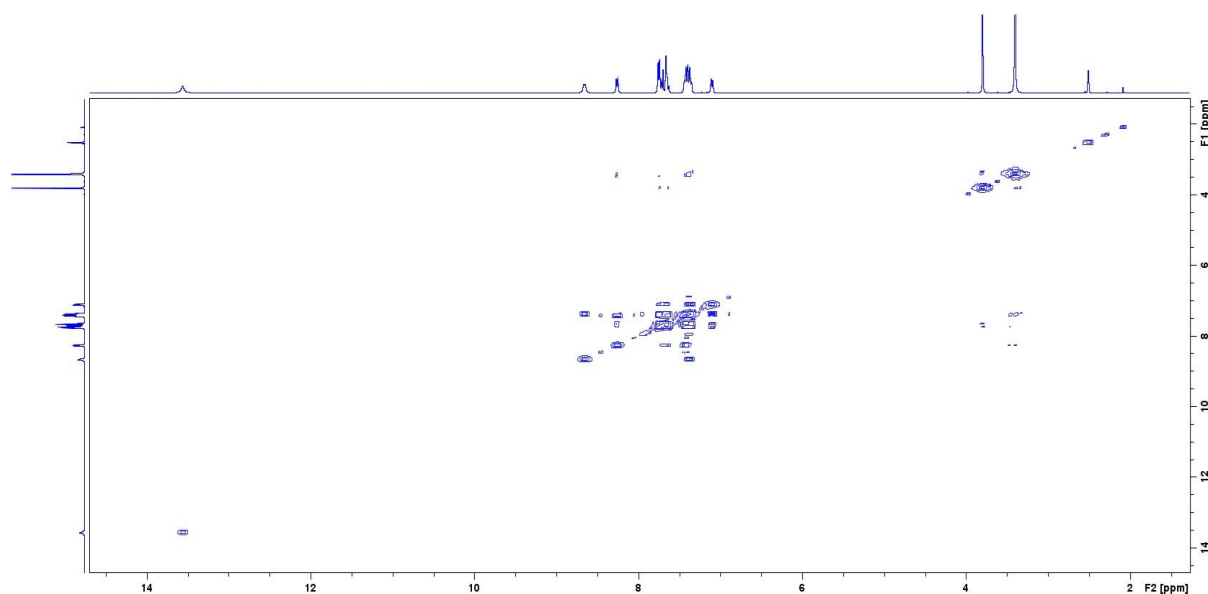


Figure 6.3 ^1H ^1H COSY spectrum of 3-methoxy-*N*-[(9*E*)-8,10,17-triazatetracyclo [8.7.0.0^{2,7}.0^{11,16}]heptadeca-1(17),2,4,6,11(16),12,14-heptaen-9-ylidene] benzamide (**34**).

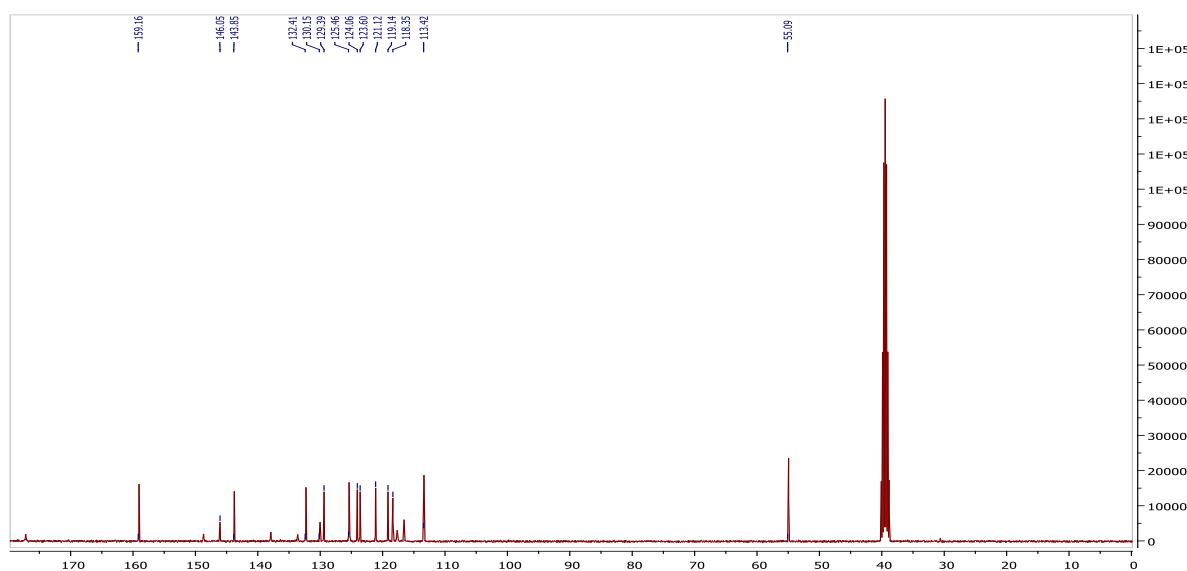


Figure 6.4 ^{13}C NMR spectrum of 3-methoxy-*N*-[(9*E*)-8,10,17-triazatetracyclo [8.7.0.0^{2,7}.0^{11,16}]heptadeca-1(17),2,4,6,11(16),12,14-heptaen-9-ylidene] benzamide (**34**).

6.6 4-Chloro-*N*-[(9*E*)-8,10,17-triazatetracyclo[8.7.0.0^{2,7}.0^{11,16}]heptadeca-1(17),2,4,6,11(16),12,14-heptaen-9-ylidene]benzamide (35)

The IR spectrum (**Figure A6.9**) showed a band at 3025 cm⁻¹ for and N–H stretch. A band at 1637 cm⁻¹ was observed for the C=O stretch. The C–N stretch was observed at 15630 cm⁻¹. The ¹H NMR (**Figure A6.10**) and ¹H–¹H COSY (**Figure A6.11**) spectra of compound **35** showed a singlet signal at 13.49 ppm for the NH proton. Signals from aromatic protons resonating between 9.40 and 6.87 ppm were observed. The ¹³C NMR spectrum (**Figure A6.12**) showed signals between 166.9 and 115.3 ppm for aromatic protons. In the characterization of compound **35** due to its low solubility in DMSO the spectra obtained for ¹H and ¹³C NMR had enhance signals for impurities when an attempt was made to obtain significant quantities of sample dissolved in the solvent used. When this was avoided extremely low signals were obtained with most peaks suppressed in the ¹H NMR spectrum and no peaks observed in the ¹³C NMR spectrum. Conclusive characterization of this compound was achieved with using IR, GC-MS and elemental analysis.

6.7 3-Nitro-*N*-[(9*E*)-8,10,17-triazatetracyclo[8.7.0.0^{2,7}.0^{11,16}]heptadeca-1(17),2,4,6,11(16),12,14-heptaen-9-ylidene]benzamide (36)

The IR spectrum (**Figure A6.13**) showed a band at 3082 cm⁻¹ for and N–H stretch. A band at 1634 cm⁻¹ was observed for the C=O stretch. The C–N stretch was observed at 1594 cm⁻¹. In the ¹H NMR (**Figure A6.14**) and ¹H–¹H COSY (**Figure A6.15**) spectra of compound **36** a singlet resonance occurred at 13.48 ppm for the NH proton. Aromatic protons were observed between 9.37 and 6.86 ppm. The ¹³C NMR spectrum (**Figure A6.16**) showed signals between 165.9 and 114.9 ppm for aromatic protons. Due to the low solubility of compound **36** in DMSO, the spectral obtained for ¹H NMR and ¹³C NMR had enhanced signals for impurities, when an attempt was made to obtain significant quantities of sample dissolved in the solvent used. When this was avoided, extremely low signals were obtained with most peaks suppressed in the ¹H NMR spectrum and no peaks observed in the ¹³C NMR spectrum. Conclusive characterization of this compound was achieved with using IR, GC-MS and elemental analysis.

6.8 3-Chloro-*N*-[(9*E*)-8,10,17-triazatetracyclo[8.7.0.0^{2,7}.0^{11,16}]heptadeca-1(17),2,4,6,11(16),12,14-heptaen-9-ylidene]benzamide (37)

The IR spectrum (**Figure A6.17**) showed a band at 1638 cm⁻¹ for the C=O stretch. The C–N stretch was observed at 1595 whilst the C=C stretch occurred at 1575 cm⁻¹. The ¹H NMR (**Figure A6.18**) spectrum of compound **37** showed a singlet at 13.50 ppm for the proton of an amide. Aromatic protons resonating between 9.41 and 6.56 ppm were observed. The ¹³C NMR spectrum (**Figure A6.19**) showed signals between 166.4 and 113.4 ppm for aromatic protons. The methoxy group was observed at 54.94 ppm.

The spectral data obtained for ¹H NMR and ¹³C NMR had enhanced signals for impurities due to its low solubility in DMSO when an attempt was made to obtain significant quantities of sample dissolved in the DMSO. When this was avoided extremely low signals were obtained with most peaks suppressed in the ¹H NMR spectrum and no peaks observed in the ¹³C NMR spectrum. Conclusive characterization of this compound was achieved with using IR, GC-MS and elemental analysis.

6.9 4-Nitro-*N*-[(9*E*)-8,10,17-triazatetracyclo[8.7.0.0^{2,7}.0^{11,16}]heptadeca-1(17),2,4,6,11(16),12,14-heptaen-9-ylidene]benzamide (38)

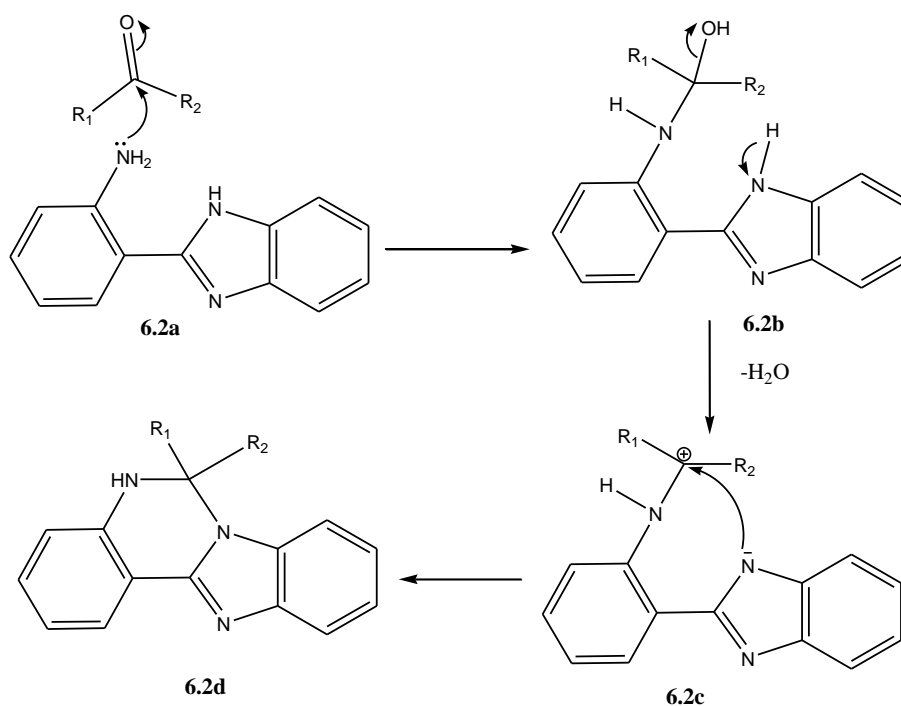
The IR spectrum (**Figure A6.20**) showed a band at 3052 cm⁻¹ for an N–H stretch. A band at 1634 cm⁻¹ was observed for the C=O stretch. The C–N stretch was observed at 1574 cm⁻¹. The ¹H NMR spectrum (**Figure A6.21**) of compound **38** showed a singlet resonance at 14.38 ppm for the proton of an amide. Aromatic protons resonating between 8.94 and 7.38 ppm were observed. Due to poor solubility of compound **38** the ¹³C NMR spectral data could not be obtained

6.10 *N*-[(9*E*)-8,10,17-triazatetracyclo[8.7.0.0^{2,7}.0^{11,16}]heptadeca-1(17),2,4,6,11(16),12,14-heptaen-9-ylidene]benzamide (39)

The IR spectrum (**Figure A6.22**) showed a band at 3056 cm⁻¹ for and N–H stretch. A band at 1633 cm⁻¹ was observed for the C=O stretch The C–N stretch was observed at 1593 cm⁻¹. In the ¹H NMR (**Figure A6.23**) and ¹H–¹H COSY (**Figure A6.24**) spectra of compound **39** the

NH proton resonated as a singlet at 14.38 ppm. Aromatic protons were observed between 8.36 and 6.92 ppm. The ^{13}C NMR spectrum (**Figure A6.25**) showed signals between 104.4 and 144.4 ppm for aromatic carbons.

The formation of triazatetracyclic have been extended to include aldehyde and ketones. The reaction is thought to proceed by the attack of the carbonyl of the ketone or aldehyde (**6.2a**) (**Scheme 6.1**) by the lone pair on the nitrogen of the 2-aminophenyl group without the presence of a base leading to the formation of the hydroxyl on the ketone or aldehyde (**6.2b**) Protonation of the hydroxyl group lead to its loss as water (**6.2c**). After which the nitrogen of the benzimidazole also attacks the carbon leading to the formation of a triazatetracyclic (**6.2d**).



Scheme 6.2 Proposed reaction mechanism for the formation of triazatetracyclics from ketones and aldehydes.

6.11 Crystal structure of compound 39

Compounds **39** was recrystallized from DMSO:Toluene (1:1). Compound **39** was obtained as white crystals. The crystallographic data, selected bond lengths and bond angles for the

crystal structure of compound **39** are provided in **Tables 6.1** and **6.2**. The ORTEP diagram for compound **39** in **Figure 6.5**. Compound **39** crystallized in the monoclinic space group $P2_1/c$.

Table 6.1 Crystallographic data and structure refinement summary for compounds **39**.

Property	39
Formula	C ₂₁ H ₁₄ N ₄ O
Formula Weight	338.36
Crystal System	Monoclinic
Space group	$P2_1/c$
a [Å]	15.8980(7)
b [Å]	4.8067(2)
c [Å]	21.0455(10)
α [°]	90
β [°]	101.153(2)
γ [°]	90
V [Å ³]	1577.86(12)
Z	4
D(calc) [g/cm ³]	1.424
Mu(MoKa) [/mm]	0.092
F(000)	704
Crystal Size [mm]	0.05 x 0.32 x 0.59
Temperature (K)	200
Radiation [Å]	MoKa 0.71073
Theta Min-Max [°]	2.0, 28.3
Dataset	-21: 21 ; -6: 6 ; -27: 28
Tot., Uniq. Data, R(int)	21774, 3928, 0.022
Observed Data [I > 2.0 sigma(I)]	3165
Nref, Npar	3928, 239
R, wR_2 , S	0.0375, 0.1047, 1.03
Max. and Av. Shift/Error	0.00, 0.00
Min. and Max. Resd. Dens. [e/Å ³]	-0.20, 0.27

The bond distance of O1–C3 in compound **39** is 1.245(1) Å, which is consistent with a carbonyl whilst the N1–C1, N1–C11, and N2–C1 bond distances in compound **39** are 1.301(2), 1.393(2), and 1.406(1) Å respectively. The bonds are not distinctly single nor double bonds suggesting the triazatetracyclic is stabilized by the quasi aromatization of the six membered ring formed after the loss of hydrogen sulphide. To make the molecule more stable. The bond angles of N1–C1–C21, N1–C1–N2 and N2–C1–C21 in compound **39** are 128.6(1), 113.3(1) and 118.1(1) Å respectively. The carbon atoms involved are all sp² hybridized but the presence of electronegative groups around them tend to distort their electron

densities and hence the bond angles. The lone pairs on the nitrogen atoms are contributed to stabilise the six membered ring.

Table 6.2 Selected bond lengths (Å) and bond angles (°) for compound **39**.

Bond lengths (Å)	
O1-C3	1.245(1)
N1-C1	1.301(2)
N1-C11	1.393(2)
N2-C1	1.406(1)
N4-C3	1.368(1)
N2-C2	1.378(1)
Bond angles (°)	
C1-N1-C11	104.8(1)
C1-N2-C2	124.1(1)
C1-N2-C12	105.9(1)
N4-C3-C31	114.8(1)
N1-C1-C21	128.6(1)
N2-C2-N3	115.4(1)
N1-C1-N2	113.3(1)
N2-C1-C21	118.1(1)

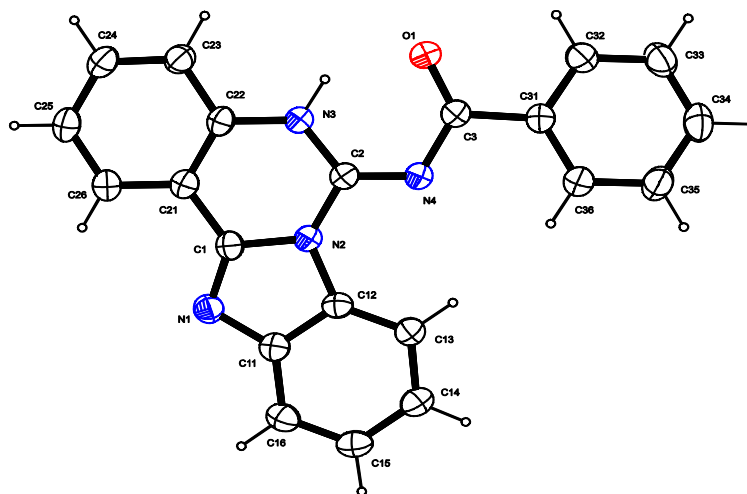


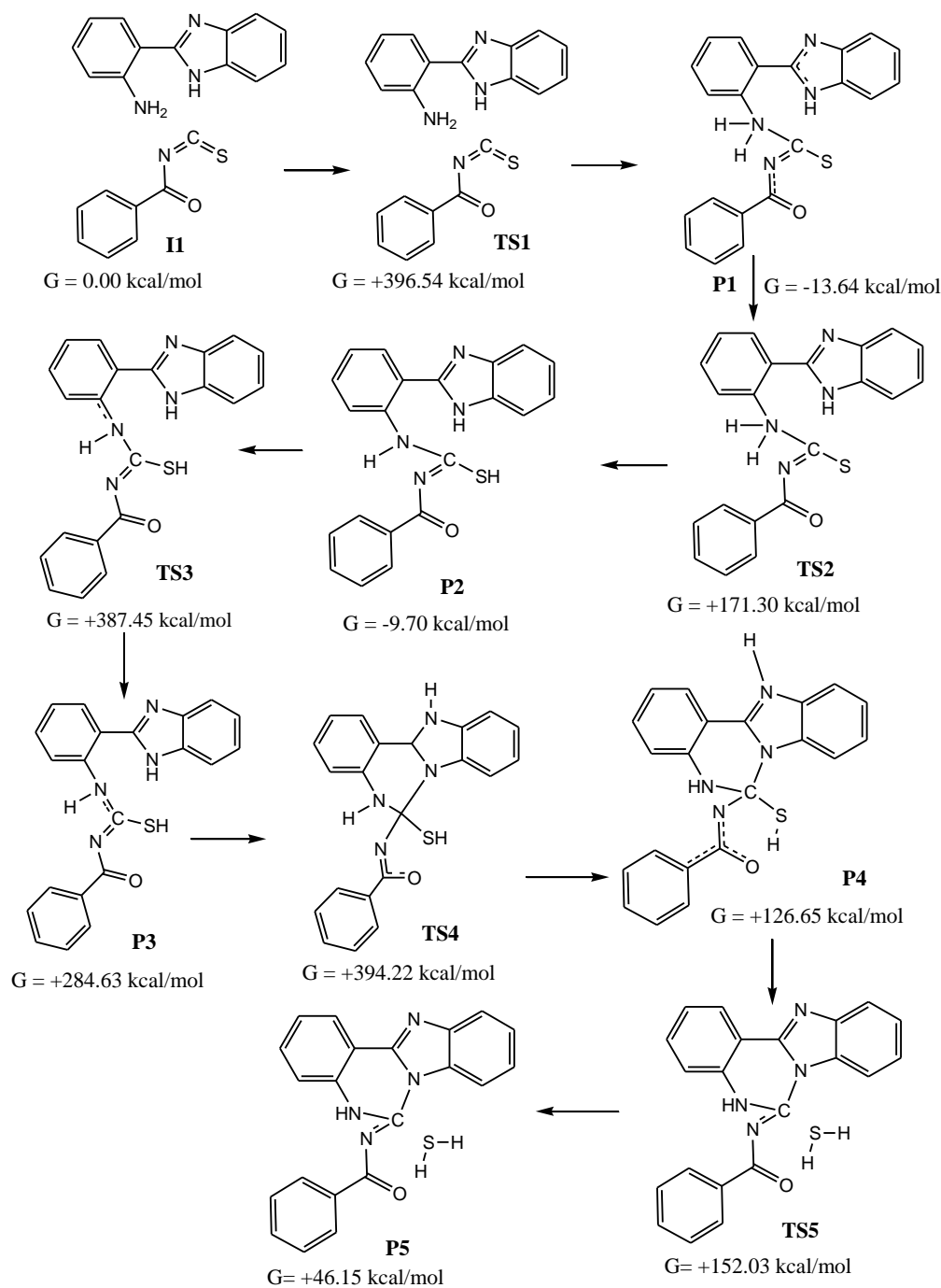
Figure 6.5 An ORTEP view of *N*-[(9*E*)-8,10,17-triazatetracyclo[8.7.0.0^{2,7}.0^{11,16}]heptadeca-1(17),2,4,6,11(16),12,14-heptaen-9-ylidene]benzamide (**39**) showing 50% probability displacement ellipsoids and the atom labelling.

6.12 Transition state studies on the formation of triazatetracyclic derivatives

The predicted reaction pathway proceeds by the attack of the thione of benzoyl isothiocyanate by the amino group attached to the benzene ring as indicated **I1** (**Scheme 6.2**) which is a singlet species of no charge and a dipole moment of 6.01 Debye. **I1** is used as reference in the computation of the relative free energies. The functional used in the computation of **I1** is B3LYP with the basis set of 6-31G(d). **I1** is obtained by optimising the starting material to a minimum and also tracing the reverse IRC path way of the transition state **TS1**. **TS1** is singlet of charge 2 with a dipole moment of 6.15 Debye It is a saddle point with a single imaginary frequency, according to the Berny algorithm and a subsequent vibrational analysis. The relative free energy of **TS1** is +396.54 kcal/mol. A forward IRC computation and optimization of the subsequent structure gave **P1** which is a singlet species of no charge and frequency with a dipole moment of 9.59 Debye. The relative free energy of **P1** is -13.64 kcal/mol.

Rearrangement of electrons leads to **TS2** which is also a doublet species with a charge of 1, a single imaginary frequency and a dipole moment of 4.47 Debye. **TS2** is a saddle point with a single imaginary frequency and a relative free energy of +171.30 kcal/mol. A forward IRC pathway from **TS2** gives **P2** which a singlet species of no charge, and a imaginary frequency of zero. The dipole moment of **P2** is 4.37 Debye, with a relative free energy of -9.70 kcal/mol. **P2** is formed by the migration of a proton from the amino group onto the sulfur. A rearrangement of electrons in **P2** leads to the formation of **TS3**, a saddle point of charge 2 with a dipole moment of 5.68 kcal/mol. The relative free energy of **TS3** is 387.45 kcal/mol. A further rearrangement gives the more stable intermediate **P3** which is also a singlet with no charge and imaginary frequency but have a relative energy of +284.63 kcal/mol. A ring closure occurs when carbon of the thiol is attacked by the lone pair of electrons on the nitrogen to form **TS4**, a singlet of no charge with a single imaginary frequency and a dipole moment of 9.99 Debye. The relative free energy of **TS4** is +394.22 kcal/mol. A forward displacement of **TS4** along the IRC and subsequent optimization of the product yields **P4**, a singlet of no charge and imaginery frequency but with a dipole moment of 16.86 Debye. The relative energy of **P4** is +126.65 kcal/mol. The rearrangement of the species, a proton shift and cleavage of the C-S bond leads to the formation of **TS5** with a loss of hydrogen sulphide. **TS5** is a transition state of no charge, with a single imaginary frequency and a dipole moment of 3.36 Debye. It has a relative energy of 152.03 kcal/mol.

A rearrangement of electrons leads to the formation of **P5** which has no charge and imaginary frequency but with a dipole moment of 2.18 Debye and a relative energy of 46.15 kcal/mol. The detailed reaction mechanism for the synthesis of triazatetracyclics has been computed to obtain five transition states of four intermediates and a product. Again these preliminary results illustrate the feasibility of the formation of product, and future work will investigate further transition states in order to find a plausible mechanism.



Scheme 6.3 DFT reaction mechanism of triazatetracyclics.

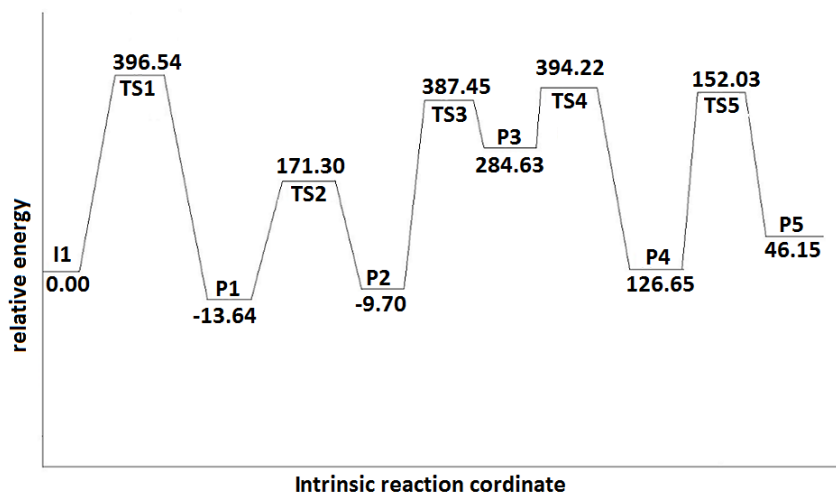


Figure 6.6 Potential energy surface for the formation of triazatetracyclics.

6.2 Biochemical studies

6.2.1 Cell viability and cytotoxicity tests

The acute cytotoxic effects of triazatetracyclics were determined by exposing them to isolated human white blood cells, for a 24-hour period. The cell viability was assessed using the MTT reduction assay and the results are presented in **Table 6.3** which indicates the compound numbers (in bold) as well as the EC₅₀ values calculated for each compound tested.

Table 6.3 Cell viability results for benzoyl isothiocyanate derivatives.

Triazatetracyclics	EC ₅₀ μM
32	45.47
33	45.09
34	131.26
35	252.77
36	136.72
37	74.95
38	164.05
39	163.67

The EC₅₀ values for the triazatetracyclics (**Figure 6.7**) showed varying effects on the cell viability of human white blood cells. Compounds **32** (4-bromo), **33** (4-methoxy) and **37** (3-chloro) derivatives were cytotoxic giving EC₅₀ values of 45.47 ± 21.92 , 45.09 ± 13.79 and 74.94 ± 13.17 μM , respectively. Substitution at position four with a bromo or a methoxy leads to an increase in cytotoxic effects of triazatetracyclics. Also a substitution at position three with a chloro makes triazatetracyclics cytotoxic.

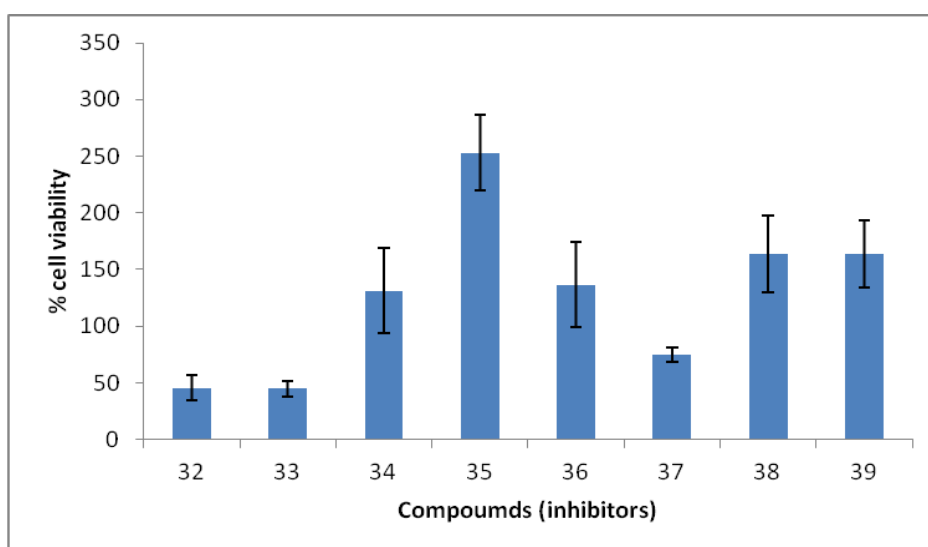


Figure 6.7 EC₅₀ values for the triazatetracyclics (μM). Error bars represent the SEM for $n = 3$.

The cytotoxicity of compounds **35** and **33**, which are the most and least cytotoxic compounds among the triazatetracyclenic derivatives, respectively is shown in **Figure 6.8**. The presence of the chloro group (**35**) at position four in the triazatetracyclenic leads to an increase in cytotoxicity, whilst the presence of a methoxy group (**33**) leads to a decrease in cytotoxicity.

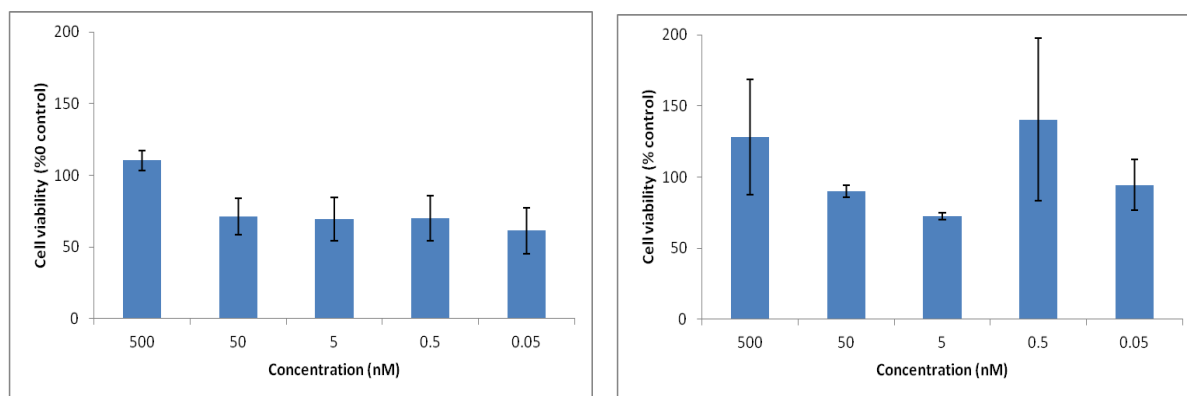


Figure 6.8 EC₅₀ values for compounds **35** and **33** (μM). Error bars represent the SEM for $n = 3$.

6.2.2 HIV-1 protease screen of triazatetracyclic derivatives

Table 6.5 and **Figure 6.9** gives the HIV-1 screening results for the triazatetracyclics. The screening of the compounds was done at 100 μM of inhibitor and that for ritonavir was done at 10 μM . Most of the triazatetracyclics do not have a significant % inhibition when compared to ritonavir. This primarily might be due to poor solubility of these compounds in the buffer used with 2% DMSO.

Table 6.4 HIV-1 protease screening results for triazatetracyclics.

Compounds	Fluorescence	Standard deviation	% Activity relative to untreated control	%Inhibition relative to untreated control
Ritonavir	36.24	1.88	9.34	90.67
32	478.51	4.7	123.36	0
33	353.86	2.68	91.22	8.78
34	354.87	8.85	91.48	8.52
35	405.49	10.65	104.53	0
36	317.61	25.8	81.88	18.12
37	157.91	10.75	69.88	30.12
38	182.64	3.29	80.82	19.18
39	380.73	9.67	98.15	1.85

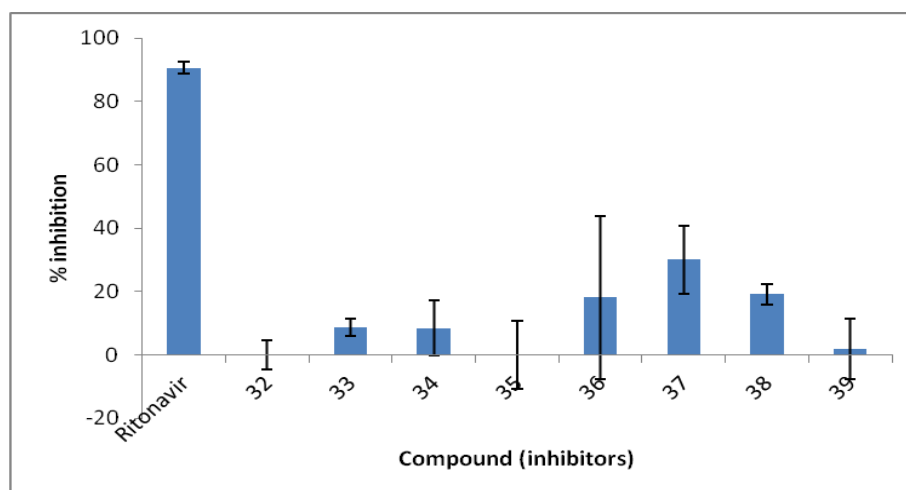


Figure 6.9 HIV-1 protease screening results illustrating % inhibition of triazatetracyclics (100 μ M) and ritonavir (10 μ M) relative to untreated control. Error bars represent SEM for $n = 3$.

Figures 6.10 and **6.11** give the 2D representation of compounds **38** and **35** in the protease active site respectively

The activity of 4-nitro-*N*-[(9*E*)-8,10,17-triazatetracyclo [8.7.0.0^{2,7}.0^{11,16}] heptadeca-1(17),2,4,6,11(16),12,14-heptaen-9-ylidene] benzamide (**35**) in the bioassay was due to the fact that it was able to undergo hydrogen bonding with aspartate B25 and aspartate A25. This makes it impossible for the natural substrate to access the active site of the enzyme.

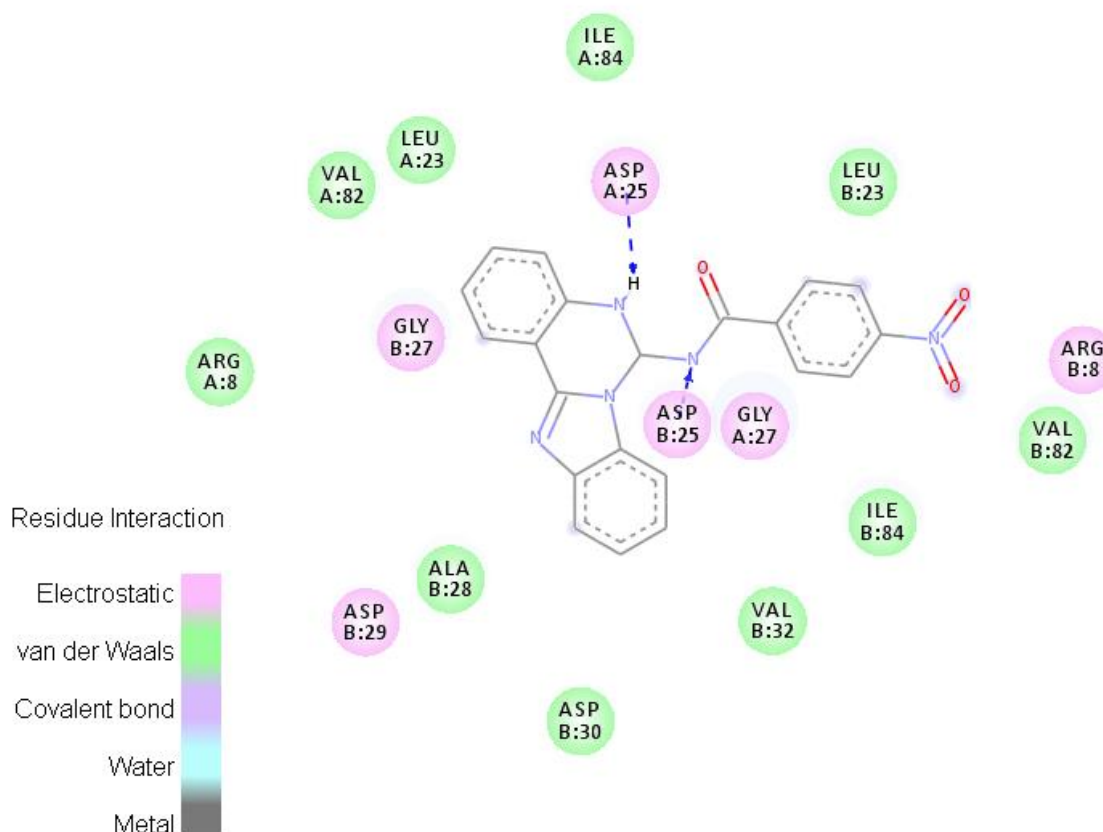


Figure 6.10 2D representation of 4-nitro-*N*-[(9*E*)-8,10,17-triazatetracyclo [8.7.0.0^{2,7}.0^{11,16}] heptadeca-1(17),2,4,6,11(16),12,14-heptaen-9-ylidene] benzamide (**38**). in the HIV-1 protease binding site

The lack of activity of 4-chloro-*N*-[(9*E*)-8,10,17-triazatetracyclo [8.7.0.0^{2,7}.0^{11,16}] heptadeca-1(17),2,4,6,11(16),12,14-heptaen-9-ylidene] benzamide (**35**) against protease was because it does not undergo any significant interaction with the groups at the active site of protease.

The predicted inhibition constants of this class of compounds range from 0.98 μM to 3.02 μM but the predicted inhibition could not be realized because of the poor solubility of these compounds in DMSO and water which was used for the bioassay.

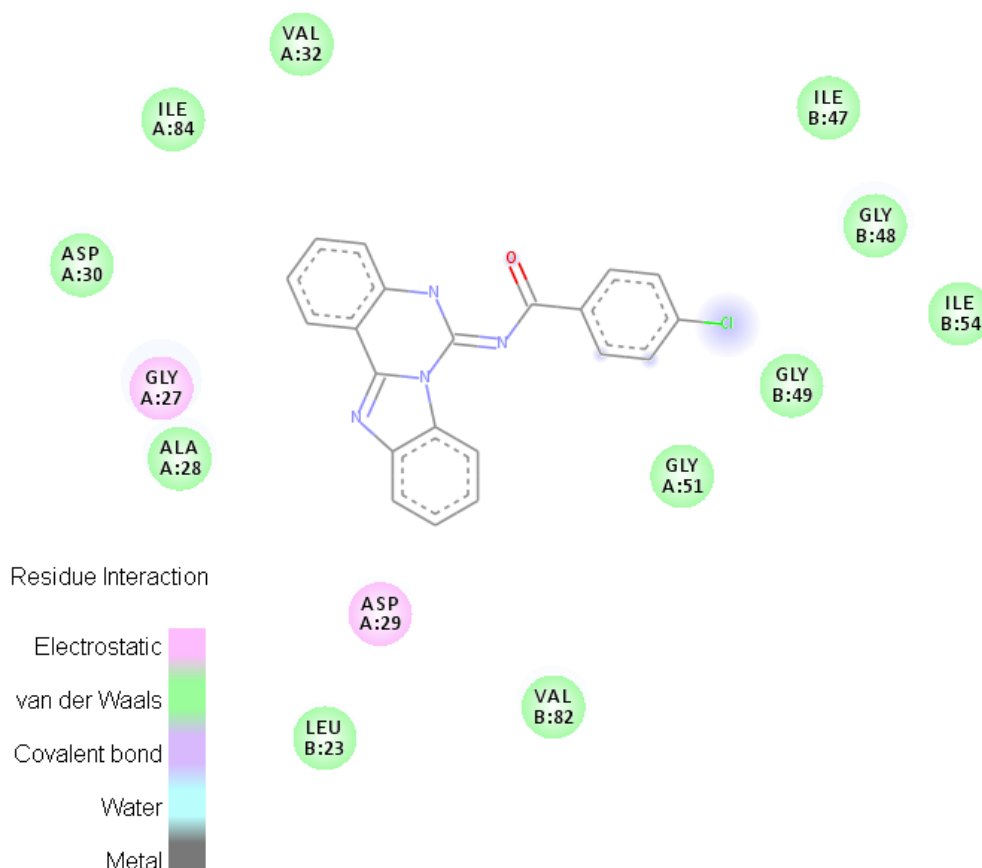


Figure 6.11 2D representation of 4-chloro-*N*-[(9*E*)-8,10,17-triazatetracyclo[8.7.0.0^{2,7}.0^{11,16}]heptadeca-1(17),2,4,6,11(16),12,14-heptaen-9-ylidene]benzamide (**35**) in the HIV-1 protease binding site

6.3 Conclusions

-Novel triazatetracyclic derivatives have been synthesized from the reaction of benzoyl isothiocyanate with 2-(2-aminophenyl)-1*H*-benzimidazole. The compounds have been characterized with spectroscopy, microanalysis and GC-MS.

-The single crystal XRD molecular structure of *N*-[(9*E*)-8,10,17-triazatetracyclo[8.7.0.0^{2,7}.0^{11,16}]heptadeca-1(17),2,4,6,11(16),12,14-heptaen-9-ylidene]benzamide (**39**) has been discussed.

-Transition state studies on the formation of *N*-[(9*E*)-8,10,17-triazatetracyclo[8.7.0.0^{2,7}.0^{11,16}]heptadeca-1(17),2,4,6,11(16),12,14-heptaen-9-ylidene]benzamide (**39**) has been carried out

using Gaussian. The various transition states in the reaction pathway and the resulting intermediates have been computed to explain a possible reaction mechanism for these compounds.

-Cell viability tests of the triazatetracyclics showed that compounds **32** (4-bromo), **33** (4-methoxy) and **37** (3-chloro) were cytotoxic giving EC_{50} values of 45.47 ± 21.92 , 45.09 ± 13.79 and $74.94 \pm 13.17 \mu\text{M}$, respectively.

-The low solubility of the triazatetracyclics is the main reason why these class of compounds exhibited a low inhibition against HIV1 protease.

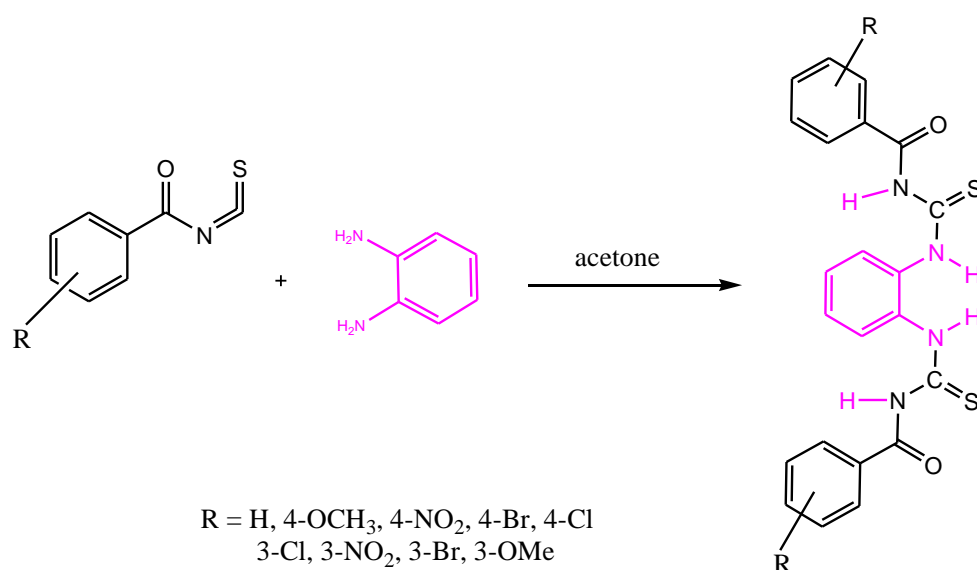
CHAPTER SEVEN

PHENYL THIOUREA COMPOUNDS AND OTHER DIAMINE DERIVATIVES

7.1 Synthesis of phenyl thiourea compounds and other diamine derivatives

A solvent-free 3-component one-pot reaction between 2,6-diaminopyridine or 1,2-diaminobenzene and NH_4SCN with subsequent addition of an aryl chloride afforded *bis*-1-(aroyl)-3-(aroyl)thioureas in excellent yields. The thiocyanate derivatives were first synthesized and then used to prepare the thiourea derivatives (**41**).³⁴¹ Benzoyl chloride has been reacted with ammonium thiocyanate in CH_2Cl_2 solution under solid-liquid phase transfer catalysis, using polyethylene glycol-400 as the catalyst, to give the corresponding benzoyl isothiocyanate. Dropwise addition of a solution of 1,4-butylenediamine in CH_2Cl_2 yielded 3,3'-dibenzoyl-1,1'-(butane-1,4-diyl)dithiourea (**54**),³⁴² while 3,3-*bis*(4-nitrophenyl)-1,10-(*p*-phenylene) dithiourea dimethylsulfoxide disolvate has been prepared by the reaction of (*p*-nitro)benzoyl isothiocyanate with *p*-phenylenediamine in CH_2Cl_2 using polyethylene glycol-400 as a phase transfer catalyst.³⁴³ This reaction has been carried using 1,6-hexyldiamine as the source of diamine to give *N,N*-(1,6-hexamethylene)-*bis*(benzoylthiourea)(**50**).³⁴⁴ Thiocarbonohydrazide has been converted into 1-aminothiocarbamoyl-4-aryloxy-3-thiosemicarbazides and 1,5-*bis*(aryloxythiocarbamoyl)thiocarbonohydrazides by the addition of one or two moles of aroyl isothiocyanate, respectively. 1-Phenyl- or 1-benzylidene-thiocarbonohydrazide and aroyl isothiocyanates gave the appropriate mono-adducts analogously. 1-Aminothiocarbamoyl-4-benzoyl-3-thiosemicarbazide, the simplest representative of these classes of compounds, is cyclized to 3-mercapto-5-phenyl-1,2,4-triazole in alkaline media, and to 2-benzamido-5-mercapto-1,3,4-thiadiazole in acid media, the action of alkyl halides in the appropriate alcohol yields 2-benzamido-5-alkylthio-1,3,4-thiadiazoles.³⁴⁵ The reaction of benzoyl isothiocyanate with *o*-phenylenediamine has been carried out in acetone using potassium thiocyanate as thiocyanate source (**40**).³⁴⁶

In this study, the phenyl thiourea derivatives are formed by the attack of the thione carbon by the two amino groups on the molecule.



Scheme 7.1 Synthesis of 1-benzoyl-3-(2-[[[(phenylformamido)methanethioyl]amino]phenyl]thiourea derivatives.

7.1.1 1-Benzoyl-3-(5-methyl-2-[[[(phenylformamido)methanethioyl]amino]phenyl]thiourea (40)

The IR spectrum (**Figure A7.1**) showed a band at 3186 cm^{-1} for an N–H stretch. A band was observed at 2981 cm^{-1} . A band for the C=O stretch of an amide was observed at 1670 cm^{-1} . The C–N stretch was observed at 1593 cm^{-1} . The ^1H NMR spectrum (**Figure A7.2**) of compound **40** showed a two doublet at signals at 12.45 ppm and 11.72 ppm for the proton of an amide. Aromatic protons were observed between 7.90 and 7.22 ppm. A singlet signal for three protons was observed at 2.31 ppm. The ^{13}C NMR spectrum (**Figure A7.3**) showed a signal at 180.4 ppm for the C=S, whilst the C=O signal was observed at 168.3 ppm. Signals for aromatic carbons occurred between 136.8 and 126.5 ppm aromatic carbons. The signal for a methyl group was observed at 20.7 ppm.

7.1.2 1-Benzoyl-3-(2-[[[(phenylformamido)methanethioyl]amino]phenyl]thiourea (41)

The IR spectrum (**Figure A7.4**) showed a bands at 3265, 3137 and 3005 cm^{-1} for an N–H stretch. A band at 1686 cm^{-1} was observed for the C=O stretch of an amide. The C–N stretch was observed at 1591 cm^{-1} . The ^1H NMR spectrum (**Figure A7.5**) of compound **40** showed a

two doublet at signals at 12.45 and 11.72 ppm for the proton of an amide. Aromatic protons were observed between 7.90 and 7.22 ppm. A singlet signal for three protons was observed at 2.31 ppm. The ^{13}C NMR spectrum (**Figure A7.6**) showed a signal at 180.4 ppm for the C=S, whilst the C=O signal was observed at 168.3 ppm. Signals for aromatic carbons occurred between 136.8 and 126.5 ppm for aromatic carbons.

7.1.3 1-(4-nitrobenzoyl)-3-[2-({[(4-nitrophenyl)formamido]methanthioyl phenyl}thiourea)amino) (42)

The IR spectrum (**Figure A7.7**) showed an N–H stretch at 3200 cm^{-1} . A band for the C=N stretch at 1683 cm^{-1} and the aromatic C=C was observed at 1601 cm^{-1} . The ^1H NMR spectrum (**Figure A7.8**) gave signals at 12.30 and 12.12 ppm for a proton of an amine whilst the aromatic protons occurred between 8.33 and 7.42 ppm. The ^{13}C NMR spectrum (**Figure A7.9**) showed a signal at 180.1 ppm for the C=S, whilst the C=O signal was observed at 161.0 ppm. Signals for aromatic carbons occurred between 149.7 and 123.2 ppm.

7.1.4 1-(4-Chlorobenzoyl)-3-[2-({[(4-chlorophenyl)formamido]methanethioyl}amino)phenylthiourea (43)

The IR spectrum (**Figure A7.10**) showed an N–H stretch at 3038 cm^{-1} , a band for the C=N stretch at 1640 cm^{-1} and the aromatic C=C was observed at 1600 cm^{-1} . The ^1H NMR spectrum (**Figure A7.11**) gave signals between 8.52–7.55 ppm for aromatic protons. The ^{13}C NMR spectrum (**Figure A7.12**) showed a signal between 143.7 and 119.6 ppm for aromatic carbons.

7.1.5 1-(3-Nitrobenzoyl)-3-[2-({[(3-nitrophenyl)formamido]methane}amino)phenyl]thourea (44)

The IR spectrum (**Figure 7.1**) showed N–H stretches at 3351 and 3204 cm^{-1} , a band for the C=O stretch was observed at 1687 cm^{-1} . Whilst bands for the C=N and C=C stretches were observed at 1603 cm^{-1} and the aromatic C=C was observed at 1515 cm^{-1} , respectively. The

^1H NMR spectrum (**Figure 7.2**) gave signals 12.34 and 12.18 ppm for a proton of an amide whilst aromatic protons occurred between 8.65 and 7.44 ppm. The ^{13}C NMR spectrum (**Figure 7.3**) gave a signal at 180.20 ppm for the C=S group, a signal for the C=O group was observed at 166.4 ppm and signals between 147.3 and 123.5 ppm were observed for aromatic carbons.

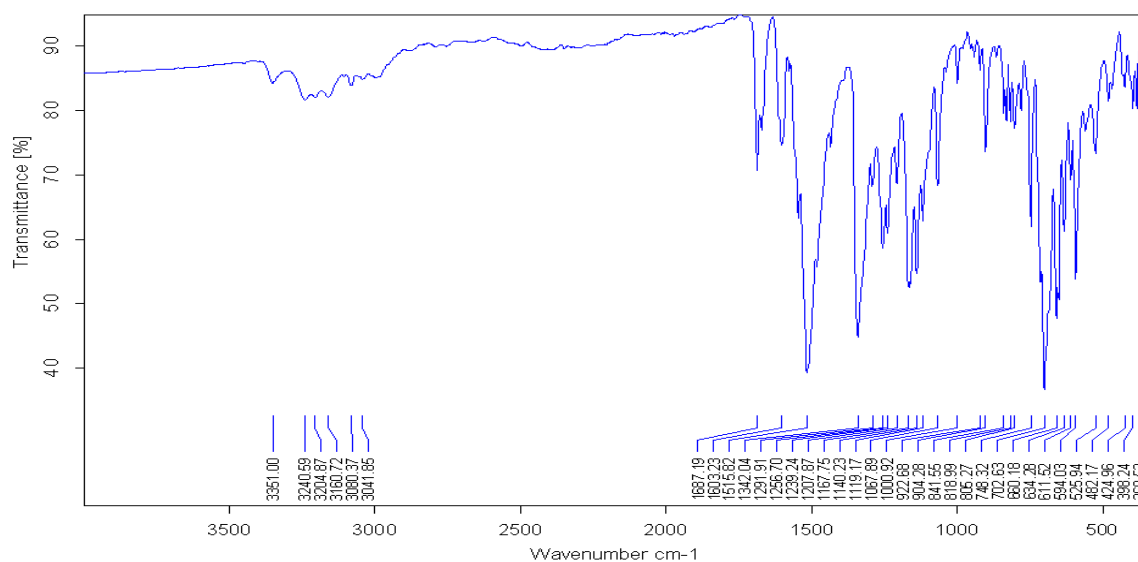


Figure 7.1 IR spectrum of 1-(3-nitrobenzoyl)-3-[2-(((3-nitrophenyl)formamido)methane)amino]phenyl]thourea (**44**).

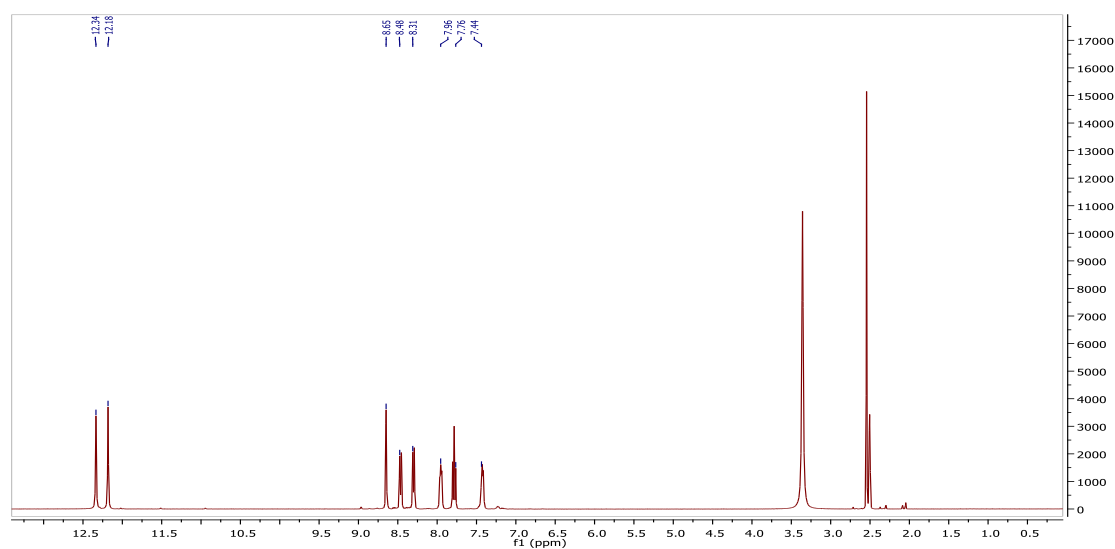


Figure 7.2 ^1H NMR spectrum of 1-(3-nitrobenzoyl)-3-[2-(((3-nitrophenyl)formamido)methane)amino]phenyl]thourea (**44**).

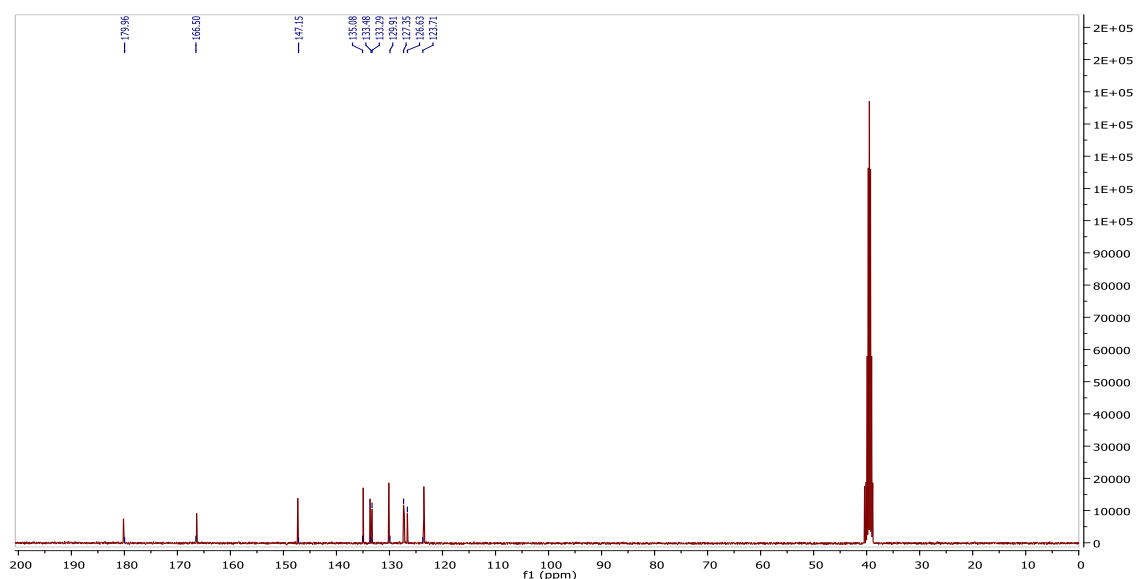


Figure 7.3 ^{13}C NMR spectrum of 1-(3-nitrobenzoyl)-3-[2-((3-nitrophenyl) formamido) methane] amino)phenyl]thiourea (**44**).

7.1.6 1-(3-Methoxybenzoyl)-3-[2-((3-methoxyphenyl)formamido)methanethioyl] amino)phenyl]thiourea (**45**)

The IR spectrum (**Figure A7.13**) showed N–H stretches at 3326 and 3184 cm^{-1} . Bands for the C=O stretch, C=C and C–N stretches were observed at 1663 cm^{-1} , 1552 and 1527 cm^{-1} respectively. The ^1H NMR spectrum (**Figure A7.14**) gave signals at 12.50 and 11.69 ppm for a proton of an amine whilst the aromatic protons occurred between 7.92 and 7.21 ppm. The methoxy protons occurred as a signal at 3.77 ppm. The ^{13}C NMR spectrum (**Figure A7.15**) showed a signal at 180.4 ppm for the C=S, whilst the C=O signal was observed at 168.1 ppm. Signals between 165.6 and 112.5 ppm were observed for aromatic carbons, whilst a signal for the methoxy group was observed at 55.5 ppm.

7.1.7 1-(4-Bromobenzoyl)-3-[2-((4-bromophenyl)formamido)methanethioyl] amino)phenyl]thiourea (**46**)

The IR spectrum (**Figure A7.16**) showed an N–H stretch at 3140 cm^{-1} . Bands for the C=O stretch, the C–N and the C=C was observed at 1681 cm^{-1} , 1585 cm^{-1} and 1517 cm^{-1} . The ^1H NMR spectrum (**Figure A7.17**) gave signals at 11.82 and 12.37 ppm for a proton of an amine

whilst the aromatic protons occurred between 7.40 and 7.91 ppm. The ^{13}C NMR spectrum (**Figure A7.18**) gave a signal at 180.5 ppm for the C=S, whilst a signal at 167.4 ppm was observed for the carbonyl. Signals were observed between 126.7 and 133.6 ppm for aromatic carbons.

7.1.8 1-(4-Methoxybenzoyl)-3-[2-([(4-methoxyphenyl)formamido]methanethiyl) amino)phenyl]thiourea (47)

The IR spectrum (**Figure A7.19**) showed N–H stretches at 3404 and 3278 cm^{-1} . Bands for the C=N and C=C stretches were observed at 1682 and 1591 cm^{-1} , respectively. The ^1H NMR spectrum (**Figure A7.20**) gave signals at 12.56 and 11.48 ppm for a proton of an amine whilst the aromatic protons occurred between 7.92 and 7.01 ppm. The protons of the methoxy group occurred at 3.82 ppm. The ^{13}C NMR spectrum (**Figure A7.21**) gave a signal at 180.8 cm^{-1} for the C=S, a signal at 167.5 and 163.2 ppm were observed for the C=O signifying the unsymmetrical nature of the molecule, and signals between 133.3 and 113.7 ppm were observed for aromatic carbons. The methoxy group was observed at 55.8 ppm.

7.1.9 1-(3-Chlorobenzoyl)-3-[2-([(3-chlorophenyl)formamido]methanethiyl) amino)phenyl]thiourea (48)

The IR spectrum (**Figure A7.22**) showed N–H stretches at 3440 and 3166 cm^{-1} . Bands for the C=O stretch, the C=N stretch and the C=C stretch were observed 1668 cm^{-1} , 1593 cm^{-1} and 1510 cm^{-1} . The ^1H NMR spectrum (**Figure A7.23**) gave signals at 11.88 and 12.40 ppm for a proton of an amide whilst the aromatic protons occurred between 8.04 and 7.41 ppm. The ^{13}C NMR spectrum (**Figure A7.24**) gave a signal at 180.4 ppm for the C=S, whilst the carbonyl occurred at 167.0 ppm and signals between 134.3 and 126.7 ppm were observed for aromatic carbons.

7.1.10 1-(3-Bromobenzoyl)-3-[2-({(3-bromophenyl)formamido]methanethioyl} amino)phenyl]thiourea (49)

The IR spectrum (**Figure A7.25**) showed an N–H stretch at 3176 cm^{-1} . Bands for the C=O stretch, the C–N stretch and the C=C stretch were observed at 1662 , 1595 and 1563 cm^{-1} , respectively. The ^1H NMR spectrum (**Figure A7.26**) gave signals at 12.37 and 11.82 ppm for a proton of an amine whilst the aromatic protons occurred between 7.91 and 7.40 ppm . The ^{13}C NMR spectrum (**Figure A7.27**) gave a signal at 180.6 ppm for the C=S, whilst a signal at 167.4 ppm was observed for the thione. Signals were observed between 136.3 and 122.1 ppm for aromatic carbons.

7.1.11 3-Benzoyl-1-(2-({(phenylformamido)methanethioyl]amino}ethyl)thiourea (50)

The IR spectrum (**Figure 7.4**) showed bands at 3420 and 3229 cm^{-1} for an N–H stretch. A band for an aliphatic C–H was observed at 3047 cm^{-1} , whilst a band at 1664 cm^{-1} was observed for the C=O stretch of an amide. The C–N stretch was observed at 1579 cm^{-1} . The ^1H NMR spectrum (**Figure 7.5**) of compound **50** showed a singlet for two protons at 10.98 ppm . Aromatic protons were observed between 7.91 and 7.51 ppm . The ^{13}C NMR spectrum (**Figure 7.6**) showed a signal at 180.8 ppm for the C=S, whilst the C=O signal was observed at 167.3 ppm . Signals for aromatic carbons occurred between 132.9 and 128.5 ppm for aromatic protons, whilst a signal for aliphatic carbons occurred at 43.4 ppm .

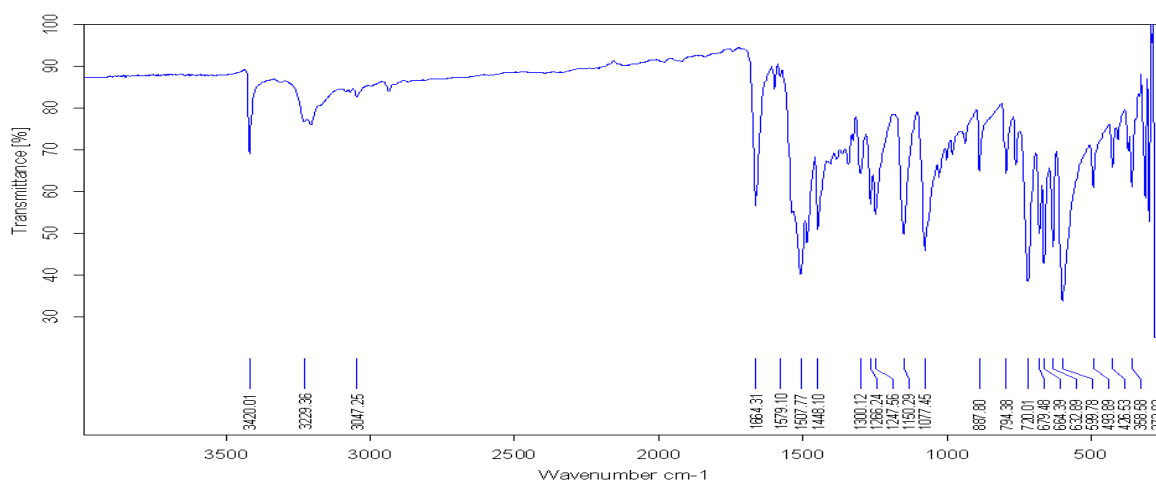


Figure 7.4 IR spectrum of 3-benzoyl-1-(2-({(phenylformamido)methanethioyl] amino}ethyl)thiourea (**50**).

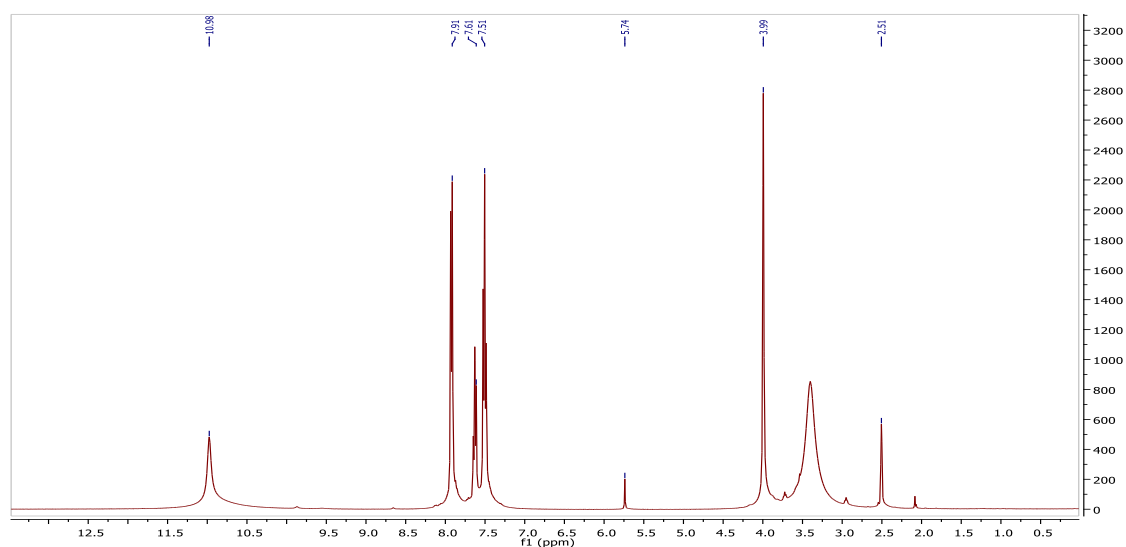


Figure 7.5 ^1H NMR spectrum of 3-benzoyl-1-(2-[[phenylformamido)methanethioyl]amino}ethyl)thiourea (**50**).

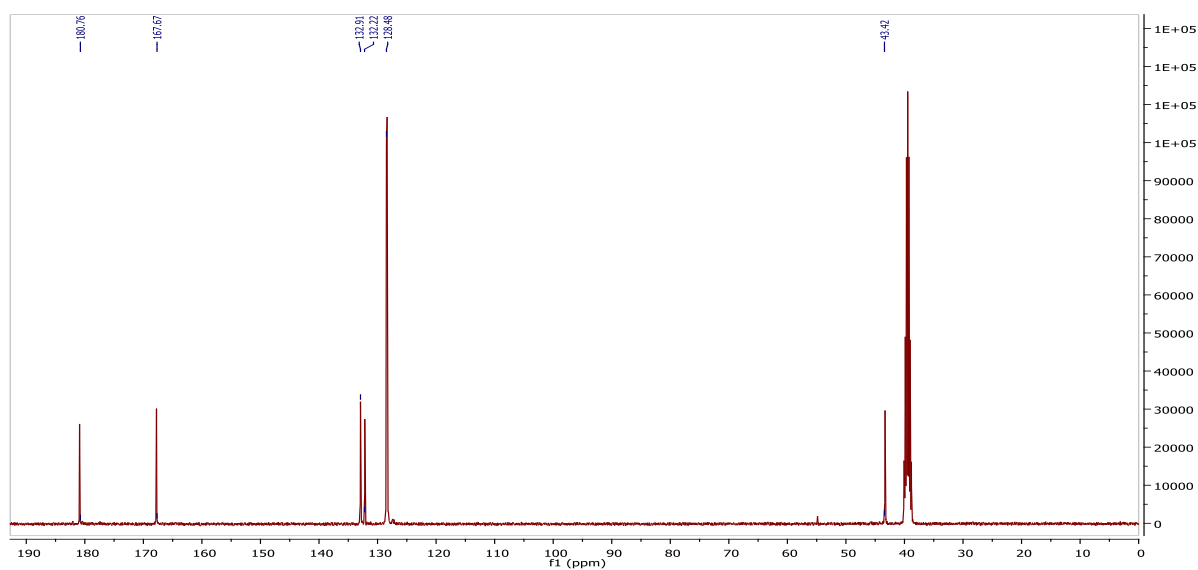


Figure 7.6 ^{13}C NMR spectrum of 3-benzoyl-1-(2-[[phenylformamido)methanethioyl]amino}ethyl)thiourea (**50**).

7.1.12 3-Benzoyl-1-[[phenylformido)methanethioyl]amino}thiourea (**51**)

The IR spectrum (**Figure A7.28**) showed a band at 2988 cm^{-1} for an N–H stretch. Bands at 1670 and 1658 cm^{-1} were observed for the C=O stretch of an amide and the C–N stretch was

observed at 1536 cm⁻¹. The ¹H NMR spectrum (**Figure A7.29**) of compound **51** showed singlet signals at 14.24 ppm and 12.12 ppm for a proton of an amide each. Aromatic protons were observed between 8.01 and 7.51 ppm. The ¹³C NMR spectrum (**Figure A7.30**) showed signals at 171.5 and 168.3 ppm for the C=S, whilst the C=O signals were observed at 167.3 and 165.0 ppm. Signals for aromatic carbons occurred between 134.2 and 125.4 ppm for aromatic carbons.

7.1.13 Crystal structures of compounds **40**, **50** and **51**

Compounds **40**, **50** and **51** were recrystallized from DMSO:Toluene (1:1). Compound **50** were obtained as white crystals, whilst compounds **40** and **49** were obtained as brown and light brown crystals respectively. The crystallographic data, selected bond lengths and bond angles for the crystal structures of compounds **40**, **50** and **51** are provided in **Tables 7.1** and **7.2**. The ORTEP diagrams for compounds **40**, **50** and **51** are presented in **Figures 7.7**, **7.8** and **7.9**. Compounds **40** and **50** crystallized in the monoclinic space group *P21/c*, while compound **51** crystallized in the monoclinic space group *P21/n*.

Table 7.1 Crystallographic data and structure refinement summary for compounds **40**, **50** and **51**

Property	40	50	51
Formula	C ₂₃ H ₂₀ N ₄ O ₂ S ₂	C ₁₈ H ₁₈ N ₄ O ₂ S ₂	C ₁₆ H ₁₄ N ₄ O ₂ S ₂ , 2(C ₂ H ₆ OS)
Formula Weight	448.57	386.50	514.73
Crystal System	Monoclinic	monoclinic	Monoclinic
Space group	<i>P2₁/c</i>	<i>P2₁/c</i>	<i>P2₁/n</i>
a [Å]	10.8288(4)	11.2036(13)	6.3738(2)
b [Å]	17.8575(7)	7.1780(8)	15.3854(5)
c [Å]	22.6276(9)	11.0901(13)	12.6585(4)
α [°]	90	90	90
β [°]	92.581(2)	100.783(5)	93.448(1)
γ [°]	90	90	90
V [Å ³]	4371.2(3)	876.11(18)	1239.09(7)
Z	8	2	2
D(calc) [g/cm ³]	1.363	1.465	1.380
Mu(MoKa) [/mm]	0.272	0.325	0.417
F(000)	1872	404	540
Crystal Size [mm]	0.23 x 0.32 x 0.54	0.14 x 0.22 x 0.25	0.15 x 0.27 x 0.33
Temperature (K)	200	200	200
Radiation [Å]	MoKa 0.71073	MoKa 0.71073	MoKa 0.71073
Theta Min-Max [°]	1.9, 28.4	3.4, 28.4	2.1, 28.3
Dataset	-14: 9 ; -23: 20 ; - 30: 30	-14: 14 ; -9: 9 ; - 13: 14	-7: 8 ; -20: 20 ; -16: 12
Tot., Uniq. Data, R(int)	40580, 10903, 0.028	2175, 2175, 0.000	11663, 3088, 0.020
Observed Data [I > 2.0 sigma(I)]	7835	1986	2596
Nref, Npar	10903, 616	2175, 128	3088, 155
R, wR ₂ , S	0.0605, 0.1408, 1.08	0.1277, 0.4138, 1.17	0.0298, 0.0821, 1.03
Max. and Av. Shift/Error	0.18, 0.00	0.00, 0.00	0.00, 0.00
Min. and Max. Resd. Dens. [e/Å ³]	-0.63, 0.71	-1.59, 1.64	-0.27, 0.33

In compound **40** the bond distances O21-C21 and O11-C11 are 1.230(1) and 1.224(1) which are consistent with carbonyls, while the bond distances of S21-C22 and S11-C12 which are 1.667(1) and 1.667(1) are typical of thiones. The bond angles of S21-C22-N22 and O11-C11-N11 are 127.6(2) and 122.4(2) respectively this confirms the carbon atoms are sp² hybridized. The bond distances of S1-C2 and O1-C1 in compound **50** are 1.662(1) and 1.218(1) for a thione and a carbonyl respectively. The bond distance of C3-C3a is 1.522(1) which is consistent with a carbon-carbon single bond. The bond angles of S1-C2-N2 and S1-C2-N1

are 126.0(1) and 118.4(1) confirming that the carbon is sp^2 hybridized, whilst the bonded of N2-C3-C3_a which is 111.1(1) confirms the carbon is sp^3 hybridized. In compound **51** the bond distance S1-C2 which was 1.668(1) was consistent with a thione, whilst the carbonyl O1-C1 occurred at 1.225(2) Å. The N2-N2a bond distance was 1.373(2) Å. The bond angles of O1-C1-N1 and O1-C1-C11 were 122.9(1) and 122.0(1) respectively, confirming that the carbon atom involved is sp^2 hybridized.

Table 7.2 Selected bond lengths (Å) and bond angles (°) for compounds **40**, **50** and **51**

Bond lengths (Å)					
40		50		51	
S21-C22	1.667(1)	S1-C2	1.662(1)	S1-C2	1.668(1)
S11-C12	1.667(1)	O1-C1	1.218(1)	O1-C1	1.225(2)
O21-C21	1.230(1)	C1-C11	1.492(1)	N1-C1	1.382(2)
O11-C11	1.224(1)	N1-C2	1.405(1)	N1-C2	1.383(2)
N21-C22	1.399(1)	N1-C1	1.371(1)	N2-N2a	1.373(2)
N22-C22	1.332(1)	C3-C3a	1.522(1)	N2-C2	1.332(2)
Bond Angles (°)					
40		50		51	
N21-C22-N22	114.5(2)	C1-N1-C2	128.6(1)	O2-S2-C4	106.2(1)
S21-C22-N22	127.6(2)	C2-N2-C3	123.3(1)	O2-S2-C3	105.6(1)
O11-C11-N11	122.4(2)	O1-C1-N1	122.4(1)	N2a-N2-C2	119.6(1)
N21-C21-C211	117.6(2)	S1-C2-N2	126.0(1)	N1-C1-C11	115.1(1)
N11-C12-N12	114.7(2)	S1-C2-N1	118.4(1)	N1-C2-N2	116.1(1)
		N1-C1-C11	115.3(1)	S1-C2-N1	121.2(1)
		O1-C1-C11	122.3(1)	C3-S2-C4	97.1(1)
		N1-C2-N2	115.6(1)	C1-N1-C2	126.5(1)
		N2-C3-C3_a	111.1(1)	O1-C1-N1	122.9(1)
				O1-C1-C11	122.0(1)
				S1-C2-N2	122.8(1)

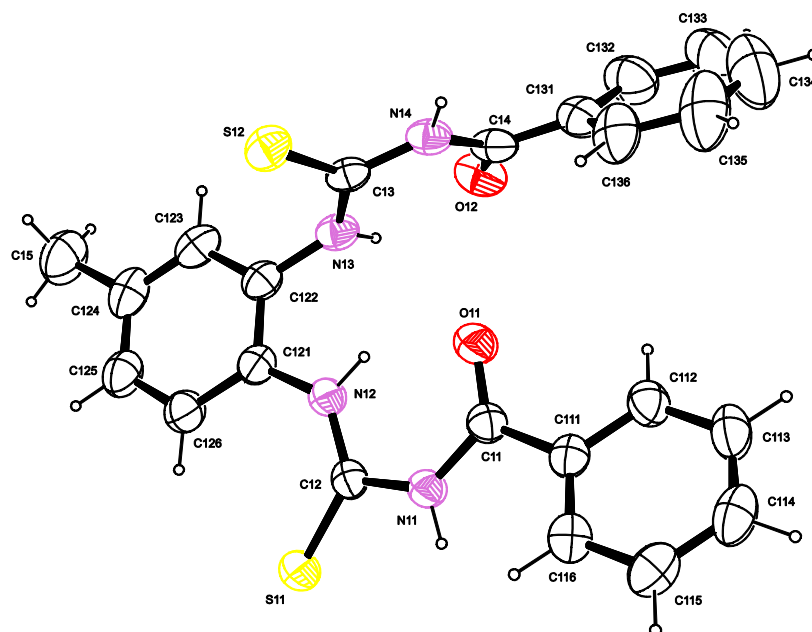


Figure 7.7 An ORTEP view of 1-benzoyl-3-(5-methyl-2-[(phenylformamido) methanethioyl]amino)phenylthiourea (**40**) showing 50% probability displacement ellipsoids and the atom labelling.

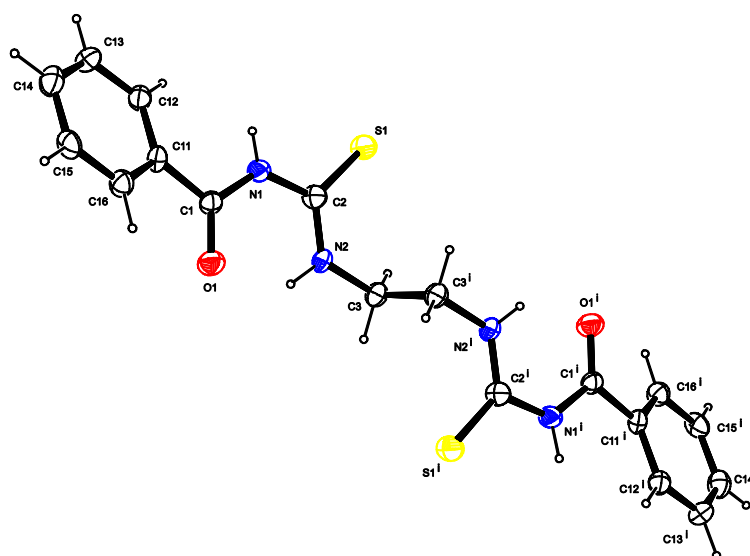


Figure 7.8 An ORTEP view of 3-benzoyl-1-(2-[(phenylformamido) methanethioyl] amino)ethylthiourea (**50**) showing 50% probability displacement ellipsoids and the atom labelling.

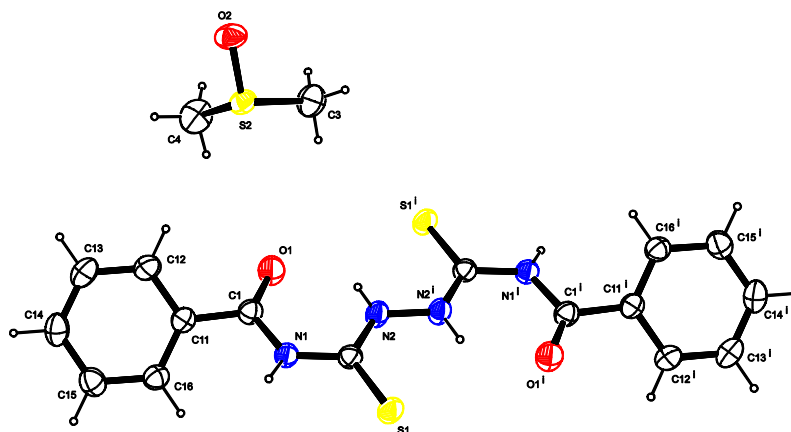


Figure 7.9 An ORTEP view of 3-benzoyl-1-[(phenylformido) methanethioyl] amino}thiourea dimethyl sulfoxide (**51**) showing 50% probability displacement ellipsoids and the atom labelling.

7.1.14 3-Benzoyl-1-(phenylamino)thiourea (**52**)

The reaction proceeds by the attack of benzoyl isothiocyanate by the primary amine of the phenylhydrazine. The IR spectrum (**Figure A7.31**) showed bands at 3060 and 3018 cm^{-1} for N–H stretches. The C–N stretch was observed at 1595 cm^{-1} whilst the aromatic C=C stretch occurred at 1561 cm^{-1} . The ^1H NMR spectrum (**Figure A7.32**) of compound **51** showed signals between 8.03-7.19 ppm for aromatic protons. The ^{13}C NMR spectrum (**Figure A7.33**) showed a signal at 162.9 ppm for the C=O signal. Signals for aromatic carbons were observed between 149.6 and 125.1 ppm.

7.1.15 1-((Benzamido)sulfanylenemethyl)urea (**53**)

Urea attacks the benzoyl isothiocyanate on one end of the molecule. Potassium thiocyanate in acetone has been reacted with benzoyl chloride at 50 °C. Urea was added and heated at 55 °C for 5 h. This gave a yield of 30%³⁴⁶ whilst refluxing in acetone for 6 h gave 86%. The IR spectrum (**Figure A7.34**) showed bands 3343 and 3197 cm^{-1} for N–H stretches. The C–N stretch was observed at 1615 cm^{-1} whilst the aromatic C=C stretch occurred at 1577 cm^{-1} . The ^1H NMR spectrum (**Figure A7.35**) of compound **45** showed singlet signals at 13.23 and 11.29 ppm for the N–H protons. Aromatic protons were observed between 7.90 and 7.56

ppm. The ^{13}C NMR spectrum (**Figure A7.36**) showed signals at 179.8 ppm for the C=S. Signals for aromatic carbons occurred between 154.8 and 128.6 ppm.

7.1.16 3-Benzoyl-1-(4-[[phenylformamido)methanethiroyl]amino]butyl)thiourea (54)

The lead ion selective electrodes have been manufactured by synthesizing a benzoyl thioureido group ionophores having two sulfur groups on the both ends of ethane, propane and butane molecules. The ionophore containing propane moiety showed the best responsivity to lead ion. With the 1,3-bis(*N,N'*-benzoylthioureido)propane ionophore, the best result was found when it included with the *o*-nitrophenyloctylether plasticizer with the highest permittivity and the oleic acid additive. The ionophores were synthesized by the reaction of ammonium thiocyanate and benzoyl chloride in acetone for 1 h. 1,2-Daminoethane, 1,3-diaminopropane or 1,4-diaminobutane dissolved in acetone was added and stirred at room temperature for 2 h.³⁴⁸

1,4-Butane diamine reacts through both amino groups hence it reacts with two moles of benzoyl isothiocyanate. The IR spectrum (**Figure 7.10**) showed bands at 3405 and 3217 cm^{-1} for N-H stretch. A band for the C=O stretch was observed at 1666 cm^{-1} . The C-N stretch was observed at 1511 cm^{-1} . The ^1H NMR spectrum (**Figure 7.11**) of compound **54** showed singlet signals at 11.22 and 10.97 ppm. Aromatic protons were observed between 7.89 and 7.50 ppm. Signals for aliphatic protons were observed at 3.76 and 2.06 ppm. The ^{13}C NMR spectrum (**Figure 7.12**) showed a signal at 180.2 ppm for the C=S, whilst a signal at 167.8 ppm was observed for the C=O. Signals for aromatic carbons occurred between 132.6 and 128.4 ppm. Signals for methylene groups were observed at 42.66 and 26.87 ppm.

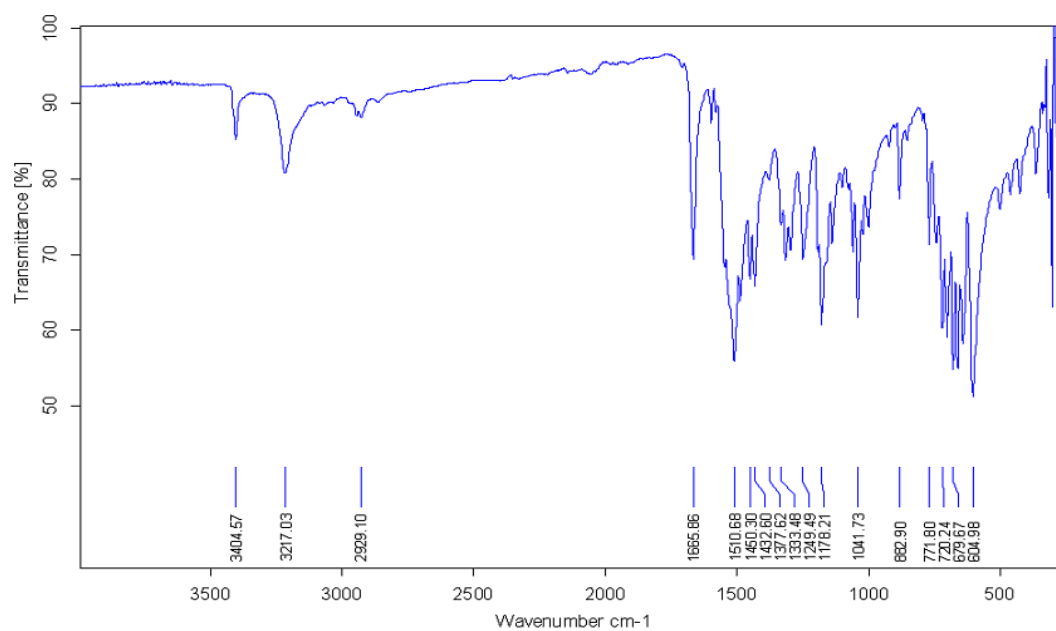


Figure 7.10 IR spectrum of 3-benzoyl-1-(4-[[phenylformamido)methanethioyl]amino]butyl)thiourea (**54**).

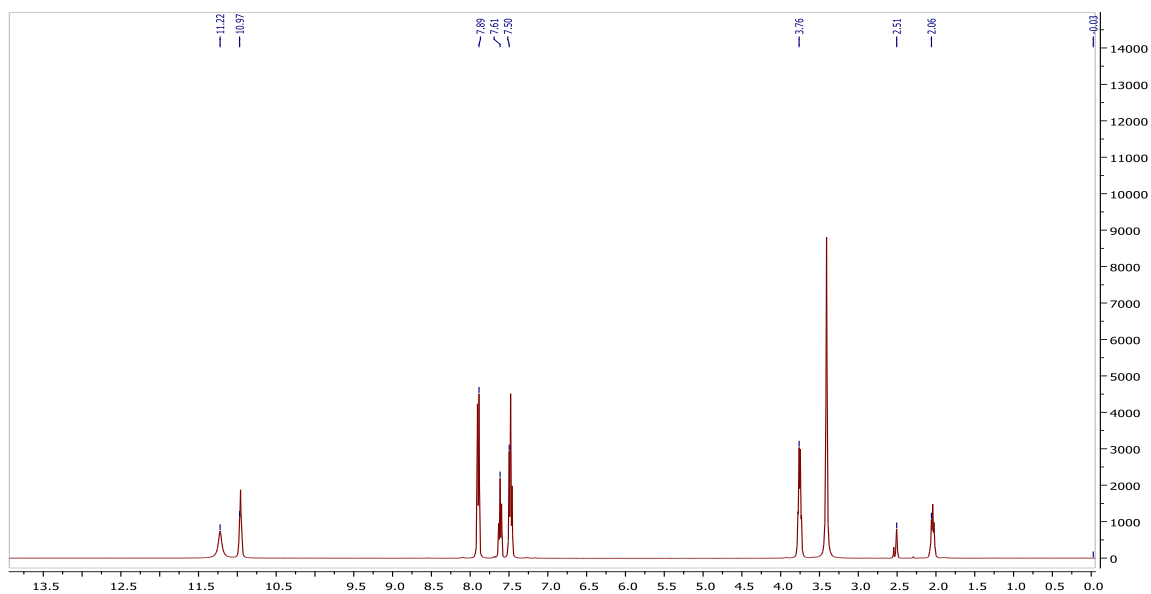


Figure 7.11 ¹H NMR spectrum of 3-benzoyl-1-(4-[[phenylformamido)methanethioyl]amino]butyl)thiourea (**54**).

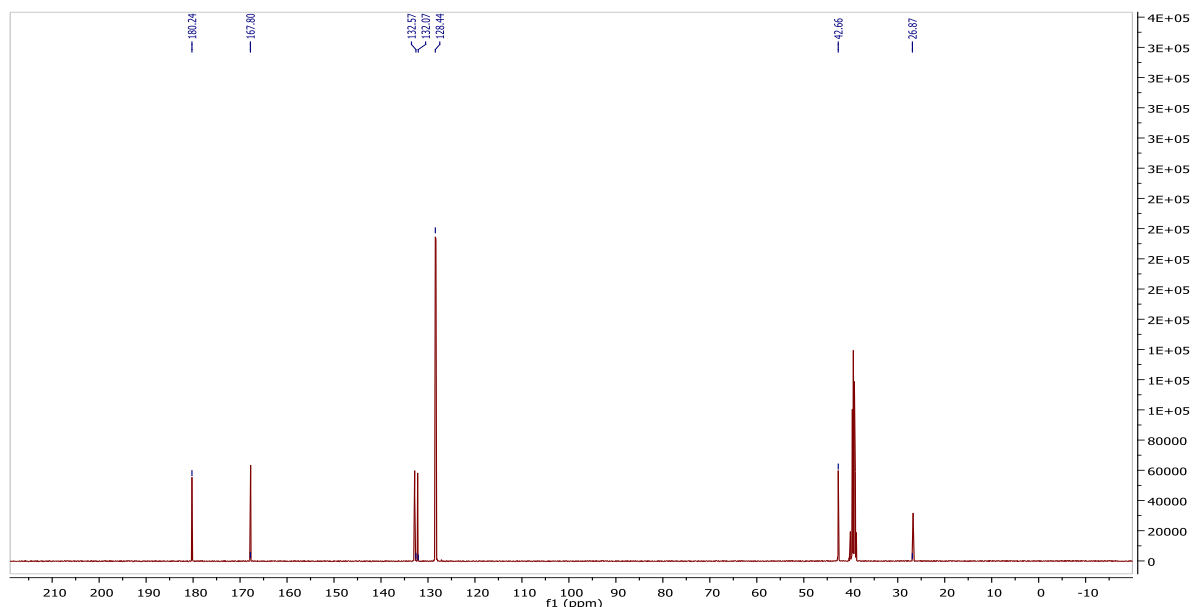


Figure 7.12 ^{13}C NMR spectrum of 3-benzoyl-1-(4-[[[(phenylformamido)methanethioyl]amino] butyl)thiourea (**54**).

7.1.17 Crystal structures of compounds **53** and **54**

Compounds **53** and **54** were recrystallized from DMSO:Toluene (1:3) and obtained as yellow solid and a light brown solid respectively. The crystallographic data, selected bond lengths and bond angles for the crystal structures of compounds **53** and **54** are provided in **Tables 3.26** and **3.27**. The ORTEP diagrams for compounds **53** and **54** are presented in **Figures 7.13** and **7.14**. Compound **53** crystallized in the monoclinic space group $C2/c$, while compound **54** crystallized in the monoclinic space group $P2_1/c$.

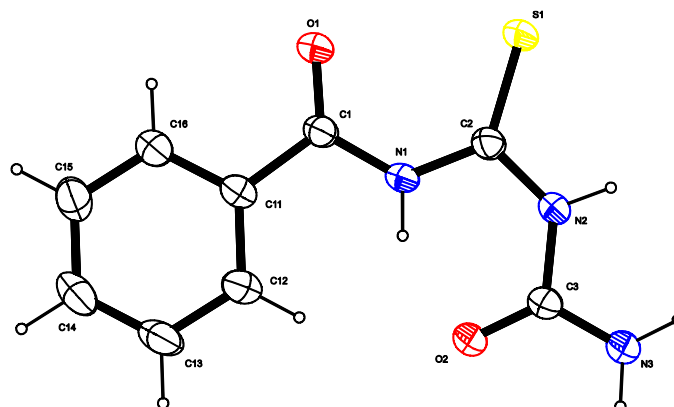
Table 7.3 Crystallographic data and structure refinement summary for compounds **53** and **54**.

Property	53	54
Formula	C ₉ H ₉ N ₃ O ₂ S	C ₂₀ H ₂₂ N ₄ O ₂ S ₂
Formula Weight	223.26	414.56
Crystal System	monoclinic	Monoclinic
Space group	<i>C2/c</i>	<i>P2₁/c</i>
a [Å]	10.2528(5)	5.9962(2)
b [Å]	12.8418(6)	23.2946(10)
c [Å]	16.0986(7)	7.1680(3)
α [°]	90	90
β [°]	106.159(2)	103.777(2)
γ [°]	90	90
V [Å ³]	2035.87(16)	972.42(7)
Z	8	2
D(calc) [g/cm ³]	1.457	1.416
Mu(MoKa) [/mm]	0.301	0.298
F(000)	928	436
Crystal Size [mm]	0.24 x 0.41 x 0.47	0.06 x 0.47 x 0.58
Temperature (K)	200	200
Radiation [Å]	MoKa, 0.71073	MoKa 0.71073
Theta Min-Max [°]	2.6, 28.3	3.1, 28.3
Dataset	-9: 13 ; -13: 17 ; -21: 21	-7: 7 ; -29: 31 ; -9: 9
Tot., Uniq. Data, R(int)	9431, 2514, 0.013	13405, 2402, 0.020
Observed Data [I > 2.0 sigma(I)]	2215	2022
Nref, Npar	2514, 152	2402, 135
R, wR ₂ , S	0.0351, 0.1000, 1.06	0.0339, 0.0931, 1.06
Max. and Av. Shift/Error	0.00, 0.00	0.00, 0.00
Min. and Max. Resd. Dens. [e/Å ³]	-0.58, 0.47	-0.20, 0.32

The bond distance of O1-C1 in compound **53** is 1.215(2) Å, which is consistent with a carbonyl whilst the N1-C1, N1-C2, and N2-C3 bond distances in compound **53** are 1.386(2), 1.367(2) and 1.402(2) Å respectively which are consistent with the C-N single bond. The bond distance of S1-C2 which is 1.648 (2) Å is consistent with a thione. The bond angles of O2-C3-N2 and S1-C2-N1 are 121.8(1) and 127.6(1) respectively shows the carbon atom is sp² hybridized. The torsion angles of C3-N2-C2-S1 and C2-N2-C3-O2 in compound **53** are 174.4(1) and 9.8(2)° suggest that there is restricted rotation in the molecule. In compound **54** the carbonyl O1-C1 was 1.223(2), whilst the thione S1-C2 was 1.673(1). The bond angles of O1-C1-C11, N1-C2-N2 and S1-C2-N2 in compound **54** were 122.1(1), 117.8(1) and 124.7(1) which is characteristic of sp² hybridized carbon.

Table 7.4 Selected bond lengths (Å) and bond angles (°) for compounds **53** and **54**.

Bond lengths (Å)			
53		54	
S1-C2	1.648(1)	S1-C2	1.673(1)
O1-C1	1.215(2)	O1-C1	1.223(2)
O2-C3	1.239(2)	N1-C1	1.374(2)
N1-C1	1.386(2)	N2-C2	1.321(2)
N1-C2	1.367(2)	N2-C3	1.461(2)
N2-C3	1.402(2)	N1-C2	1.390(2)
N3-C3	1.325(2)	C3-C4	1.521(2)
N2-C2	1.374(2)	C4-C4_a	1.522(2)
Bond angles (°)			
53		54	
C1-N1-C2	128.8(1)	C1-N1-C2	129.3(1)
C2-N2-C3	128.6(1)	C2-N2-C3	122.3(1)
N2-C3-N3	113.9(1)	O1-C1-C11	122.1(1)
O2-C3-N3	124.4(1)	N1-C2-N2	117.8(1)
S1-C2-N2	118.2(1)	S1-C2-N2	124.7(1)
N1-C2-N2	114.2(1)	N2-C3-C4	112.4(1)
O2-C3-N2	121.8(1)	S1-C2-N1	117.5(1)
S1-C2-N1	127.6(1)	N1-C1-C11	115.4(1)
O1-C1-N1	123.2(1)	O1-C1-N1	122.5(1)

**Figure 7.13** An ORTEP view of 3-benzoyl-1-[(phenylformido)methanethioyl]amino}thiourea (**53**) showing 50% probability displacement ellipsoids and the atom labelling.

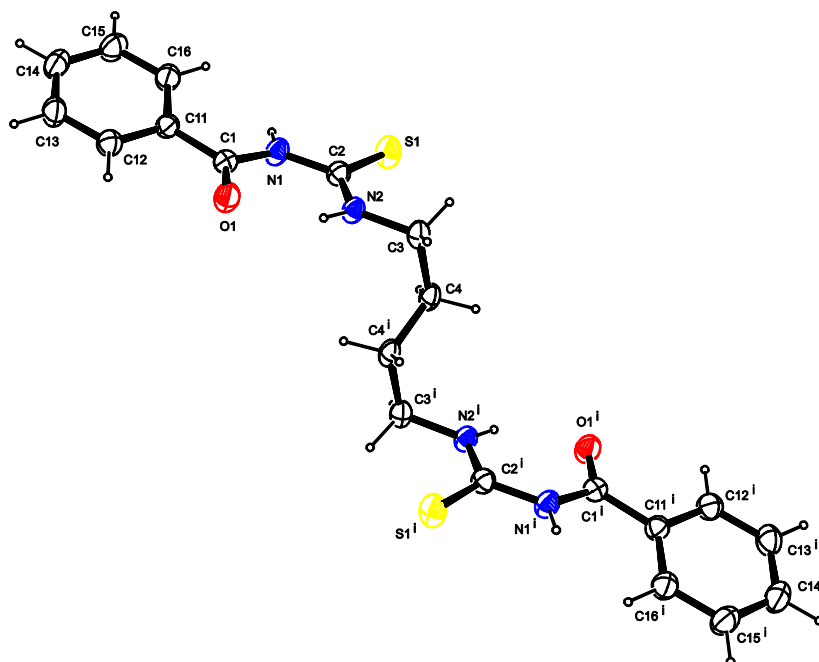


Figure 7.14 An ORTEP view of 3-benzoyl-1-(4-((phenylformamido) methanethioyl) amino)butyl)thiourea (**54**) showing 50% probability displacement ellipsoids and the atom labelling.

7.2 Biochemical studies

7.2.1 Cell viability and cytotoxicity tests

The acute cytotoxic effects of benzoyl isothiocyanate derivatives of diamines were determined by exposing them to isolated human white blood cells, for a 24-hour period. The cell viability was assessed using the MTT reduction assay and the results are presented in **Table 7.4** which indicates the compound numbers (in bold) as well as the EC₅₀ values calculated for each compound tested.

Table 7.5 Cell viability results for diamine derivatives of benzoyl isothiocyanate derivatives.

Diamines	EC ₅₀ μM
40	204.5
41	191.7
42	147.9
43	130.5
44	481.7
45	264.0
46	17.0
47	100.0
48	69.2
49	35.9
50	211.6
51	479.3
52	279.6
53	260.5
54	68.4

The EC₅₀ values for the diamine derivatives (**Figure 7.15**) of benzoyl isothiocyanate showed varying effects of the inhibitors on the cell viability of human white blood cells. Compounds **46** (4-bromo derivative) and **48** (3-chloro derivative) gave EC₅₀ values of $17.04 \pm 9.75 \mu\text{M}$ and $69.20 \pm 38.160 \mu\text{M}$, respectively, whilst compound **54** (1,4-butane diamine) and **49** (3-bromo), which were also cytotoxic, gave EC₅₀ values of $68.37 \pm 26.45 \mu\text{M}$ and $35.90 \pm 20.55 \mu\text{M}$. Substitution at position three with a bromo and a chloro leads to an increase in its cytotoxic effects among the diamine derivatives. Similarly, a substitution at position four with bromo also leads to an increase in cytotoxic effects among the diamine derivatives.

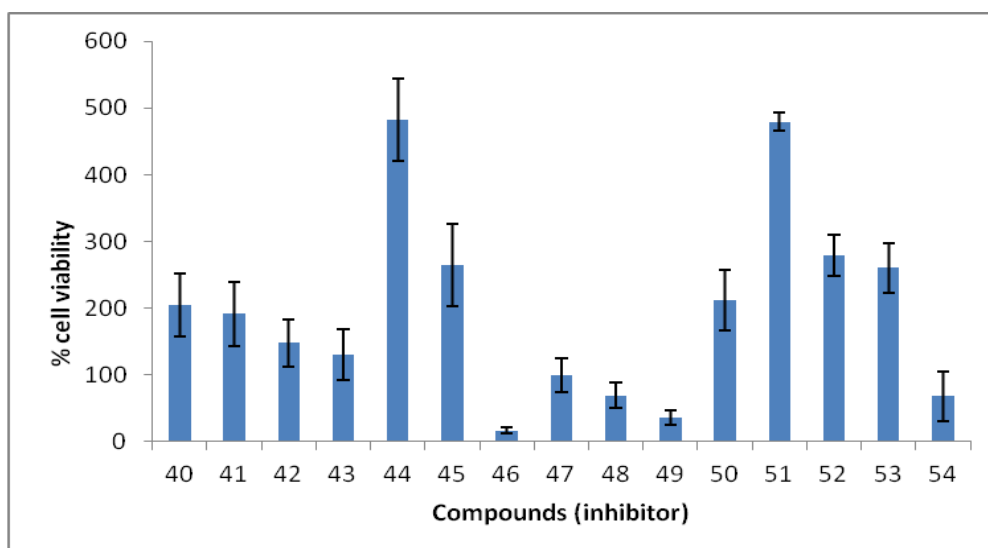


Figure 7.15 EC_{50} values for the diamine derivatives of benzoyl isothiocyanate (μM). Error bars represent the SEM for $n = 3$.

The cytotoxicity test of compounds **46** and **40** which are the most and least cytotoxic compounds, respectively, among the diamine derivatives of benzoyl isothiocyanate, depicted in **Figure 7.16**. The presence of the bromo group (**46**) at position four in the diamines leads to an increase in cytotoxicity, whilst the presence of the methyl group (**40**) at position three on the phenylenediamine in the diamines leads to a decrease in cytotoxicity.

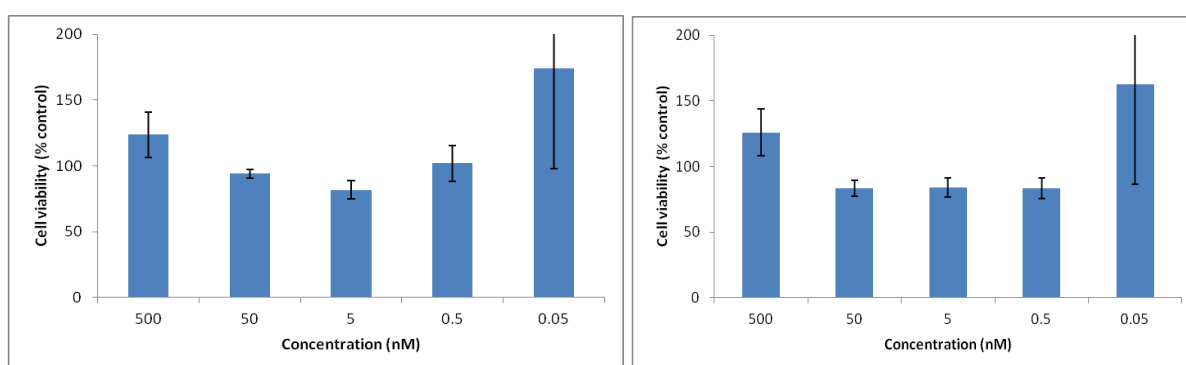


Figure 7.16 EC_{50} values for compounds **46** and **40** (μM). Error bars represent the SEM for $n = 3$.

7.2.2 HIV-1 protease screen of structurally diverse diamine derivatives of benzoyl isothiocyanate

Table 7.6 and **Figure 7.17** gives the HIV-1 screening results for the diamine derivatives of benzoyl isothiocyanate. The screening of the compounds was done at 100 μM of inhibitor and that for ritonavir was done at 10 μM . All the compounds gave a percentage inhibition lower than 40% of the untreated control except compound **49** which gave a percentage inhibition of $97.03 \pm 10.61\%$ compared to the untreated control. Compound **48** gave the best inhibition constant of 0.060 μM in the *in silico* results among the diamine derivatives does not inhibit HIV-1 protease significantly at 100 μM . The deviation from the predicted inhibition constants observed in the *in silico* results may be due to solvent effect and the complex matrix introduced by the presence of buffers and intermolecular interaction between inhibitor molecules. In the model, the inhibitor was placed in a defined space in the active site and the interactions were computed whilst in the actual assay the inhibitor had to navigate the solvent matrix to the active site to elicit any activity. Compound **49** (3-bromo derivative) gave high % inhibition it should be noted it is cytotoxic to white blood cells. That notwithstanding derivatizing compound **49** might improve its activity and reduce the cytotoxic effects in its analogues.

Table 7.6 HIV-1 protease screening results of some diamines derivatives of benzoyl isothiocyanate.

Compound	Fluorescence	Standard deviation	% Activity relative to untreated control	% Inhibition relative to untreated control
Ritonavir	36.24	1.88	9.34	90.66
40	186.01	9.605	82.31	17.69
41	202.70	6.12	89.70	10.30
42	155.85	0.418	68.97	31.03
43	402.60	4.103	103.79	0
44	152.13	11.03	67.32	32.68
45	243.51	4.6	107.76	0
46	159.05	4.103	70.38	29.62
47	446.80	2.43	115.18	0
48	381.00	11	98.22	1.78
49	11.522	0.37	2.97	97.03
51	147.94	20.69	65.4	34.53
52	145.79	5.238	64.516	35.49
53	268.44	10.605	69.20	30.80
54	151.00	0.1584	66.82	33.18

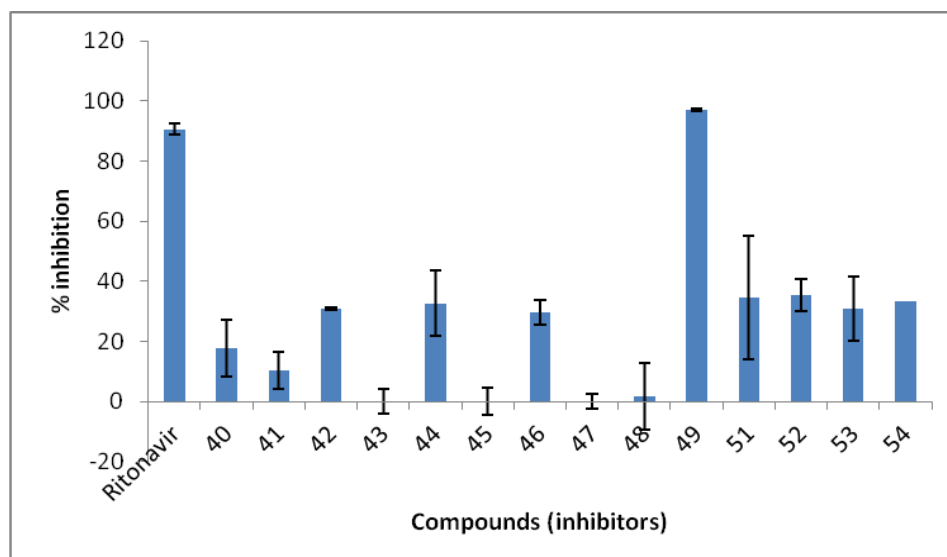


Figure 7.17 HIV-1 protease screening results illustrating % inhibition of selected diamine derivatives of benzoyl isothiocyanate (100 μM) and ritonavir (10 μM) relative to untreated control. Error bars represent SEM of $n = 3$.

The predicted inhibition constants of between 0.06 and 1.90 μM were the best predicted inhibition constants and this was consistent with the results from the bioassay as these compounds gave the best inhibition against HIV-1 protease. This is due to the fact that these compounds are bigger and fit into the active site better and interact or binds to more amino acid residues in the active site of protease making them more effective inhibitors. This can be seen in **Figures 7.18, 7.19, 7.20** and **7.21** which give the 2D representation of compounds **47, 54, 46** and **49** respectively in the protease active site. The presence of polar group on this class of compounds improves the extent of interaction at the active site both in the docking studies and the bioassays making this class of compounds more active against protease.

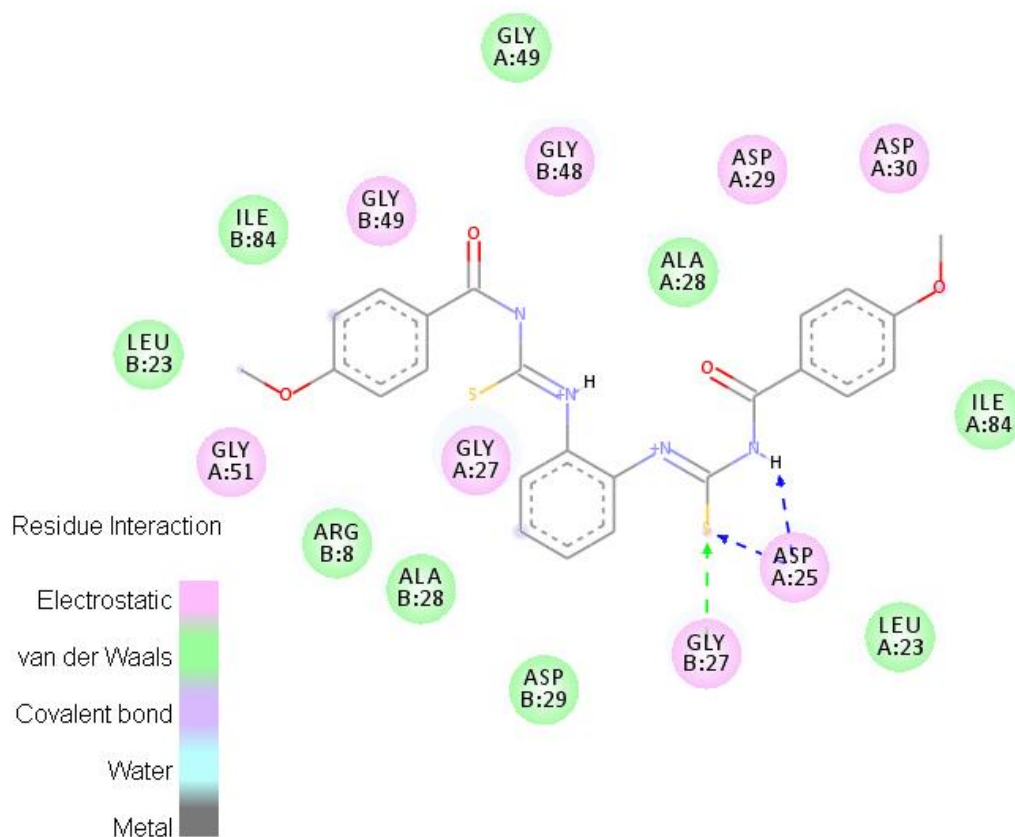


Figure 7.18 2D representation of 1-(4-methoxybenzoyl)-3-[2-((4-methoxyphenyl)formamido)methanethiyl]amino)phenyl]thiourea (**47**) in the HIV-1 protease binding site.

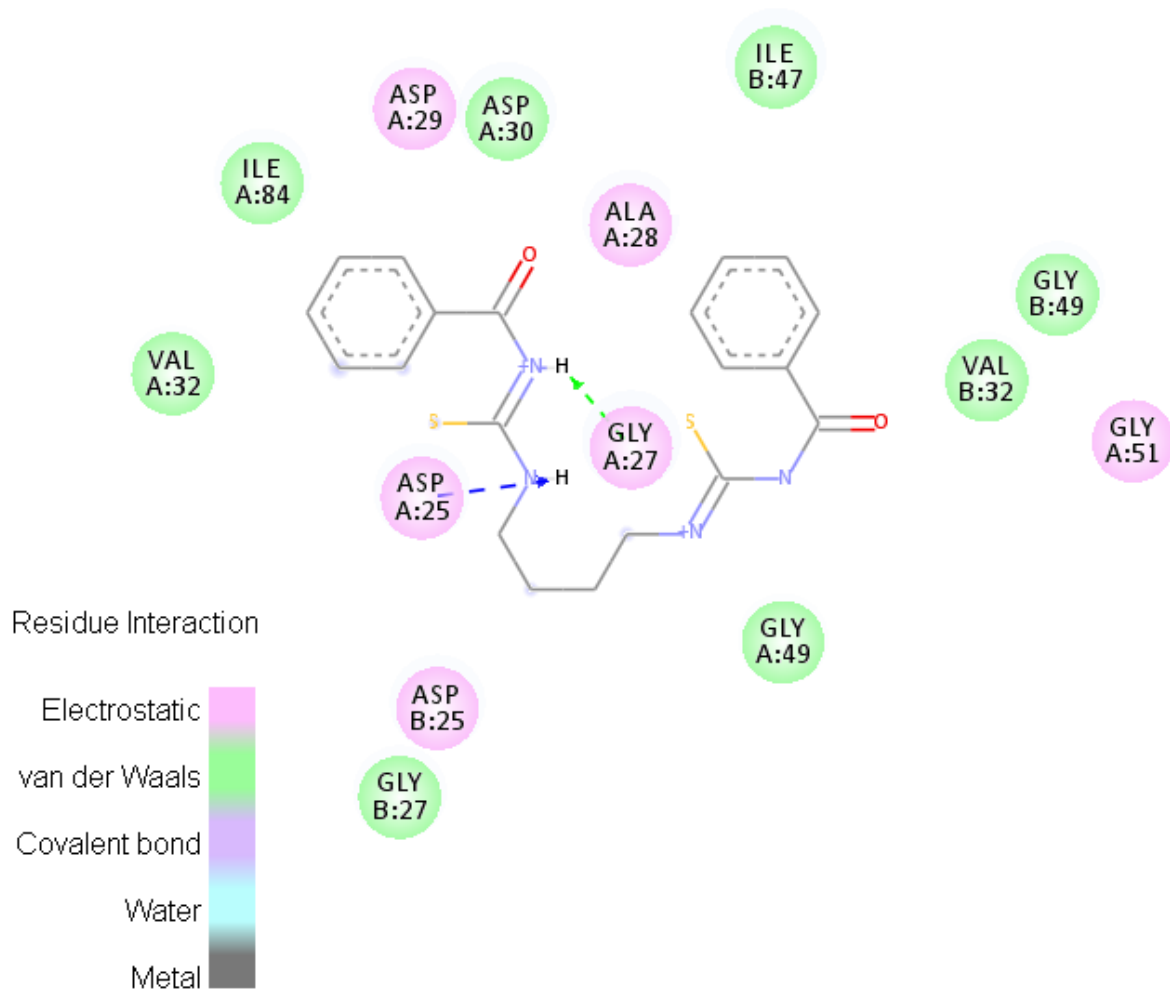


Figure 7.19 2D representation of 3-benzoyl-1-(4-((phenylformamido)methanethioyl)amino)butylthiourea (**54**) in the HIV-1 protease binding site.

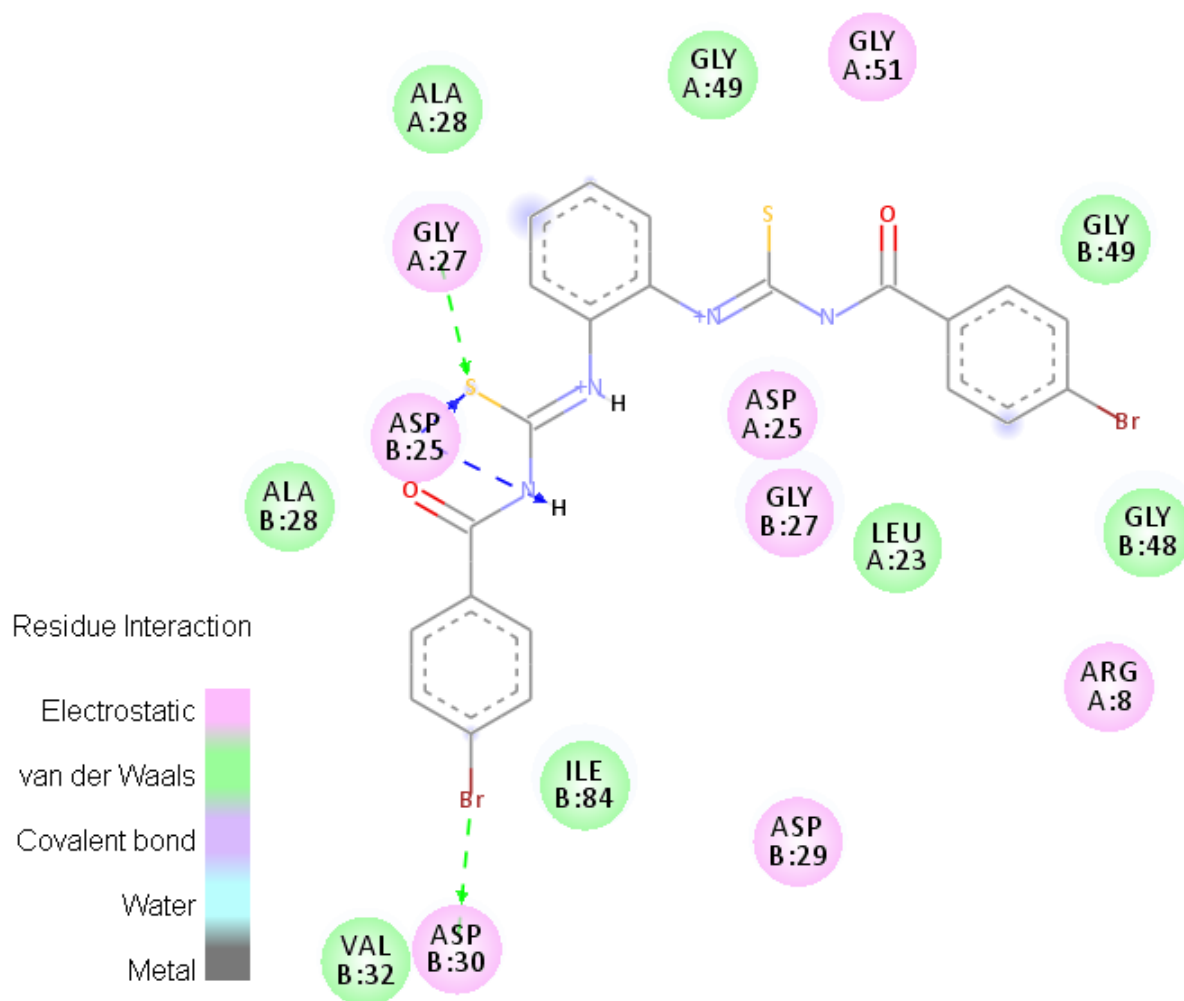


Figure 7.20 2D representation of 1-(4-bromobenzoyl)-3-[2-((4-bromophenyl)formamido)methanethioyl]amino)phenyl]thiourea (**46**) in the HIV-1 protease binding site.

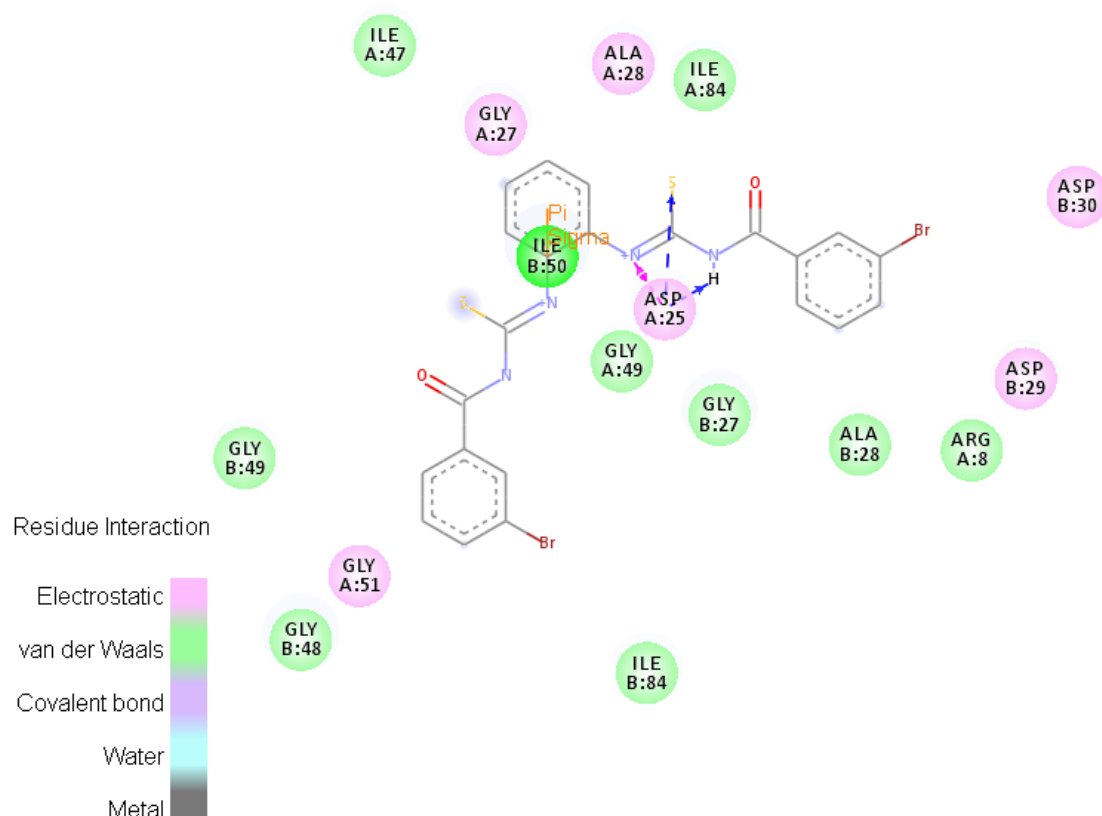


Figure 7.21 2D representation of 1-(3-bromobenzoyl)-3-[2-(((3-bromophenyl)formamido)methanethioyl)amino)phenyl]thiourea (**49**) in the HIV-1 protease binding site.

7.3 Conclusions

-Structurally diverse aromatic and aliphatic diamine derivatives of benzoyl isothiocyanates have been synthesized and characterized by spectroscopy, microanalysis and GC-MS.

-The single crystal XRD molecular structures of 1-benzoyl-3-(5-methyl-2-(((phenylformamido)methanethioyl)amino)phenyl)thiourea (**40**), 3-benzoyl-1-(2-(((phenylformamido)methanethioyl)amino)ethyl)thiourea (**50**), 3-benzoyl-1-(((phenylformido)methanethioyl)amino)thiourea (**51**), 3-benzoyl-1-(((phenylformido)methanethioyl)amino)thiourea (**53**), 3-benzoyl-1-(4-(((phenylformamido)methanethioyl)amino)butyl)thiourea (**54**) have been discussed.

-The cell viability tests of the diamines derivatives showed that 1-(4-bromobenzoyl)-3-[2-(((4-bromophenyl)formamido)methanethiyl)amino)phenyl]thiourea (**46**) and 1-(3-chlorobenzoyl)-3-[2-(((3-chlorophenyl)formamido)methanethiyl)amino)phenyl]thiourea (**48**) were cytotoxic with EC_{50} values of $17.04 \pm 9.75 \mu\text{M}$ and $69.20 \pm 38.160 \mu\text{M}$ respectively, whilst 1-(3-bromobenzoyl)-3-[2-(((3-bromophenyl)formamido)methanethiylamino)phenyl]thiourea (**49**), 3-benzoyl-1-(4-(((phenylformamido)methanethiyl)amino)butyl)thiourea (**54**) which were also cytotoxic gave EC_{50} values of 35.90 ± 20.55 and $68.37 \pm 26.45 \mu\text{M}$.

-The HIV-1 protease assay of 1-(3-bromobenzoyl)-3-[2-(((3-bromophenyl)formamido)methanethiylamino)phenyl]thiourea (**49**) gave an inhibition of 97% at an inhibitor concentration of $100 \mu\text{M}$ and a protease concentration of 20 nM .

CHAPTER EIGHT

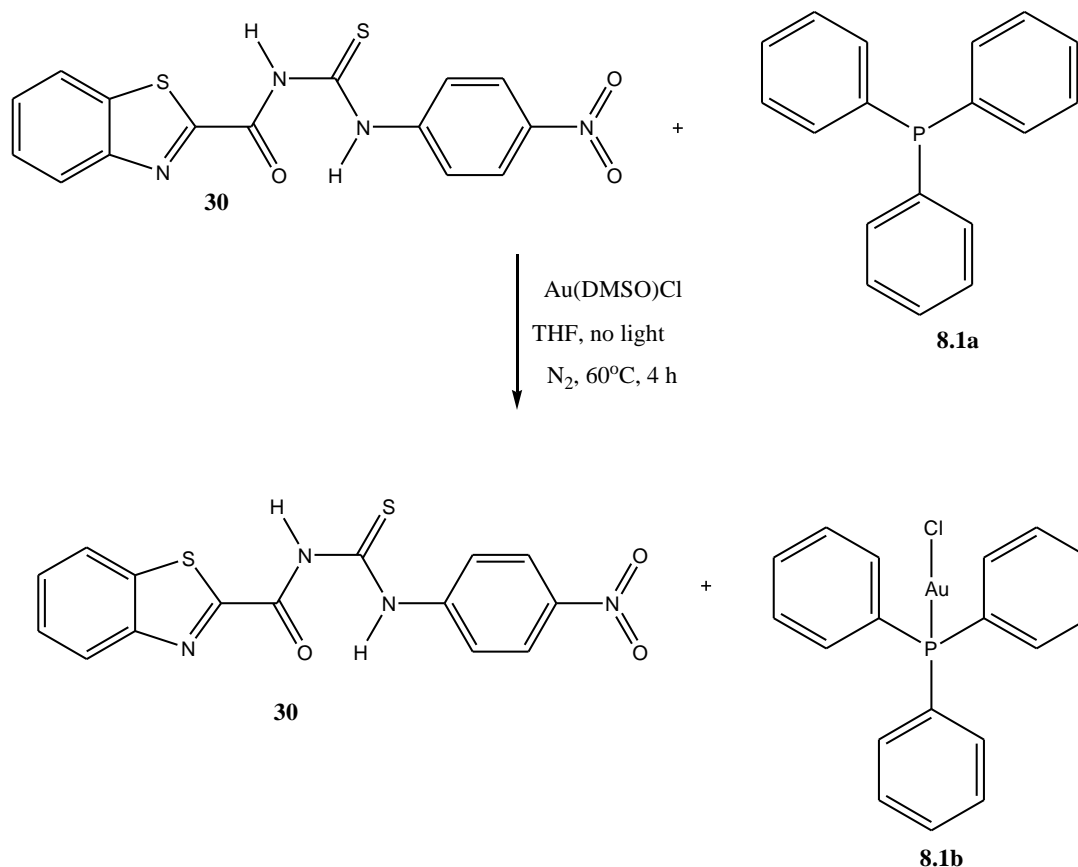
GOLD AND SILVER CATALYZED REACTIONS OF BENZOYL ISOTHIOCYANATE DERIVATIVES

8.1 Attempted synthesis of gold compounds

The attempted synthesis of gold compounds using 3-(1,3-benzothiazol-2-yl)-1-(benzoyl)thiourea derivatives led to the formation of benzamides. Benzamides have been developed through the cleavage of sp^3 C-Ph bond of methyl arenes with *N*-substituted formamides.³⁴⁹ Various benzamides have been prepared in low to moderate yields.³⁴⁹ A procedure for the oxidative synthesis of amides from styrenes and amines has been developed.³⁵⁰ Various primary and secondary amides were formed in moderate yields (25–81%).³⁵⁰ Synthesis of amides by aerobic oxidative coupling of alcohols or aldehydes with amines using a catalytic system comprised of supported gold nanoparticles in methanol has been reported as a highly efficient and selective process.³⁵¹ Pathway for both *N*-benzoylation and *N*-acetylation of anilines, amines, diamines, and aminoalcohols using enol esters have been accessed in good yields.³⁵² The enantioselective synthesis of atropisomeric tertiary benzamides employing catalytic electrophilic aromatic substitution reactions have been reported.³⁵³ $PtCl_2$ or $AuBr_3$ (1–3 mol %) has been used to promote the generation and [3+2] cycloaddition of transition-metal-containing azomethine ylides derived from *N*-(*o*-alkynylphenyl)imines bearing an internal alkyne moiety. Tricyclic indole derivatives having a substituent at the 3-position of the indole nucleus have been accessed by this method.³⁵⁴ A gold-catalyzed nitrene transfer reaction has been reported in which a gold(I) compound, supported by 4,4',4''-*tri-tert*-butyl-2,2':6',2''-terpyridine (tBu_3tpy) as the ligand, efficiently catalyzes olefin aziridination with the use of $PhI(OAc)_2$ and sulfonamides. This system also mediates carbene insertion into benzene.³⁵⁵ A complimentary diamination of alkenes by using homogeneous gold catalysts has been reported. The key step is an intramolecular alkyl–nitrogen bond formation from a gold(III) intermediate. This process validates the concept of reductive elimination from high oxidation catalyst states for this type of C–N bond forming reactions.³⁵⁶

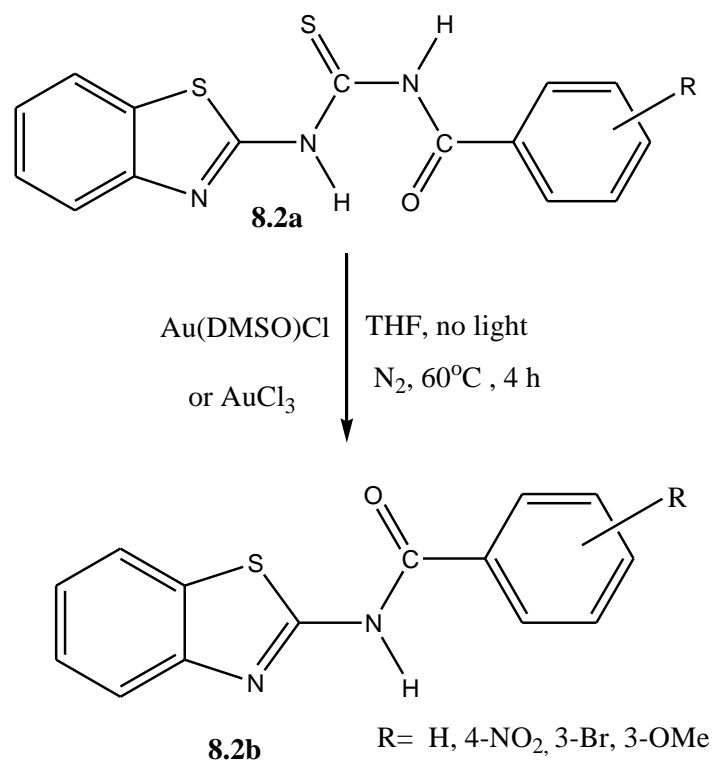
Our attempt to make gold complexes of sulfur-containing ligands gave varying results. An attempted reaction of chlorotriphenylphosphinegold(I) with the ligands in the presence of

silver oxide in acetonitrile and dichloromethane led to the recovery of the triphenylphosphine whilst the ligand was decomposed. Another attempt with triphenylphosphine, the ligands and chlorodimethylsulfoxidegold(I) also resulted in the formation of chlorotriphenylphosphine gold(I) (**Scheme 8.1**) Another attempt with 3-(1,3-benzothiazol-2-yl)-1-(4-nitrobenzoyl) thiourea, triphenylphosphine and chlorodimethylsulfoxidegold(I) in tetrahydrofuran under nitrogen and the absence of light also gave chlorotriphenylphosphinegold(I) whilst the ligand was recovered.



Scheme 8.1 Attempted synthesis of gold complex of benzothiazole derivatives.

Another to synthesize the gold complexes of the 3-(1,3-benzothiazol-2-yl)-1-(4-benzoyl)thiourea derivatives (**Scheme 8.2**) led to the gold catalyzed dethiocyanation of 3-(1,3-benzothiazol-2-yl)-1-(4-benzoyl)thiourea derivatives to give benzamides.



Scheme 8.2 Attempted synthesis of gold complexes of 3-(1,3-benzothiazol-2-yl)-1-(4-benzoyl)thiourea derivatives.

Due to the very small quantities of material used in the synthesis of these compounds very small amounts of products were obtained hence concentrated samples were not obtained for the ^{13}C NMR spectral analysis of these compounds. Hence the products were conclusively characterized using IR, GC-MS, microanalysis and single crystal XRD in tandem.

8.1.1 *N*-(Benzothiazol-2-yl)-4-nitrobenzamide (55)

This is thought to proceed by the attack of gold by the sulfur due to its strong affinity for gold. A suspected electron redistribution converts the gold(I) to with a gold(0) which is a by-product whilst the thiocyanate is lost from the ligand in the process. A detailed mechanism has not been investigated yet but the final product suggests a gold-catalysed dethiocyanation and a C-N coupling to form an amide. The IR spectrum (**Figure A8.1**) showed an N-H stretch of an amide at 3117 cm^{-1} , a band for the C=O stretch was observed at 1686 cm^{-1} and the C=N stretch was observed at 1599 cm^{-1} . Whilst the aromatic C=C stretch was observed at 1522 cm^{-1} . The ^1H NMR spectrum (**Figure A8.2**) gave signals between 8.39 and 7.37 ppm

for aromatic protons. The ^{13}C NMR spectrum (**Figure A8.3**) gave signals between at 130.4 and 124.1 for aromatic carbons.

8.1.2 *N*-(Benzothiazol-2-yl)-3-bromobenzamide (56)

The reaction is thought to proceed in a similar manner to compound **55**. The IR spectrum (**Figure A8.4**) showed an N–H stretch at 3066 cm^{-1} , a band for the C=O stretch was observed at 1677 cm^{-1} and the aromatic C=C was observed at 1555 cm^{-1} . The ^1H NMR spectrum (**Figure A8.5**) ^{13}C NMR spectrum of *N*-(benzothiazol-2-yl)-4-nitrobenzamide (**55**) gave signals between 8.35 and 7.36 ppm for aromatic protons. The ^{13}C NMR spectrum (**Figure A8.6**) gave signals between at 131.5 and 122.5 for aromatic carbons.

8.1.3 *N*-(Benzothiazol-2-yl)-3-methoxybenzamide (57)

The reaction is thought to proceed in a similar manner to compound **55**. The IR spectrum (**Figure A8.7**) showed an N–H stretch at 3458 cm^{-1} , the bands for the aliphatic C–H stretch were observed at 2922 and 2852 cm^{-1} , a band for the C=O stretch was observed at 1686 cm^{-1} and the aromatic C=C and the C–N stretch were observed at 1604 and 1578 cm^{-1} , respectively. The ^1H NMR spectrum (**Figure A8.8**) gave a signal at 11.580 ppm for the proton of an amine. Signals between 8.02 and 7.21 ppm were observed for aromatic protons. The ^{13}C NMR spectrum (**Figure A8.9**) gave signals between at 159.7 and 109.5 for aromatic carbons, whilst a signal for the methoxy group was observed at 55.8 ppm.

8.1.4 *N*-(Benzothiazol-2-yl)benzamide (58)

The reaction is thought to proceed in a similar manner to compound **55**. The IR spectrum (**Figure 8.1**) showed an N–H stretch at 3273 cm^{-1} , a band for the C=O stretch was observed at 1693 cm^{-1} and the aromatic C=C and the C–N stretches were observed at 1599 and 1549 cm^{-1} , respectively. The ^1H NMR spectrum (**Figure 8.2**) gave signals between 8.35 and 7.36 ppm for aromatic protons. The ^{13}C NMR spectrum (**Figure 8.3**) gave signals between at 136.1 and 122.3 for aromatic carbons.

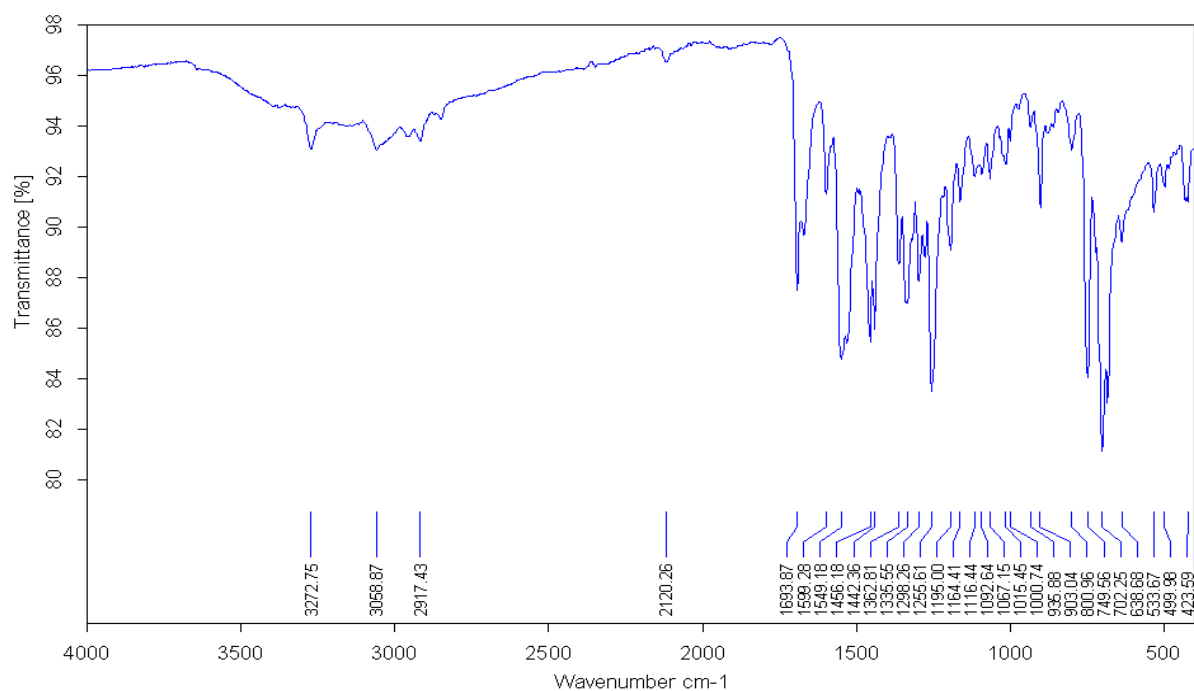


Figure 8.1 IR spectrum of *N*-(benzothiazol-2-yl)-benzamide (**58**).

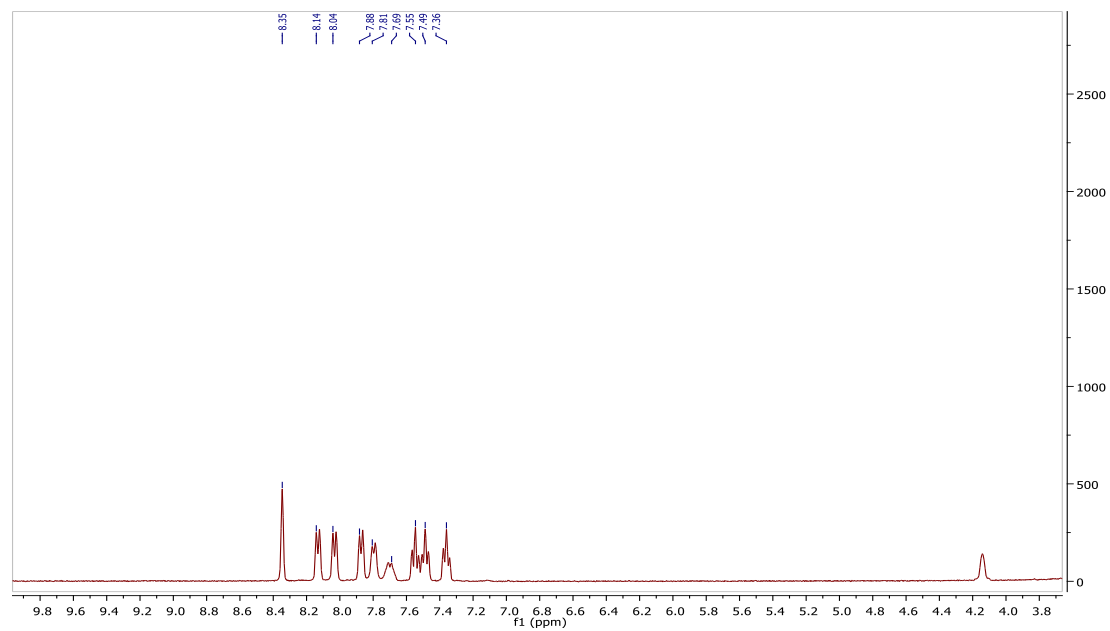


Figure 8.2 ¹H NMR spectrum of *N*-(benzothiazol-2-yl)-benzamide (**58**).

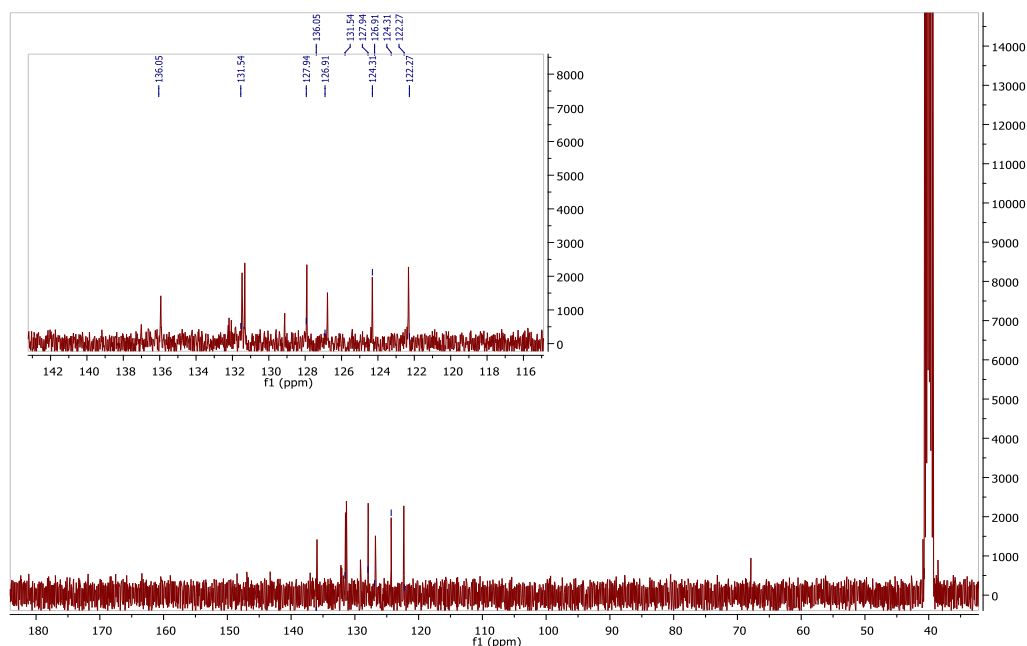


Figure 8.3 ^{13}C NMR spectrum of *N*-(benzothiazol-2-yl)-benzamide (**58**).

8.1.5 Crystal structures of compounds **55**, **56**, **58** and chlorotriphenylphosphinegold(I).

Compounds **55**, **56**, **58** and chlorotriphenylphosphinegold(I) were recrystallized from methanol. The crystallographic data, selected bond lengths and bond angles for the crystal structures of compounds **55**, **56**, **58** and triphenyl phosphine are provided in **Tables 8.1** and **8.2**. The ORTEP diagrams for compounds **55**, **56**, **58** and triphenyl phosphine are presented in **Figures 8.4**, **8.5** and **8.6** respectively. Compound **55** crystallized in the orthorhombic space group *Pbcn* while compound **56** crystallized in the triclinic space group *P-1*. Compound **58** crystallized in the monoclinic space group *P21/n*. The ORTEP diagram of chlorotriphenylphosphinegold(I) is presented in **Figure 8.7** and the complex crystallized in the orthorhombic space *P2₁2₁2₁*.

Table 8.1 Crystallographic data and structure refinement summary for compounds **55**, **56**, **58** and chlorotriphenylphosphinegold(I)

Property	55	56	58	Au(PPh₃)Cl
Formula	C ₁₄ H ₉ N ₃ O ₃ S	C ₁₄ H ₉ BrN ₂ OS	C ₁₄ H ₁₀ N ₂ OS	C ₁₈ H ₁₅ AuCIP
Formula Weight	299.30	333.19	254.30	494.69
Crystal System	Orthorhombic	Triclinic	Monoclinic	Orthorhombic
Space group	<i>Pbcn</i>	<i>P-1</i>	<i>P21/n</i>	<i>P2₁2₁2₁</i>
a [Å]	29.023(4)	5.9083(3)	5.9236(4)	10.1354(4)
b [Å]	7.7882(10)	7.6853(4)	16.7628(10)	12.3093(5)
c [Å]	11.5676(17)	14.4978(8)	11.8749(7)	13.0568(5)
α [°]	90	77.501(2)	90	90
β [°]	90	78.463(3)	102.305(2)	90
γ [°]	90	89.036(3)	90	90
V [Å ³]	2614.7(6)	629.47(6)	1152.04(12)	1628.96(11)
Z	8	2	4	4
D(calc) [g/cm ³]	1.521	1.758	1.466	2.017
Mu(MoKa) [/mm]	0.262	3.422	0.268	9.283
F(000)	1232	332	528	936
Crystal Size [mm]	0.15 x 0.30 x 0.51	0.03 x 0.17 x 0.50	0.34 x 0.40 x 0.74	0.26 x 0.31 x 0.63
Temperature (K)	273	200	200	200
Radiation [Å]	MoKa 0.71073	MoKa 0.71073	MoKa 0.71073	MoKa 0.71073
θ Min-Max [°]	2.7, 28.4	2.7, 28.3	2.1, 28.3	2.3, 28.3
Dataset	-38: 38 ; -10: 6 ; -15: 15	-7: 7 ; -8: 10 ; -18: 19	-7: 7 ; -22: 20 ; -15: 14	-11: 13 ; -16: 16 ; -17: 17
Tot., Uniq. Data, R(int)	29350, 3272, 0.025	11395, 3118, 0.029	10261, 2851, 0.012	27916, 4037, 0.036
Observed data [I > 2.0 sigma(I)]	2537	2603	2659	3887
Nref, Npar	3272, 194	3118, 176	2851, 167	4037, 190
R, wR ₂ , S	0.0440, 0.1303, 1.09	0.0283, 0.0710, 1.05	0.0302, 0.0820, 1.05	0.0182, 0.0455, 1.09
Max. and Av. Shift/Error	0.00, 0.00	0.00, 0.00	0.00, 0.00	0.00, 0.00
Min. and Max. Resd. Dens. [e/Å ³]	-0.37, 0.34	0.42, 0.52	-0.24, 0.38	-1.52, 0.69

The bond distance of O1-C2 in compounds **55**, **56** and **58** are 1.213(2), 1.216(1) and 1.221(1) respectively, which is consistent with a carbonyl whilst the S1-C1 bond distances were 1.737(2), 1.747(2) and 1.750(1) Å respectively are consistent with the C=S bond. The bond angle of C1-S1-C12 in compounds **55**, **56** and **58** are 88.3(1), 87.9(1) and 88.10(5) (°) respectively whilst the bond angle of S1-C1-N1 in compounds **55**, **56** and **58** are 116.9(1), 117.5(2) and 117.2(1) (°). The bond distances of Au1-P1 and Au-Cl1 in Au(PPh₃)Cl

triphenylphosphine is 1.816(4) and 2.229(1) respectively whilst the bond angles of Cl1-Au1-P1 and Au1-P1-C11 are 114.2(1) and 11.9(1) respectively.

Table 8.2 Selected bond lengths (Å) and bond angles (°) for compounds for compounds **55**, **56**, **58** and chlorotriphenylphosphinegold(I)

Bond lengths (Å)					
55		56	58	Au(PPh ₃)Cl	
S1-C1	1.737(2)	1.747(2)	1.750(1)	P1-C31	1.378(6)
S1-C12	1.734(2)	1.741(2)	1.741(1)	Au1-Cl1	2.229(1)
O1-C2	1.213(2)	1.216(2)	1.221(1)	Au1-P1	1.816(4)
N1-C11	1.393(2)	1.391(3)	1.397(1)	P1-C11	1.813(4)
N1-C1	1.296(2)	1.301(2)	1.300(1)	P1-C21	1.816(4)
N2-C2	1.367(2)	1.370(2)	1.375(1)		
N2-C1	1.375(2)	1.375(3)	1.381(1)		
Bond Angles (°)					
55		56	58	Au(PPh ₃)Cl	
C1-S1-C12	88.3(1)	87.9(1)	88.1(1)	C11-P1-C21	103.9(2)
C1-N1-C11	109.8(2)	109.3(2)	109.7(1)	Cl1-Au1-P1	114.2(1)
C1-N2-C2	123.2(2)	124.0(2)	124.1(1)	Au1-P1-C11	111.9(1)
S1-C1-N1	116.9(1)	117.5(2)	117.2(1)	Au1-P1-C21	112.8(1)
S1-C1-N2	121.8(1)	121.4(1)	121.8(1)	Au1-P1-C31	105.8(2)

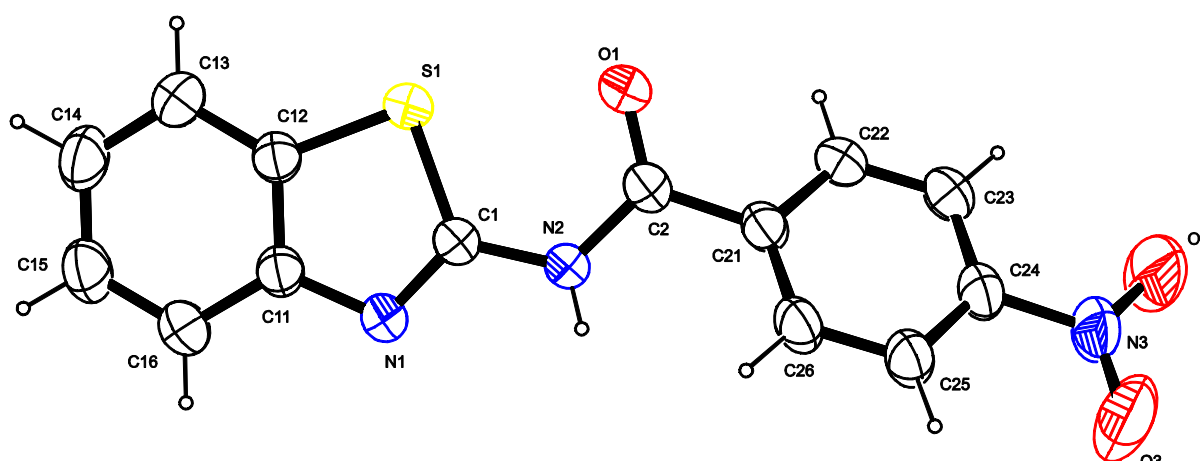


Figure 8.4 An ORTEP view of *N*-(benzothiazol-2-yl)-4-nitrobenzamide (**55**) showing 50% probability displacement ellipsoids and the atom labelling.

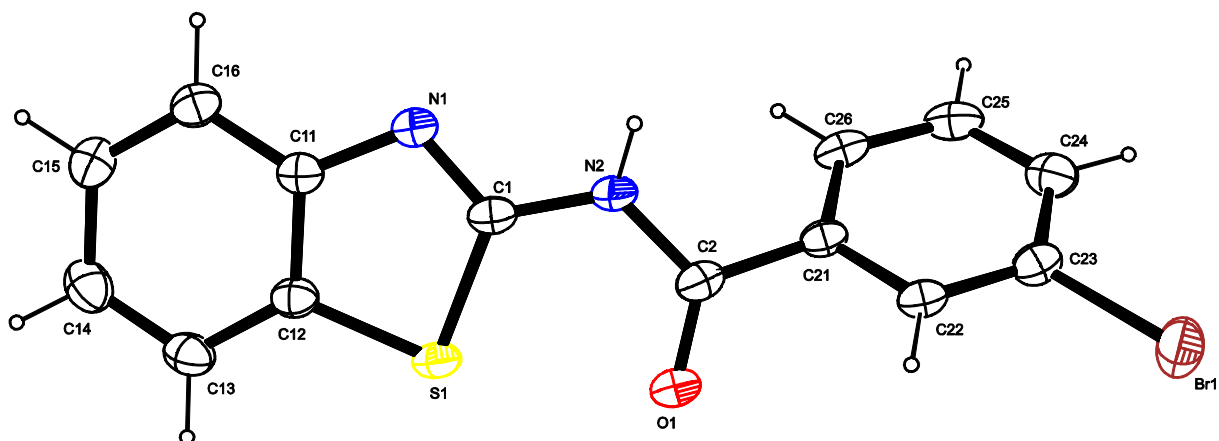


Figure 8.5 An ORTEP view of *N*-(benzothiazol-2-yl)-3-bromobenzamide (**56**) showing 50% probability displacement ellipsoids and the atom labelling.

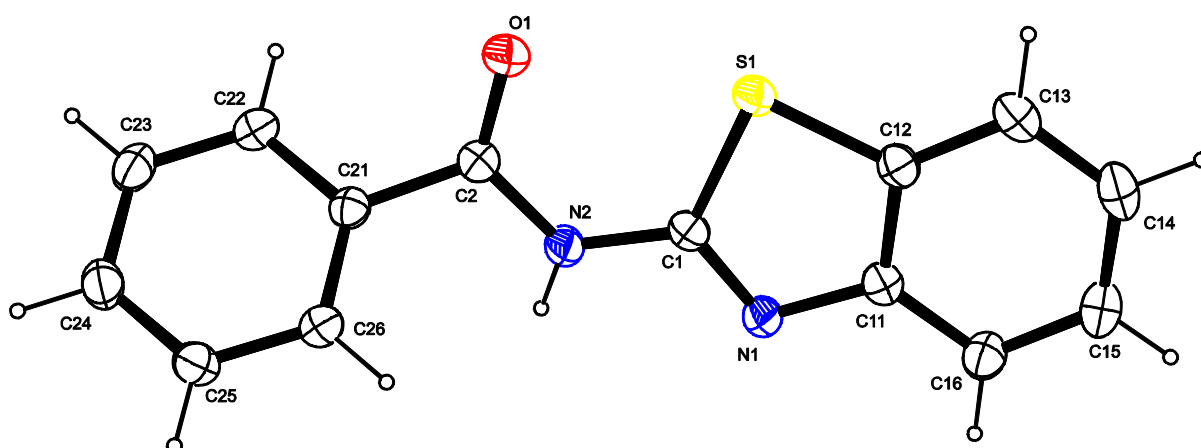


Figure 8.6 An ORTEP view of *N*-(benzothiazol-2-yl)benzamide (**58**) showing 50% probability displacement ellipsoids and the atom labelling.

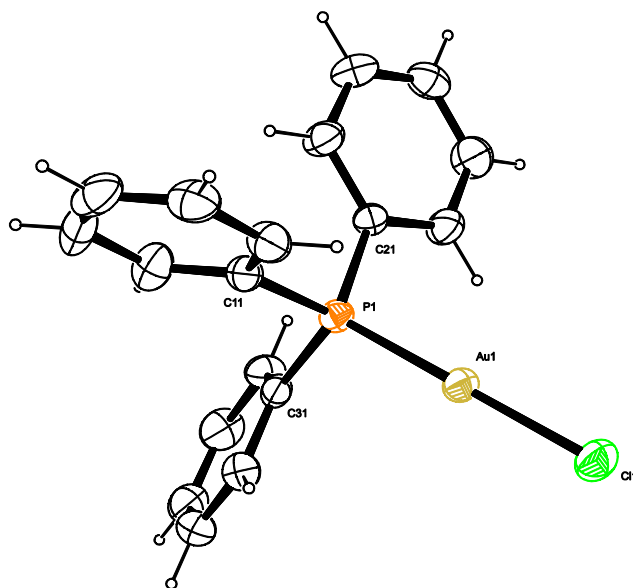
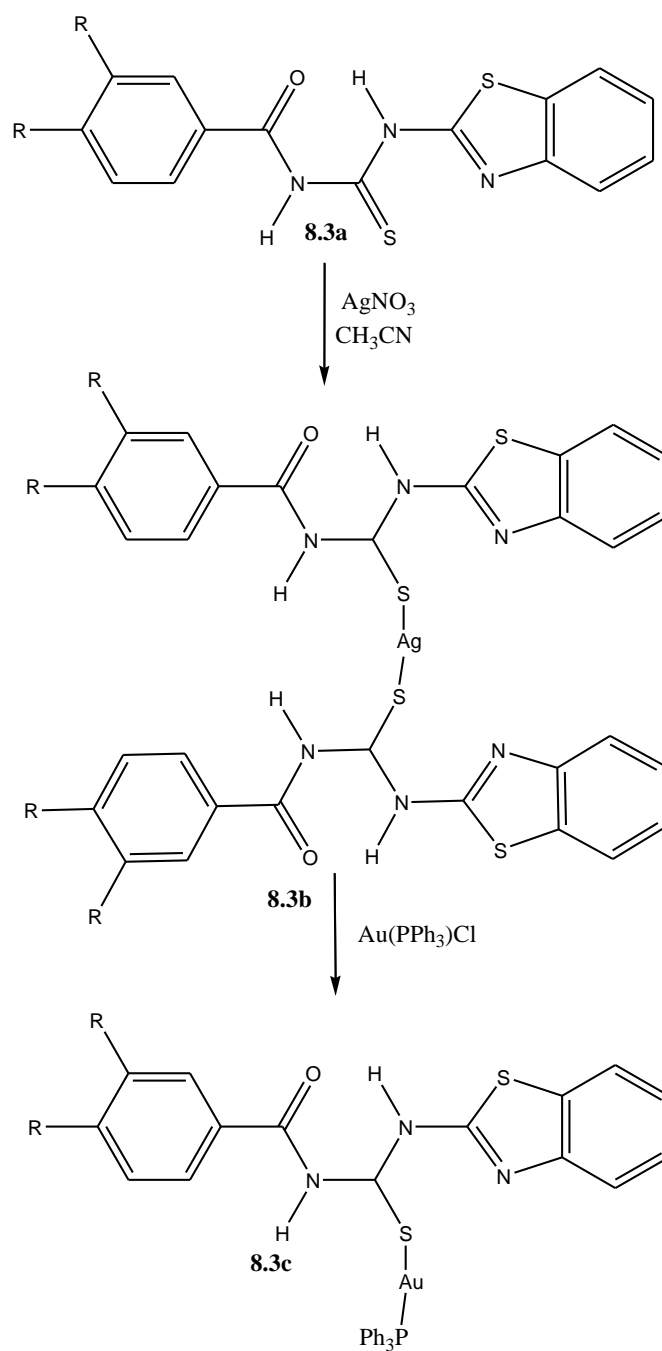


Figure 8.7 An ORTEP view of chlorotriphenylphosphinegold(I).

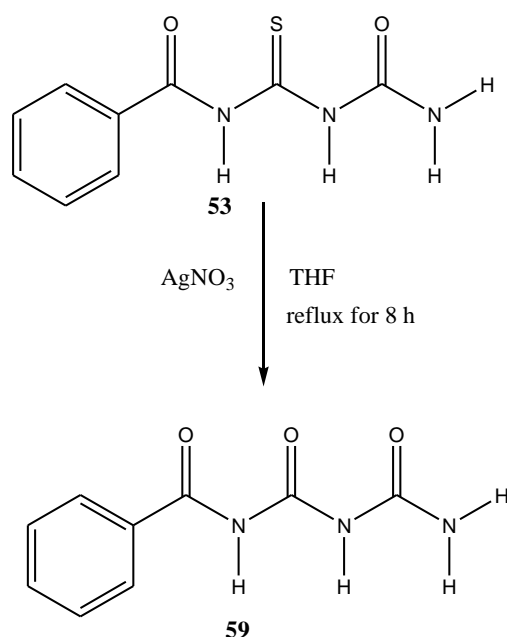
8.2 Silver catalyzed transformations

In the silver catalyzed transformation, the approach was to synthesize silver complexes and substitute it with gold in the complex.³⁵⁷ Gold(I) *N*-heterocyclic carbene (NHC) complexes have been obtained in good yields from the corresponding silver complexes by treatment with [AuCl(PPh₃)] following the silver carbene transfer route. The silver complexes were synthesized from the benzimidazolium halide salts by the *in situ* reactions with Ag₂O in dichloromethane as a solvent at room temperature.³⁵⁸ An attempt was made to carry out the synthesis of silver(I) complexes so as to carry out the transmetalation reaction.



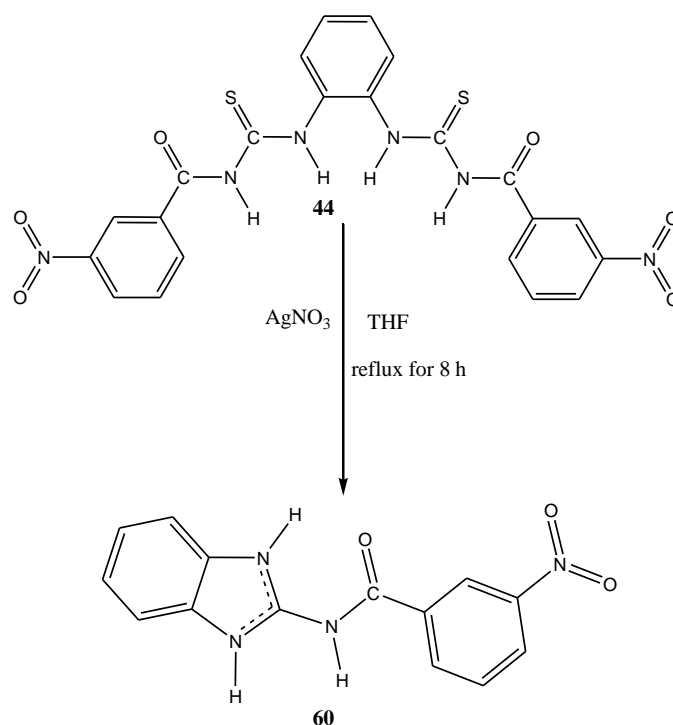
Scheme 8.3 Synthesis of gold compounds *via* silver complexes.

8.2.1 1-((Benzamido)formyl)urea (**59**)



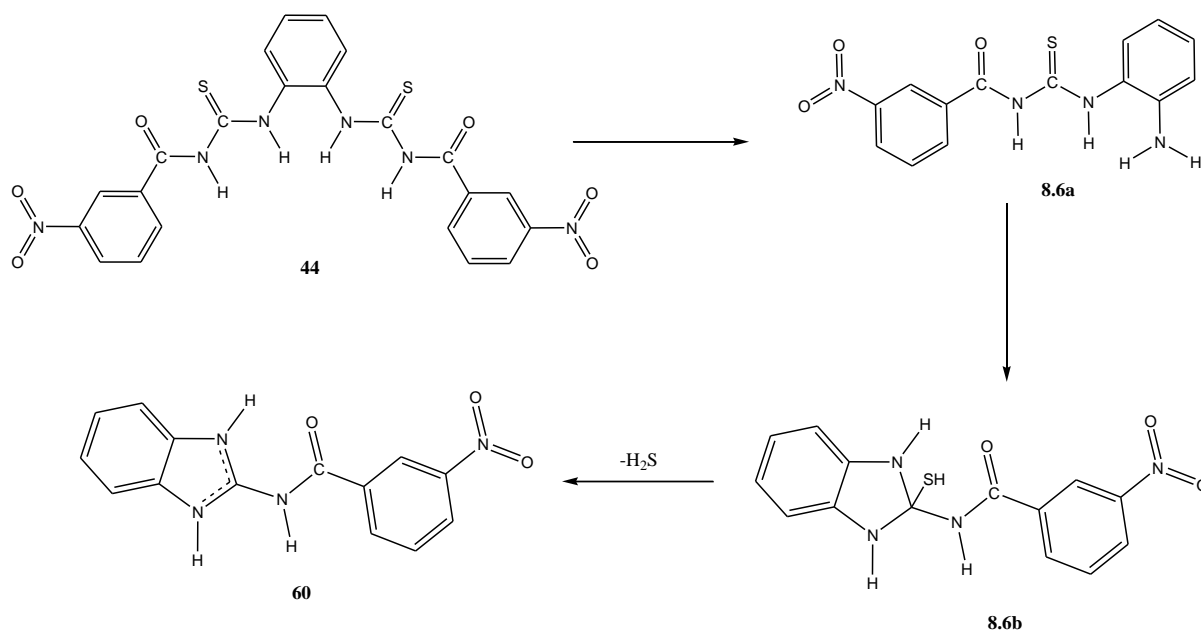
Scheme 8.4 Synthesis of 1-((benzamido)formyl)urea (**59**).

1-((Benzamido)formyl)urea **56** is formed by the silver catalysed substitution of sulfur with oxygen, the source of oxygen is presumably water. The IR spectrum (**Figure A8.10**) showed bands for the N–H stretches at 3345 and 3225 cm⁻¹. The band for the C=O stretch was observed at 1710 cm⁻¹. A band for the C=N and the aromatic C=C were observed at 1663 and 1598 cm⁻¹, respectively. The ¹H NMR spectrum (**Figure A8.11**) gave signals between 8.05 and 7.27 ppm for aromatic protons. The ¹³C NMR spectrum (**Figure A8.12**) gave a signal at 169.6 ppm for the carbonyl and signals between 132.1 and 127.8 ppm were observed for aromatic carbons.

8.2.2 *N*-(2,3-Dihydro-1*H*-benzo[d]imidazol-2-yl)-3-nitrobenzamide (60)

Scheme 8.5 Synthesis of *N*-(2,3-dihydro-1*H*-benzo[d]imidazol-2-yl)-3-nitrobenzamide (**60**).

The reaction is thought to proceed by the loss of a benzoyl isothiocyanate unit to form **8.6a**. The attack of the thione carbon by the lone electrons on the nitrogen leads to the formation of **8.6b** which forms leads to **60** upon rearrangement and possible loss of hydrogen sulfide.



Scheme 8.6 Proposed pathway for the synthesis of *N*-(2,3-dihydro-1*H*-benzo[*d*]imidazol-2-yl)-3-nitrobenzamide (**60**).

N-(2,3-Dihydro-1*H*-benzo[*d*]imidazol-2-yl)-3-nitrobenzamide (**60**) was formed by the silver-catalysed cleavage and cyclization of compound **44**. The IR spectrum (**Figure A8.13**) showed signals at 3321 and 3100 cm^{-1} for the N–H stretch, a signal was observed for the C=N stretch at 1682 cm^{-1} and the aromatic C=C was observed at 1591 cm^{-1} . The ^1H NMR spectrum (**Figure A8.14**) gave signals for aromatic protons between 8.88 and 7.29 ppm. The ^{13}C NMR spectrum (**Figure A8.15**) gave signals between 148.1 and 113.1 ppm for aromatic carbons.

8.2.3 Crystal structures of compounds **59** and **60**

Compounds **59** and **60** were recrystallized from DMSO:Toluene(4:1). The crystallographic data, selected bond lengths and bond angles for the crystal structures of compounds **59** and **60** are provided in **Tables 8.3** and **8.4**. The ORTEP diagrams for compounds **59** and **60** are presented in **Figures 8.8** and **8.9** respectively. Compound **59** crystallized in the monoclinic space group P21/*c* while compound **60** crystallized in the triclinic space group *P*-1.

Table 8.3 Crystallographic data and structure refinement summary for compounds **59** and **60**.

Property	59	60
Formula	C ₉ H ₉ N ₃ O ₃	2(C ₁₄ H ₁₁ N ₄ O ₃), O ₄ S, 2(C ₂ H ₆ OS), C ₂ H ₆ O, H ₂ O
Formula Weight	207.19	882.94
Crystal System	Monoclinic	Triclinic
Space group	<i>P21/c</i>	<i>P-1</i>
a [Å]	7.8993(4)	11.5334(7)
b [Å]	22.3734(10)	13.6711(8)
c [Å]	5.1861(2)	15.0439(9)
α [°]	90	66.063(2)
β [°]	99.912(2)	77.082(3)
γ [°]	90	69.274(3)
V [Å ³]	902.88(7)	2018.8(2)
Z	4	2
D(calc) [g/cm ³]	1.524	1.452
Mu(MoKa) [/mm]	0.118	0.260
F(000)	432	924
Crystal Size [mm]	0.04 x 0.32 x 0.62	0.12 x 0.48 x 0.64
Temperature (K)	200	200
Radiation [Å]	MoKa 0.71073	MoKa 0.71073
θ Min-Max [°]	1.8, 28.3	1.7, 28.4
Dataset	-9: 10 ; -29: 29 ; -6: 6	-15: 14 ; -18: 18 ; -18: 20
Tot., Uniq. Data, R(int)	12790, 2244, 0.022	36051, 10032, 0.019
Observed data [I > 2.0 sigma(I)]	1939	7758
Nref, Npar	2244, 152	10032, 566
R, wR ₂ , S	0.0354, 0.0948, 1.06	0.0497, 0.1462, 1.05
Max. and Av. Shift/Error	0.00, 0.00	0.00, 0.00
Min. and Max. Resd. Dens. [e/Å ³]	-0.22, 0.30	-0.71, 0.91

The bond distances of O1-C1 and N1-C1 in compound **59** are 1.220(1) and 1.377(1) respectively, confirming a carbonyl and a C-N which is neither distinctly single or a double bond suggesting delocalization of the electrons between the atoms. The bond angles of O1-C1-N1 and O2-C2-N1 are 129.1(1) and 118.6(1) respectively are consistent with Sp² hybridized carbon. In compound **60** bond distances of N22-C21 and O21-C22 are 1.337(3) and 1.218(3) Å respectively, which confirms a C-N bond with the electrons delocalized between the atoms whilst the C=O confirms the carbonyl bond. The bond angles of N22-C21-N23 and O22-N24-O23 are 23.0(2) and 122.7(2) (°)

Table 8.4 Selected bond lengths (Å) and bond angles (°) compounds for compounds **59** and **60**.

Bond lengths(Å)			
59		60	
O1-C1	1.220(1)	N22-C21	1.337(3)
O2-C2	1.218(1)	N23-C22	1.383(3)
O3-C3	1.229(1)	N23-C21	1.358(2)
N1-C1	1.377(1)	N24-C223	1.469(3)
N1-C2	1.396(1)	O21-C22	1.218(3)
N2-C2	1.359(1)	O22-N24	1.215(3)
N2-C3	1.410(1)	O23-N24	1.215(3)
N3-C3	1.327(1)		
Bond angles(°)			
59		60	
C1-N1-C2	129.1(1)	O22-N24-C223	118.6(2)
O1-C1-N1	121.7(1)	O22-N24-O23	123.0(2)
N1-C2-N2	116.6(1)	N22-C21-N23	122.7(2)
O2-C2-N2	124.9(1)	N21-C21-N23	127.4(2)
O2-C2-N1	118.6(1)	N21-C21-N22	109.9(2)
O3-C3-N3	124.9(1)	O21-C22-N23	121.4(2)
N2-C3-N3	117.9(1)	N23-C22-C221	117.1(2)
O3-C3-N2	117.2(1)		

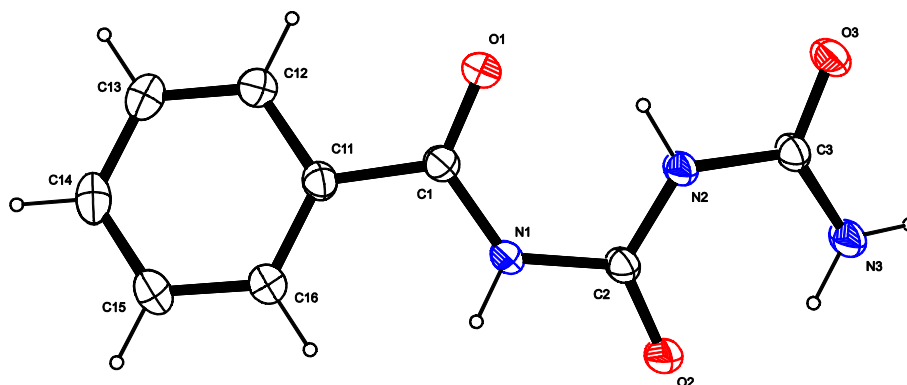


Figure 8.8 An ORTEP view of 1-((benzamido)formyl)urea (**59**).

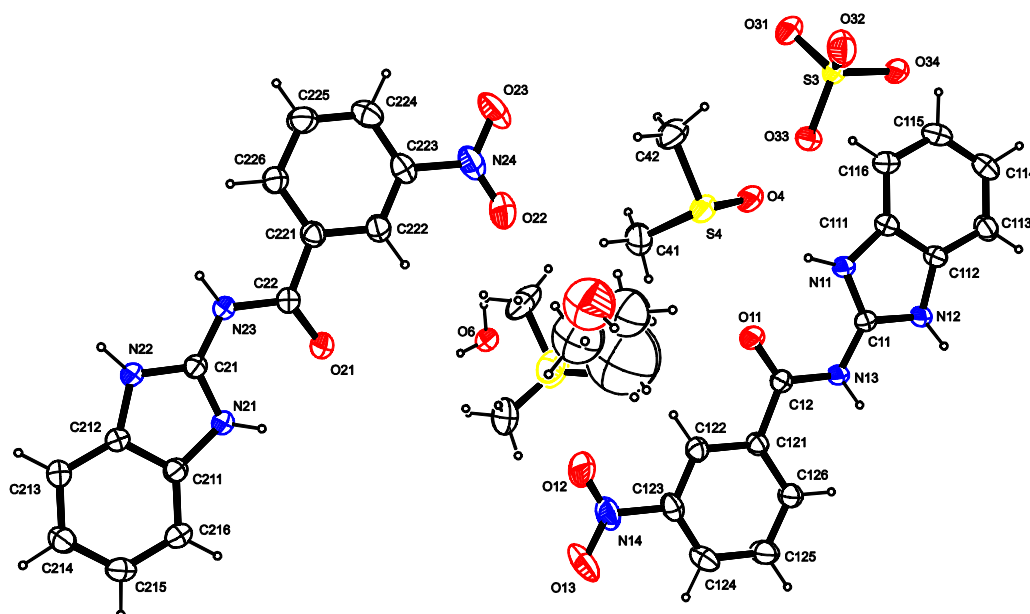


Figure 8.9 An ORTEP view of *N*-(2,3-dihydro-1*H*-benzo[*d*]imidazol-2-yl)-3-nitrobenzamide (**60**)

8.3 Conclusions

-An attempted synthesis of the gold compounds of the benzothiazole derivatives led to C-N coupling with the loss of the thiocyanate unit. The same products were obtained for both gold(I) dimethylsulfoxide chloride or gold(III) chloride with gold(0) being a side product in both cases. The reaction is thought to proceed by the attack of the thione moiety by the gold ion leading to the formation of a possible gold complex as intermediate. The reduction of gold to gold (0) and the dethiocyanation allows the C–N couple to occur leading to the formation of the benzamides. The products obtained were *N*-(benzothiazol-2-yl)-4-nitrobenzamide (**55**), *N*-(benzothiazol-2-yl)-3-bromobenzamide (**56**), *N*-(benzothiazol-2-yl)-3-methoxybenzamide (**57**) and *N*-(benzothiazol-2-yl)benzamide (**58**). The compounds have been fully characterized and the crystal structures of compounds **55**, **56** and **58** have been discussed. However, a full mechanism is yet to be investigated. This work present the first report of such a gold catalysed transformation.

-An attempted synthesis of a silver complex of 1-((benzamido)sulfanylenemethyl)urea (**53**) led to the silver catalysed conversion of compound **53** to 1-((benzamido)formyl)urea (**56**).

The product has been characterized by spectroscopy, microanalysis and GC-MS. The crystal structure of compound **56** has been discussed.

-Another attempt at synthesizing a silver complex of compound **44** led to the formation *N*-(2,3-dihydro-1*H*-benzo[d]imidazol-2-yl)-3-nitrobenzamide (**60**) by the silver-catalyzed cleavage and cyclization of compound **44**. The compound **60** has been characterized by spectroscopy, microanalysis and GC-MS. The crystal structure of compound **60** has been discussed.

CHAPTER NINE

CONCLUSIONS AND FUTURE WORK

9.1 Conclusions

In this study a set of amino acid-linked benzimidazole derivatives were designed using Autodock 4.2 (**Chapter 3**) and the attempted synthesis of these compounds led to the novel synthesis of 2,2,4-trimethyl-2,3-dihydro-1*H*-benzodiazepin-5-ium isophthalate (**3**) via microwave irradiation of *o*-phenylenediamine and isophthalic acid in the presence of acetone. A new set of amino acid derivatives were also designed using Autodock 4.2. The synthesis of the amino acid derivatives was successfully carried out. It was observed that the proline derivative exhibited the existence of rotamers in solutions which has been observed for the first time among these compounds. Conversion of the amino acid derivatives to benzimidazoles on the carboxylic acid was not successful.

In **Chapter 4**, novel tetraazatricyclic derivatives were prepared by the reaction of 2-aminobenzimidazole and benzoyl isothiocyanate derivatives. Though aliphatic derivatives of sulfur-containing tetraazatricyclics have been synthesized before this work presents the first synthesis of the aromatic derivatives of tetraazatricyclics from benzoyl isothiocyanates. Tautomerism of the thione residue has been observed when a nitro group is substituted at position 3 in the aryl ring leading to the existence of two different species in solution. Density functional theory transition state studies of the reaction mechanism of tetraazatricyclics have been carried in this work to compute a reaction pathway for tetraazatricyclics through the various intermediates and transition states. This thesis also presents the first base catalyzed degradation of sulfur containing tetraazatricyclics to give *N*-(1*H*-benzimidazol-2-yl)benzamide (**21**). The DFT transition state studies of this degradation has also been carried out. The cell viability tests of the tetraazatricyclics showed that compound **18** (unsubstituted), **12** (4-chloro) and **14** (4-methoxy) derivatives were cytotoxic, with EC₅₀ values of 0.15 ± 0.051 , 37.96 ± 21.87 and 5.28 ± 2.95 μ M, respectively. The HIV-1 protease screen of the tetraazatricyclic derivatives have been presented. Compounds **19** (4-nitro derivative) and **16** (3-nitro derivative) showed good activity against HIV-1 protease with % inhibition of 59.57 ± 13.59 and 79.97 ± 11.97 respectively. This is consistent with the docking studies, the orientation adapted by compound **16** at the active site of protease ensures that it binds more strongly to amino acid residues than the other derivatives. The reaction of benzoyl isothiocyanate with 2-aminobenzoxazole yielded 3-benzoyl-1-(2-hydroxyphenyl)urea (**22**) and the postulated

reaction mechanism suggests a ring opening of the 2-aminobenzoxazole ring and there is no precedent to this type of benzoyl isothiocyanate catalyzed ring opening in literature.

2-Aminobenzothiazole derivatives of benzoyl isothiocyanates have been synthesized and the DFT transition state studies of the formation of 3-(1,3-benzothiazol-2-yl)-1-(benzoyl)thiourea (**23**) carried to compute the possible reaction pathway with intermediates and transition states in **Chapter 5**. Cell viability test on the benzothiazole derivatives showed that compounds **31** (3-bromo) and **30** (4-nitro) were cytotoxic with EC₅₀ values of 1.207 ± 0.58 and 24.08 ± 13.14 μM , respectively. In the HIV-1 protease screen for the benzothiazole derivatives, all the compounds in this set gave percentage inhibition lower than 40% at a concentration of 100 μM of inhibitor and 20 μM of protease. The low reactivity of these compounds could be due to the presence of polar groups that make them interact to greater extent with the constituents of the buffer used. The compounds did not interact sufficiently with the target molecule.

Novel triazatetracyclics derivatives have been synthesized from the reaction of benzoyl isothiocyanate with 2(2-aminophenyl)-1*H*-benzimidazole in **Chapter 6**. Transition state studies on the formation of *N*-[(9*E*)-8,10,17-triazatetracyclo[8.7.0.0^{2,7}.0^{11,16}] heptadeca-1(17),2,4,6,11(16),12,14-heptaen-9-ylidene]benzamide (**39**) has been computed to obtain the various transition states in the reaction pathway and the resulting intermediates to explain a possible reaction mechanism for these compounds. The cell viability tests of the triazatetracyclics showed that compounds **32** (4-bromo), **33** (4-methoxy) and **37** (3-chloro) were cytotoxic giving EC₅₀ values of 45.47 ± 21.92 , 45.09 ± 13.79 and 74.94 ± 13.17 μM , respectively. This class of compounds exhibited a low inhibition against HIV1 protease because of their low solubility in the acetate buffer used for the assay.

In **Chapter 7**, the cell viability tests of aromatic and aliphatic diamine derivatives of benzoyl isothiocyanates have been carried out and this showed that 1-(4-bromobenzoyl)-3-[2-({[(4-bromophenyl)formamido]methanethioyl}amino)phenyl]thiourea (**46**) and 1-(3-chlorobenzoyl)-3-[2-({[(3-chlorophenyl)formamido]methanethioyl}amino)phenyl]thiourea (**48**) were cytotoxic with EC₅₀ values of 17.04 ± 9.75 μM and 69.20 ± 38.160 μM respectively, whilst 1-(3-bromobenzoyl)-3-[2-({[(3-bromophenyl)formamido]methanethioylamino)phenyl]thiourea (**49**), 3-benzoyl-1-(4-{{[(phenylformamido)methanethioyl]amino}butyl]thiourea (**54**) which were also cytotoxic gave EC₅₀ values of 35.90 ± 20.55 and 68.37 ± 26.45

μM . In the HIV-1 protease assay of the aromatic and aliphatic diamine derivatives of benzoyl isothiocyanates, 1-(3-bromobenzoyl)-3-[2-({[(3-bromophenyl)formamido]methanethiolyamino) phenyl]thiourea (**49**) gave an inhibition of 97% at an inhibitor concentration of 100 μM and a protease concentration of 20 nM. This was the best result from the bioassays. The attempt to obtain an IC_{50} for these assays was not possible with the concentration range chosen because the data obtained did not fit an exponential curve with a 99.5% confidence level.

An attempted synthesis of the gold compounds of the benzothiazole derivatives in **Chapter 8** led to C–N coupling with the loss of the thiocyanate unit. The same products were obtained for both gold(I) dimethylsulfoxide chloride or gold(III) chloride with gold(0) being a side product in both cases. The reaction is thought to proceed by the attack of the thione moiety by the gold ion leading to the formation of a possible gold complex as intermediate. The reduction of gold to gold (0) and the dethiocyanation allows the C–N couple to occur leading to the formation of the benzamides. This work presents the first report of such a gold catalyzed transformation. An attempted synthesis of a silver complex of 1-((benzamido)sulfanylenemethyl)urea (**53**) led to the silver catalyzed conversion of compound **53** to 1-((benzamido)formyl)urea (**56**), where water is presumed to be the source of oxygen. Another attempt at synthesizing a silver complex of compound **44** led to the formation *N*-(2,3-dihydro-1*H*-benzo[d]imidazol-2-yl)-3-nitrobenzamide (**60**) the silver-catalysed cleavage and cyclization of compound **44**.

9.2 Future Work

Though compound **49** is the most active against HIV-1 protease but it is also cytotoxic hence derivatizing by introducing other groups in place of the bromide might reduce its cytotoxicity. This could be achieved by the addition of aliphatic side chains could be introduced onto compounds **16** and **19**. Derivatization of compound **49** should also achieve acceptable cytotoxicity levels.

The synthesis of the gold complexes using chlorotetrahydrothiophenogold(I) would be explored, since introduction of gold into these compounds is known to improve their activity against HIV-1. The novel gold-catalysed dethiocyanation reaction coupled with C–N

coupling to form an amide would be further investigated and the detailed reaction mechanism studied.

Further work on the HIV-1 protease assay would be carried out to obtain kinetic information. The data obtained would be interpreted using the Michaelis-Menten equation to ascertain the type of inhibition exhibited by these compounds.

Thermodynamic data would be obtained by displacement titration calorimetry. Pepstatin would be used as a weak binder and the number of active sites obtained from its titration with HIV-1 protease. A subsequent titration with selected benzoyl isothiocyanate derivatives (eg compounds **16**, **19** or **49**) and this could be completed to obtain data about the binding energy, Gibbs free energy, the entropy and enthalpy. This could contribute to determining the therapeutic potential of compound **49**.

REFERENCES

- [1] United Nations. 2010 Report on the global HIV/AIDS Epidemic: global report; UN: New York, **2010**.
- [2] A cluster of Kaposi's sarcoma and Pneumocystis carinii pneumonia among homosexual male residents of Los Angeles and Orange Counties, California. *MMWR. Morb. Mortal Wkly. Rep.* **1982**, 31, 305–307
- [3] P.M. Sharp, B.H. Hahn. The evolution of HIV-1 and the origin of AIDS. *Phil. Trans. R. Soc. B.* **2010**, 365, 2487–2494.
- [4] L.V. Wain, E. Bailes, F. Bibollet-Ruche, J.M. Decker, B.F. Keele, F.V. Heuverswyn, Y. Li, J. Takehisa, E.M. Ngole, G.M. Shaw, M. Peeters, B. H. Hahn, P.M. Sharp. Adaptation of HIV-1 to its human host. *J. Mol. Biol. Evol.* **2007**, 24(8), 1853–1860.
- [5] Y. Shao and C. Williamson. The HIV-1 epidemic: low-to middle-income countries. *Cold Spring Harb. Perspect. Med.* **2012**, 2, 71–87.
- [6] K.D. Jayappa, Z. Ao, X. Yao. The HIV-1 passage from cytoplasm to nucleus: the process involving a complex exchange between the components of HIV-1 and cellular machinery to access nucleus and successful integration. *Int. J Biochem. Mol. Biol.* **2012**, 3(1), 70–85.
- [7] B.G. Turner, M.F. Summers. Structural biology of HIV. *J. Mol. Biol.* **1999**, 285, 1–32.
- [8] L.O. Arthur, J. W. Bess Jr, R.C.I. Sowder, R.E. Benveniste, D.L Mann, J.C. Chermann, L. E Henderson. Cellular proteins bound to immunodeficiency viruses: implications for pathogenesis and vaccines. *Science* **1992**, 258, 1935–1938.
- [9] P.R. Chapham, R.A Weiss. Immunodeficiency viruses: Spoilt for choice of co-receptors. *Nature* **1997**, 388, 230–231.
- [10] B.J. Doranz, J. Rucker, Y. Yi, R.J. Smyth, M. Samson, S.C. Peiper, M. Parmentier, R. G. Collman, R.W. Doms. A dual-tropic primary HIV-1 isolate that uses fusin and the β -chemokine receptors CKR-5, CKR-3, and CKR-2b as fusion cofactors. *Cell* **1996**, 85, 1149–1158.
- [11] F. Feng, C.C. Broder, P.E. Kennedy, E.A Berger. HIV-1 entry cofactor: functional cDNA cloning of a seven-transmembrane, G protein-coupled receptor. *Science* **1996**, 272, 872–877.
- [12] J.P. Moore. Co-receptors: implications for HIV pathogenesis and therapy. *Science* **1997**, 276, 51–52.

- [13] S.P. Goff, Retroviral reverse transcriptase: Synthesis, structure, and function. *J. Acquired Immune Defic. Syndr.* **1990** 3, 817–831.
- [14] R. A. Katz, A. M. Skalka. The retroviral enzymes, *Annu. Rev. Biochem.* **1994**. 63, 133–173.
- [15] A. Telesnitsky, S. P. Goff, (Coffin, J. M, Hughes, S. H. & Varmus, H. E., eds), **1997**, 1, 121–160.
- [16] J.M.Whitcomb, S. H. Hughes. Retroviral reverse transcription and integration: progress and problems. *Annu. Rev. Cell Biol.* **1992**, 8, 275–306.
- [17] M.D. Miller, C.M. Farnet, F.D.Bushman. Human immunodeficiency virus type 1 preintegration complexes: studies of organization and composition. *J. Virol.* **1997**, 71, 5382–5390.
- [18] B. Bowerman, P.O. Brown, J.M. Bishop, H.E. Varmus. A nucleoprotein complex mediates the integration of retroviral DNA. *Genes Dev.* **1989**, 3, 469–478.
- [19] R.A.M. Fouchier, B.E. Meyer, J.H. M, Simon, U.Fischer, M.H. Malim. HIV-1 infection of non-dividing cells: evidence that the amino-terminal basic region of the viral matrix protein is important for Gag processing but not for post-entry nuclear import. *EMBO J.* **1997**, 16, 4531–4539.
- [20] E.O. Freed, A.M. Martin. Virion incorporation of envelope glycoproteins with long but not short cytoplasmic tails is blocked by specific, single amino acid substitutions in the human immunodeficiency virus type 1 matrix. *J. Virol.* **1995**, 69, 1984–1989.
- [21] Z. Nie, D. Bergeron, R.A. Subbramanian, X.J. Yao, F. Checroune, N. Rougeau, E.A. Cohen. The putative alpha helix 2 of human immunodeficiency virus type 1 Vpr contains a determinant which is responsible for the nuclear translocation of proviral DNA in growth-arrested cells. *J. Virol.* **1998**, 72, 4104–4115.
- [22] R.A.M. Fouchier, B.E. Meyer, J.H. Simon, U. Fischer, A.V. Albright, F. Gonzalez-Siarano, M.H. Malim. Interaction of the human immunodeficiency virus type 1 Vpr protein with the nuclear pore complex. *J. Virol.* **1998**, 72, 6004–6013.
- [23] S. Popov, M. Rexach, G. Zybarth, N. Reiling, M.A. Lee, L. Ratner, C.M. Lane, M.S. Moore, G. Blobel, M. Bukrinsky. Viral protein R regulates nuclear import of the HIV-1 pre-integration complex. *EMBO J.* **1998**, 17, 909–917.
- [24] M.A.Vodicka, D.M. Koepp, P.A. Silver, M. Emerman. HIV-1 Vpr interacts with the nuclear transport pathway to promote macrophage infection. *Genes Dev.* **1998**, 12, 175–185.

- [25] J.B.M. Jowett, V. Planelles, B. Poon, N.P. Shah, M.L. Chen, I.S.Y. Chen. The human immunodeficiency virus type 1 vpr gene arrests infected T cells in the G2 + M phase of the cell cycle. *J. Virol.* **1995**, 69, 6304–6313.
- [26] F. Re, D. Braaten, E.K. Franke, J. Luban. Human immunodeficiency virus type 1 Vpr arrests the cell cycle in G2 by inhibiting the activation of p34cdc2-cyclin B. *J. Virol.* **1995**, 69, 6859–6864.
- [27] M.E. Rogel, L.I. Wu, M. Emerman. The human immunodeficiency virus type 1 vpr gene prevents cell proliferation during chronic infection. *J. Virol.* **1995**, 69, 882–888.
- [28] M.I. Bukrinsky, S. Haggerty, M.P. Dempsey, N. Sharova, A. Adzhubei, L. Spitz, P. Lewis, D. Goldfarb, M. Emerman, M. Stevenson. A nuclear localization signal within HIV-1 matrix protein that governs infection of non-dividing cells. *Nature* **1993**, 365, 666–669.
- [29] U. von Schwedler, R.S. Kornbluth, D. Trono. The nuclear localization signal of the matrix protein of human immunodeficiency virus type 1 allows the establishment of infection in macrophages and quiescent T lymphocytes. *Proc. Natl Acad. Sci. USA*, **1994**, 91, 6992–6996.
- [30] P. Wei, M.E. Garber, S.M. Fang, W.H. Fischer, K.A. Jones. A novel CDK9-associated C-type cyclin interacts directly with HIV-1 Tat and mediates its high-affinity loop-specific binding to TAR RNA. *Cell* **1998**, 92, 451–462.
- [31] C.H. Herrmann, A.P. Rice. Lentivirus Tat proteins specifically associate with a cellular protein kinase, TAK that hyperphosphorylates the carboxyl-terminal domain of the large subunit of RNA polymerase II: candidate for a Tat cofactor. *J. Virol.* **1995**, 69, 1612–1620.
- [32] D. Reines, J.W. Conaway, R.C. Conaway. The RNA polymerase II general elongation factors. *Biochem. Sci.* **1996**, 9, 351–355.
- [33] M. Ohno, M. Fornerod, I.W. Mattaj. Nucleocytoplasmic transport: the last 200 nanometers. *Cell* **1998**, 92, 327–336.
- [34] M. Emerman, M.H. Malim. HIV-1 regulatory/accessory genes: keys to unraveling Viral and host cell biology. *Science* **1998**, 280, 1880–1884.
- [35] D.C. Chan, D. Fass, J.M. Berger, P.S. Kim. Core structure of gp41 from the HIV envelope glycoprotein. *Cell* **1997**, 89, 263–273.
- [36] P.L. Earl, B. Moss, R.W. Doms. Folding interaction with GRP78-BiP assembly and transport of the human immunodeficiency virus type 1 envelope protein. *J. Virol.* **1991**, 65, 2047–2055.

- [37] C.K. Leonard, M.W. Spellman, L. Riddle, R.J. Harris, J.N. Thomas, T.J. Gregory. Assignment of intrachain disulfide bonds and characterization of potential glycosylation sites of the type 1 recombinant human immunodeficiency virus envelope glycoprotein (gp120) expressed in Chinese hamster ovary cells. *J. Biol. Chem.* **1990**, 265, 10373–10382.
- [38] M. Lu, S.C. Blacklow, P.S. Kim. A trimeric structural domain of the HIV-1 transmembrane glycoprotein. *Nature Struct. Biol.* **1995**, 2, 1075–1082.
- [39] R. Wyatt, J. Sodroski. The HIV-1 envelope glycoproteins: fusogens, antigens, and immunogens. *Science.* **1998**, 280, 1884–1888.
- [40] J.A. Hoxie, J.D. Alpers, J.L. Rackowski, K. Huebner, B.S. Haggarty, A.J Cedarbaum, J.C. Reed. Alterations in T4 (CD4) protein and mRNA synthesis in cells infected with HIV. *Science.* **1986**, 234, 1123–1127.
- [41] B. Crise, L. Buonocore, J.K. Rose. CD4 is retained in the endoplasmic reticulum by the human immunodeficiency virus type 1 glycoprotein precursor. *J. Virol.* **1990**, 64, 5585–5593.
- [42] F. Margottin, S.P. Bour, H. Durand, L. Selig, S. Benichou V. Richard, D. Thomas, K.Strebel, R.A Benarous. A Novel Human WD Protein h-bTrCP that Interacts with HIV-1 Vpu Connects CD4 to the ER Degradation Pathway through an F-Box Motif. *Mol. Cell.* **1998**, 1, 565–574.
- [43] M. Foti, A. Mangasarian, V. Piguet, D.P. Lew, K.H. Krause, D Trono, J.L. Carpentier. Nef-mediated Clathrin-coated Pit Formation. *J. Cell Biol.* 1997, 139, 37–47.
- [44] F. Dyda, B Hickman, T.M. Jenkins, A. Engelman, R. Craigie, D.R. Davies. Crystal structure of the catalytic domain of HIV-1 integrase: similarity to other polynucleotidyl transferases. *Science* **1994**, 266 (5193):1981–1986.
- [45] P.A. Rice, T.A. Baker. Comparative architecture of transposase and integrase complexes. *Nat. Struct. Biol.* **2001**, 8(4), 302–307.
- [46] P.O. Brown. Integration of retroviral DNA. *Curr Top Microbiol Immunol.* **1990**, 157, 19–48.
- [47] F.D. Bushman, R. Craigie. Activities of human immunodeficiency virus (HIV) integration protein in vitro: specific cleavage and integration of HIV DNA. *Proc. Natl. Acad. Sci. U S A.* **1991**, 88(4), 1339–1343.
- [48] R.A.P. Lutzke, N.A. Eppens, P.A. Weber, R.A. Houghten, R.H.A. Plasterk. Identification of a hexapeptide inhibitor of the human immunodeficiency virus

- integrase protein by using a combinatorial chemical library. *Biochemistry* **1995**, 92, 11456–11460.
- [49] J. Kulkosky, R.A. Katz, G. Merkel, A.M. Skalka. Activities and substrate specificity of the evolutionarily conserved central domain of retroviral integrase. *J. Virol.* **1995**, 206, 448–456.
- [50] J. Kulkosky, R.A. Katz, G. Merkel, A.M. Skalka. Activities and substrate specificity of the evolutionarily conserved central domain of retroviral integrase. *J. Virol.* **1995**, 206(1):448–456.
- [51] D.C. Van Gent, A.A. Groeneger, R.H. Plasterk. Mutational analysis of the integrase protein of human immunodeficiency virus type 2. *Proc. Natl. Acad. Sci. USA*, **1992**, 89, 9598–9602.
- [52] C. Vink, A.M. Oude Groeneger, R.H. Plasterk. Identification of the catalytic and DNA-binding region of the human immunodeficiency virus type I integrase protein. *Nucleic Acids Res.* **1993**, 21, 1419–1425.
- [53] A. Engelman, F.D. Bushman, R. Craigie. Identification of discrete functional domains of HIV-1 integrase and their organization within an active multimeric complex. *EMBO J.* **1993**, 12(8), 3269–3275.
- [54] M. Drelich, M. Haenggi, J. Mous. Conserved residues Pro-109 and Asp-116 are required for interaction of the human immunodeficiency virus type 1 integrase protein with its viral DNA substrate. *J. Virol.* **1993**, 5041–5044.
- [55] S.R. Mumm, D.P. Grandgenett. Defining nucleic acid-binding properties of avian retrovirus integrase by deletion analysis, *Virology.* **1991**, 1160–1167.
- [56] F.D. Bushman, B. Wang. Rous sarcoma virus integrase protein: mapping functions for catalysis and substrate binding. *Virology.* **1994**, 2215–2223.
- [57] M. Schauer, A. Billich. The N-terminal region of HIV-1 integrase is required for integration activity, but not for DNA-binding. *Biochem Biophys Res Commun.* **1992**, 30, 185 (3), 874–80.
- [58] D.C. van Gent, Y. Elgersma, M.W.J. Bolk, C. Vink, R.H.A. Plasterk. DNA binding properties of the integrase proteins of human immunodeficiency viruses types 1 and 2. *Nucleic Acids Research.* **1991**, 19 (14), 3821–3827.
- [59] R.A.P. Lutzke, C. Vink, R.H.A. Plasterk. Characterization of the minimal DNA-binding domain of the HIV integrase protein. *Nucleic Acids Research.* **1994**, 22(20), 4125–4131.

- [60] E. Asante–Appiah, A. M. Skalka. Molecular mechanisms in retrovirus DNA integration. *Antiviral Research* **1997**, 36, 139–156.
- [61] T.S. Heuer, P.O. Brown. Mapping features of HIV-1 integrase near selected sites on viral and target DNA molecules in an active enzyme-DNA complex by photo-cross-linking. *Biochemistry* **1997**, 36, 10655–10665.
- [62] P. Hindmarsh, J. Leis. Retroviral DNA integration. *Microbiol. Mol. Biol. Rev.* **1999**, 63(4), 836–843.
- [63] R. Craigie. HIV Integrase, a brief overview from chemistry to therapeutics. *J. Bio Chem.* **2001**, 276(26), 23213–23216.
- [64] A. Engelman, K. Mizuuchi, R. Craigie. HIV-1 DNA integration: mechanism of viral DNA cleavage and DNA strand transfer. *Cell* **1991**, 67, 1211–1221.
- [65] A. Engelman, R. Craigie. Identification of conserved amino acid residues critical for human immunodeficiency virus type 1 integrase function in vitro. *J. Virol.* **1992**, 66(11), 6361–6369.
- [66] A.D. Leavitt, L. Shiue, H.E. Varmus. Site-directed mutagenesis of HIV-1 integrase demonstrates differential effects on integrase functions in vitro. *J. Bio.Chem.* **1993**, 268(3), 2113–2119.
- [67] J. Kulkosky, K.S. Jones, R.A. Katz, J.P.G. Mack, A.M. Skalka. Residues critical for retroviral integrative recombination in a region that is highly conserved among retroviral/retrotransposon integrases and bacterial insertion sequence transposases. *Mol. Cell. Biol.* **1992**, 12 (5), 2331–2338.
- [68] G. Bujacz, M. Jaskólski, J. Alexandratos, A. Wlodawer, G. Merkel, R.A. Katz, A.M. Skalka. High-resolution structure of the catalytic domain of Avian Sarcoma virus integrase. *J. Mol. Biol.* **1995**, 253, 333–346.
- [69] G. Bujacz, M. Jaskólski, J. Alexandratos, A. Wlodawer, G. Merkel, R.A. Katz, A.M. Skalka. The catalytic domain of Avian Sarcoma virus integrase: conformation of the active-site residues in the presence of divalent cations. *Structure* **1996**, 4(1), 89–96.
- [70] Y. Goldgur, F. Dyda, A.B. Hickman, T.M. Jenkins, R. Craigie, D. R.Davies. Three new structures of the core domain of HIV-1 integrase: An active site that binds magnesium. *Proc. Natl. Acad. Sci. USA.* **1998**, 95, 9150–9154.
- [71] Z. Chen, Y. Yan, S. Munshi, Y. Li, J.Z. Murphy, B. Xu, M. Witmer, P. Felock, A. Wolfe V. Sardana, E.A. Emini, D. Hazuda, L.C. Kuo. X-ray structure of simian immunodeficiency virus integrase containing the core and C-terminal domain

- (Residues 50-293) - An Initial glance of the viral DNA binding platform. *J. Mol. Biol.* **2000**, 296, 521–533.
- [72] J.C.H. Chen, J. Krucinski, L.J.W. Miercke, J.S. Finer-Moore, A.H. Tang, A.D. Leavitt, R. M. Stroud. Crystal structure of the HIV-1 integrase catalytic core and C-terminal domains: A model for viral DNA binding. *Proc. Natl. Acad. Sci. U S A.* **2000**; 97(15): 8233–8238.
- [73] Z.N. Yang, T.C. Mueser, F.D. Bushman, C.C. Hyde1. Crystal structure of an active two-domain derivative of Rous Sarcoma virus integrase. *J. Mol. Biol.* **2000**, 296, 535–548.
- [74] P. Rice, K. Mizuuchi. Structure of the bacteriophage Mu transposase core: a common structural motif for DNA transposition and retroviral integration. *Cell* **1995**, 82, 209–220.
- [75] H. Aldaz, E. Schuster, T.A. Baker. The interwoven architecture of the Mu transposase couples DNA synapsis to catalysis. *Cell* **1996**, 85, 257–269.
- [76] T.L. Williams, E.L. Jackson, A. Carritte, T.A. Baker. Organization and dynamics of the Mu transpososome: recombination by communication between two active sites. *Genes Dev.* **1999**, 13, 2725–2737.
- [77] L.A. Kohlstaedt, J. Wang, J.M. Friedman, P.A. Rice, T.A. Steitz. Crystal structure at 3.5 Å resolution of HIV-1 reverse transcriptase complexed with an inhibitor. *Science*.**1992**, 26, **256** (5065), 1783–1790.
- [78] A. Jacobo-Molina, J. Ding, R.G. Nanni, A.D. Ckark, JR, X. Lu, C. Tantillo, R.L. Williams, G. Kamer, A.L. Ferris, P. Clark, A. Hizi, S.H. Hughes, E. Arnold. Crystal structure of human immunodeficiency virus type 1 reverse transcriptase complexed with double-stranded DNA at 3.0 Å resolution shows bent DNA. *Proc. Natl. Acad. Sci. USA*, **1993**, 90, 6320–6324.
- [79] D.W. Rodgers, S.J. Gamblin, B.A. Harris, S. Ray, J.S. Culp, B. Hellmig, D.J. Woolf, C. Debouck, S.C. Harrison. The structure of unliganded reverse transcriptase from the human immunodeficiency virus type 1. *Proc. Natl. Acad. Sci. USA.* **1995**, 92, 1222–1226.
- [80] J. Ding, K. Das, Y. Hsiou, S.G. Sarafianos, A.D. Clark Jr, A. Jacobo-Molina, C. Tantillo, S.H. Hughes, E. Arnold. Structure and functional implications of the polymerase active site region in a complex of HIV-1 RT with a double-stranded DNA template-primer and an antibody fab fragment at 2.8 Å resolution. *J. Mol. Biol.* **1998**, 284, 1095–1111.

- [81] S.G. Sarafianos, K. Das, C. Tantillo, A.D. Clark Jr, J.Ding, J.M. Whitcomb, P.L.Boyer, S.H. Hughes, E. Arnold. Crystal structure of HIV-1 reverse transcriptase in complex with a polypurine tract RNA:DNA. *EMBO J.* **2001**, 20(6), 1449–1461.
- [82] S. Tuske, S.G. Sarafianos, A.D Clark Jr, J. Ding, L.K. Naeger, K.L. White, M.D. Miller, C.S. Gibbs, P.L Boyer, P. Clark, G. Wang, B.L. Gaffney, R.A. Jones, D.M. Jerina, S.H. Hughes, E. Arnold. Structures of HIV-1 RT–DNA complexes before and after incorporation of the anti-AIDS drug tenofovir. *Nat. Struct. Mol. Biol.* **2004**. 11, 469–474.
- [83] H. Huang, R. Chopra, G.L. Verdine, S.C. Harrison. Structure of a covalently trapped catalytic complex of HIV-1 reverse transcriptase: implications for drug resistance. *Science* **1998**, 27, 282(5394), 1669–1675.
- [84] S.G. Sarafianos, B. Marchand, K. Das, D. Himmel, M.A. Parniak, S.H. Hughes, E. Arnold. Structure and function of HIV-1 reverse transcriptase: molecular mechanisms of polymerization and inhibition. *J. Mol. Biol.* **2009**, 23, 385(3), 693–713.
- [85] M.D. Powell, M. Ghosh, P.S. Jacques, K.J. Howard, S.F.J. Le Grice, J.G. Levin. Alanine-scanning mutations in the “primer grip” of p66 HIV-1 reverse transcriptase result in selective loss of RNA priming activity. *J. Bio. Chem.* **1997**, 272(20), 13262–13269.
- [86] M. Götte, G. Maier, H.J. Gross, H. Heumann. Localization of the active site of HIV-1 reverse transcriptase-associated RNase H domain on a DNA template using site-specific generated hydroxyl radicals. *J. Bio. Chem.* **1998**, 273(17), 10139–10146.
- [87] J. Deval, K.L. White, M.D. Miller, N.T. Parkin, J. Courcambeck, P. Halfon, B. Selmi, J. Boretto, B. Canard. Mechanistic basis for reduced viral and enzymatic fitness of HIV-1 reverse transcriptase containing both K65R and M184V mutations. *J. Bio. Chem.* **2004**, 279, 1, 509–516.
- [88] D.R. Davies. The structure and function of the aspartic proteinases. *Annu. Rev. Biophys. Biophys. Chem.* **1990**, 19, 189–215.
- [89] A. Brik, C.H. Wong. HIV-1 protease: mechanism and drug discovery. *Org. Biomol. Chem.* **2003**, 1(1), 5–14.
- [90] H.G. Kräusslich, R.H. Ingraham, M.T. Skoog, E. Wimmer, P.V. Pallai, C.A. Carter. Activity of purified biosynthetic proteinase of human immunodeficiency virus on natural substrates and synthetic peptides. *Proc. Natl. Acad. Sci. U.S.A.* **1989**, 86(3), 807–811.

- [91] S. Seelmeier, H. Schmidt, V. Turk, K von der Helm. Human immunodeficiency virus has an aspartic-type protease that can be inhibited by pepstatin A. *Proc. Natl. Acad. Sci. U.S.A.* **1988**, 85(18), 6612–6616.
- [92] F. McPhee, A.C. Good, I.D. Kuntz, C.S. Craik. Engineering human immunodeficiency virus 1 protease heterodimers as macromolecular inhibitors of viral maturation. *Proc. Natl. Acad. Sci. U.S.A.* **1996**, 93(21), 11477–11481.
- [93] M. Jaskólski, A.G. Tomasselli, T.K Sawyer, D.G. Staples, R.L. Heinrikson, J Schneider, S.B. Kent, A. Wlodawer. Structure at 2.5Å. resolution of chemically synthesized human immunodeficiency virus type 1 protease complexed with a hydroxyethylene-based inhibitor. *Biochemistry* **1991**, 30(6), 1600–1609.
- [94] K.A. Sepkowitz. AIDS-the first 20 years. *N. Eng. J. Med.* **2001**, 344, 1764–1772.
- [95] F.J. Palella Jr, K.M. Delaney, A.C. Moorman, M.O. Loveless, J. Fuhrer, G.A. Satten, D.J. Aschman, S.D. Holmberg. Declining morbidity and mortality among patients with advanced human immunodeficiency virus infection. *N. Engl. J. Med.* **1998**, 338, 853–860.
- [96] S.M. Hammer, K.E. Squires, M.D. Hughes, J.M. Grimes, L.M. Demeter, J.S. Currier, J.J. Eron. Jr, J.E. Feinberg, H.H. Balfour Jr, L.R. Deyton, J.A. Chodakewitz, M.A Fischl. A controlled trial of two nucleoside analogues plus Indinavir in persons with human immunodeficiency virus infection and CD4 cell counts of 200 per cubic millimetre or less. *N. Engl. J. Med.* **1997**, 337, 725–733.
- [97] A.K. Ghosh, B.D. Chapsal, I.T. Weber, H. Mitsuya. Design of HIV protease inhibitors targeting protein backbone: an effective strategy for combating drug resistance. *Acc. Chem. Res.* **2008**, 41, 78–86.
- [98] A.K. Ghosh, S. Leshchenko-Yashchuk, D.D. Anderson, A. Baldrige, M. Noetzel, H.B. Miller, Y. Tie, Y.F. Wang, Y. Koh, I.T. Weber, H. Mitsuya. Design of HIV-1 protease inhibitors with pyrrolidinones and oxazolidinones as novel P1'-Ligands to enhance backbone-binding interactions with protease: synthesis, biological evaluation, and protein–ligand X-ray studies. *J. Med. Chem.* **2009**, 52, 3902–3914.
- [99] A. Mocroft, L. Ruiz, P. Reiss, B. Ledergerber, C. Katlama, A. Lazzarin, F.D. Goebel, A. N. Phillips, B. Clotet, J.D. Lundgren. Virological rebound after suppression on highly active antiretroviral therapy. *AIDS* **2003**, 17, 1741–1751.
- [100] A.J. Leigh Brown, S.D. Frost, W.C. Mathews, K. Dawson, N.S. Hellmann, E.S. Daar, D.D. Richman, S.J. Little. Transmission fitness of drug-resistant human

- immunodeficiency virus and the prevalence of resistance in the antiretroviral-treated population. *J. Infect. Dis.* **2003**, 187, 683–686.
- [101] D.D. Richman, S.C. Morton, T. Wrin, N. Hellmann, S. Berry, M.F. Shapiro, S.A. Bozzette. The prevalence of antiretroviral drug resistance in the United States. *AIDS* **2004**, 18, 1393–1401.
- [102] C.B. Hurt, S.I. McCoy, J. Kuruc, J.A. Nelson, M. Kerkau, S. Fiscus, K. McGee, J. Sebastian, P. Leone, C. Pilcher, C. Hicks. Transmitted antiretroviral drug resistance among acute and recent HIV infections in North Carolina from 1998 to 2007. *Antivir. Ther.* **2009**, 14, 673–678.
- [103] Z. Grossman, M. Lorber, S. Maayan, N. Bar-Yacov, I. Levy, D. Averbuch, V. Istomin, M. Chowers, Z. Stoeber, D. Ram, H. Rudich, F. Mileguir, R. Pavel, R. Almaliach, F. Schlaeffer, Z. Kra-Oz, E. Mendelson, J. M. Schapiro, K. Riesenber. Drug-resistant HIV infection among drug-naïve patients in Israel. *Clin. Infect. Dis.* **2005**, 40, 294–302.
- [104] R.M. Grant, F. Hecht, M. Warmerdam, L. Liu, T. Liegler, C.J. Petropoulos, N.S. Hellmann, M. Chesney, M.P. Busch, J.O. Kahn. Time trends in primary HIV-1 drug resistance among recently infected persons. *JAMA*. **2002**, 288, 181–188.
- [105] V. Miller. International perspectives on antiretroviral resistance. Resistance to protease inhibitors. *J. Acquir. Immune. Defic. Syndr.* **2001**, 26(1), S34–S50.
- [106] R.W. Shafer, J.M. Schapiro. HIV-1 Drug resistance mutations: an updated framework for the second decade of HAART. *AIDS Rev.* **2008**, 10, 67–84.
- [107] S.M. Hammer, M.S. Saag, M. Schechter, J.S. Montaner, R.T. Schooley, D.M. Jacobsen, M.A. Thompson, C.C. Carpenter, M.A. Fischl, B.G. Gazzard, J.M. Gatell, M.S. Hirsch, D.A. Katzenstein, D.D. Richman, S. Vella, P.G. Yeni, P.A. Volberding. Treatment for adult HIV infection: recommendations of the International AIDS Society-USA panel. *Top. HIV. Med.* **2006**, 14, 827–843.
- [108] A. H. Kaplan, J.A. Zack, M. Knigge, D.A. Paul, D.J. Kempf, D.W. Norbeck, R. Swanstrom. Partial inhibition of the human immunodeficiency virus type 1 protease results in aberrant virus assembly and the formation of noninfectious particles. *J. Virol.* **1993**, 67, 4050–4055.
- [109] J.R. Rose, L.M. Babe, C.S. Craik. Defining the level of human immunodeficiency virus type 1 (HIV-1) protease activity required for HIV-1 particle maturation and infectivity. *J. Virol.* **1995**, 69, 2751–2758.

- [110] N.E. Kohl, E.A. Emini, W.A. Schleif, L.J. Davis, J.C. Heimbach, R.A. Dixon, E.M. Scolnick, I.S. Sigal. Active human immunodeficiency virus protease is required for viral infectivity, *Proc. Natl. Acad. Sci. U.S.A.* **1988**, 85, 4686–4690.
- [111] C. Peng, B.K. Ho, T. W. Chang, N.T. Chang. Role of human immunodeficiency virus type 1-specific protease in core protein maturation and viral infectivity. *J. Virol.* **1989**, 63, 2550–2556.
- [112] A. Wlodawer, J. Vondrasek. Inhibitors of HIV-1 protease: a major success of structure-assisted drug design. *Annu. Rev. Biophys. Biomol. Struct.* **1998**, 27, 249–284.
- [113] M.E. Noble, J.A. Endicott, L.N. Johnson. Protein kinase inhibitors: insights into drug design from structure. *Science* **2004**, 303, 1800–1805.
- [114] I.V. Alymova, G. Taylor, A. Portner. Neuraminidase Inhibitors as Antiviral Agents. *Curr. Drug Targets Infect. Disord.* **2005**, 5, 401–409.
- [115] P.R. Mittl, M.G. Grutter. Opportunities for structure-based design of protease-directed drugs. *Curr. Opin. Struct. Biol.* **2006**, 16, 769–775.
- [116] A.K. Ghosh. Harnessing nature's insight: design of aspartyl protease inhibitors from treatment of drug-resistant HIV to Alzheimer's disease. *J. Med. Chem.* **2009**, 52, 2163–2176.
- [117] R.B. Rose, C.S. Craik, R.M. Stroud. Domain flexibility in retroviral proteases: structural implications for drug resistant mutations. *Biochemistry* **1998**, 37, 2607–2621.
- [118] W.R. Scott, C.A. Schiffer. Curling of flap tips in HIV-1 protease as a mechanism for substrate entry and tolerance of drug resistance. *Structure* **2000**, 8, 1259–1265.
- [119] A.L. Perryman, J. H. Lin, J.A. McCammon. HIV-1 protease molecular dynamics of a wild-type and of the V82F/I84V mutant: Possible contributions to drug resistance and a potential new target site for drugs, *Protein Sci.* **2004**, 13, 1108–1123.
- [120] F. Liu, A.Y. Kovalevsky, J.M. Louis, P.I. Boross, Y.F. Wang, R.W. Harrison, I.T. Weber. Mechanism of drug resistance revealed by the crystal structure of the unliganded HIV-1 protease with F53L mutation. *J. Mol. Biol.* **2006**, 358, 1191–1199.
- [121] S. Spinelli, Q. Z. Liu, P. M. Alzari, P. H. Hirel, R. J. Poljak. The three-dimensional structure of the aspartyl protease from the HIV-1 isolate BRU. *Biochimie.* **1991**, 73, 1391–1396.
- [122] Y. Tie, P.I. Boross, Y.F. Wang, L. Gaddis, F. Liu, X. Chen, J. Tozser, R.W. Harrison, I.T. Weber. Molecular basis for substrate recognition and drug resistance from 1.1 to

- 1.6 Å resolution crystal structures of HIV-1 protease mutants with substrate analogs. *FEBS J.* **2005**, 272, 5265–5277.
- [123] Z.Q. Beck, G.M. Morris, J. H. Elder. Defining HIV-1 protease substrate selectivity, *Curr. Drug Targets. Infect. Disord.* **2002**, 2, 37–50.
- [124] N.A. Roberts, J.A. Martin, D. Kinchington, A.V. Broadhurst, J.C. Craig, I.B. Duncan, S.A. Galpin, B.K. Handa, J. Kay, A. Krohn. Rational design of peptide-based HIV proteinase inhibitors. *Science* **1990**, 248, 358–361.
- [125] S. Mehandru, M. Markowitz. Tipranavir: a novel non-peptidic protease inhibitor for the treatment of HIV infection. *Expert. Opin. Investig. Drugs* **2003**, 12, 1821–1828.
- [126] Y. Koh, H. Nakata, K. Maeda, H. Ogata, G. Bilcer, T. Devasamudram, J.F. Kincaid, P. Boross, Y.F. Wang, Y. Tie, P. Volarath, L. Gaddis, R.W. Harrison, I.T. Weber, A.K. Ghosh, H. Mitsuya. Novel *bis*-tetrahydrofuranylurethane-containing nonpeptidic protease inhibitor (PI) UIC-94017 (TMC114) with potent activity against multi-PI-resistant human immunodeficiency virus in vitro. *Antimicrob. Agents Chemother.* **2003**, 47, 3123–3129.
- [127] H. Jacobsen, K. Yasargil, D.L. Winslow, J.C. Craig, A. Krohn, I.B. Duncan, J. Mous. Characterization of human immunodeficiency virus type 1 mutants with decreased sensitivity to proteinase inhibitor Ro 31-8959. *J. Virol.* **1995**, 206, 527–534.
- [128] P.R. Harrigan, R.S. Hogg, W.W. Dong, B. Yip, B. Wynhoven, J. Woodward, C.J. Brumme, Z.L. Brumme, T. Mo, C.S. Alexander, J.S. Montaner. Predictors of HIV drug-resistance mutations in a large antiretroviral-naive cohort initiating triple antiretroviral therapy. *J. Infect. Dis.* **2005**, 191, 339–347.
- [129] S.D. Weiser, D. Guzman, E.D. Riley, R. Clark, D.R. Bangsberg. Higher rates of viral suppression with nonnucleoside reverse transcriptase inhibitors compared to single protease inhibitors are not explained by better adherence. *HIV. Clin. Trials.* **2004**, 5, 278–287.
- [130] J.M. Yasuda, C. Miller, J.S. Currier, D.N. Forthal, C.A. Kemper, G.N. Beall, J.G. Tilles, E.V. Capparelli, J.A. McCutchan, R.H. Haubrich. The correlation between plasma concentrations of protease inhibitors, medication adherence and virological outcome in HIV-infected patient. *Antivir. Ther.* **2004**, 9, 753–761.
- [131] D.L. Paterson, S. Swindells, J. Mohr, M. Brester, E.N. Vergis, C. Squier, M.M. Wagener, N. Singh. Adherence to protease inhibitor therapy and outcomes in patients with HIV infection. *Ann. Intern. Med.* **2000**, 133, 21–30.

- [132] D. Nolan, P. Reiss, S. Mallal. Adverse effects of antiretroviral therapy for HIV infection: a review of selected topics. *Expert. Opin. Drug Saf.* **2005**, 4, 201–218.
- [133] A.M. Wensing, C.A. Boucher. Worldwide transmission of drug-resistant HIV. *AIDS Rev.* **2003**, 5, 140–155.
- [134] D.R. Kuritzkes. Resistance to protease inhibitors. *J. HIV. Ther.* **2002**, 7, 87–91.
- [135] R.W. Shafer. Genotypic testing for human immunodeficiency virus type 1 drug resistance. *Clin. Microbiol. Rev.* **2002**, 15, 247–277.
- [136] L. Vergne, M. Peeters, E. Mpoudi-Ngole, A. Bourgeois, F. Liegeois, C. Toure-Kane, S. Mboup, C. Mulanga-Kabeya, E. Saman, J. Jourdan, J. Reynes, E. Delaporte. Genetic diversity of protease and reverse transcriptase sequences in non-subtype-B human immunodeficiency virus type 1 strains: evidence of many minor drug resistance mutations in treatment-naive patients. *J. Clin. Microbiol.* **2000**, 38, 3919–3925.
- [137] J.L. Martinez-Cajas, M.A. Wainberg. Protease inhibitor resistance in HIV-infected patients: Molecular and clinical perspectives. *Antiviral Res.* **2007**, 76, 203–221.
- [138] M. Kozisek, K.G. Saskova, P. Rezacova, J. Brynda, N.M. van Maarseveen, D. de Jong, C.A. Boucher, R.M. Kagan, M. Nijhuis, J. Konvalinka. Ninety-nine is not enough: molecular characterization of inhibitor-resistant human immunodeficiency virus type 1 protease mutants with insertions in the flap region. *J. Virol.* **2008**, 82, 5869–5878.
- [139] F. Tramuto, F. Bonura, S. Mancuso, N. Romano, F. Vitale. Detection of a new 3-Base pair insertion mutation in the protease gene of human immunodeficiency virus type 1 during Highly Active Antiretroviral Therapy (HAART). *AIDS Res. Hum. Retroviruses.* **2005**, 21, 420–423.
- [140] J. Friend, N. Parkin, T. Liegler, J.N. Martin, S.G. Deeks. Isolated lopinavir resistance after virological rebound of a ritonavir/lopinavir-based regimen. *AIDS* **2004**, 18, 1965–1966.
- [141] A. Velazquez-Campoy, S. Muzammil, H. Ohtaka, A. Schon, S. Vega, E. Freire. Structural and thermodynamic basis of resistance to HIV-1 protease inhibition: implications for inhibitor design. *Curr. Drug Targets. Infect. Disord.* **2003**, 3, 311–328.
- [142] S.S. Birajdar, G.D. Hatnapure, A.P. Keche, V.M. Kamble. Synthesis of 2-substituted-1*H*-benzo[d]imidazoles through oxidative cyclization of *o*-phenylenediamine and substituted aldehydes using dioxane dibromide. *RJPBCS.* **2014**, 5(1), 487–493.

- [143] R. Fazaeli, H. Aliyan. A heterogeneous catalyst for efficient and green synthesis of 2-arylbenzothiazoles and 2-arylbenzimidazoles. *Appl. Catal. A*. **2009**, 353, 74–79.
- [144] R. Zhang, L. Lei, Y.G. Xu, W.Y. Hua, G.Q.Gong. Benzimidazol-2-yl or benzimidazol-2-ylthiomethyl benzoylguanidines as novel Na⁺ /H⁺ exchanger inhibitors, synthesis and protection against ischemic-reperfusion injury. *Bioorg. Med. Chem. Lett.* **2007**, 17, 2430–2433.
- [145] Y. Riadi, R. Mamouni, R. Azzalou, M. El Haddad, S. Routier, G. Guillaumet, S. Lazar. An efficient and reusable heterogeneous catalyst Animal Bone Meal(ABM) for facile synthesis of benzimidazoles, benzoxazoles, and benzothiazoles. *Tetrahedron Lett.* **2011**, 52, 3492–3495.
- [146] M.G. Shen, C. Cai. Ytterbium perfluorooctanesulfonates catalyzed synthesis of benzimidazole derivatives in fluoruous solvents. *J. Fluor. Chem.* **2007**, 128, 232–235.
- [147] T. Fonseca, B. Gigantea, T.L. Gilchrist. A short synthesis of phenanthro[2,3-d]imidazoles from dehydroabiatic acid application of the methodology as a convenient route to benzimidazoles. *Tetrahedron* **2001**, 57, 1793–1799.
- [148] J. Kim, J. Kim, H. Lee, B.M. Lee, B.H. Kim. Indium-mediated one-pot benzimidazole synthesis from 2-nitroanilines or 1,2-dinitroarenes with orthoesters. *Tetrahedron*. **2011**, 67, 8027–8033.
- [149] S. Lin, L. Yang. A simple and efficient procedure for the synthesis of benzimidazoles using air as the oxidant. *Tetrahedron Lett.* **2005**, 46, 4315–4319.
- [150] C. Mukhopadhyay, P.K. Tapaswi. PEG-mediated catalyst-free expeditious synthesis of 2-substituted benzimidazoles and bis-benzimidazoles under solvent-less conditions. *Tetrahedron Lett.* **2008**, 49, 6237–6240.
- [151] M.A. Chari, D. Shobha, E.R. Kenawy, S.S. Al-Deyab, B.V.S. Reddy, A. Vinu. Nanoporous aluminosilicate catalyst with 3D cage-type porous structure as an efficient catalyst for the synthesis of benzimidazole derivatives. *Tetrahedron Lett.* **2010**, 51, 5195–5199.
- [152] S. Nandi, S. Samanta, S. Jana, J.K. Ray. Synthesis of substituted benzimidazo[2,1-a]isoquinolines and its condensed analogues using Pd(0)-catalyzed cyclization/C–H activation. *Tetrahedron Lett.* **2010**, 51, 5294–5297.
- [153] A. Dhakshinamoorthy, K. Kanagaraj, K. Pitchumani. Novel cytotoxic constituents of *Orthosiphon diffusus*. *Tetrahedron Lett.* **2011**, 52, 69–73.

- [154] H. Leutbecher, M.A. Constantin, S. Mika, J. Conrad, U. Beifuss. A new laccase-catalyzed domino process and its application to the efficient synthesis of 2-aryl-1H-benzimidazoles. *Tetrahedron Lett.* **2011**, 52, 604–607.
- [155] I. Hutchinson, M.F.G. Stevens, A.D. Westwell. The regiospecific synthesis of 5- and 7-monosubstituted and 5,6-disubstituted 2-arylbenzothiazoles. *Tetrahedron Lett.* **2000**, 41, 425–428.
- [156] L.S. Gadekar, B.R. Arbad, M.K. Lande. Eco-friendly synthesis of benzimidazole derivatives using solid acid scolecite catalyst. *Chin. Chem. Lett.* **2010**, 21, 1053–1056.
- [157] Z.W. Xu, J. Tang, H. Tian. A highly sensitive colorimetric and ratiometric sensor for fluoride ion. *Chin. Chem. Lett.* **2008**, 19, 1353–1357.
- [158] G.R. Jadhav, M.U. Shaikh, R.P. Kale, C.H. Gill. Ammonium metavanadate: A novel catalyst for synthesis of 2-substituted benzimidazole derivatives. *Chin. Chem. Lett.* **2009**, 20, 292–295.
- [159] S.K. Dabhade, R.O. Bora, M. Farooqui, C.H. Gill. DMP (1,1,1-triacetoxy-1,1-dihydro-1,2-benziodoxol-3(1H)-one): A novel catalyst for synthesis of 2-substituted benzimidazoles derivatives. *Chin. Chem. Lett.* **2009**, 20, 893–897.
- [160] M. Dey, K. Deb, S.S. Dhar. VO(acac)₂ catalyzed condensation of *o*-phenylenediamine with aromatic carboxylic acids/aldehydes under microwave radiation affording benzimidazoles. *Chin. Chem. Lett.* **2011**, 22, 296–299.
- [161] K. Khosravi, S. Kazemi. Synthesis of 2-arylbenzimidazoles and 2-arylbenzothiazoles in both room temperature and microwave condition catalyzed by hexamethylenetetramine–bromine complex. *Chin. Chem. Lett.* **2012**, 23, 61–64.
- [162] R.N. Nadaf, S.A. Siddiqui, T. Daniel, R.J. Lahoti, K.V. Srinivasan. Room temperature ionic liquid promoted regioselective synthesis of 2-aryl benzimidazoles, benzoxazoles and benzthiazoles under ambient conditions. *J. Mol. Cat. A: Chem.* **2004**, 214, 155–160.
- [163] R. Trivedi, S.K. De, R.A. Gibbs. A convenient one-pot synthesis of 2-substituted benzimidazoles. *J. Mol. Cat. A: Chem.* **2006**, 245, 8–11.
- [164] M.M. Heravi, S. Sadjadi, H.A. Oskooie, R.H. Shoar, F.F. Bamoharram. Heteropolyacids as heterogeneous and recyclable catalysts for the synthesis of benzimidazoles. *Cat. Commun.* **2008**, 9, 504–507.
- [165] C. Mukhopadhyay, P.K. Tapaswi. Dowex 50W: A highly efficient and recyclable green catalyst for the construction of the 2-substituted benzimidazole moiety in aqueous medium. *Cat. Commun.* **2008**, 9, 2392–2394.

- [166] S.S. Panda, S.C. Jain. Synthesis of 2-arylbenzimidazoles in water. *Synth. Commun.* **2011**, 41, 729–735.
- [167] J.V. Madhav, B.S. Kuarm, B. Rajitha. Dipyrindine copper chloride as a mild and efficient catalyst for the solid state synthesis of 2-substituted benzimidazoles. *ARKIVOC*. **2008** (xiii) 145–150.
- [168] F.K. Behbahani, A. Lotfi. Catalytic performance of SiO₂ supported Fe(ClO₄)₃.6H₂O in synthesis of 2-substituted benzimidazoles. *Eur. Chem. Bull.* **2013**, 2(9), 694–697.
- [169] S. Rostamizadeh, R. Aryan, H.R. Ghaieni. Aqueous 1 M glucose solution as a novel and fully green reaction medium and catalyst for the oxidant-free synthesis of 2-arylbenzimidazoles. *Synth. Commun.* **2011**, 41, 1794–1804.
- [170] Y.Q. Yuan, S.R. Guo. TMSCl/Fe(NO₃)₃-catalyzed synthesis of 2-arylbenzothiazoles and 2-arylbenzimidazoles under ultrasonic irradiation. *Synth. Commun.* **2011**, 41, 2169–2177.
- [171] H. Alinezhad, F. Salehian, P. Biparva. Synthesis of benzimidazole derivatives using heterogeneous ZnO nanoparticles. *Synth. Commun.* **2012**, 42, 102–108.
- [172] L.J. Zhang, J. Xia, Y.Q. Zhou, H. Wang, S.W. Wang. Rare-earth metal chlorides as efficient catalysts for the simple and green synthesis of 1,2-disubstituted benzimidazoles and 2-substituted benzothiazoles under ultrasound irradiation. *Synth. Commun.* **2012**, 42, 328–336.
- [173] B.P. Bandgar, B. Hote, B.L. Korbad, S.A. Patil. ZnO as an efficient and inexpensive catalyst for one pot synthesis of 2, 4, 5-triphenyl-1*H*-imidazole derivatives at room temperature. *E-J. Chem.* **2011**, 8(3), 1339–1345.
- [174] J. Cheng, N. Xiu, X. Li, X. Luo. Convenient method for the preparation of 2-aryl-1*H*-benzimidazole-4-carboxylic acids. *Synth. Commun.* **2005**, 35, 2395–2399.
- [175] S. Kaul, A. Kumar, B. Sain, A. K. Bhatnagar. Simple and convenient one-pot synthesis of benzimidazoles and benzoxazoles using *N,N*-dimethylchloro sulfitemethaniminium chloride as condensing agent. *Synth. Commun.* **2007**, 37, 2457–2460.
- [176] G.M. Coppola. *N*-hydroxyphthalimide/Cobalt acetate a new catalytic oxidative system for the synthesis of benzimidazoles. *Synth. Commun.* **2008**, 38, 3500–3507.
- [177] B.C. Raju, N.D. Theja, J.A. Kumar. Efficient and inexpensive synthesis of benzimidazoles and quinoxalines. *Synth. Commun.* **2008**, 39, 175–188.

- [178] A.T. Khan, T. Parvin, L.H. Choudhury. A Simple and convenient one-pot synthesis of benzimidazole derivatives using cobalt(II) chloride hexahydrate as catalyst. *Synth. Commun.* **2009**, 39, 2339–2346.
- [179] Z. Mao, Z. Wang, J. Li, X. Song, Y. Luo. Rapid and cheap synthesis of benzimidazoles via intermittent microwave promotion: a simple and potential industrial application of air as oxidant. *Synth. Commun.* **2010**, 40, 1963–1977.
- [180] M. Abdollahi-Alibeik, M. Moosavifard. FeCl₃-doped polyaniline nanoparticles as reusable heterogeneous catalyst for the synthesis of 2-substituted benzimidazoles. *Synth. Commun.* **2010**, 40, 2686–2695.
- [181] V.D. Patil, J. Patil, P. Rege, G. Dere. Mild and efficient synthesis of benzimidazole using lead peroxide under solvent-free conditions. *Synth. Commun.* **2011**, 41, 58–62.
- [182] A.V. Narsaiah, A.R. Reddy, J.S. Yadav. Mild and highly efficient protocol for the synthesis of benzimidazoles using Samarium triflate [Sm(OTf)₃]. *Synth. Commun.* **2011**, 41, 262–267.
- [183] K.R. Kumar, P.V.V. Satyanarayana, B.S. Reddy. NaHSO₄-SiO₂ promoted synthesis of benzimidazole derivatives. *Arch. of Appl.Sci. Res.* **2012**, 4 (3):1517–1521.
- [184] K. Niknam, A. Fatehi-Raviz, Synthesis of 2-Substituted Benzimidazoles and Bis-benzimidazoles by Microwave in the Presence of Alumina-Methanesulfonic Acid *J. Iran. Chem. Soc.* **2007**, 4(4), 438–443.
- [185] R.K. Sodhi, S. Paul. Nanosized Mn(acac)₃ Anchored on amino functionalized silica for the selective oxidative synthesis of 2-arylbenzimidazoles, 2-arylbenzothiazoles and aerobic oxidation of benzoin in water. *Catal. Lett.* **2011**, 141, 608–615.
- [186] H. Sharghi, R. Khalifeh, S. Gholamhossein, M. Mahdi, A. Mohammad, M. Eskandar. Simple, efficient and applicable route for synthesis of 2-aryl(heteroaryl)-benzimidazoles at room temperature using copper nanoparticles on activated carbon as a reusable heterogeneous catalyst. *Catal. Lett.* **2011**, 141,1845–1850.
- [187] A. Kumar, R.A. Maurya D. Saxena. Diversity-oriented synthesis of benzimidazole, benzoxazole, benzothiazole and quinazolin-4(3H)-one libraries via potassium persulfate–CuSO₄-mediated oxidative coupling reactions of aldehydes in aqueous micelles. *Mol Divers.* **2010**, 14, 331–341.
- [188] C.A.O Ke, T.U.Y. Qiang, Z. FuMinP. Synthesis of substituted benzoxazoles by the iron(III)-catalyzed aerobic oxidation process. *Sci. China Chem.* **2010**, 53 (1), 130–134.

- [189] M. Kidwai, A. Jahan, D. Bhatnagar. Polyethylene glycol: a recyclable solvent system for the synthesis of benzimidazole derivatives using CAN as catalyst. *J. Chem. Sci.* **2010**, 122(4) 607–612.
- [190] L. M. Dudd, E. Venardou, E. Garcia-Verdugo, P. Licence, A.J. Blake, C. Wilson, M. Poliakoff. Synthesis of benzimidazoles in high-temperature water. *Green Chem.* **2003**, 5, 187–192.
- [191] G. Renard, D.A. Lerner. First simple and mild synthesis of 2-alkylbenzimidazoles involving a supported enzymatic catalyst. *New J. Chem.* **2007**, 31, 1417–1420.
- [192] A.K. Chaturvedi, A.S. Negi, P. Khare. A simple and straightforward synthesis of substituted 2-arylbenzimidazoles over silica gel. *RSC Adv.* **2013**, 3, 4500–4504.
- [193] K. Bahrami, M. M. Khodaei, A. Nejadi. Synthesis of 1,2-disubstituted benzimidazoles, 2-substituted benzimidazoles and 2-substituted benzothiazoles in SDS micelles. *Green Chem.* **2010**, 12, 1237–1241.
- [194] A. Kumar, R.A. Maurya, P. Ahmad. Diversity oriented synthesis of benzimidazole and benzoxa/(thia)zole libraries through polymer-supported hypervalent iodine reagent. *J. Comb. Chem.* **2009**, 11, 198–201.
- [195] S.B. Mohan, T.P. Behera, B.V.V Ravi Kumar. Microwave irradiation versus conventional method: synthesis of benzimidazolyl chalcone derivatives. *Int. J. Chem. Tech Res.* **2010**, 2(3), 1634–1637.
- [196] M.C. Sharma, D.V. Kohli, S. Sharma, A.D. Sharma. Synthesis and antihypertensive activity of some new benzimidazole derivatives of 4'-(6-methoxy-2-substituted-benzimidazole-1-ylmethyl)-biphenyl-2-carboxylic acid in the presences of $\text{BF}_3 \cdot \text{OEt}_2$, *Der Pharmacia Sinica* **2010**, 1(1), 104–115
- [197] A. Mobinikhaledi, A. Hamta, M. Kalhor, M. Shariatzadeh. simple synthesis and biological evaluation of some benzimidazoles using sodium hexafluoroaluminate, Na_3AlF_6 , as an efficient catalyst. *IJPR.* **2014**, 13(1): 95–101.
- [198] A Fazlinia, M. H. Mosslemin, H. Sadoughi. An efficient procedure for the synthesis of benzimidazoles using $\text{H}_2\text{O}_2/\text{SiO}_2\text{-FeCl}_3$ system. *J. Korean Chem. Soc.* **2010**, 54 (5) 579–581.
- [199] P. Saha, T. Ramana, N. Purkait, M.A. Ali, R. Paul, T. Punniyamurthy. Ligand-free copper-catalyzed synthesis of substituted benzimidazoles, 2-aminobenzimidazoles, 2-aminobenzothiazoles, and benzoxazoles. *J. Org. Chem.* **2009**, 74, 8719–8725.

- [200] Y. Kim, M.R. Kumar, N. Park, Y. Heo, S. Lee. Copper-catalyzed, one-pot, three-component synthesis of benzimidazoles by condensation and C–N Bond formation. *J. Org. Chem.* **2011**, 76, 9577–9583.
- [201] K. Bahrami, M.M. Khodaei, F. Naali. Mild and highly efficient method for the synthesis of 2-arylbenzimidazoles and 2-arylbenzothiazoles. *J. Org. Chem.* **2008**, 73, 6835–6837.
- [202] M.M. Heravi, S. Sadjadi, H.A. Oskooie, R.H. Shoar, F.F. Bamoharram. Heteropolyacids as green and reusable catalysts for the synthesis of 3,1,5-benzoxadiazepines. *Molecules* **2007**, 12, 255–262.
- [203] K.U. Sadek, R.A. Mekheimer, A.M.A. Hameed, F. Elnahas, M.H. Elnagdi. Green and highly efficient synthesis of 2-arylbenzothiazoles using glycerol without catalyst at ambient temperature. *Molecules* **2012**, 17, 6011–6019.
- [204] S. Oda, H. Shimizu, Y. Aoyama, T. Ueki, S. Shimizu, H. Osato, and Yoshiyuki Takeuchi. Development of Safe One-Pot Synthesis of N-1- and C-2-Substituted benzimidazole *via* reductive cyclization of *o*-nitroarylamine using Na₂S₂O₄, *Org. Process Res. Dev.* **2012**, 16, 96–101.
- [205] M.M. Heravi, B. Baghernejad, H.A. Oskooie, R. Malakooti. Mesoporous molecular sieve MCM-41 as a novel and efficient catalyst to synthesis of 2-substituted benzimidazoles. *J. Chin. Chem. Soc.* **2008**, 55, 1129–1132.
- [206] J. Lu, B. Yang, Y. Bai. Microwave irradiation synthesis of 2-substituted benzimidazoles using PPA as a catalyst under solvent free conditions. *Synth Commun.* **2002**, 32 (24). 3703–3709.
- [207] M.P. Surpur, P.R. Singh, S.B. Patil, S.D. Samant. One-pot synthesis of benzimidazoles from *o*-nitroanilines under microwaves *via* a reductive cyclization. *Synth Commun.* **2007**, 37, 1375–1379.
- [208] S. Budow, M. Kozłowska, A. Gorska, Z. Kazimierczuk, H. Eickmeier, P.L. Colla, G. Gosselin, F. Seela. Substituted benzimidazoles: antiviral activity and synthesis of nucleosides. *ARKIVOC*, **2009** (iii) 225–250.
- [209] M. Tonelli, M. Simone, B. Tasso, F. Novelli, V. Boido, F. Sparatore, G. Paglietti, S. Pricl, G. Giliberti, S. Blois, C. Ibba, G. Sanna, R. Loddo, P.L. Colla. Antiviral activity of benzimidazole derivatives. II. Antiviral activity of 2-phenylbenzimidazole derivatives. *Bioorg. Med. Chem.* **2010**, 18, 2937–2953.
- [210] X. Wu, P. Öhrngren, A.A. Joshi, A. Trejos, M. Persson, R.K. Arvela, H. Wallberg, L. Vrang, Å. Rosenquist, B. B. Samuelsson, J. Unge, M. Larhed. Synthesis, X-ray

- analysis and biological evaluation of a new class of stereopure lactam-based HIV-1 protease inhibitors. *J. Med. Chem.* **2012**, 55, 2724–2736.
- [211] J.D.A. Tyndall, R.C. Reid, D.P. Tyssen, D.K. Jardine, B. Todd, M. Passmore, D.R. March, L.K. Pattenden, D.A. Bergman, D. Alewood, S.H. Hu, P.F. Alewood, C.J. Birch, J.L. Martin, D.P. Fairlie. Synthesis, stability, antiviral activity, and protease-bound structures of substrate-mimicking constrained macrocyclic inhibitors of HIV-1 protease. *J. Med. Chem.* **2000**, 43, 3495–3504.
- [212] C.T. Lemke, S. Titolo, U. von Schwedler, N. Goudreau, J.F. Mercier, E. Wardrop, A.M. Faucher, R. Coulombe, S.S.R. Banik, L. Fader, A. Gagnon, S.H. Kawai, J. Rancourt, M. Tremblay, C. Yoakim, B. Simoneau, J. Archambault, W.I. Sundquist, S.W. Mason. Distinct effects of two HIV-1 capsid assembly inhibitor families that bind the same site within the *N*-terminal domain of the viral CA protein. *J. Virol.* **2012**, 86(12), 6643–6655
- [213] T.K. Venkatachalam, E.A. Sudbeck, F.M. Uckun. Regiospecific synthesis, X-ray crystal structure and biological activities of 5-bromothiophenethyl thioureas. *Tetrahedron Lett.* **2001**, 42, 6629–6632.
- [214] A.M. Bowser, J.S. Madalengoitia. Synthesis of highly substituted ureas and thioureas through 1,3-diaza-Claisen rearrangements. *Tetrahedron Lett.* **2005**, 46, 2869–2872.
- [215] X.N. Wang, L.T. Shen, S. Ye. NHC-catalyzed enantioselective [2 + 2] and [2 + 2 + 2] cycloadditions of ketenes with isothiocyanates. *Org. Lett.* **2011**, 13(24), 6382–6385.
- [216] I. Yavari, H. Djahaniani. One-step synthesis of substituted 4,7-bis[alkyl(aryl)imino]-3-oxa-6-thia-1-azaspiro[4.4]nona-1,8-dienes. *Tetrahedron Lett.* **2005**, 46, 7491–7493.
- [217] T. Shinada, T. Umezawa, T. Ando, H. Kozuma, Y. Ohfuné. A new entry for the synthesis of *N*-acyl-*N'*-substituted guanidines. *Tetrahedron Lett.* **2006**, 47, 1945–1947.
- [218] I. Yavari, H. Djahaniani. Synthesis of 4*H*-[1,3]dithiolo[4,5-*b*]pyrroles through the reaction of benzoyl isothiocyanate and dialkyl acetylenedicarboxylates in the presence of Ph₃P. *Tetrahedron Lett.* **2006**, 47, 2953–2956.
- [219] I. Yavari, Z. Hossaini, M. Sabbaghan. Efficient synthesis of tetrasubstituted thiophenes by reaction of benzoyl isothiocyanates, ethyl bromopyruvate and enamines. *Tetrahedron Lett.* **2008**, 49, 844–846.
- [220] C.Y. Chen, F.F. Wonga, J.J. Huang, S.K. Lin, M.Y. Yeh. Desulfurization and transformation of isothiocyanates to cyanamides by using sodium bis(trimethylsilyl)amide. *Tetrahedron Lett.* **2008**, 49, 6505–6507.

- [221] S. Cunha, T. Lima da Silva. One-pot and catalyst-free synthesis of thiosemicarbazones via multicomponent coupling reactions. *Tetrahedron Lett.* **2009**, 50, 2090–2093.
- [222] V. Golubev, F. Zubkov, M. Krasavin. A simple, three-component synthesis of 2-aminothiazoles using trimethylsilyl isothiocyanate. *Tetrahedron Lett.* **2013**, 54, 4844–4847.
- [223] H.B. Jalani, A.N. Pandya, D.H. Pandya, J.A. Sharma, V. Sudarsanam, K.K. Vasu. An efficient one-pot synthesis of functionally diverse 2-aminothiazoles from isothiocyanates, amidines/guanidines and halomethylenes. *Tetrahedron Lett.* **2013**, 54, 5403–5406.
- [224] A. Senthilvelan, V.T. Ramakrishnan. A new base-mediated photocyclization to 1,2,4-triazolo[3,4-b]-1,3-(4*H*)-benzothiazines via 1,2,4-triazole-3-thiones. *Tetrahedron Lett.* **2002**, 43, 5119–5121.
- [225] J. Zhang, Y. Shi, P. Stein, K. Atwal, C. Li. One-pot synthesis of *N,N*-disubstituted acylguanidines. *Tetrahedron Lett.* **2002**, 43, 57–59
- [226] J. Ravn, M. Ankersen, M. Begtrup, J.F. Lau. A novel solid-phase synthesis of di- and tri-substituted *N*-acyl ureas. *Tetrahedron Lett.* **2003**, 44, 6931–6935.
- [227] V.J. Cee, N.S. Downing. A one-pot method for the synthesis of 2-aminobenzimidazoles and related heterocycles. *Tetrahedron Lett.* **2006**, 47, 3747–3750.
- [228] B.A. Burkett, J.M. Kane-Barber, R.J. O'Reilly, L. Shi. Polymer-supported thiobenzophenone: a self-indicating traceless 'catch and release' linker for the synthesis of isothiocyanates. *Tetrahedron Lett.* **2007**, 48, 5355–5358.
- [229] H. Stephan, A. Röhrich, S. Noll, J. Steinbach, R. Kirchnerb, J. Seidel. Carbohydration of 1,4,8,11-tetraazacyclotetradecane (cyclam): synthesis and binding properties toward concanavalin A. *Tetrahedron Lett.* **2007**, 48, 8834–8838.
- [230] K.G. Sreejalekshmi, K.N. Rajasekharan. One-pot sequential multicomponent route to 2,4-diaminothiazoles—a facile approach to bioactive agents for cancer therapeutics. *Tetrahedron Lett.* **2012**, 53, 3627–3629.
- [231] C.K. Mirabelli, R.K. Johnson, D.T. Hill, L.F. Faucette, G.R. Girard, G.Y. Kuo, C.M. Sung, S.T. Crooket. Correlation of the *in vitro* cytotoxic and *in vivo* antitumor activities of gold(1) coordination complexes. *J. Med. Chem.* **1986**, 29, 218–223.
- [232] L. Ronconi, C. Marzano, P. Zanello, M. Corsini, G. Miolo, C. Macca, A. Trevisan, D. Fregona. Gold(III) dithiocarbamate derivatives for the treatment of cancer: solution

- chemistry, DNA binding, and hemolytic properties. *J. Med. Chem.* **2006**, 49, 1648–1657.
- [233] R.G. Balasingham, C.F. Williams, H.J. Mottram, M.P. Coogan, S.J.A. Pope. Gold(I) complexes derived from alkynoxy-substituted anthraquinones: syntheses, luminescence, preliminary cytotoxicity, and cell imaging studies. *Organometallics* **2012**, 31, 5835–5843.
- [234] B.A. Al-Maythalony, M. Monim-ul-Mehboob, M. Altaf, M.I.M. Wazeer, A.A. Isab, S. Altuwaijri, A. Ahmed, V. Dhuna, G. Bhatia, K. Dhuna, S.S. Kamboj. Some new [(thione)₂Au(diamine)]Cl₃ complexes: Synthesis, spectroscopic characterization, computational and in vitro cytotoxic studies. *Spectrochim. Acta A: Mol. Biomol. Spectrosc.* **2013**, 115, 641–647.
- [235] R. Visbal, A. Laguna, M.C. Gimeno. Simple and efficient synthesis of [MCl(NHC)] (M = Au, Ag) complexes. *Chem. Commun.* **2013**, 49, 5642–5644.
- [236] J. Arcau, V. Andermark, E. Aguiló, A. Gandioso, A. Moro, M. Cetina, J.C. Lima, K. Rissanen, I. Ott, L. Rodríguez. Luminescent alkynyl-gold(I) coumarin derivatives and their biological activity. *Dalton Trans.* **2014**, 43, 4426–4436.
- [237] S. Newcombe, M. Bobin, A. Shrikhande, C. Gallop, Y. Pace, H. Yong, R. Gates, S. Chaudhuri, M. Roe, E. Hoffmann, E.M.E. Viseux. Gold amides as anticancer drugs: synthesis and activity studies. *Org. Biomol. Chem.* **2013**, 11, 3255–3260.
- [238] C.M. Che, R.W.Y. Sun. Therapeutic applications of gold complexes: lipophilic gold(III) cations and gold(I) complexes for anti-cancer treatment. *Chem. Commun.* **2011**, 47, 9554–9560.
- [239] M.J. McKeage, L. Maharaj, S.J. Berners-Price. Mechanisms of cytotoxicity and antitumor activity of gold(I)phosphine complexes: the possible role of mitochondria. *Coord. Chem. Rev.* **2002**, 232, 127–135.
- [240] A. Molter, J. Rust, C.W. Lehmann, G. Deepa, P. Chiba, F. Mohr. Synthesis, structures and anti-malaria activity of some gold(I) phosphine complexes containing seleno- and thiosemicarbazonato ligands. *Dalton Trans.* **2011**, 40, 9810–9820.
- [241] D. Clajus, R. Kramolowsky, G. Siasios, E.R.T. Tiekink. Binuclear diorganophosphinothioformamido complexes of gold(I) synthesis and crystal structure of [Au(PhPC(S)NPh)]₂ and related systems. *Inorg. Chim. Acta.* **1998**, 281, 64–69.
- [242] M.E. Naggar, I. Shehadi, H.E. Abdou, A.A. Mohamed. Gilded hope for medicine. *Inorganics* **2015**, 3, 139–154.

- [243] P.N. Fonteh, F.K. Keter, D. Meyer, I.A. Guzei, J. Darkwa. Tetra-chloro-(bis-(3,5-dimethylpyrazolyl)methane)gold(III) chloride: An HIV-1 reverse transcriptase and protease inhibitor. *J. Inorg. Biochem.* **2009**, 103, 190–194.
- [244] S.D. Khanye, G.S. Smith, C. Lategan, P.J. Smith, J. Gut, P.J. Rosenthal, K. Chibale. Synthesis and in vitro evaluation of gold(I) thiosemicarbazone complexes for antimalarial activity. *J. Inorg. Biochem.* **2010**, 104, 1079–1083.
- [245] D.I. Bezuidenhout, B. van der Westhuizen, A.J. Rosentha, M. Wörle, D.C. Lilesa, I. Fernández. Fischer-type gold(I) carbene complexes stabilized by aurophilic interactions. *Dalton Trans.* **2014**, 43, 398–401.
- [246] K.J. Akerman, A.M. Fagenson, V. Cyril, M. Taylor, M. T. Muller, M.P. Akerman, O.Q. Munro. Gold(III) macrocycles: nucleotide-specific unconventional catalytic inhibitors of human topoisomerase I. *J. Am. Chem. Soc.* **2014**, 136, 5670–5682.
- [247] P. Gu, Q. Xu, M. Shi. Development and outlook of chiral carbene–gold(I) complexes catalyzed asymmetric reactions. *Tetrahedron Lett.* **2014**, 55, 577–584.
- [248] I.S. Nielsen, E. Taarning, K. Egeblad, R. Madsen, C.H. Christensen. Direct aerobic oxidation of primary alcohols to methyl esters catalyzed by a heterogeneous gold catalyst. *Catal. Lett.* **2007**, 116, 1–2, 35–40.
- [249] A.M. Echavarren, E. Jiménez-Núñez, Complexity via gold-catalyzed molecular gymnastics. *Top. Catal.* **2010**, 53, 924–930.
- [250] K.P. Bhabak, G. Muguesh. Gold(I)-selenolate complexes: Synthesis, characterization and ligand exchange reactions. *J. Chem. Sci.* **2011**, 123(6), 783–789.
- [251] M. Navarro. Gold complexes as potential anti-parasitic agents. *Coord. Chem. Rev.* **2009**, 253, 1619–1626.
- [252] R.G. Buckley, A.M. Elsome, S.P. Fricker, G.R. Henderson, B.R.C. Theobald, R. V. Parish, B.P. Howe, L.R. Kelland. Antitumor properties of some 2-[(dimethylamino)methyl]phenylgold(III) complexes. *J. Med. Chem.* **1996**, 39, 5208–5214.
- [253] J. A. Kovacs, M. Baseler, R.J. Dewar, S. Vogel, R.T. Davey, J. Falloon, M.A. Polis, R.E. Walker, R. Stevens, N. P. Salzman, J.A. Metcalf, H. Masur, H.C. Lane. Controlled trial of interleukin-2 infusions in patients infected with the human immunodeficiency virus. *N. Eng. J. Med.* **1996**, 335, 1350–1356.
- [254] P.N. Fonteh, F.K. Keter, D Meyer. HIV therapeutic possibilities of gold compounds. *BioMetals* **2010**, 23,185–196.

- [255] P. Fonteh, D. Meyer. Novel gold(I) phosphine compounds inhibit HIV-1 enzymes. *Metallomics* **2009**, 1, 427–433.
- [256] S. Ahmad. The chemistry of cyano complexes of gold(I) with emphasis on the ligand scrambling reactions. *Coord. Chem. Rev.* **2004**, 248, 231–243.
- [257] T. Okada, B.K. Patterson, S.Q. Ye, M.E. Gurney. Aurothiolates inhibit HIV-1 infectivity by gold(I) ligand exchange with a component of the virion surface. *Virology* **1993**, 192, 631–642.
- [258] P.J. Sadler, Z. Guo. Metal complexes in medicine: design and mechanism of action. *Pure & Appl. Chem.* **1998**, 70(4), 863–871.
- [259] B.M. Sutton. Gold compounds for rheumatoid arthritis. *Gold Bulletin* **1986**, 19(1), 15–16.
- [260] K. Tepperman, Y. Zhang, P.W. Roy, R. Floyd, Z. Zhao, J.G. Dorsey, R.C. Elder. Transport of the dicyanogold(I) anion. *Met. Based Drugs* **1994**, 1(5–6), 433–443.
- [261] C.F. Shaw, A.A. Isab, J.D. Hoeschele, M. Starich, J. Locke, P. Schulteis, J. Xiao. Oxidation of the phosphine from the auranofin analog, triisopropylphosphine(2,3,4,6-tetra-*O*-acetyl-1-thio-beta-*D*-glucopyranosato-*S*)gold(I), via a protein-bound phosphonium intermediate. *J. Am. Chem. Soc.* **1994**, 116, 2254–2260.
- [262] Y. Zhang, E.V. Hess, K.G. Pryhuber, J.G. Dorsey, K. Tepperman, R.C. Elder. Gold binding sites in red blood cells. *Inorg. Chim. Acta.* **1995**, 229, 271–28.
- [263] Elementar Analysensysteme GmbH, 2005, CHNOS Elemental Analyzer Vario Micro operating instruction.
- [264] Elementar.de, **2000**, Tecnologia Aplicada Internacionan, San Jose, Costa Rica, America Central.
- [265] Bruker, **1999**, SHELXTL-5.1. (includes XS, XL, XP, XSHELL), Bruker AXS Inc., Madison, Wisconsin, USA.
- [266] A.L. Spek. Single-crystal structure validation with the program PLATON *J. Appl. Crystallogr.* **2003**, 36, 7–13.
- [267] L.J. Farrugia. ORTEP-3 for Windows - a version of ORTEP-III with a Graphical User Interface (GUI). *J. Appl. Crystallogr.* **1997**, 30, 565–566.
- [268] D.S. Goodsell, G.M. Morris, A.J. Olson. Automated docking of flexible ligands: applications of AutoDock. *J. Mol. Recogn.* **1996**, 9 (1), 1–5.
- [269] G.M. Morris, D.S. Goodsell, M.E. Pique, W. Lindstrom, R. Huey, S. Forli, W.E. Hart, S. Halliday, R. Belew, A.J. Olson. AutoDock Version 4.2, User Guide, **2002**, 1–66.

- [270] M. J. Frisch, G. W. Trucks, H.B. Schlegel, G. E. Scuseria, M. A. Robb, J. R. Cheeseman, G. Scalmani, V. Barone, B. Mennucci, G. A. Petersson, H. Nakatsuji, M. Caricato, X. Li, H. P. Hratchian, A. F. Izmaylov, J. Bloino, G. Zheng, J. L. Sonnenberg, M. Hada, M. Ehara, K. Toyota, R. Fukuda, J. Hasegawa, M. Ishida, T. Nakajima, Y. Honda, O. Kitao, H. Nakai, T. Vreven, J.A. Montgomery, Jr., J. E. Peralta, F. Ogliaro, M. Bearpark, J. J. Heyd, E. Brothers, K. N. Kudin, V. N. Staroverov, T. Keith, R. Kobayashi, J. Normand, K. Raghavachari, A. Rendell, J.C. Burant, S. S. Iyengar, J. Tomasi, M. Cossi, N. Rega, J. M. Millam, M. Klene, J. E. Knox, J. B. Cross, V. Bakken, C. Adamo, J. Jaramillo, R. Gomperts, R.E. Stratmann, O. Yazyev, A. J. Austin, R. Cammi, C. Pomelli, J. W. Ochterski, R. L. Martin, K. Morokuma, V. G. Zakrzewski, G. A. Voth, P. Salvador, J. J. Dannenberg, S. Dapprich, A. D. Daniels, O. Farkas, J. B. Foresman, J. V. Ortiz, J. Cioslowski, D. J. Fox, Gaussian 09, Revision C.01; Gaussian Inc., Wallingford, CT, Gaussian 09, **2010**.
- [271] Y. Qiao, K. L. Han. Elucidation of the reaction mechanisms and diastereoselectivities of phosphine-catalyzed [4 + 2] annulations between allenolates and ketones or aldimines. *Org. Biomol. Chem.* **2012**, 10, 7689–7706.
- [272] C. Gonzalez, H. B. Schlegel. Reaction path following in mass-weighted internal coordinates. *J. Phys. Chem.* **1990**, 94, 5523–5527.
- [273] C. Gonzalez, H. B. Schlegel. An improved algorithm for reaction path following. *J. Chem. Phys.* **1989**, 90, 2154–2161.
- [274] D.T. Vistica, P. Skehan, D. Scudiero, A. Monks, A. Pittman. M. R. Boyd, Tetrazolium-based assays for cellular viability: A critical examination of selected parameters affecting formazan production. *Cancer Res.* 1991, 51, 2515–2520.
- [275] J. L. Sebaugh. Guidelines for accurate EC50/IC50 estimation. *Pharm. Stat.* **2011**, 10(2), 128–134.
- [276] I. Moreno-Garrido, L. M. Lubián, A. M. V. M. Soares. Influence of cellular density on determination of EC50 in microalgal growth inhibition tests. *Ecotoxicol. Environ. Saf.* **2000**, 47, 112–116.
- [277] Z. Chen, R. Bertin, G. Froidi. EC50 estimation of antioxidant activity in DPPH– assay using several statistical programs. *Food Chem.* **2013**, 138, 414–420.
- [278] B. Alexander, D. J. Browse, S. J. Reading, I. S. Benjamin. accurate mathematical method for calculation of the EC50. *J. Pharmacol. Toxicol.* **1999**, 41, 55–58.

- [279] S. O. Vartanyan, A. B. Sargsyam, A. S. Avakyam, E. A. Markaryn, T. O. Asatryan. Synthesis of Diamides from 1,4-Benzodioxane-2- and Isochroman-1-carboxylic Acids. *Russ. J. Org. Chem.* **2012**, 4,8 (7), 972–976.
- [280] A. G. N. Christian, V. F. Montalbetti. Amide bond formation and peptide coupling *Tetrahedron* **2005**, 61,10827–10852.
- [281] M. Hosseini-Sarvari, H. Sharghi. ZnO as a new catalyst for *N*-formylation of amines under solvent-free conditions. *J. Org. Chem.* **2006**, 71, 6652–6654.
- [282] B. C. Ranu, P. Dutta. A simple and convenient procedure for the conversion of esters to secondary amides. *Synth. Commun.* **2003**, 33, 297–301.
- [283] C. Han, J. P. Lee, E. Lobkovsky, J. A. Porco Jr. Catalytic ester–amide exchange using group (IV) metal alkoxide–activator complexes. *J. Am. Chem. Soc.* **2005**, 127, 10039–10044.
- [284] Y. Suto, N. Yamagiwa, Y. Torisawa. Pd-catalyzed oxidative amidation of aldehydes with hydrogen peroxide *Tetrahedron* **2008**, 49(40) 5732–5735.
- [285] Y. Zhang, C. Chan, S. C. Ghosh, Y. Li, S. H. Hong. Well-defined *N*-heterocyclic carbene based ruthenium catalysts for direct amide synthesis from alcohols and amines *Organometallics* **2010**, 29, 1374–1378.
- [286] M. Sugumaran, M. Y. Kumar. Synthesis and biological activity of novel 2, 5-disubstituted benzimidazole derivatives. *IJPSDR*. **2012**, 4, 80–83
- [287] S. B. Mohan, T. R. Behera, B. V. V. Kumar. Synthesis and biological activity of novel 2, 5-disubstituted benzimidazole derivatives, *Int. J. Chem. Tech. Res.*, **2010**, 2 1634–1637.
- [288] K. Niknam, F Raviz. Synthesis of 2-substituted benzimidazoles and bis-benzimidazoles by microwave in the presence of alumina-methanesulfonic acid. *J. Iran. Chem. Soc.* **2007**, 4, 438–443.
- [289] V.D. Patil, G. Medha, M. Shramesha, J. Aarti. A mild and efficient synthesis of Benzimidazole by using lead peroxide under solvent free condition. *Der Chemica Sinca* **2010**, 1, 125–129.
- [290] R. R. Nagawade, D. B. Shinde. BF₃.OEt₂ promoted solvent free synthesis of benzimidazole derivatives. *Chin. Chem. Lett.* **2006**, 17, 453–456.
- [291] S.E. López, J. Restrepo, B. Pérez, S. Ortiz, J. Salazar. One pot microwave promoted synthesis of 2-aryl-1*H*-benzimidazoles using sodium hydrogen sulfite, *Bull. Korean Chem. Soc.* **2009**, 30(7), 1628–1630.

- [292] M Shen, T. Driver. Iron(II) bromide-catalyzed synthesis of benzimidazoles from aryl azides, *Org. Lett.* **2008**, 10(15), 3367–3370.
- [293] F.H. Allen. The Cambridge Structural Database: a quarter of a million crystal structures and rising, *Acta. Cryst. B* **2002**, 580, 380–388.
- [294] M. Rekha, A. Hamza, B. R. Venugopal, N. Nagaraju. Synthesis of 2-substituted benzimidazoles and 1,5-disubstituted benzodiazepines on alumina and zirconia catalysts. *Chin. J. Catal.* **2012**, 33, 439–446.
- [295] J.S. Yadav, Y. K. Srivastava. An efficient microwave-assisted synthesis of some novel 1,4-diazepine derivatives as possible antimicrobial agents. *Rasayan J. Chem.* **2010**, 3, 726–730.
- [296] F. Odame, P. Kleyi, E. Hosten, R. Betz, K. Lobb, Z. Tshentu. The formation of 2,2,4-trimethyl-2,3-dihydro-1*H*-1,5-benzodiazepine from 1,2-diaminobenzene in the presence of acetone. *Molecules* **2013**, 18, 14293–14305.
- [297] S A. Majid, W. A. Khanday, R. Tomar. Synthesis of 1,5-benzodiazepine and Its derivatives by condensation reaction using H-MCM-22 as catalyst. *J. Biomed. Biotechnol.* **2012**, 1–6
- [298] C.W. Kuo, C.C. Wang, V. Kavala, C.F. Yao. Efficient TCT-catalyzed synthesis of 1,5-benzodiazepine derivatives under mild conditions. *Molecules* **2008**, 13, 2313–2325.
- [299] J.A.P.S. Gomez, T. Maschmeyer. The reductive amination of aldehydes and ketones and the hydrogenation of nitriles: Mechanistic aspects and selectivity control. *Adv. Synth. Catal.* **2002**, 344, 1037–1057.
- [300] P.S Bailey Jr.; C.A Bailey. *Organic Chemistry—A Brief Survey of Concepts and Applications*, 6th ed.; Prentice Hall: Upper Saddle River, NJ, USA, **1999**, 208–210.
- [301] M.A. Ibrahim, M.S.M. Yusof, N.M. Amin. Anti-amoebic properties of carbonyl thiourea derivatives. *Molecules* **2014**, 19, 5191–5204.
- [302] Y. M. Zhang, T. B. Wei, L. Xian, L M. G. An efficient synthesis of polymethylene-bis-aryl thiourea derivatives under the condition of a phase transfer catalysis. *Phosphorus, Sulfur, and Silicon.* **2004**, 1790, 2007–2013.
- [303] A. Yahyazadeh, Z. Ghasemi, Synthesis of unsymmetrical thiourea derivatives. *Eur. Chem. Bull.* **2013**, 573–575.
- [304] S. Saeed, N. Rashid, M.H. Bhatt, P.G. Jones, Synthesis, spectroscopic characterization, mass spectrometry, and crystal structure of N-[(4-bromophenyl)amino] carbonthioyl}benzamide. *Turk J. Chem.* **2010**, 34, 761–770

- [305] S. Saeed, R. Hussain. A convenient way for the preparation of novel thiourea derivatives containing biologically active quinazoline moiety. *Eur. Chem. Bull.* **2013**, 2, 465–467.
- [306] J. Wu, Q. Shi, Z. Chen, M. He, L. Jin, D. Hu, Synthesis and Bioactivity of Pyrazole Acyl Thiourea Derivatives. *Molecules* **2012**, 17, 5139–5150.
- [307] S.J. Xue, S.Y. Ke, T.B. Wei, L. P. Duan, Y. L. Guo. Ultrasonic irradiated synthesis of *N*-(5-aryl-2-furoyl)thiourea derivatives containing substituted pyrimidine ring under phase transfer catalysis. *J. Chin. Chem. Soc.* **2004**, 51, 1013–1018.
- [308] H.M. Fadallah, K.A. Khan, A.M. Asir. Synthesis and biological evaluation of new 3-trifluoromethylpyrazolesulfonyl-urea and thiourea derivatives as antidiabetic and antimicrobial agents. *J. Fluor. Chem.* **2011**, 132, 131–137.
- [309] G.W. Lee, N. Singh, D.O. Jang. Benzimidazole and thiourea conjugated fluorescent hybrid receptor for selective recognition of PO_4^{3-} . *Tetrahedron Lett.* **2008**, 49, 1952–1956.
- [310] J.M. Marquez, O. Lopez, I. Maya, J. Fuentes, J.G. Fernandez-Bolanos. Taurine isothiocyanate: a versatile intermediate for the preparation of ureas, thioureas, and guanidines. Taurine-derived cyclodextrins. *Tetrahedron Lett.* **2008**, 49, 3912–3915.
- [311] G. Madhava, V.K. Subbaiah, R. Srenivasulu, C.N. Raju. Synthesis of novel urea and thiourea derivatives of diphenylphosphoramidate and their antimicrobial activity. *Der Pharm. Lett.* **2012**, 4, 1194–1201.
- [312] K. Takasu, T. Azuma, I. Enkhtaivan, Y. Takemoto. Synthesis and Properties of Chiral Thioureas Bearing an Additional Function at a Remote Position Tethered by a 1,5-Disubstituted Triazole. *Molecules* **2010**, 15, 8327–8348.
- [313] C. K. Özer, H. Arslan, D. VanDerveer, N. Külçü. Synthesis and characterization of *N*-(arylcabamothioyl)-cyclohexanecarboxamide derivatives: the crystal structure of *N*-(naphthalen-1-ylcabamothioyl)cyclohexanecarboxamide. *Molecules* **2009**, 14, 655–666.
- [314] Z. Li, Y. Zhang, Y. Wang. Synthesis and characterization of *N*-benzoyl-*N'*-carboxylalkyl-substituted thiourea derivatives. *Phosphorus, Sulfur and Silicon* **2003**, 178, 293–297.
- [315] A.T. Kabbani, H. Ramadam, H.H. Hammud, A.M. Ghannoum. Synthesis of some metal complexes of *N*-[(benzoylamino)-thioxomethyl]-amino acid (HL). *JUCTM.* **2005**, 40, 339–344.

- [316] D. M. H. AL-Mudhaffar, D.S. Al-Edani, S.M. Dawood. Synthesis, characterization and biological activity of some complexes of some new amino acid derivatives *N*-[(benzoylamino)-thioxomethyl]-amino acid(HL) *J. Korean Chem. Soc.* **2010**, 54, 506–514.
- [317] N. Ngah, M.B. Kassim, B.M. Yamin. (2*S*)-1-(benzoyl thio carbamo-yl)pyrrolidine-2-carboxylic acid monohydrate *Acta Cryst.* **2006**, E62, 4501–4502.
- [318] S. Saeed, N. Rashid, P.G. Jones, M. Ali, R. Hussain. Synthesis, characterization and biological evaluation of some thiourea derivatives bearing benzothiazole moiety as potential antimicrobial and anticancer agents. *Eur. J. Med. Chem.* **2010**, 45, 1323–1331
- [319] C.H. Choi, M. Kertez. Conformational information from vibrational spectra of styrene, *trans*-stilbene, and *cis*-stilbene. *J. Phys. Chem. A.* **1997**, 101, 3823–3831.
- [320] M. Kurt, P. Chinna Babu, N. Sundaraganesan, M. Cinar, M. Karabacak. Molecular structure, vibrational, UV and NBO analysis of 4-chloro-7-nitrobenzofurazan by DFT calculations. *Spectrochim. Acta A.* **2011**, 79 1162–1170.
- [321] F.V. Lewis, C. Ioannides, D.V Parke. Interaction of a series of nitriles with the alcohol-inducible isoform of P450: Computer analysis of structure—activity relationships. *Xenobiotica* **1994**, 24, 401–408.
- [322] L. Padmaja, R.C. Kunar, D. Sajan, I.H. Joe, V.S. Jayakumar, G.R. Pettit, O.F. Nielsen. Density functional study on the structural conformations and intramolecular charge transfer from the vibrational spectra of the anticancer drug combretastatin-A2. *J. Raman Spectrosc.* **2009**, 40, 419–428.
- [323] A. Poiyamozhi, N. Sundaraganesan, M. Karabacak, O. Tanriverdi, M. Kurt. The spectroscopic (FTIR, FT-Raman, UV and NMR), first-order hyperpolarizability and HOMO–LUMO analysis of 4-amino-5-chloro-2-methoxybenzoic acid. *J. Mol. Struct.* **2012**, 1024, 1–12.
- [324] P. Udhayakala, A. Jayanthi, T.V. Rajendiran, S. Gunasekaran. Molecular structure, FT-IR and FT-Raman spectra and HOMO-LUMO analysis of 2-methoxy-4-nitroaniline using ab initio HF and DFT (B3LYP/B3PW91) calculations. *Arch. Appl. Sci. Res.* **2011**, 3, 424–439.
- [325] R.G. Pearson. Absolute electronegativity and hardness correlated with molecular orbital theory. *Proc. Natl. Acad. Sci. U. S. A.* **1986**, 83, 8440–8441.

- [326] R.H. Chen, J.F. Xiang, P. Peng, G.Z. Mo, X.S. Tang, Z.Y. Wang, X.F. Wang. Synthesis of benzimidazoles from amino acids with solvent-free melting method, *Asian J. Chem.* **2014**, 26, 926–932.
- [327] P. Peng, J.F. Xiong, G.Z. Mo, J.L. Zheng, R.H. Chen, X.Y. Chen, Z.Y. Wang. A concise synthesis of benzimidazoles via the microwave-assisted one-pot batch reaction of amino acids up to a 10 g scale. *Amino Acids* **2014**, 2427–2433.
- [328] F. Odame, E. Hosten, Z.R. Tshentu, R. Betz. Crystal structure of dimethyl 2-(4-oxo-2-thio-4-phenyl-1,3-diazabutyl)- succinate, at 200 K, C₁₄H₁₆N₂O₅S. *Z. Kristallogr. NCS* **2014**, 229, 337–338.
- [329] F. Odame, E. Hosten, Z.R. Tshentu, R. Betz. Crystal structure of 3,5-diaza-methyl-2-methyl-6-oxo-6-phenyl-4-thioxohexanoate, at 200 K, C₁₂H₁₄N₂O₃S. *Z. Kristallogr. NCS* **2015**, 230, 9–10.
- [330] F. Odame, E. Hosten, Z.R. Tshentu, R. Betz. Crystal structure of N-(methoxy)methanethiylbenzamide, C₉H₉NO₂S. *Z. Kristallogr. NCS* **2014**, 229, 329–330.
- [331] D. T. Elmore, P.A. Toseland. Degradative studies on peptides and proteins. Part IV. The formation of salts of 2-acylaminothiazol-5-ones by acid-catalysed degradation of N-acylthiocarbamoylpeptides and their behaviour towards nucleophilic reagents. *J. Chem. Soc.* **1957**, 2460–2466
- [332] A. Hajri, R. Abderrahim. Synthesis of [1,2-*a*] benzimidazolo-1,3,5-triazin-2-thione, [1,2-*a*] benzimidazolo-1,3,5-thiadiazin-2-thione, [1,2-*a*] benzimidazolo-1,3,5-triazin-2-amine, and [1,2-*a*] benzimidazol-2-yl amidrazone. *Heteroatom Chem.* **2010**, 21 (5), 279–28.
- [333] S. Kato, Y. Kawahara, H. Kageyama, R. Yamada, O. Niyomura, T. Murai, T. Kanda. Thion (RCSOH), selenon (RCSeOH), and telluron (RCTeOH) acids as predominant species. *J. Am. Chem. Soc.* **1996**, 118, 1262–1267.
- [334] E.D. Jemmis, K.T. Giju, J. Leszczynski, Tautomeric rearrangements in mono- and dichalcogenide analogs of formic acid, HC(X)YH (X, Y = O, S, Se, Te): A theoretical study. *J. Phys. Chem. A*, **1997**, 101 (40), 7389–7395
- [335] P. Gupta, H. L. Yadav, G. Garg, R.S. Pawar, U.K. Patil, P.K. Singour. Synthesis and biological evaluation of some novel 2-aminobenzothiazole derivatives as potential analgesic agents. *Asian J. Research Chem.* **2010**, 3 (1), 47–50
- [336] T. M. Das, C. P. Rao, E. Kolehmainen. Synthesis and characterisation of N-glycosyl amines from the reaction between 4,6-*O*-benzylidene-d-glucopyranose and substituted

- aromatic amines and also between 2-(*o*-aminophenyl)benzimidazole and pentoses or hexoses. *Carbohydr. Res.* **2001**, 334, 261–269.
- [337] Y S. Chhonker, B. Veenu, S R. Hasim, N. Kaushik, D. Kumar, P. Kumar. Synthesis and pharmacological evaluation of some new 2-phenyl benzimidazoles derivatives and their Schiff's bases. *E-J. Chem.* **2009**, 6(S1), S342–S346.
- [338] H. Pessoa-Mahana, C.D. Pessoa-Mahana, R. Salazar, J.A. Valderrama, E. Saez R. Araya-Maturana. Solvent-free synthesis of 6-arylbenzimidazo[1,2-*c*]quinazolines under microwave irradiation. *Synthesis* **2004**, 3, 436–440.
- [339] P. P. Joshi, S.G. Shirodkar. A new approach for the synthesis of 6-aryl -5,6-dihydro benzimidazo[1,2-*c*]quinazoline derivatives and its biological study. *WJPPS.* **2014**, 3(9), 950–958.
- [340] B.A. Insuasty, H. Torres, J. Quiroga, R. Abonia, R. Rodriguez, M. Nogeras, A. Sanchez, C. Saitz, S. L. Alvarez, S.A. Zacchino. Synthesis characterization and in vitro antifungal evaluation of novel benzimidazo[1,2-*c*] quinazolines. *J. Chil. Chem. Soc.* **2006**, 51, 2, 927–932.
- [341] R. Mohebat; G. Mohammadian. An efficient one-pot synthesis of bis-1-(aroyl)-3-(aryl)thiourea. *J Chem. Res.* **2012**, 36, (11), 626–628
- [342] Y.J. Ding, X.B. Chang, X.Q. Yang, W.K. Dong. 3,3'-Dibenzoyl-1,1'-(butane-1,4-diyl)dithiourea. *Acta Cryst.* **2008**. E64, o658
- [343] W.K. Dong, H.B. Yan, L.Q. Chai, Z.W. Lv, C.Y. Zhao. 3,3-Bis(4-nitrophenyl)-1,10-(*p*-phenylene) dithiourea dimethylsulfoxidedisolvate. *Acta Cryst.* **2008**, E64, o1097
- [344] W.K. Dong, X.Q. Yang, L. Xu, L. Wang, G.L. Liu, J.H. Feng. Crystal structure of *N,N*-(1,6-hexamethylene)-bis(benzoylthiourea), C₂₂H₂₆N₄O₂S₂, *Z. Kristallogr. NCS* **2007**, 222, 279–280.
- [345] F. Kurzer. Heterocyclic compounds from urea derivatives. Part XX1.1 adducts from thiocarbonohydrazides and aroyl Isothiocyanates and their cyclisation. *J. Chem. Soc. (C)*, **1971**, 2932–2938.
- [346] S.K. Kang, N. S. Cho, M.K. Jeon. 1-Benzoyl-2-thiobiuret. *Acta Cryst.* **2012**, E68, o395
- [347] E.I. Thiam, M. Diop, M. Gaye, A.S. Sall, A.H. Barry. 1,2-Bis(*N'*-benzoylthioureido) benzene. *Acta Cryst.* **2008**, E64, o776
- [348] Y.H. Lee, W.S. Han, H.J. Lee, S.M. Ahn, T.K. Hong. Lead(II) ion selective poly(aniline) solid contact electrode based on 1,2-bis(*N'*-benzoylthioureido)ethane, propane and butane ionophores. *J. Anal. Chem.* **2015**, 70 (5), 621–626.

- [349] G. Dou, M. Wang, D. Shi. One-pot synthesis of quinazolinone derivatives from nitro-compounds with the aid of low-valent titanium. *J. Comb. Chem.* **2009**, 11, 151–154.
- [350] J.B. Feng, D. Wei, J.L. Gong, X. Qi, X.F. Wu. Oxidative synthesis of benzamides from toluenes and DMF, *Tetrahedron Lett.* **2014**, 55, 5082–5084
- [351] M. Sharif, J.L. Gong, P. Langer, M. Beller, X.F. Wu. A novel oxidative procedure for the synthesis of benzamides from styrenes and amines under metal-free conditions, *Chem. Commun.* **2014**, 50, 4747–4750
- [352] S. Kegnæs, J. Mielby, U. V. Mentzel, T. Jensen, P. Fristrup, A. Riisager. One-pot synthesis of amides by aerobic oxidative coupling of alcohols or aldehydes with amines using supported gold and base as catalysts. *Chem. Commun.* **2012**, 48, 2427–2429.
- [353] A. Alalla, M. Merabet-Khelassi, L. Aribi-Zouiouche, O. Rian. Green synthesis of benzamides in solvent and activation free conditions. *Synth. Commun.* **2014**, 44: 2364–2376.
- [354] K.T. Barrett, S.J. Miller. Enantioselective synthesis of atropisomeric benzamides through peptide-catalyzed bromination. *J. Am. Chem. Soc.* **2013**, 135, 2963–2966.
- [355] H. Kusama, Y. Miyashita, J. Takaya, N. Iwasawa. Pt(II)- or Au(III)-catalyzed [3+2] cycloaddition of metal-containing azomethine ylides: highly efficient synthesis of the mitosene skeleton. *Org. Lett.* **2006**, 8(2), 289–292
- [356] Z. Li, X. Ding, C. He. Nitrene transfer reactions catalyzed by gold complexes. *J. Org. Chem.* **2006**, 71, 5876–5880.
- [357] A. Iglesias, K. Muñoz. Oxidative interception of the hydroamination pathway: A gold-catalyzed diamination of alkenes. *Chem. Eur. J.* **2009**, 15(40) 10563–10569
- [358] J. Vicente, M.T. Chicote. The ‘acac method’ for the synthesis of coordination and organometallic compounds: synthesis of gold complexes. *Coord. Chem. Rev.* **1999**, 193–195, 1143–1161.
- [359] Özdemir, N. Temelli, S. Günal, S. Demir. Gold(I) complexes of *N*-heterocyclic carbene ligands containing benzimidazole: synthesis and antimicrobial activity. *Molecules* **2010**, 15, 2203–2210.

APPENDIX A

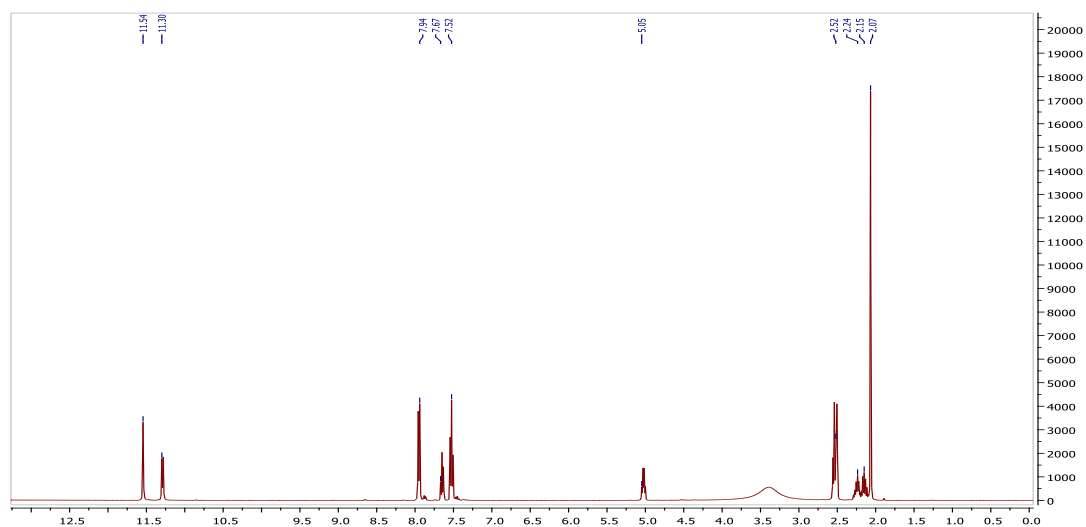
CHARACTERIZATION SPECTRAL FOR AMINO ACID DERIVATIVES OF
BENZOYL ISOTHIOCYANATE

Figure A3.1 ^1H NMR spectrum of 2-[(benzoylcarbamothioyl)amino]-4-(methylsulfonyl)butanoic acid (**7**).

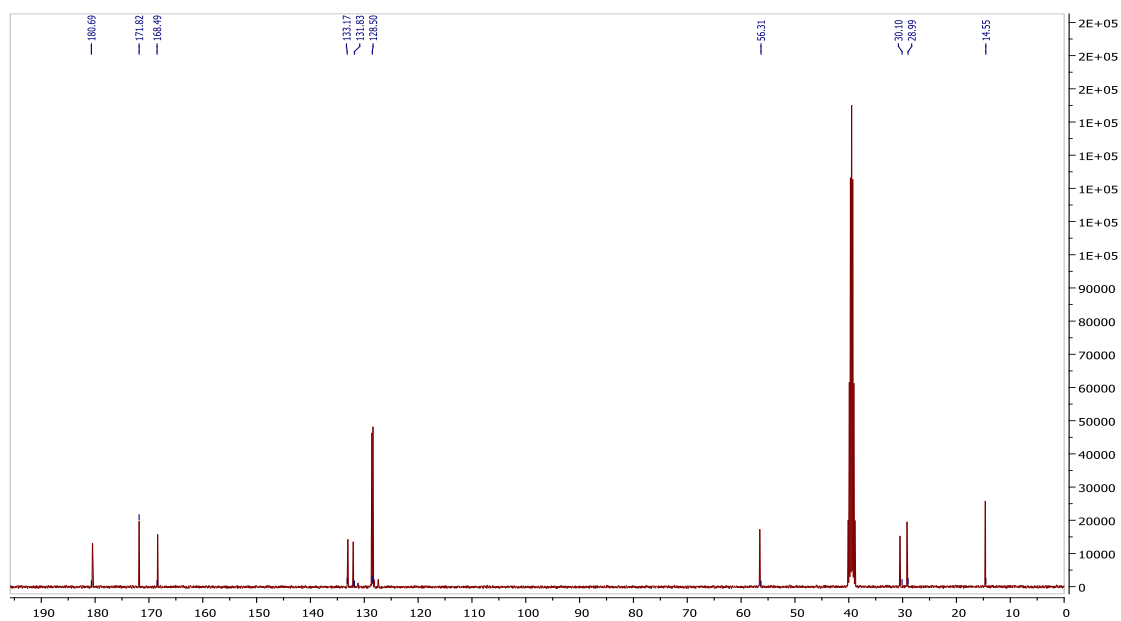


Figure A3.2 ^{13}C NMR spectrum of 2-[(benzoylcarbamothioyl)amino]-4-(methylsulfanyl)butanoic acid (**7**).

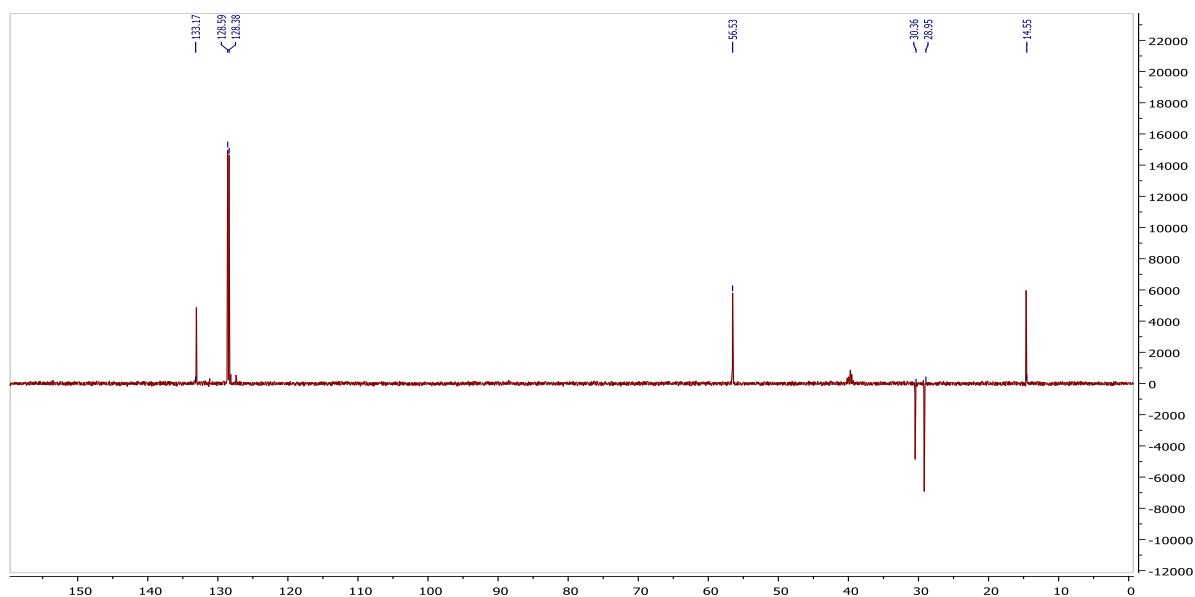


Figure A3.3 DEPT spectrum of 2-[(benzoylcarbamothioyl)amino]-4-(methylsulfanyl)butanoic acid (**7**).

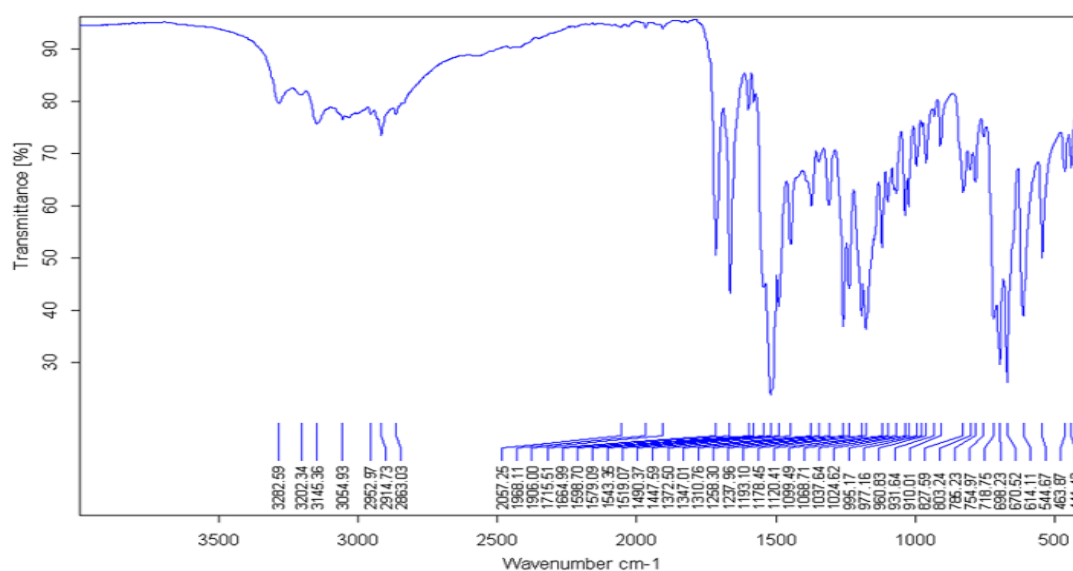


Figure A3.4 IR spectrum of 2-[(benzoylcarbamothioyl)amino]-4-(methylsulfanyl)butanoic acid (**7**).

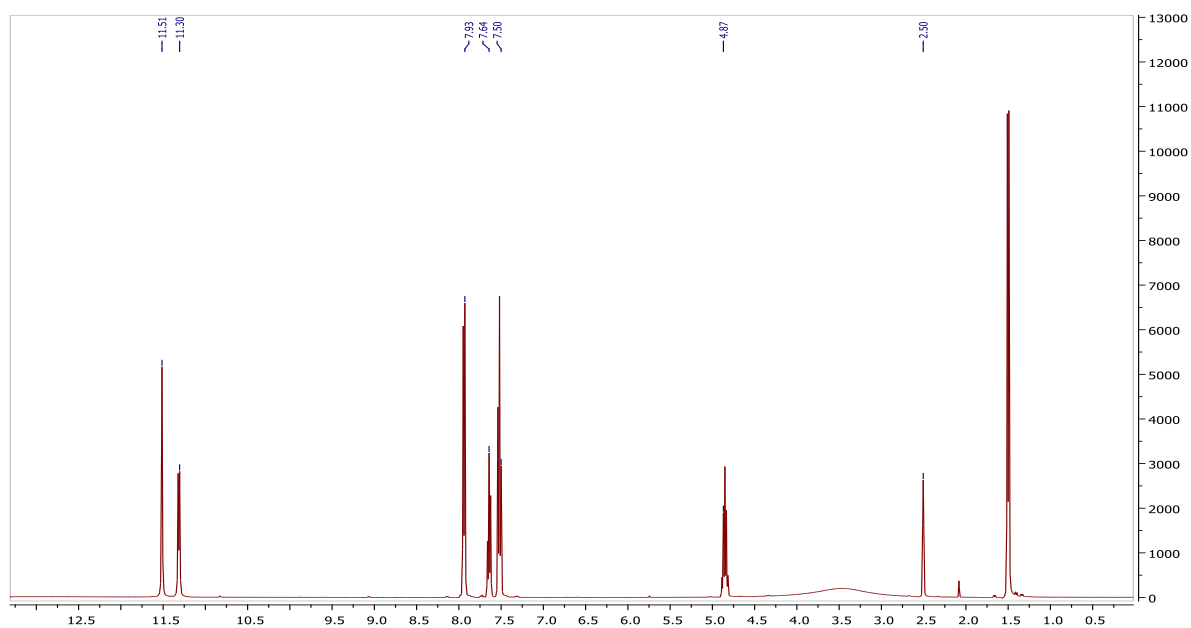


Figure A3.5 ^1H NMR spectrum of 2-[(benzoylcarbamothioyl)amino]propanoic acid (**8**).

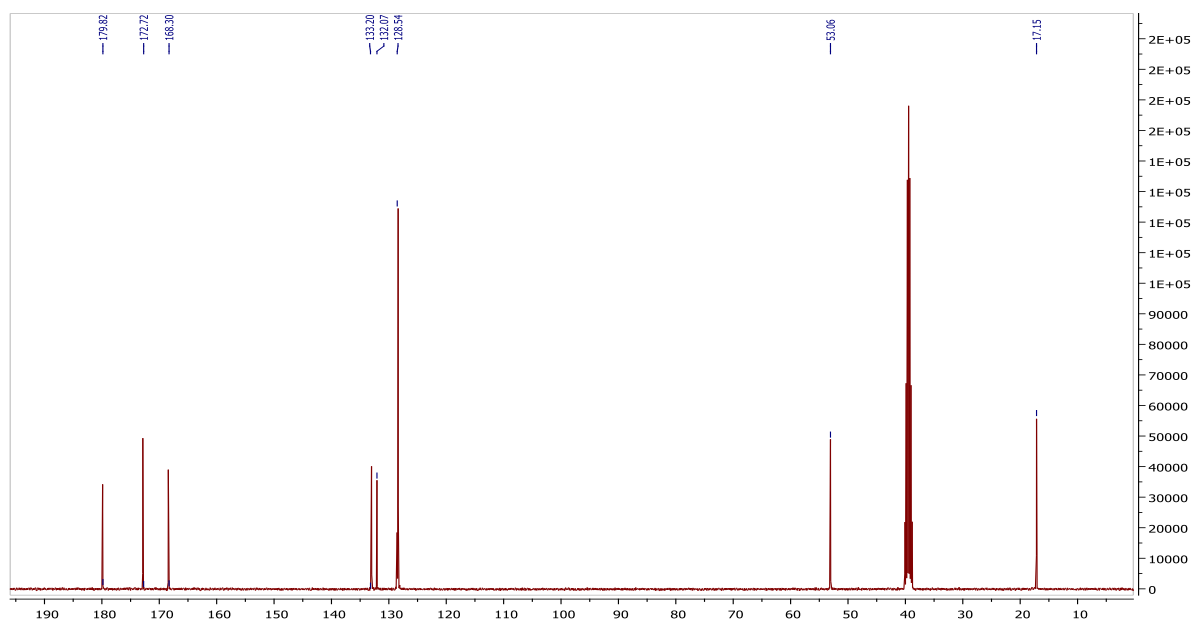


Figure A3.6 ^{13}C NMR spectrum of 2-[(benzoylcarbamothioyl)amino]propanoic acid (**8**).

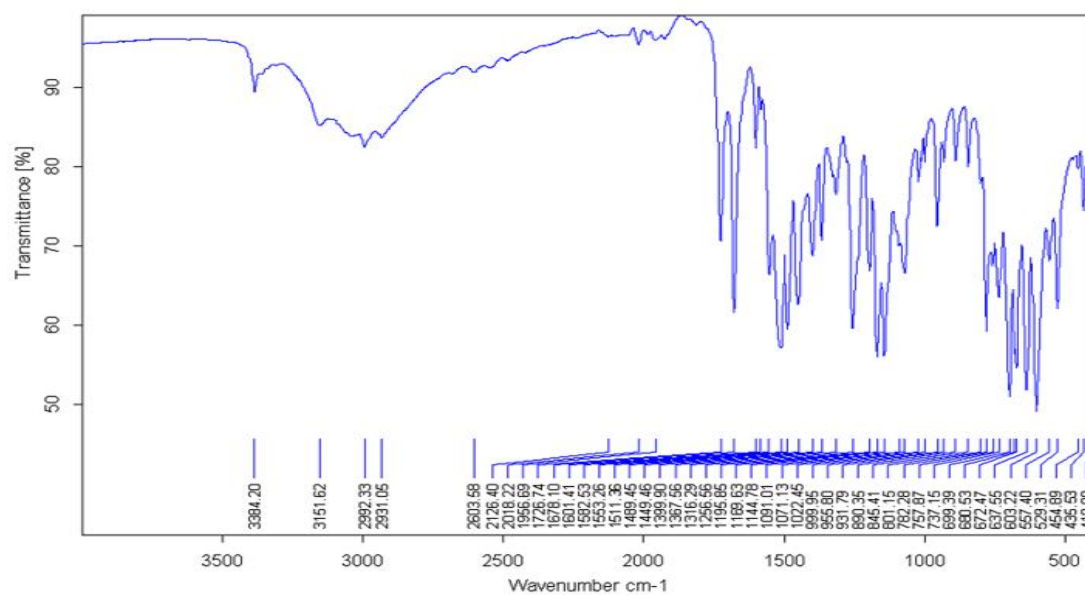


Figure A3.7 IR spectrum of 2-[(benzoylcarbamothioyl)amino]propanoic acid (**8**).

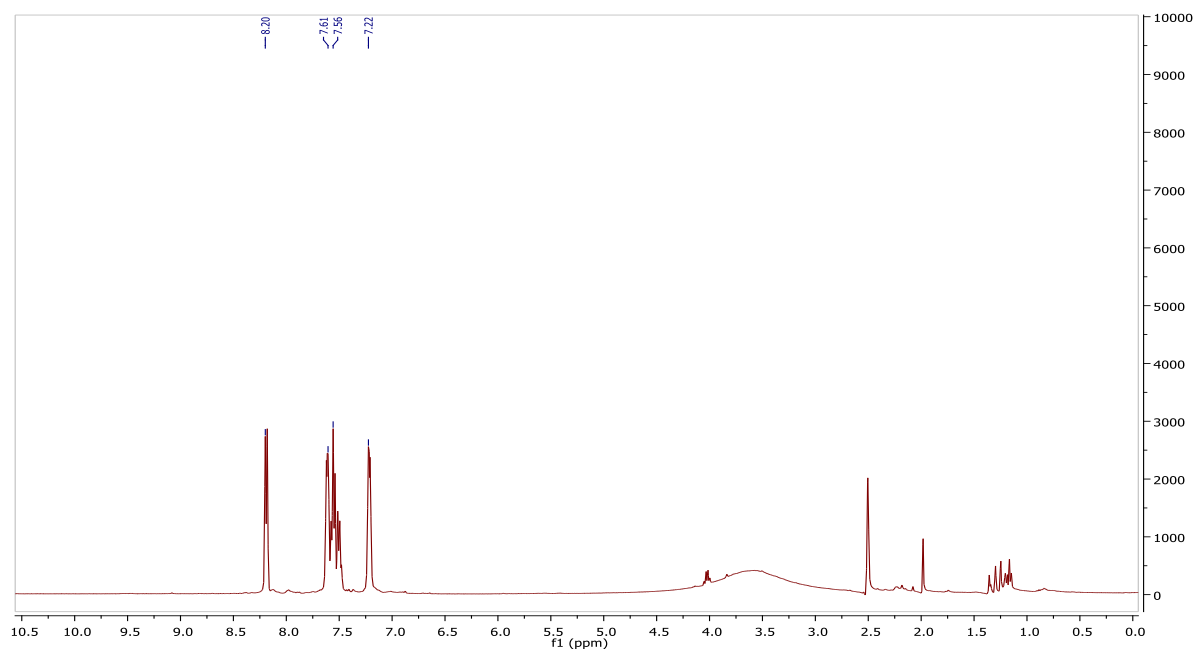


Figure A3.8 ^1H NMR spectrum of 2-phenyl-1*H*-benzimidazole (**9**).

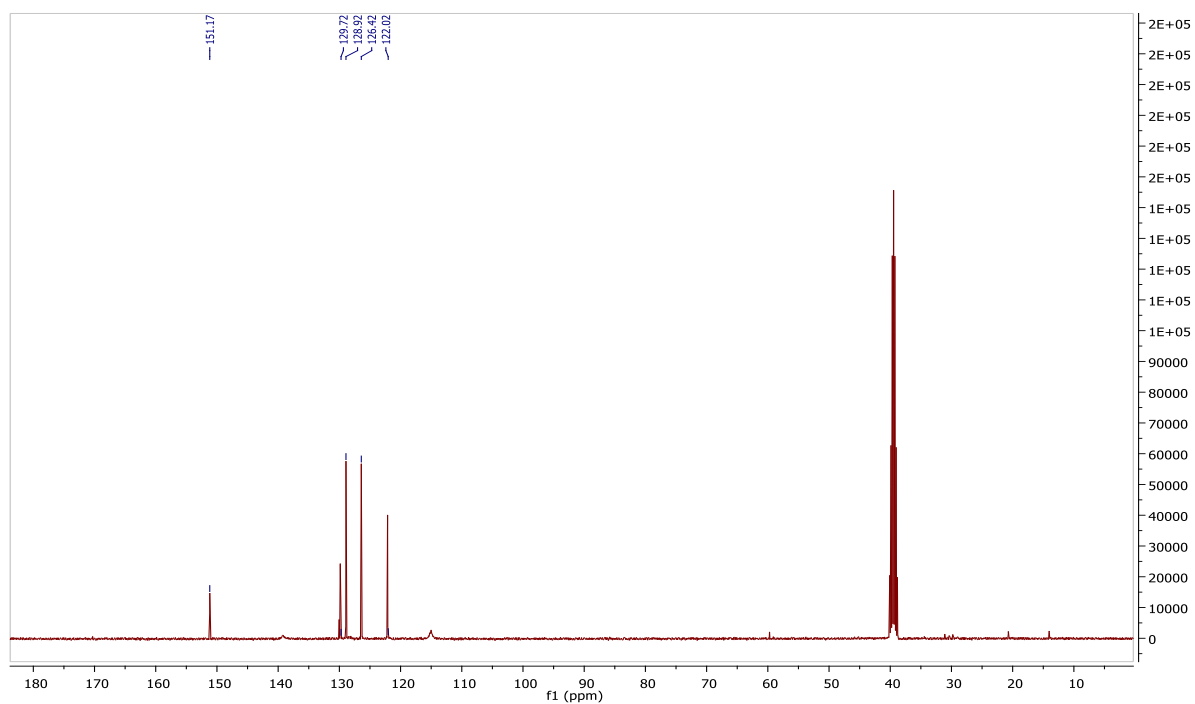


Figure A3.9 ¹³C NMR spectrum of 2-phenyl-1H-benzimidazole (9).

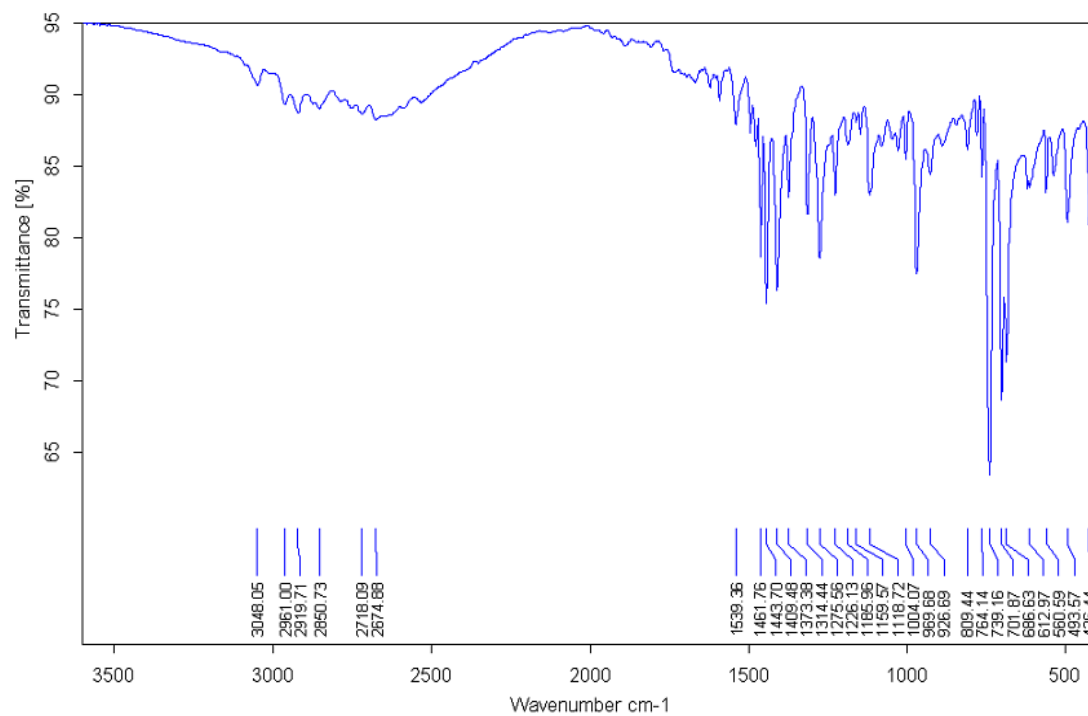


Figure A3.10 IR spectrum of 2-phenyl-1H-benzimidazole (9).

APPENDIX B

CHARACTERIZATION DATA FOR TETRAAZATRICYCLIC DERIVATIVES

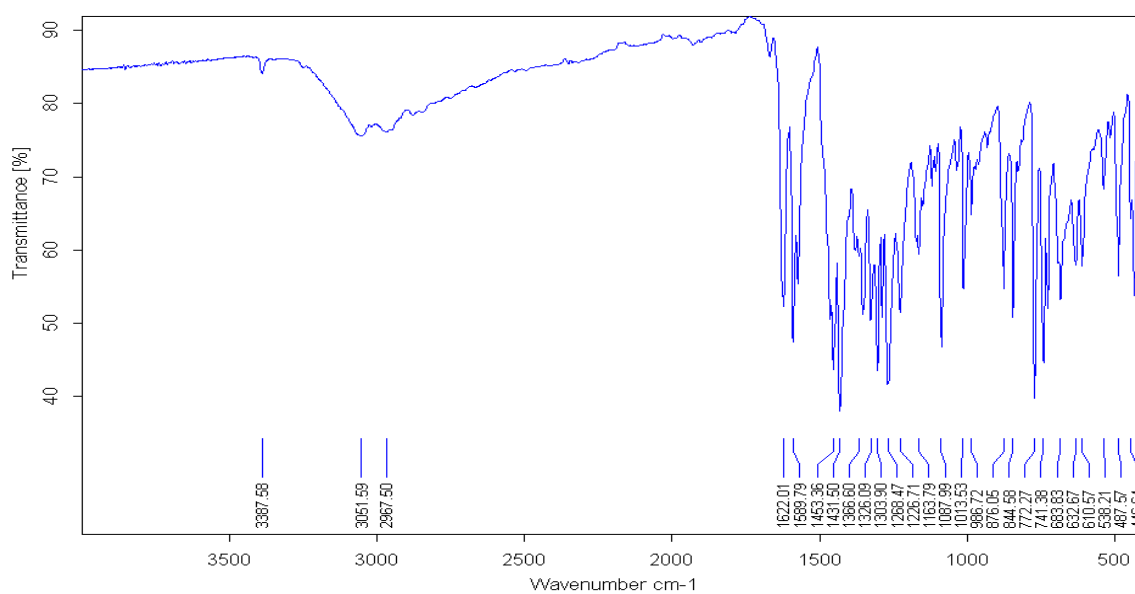


Figure A4.1 IR spectrum of 11-(4-chlorophenyl-1,8,10,12-tetraazatricyclo[7.4.0.0^{2,7}]trideca-2(7),3,5,9,11-pentaene-13-thione (**12**).

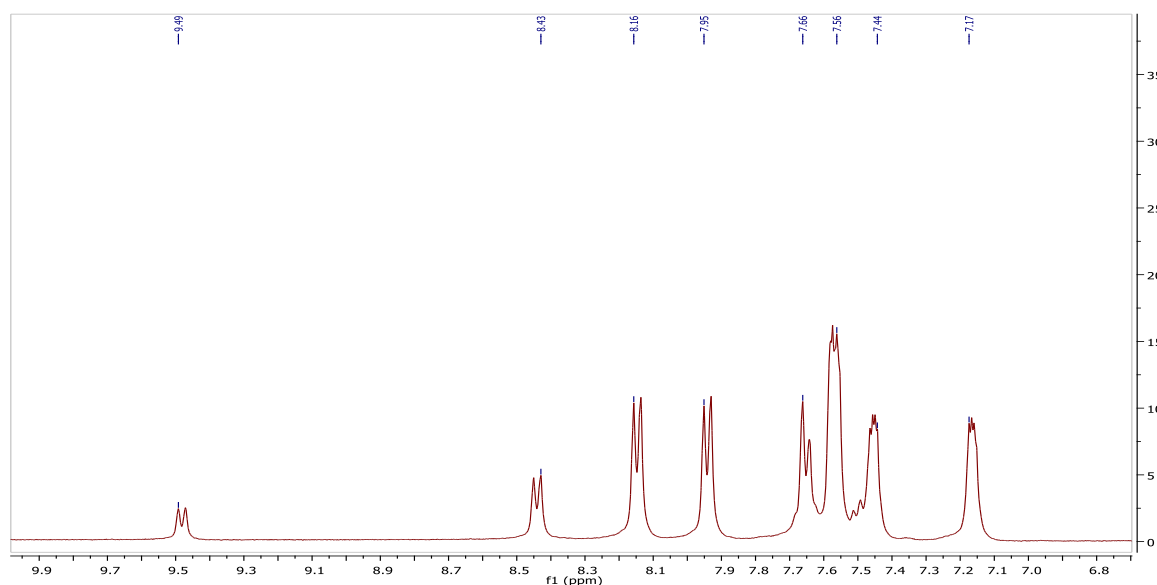


Figure A4.2 ¹H NMR spectrum of 11-(4-chlorophenyl-1,8,10,12-tetraazatricyclo[7.4.0.0^{2,7}]trideca-2(7),3,5,9,11-pentaene-13-thione (**12**).

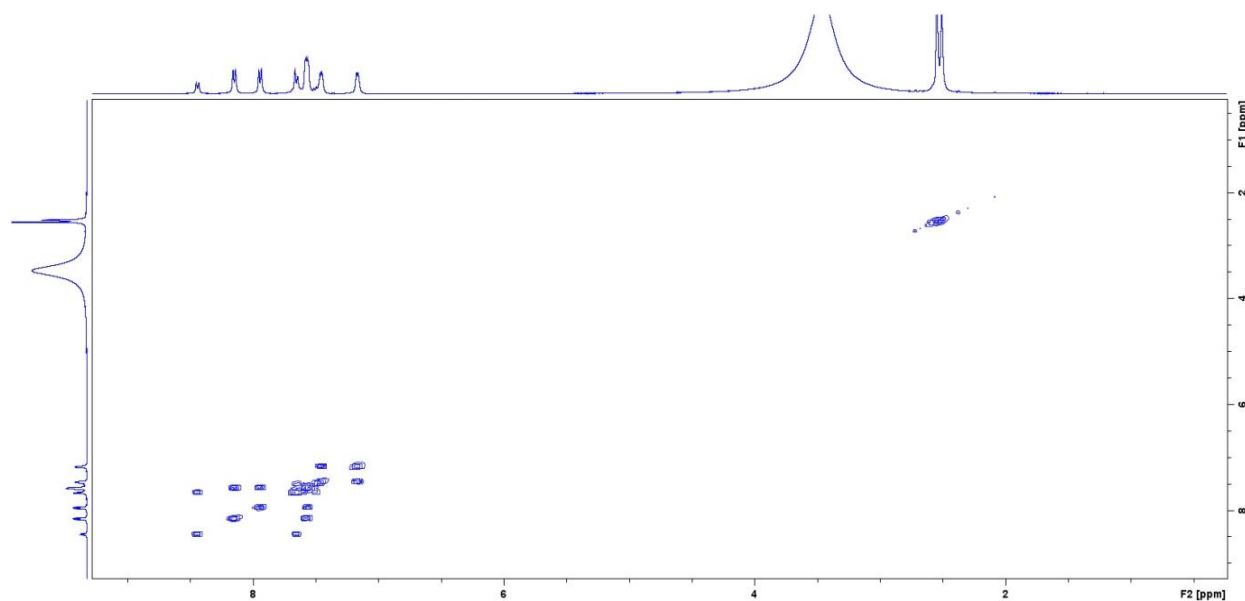


Figure A4.3 ^1H - ^1H COSY spectrum of 11-(4-chlorophenyl)-1,8,10,12-tetraazatricyclo[7.4.0.0^{2,7}]trideca-2(7),3,5,9,11-pentaene-13-thione (**12**).

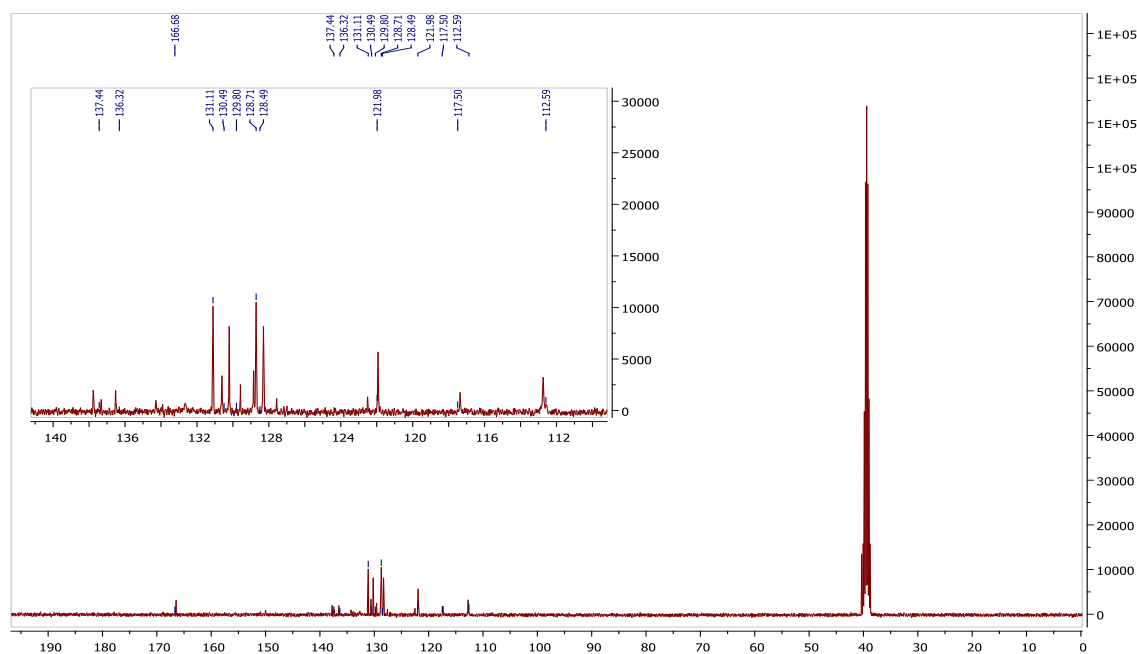


Figure A4.4 ^{13}C NMR spectrum of 11-(4-chlorophenyl)-1,8,10,12-tetraazatricyclo[7.4.0.0^{2,7}]trideca-2(7),3,5,9,11-pentaene-13-thione (**12**).

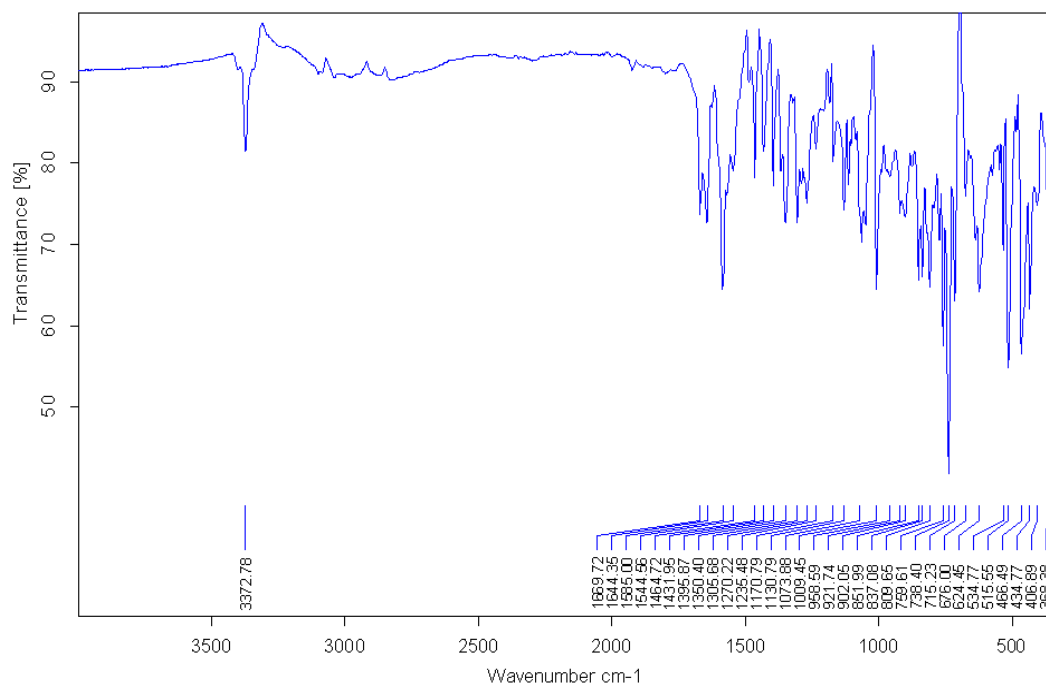


Figure A4.5 IR spectrum of 11-(4-bromophenyl)-,8,10,2-tetraazatricyclo[7.4.0.0^{2,7}]trideca-2(7),3,5,9,11-pentaene-13-thione (**13**).

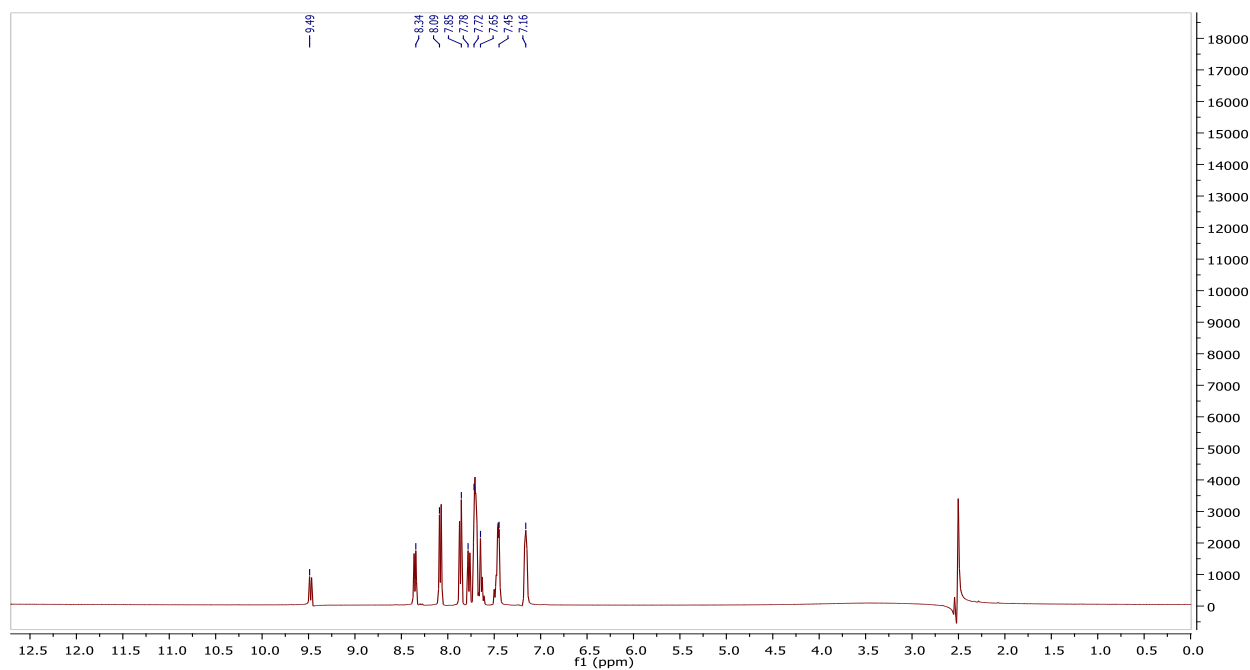


Figure A4.6 ¹H NMR spectrum of 11-(4-bromophenyl)-,8,10,2-tetraazatricyclo [7.4.0.0^{2,7}]trideca-2(7),3,5,9,11-pentaene-13-thione (**13**).

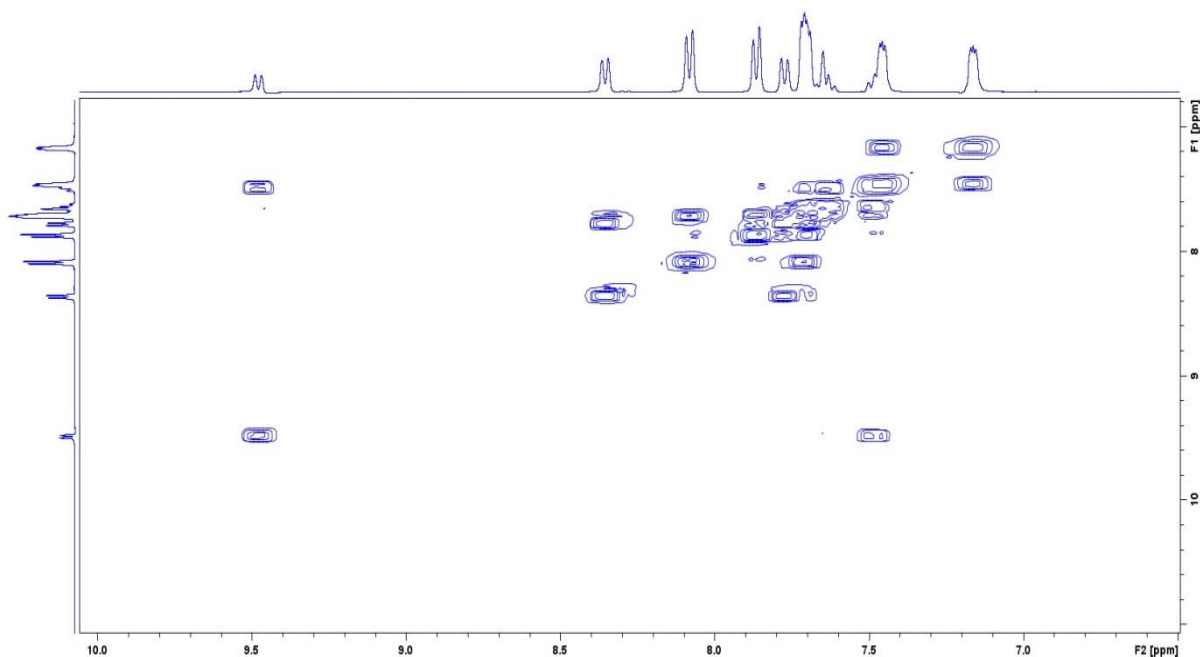


Figure A4.7 ^1H ^1H COSY spectrum of 11-(4-bromophenyl)-,8,10,2-tetraazatricyclo[7.4.0.0^{2,7}]trideca-2(7),3,5,9,11-pentaene-13-thione (**13**).

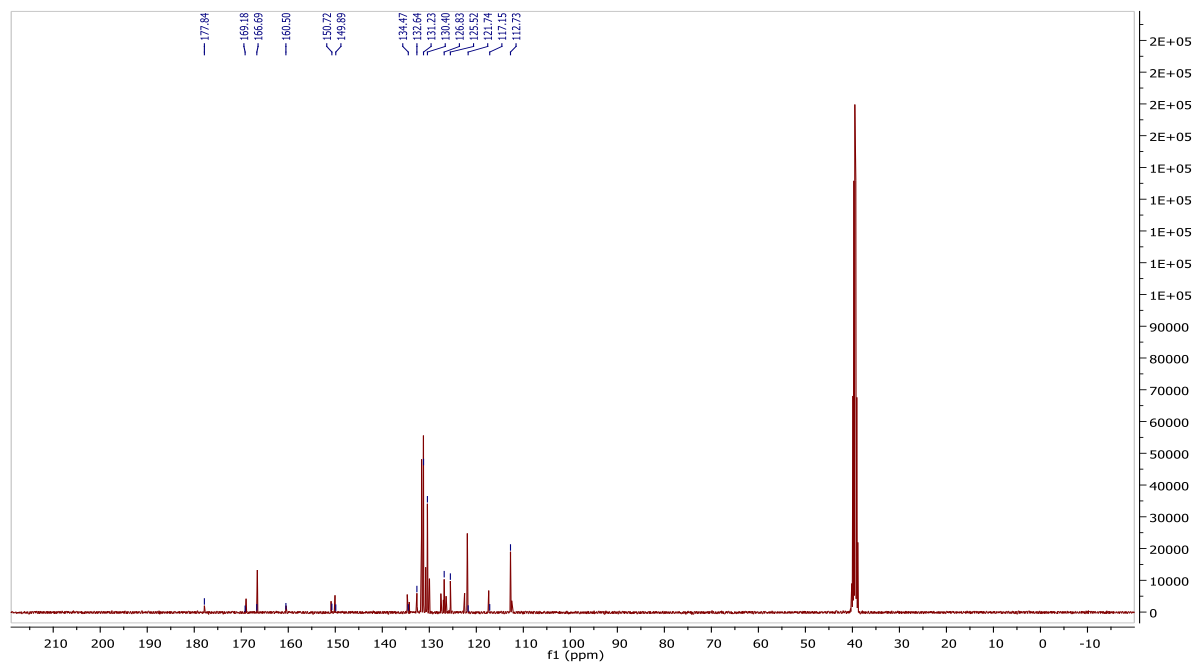


Figure A4.8 ^{13}C NMR spectrum of 11-(4-bromophenyl)-,8,10,2-tetraazatricyclo[7.4.0.0^{2,7}]trideca-2(7),3,5,9,11-pentaene-13-thione (**13**).

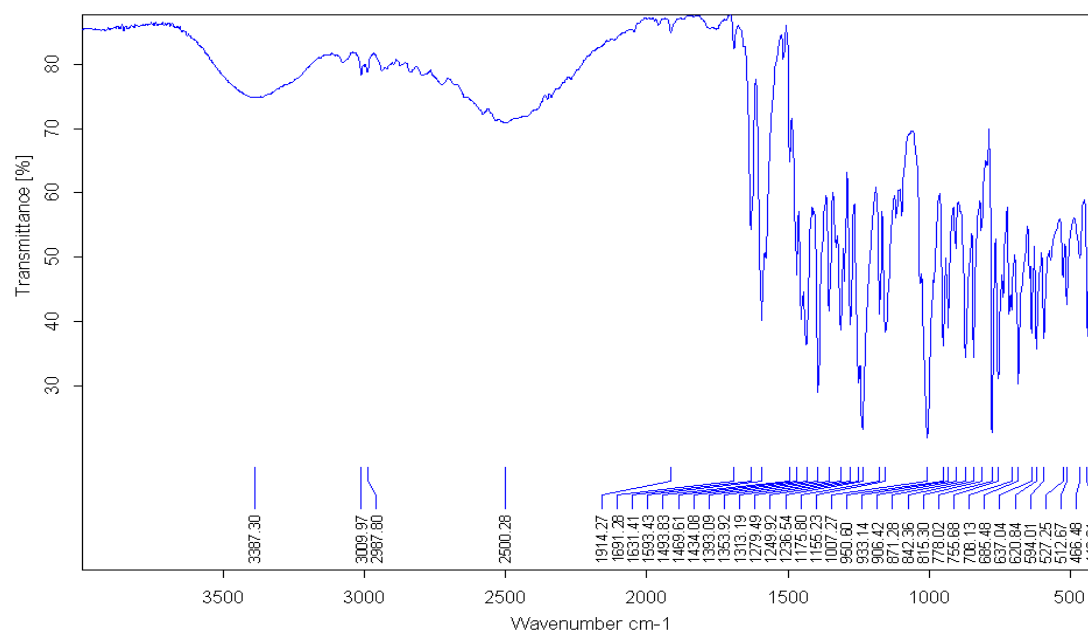


Figure A4.9 IR spectrum of 11-(4-methoxyphenyl)-1,8,10,12-tetraazatricyclo[7.4.0.0^{2,7}] trideca-2(7),3,9,1-pentaene-13-thione (**14**).

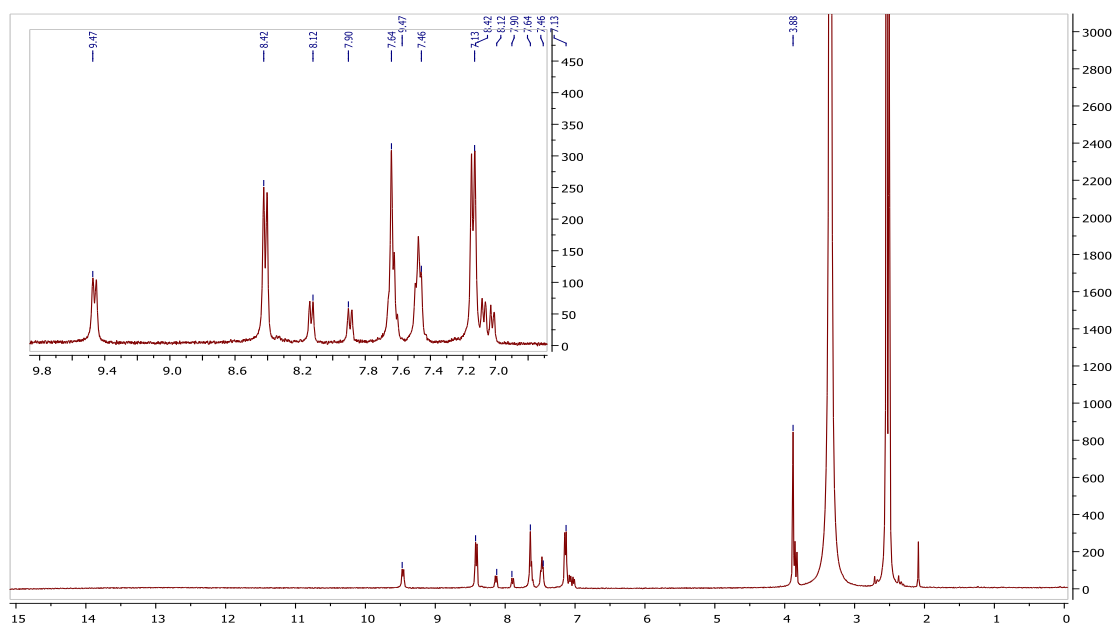


Figure A4.10 ¹H NMR spectrum of 11-(4-methoxyphenyl)-1,8,10,12-tetraazatricyclo[7.4.0.0^{2,7}] trideca-2(7),3,9,1-pentaene-13-thione (**14**).

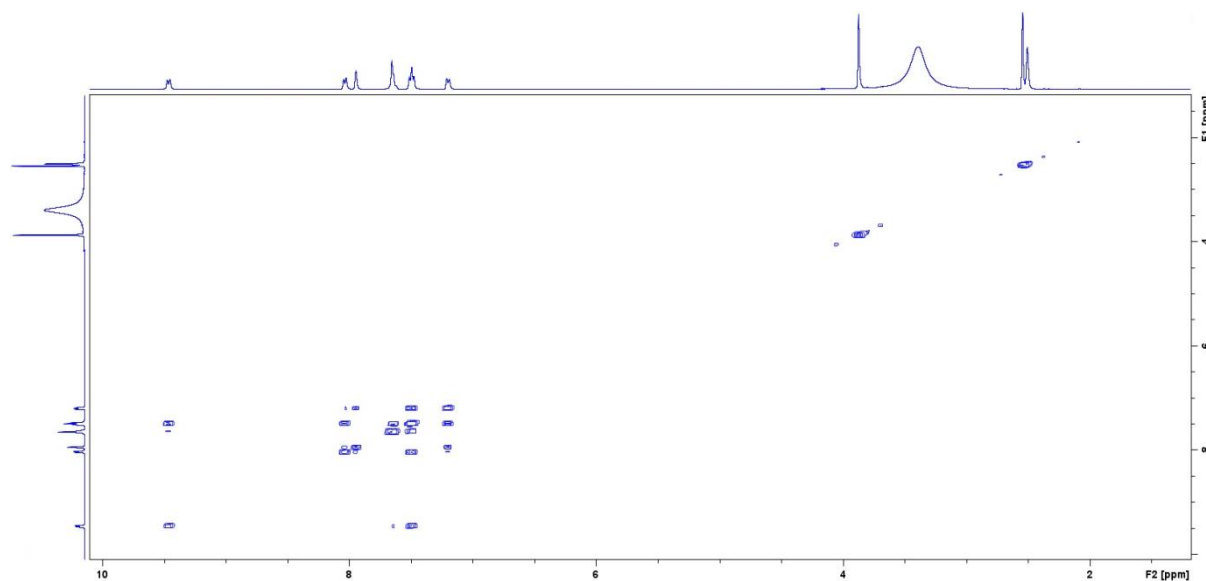


Figure A4.11 ^1H ^1H COSY spectrum of 11-(4-methoxyphenyl)-1,8,10,12-tetraazatricyclo[7.4.0.0^{2,7}]trideca-2(7),3,9,1-pentaene-13-thione (**14**).

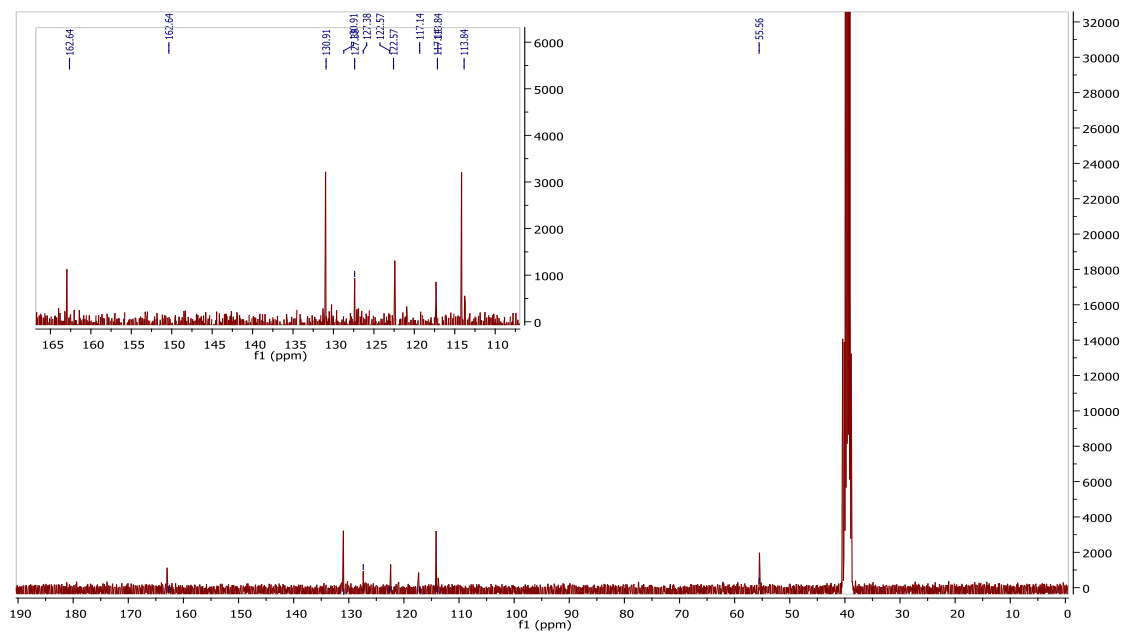


Figure A4.12 ^{13}C NMR spectrum of 11-(4-methoxyphenyl)-1,8,10,12-tetraazatricyclo[7.4.0.0^{2,7}]trideca-2(7),3,9,1-pentaene-13-thione (**14**).

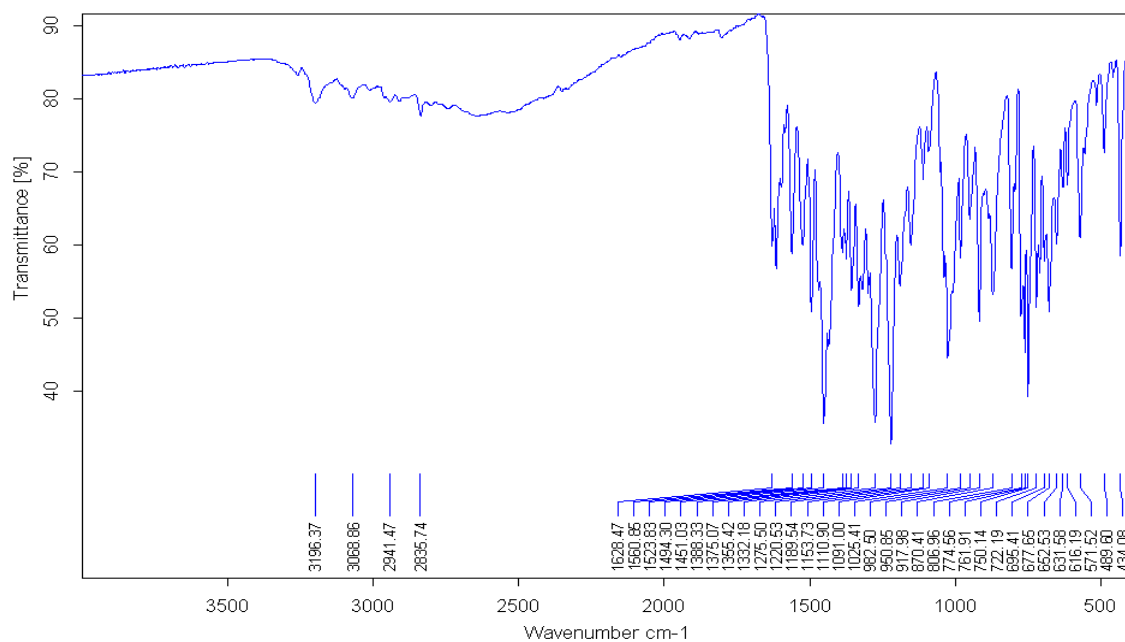


Figure A4.13 IR spectrum of 11-(3-methoxyphenyl)-1,8,10,12-tetraazatricyclo[7.4.0.0^{2,7}]trideca-2(7),3,5,9,11-pentaene-13-thione (**15**).

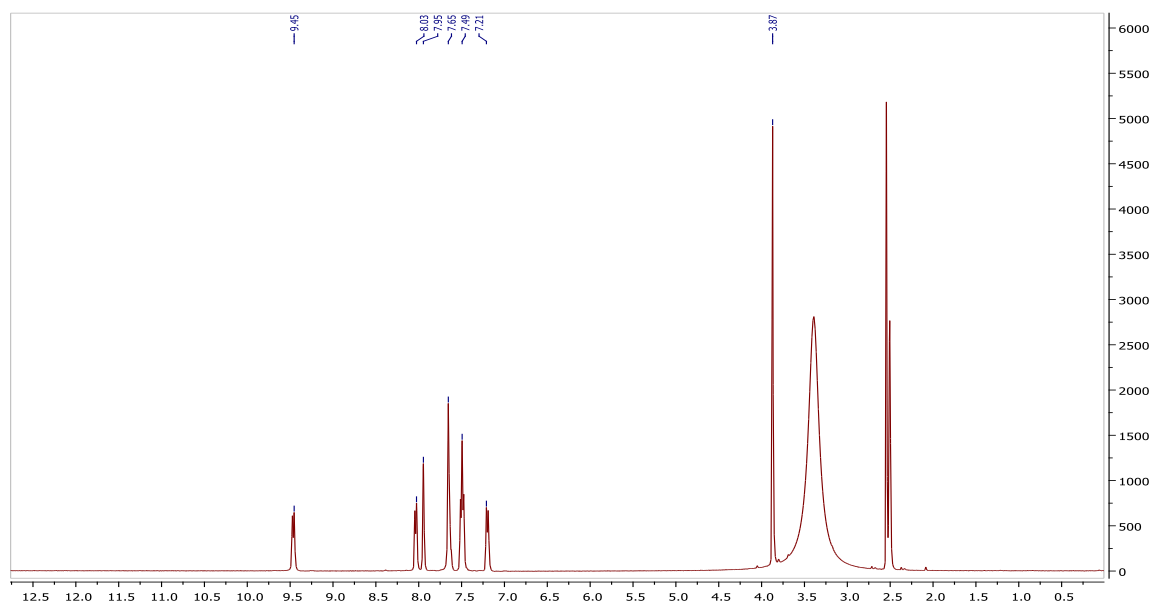


Figure A4.14 ¹H NMR spectrum of 11-(3-methoxyphenyl)-1,8,10,12-tetraazatricyclo[7.4.0.0^{2,7}]trideca-2(7),3,5,9,11-pentaene-13-thione (**15**).

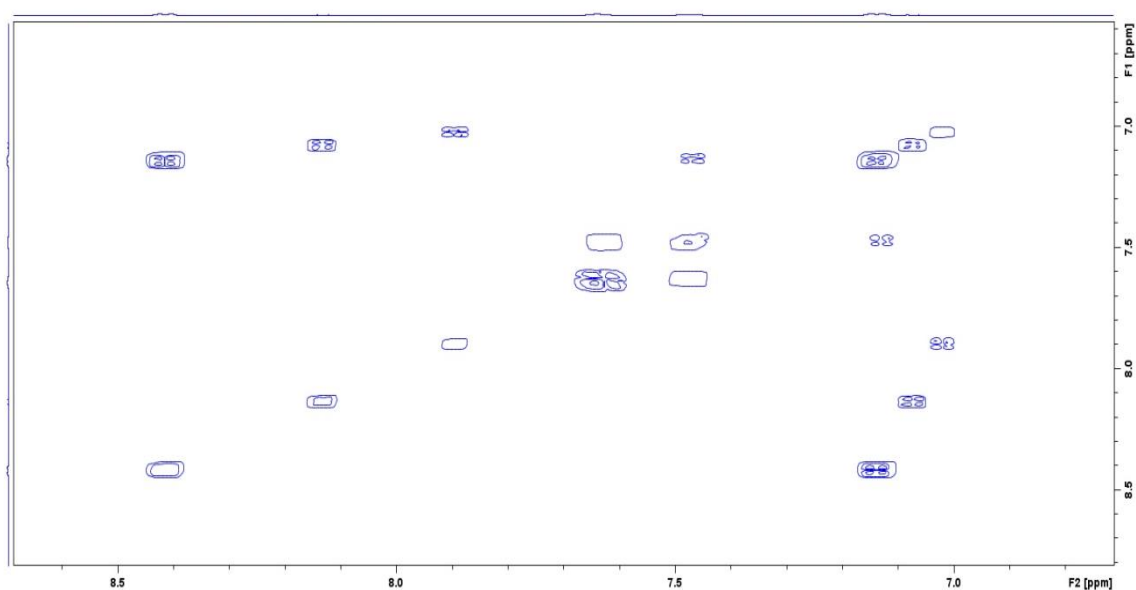


Figure A4.15 ¹H H COSY spectrum of 11-(3-methoxyphenyl)-1,8,10,12-tetraazatricyclo [7.4.0.0^{2,7}]trideca-2(7),3,5,9,11-pentaene-13-thione (**15**).

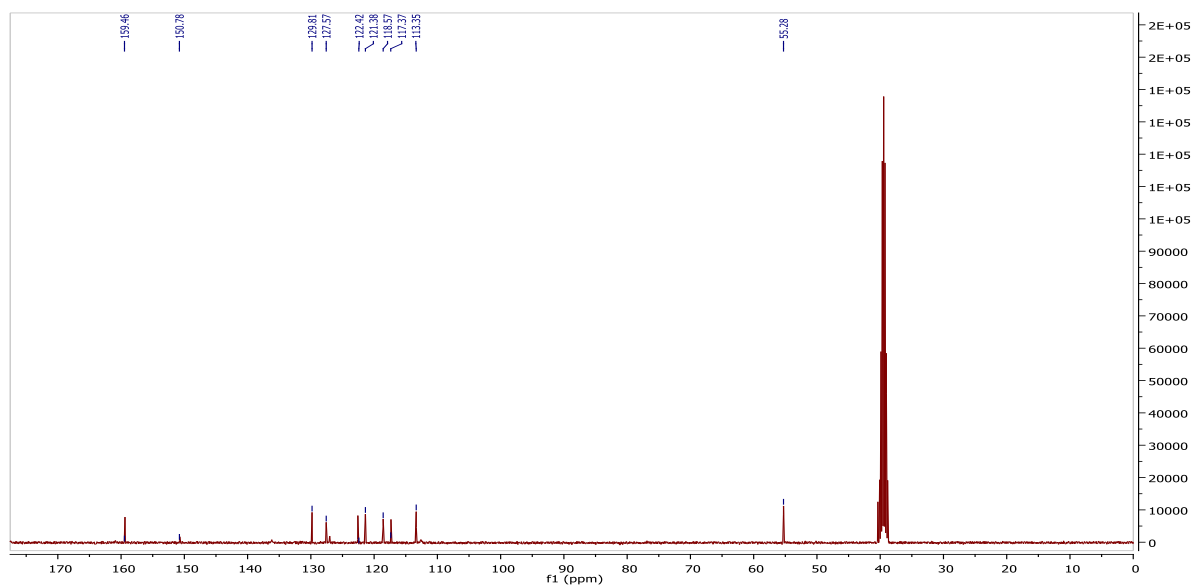


Figure A4.16 ¹³C NMR spectrum of 11-(3-methoxyphenyl)-1,8,10,12-tetraazatricyclo [7.4.0.0^{2,7}] trideca-2(7),3,5,9,11-pentaene-13-thione (**15**).

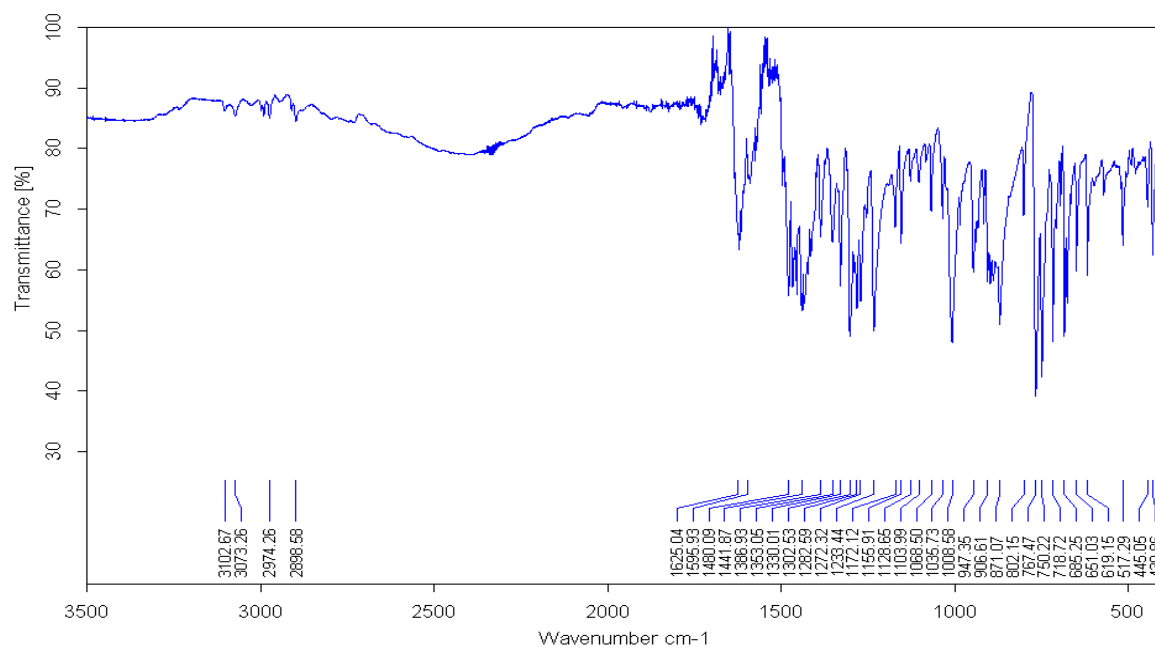


Figure A4.17 IR spectrum of 11-(3-chlorophenyl)-1,8,10,12-tetraazatricyclo[7.4.0.0^{2,7}] trideca-2(7),3,5,9,11-pentaene-13-thione (**17**).

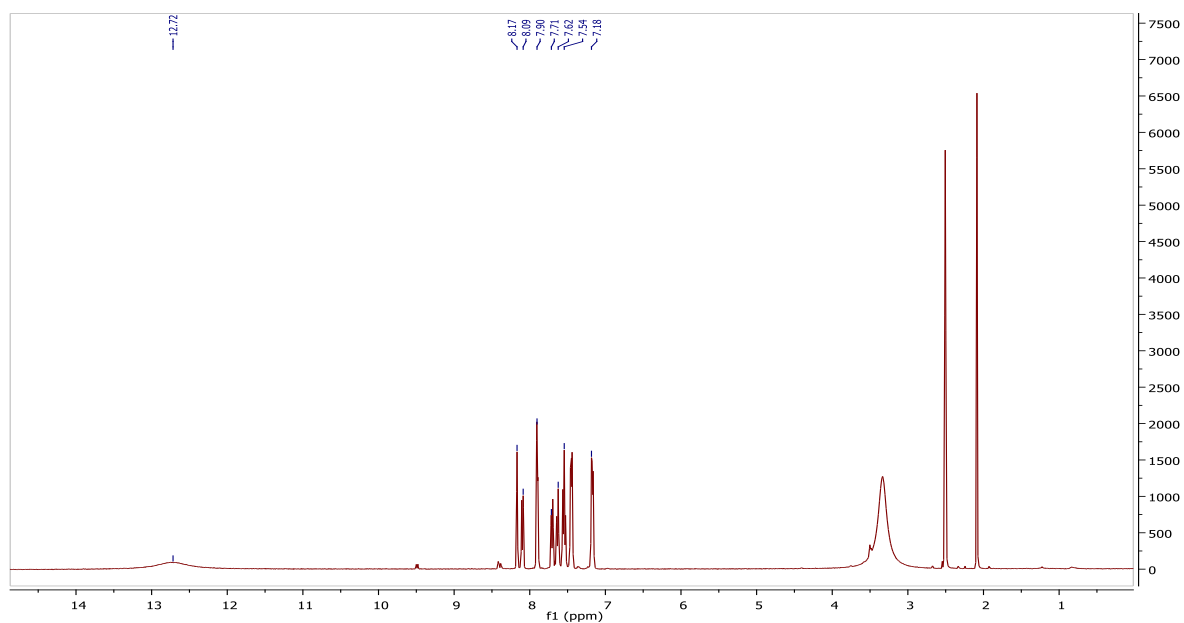


Figure A4.18 ¹H NMR spectrum of 11-(3-chlorophenyl)-1,8,10,12-tetraazatricyclo[7.4.0.0^{2,7}] trideca-2(7),3,5,9,11-pentaene-13-thione (**17**).

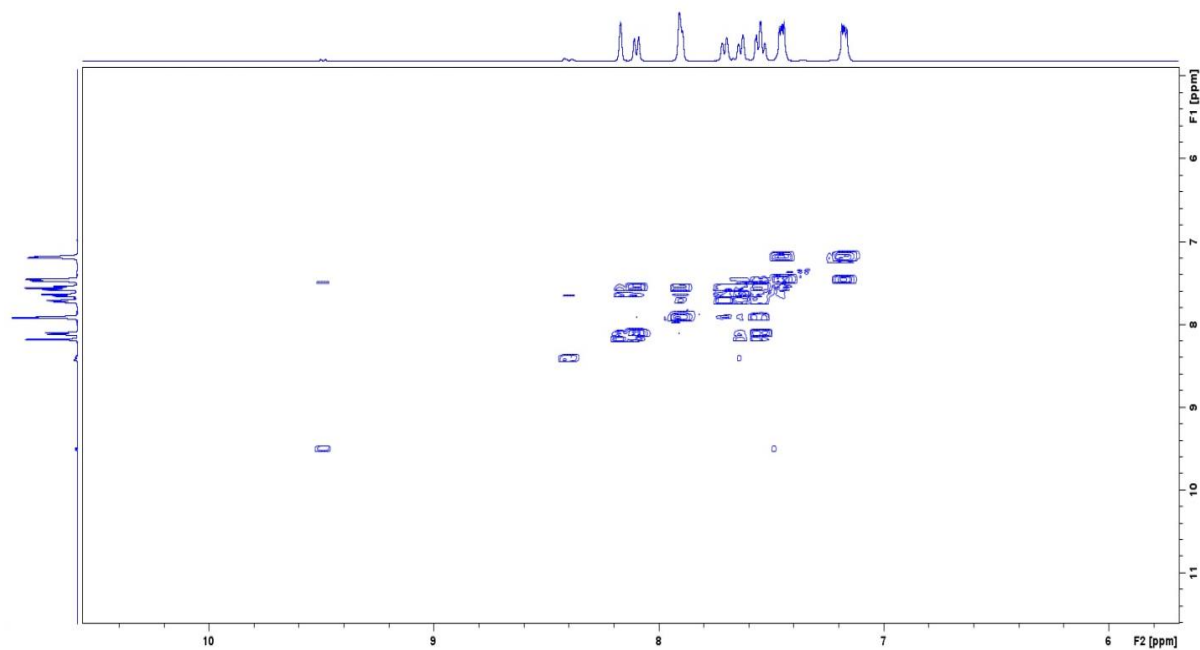


Figure A4.19 ^1H H COSY spectrum of 11-(3-chlorophenyl)-1,8,10,12-tetraazatricyclo[7.4.0.0^{2,7}]trideca-2(7),3,5,9,11-pentaene-13-thione (**17**).

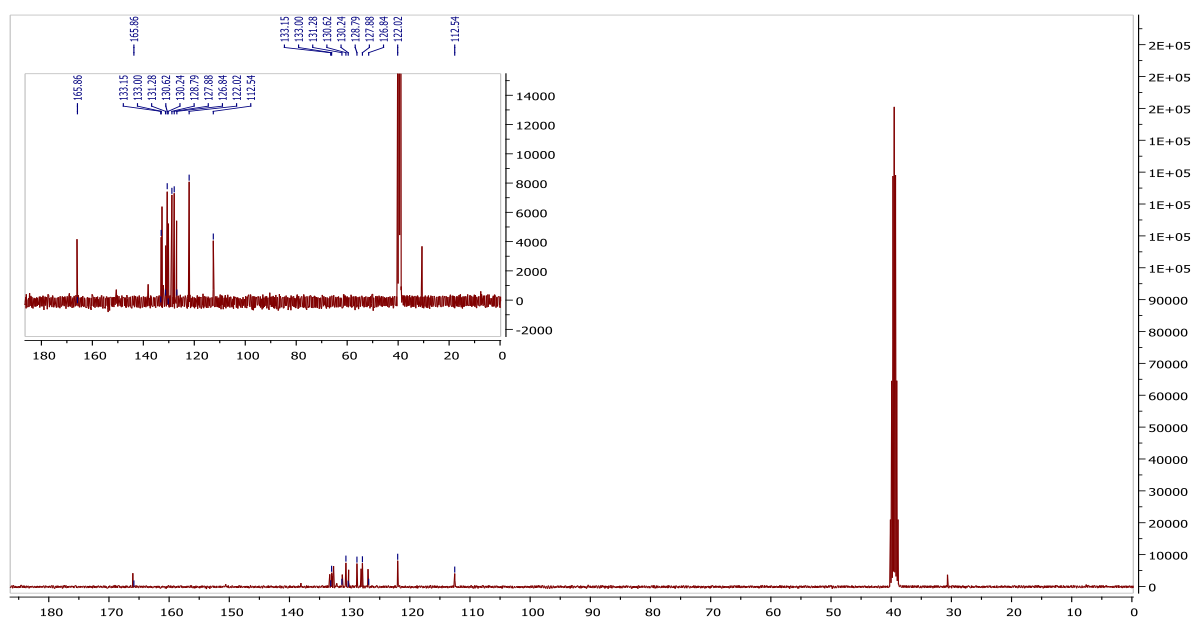


Figure A4.20 ^{13}C NMR spectrum of 11-(3-chlorophenyl)-1,8,10,12-tetraazatricyclo[7.4.0.0^{2,7}]trideca-2(7),3,5,9,11-pentaene-13-thione (**17**).

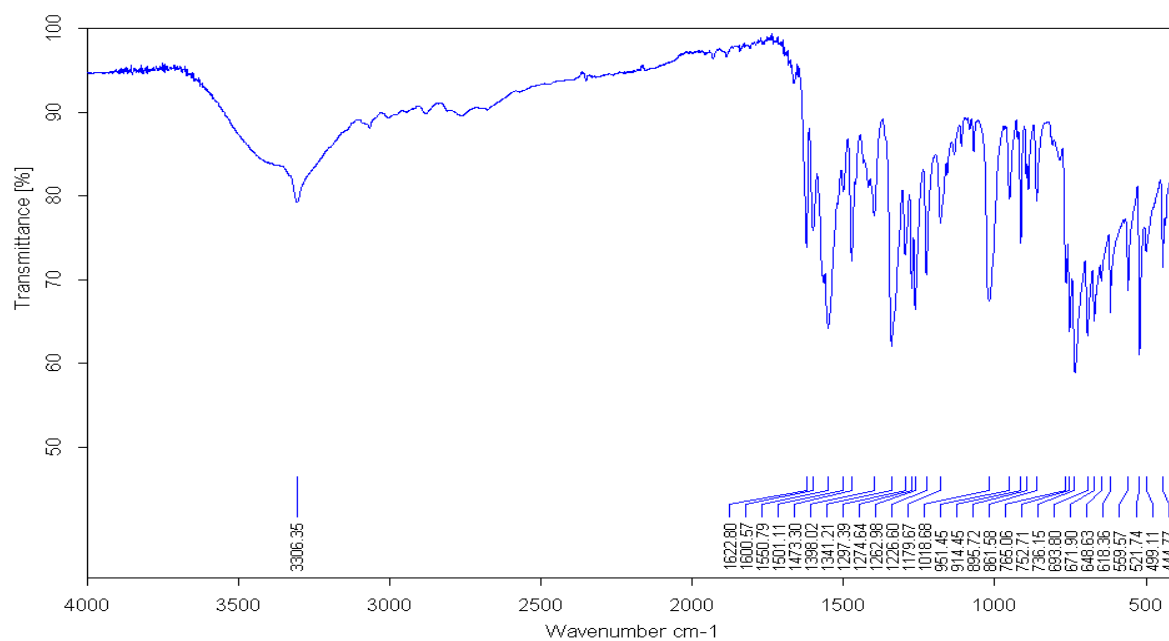


Figure A4.21 ^{13}C NMR spectrum of 11-(3-bromophenyl)-1,8,10,12-tetraazatricyclo [7.4.0.0^{2,7}]trideca-2(7),3,5,9,11-pentaene-13-thione (**18**).

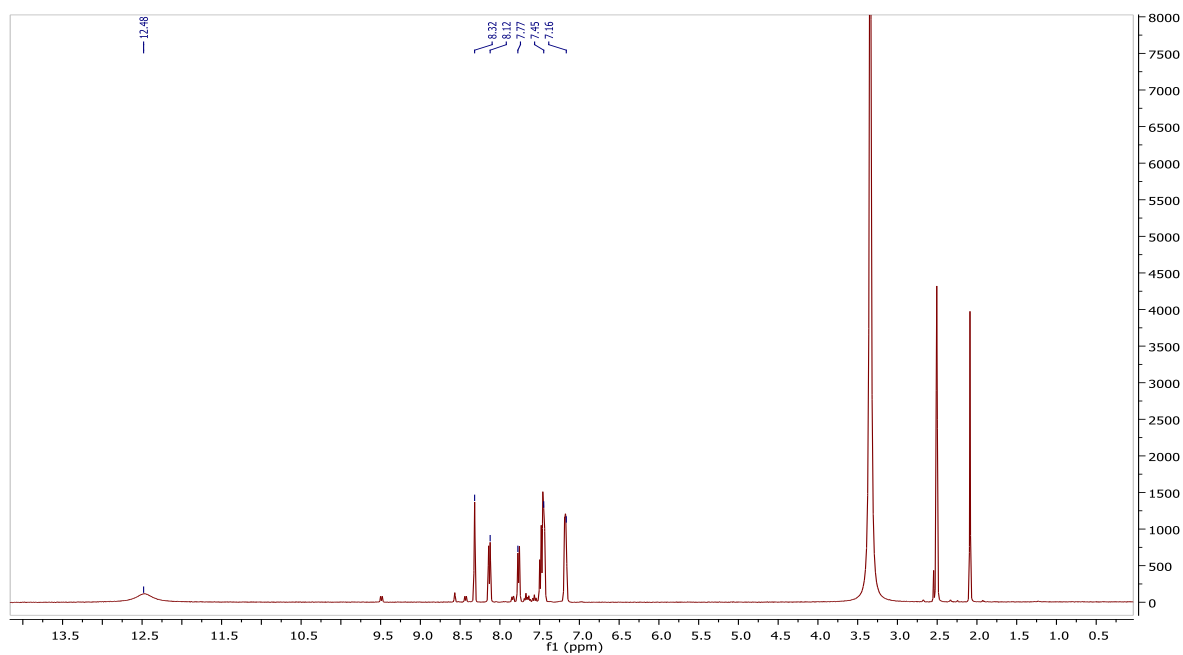


Figure A4.22 ^1H NMR spectrum of 11-(3-bromophenyl)-1,8,10,12-tetraazatricyclo [7.4.0.0^{2,7}]trideca-2(7),3,5,9,11-pentaene-13-thione (**18**).

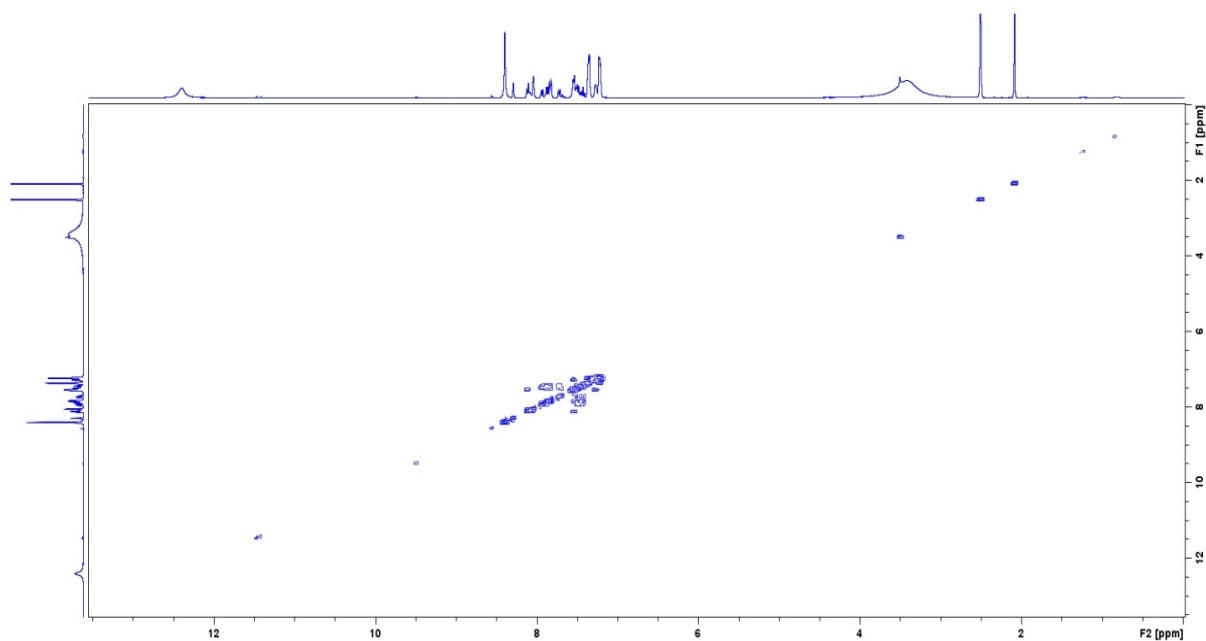


Figure A4.23 ^1H ^1H COSY spectrum of 11-(3-bromophenyl)-1,8,10,12-tetraazatricyclo [7.4.0.0^{2,7}]trideca-2(7),3,5,9,11-pentaene-13-thione (**18**).

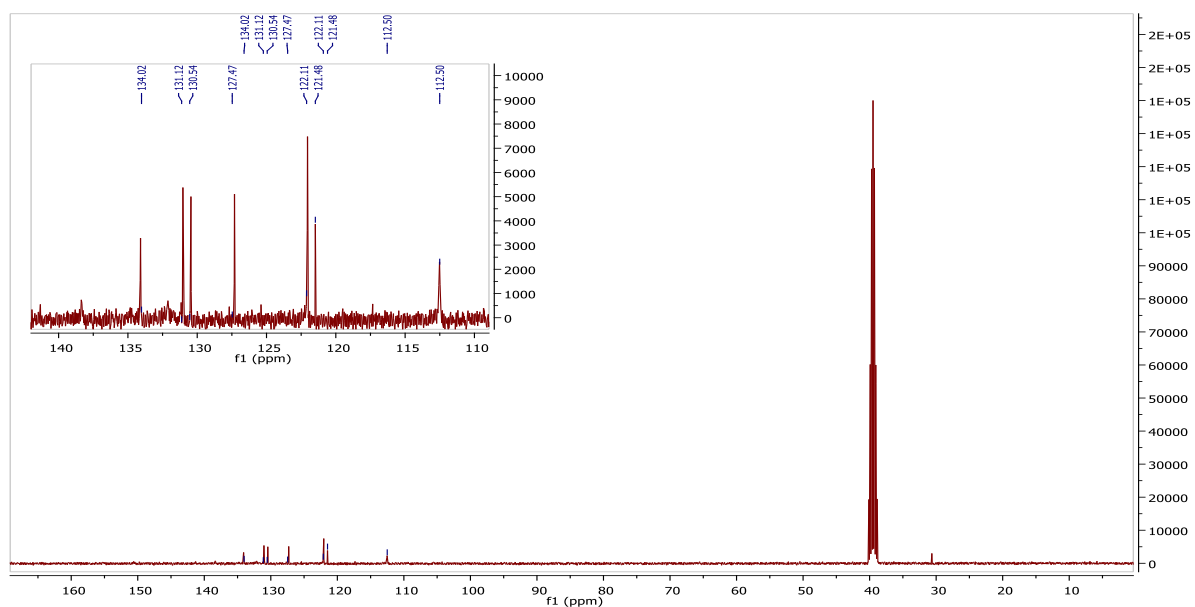


Figure A4.24 ^{13}C NMR spectrum of 11-(3-bromophenyl)-1,8,10,12-tetraazatricyclo [7.4.0.0^{2,7}]trideca-2(7),3,5,9,11-pentaene-13-thione (**18**).

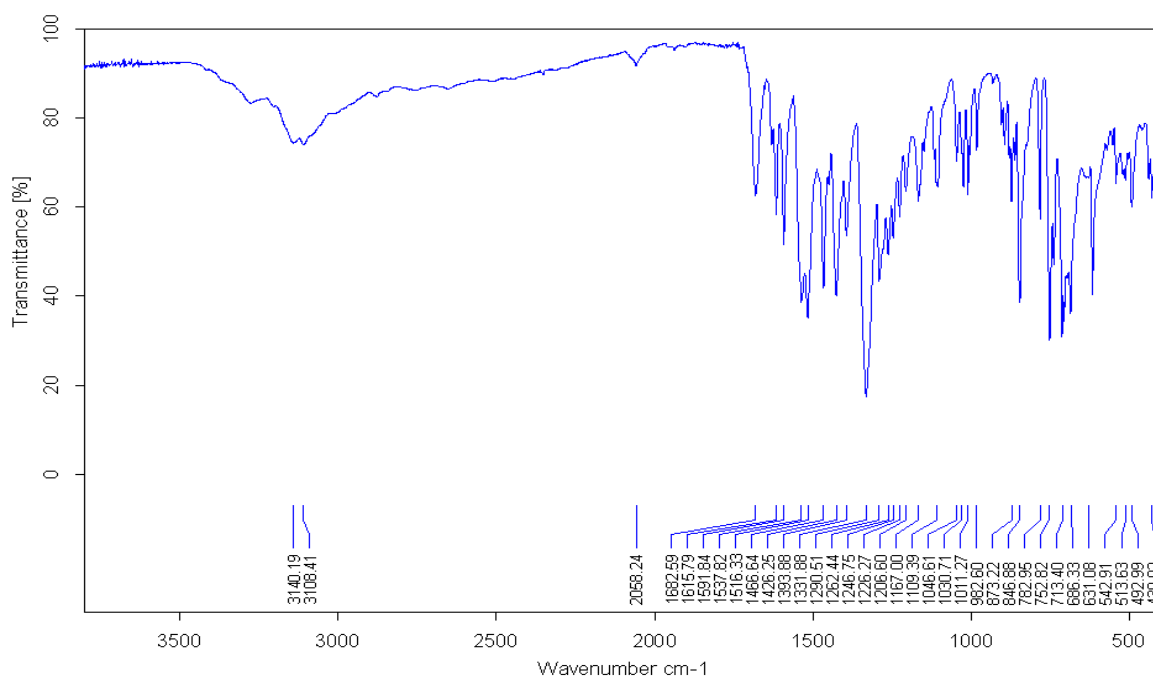


Figure A4.25 IR spectrum of 11-(4-nitrophenyl)-1,8,10,12-tetraazatricyclic [7.4.0.0^{2,7}] trideca-2(7),3,5,9,11-pentaene-13-thione (**19**).

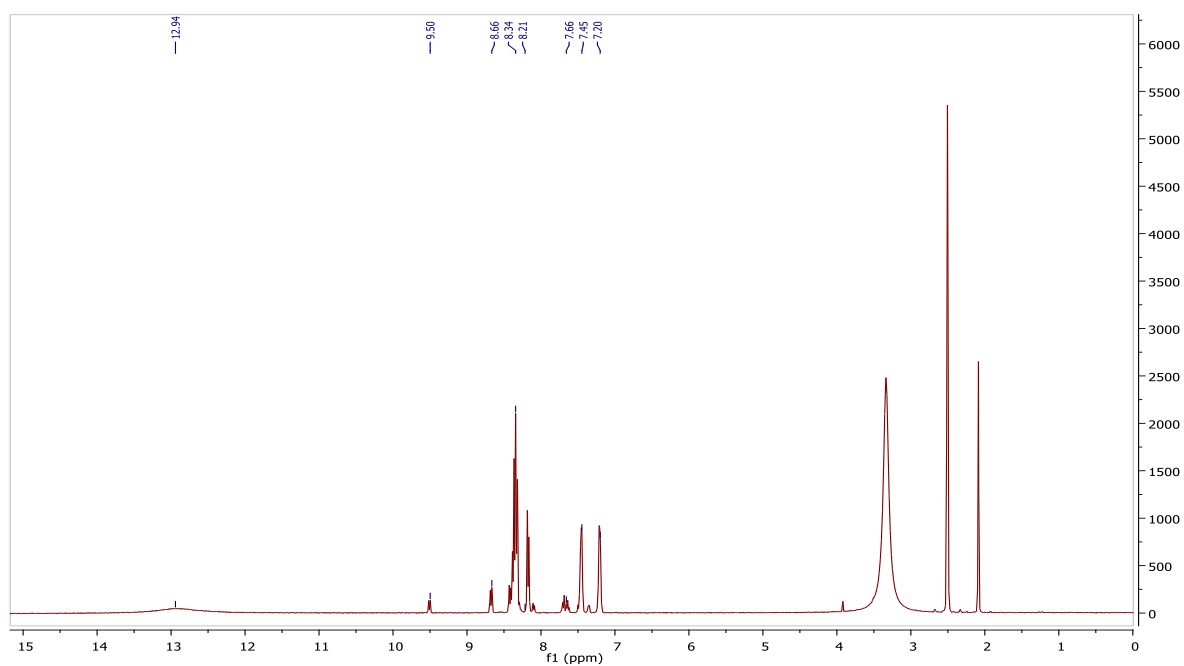


Figure A4.26 ¹H NMR spectrum of 11-(4-nitrophenyl)-1,8,10,12-tetraazatricyclic [7.4.0.0^{2,7}] trideca-2(7),3,5,9,11-pentaene-13-thione (**19**).

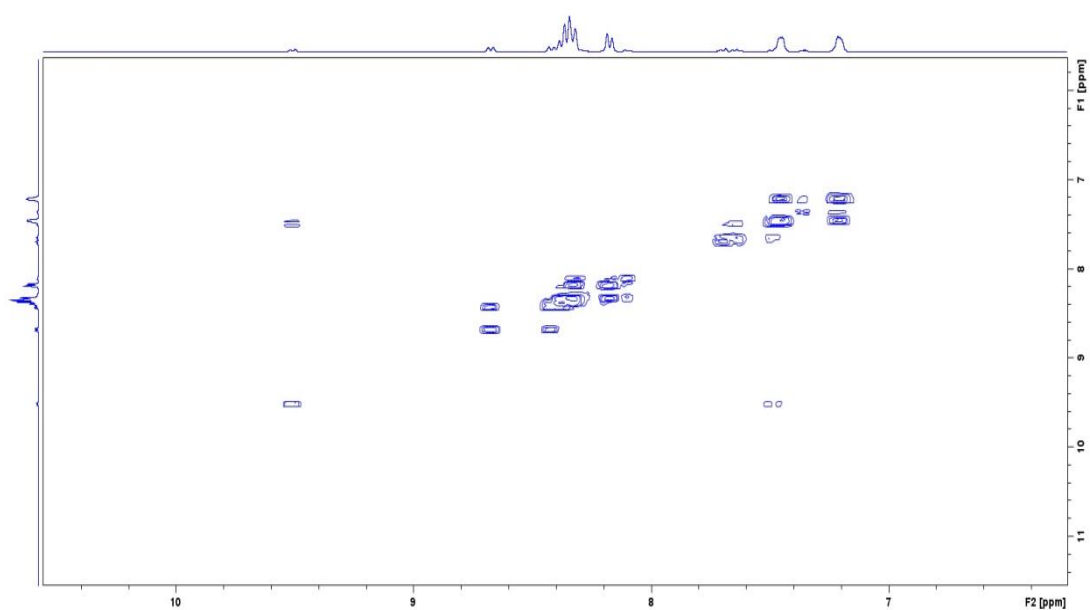


Figure A4.27 ^1H ^1H COSY spectrum of 11-(4-nitrophenyl)-1,8,10,12-tetraazatricyclic [7.4.0.0^{2,7}] trideca-2(7),3,5,9,11-pentaene-13-thione (**19**).

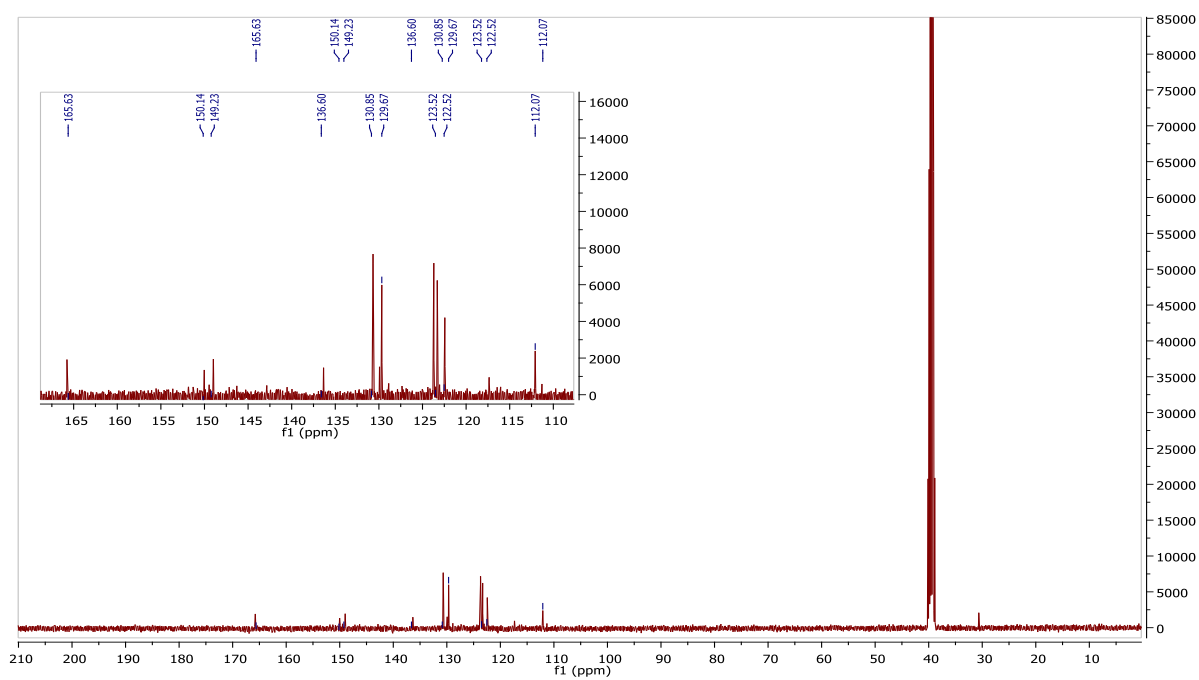


Figure A4.28 ^{13}C NMR spectrum of 11-(4-nitrophenyl)-1,8,10,12-tetraazatricyclic [7.4.0.0^{2,7}] trideca-2(7),3,5,9,11-pentaene-13-thione (**19**).

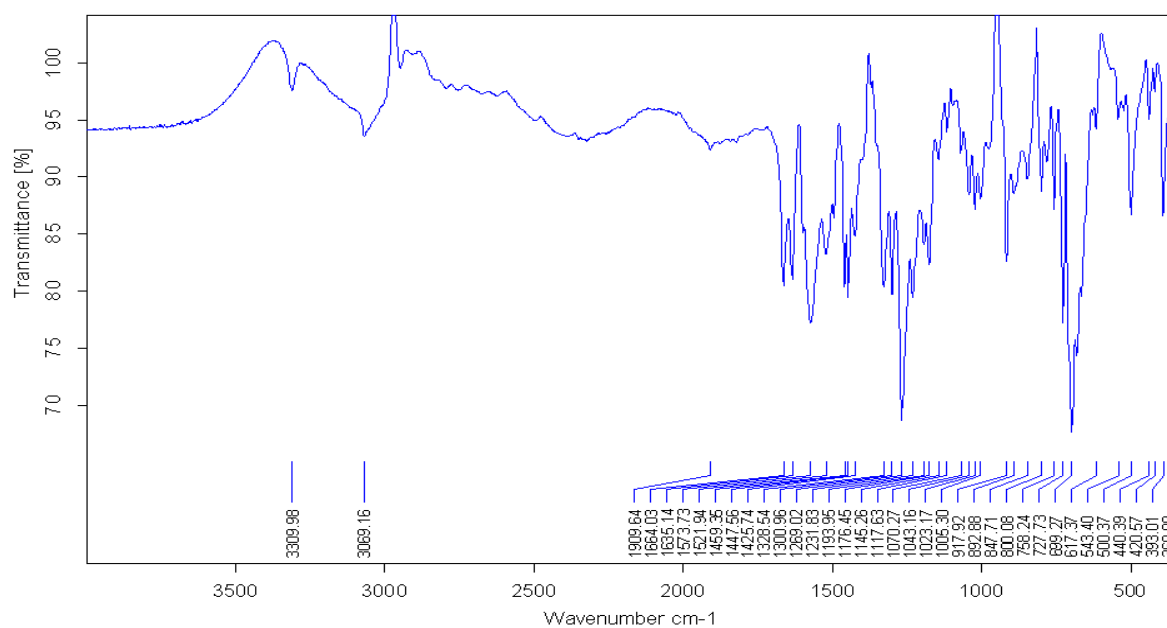


Figure A4.29 IR spectrum of 11-phenyl-1,8,10,12-tetraazatricyclo[7.4.0.0^{2,7}]trideca-2(7),3,5,9,11-pentaene-13-thione (**20**).

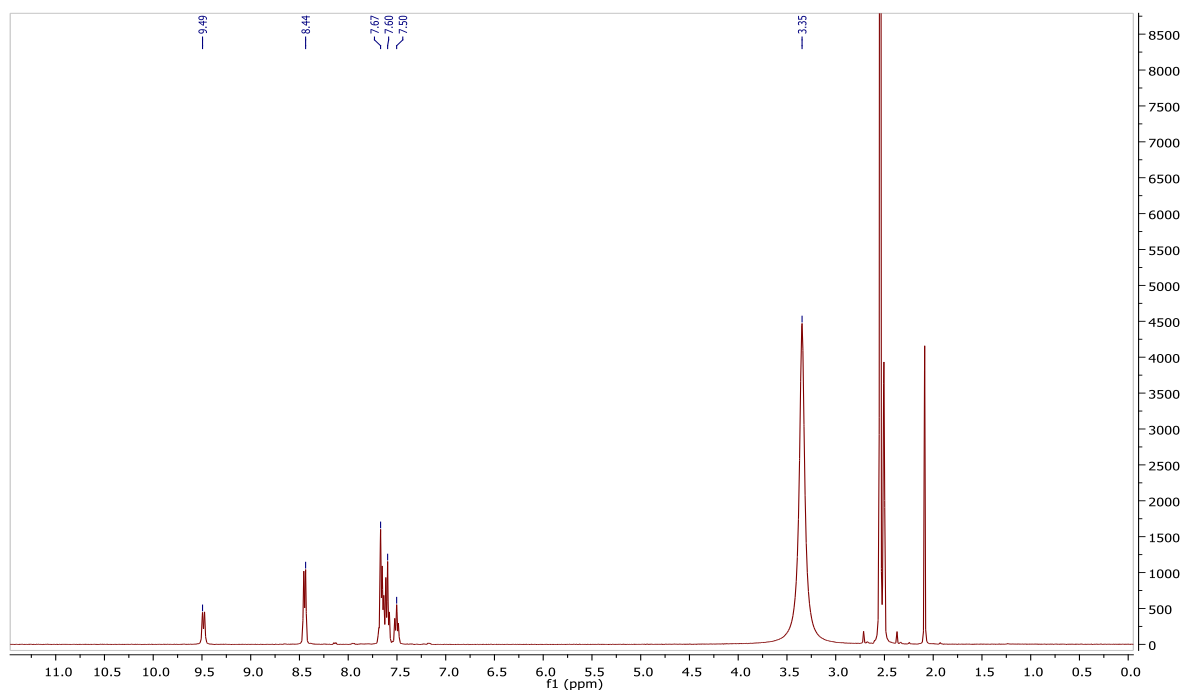


Figure A4.30 ¹H NMR spectrum of 11-phenyl-1,8,10,12-tetraazatricyclo[7.4.0.0^{2,7}]trideca-2(7),3,5,9,11-pentaene-13-thione (**20**).

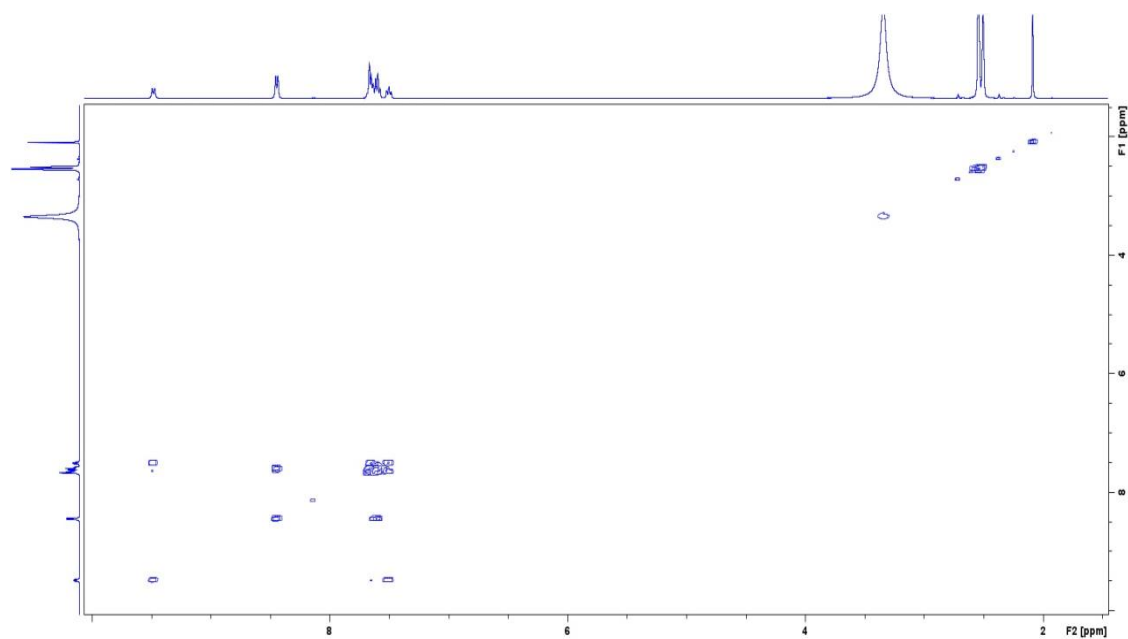


Figure A4.31 ^1H - ^1H COSY spectrum of 11-phenyl-1,8,10,12-tetraazatricyclo[7.4.0.0^{2,7}]trideca-2(7),3,5,9,11-pentaene-13-thione (**20**).

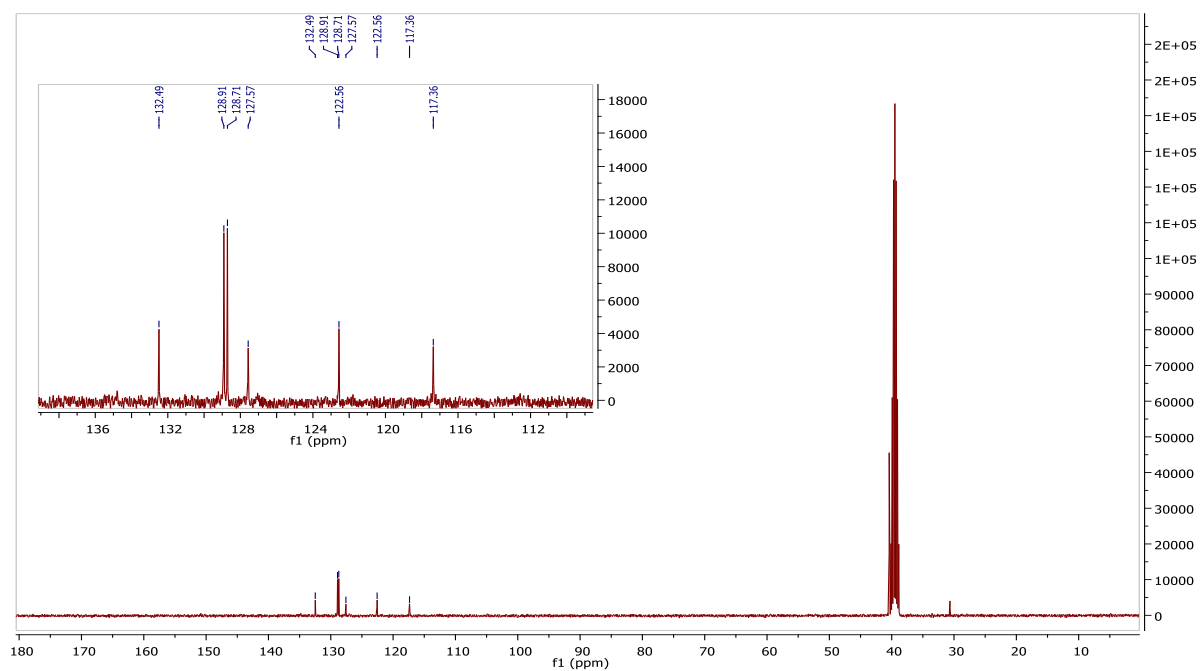


Figure A4.32 ^{13}C NMR spectrum of 11-phenyl-1,8,10,12-tetraazatricyclo[7.4.0.0^{2,7}]trideca-2(7),3,5,9,11-pentaene-13-thione (**20**).

APPENDIX C

CHARACTERIZATION DATA FOR 3-(1,3-BENZOTHAZOL-2-YL)-1-(BENZOYL)THIOUREA DERIVATIVES

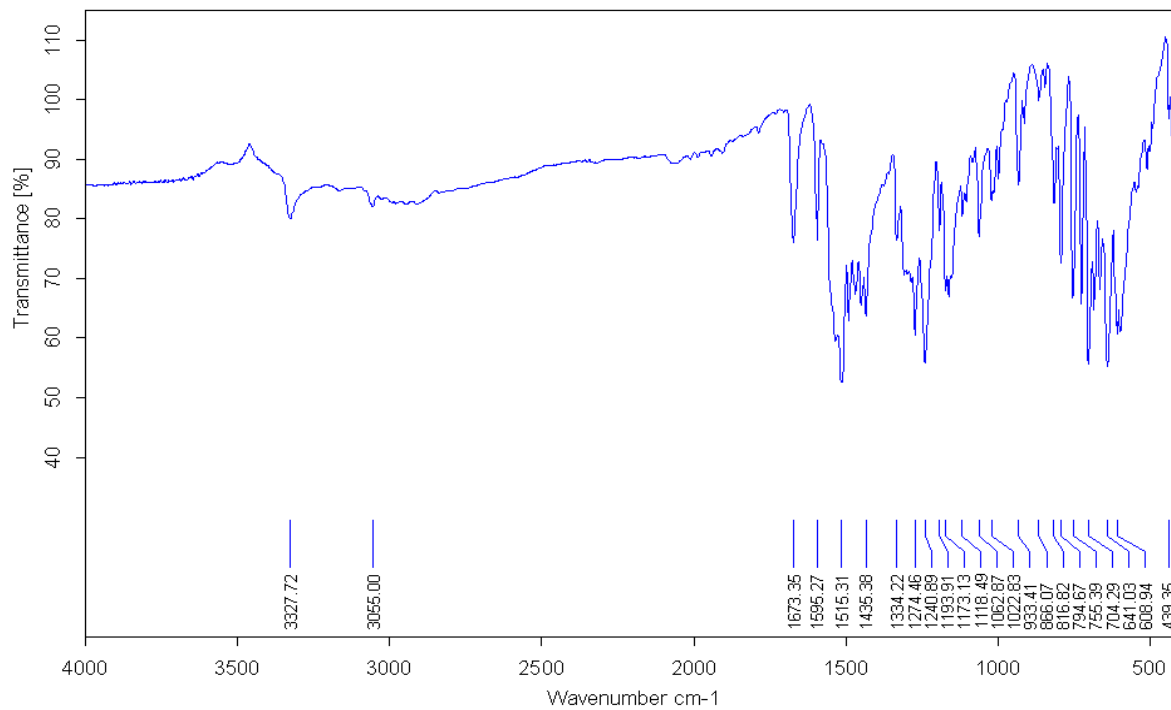


Figure A5.1 IR spectrum 3-(1,3-benzothiazol-2-yl)-1-(benzoyl)thiourea (**23**).

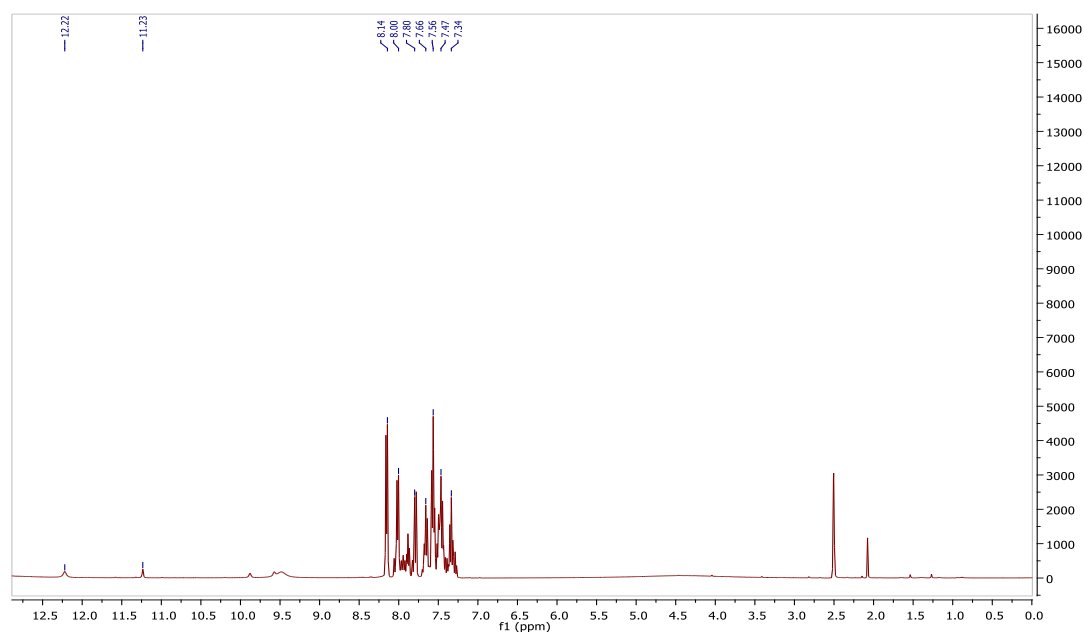


Figure A5.2 ¹H NMR spectrum 3-(1,3-benzothiazol-2-yl)-1-(benzoyl)thiourea (**23**).

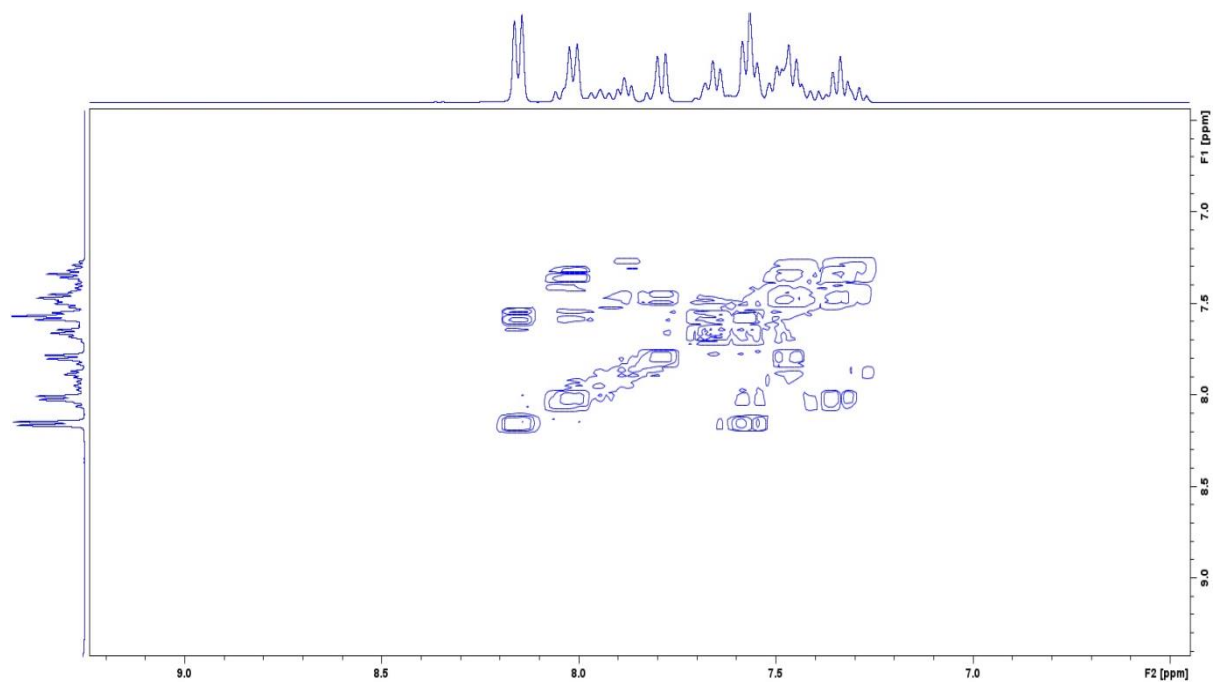


Figure A5.3 ^1H - ^1H COSY spectrum 3-(1,3-benzothiazol-2-yl)-1-(benzoyl)thiourea (**23**).

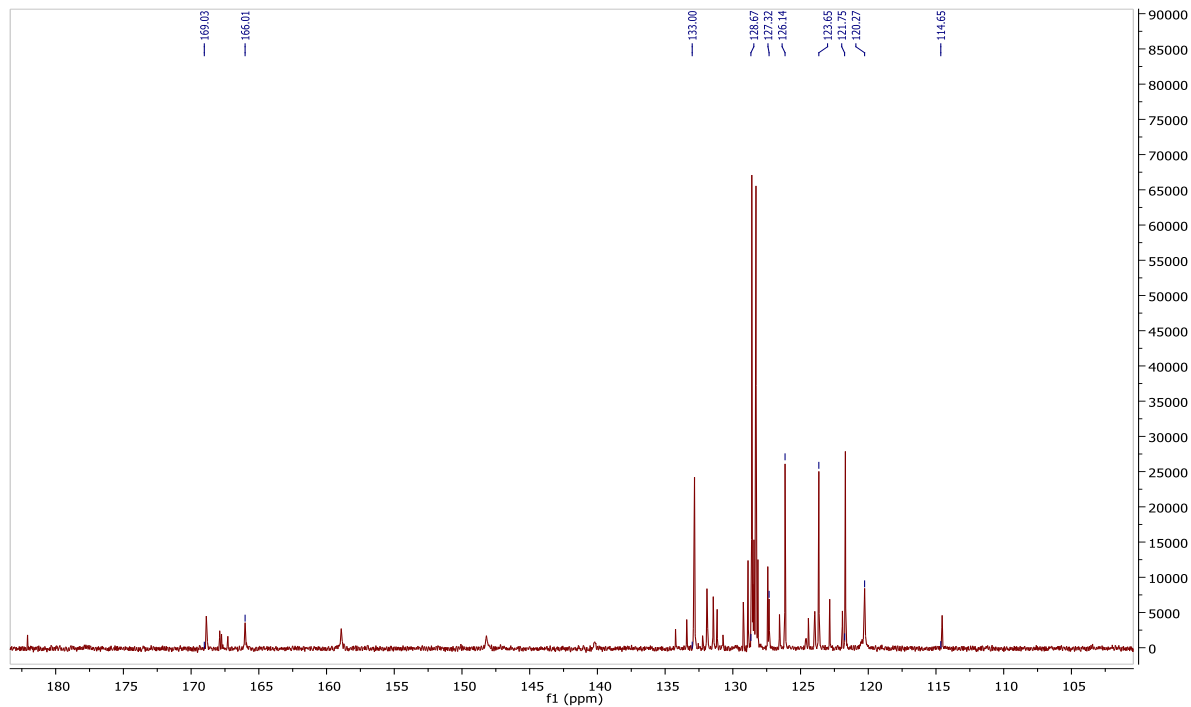


Figure A5.4 ^{13}C NMR spectrum 3-(1,3-benzothiazol-2-yl)-1-(benzoyl)thiourea (**23**).

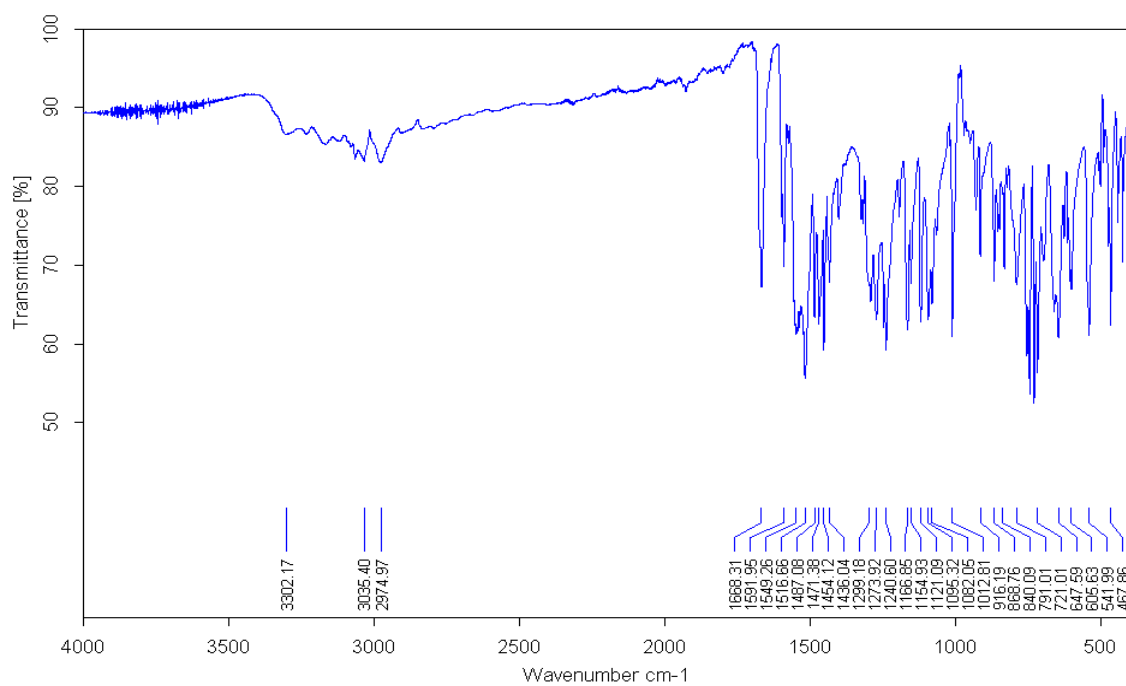


Figure A5.5 IR spectrum of 3-(1,3-benzothiazol-2-yl)-1-(4-chlorobenzoyl)thiourea (24).

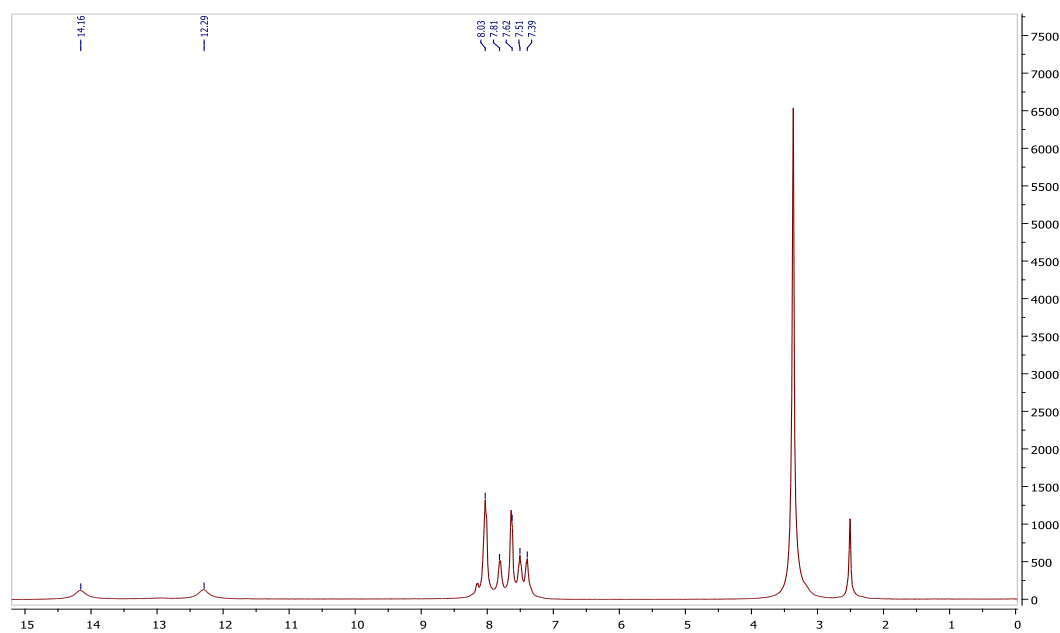


Figure A5.6 ¹H NMR spectrum of 3-(1,3-benzothiazol-2-yl)-1-(4-chlorobenzoyl)thiourea (24).

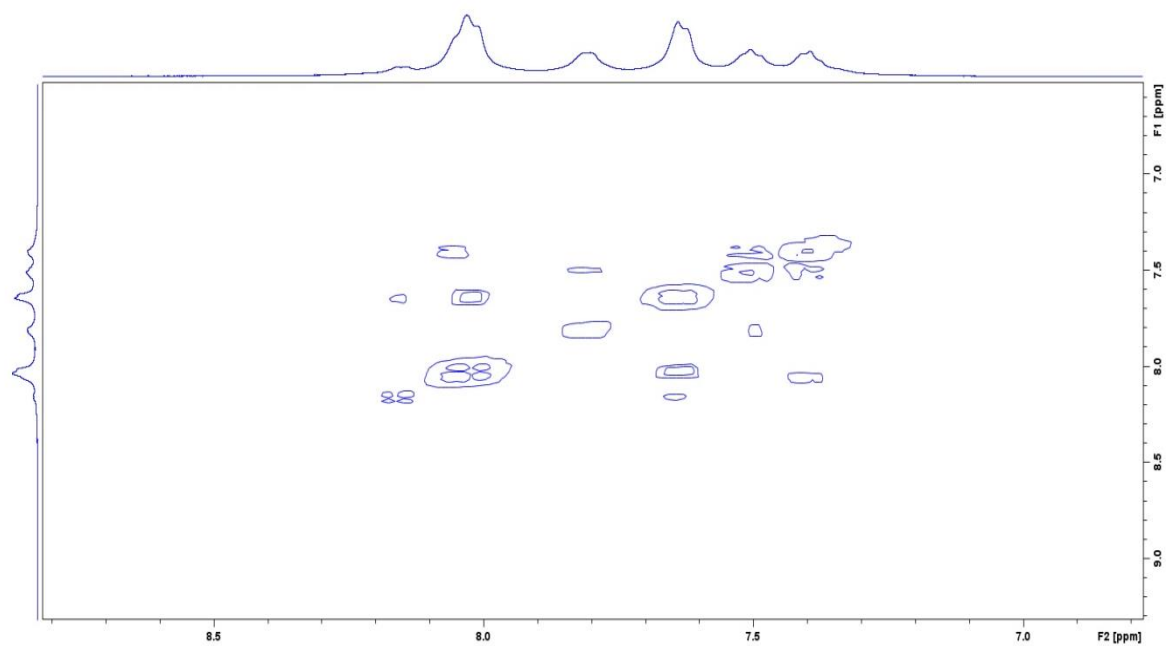


Figure A5.7 ^1H - ^1H COSY spectrum of 3-(1,3-benzothiazol-2-yl)-1-(4-chlorobenzoyl)thiourea (**24**).

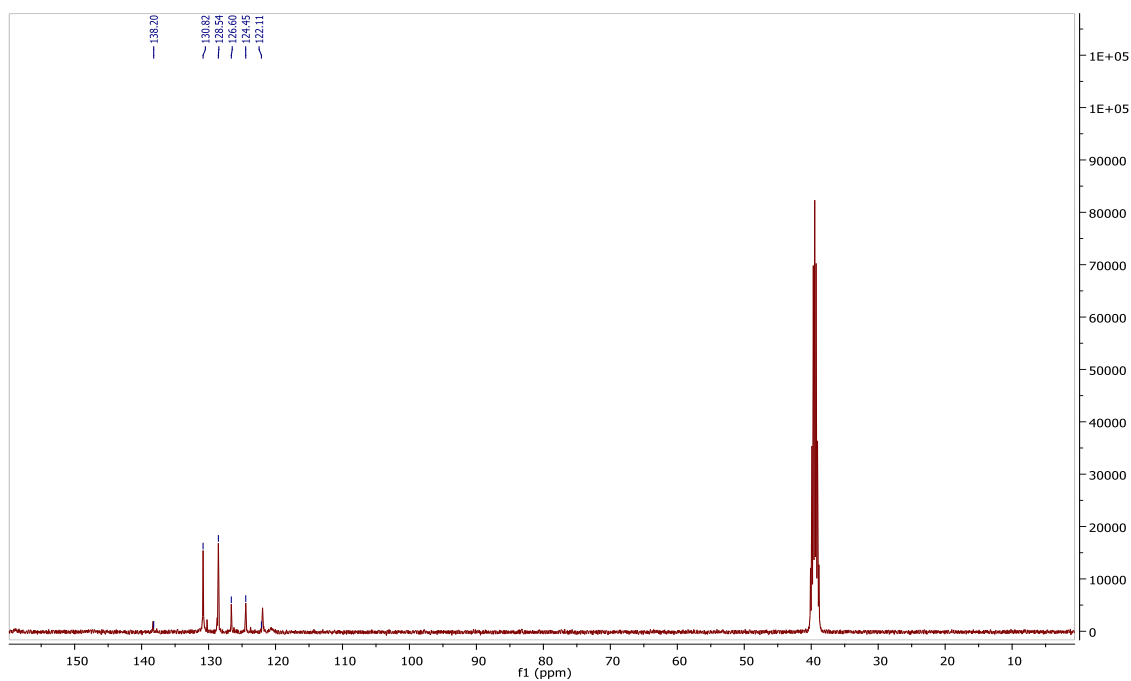


Figure A5.8 ^{13}C NMR spectrum of 3-(1,3-benzothiazol-2-yl)-1-(4-chlorobenzoyl)thiourea (**24**).

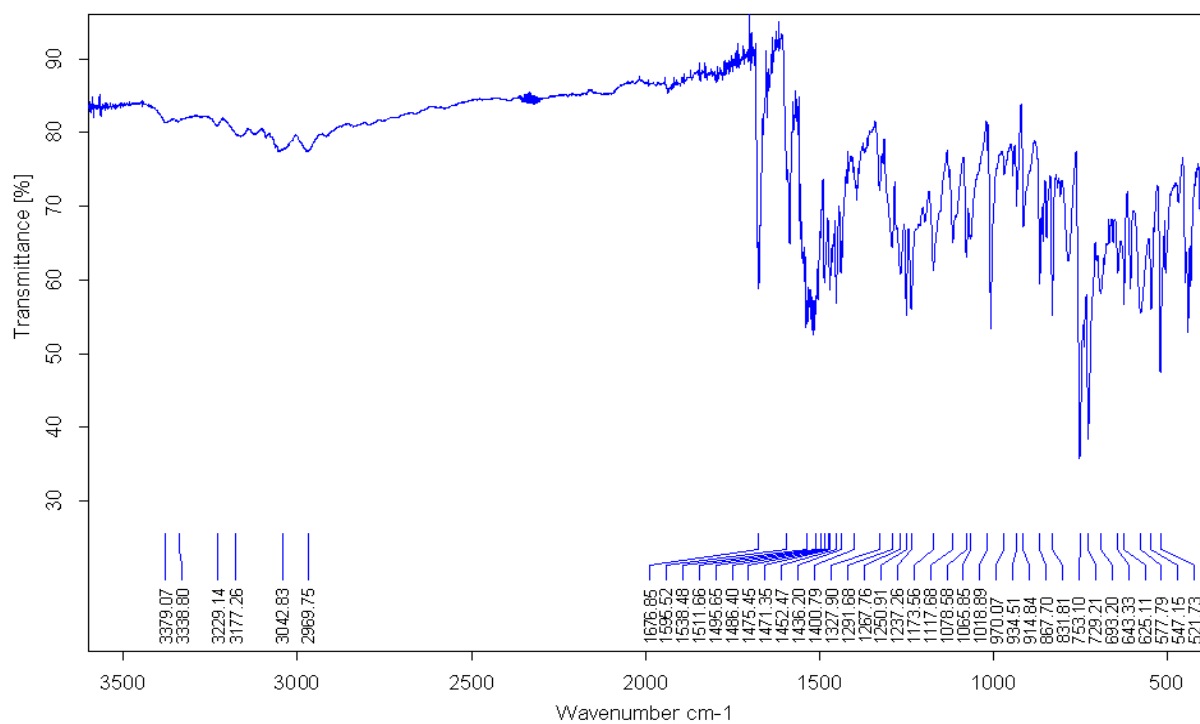


Figure A5.9 IR spectrum of 3-(1,3-benzothiazol-2-yl)-1-(4-bromobenzoyl)thiourea (**25**).

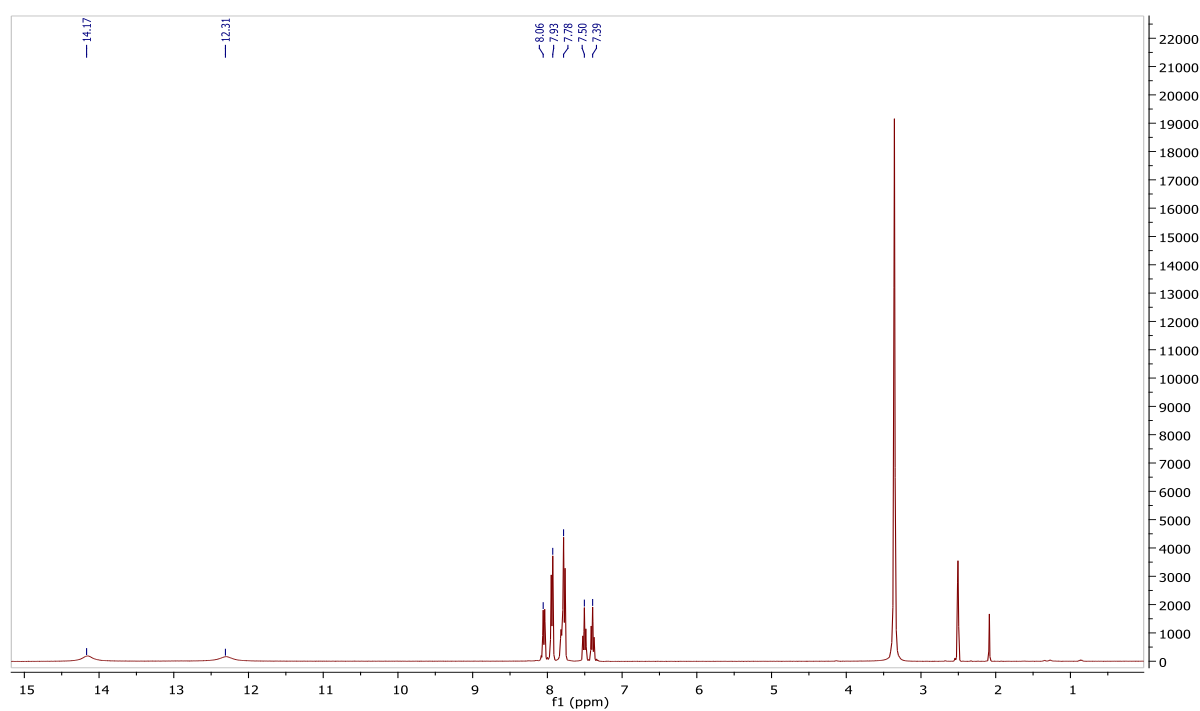


Figure A5.10 ^1H NMR spectrum of 3-(1,3-benzothiazol-2-yl)-1-(4-bromobenzoyl)thiourea (**25**).

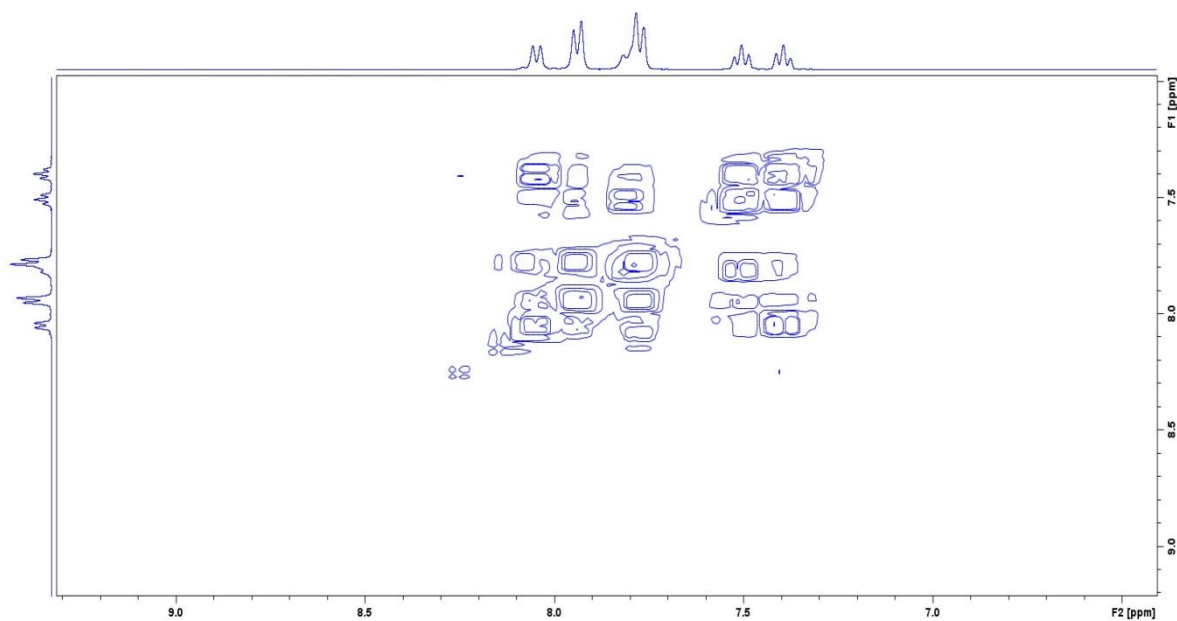


Figure A5.11 ^1H ^1H COSY spectrum of 3-(1,3-benzothiazol-2-yl)-1-(4-bromobenzoyl)thiourea (**25**).

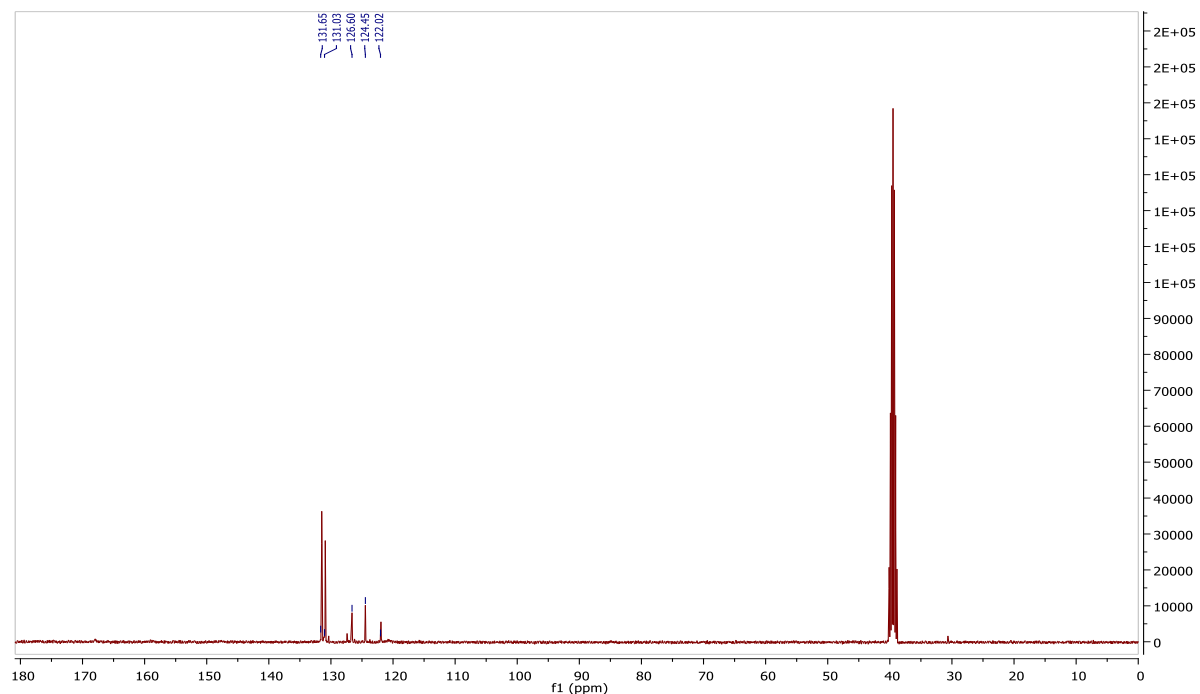


Figure A5.12 ^{13}C NMR spectrum of 3-(1,3-benzothiazol-2-yl)-1-(4-bromobenzoyl)thiourea (**25**).

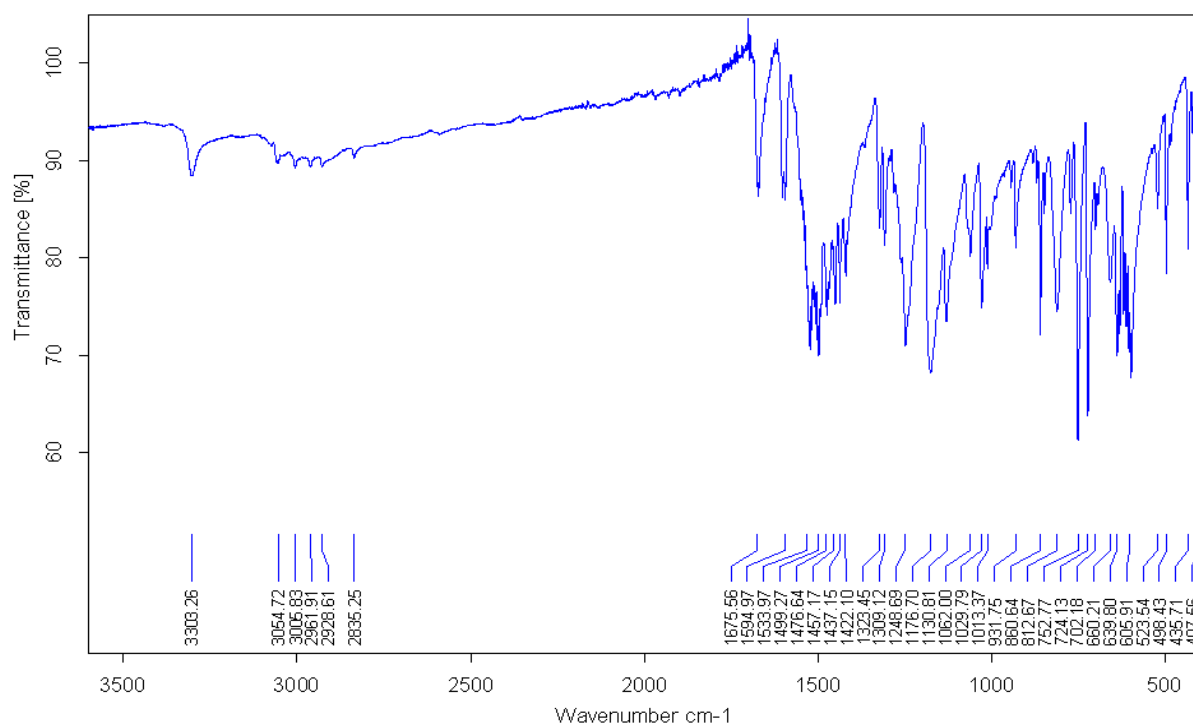


Figure A5.13 IR spectrum of 3-(1,3-benzothiazol-2-yl)-1-(4-methoxybenzoyl)thiourea (**26**).

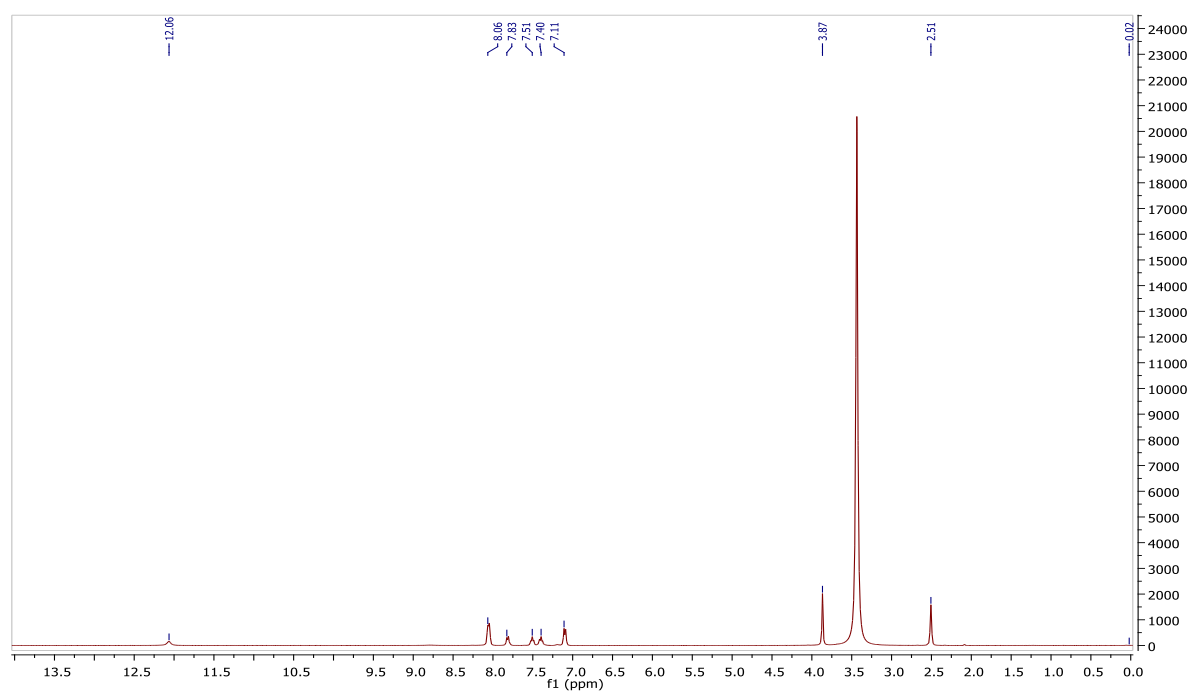


Figure A5.14 ^1H NMR spectrum of 3-(1,3-benzothiazol-2-yl)-1-(4-methoxybenzoyl)thiourea (**26**).

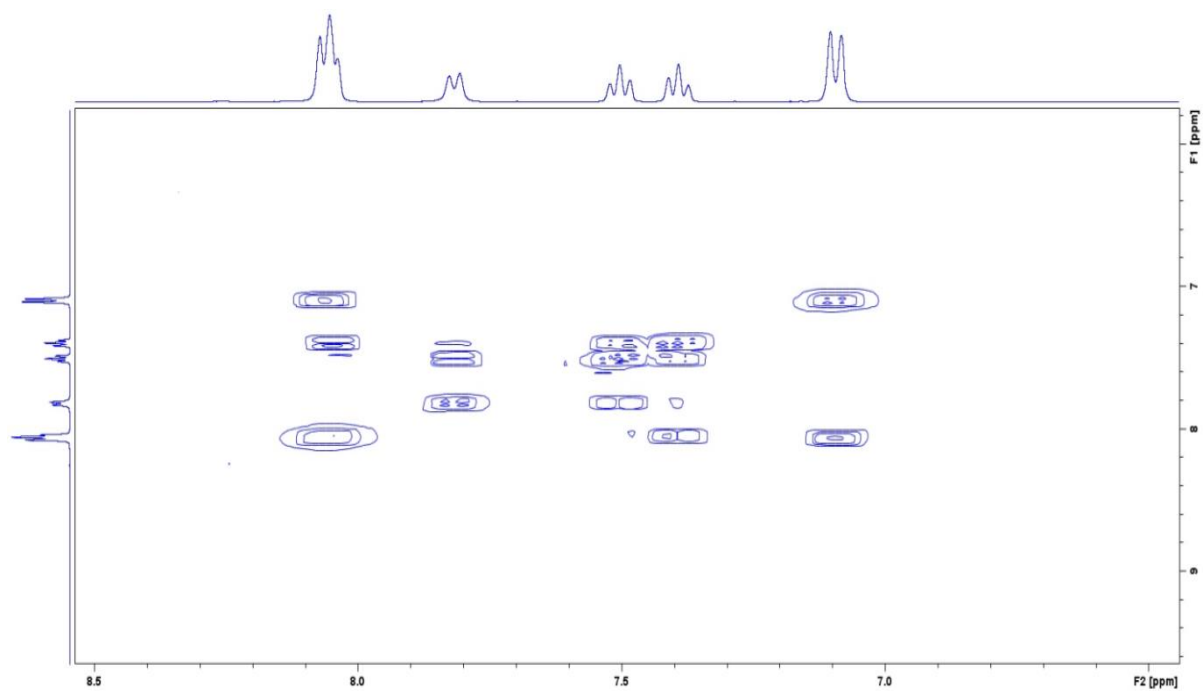


Figure A5.15 ^1H ^1H COSY spectrum of 3-(1,3-benzothiazol-2-yl)-1-(4-methoxybenzoyl)thiourea (**26**).

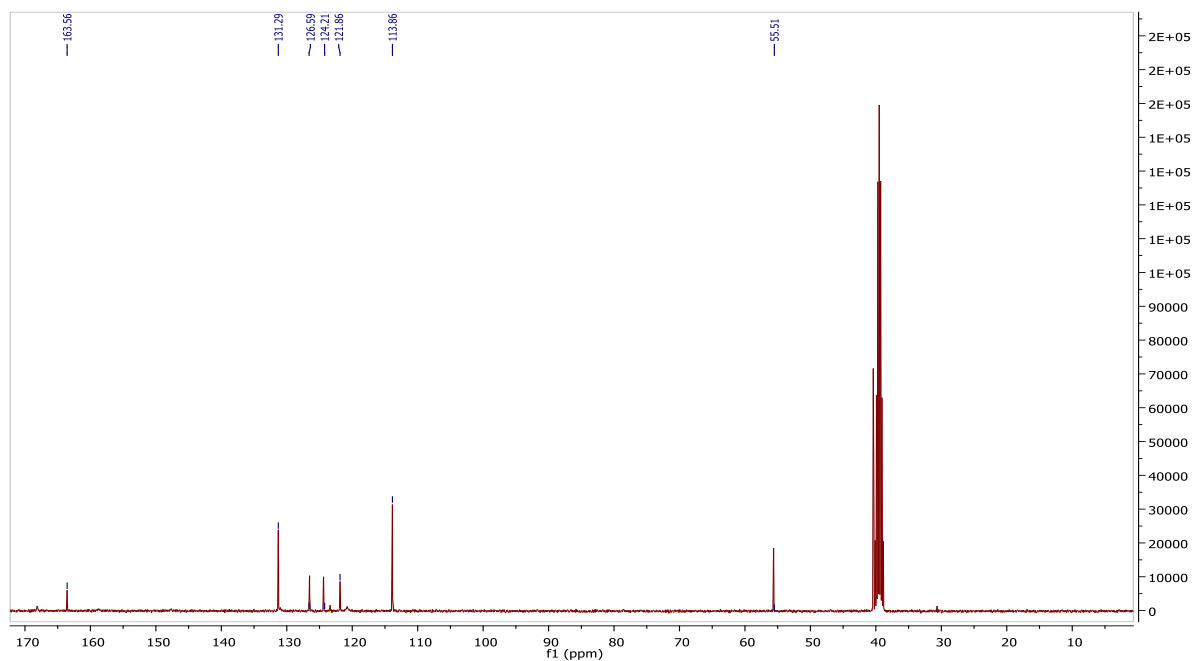


Figure A5.16 ^{13}C NMR spectrum of 3-(1,3-benzothiazol-2-yl)-1-(4-methoxybenzoyl)thiourea (**26**).

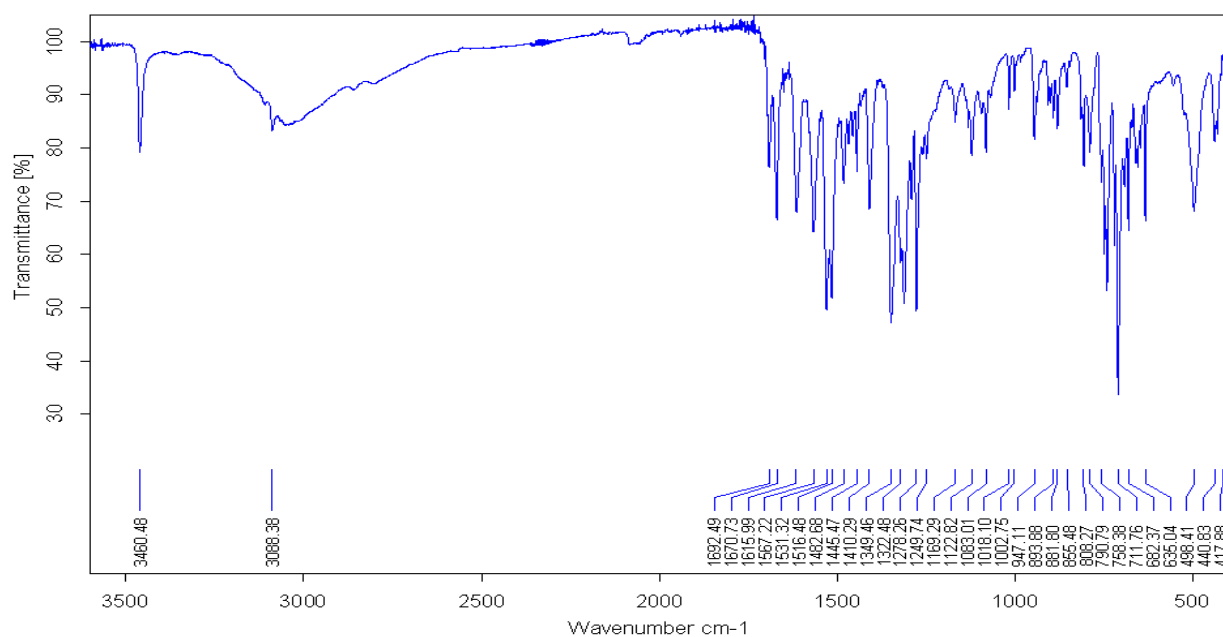


Figure A5.17 IR spectrum of 3-(1,3-benzothiazol-2-yl)-1-(3-nitrobenzoyl)thiourea (**28**).

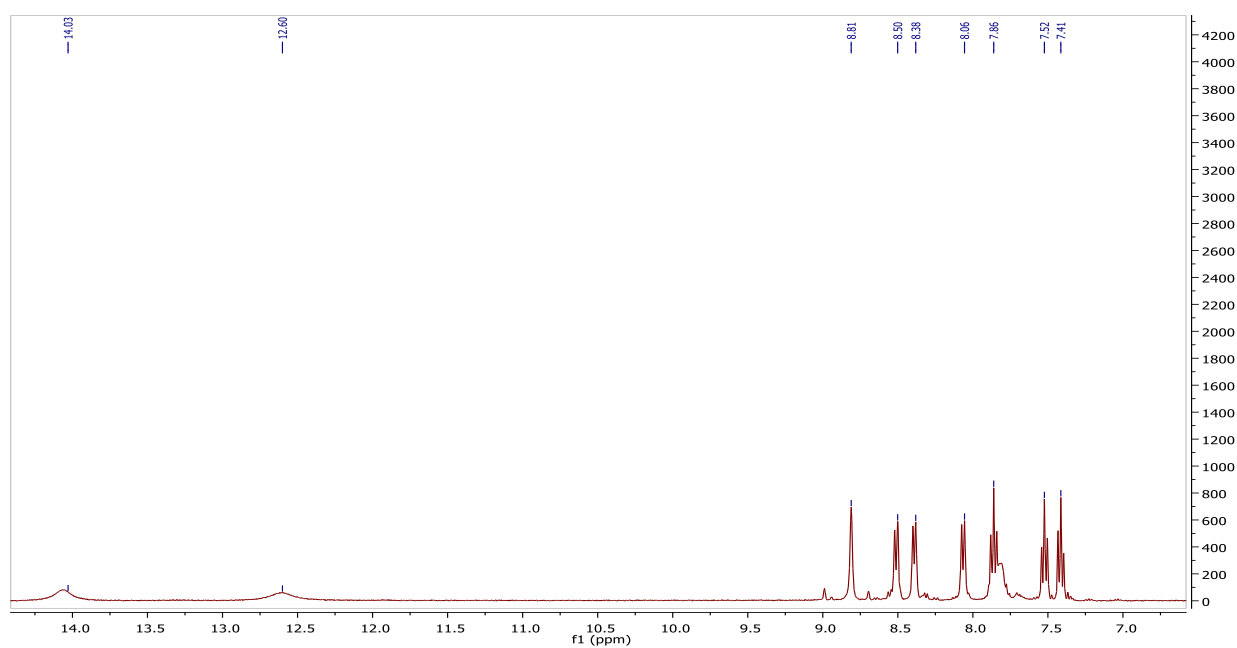


Figure A5.18 ^1H NMR spectrum of 3-(1,3-benzothiazol-2-yl)-1-(3-nitrobenzoyl)thiourea (**28**).

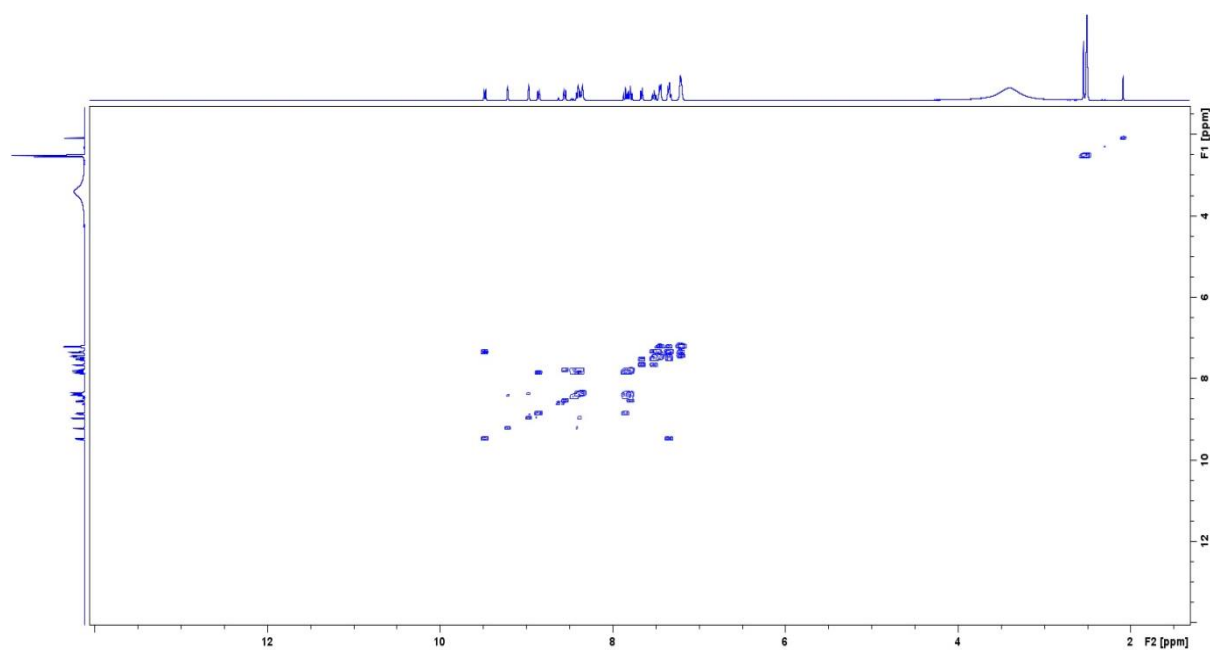


Figure A5.19 ^1H - ^1H COSY spectrum of 3-(1,3-benzothiazol-2-yl)-1-(3-nitrobenzoyl)thiourea (**28**).

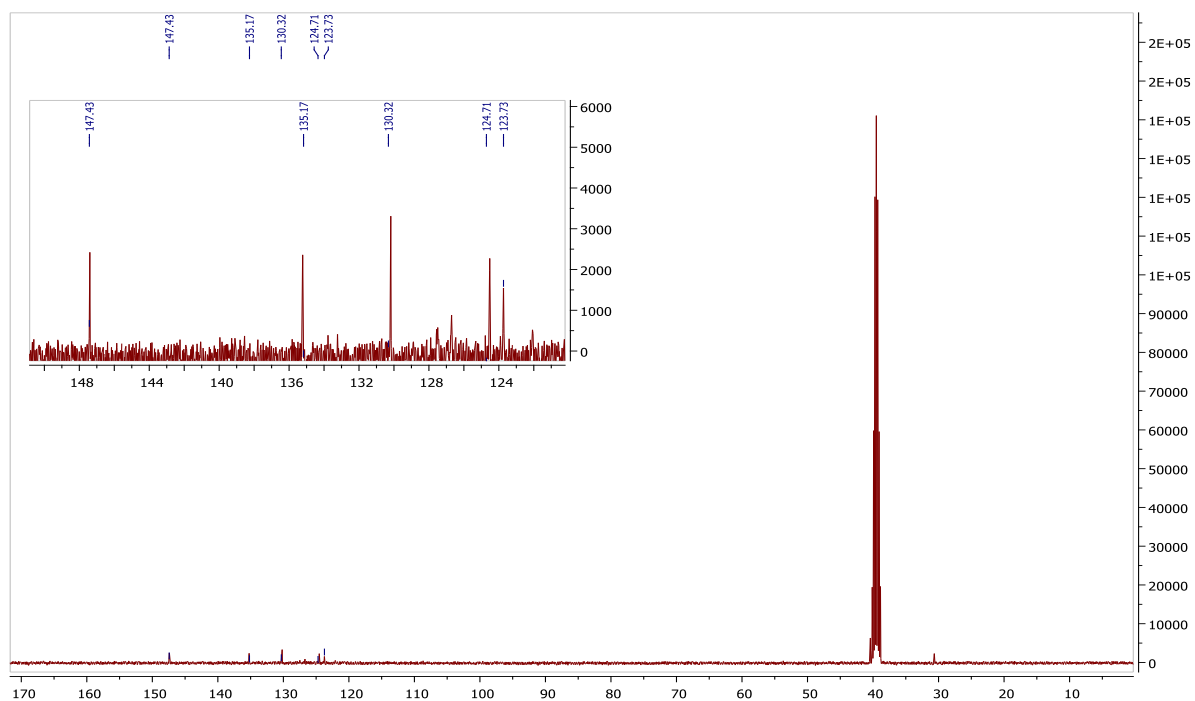


Figure A5.20 ^{13}C NMR spectrum of 3-(1,3-benzothiazol-2-yl)-1-(3-nitrobenzoyl)thiourea (**28**).

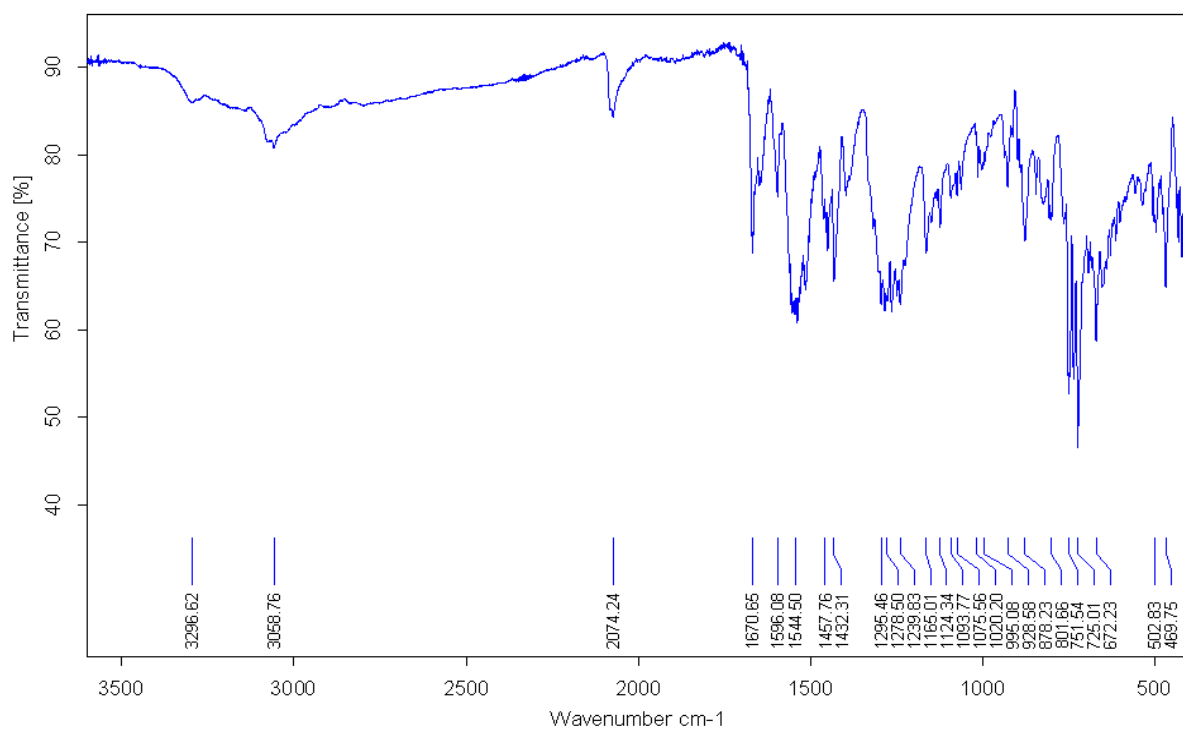


Figure A5.21 IR spectrum of 3-(1,3-benzothiazol-2-yl)-1-(3-chlorobenzoyl)thiourea (29).

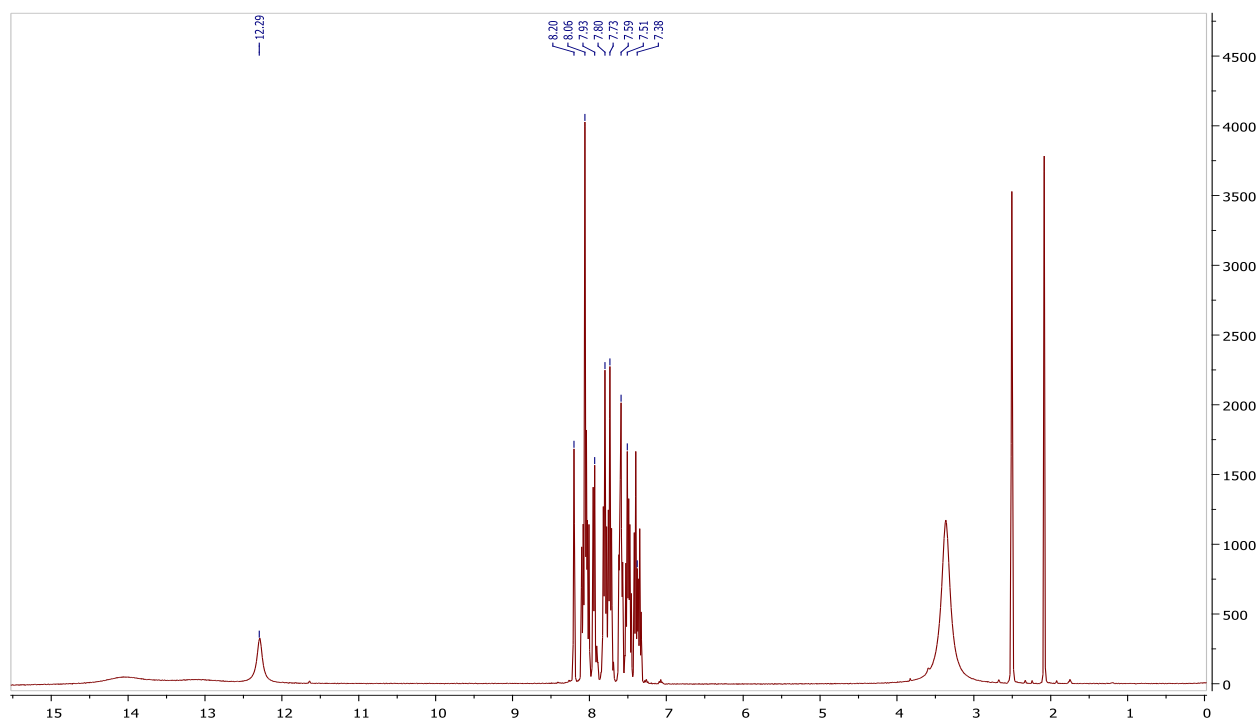


Figure A5.22 ¹H NMR spectrum of 3-(1,3-benzothiazol-2-yl)-1-(3-chlorobenzoyl)thiourea (29).

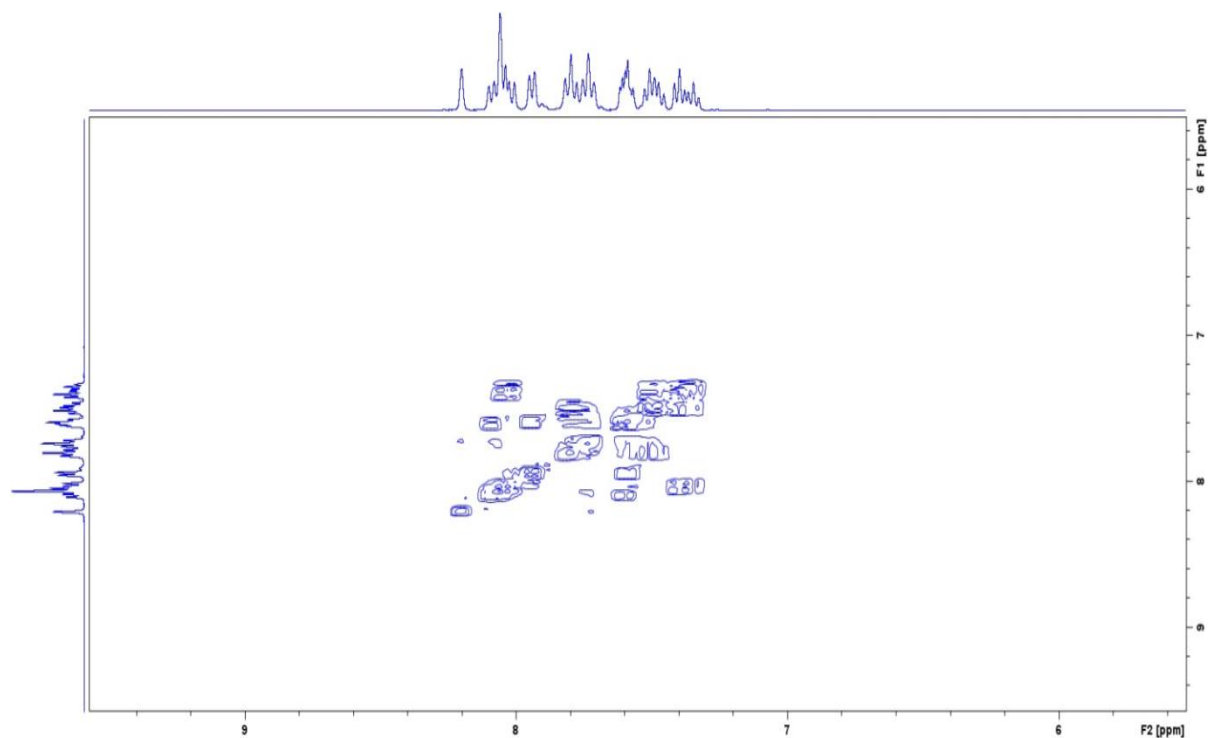


Figure A5.23 ^1H - ^1H COSY spectrum of 3-(1,3-benzothiazol-2-yl)-1-(3-chlorobenzoyl)thiourea (**29**).

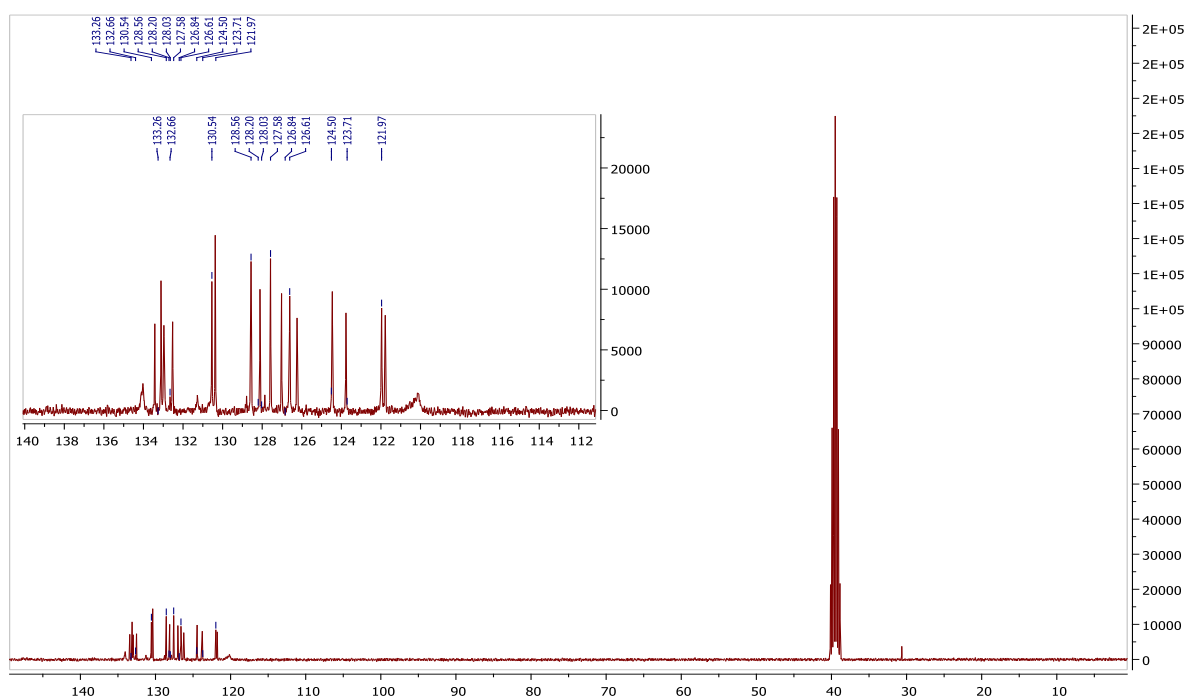


Figure A5.24 ^{13}C NMR spectrum of 3-(1,3-benzothiazol-2-yl)-1-(3-chlorobenzoyl)thiourea (**29**).

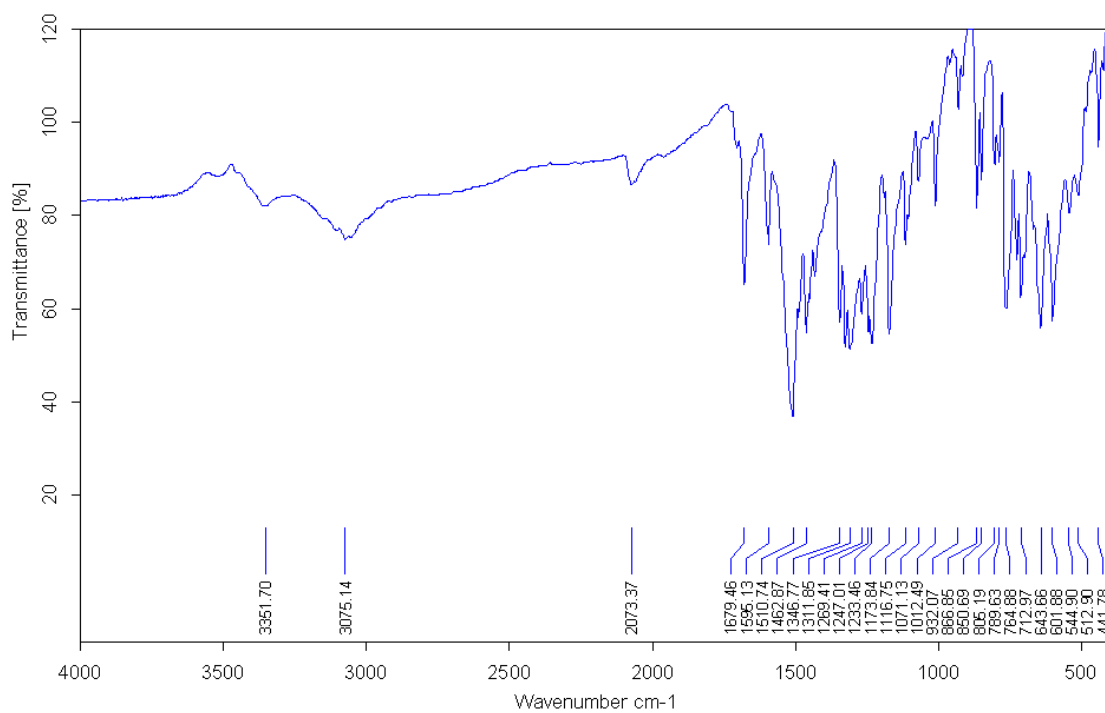


Figure A5.25 IR spectrum of 3-(1,3-benzothiazoyl-2-yl)-1-(4-nitrobenzoyl)thiourea (**30**).

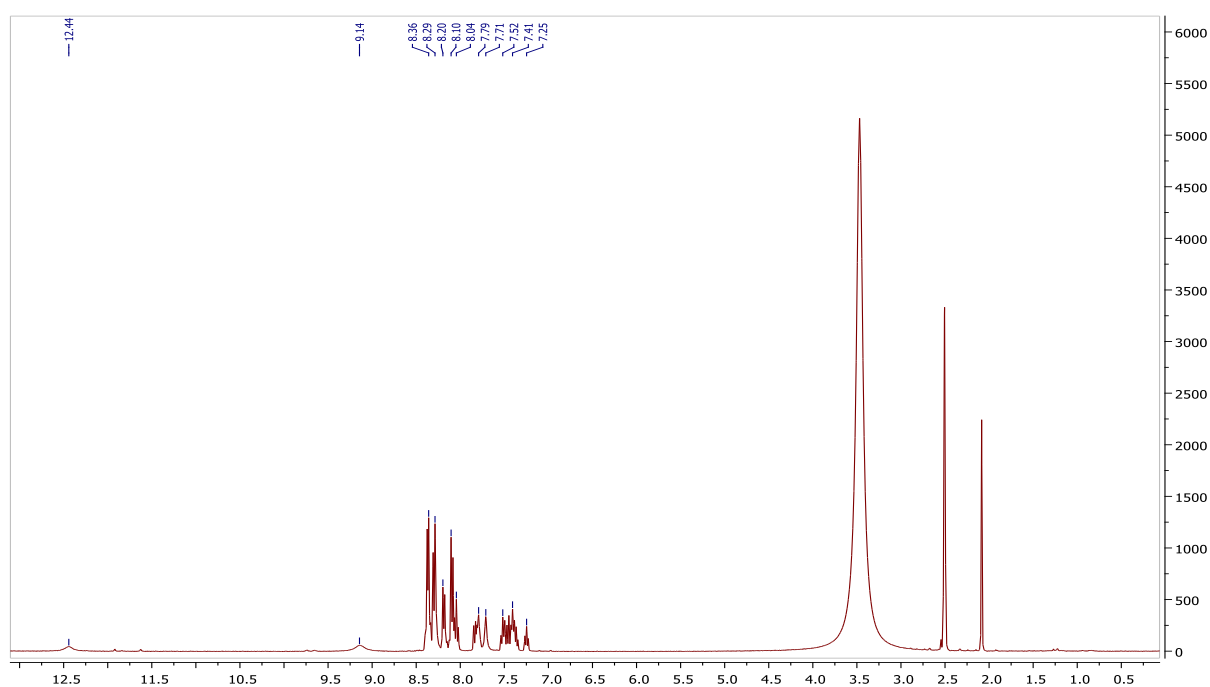


Figure A5.26 ^1H NMR spectrum of 3-(1,3-benzothiazoyl-2-yl)-1-(4-nitrobenzoyl)thiourea (**30**).

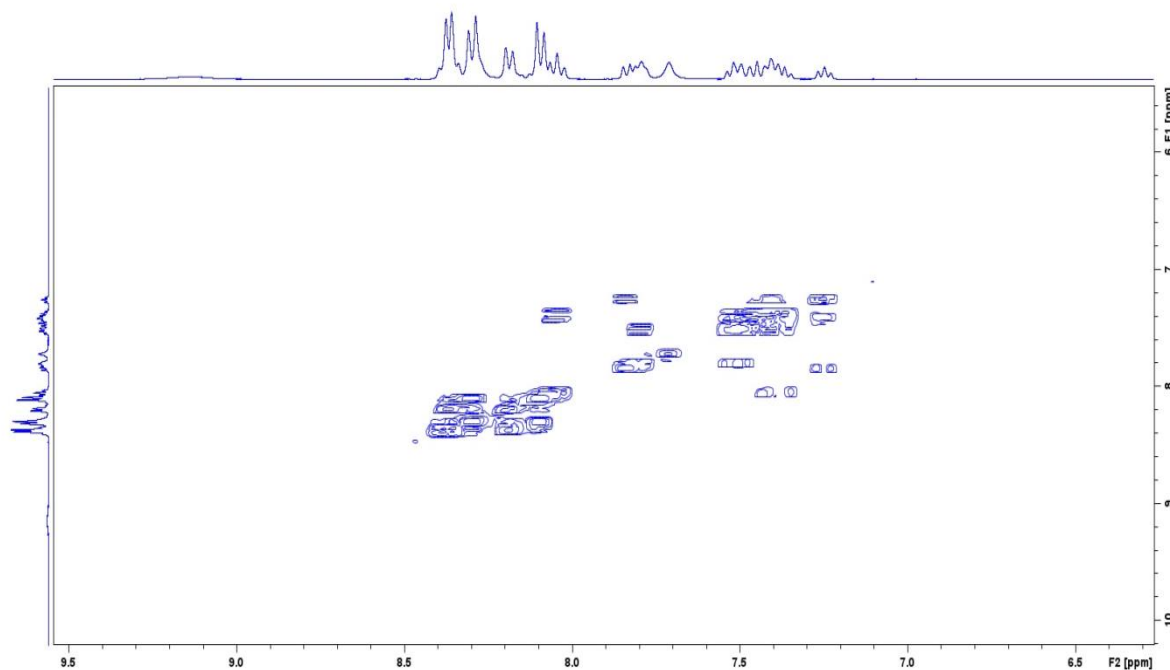


Figure A5.27 ^1H - ^1H COSY spectrum of 3-(1,3-benzothiazoyl-2-yl)-1-(4-nitrobenzoyl)thiourea (**30**).

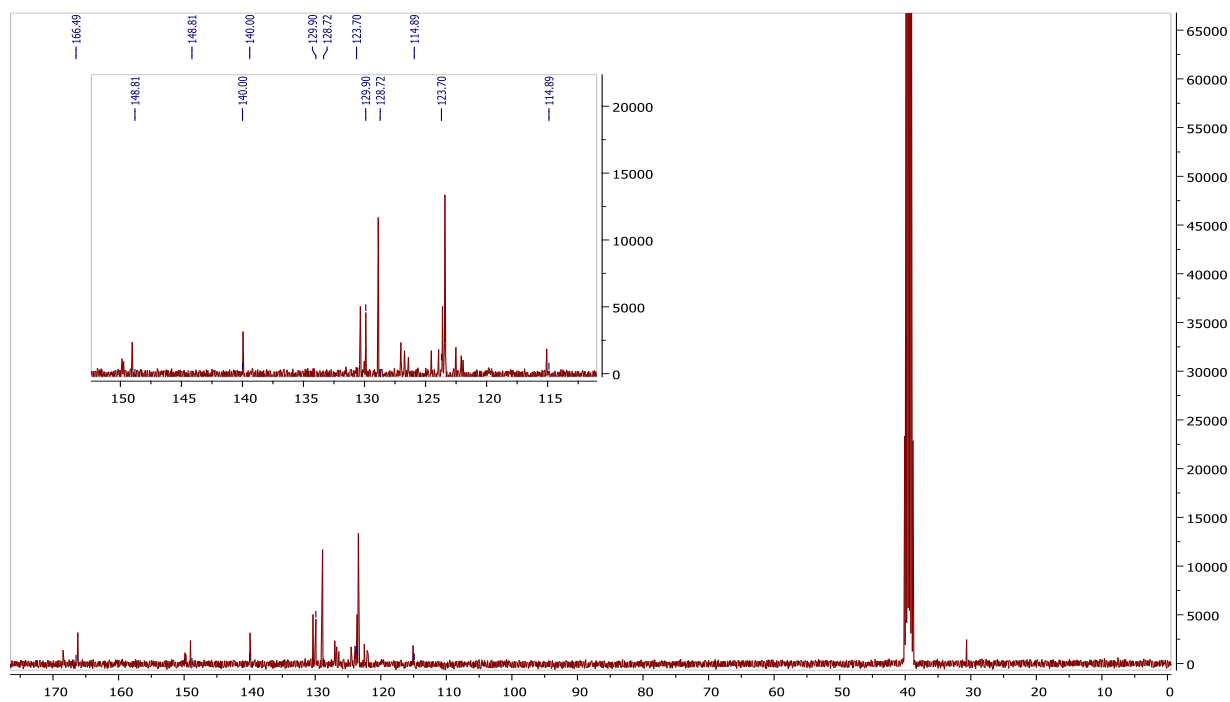


Figure A5.28 ^{13}C NMR spectrum of 3-(1,3-benzothiazoyl-2-yl)-1-(4-nitrobenzoyl)thiourea (**30**).

APPENDIX D

CHARACTERIZATION DATA OF TRIAZATETRACYCLIC DERIVATIVES

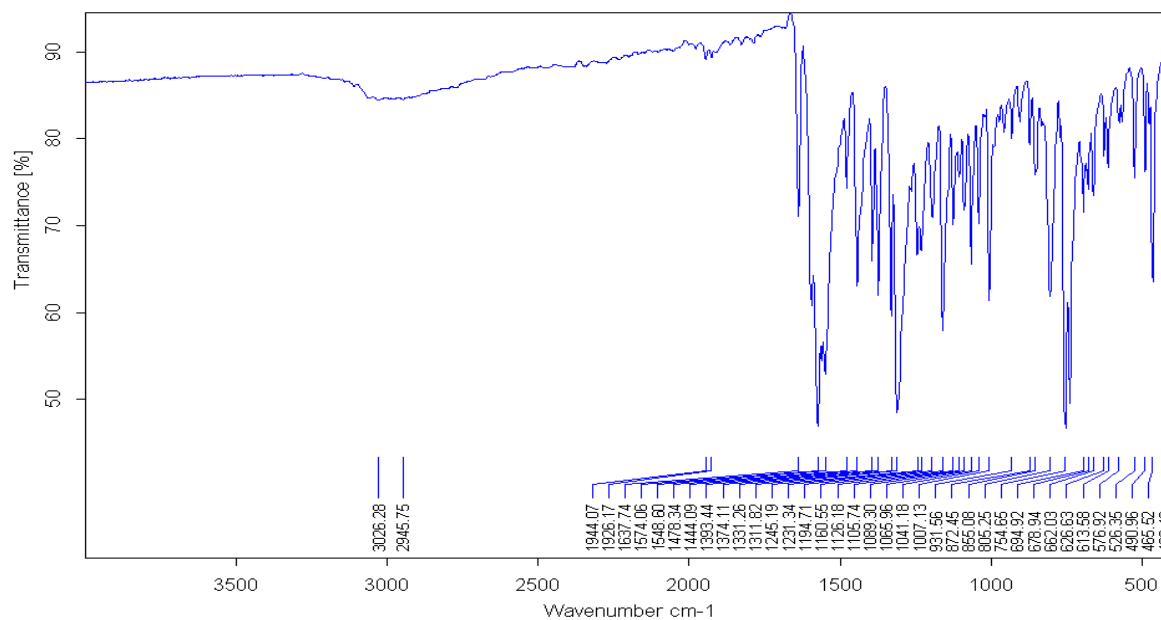


Figure A6.1 IR spectrum of 4-bromo-*N*-[(9*E*)-8,10,17-triazatetracyclo [8.7.0.0^{2,7}.0^{11,16}]heptadeca-1(17),2,4,6,11(16),12,14-heptaen-9-ylidene]benzamide (**32**).

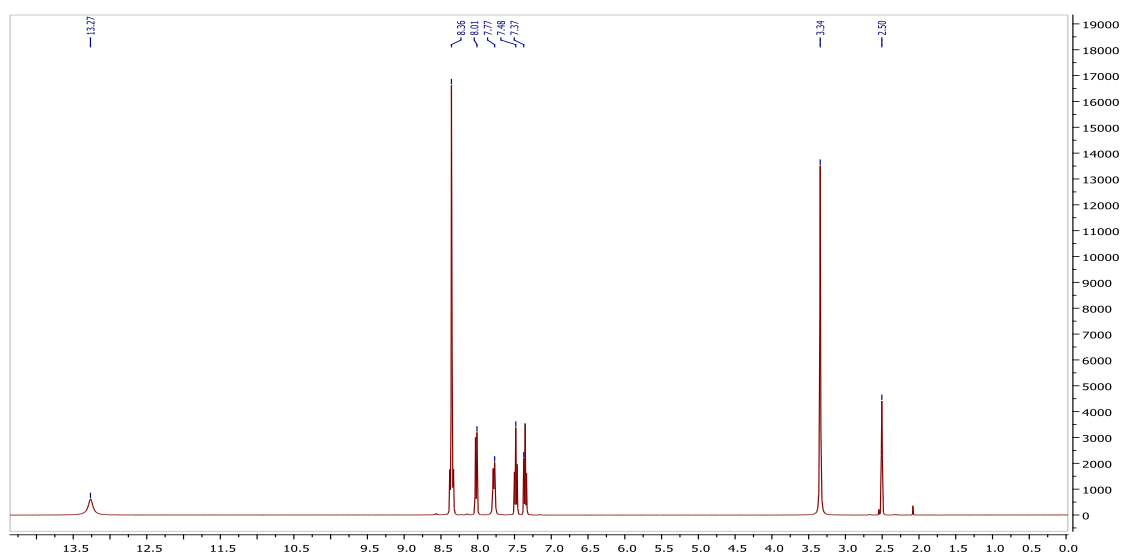


Figure A6.2 ¹H NMR spectrum of 4-bromo-*N*-[(9*E*)-8,10,17-triazatetracyclo [8.7.0.0^{2,7}.0^{11,16}]heptadeca-1(17),2,4,6,11(16),12,14-heptaen-9-ylidene]benzamide (**32**).

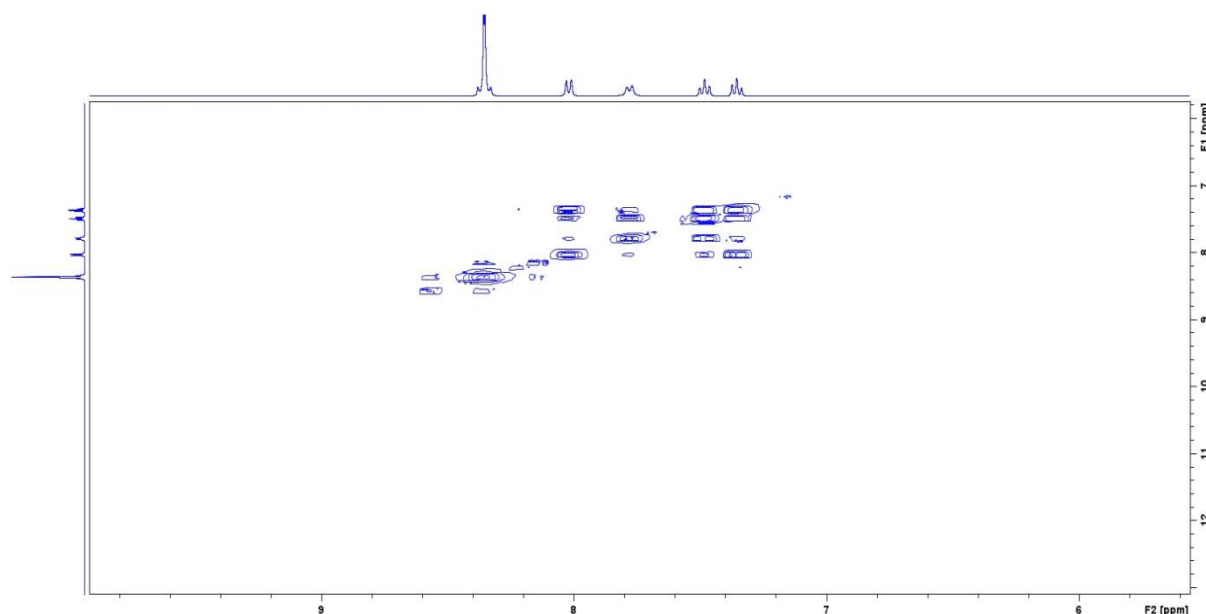


Figure A6.3 ^1H - ^1H COSY spectrum of 4-bromo-*N*-[(9*E*)-8,10,17-triazatetracyclo 8.7.0.0^{2,7}.0^{11,16}]heptadeca-1(17),2,4,6,11(16),12,14-heptaen-9-ylidene] benzamide (**32**).

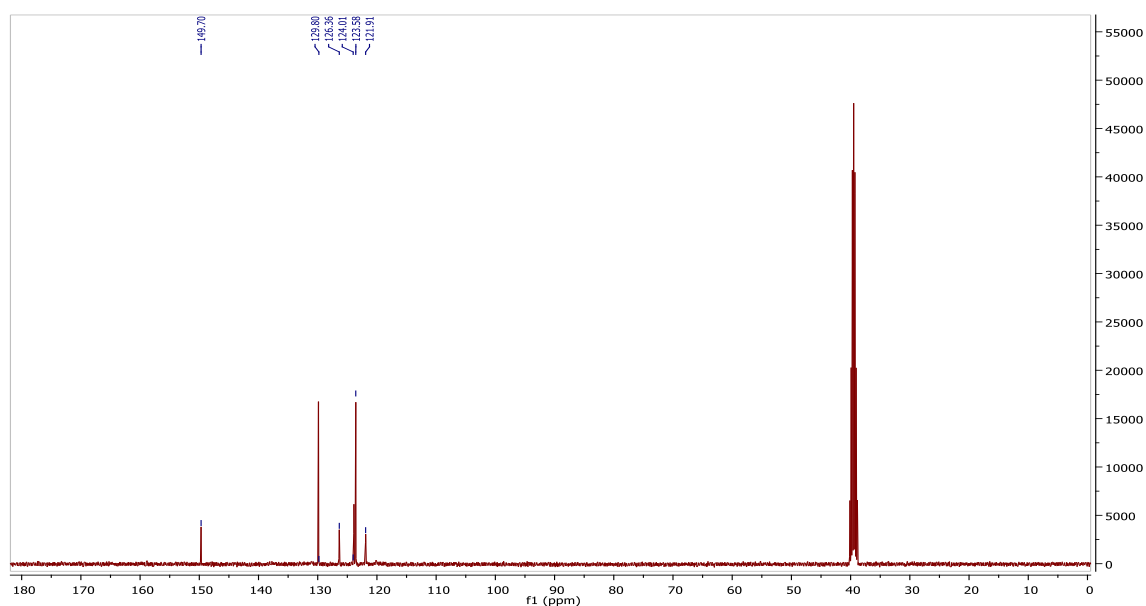


Figure A6.4 ^{13}C NMR spectrum of 4-bromo-*N*-[(9*E*)-8,10,17-triazatetracyclo [8.7.0.0^{2,7}.0^{11,16}]heptadeca-1(17),2,4,6,11(16),12,14-heptaen-9-ylidene] benzamide (**32**).

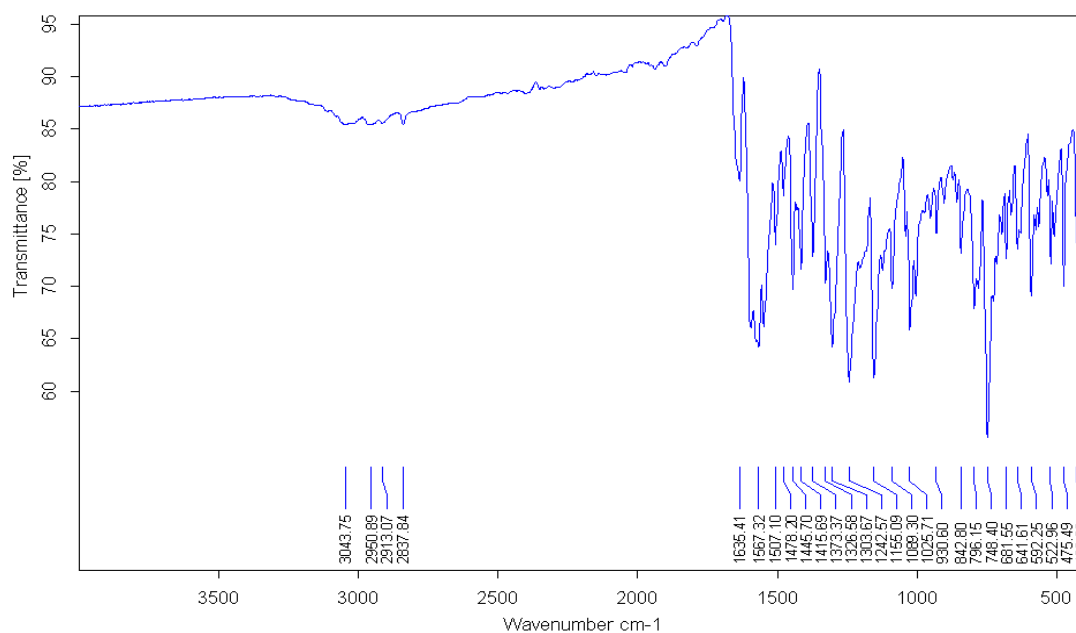


Figure A6.5 IR spectrum of 4-methoxy-*N*-[(9*E*)-8,10,17-triazatetracyclo[8.7.0.0^{2,7}.0^{11,16}]heptadeca-1(17),2,4,6,11(16),12,14-heptaen-9-ylidene]benzamide (**33**).

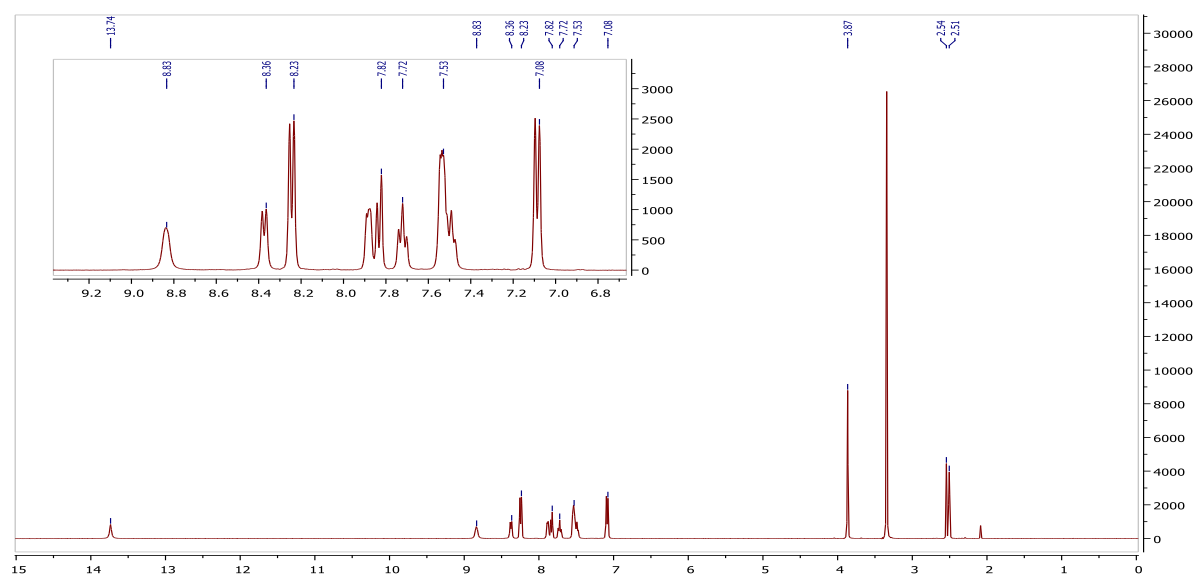


Figure A6.6 ¹H NMR spectrum of 4-methoxy-*N*-[(9*E*)-8,10,17-triazatetracyclo[8.7.0.0^{2,7}.0^{11,16}]heptadeca-1(17),2,4,6,11(16),12,14-heptaen-9-ylidene]benzamide (**33**).

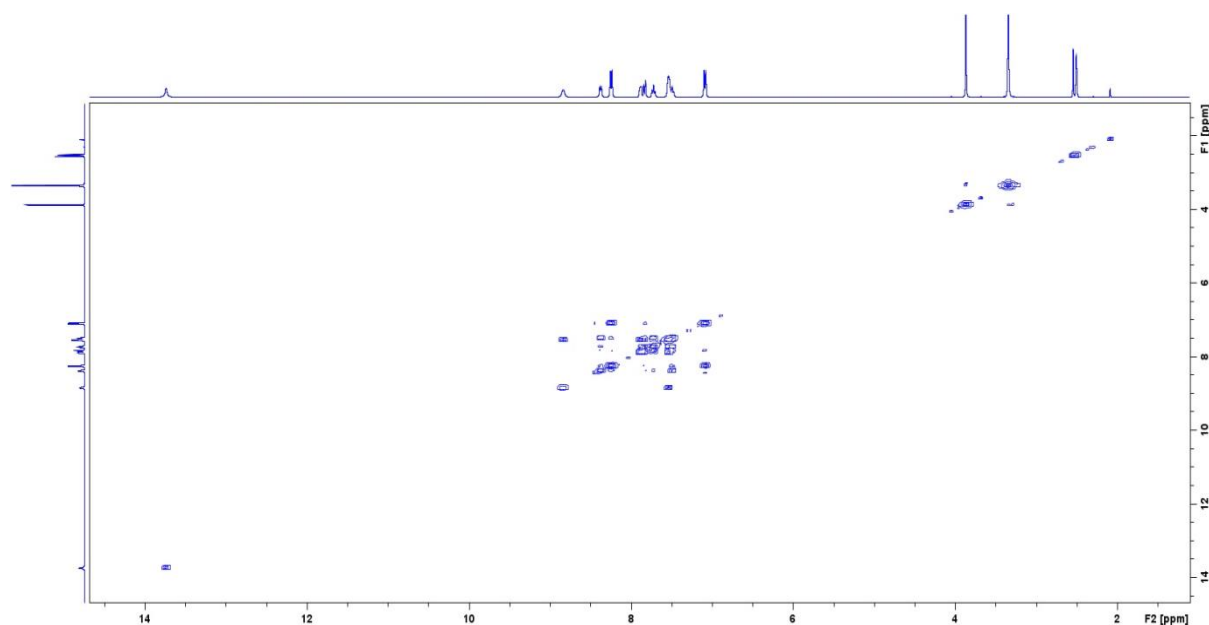


Figure A6.7 ^1H - ^1H COSY spectrum of 4-methoxy-*N*-[(9*E*)-8,10,17-triazatetracyclo [8.7.0.0^{2,7}.0^{11,16}] heptadeca-1(17),2,4,6,11(16),12,14-heptaen-9-ylidene] benzamide (**33**).

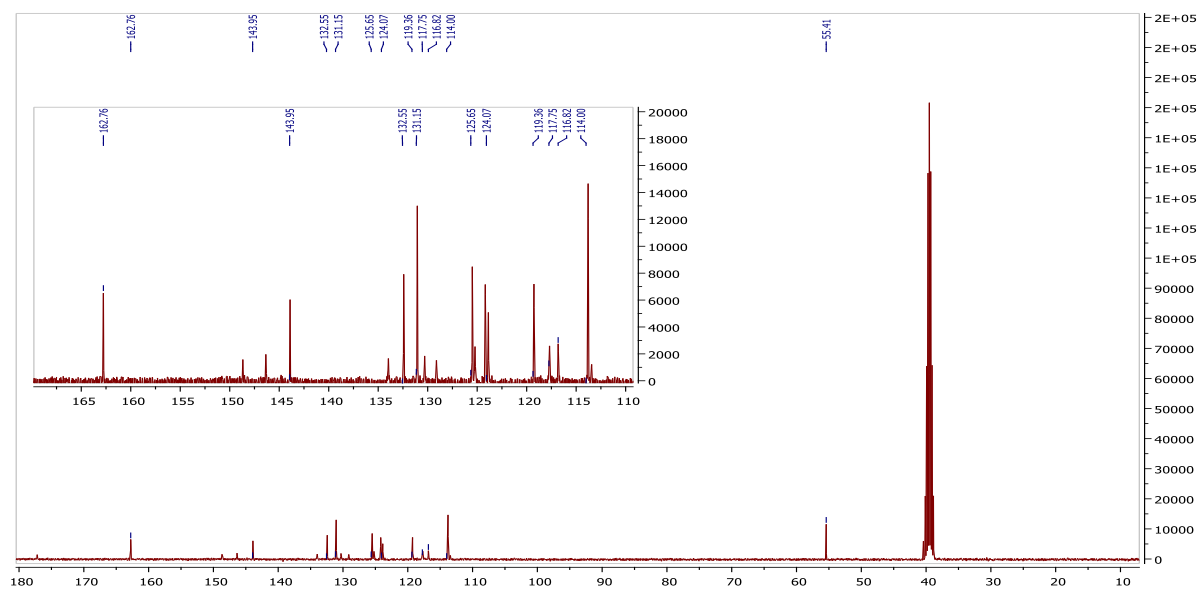


Figure A6.8 ^{13}C NMR spectrum of 4-methoxy-*N*-[(9*E*)-8,10,17-triazatetracyclo [8.7.0.0^{2,7}.0^{11,16}]heptadeca-1(17),2,4,6,11(16),12,14-heptaen-9-ylidene] benzamide (**33**).

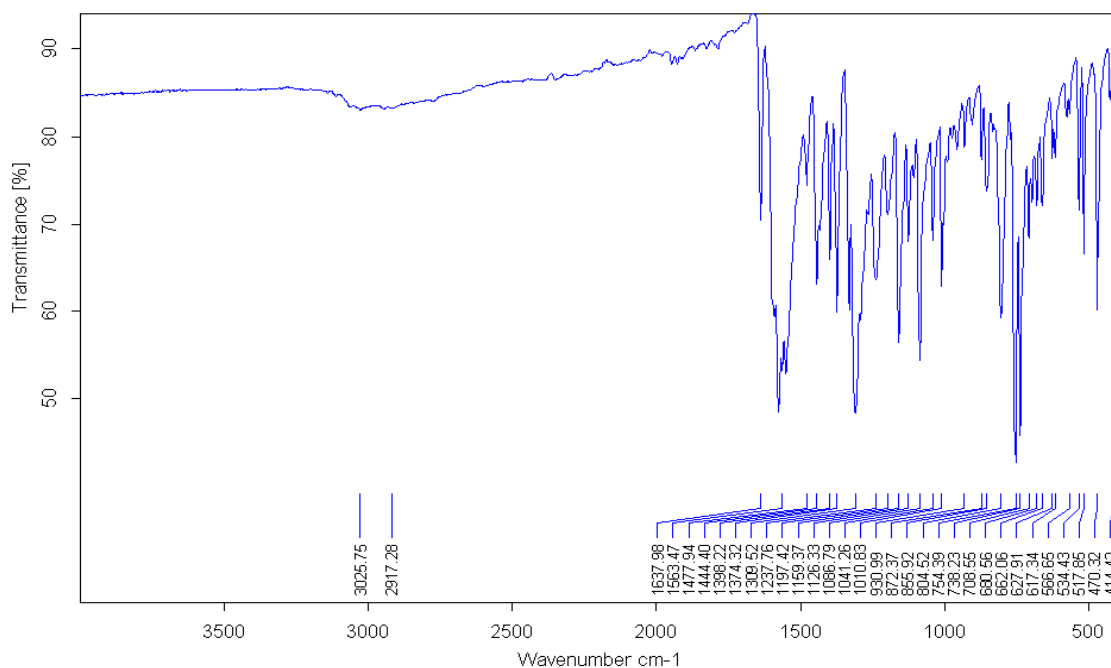


Figure A6.9 IR spectrum of 4-chloro-*N*-[(9*E*)-8,10,17-triazatetracyclo [8.7.0.0^{2,7}.0^{11,16}]heptadeca-1(17),2,4,6,11(16),12,14-heptaen-9-ylidene] benzamide (**35**).

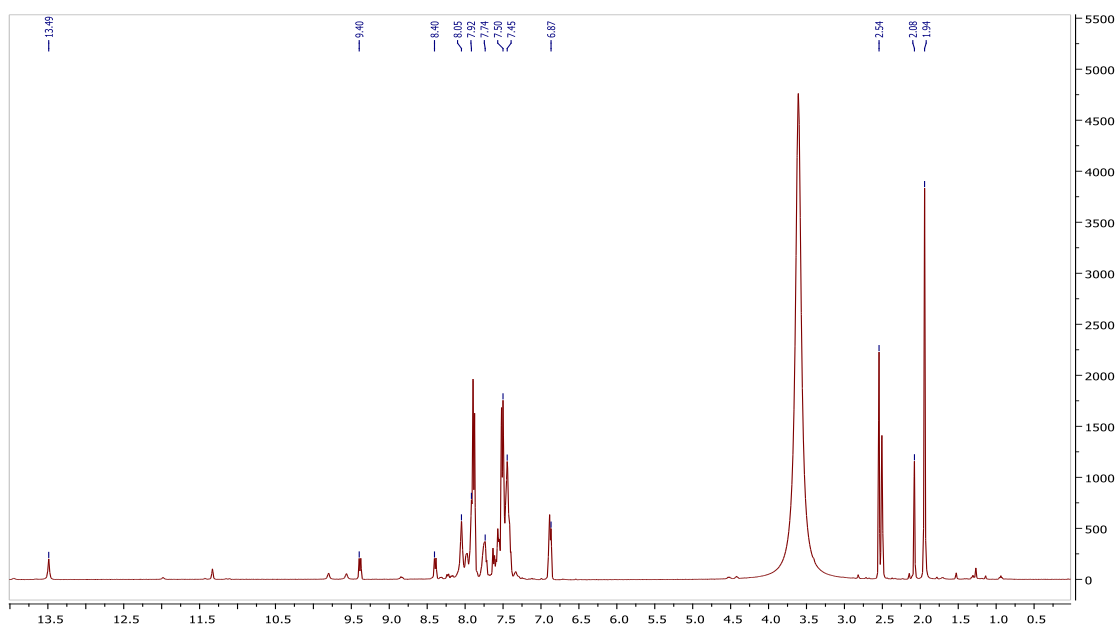


Figure A6.10 ¹H NMR spectrum of 4-chloro-*N*-[(9*E*)-8,10,17-triazatetracyclo [8.7.0.0^{2,7}.0^{11,16}]heptadeca-1(17),2,4,6,11(16),12,14-heptaen-9-ylidene] benzamide (**35**).

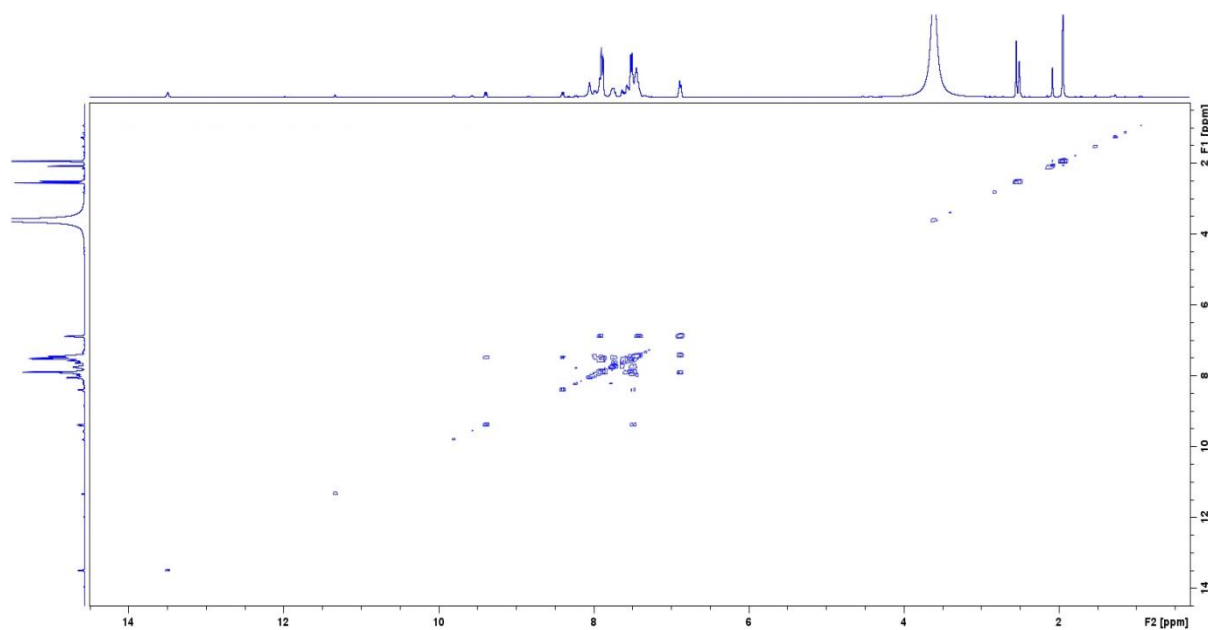


Figure A6.11 ^1H ^1H COSY spectrum of 4-chloro-*N*-[(9*E*)-8,10,17-triazatetracyclo [8.7.0.0^{2,7}.0^{11,16}]heptadeca-1(17),2,4,6,11(16),12,14-heptaen-9-ylidene] benzamide (**35**).

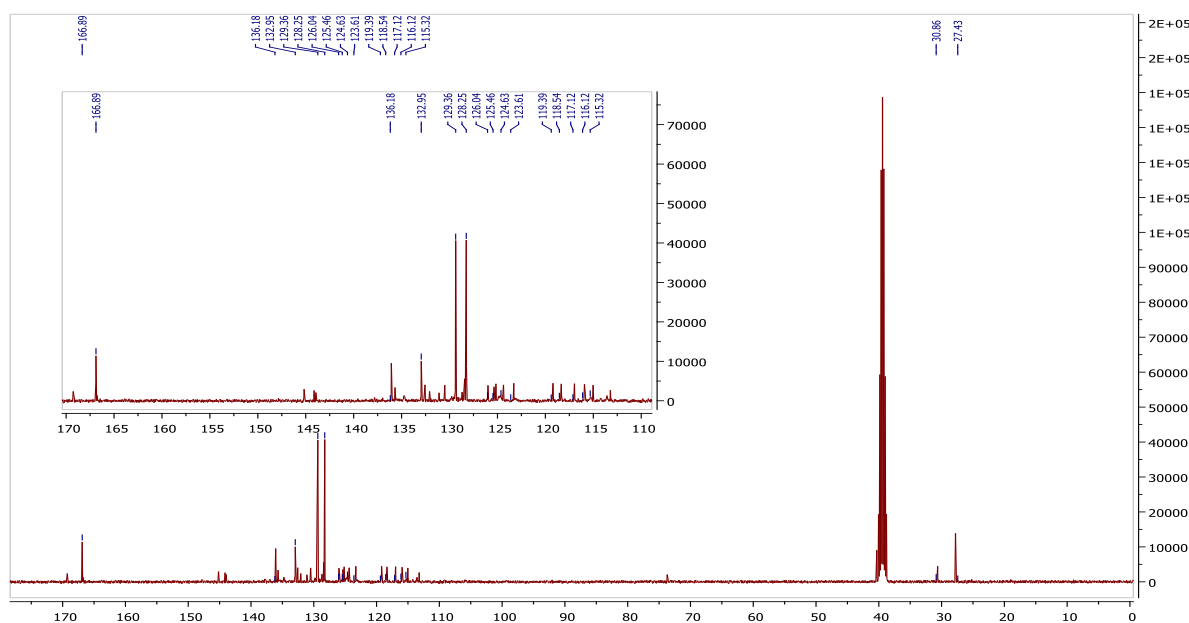


Figure A6.12 ^{13}C NMR spectrum of 4-chloro-*N*-[(9*E*)-8,10,17-triazatetracyclo [8.7.0.0^{2,7}.0^{11,16}]heptadeca-1(17),2,4,6,11(16),12,14-heptaen-9-ylidene] benzamide (**35**).

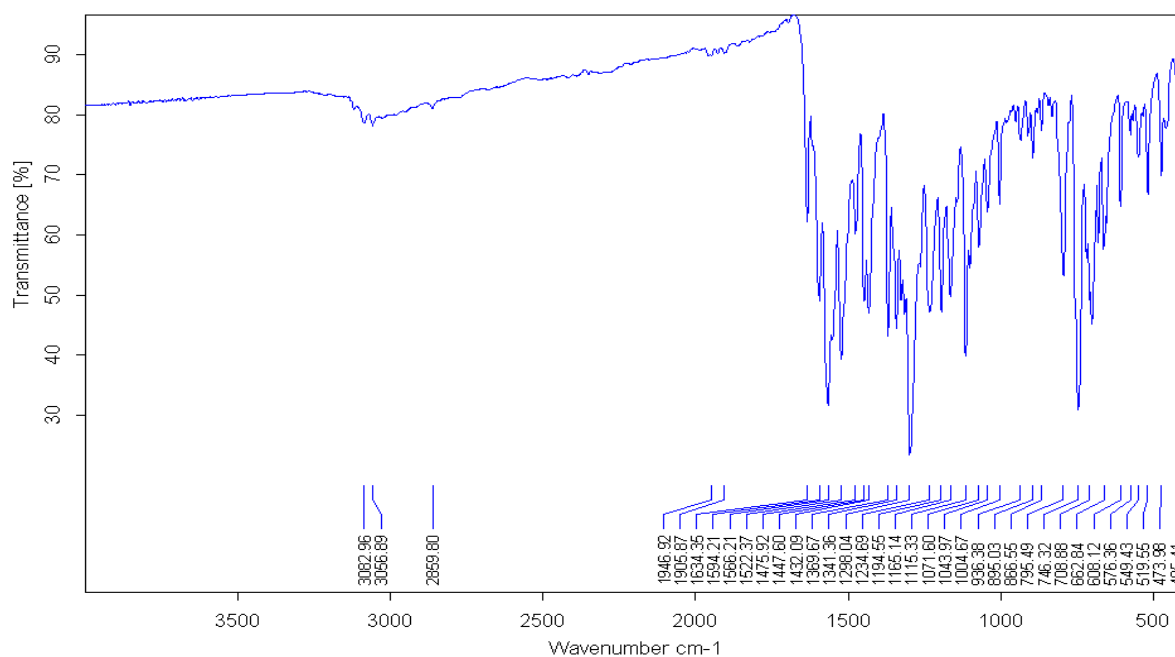


Figure A6.13 IR spectrum of 3-nitro-*N*-[(9*E*)-8,10,17-triazatetracyclo [8.7.0.0^{2,7}.0^{11,16}]heptadeca-1(17),2,4,6,11(16),12,14-heptaen-9-ylidene] benzamide (**36**).

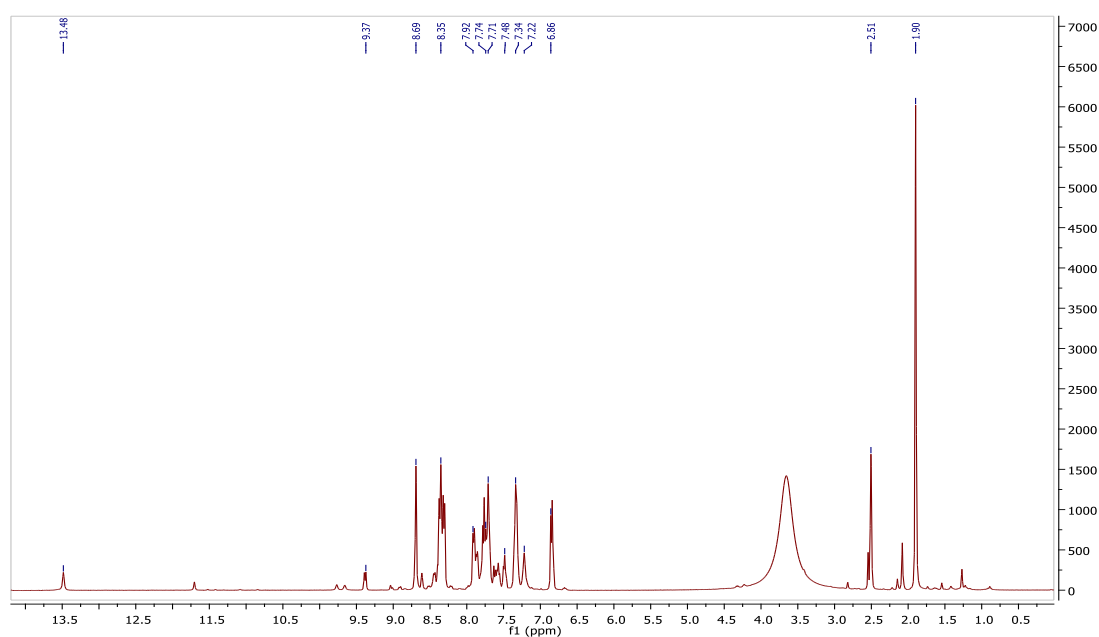


Figure A6.14 ¹H NMR spectrum of 3-nitro-*N*-[(9*E*)-8,10,17-triazatetracyclo [8.7.0.0^{2,7}.0^{11,16}]heptadeca-1(17),2,4,6,11(16),12,14-heptaen-9-ylidene] benzamide (**36**).

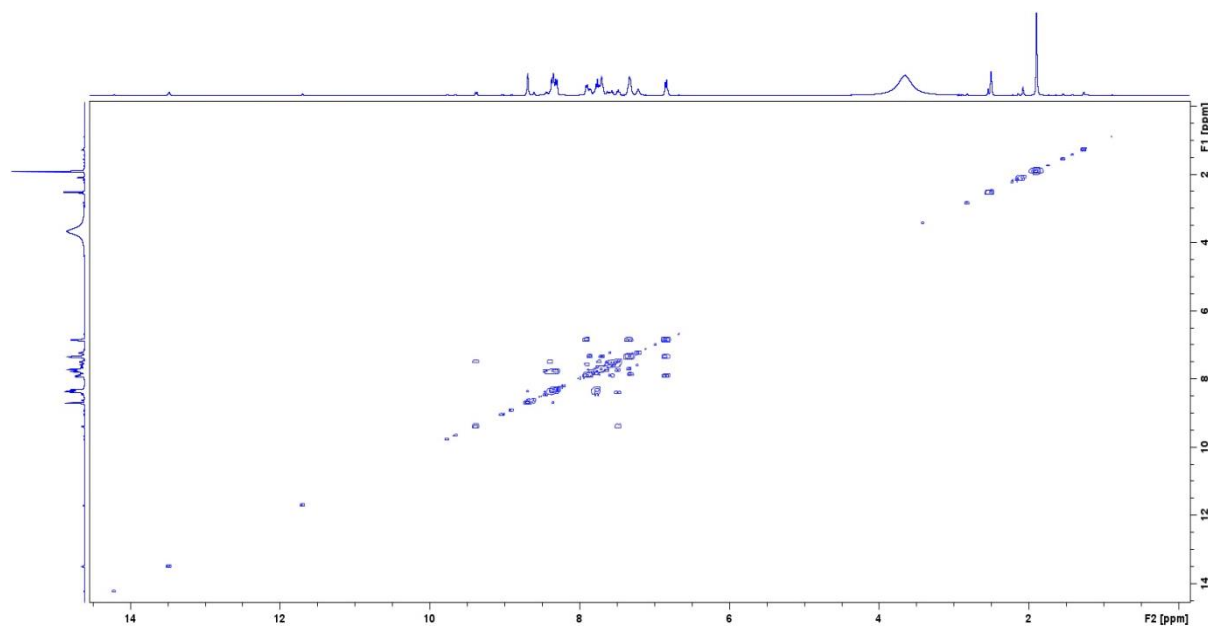


Figure A6.15 ^1H ^1H COSY spectrum of 3-nitro-*N*-[(9*E*)-8,10,17-triazatetracyclo [8.7.0.0^{2,7}.0^{11,16}]heptadeca-1(17),2,4,6,11(16),12,14-heptaen-9-ylidene] benzamide (**36**).

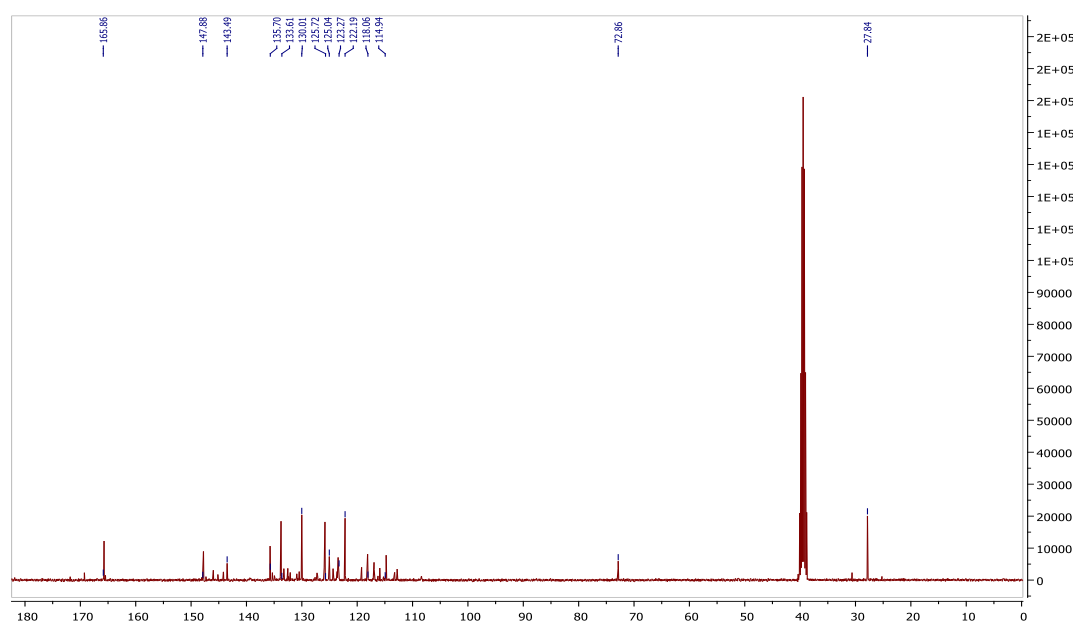


Figure A6.16 ^{13}C NMR spectrum of 3-nitro-*N*-[(9*E*)-8,10,17-triazatetracyclo [8.7.0.0^{2,7}.0^{11,16}]heptadeca-1(17),2,4,6,11(16),12,14-heptaen-9-ylidene] benzamide (**36**).

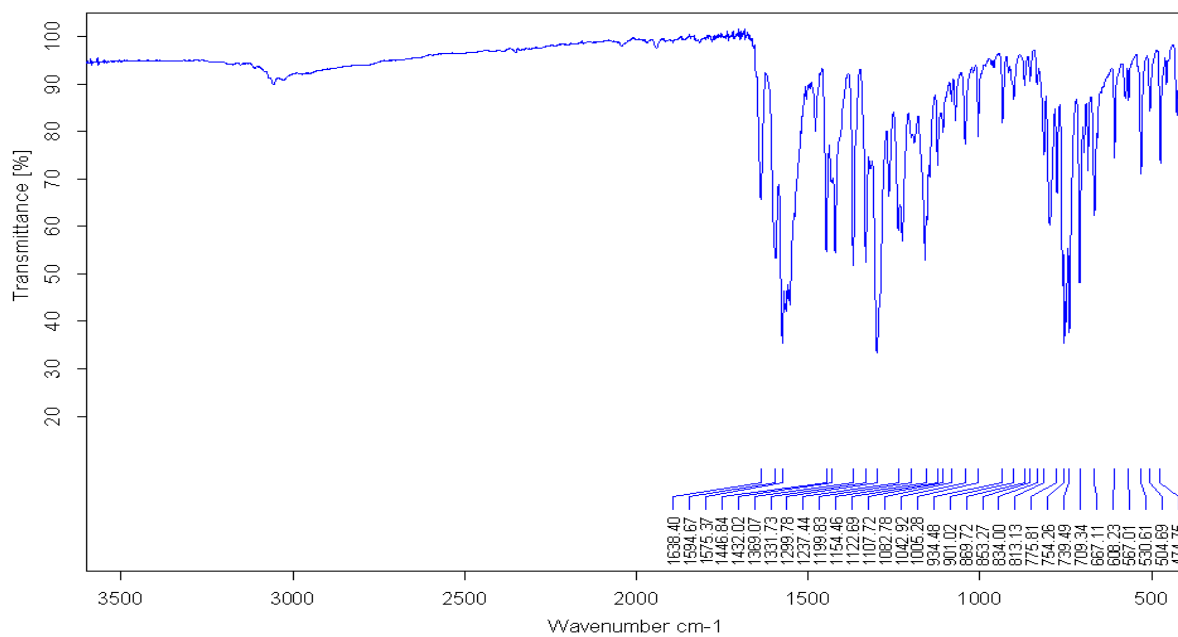


Figure A6.17 IR spectrum of 3-chloro-*N*-[(9*E*)-8,10,17-triazatetracyclo[8.7.0.0^{2,7}.0^{11,16}]heptadeca-1(17),2,4,6,11(16),12,14-heptaen-9-ylidene]benzamide (**37**).

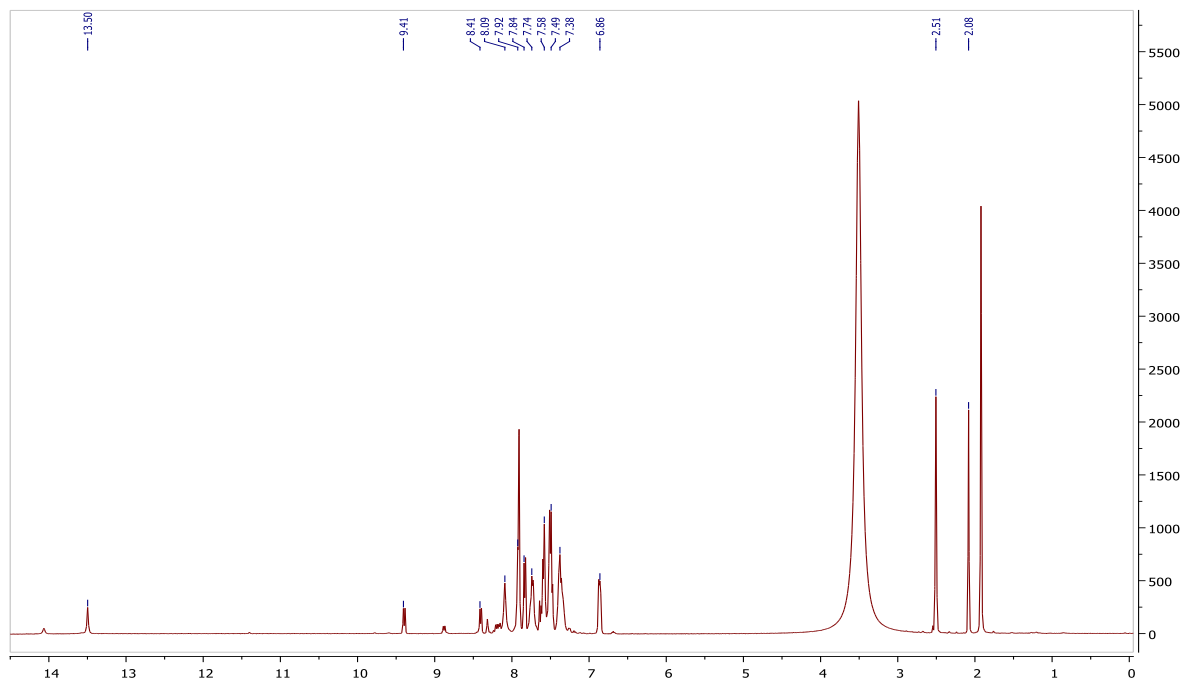


Figure A6.18 ¹H NMR spectrum of, 3-chloro-*N*-[(9*E*)-8,10,17-triazatetracyclo[8.7.0.0^{2,7}.0^{11,16}]heptadeca-1(17),2,4,6,11(16),12,14-heptaen-9-ylidene]benzamide (**37**).

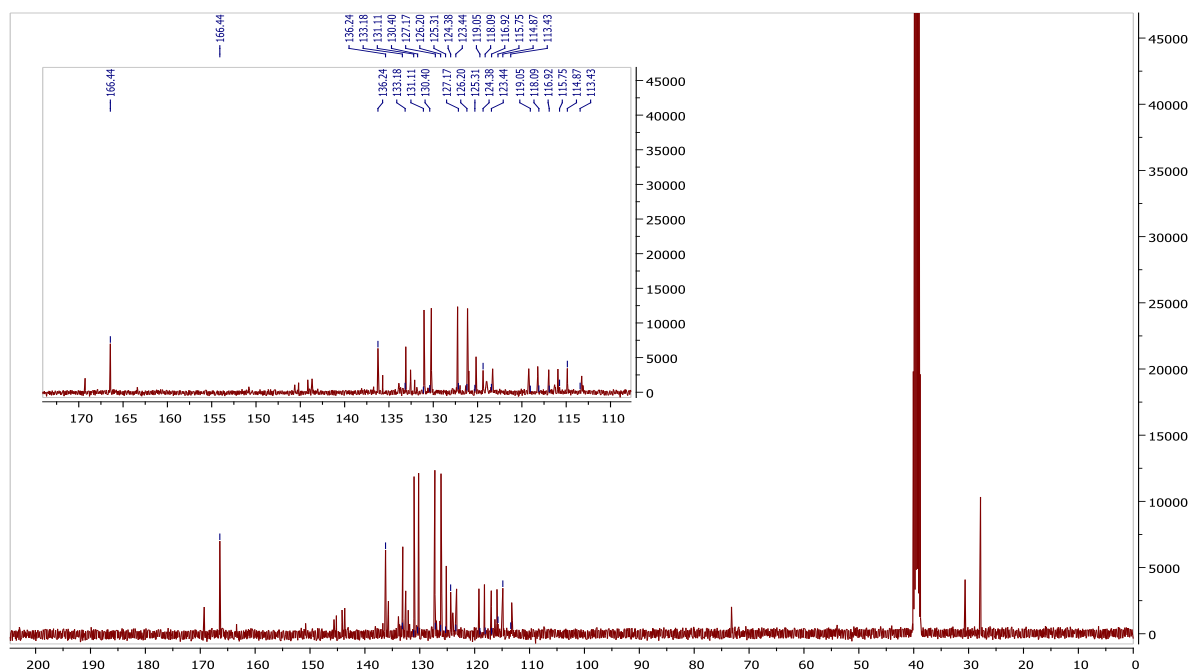


Figure A6.19 ^{13}C NMR spectrum of 3-chloro-*N*-[(9*E*)-8,10,17-triazatetracyclo [8.7.0.0^{2,7}.0^{11,16}]heptadeca-1(17),2,4,6,11(16),12,14-heptaen-9-ylidene] benzamide (**37**).

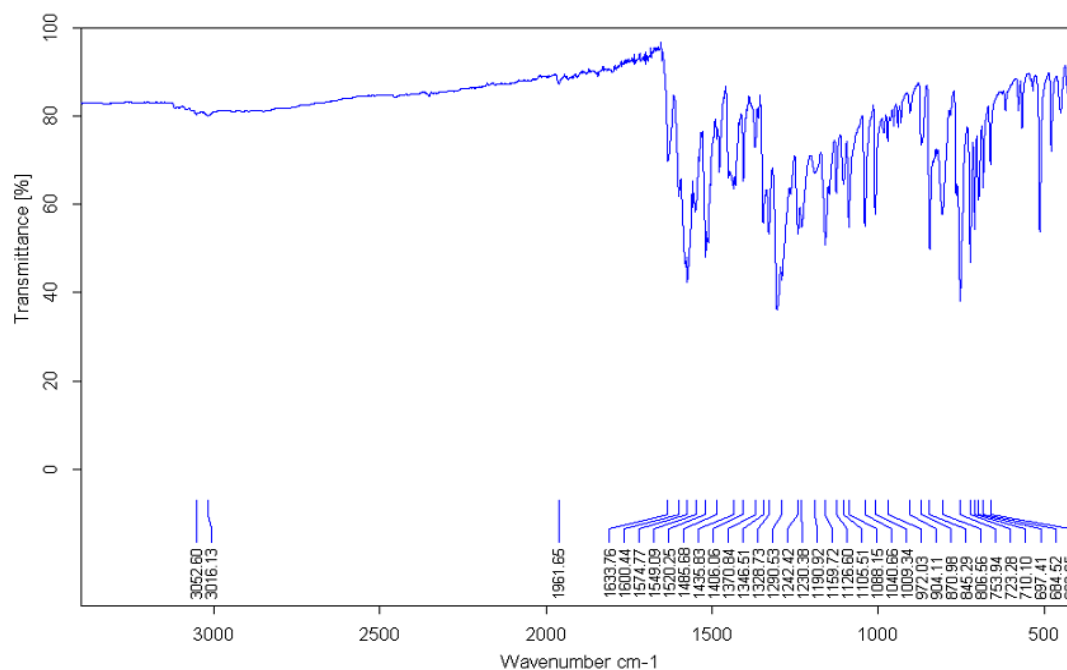


Figure A6.20 IR spectrum of 4-nitro-*N*-[(9*E*)-8,10,17-triazatetracyclo [8.7.0.0^{2,7}.0^{11,16}]heptadeca-1(17),2,4,6,11(16),12,14-heptaen-9-ylidene] benzamide (**38**).

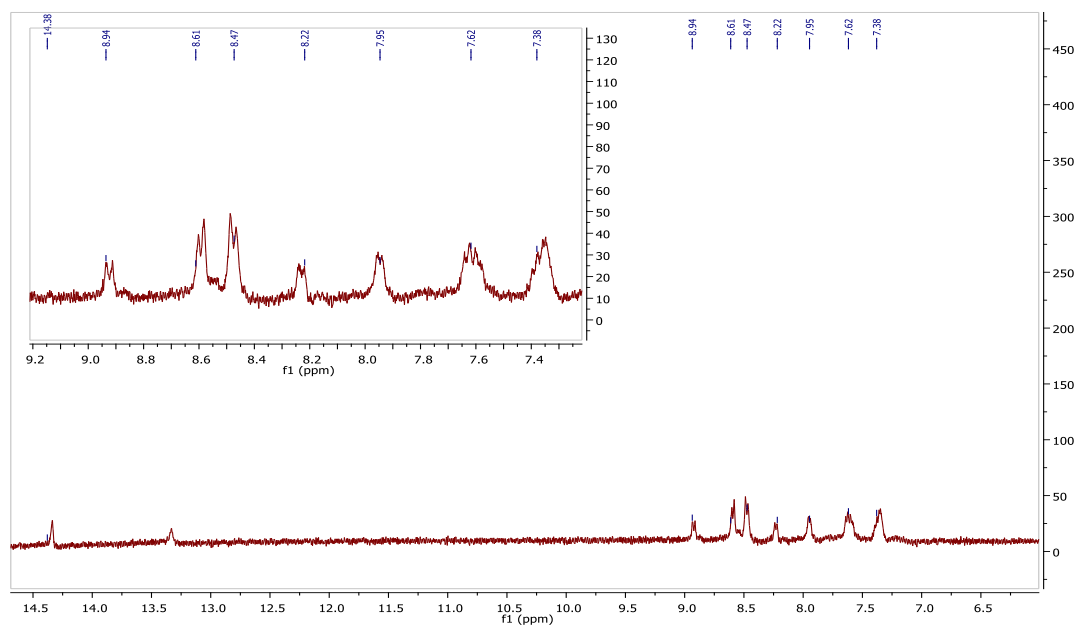


Figure A6.21 ^1H NMR spectrum of 4-nitro-*N*-[(9*E*)-8,10,17-triazatetracyclo[8.7.0.0^{2,7}.0^{11,16}]heptadeca-1(17),2,4,6,11(16),12,14-heptaen-9-ylidene]benzamide (**38**).

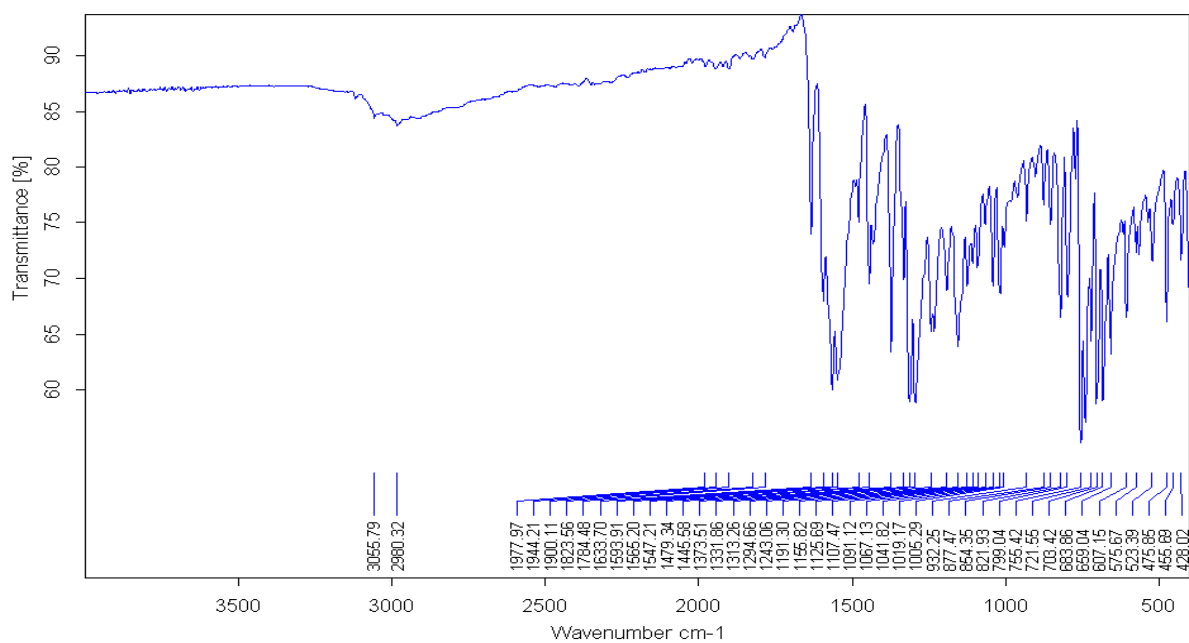


Figure A6.22 IR spectrum of *N*-[(9*E*)-8,10,17-triazatetracyclo[8.7.0.0^{2,7}.0^{11,16}]heptadeca-1(17),2,4,6,11(16),12,14-heptaen-9-ylidene]benzamide (**39**).

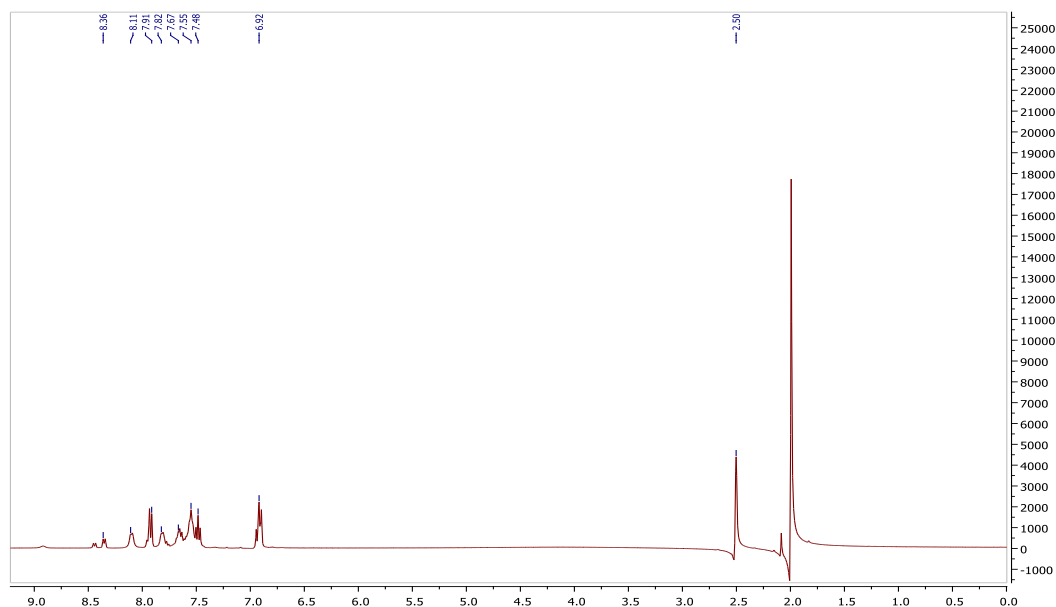


Figure A6.23 ^1H NMR spectrum of 3-bromo-*N*-[(9*E*)-8,10,17-triazatetracyclo [8.7.0.0^{2,7}.0^{11,16}]heptadeca-1(17),2,4,6,11(16),12,14-heptaen-9-ylidene] benzamide (**39**).

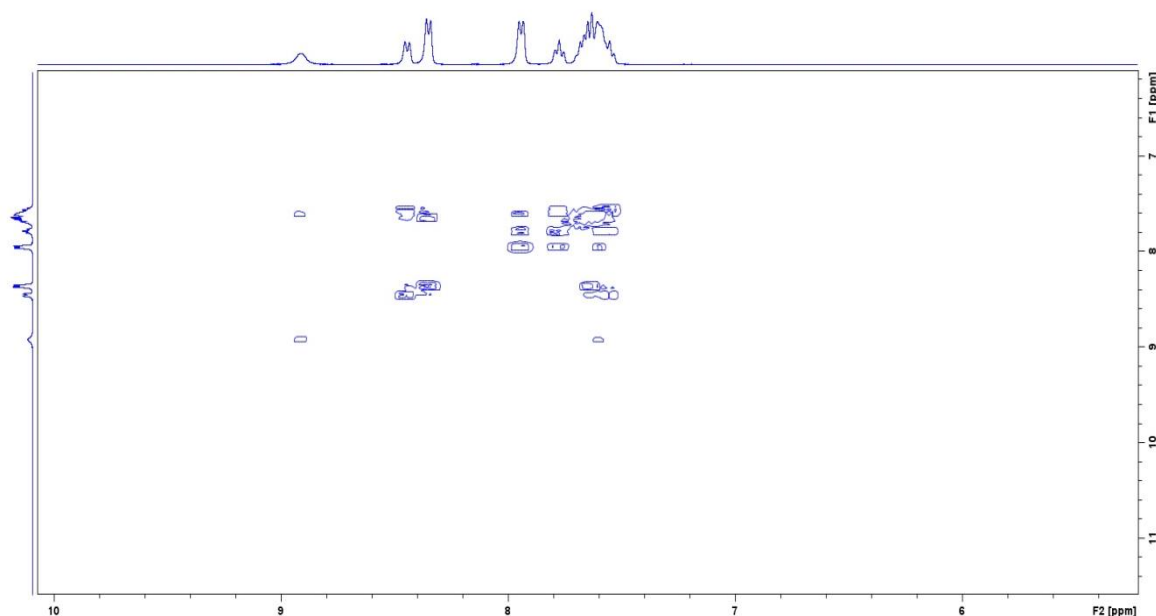


Figure A6.24 ^1H ^1H COSY spectrum of 3-bromo-*N*-[(9*E*)-8,10,17-triazatetracyclo [8.7.0.0^{2,7}.0^{11,16}]heptadeca-1(17),2,4,6,11(16),12,14-heptaen-9-ylidene] benzamide (**39**).

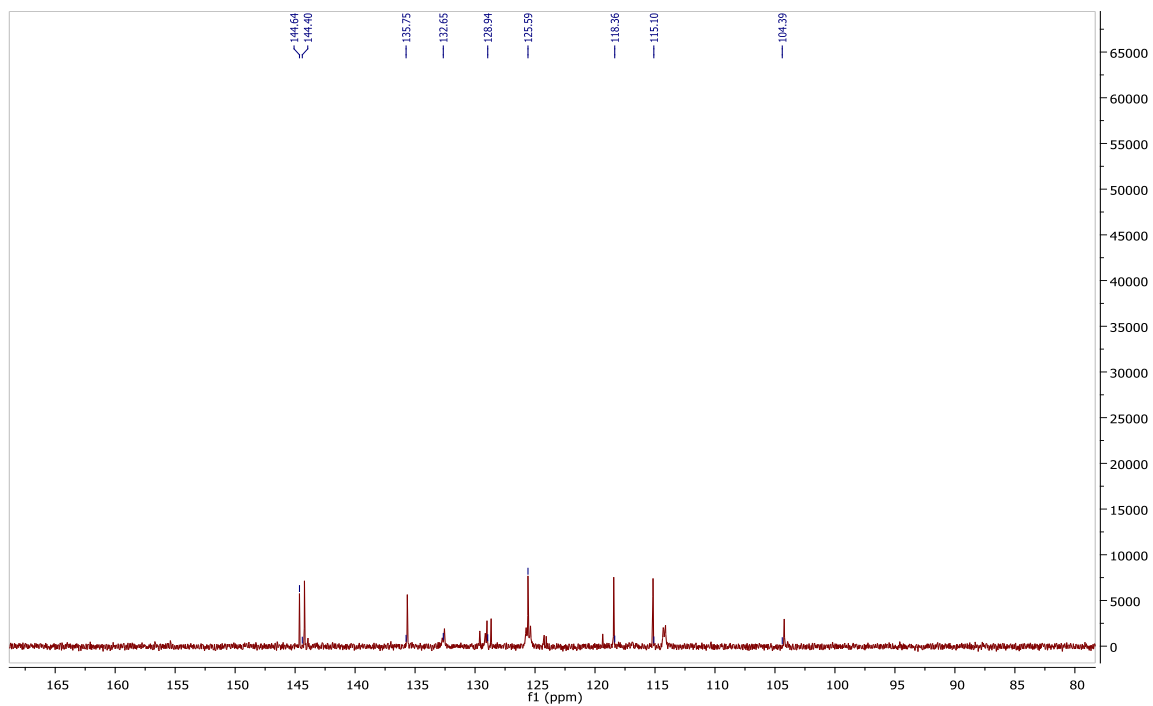


Figure A6.25 ^{13}C NMR spectrum of 3-bromo-*N*-[(9*E*)-8,10,17-triazatetracyclo [8.7.0.0^{2,7}.0^{11,16}]heptadeca-1(17),2,4,6,11(16),12,14-heptaen-9-ylidene] benzamide (**39**).

APPENDIX E

PHENYL THIOUREA COMPOUNDS AND OTHER DIAMINE DERIVATIVES

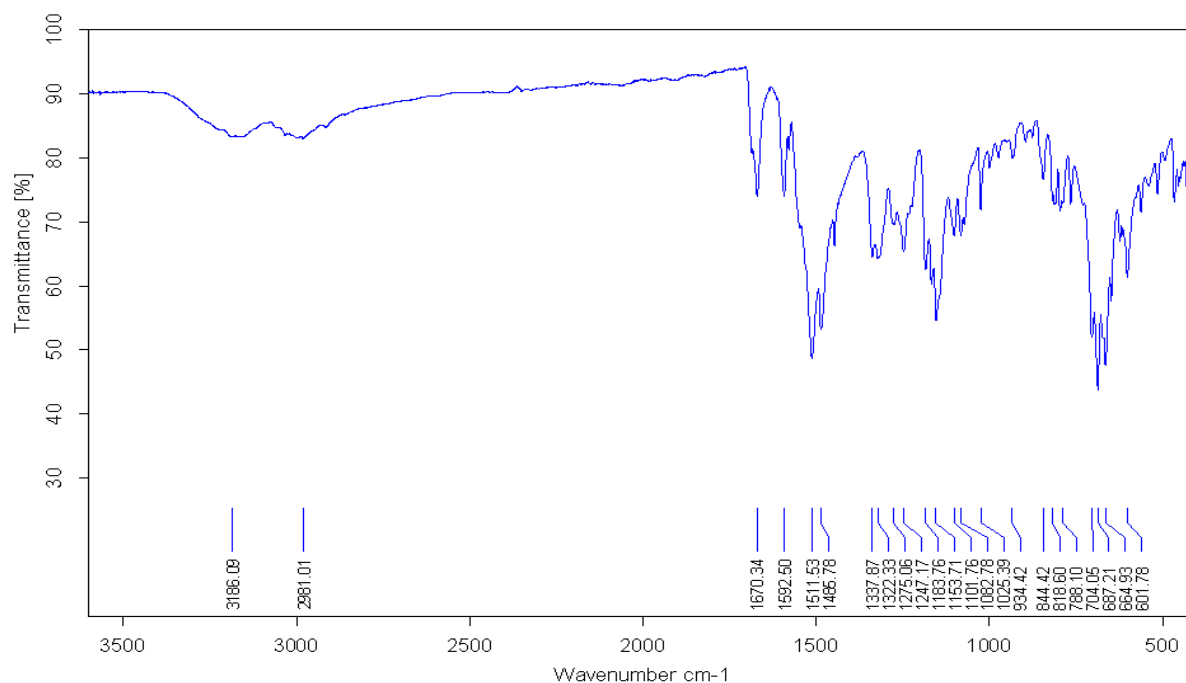


Figure A7.1 IR spectrum of 1-benzoyl-3-(5-methyl-2-[(phenylformamido)methanethioyl] amino)phenylthiourea (**40**).

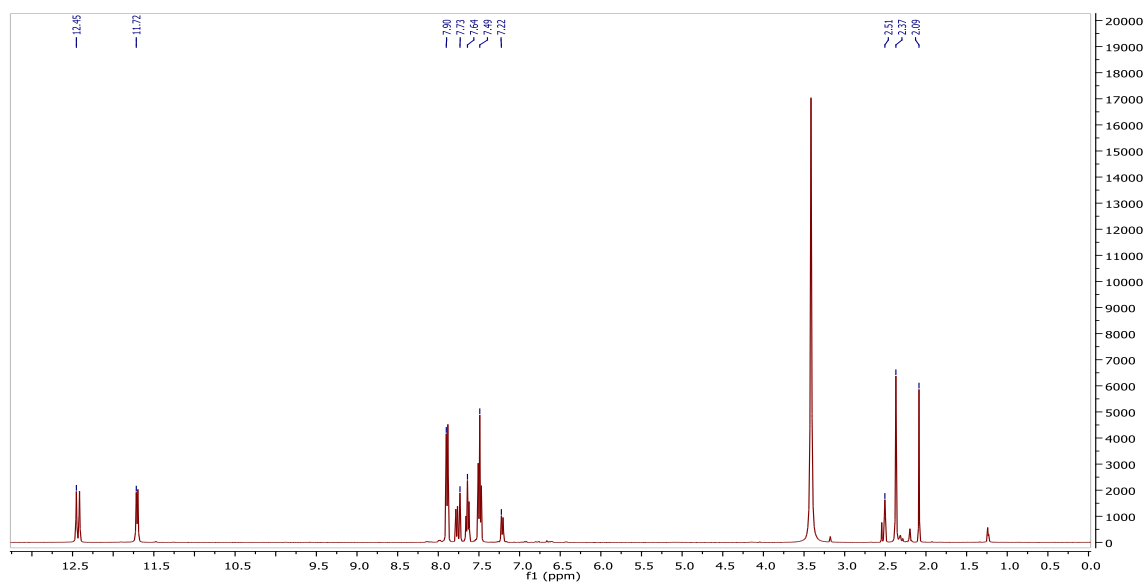


Figure A7.2 ^1H NMR spectrum of 1-benzoyl-3-(5-methyl-2-[(phenylformamido)methanethioyl] amino)phenylthiourea (**40**).

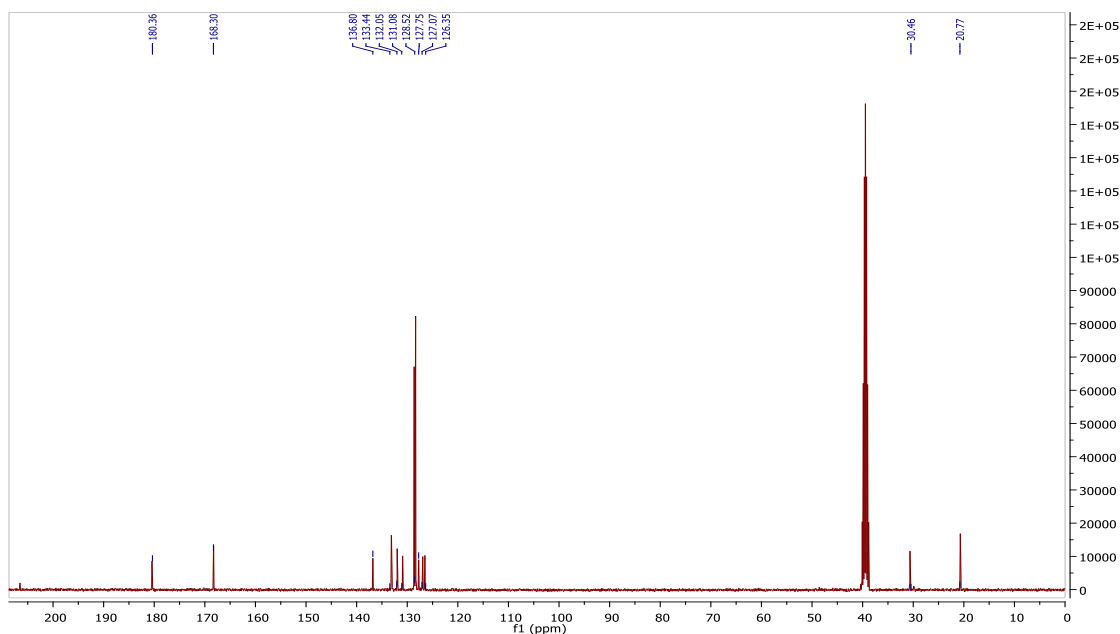


Figure A7.3 ^{13}C NMR spectrum of 1-benzoyl-3-(5-methyl-2-((phenylformamido) methanethiyl) amino) phenylthiourea (**40**).

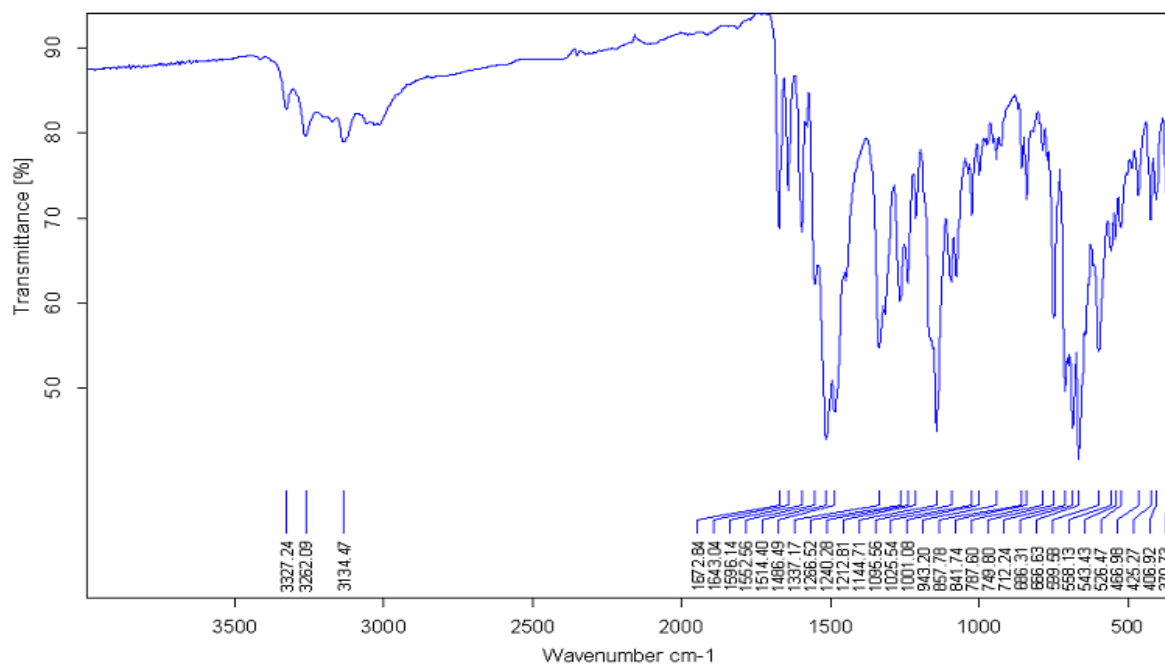


Figure A7.4 IR spectrum of 1-benzoyl-3-(2-((phenylformamido) methanethiyl) amino) phenylthiourea (**41**).

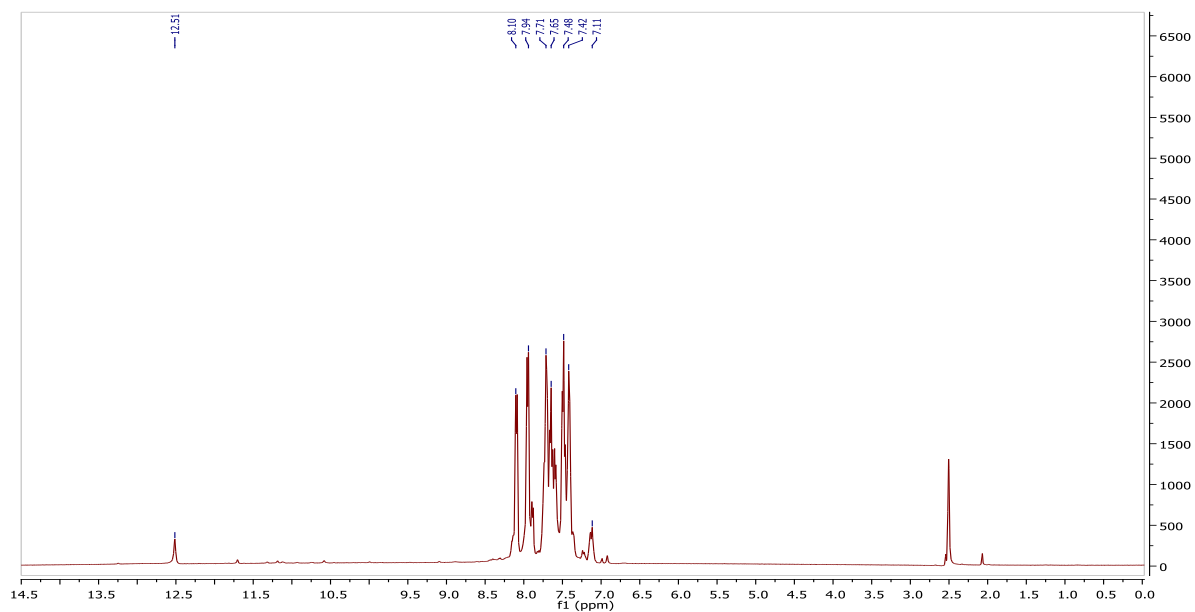


Figure A7.5 ¹H NMR spectrum of 1-benzoyl-3-(2-((phenylformamido)methanethioyl)amino)phenylthiourea (**41**).

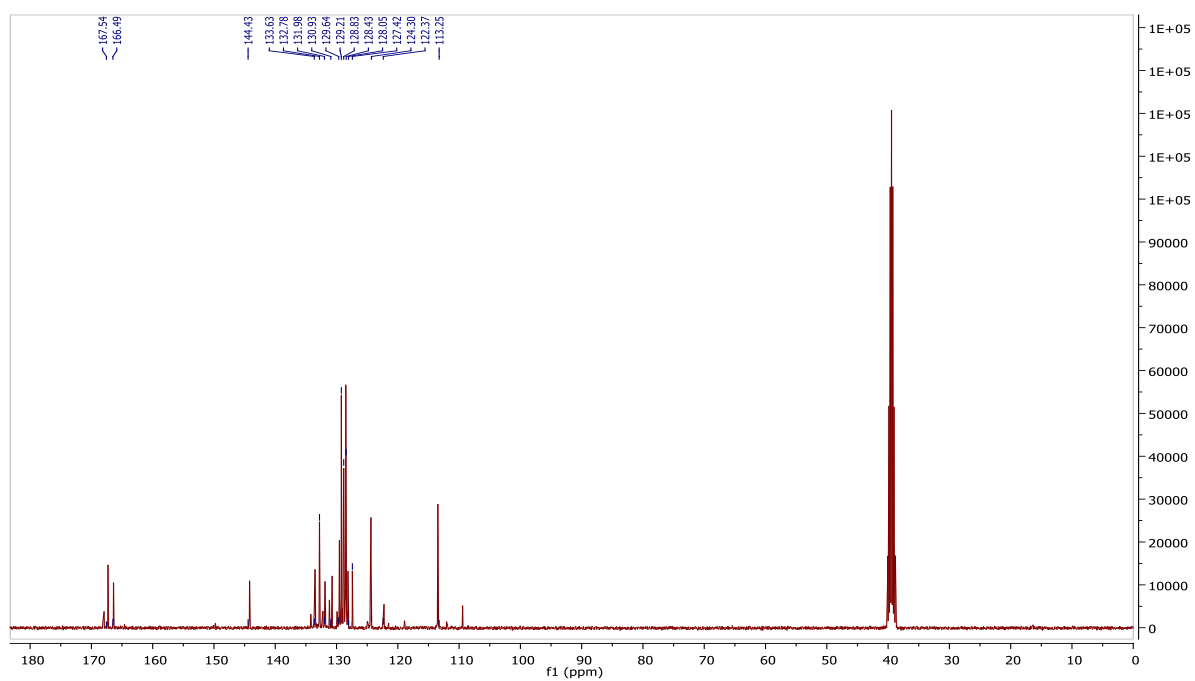


Figure A7.6 ¹³C NMR spectrum of 1-benzoyl-3-(2-((phenylformamido)methanethioyl)amino)phenylthiourea (**41**).

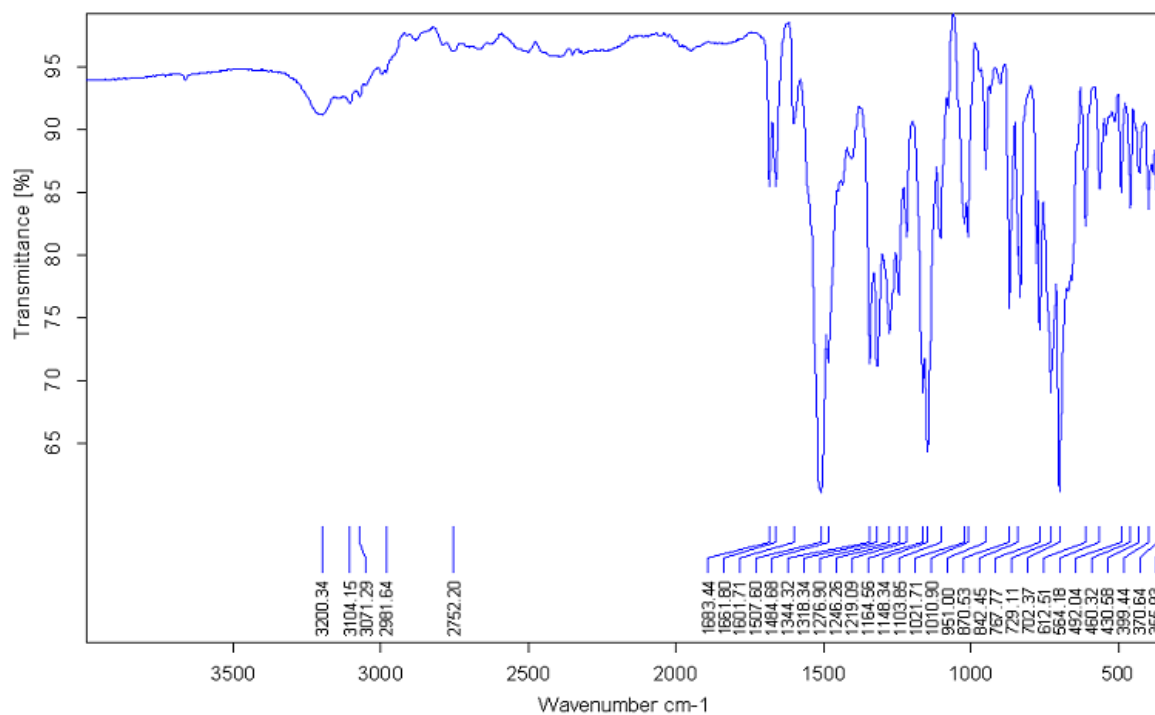


Figure A7.7 IR spectrum of 1-(4-nitrobenzoyl)-3-[2-({[(4-nitrophenyl)formamido]methanthiophenyl}thiourea)amino) (**42**).

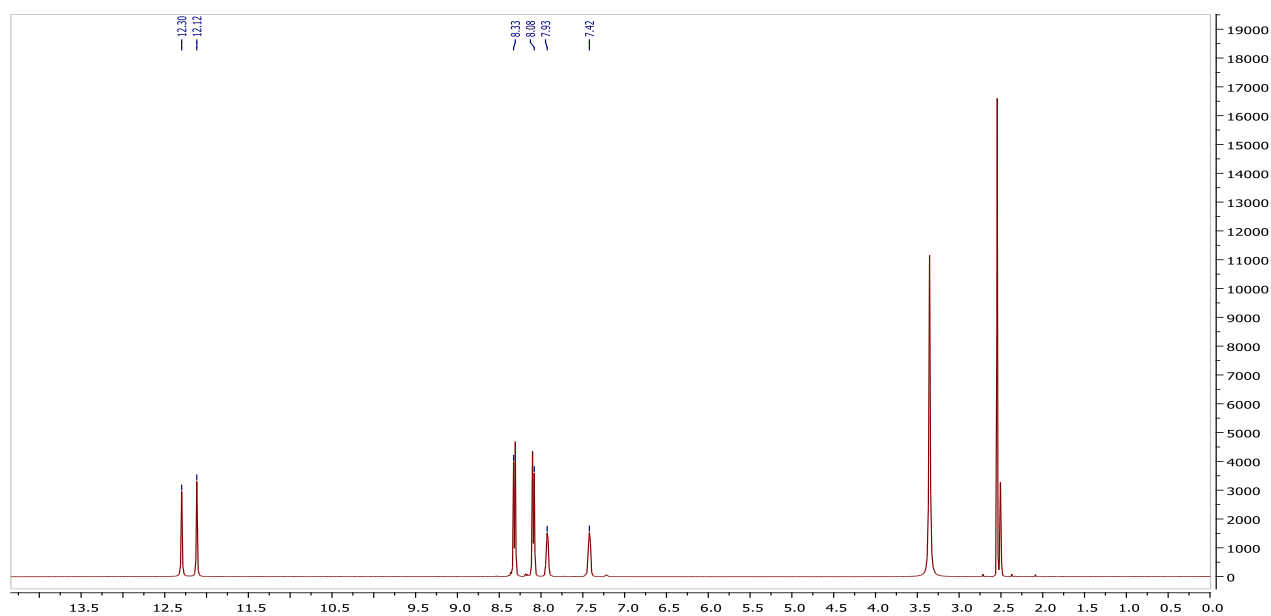


Figure A7.8 ^1H NMR spectrum of 1-(4-nitrobenzoyl)-3-[2-({[(4-nitrophenyl)formamido]methanthiophenyl}thiourea)amino) (**42**).

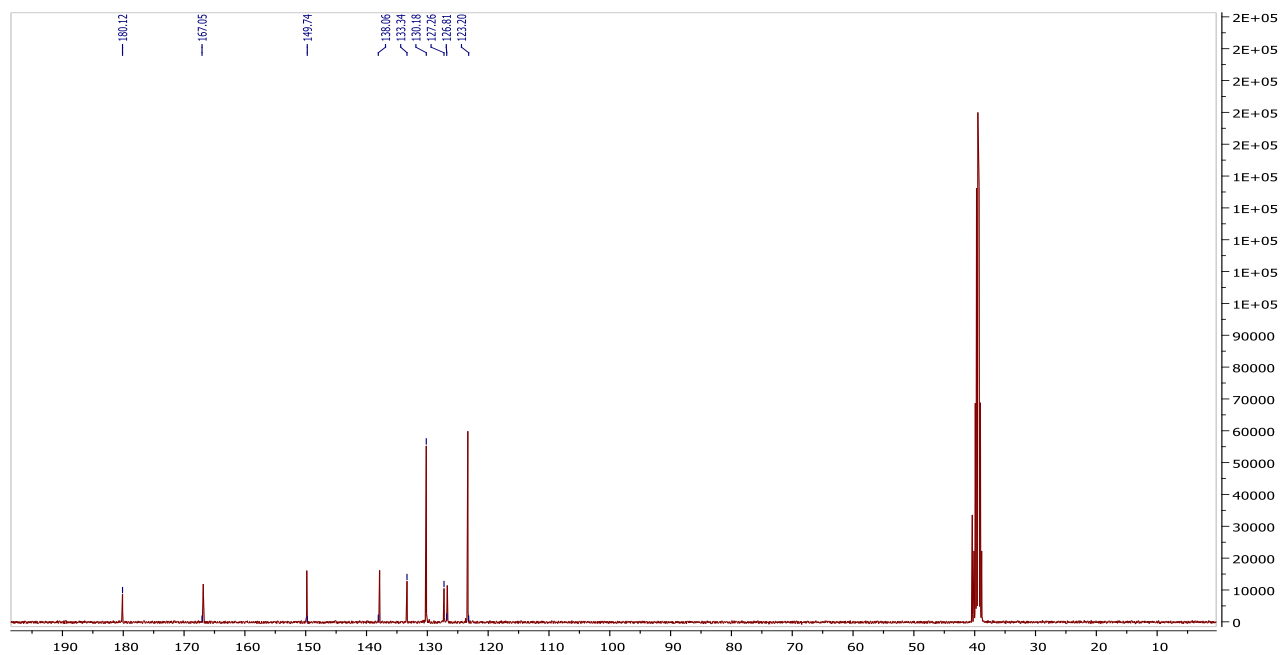


Figure A7.9 ^{13}C NMR spectrum of 1-(4-nitrobenzoyl)-3-[2-({[(4-nitrophenyl)formamido]methanthioyl phenyl}thiourea)amino) (42).

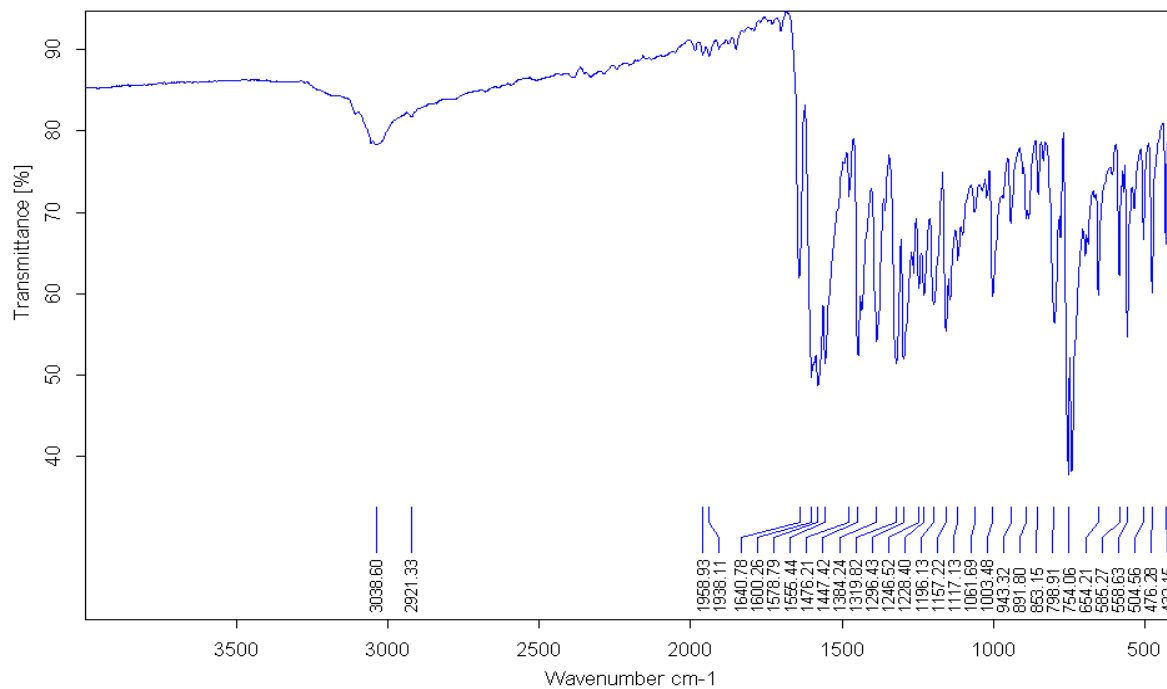


Figure A7.10 IR spectrum of 1-(4-chlorobenzoyl)-3-[2-({[(4-chlorophenyl)formamido]methanethioyl}amino)phenylthiourea (43).

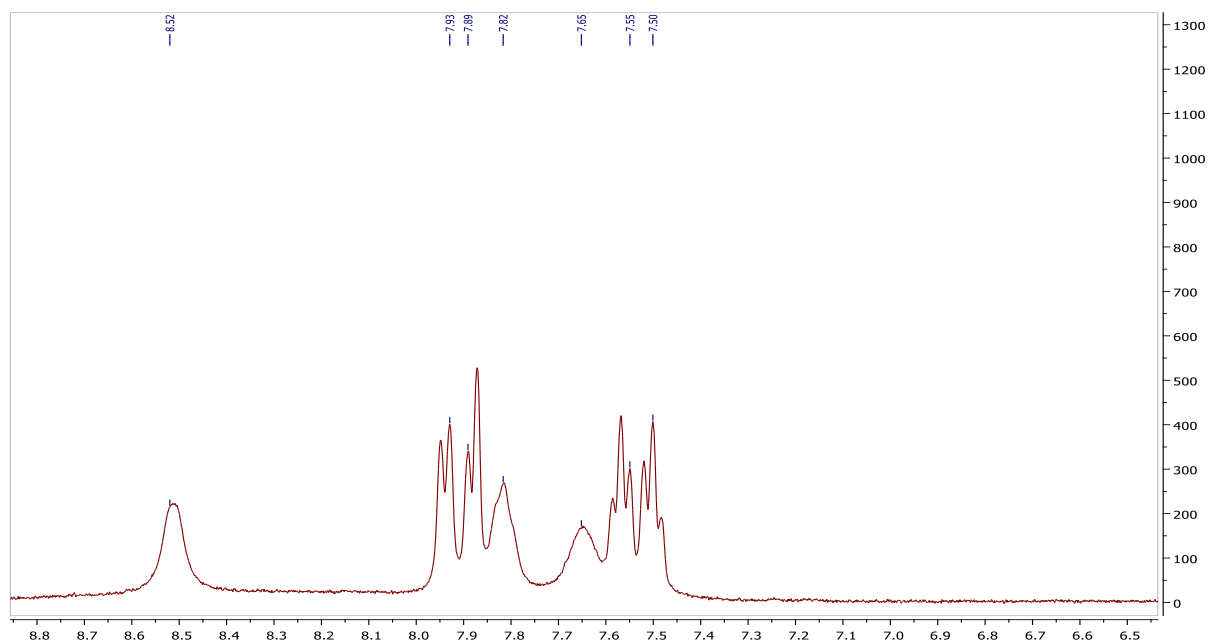


Figure A7.11 ¹H NMR spectrum of 1-(4-chlorobenzoyl)-3-[2-([(4-chlorophenyl)formamido]methanethiyl)amino)phenylthiourea (**43**).

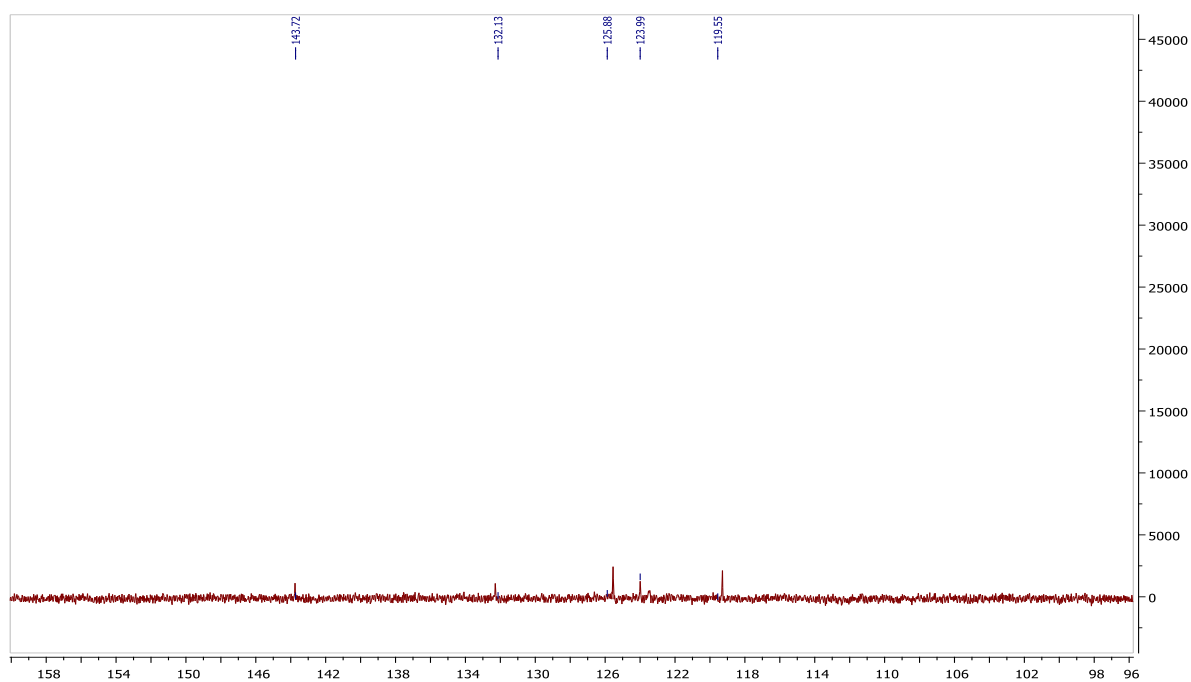


Figure A7.12 ¹³C NMR spectrum of 1-(4-chlorobenzoyl)-3-[2-([(4-chlorophenyl)formamido]methanethiyl)amino)phenylthiourea (**43**).

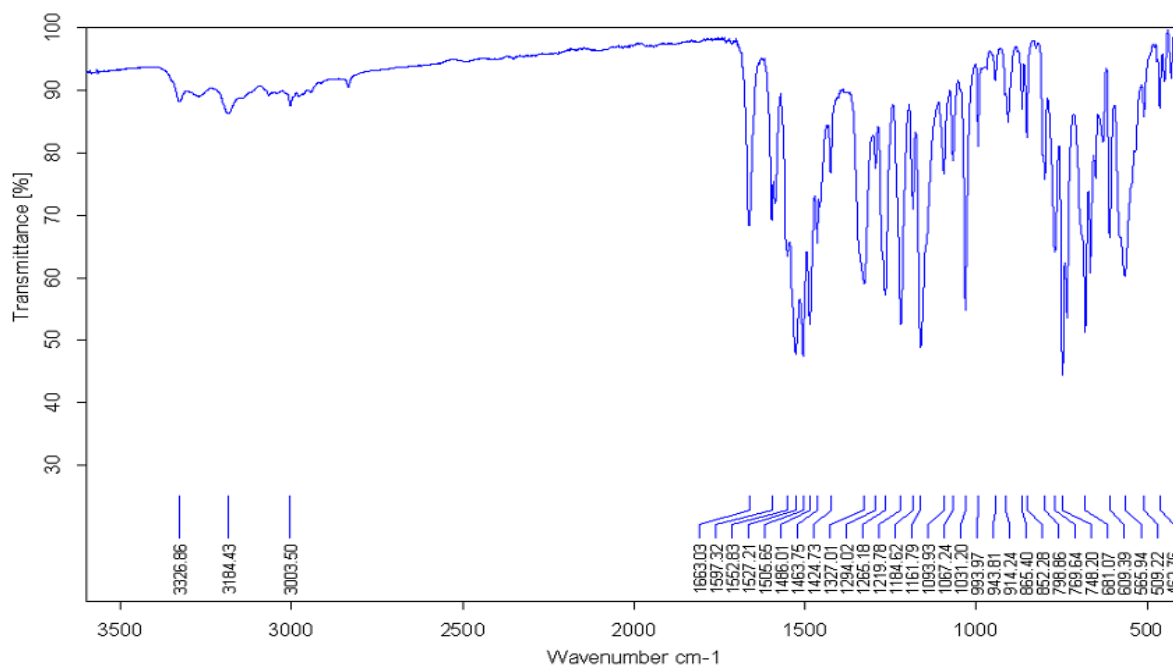


Figure A7.13 IR spectrum of 1-(3-methoxybenzoyl)-3-[2-({[(3-methoxyphenyl)formamido]methanethiyl}amino)phenyl]thiourea (**45**).

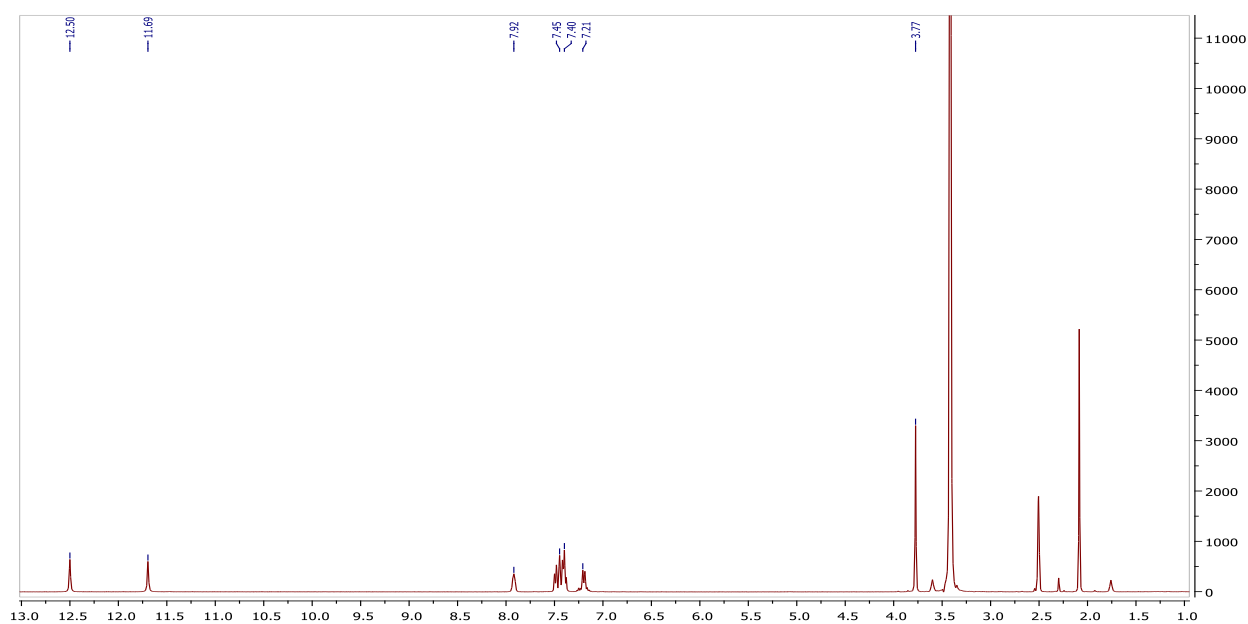


Figure A7.14 ¹H NMR spectrum of 1-(3-methoxybenzoyl)-3-[2-({[(3-methoxyphenyl)formamido]methanethiyl}amino)phenyl]thiourea (**45**).

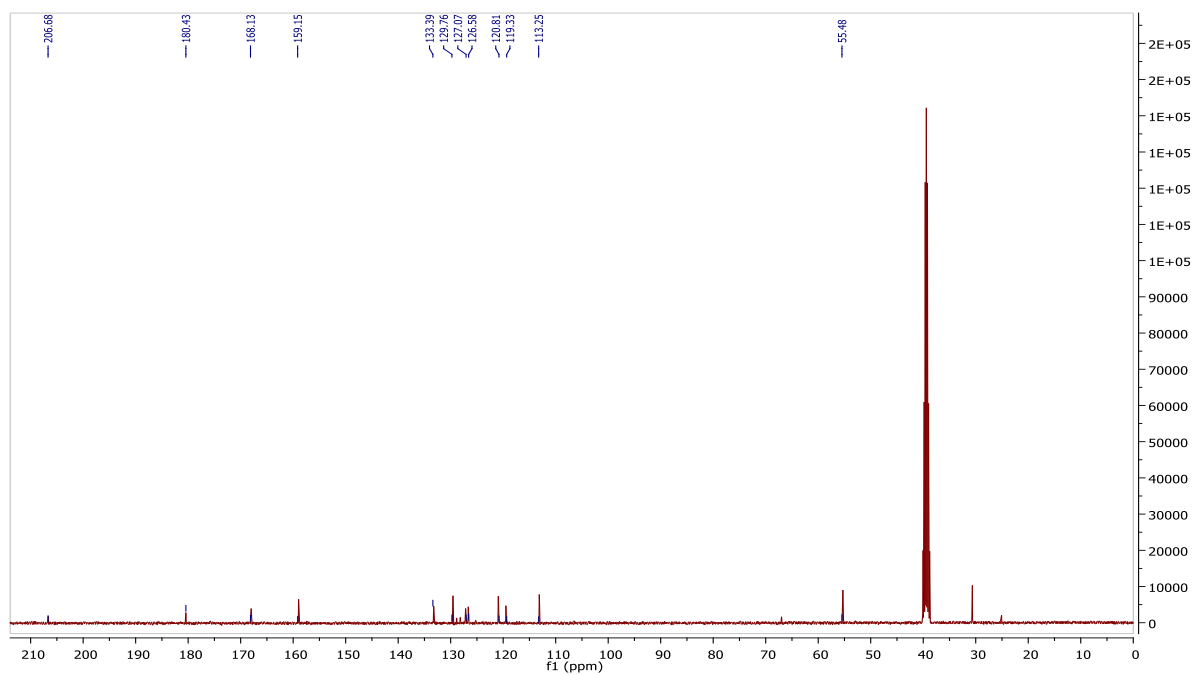


Figure A7.15 ^{13}C NMR spectrum of 1-(3-methoxybenzoyl)-3-[2-(((3-methoxyphenyl)formamido] methanethiyl)amino)phenyl]thiourea (**45**).

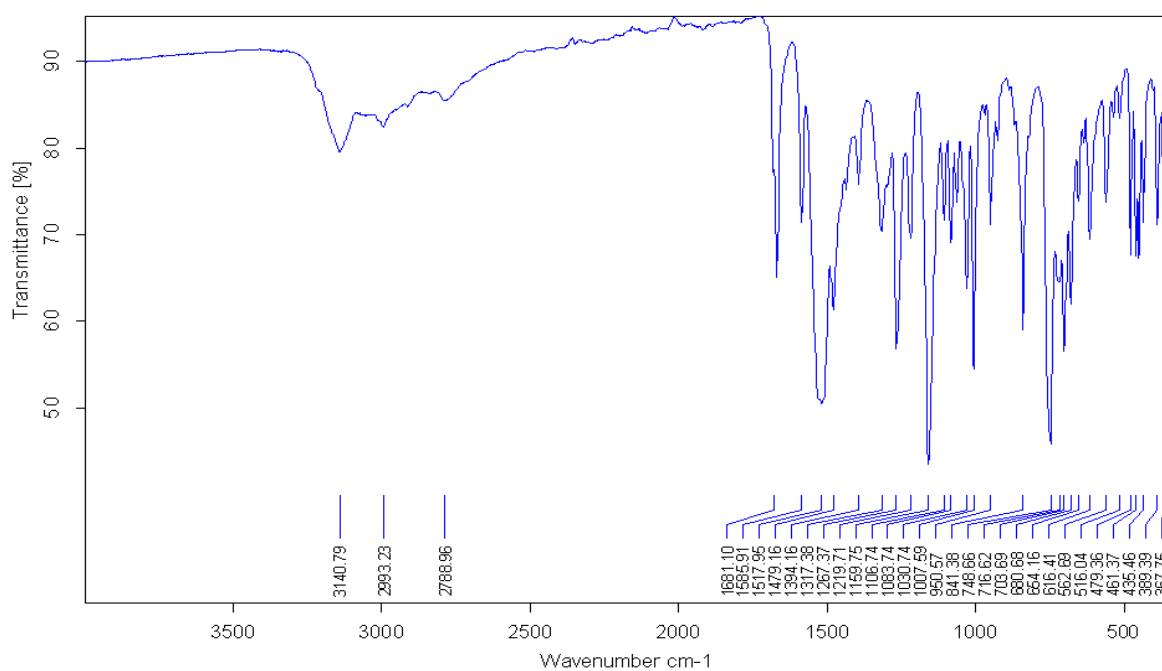


Figure A7.16 IR spectrum of 1-(4-bromobenzoyl)-3-[2-(((4-bromophenyl)formamido] methanethiyl)amino)phenyl]thiourea (**46**).

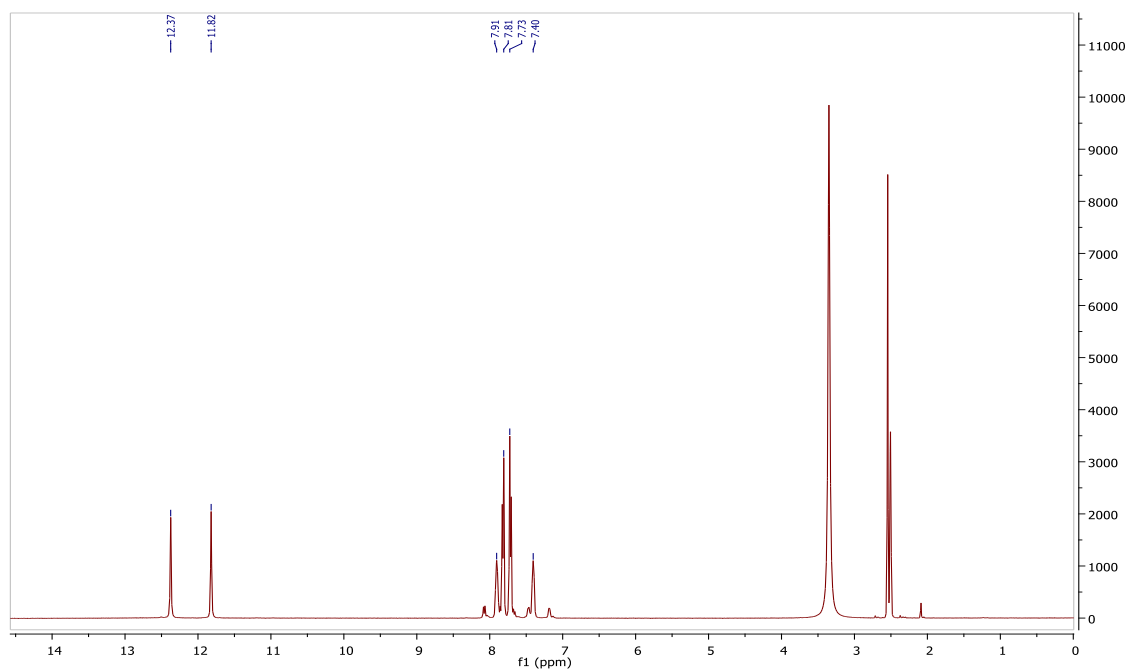


Figure A7.17 ¹H NMR spectrum 1-(4-bromobenzoyl)-3-[2-({[(4-bromophenyl)formamido]methanethiyl}amino)phenyl]thiourea (**46**).

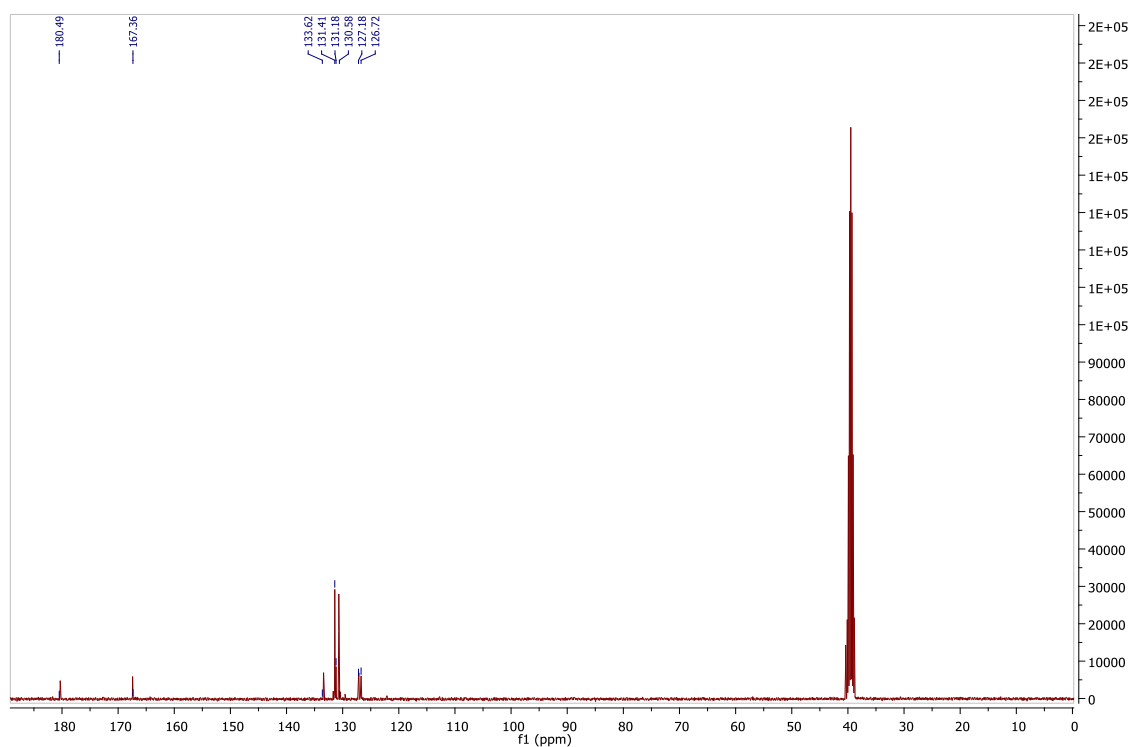


Figure A7.18 ¹³C NMR spectrum of 1-(4-bromobenzoyl)-3-[2-({[(4-bromophenyl)formamido]methanethiyl}amino)phenyl]thiourea (**46**).

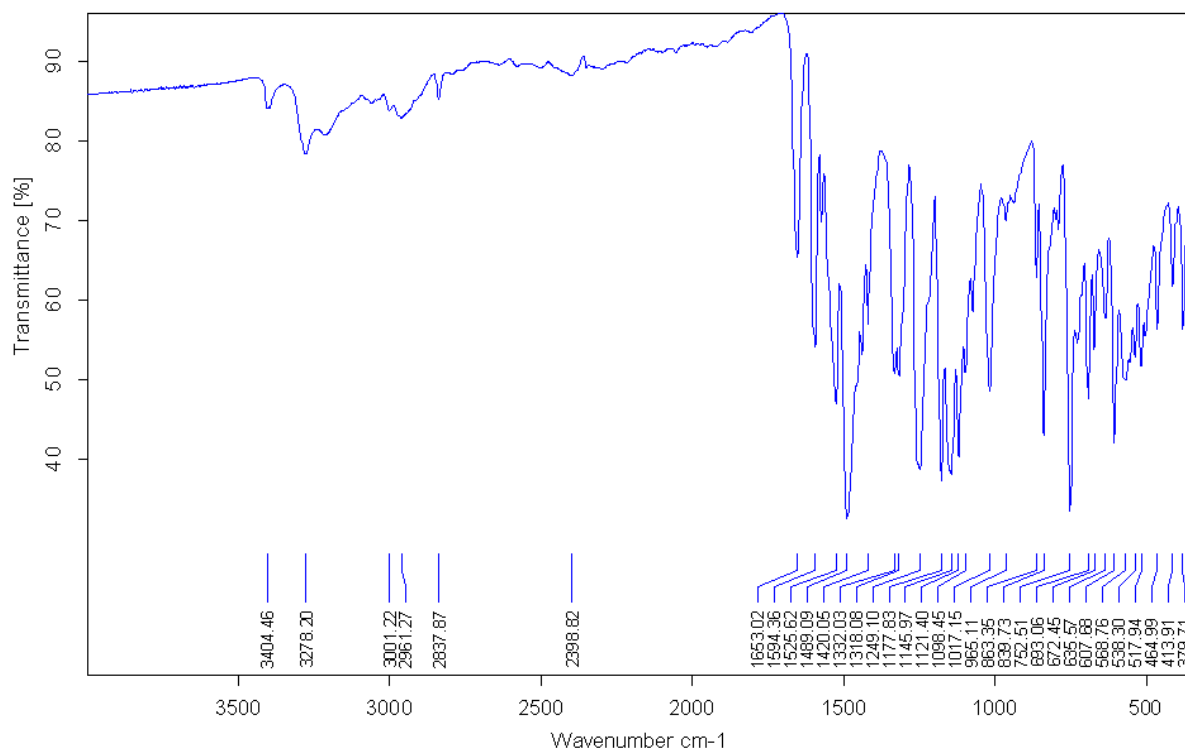


Figure A7.19 IR spectrum of 1-(4-methoxybenzoyl)-3-[2-(((4-methoxyphenyl)formamido)methanethioyl)amino)phenyl]thiourea (**47**).

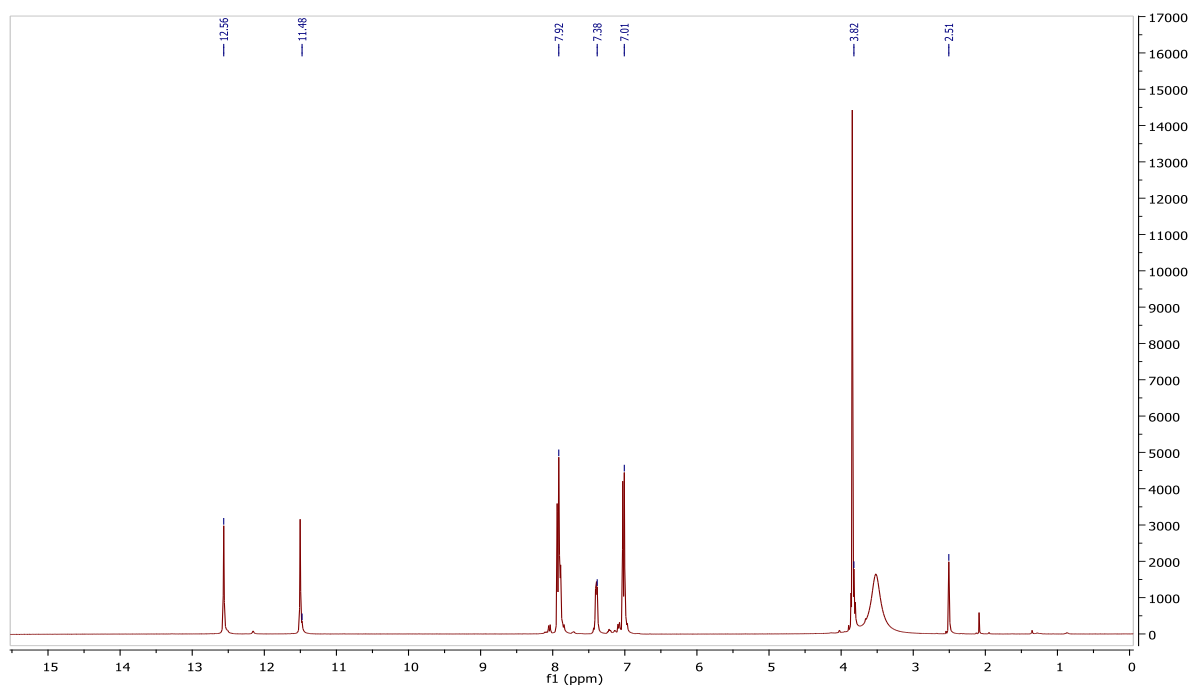


Figure A7.20 ¹H NMR spectrum of 1-(4-methoxybenzoyl)-3-[2-(((4-methoxyphenyl)formamido)methanethioyl)amino)phenyl]thiourea (**47**).

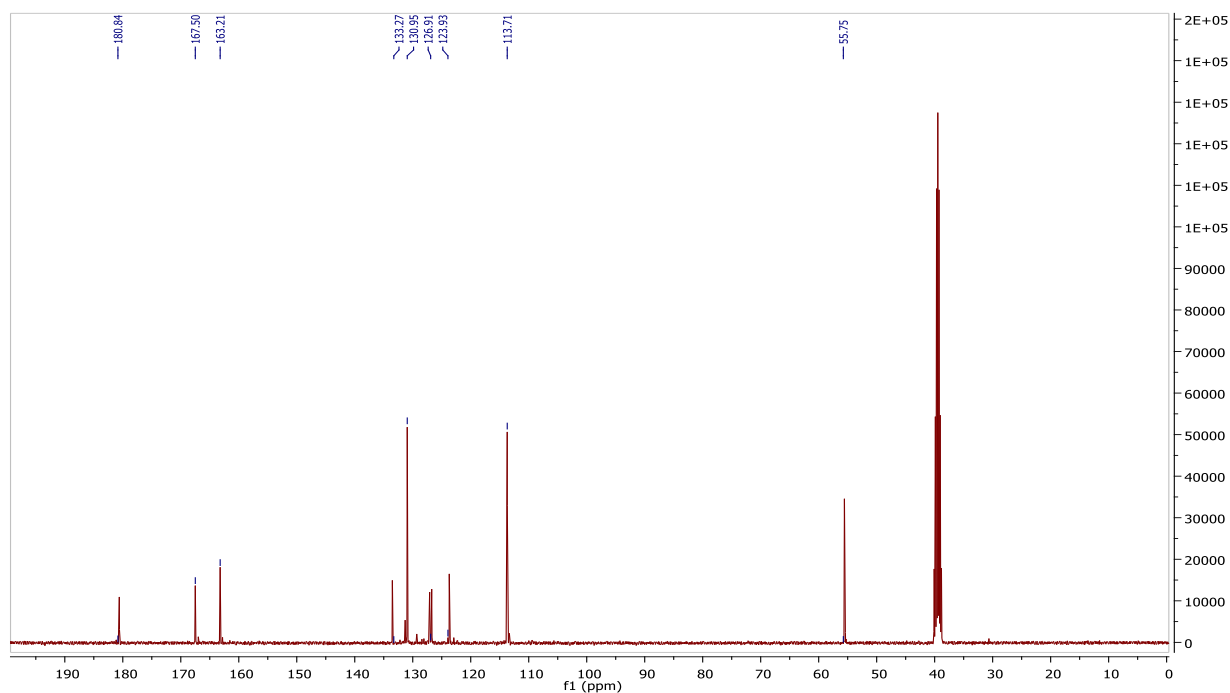


Figure A7.21 ^{13}C NMR spectrum of 1-(4-methoxybenzoyl)-3-[2-(((4-methoxyphenyl)formamido)methanethioyl)amino)phenyl]thiourea (47).

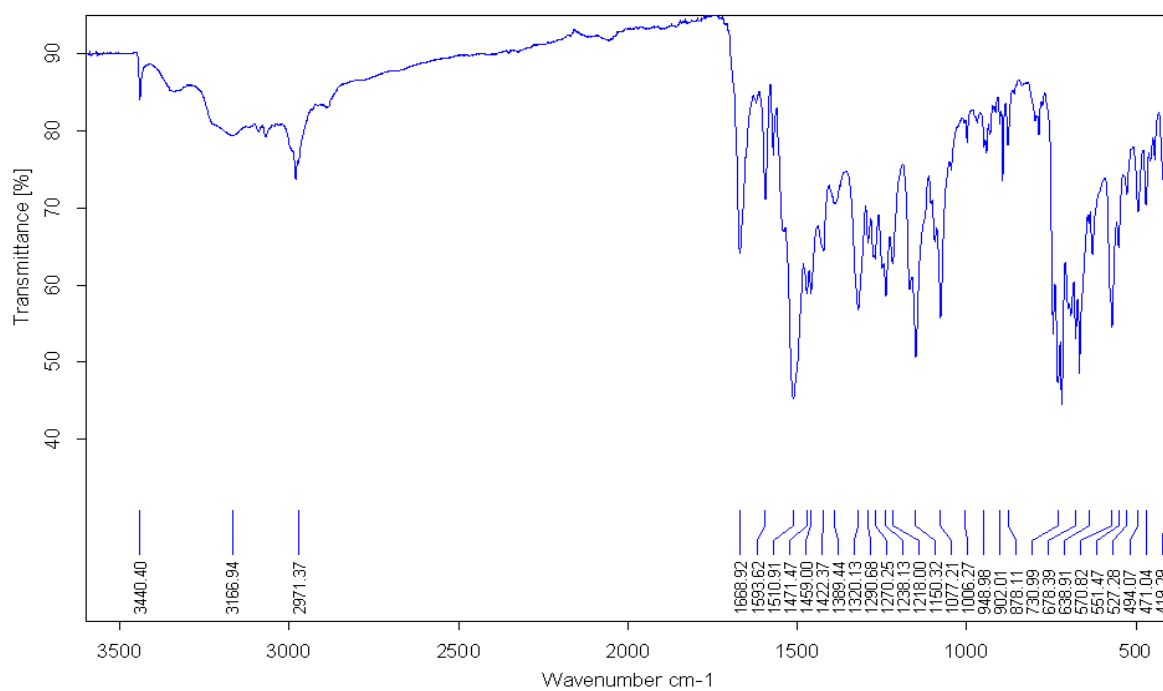


Figure A7.22 IR spectrum of 1-(3-chlorobenzoyl)-3-[2-(((3-chlorophenyl)formamido)methanethioyl)amino)phenyl]thiourea (48).

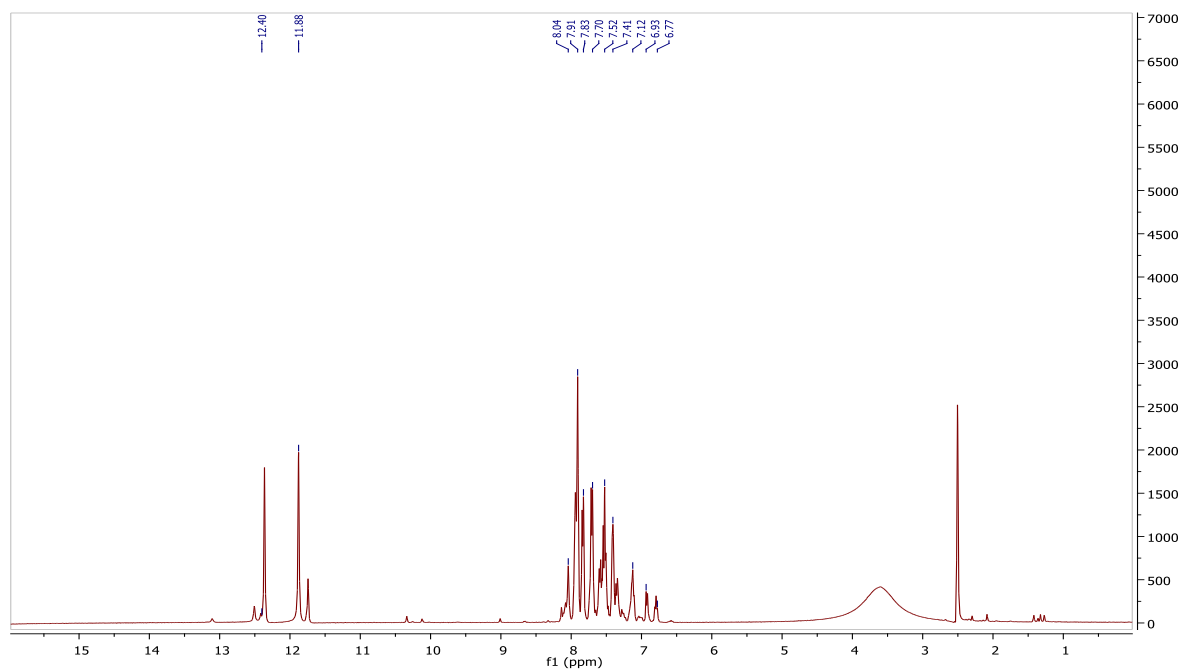


Figure A7.23 ^1H NMR spectrum of 1-(3-chlorobenzoyl)-3-[2-((3-chlorophenyl)formamido)methanethiyl]amino)phenyl]thiourea (**48**).

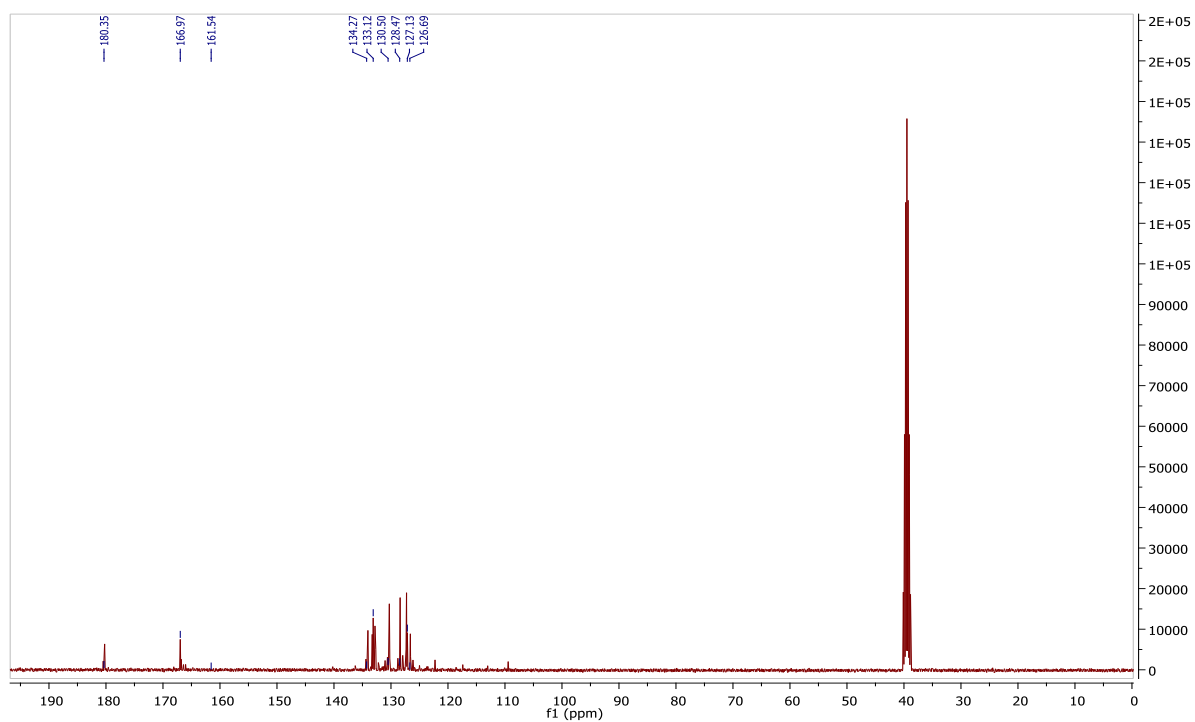


Figure A7.24 ^{13}C NMR spectrum of 1-(3-chlorobenzoyl)-3-[2-((3-chlorophenyl)formamido)methanethiyl]amino)phenyl]thiourea (**48**).

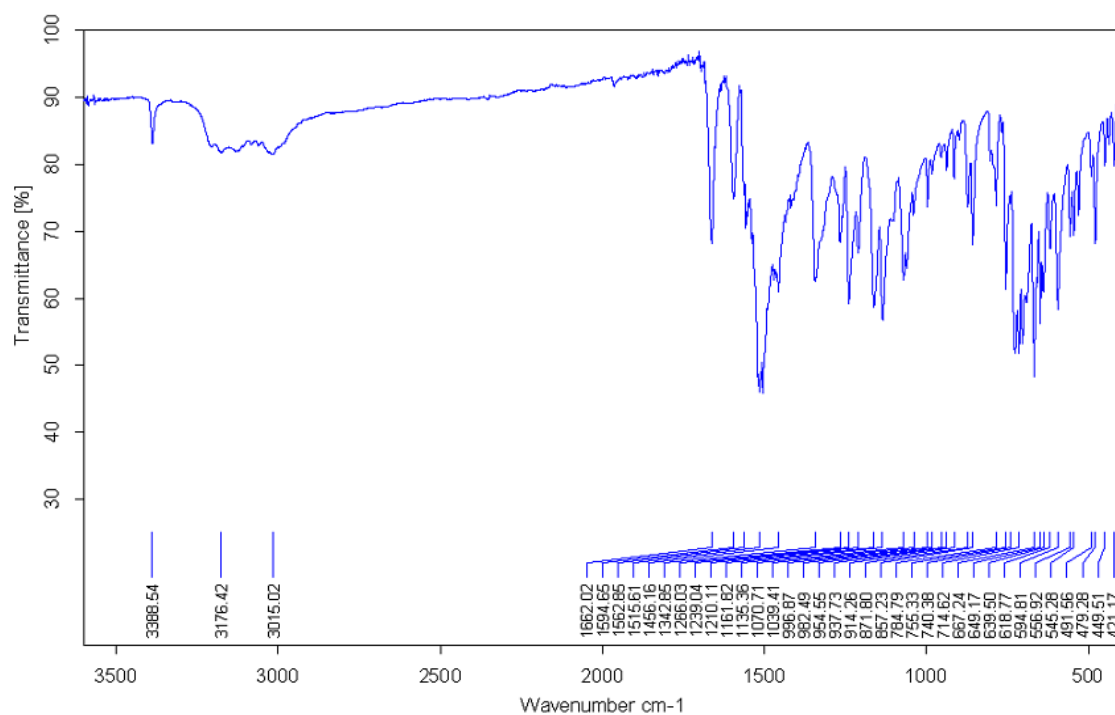


Figure A7.25 IR spectrum of 1-(3-bromobenzoyl)-3-[2-(((3-bromophenyl)formamido]methanethiyl}amino)phenyl]thiourea (**49**).

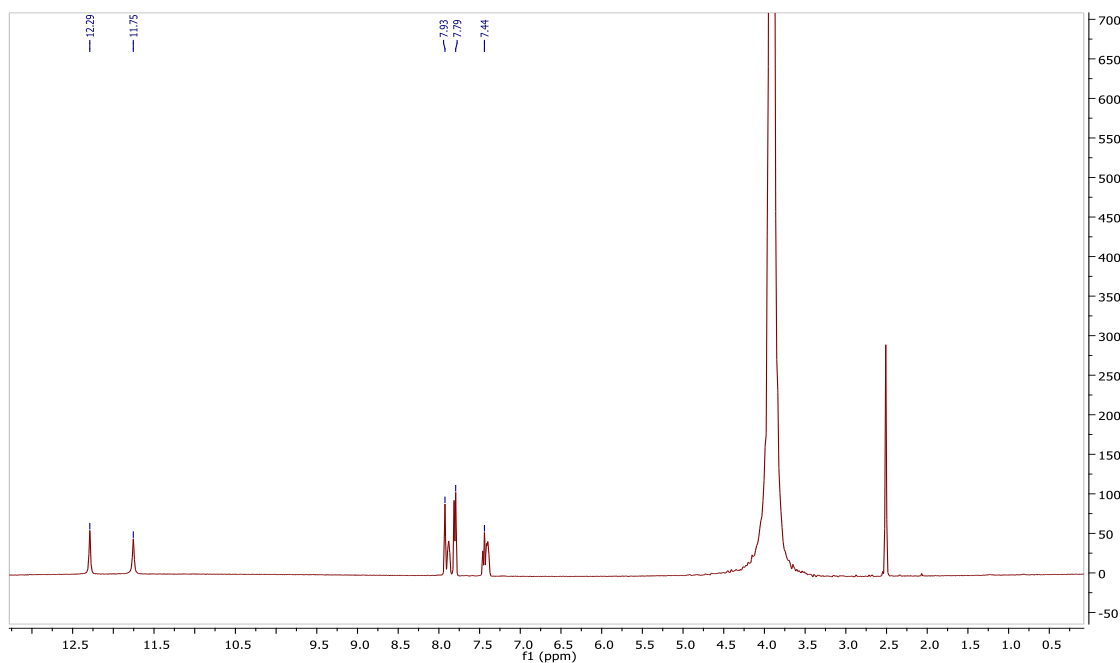


Figure A7.26 ¹H NMR spectrum of 1-(3-bromobenzoyl)-3-[2-(((3-bromophenyl)formamido]methanethiyl}amino)phenyl]thiourea (**49**).

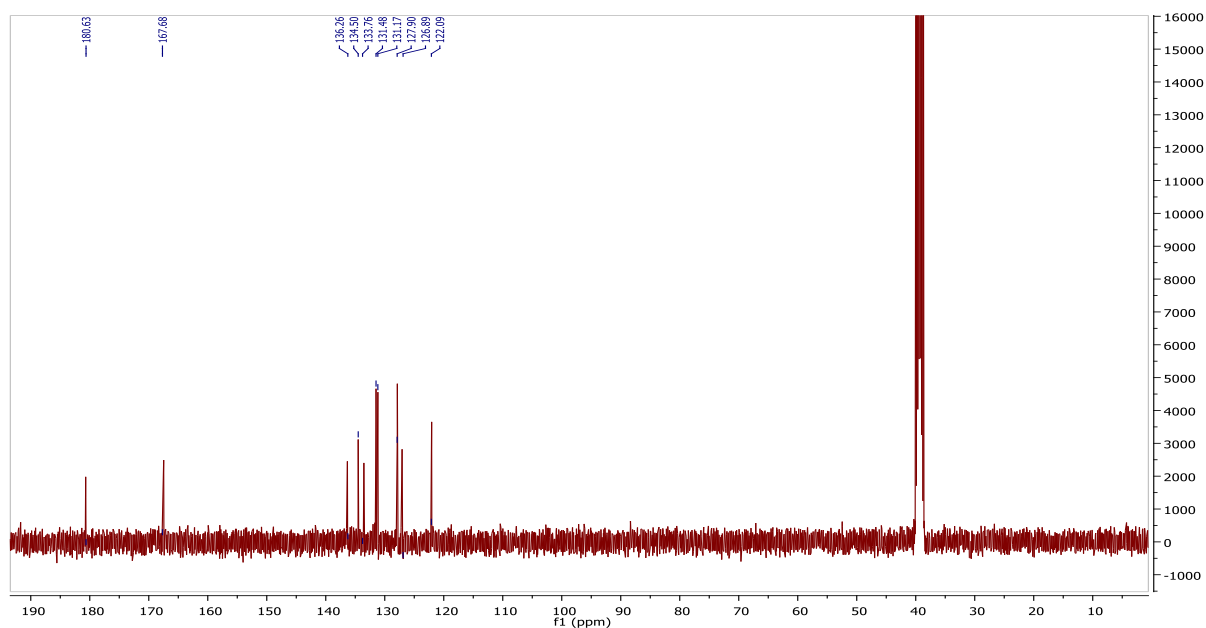


Figure A7.27 ^{13}C NMR spectrum of 1-(3-bromobenzoyl)-3-[2-((3-bromophenyl)formamido)methanethiyl]amino)phenyl]thiourea (**49**).

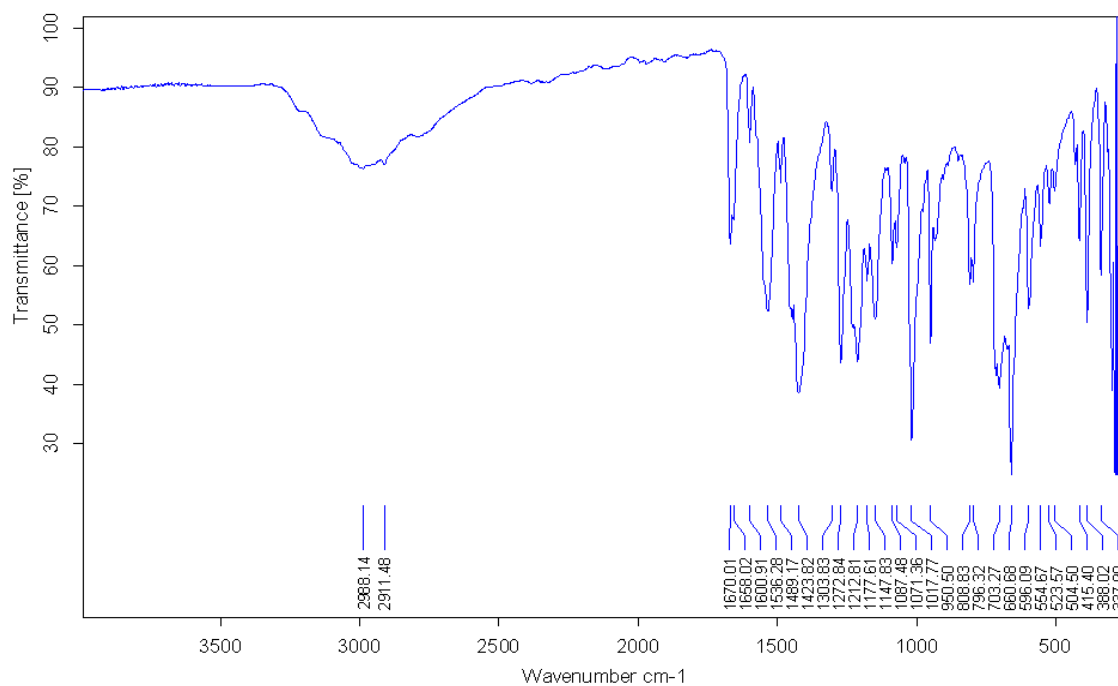


Figure A7.28 IR spectrum of 3-benzoyl-1-((phenylformido)methanethiyl)amino)thiourea (**51**).

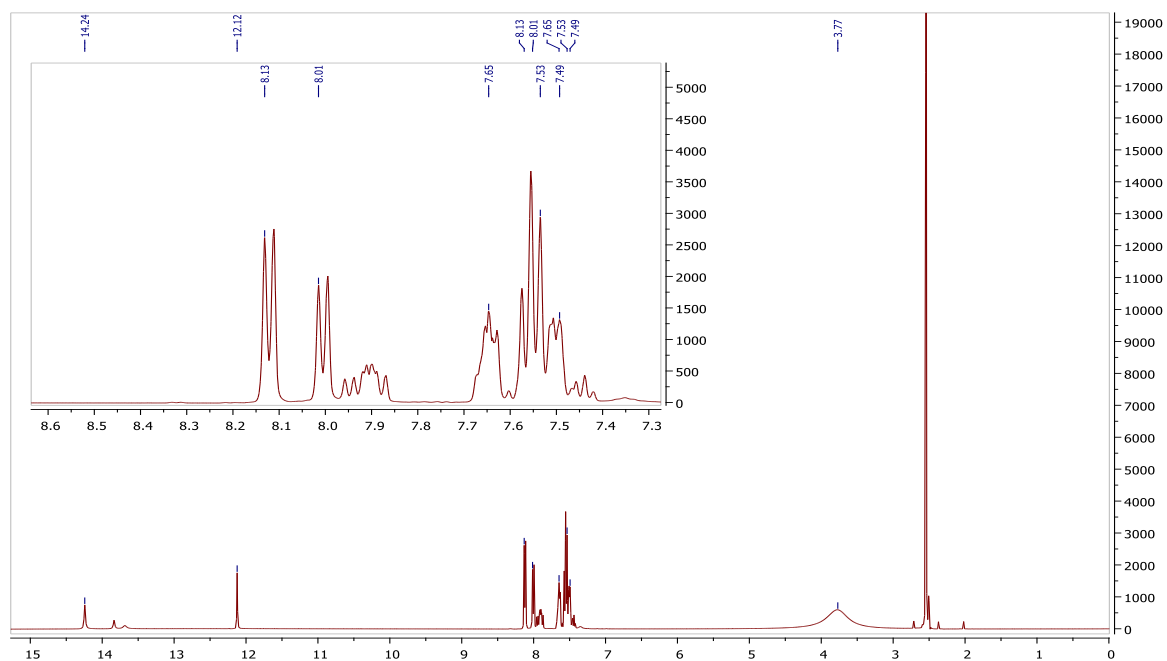


Figure A7.29 ^1H NMR spectrum of 3-benzoyl-1-[[[(phenylformido)methanethioyl]amino]thiourea (**51**).

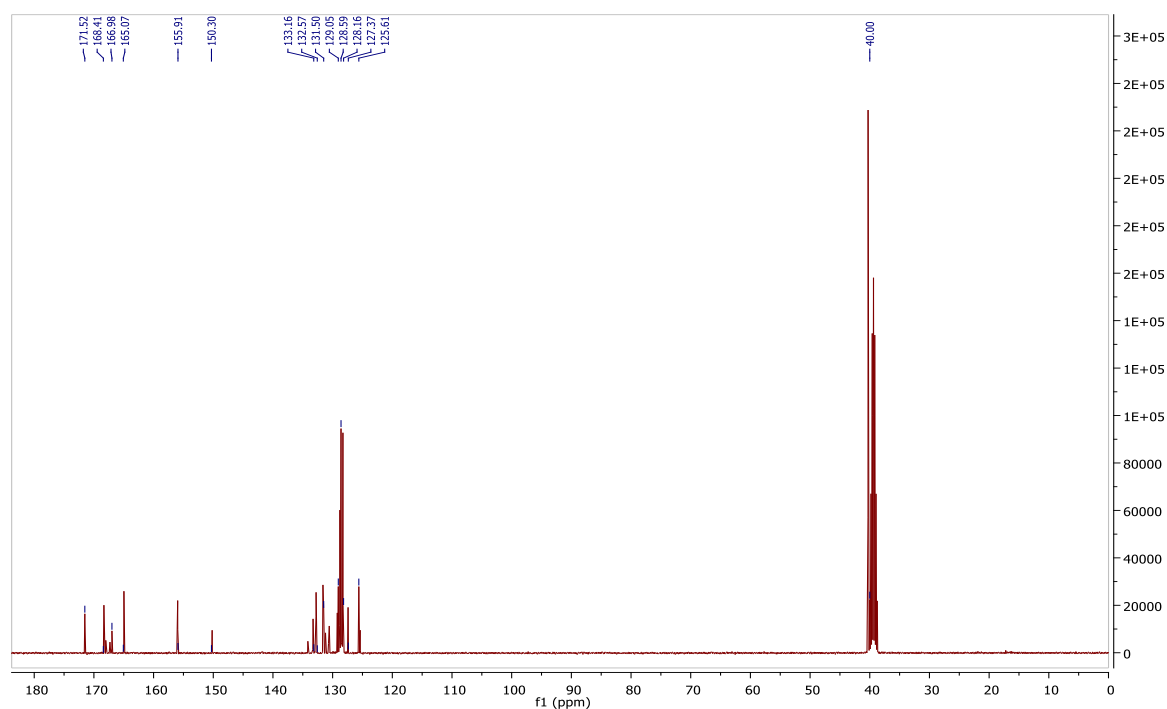


Figure A7.30 ^{13}C NMR spectrum of 3-benzoyl-1-[[[(phenylformido)methanethioyl]amino]thiourea (**51**).

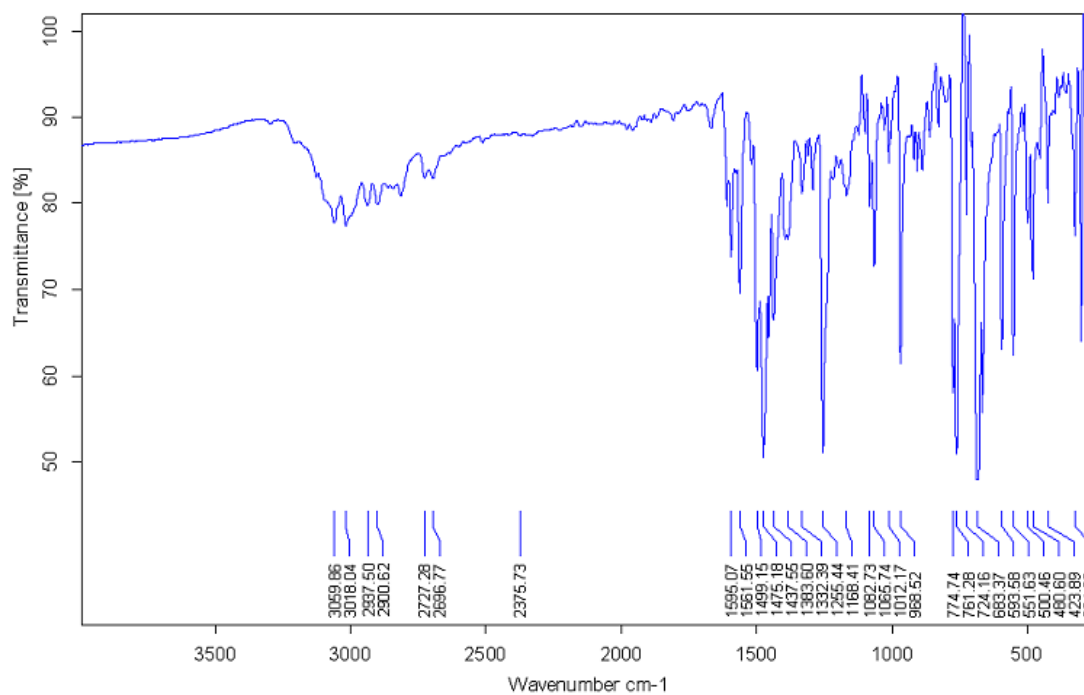


Figure A7.31 IR spectrum of 3-benzoyl-1-(phenylamino)thiourea (52).

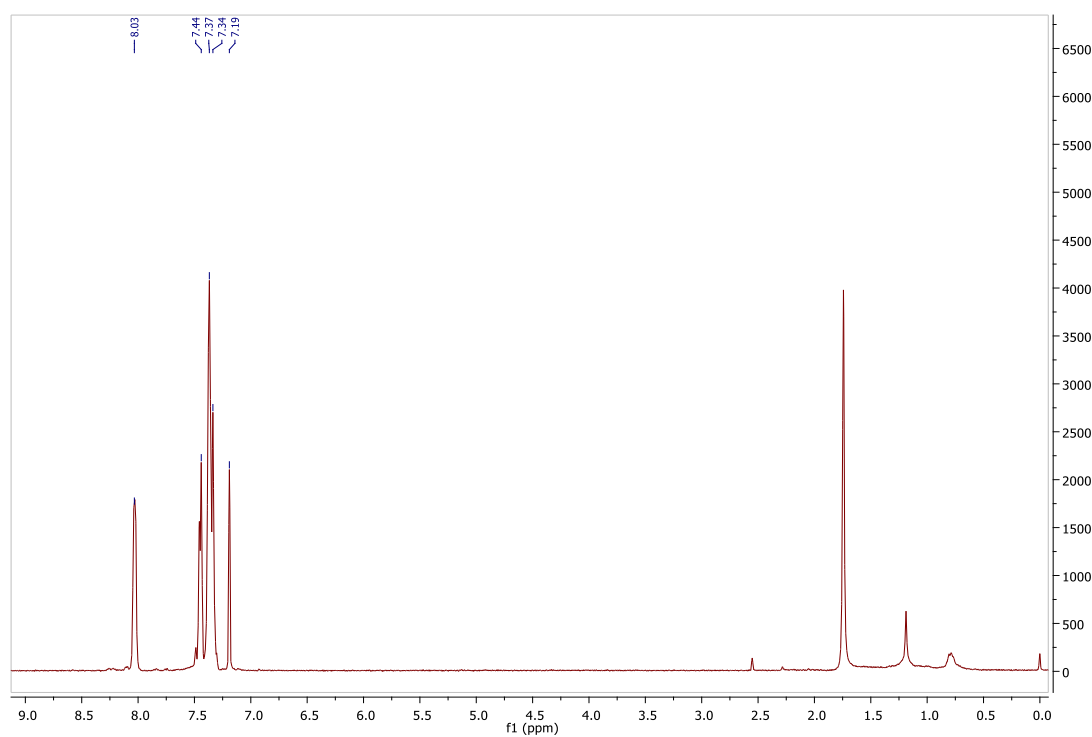


Figure A7.32 ¹H NMR spectrum of 3-benzoyl-1-(phenylamino)thiourea (52).

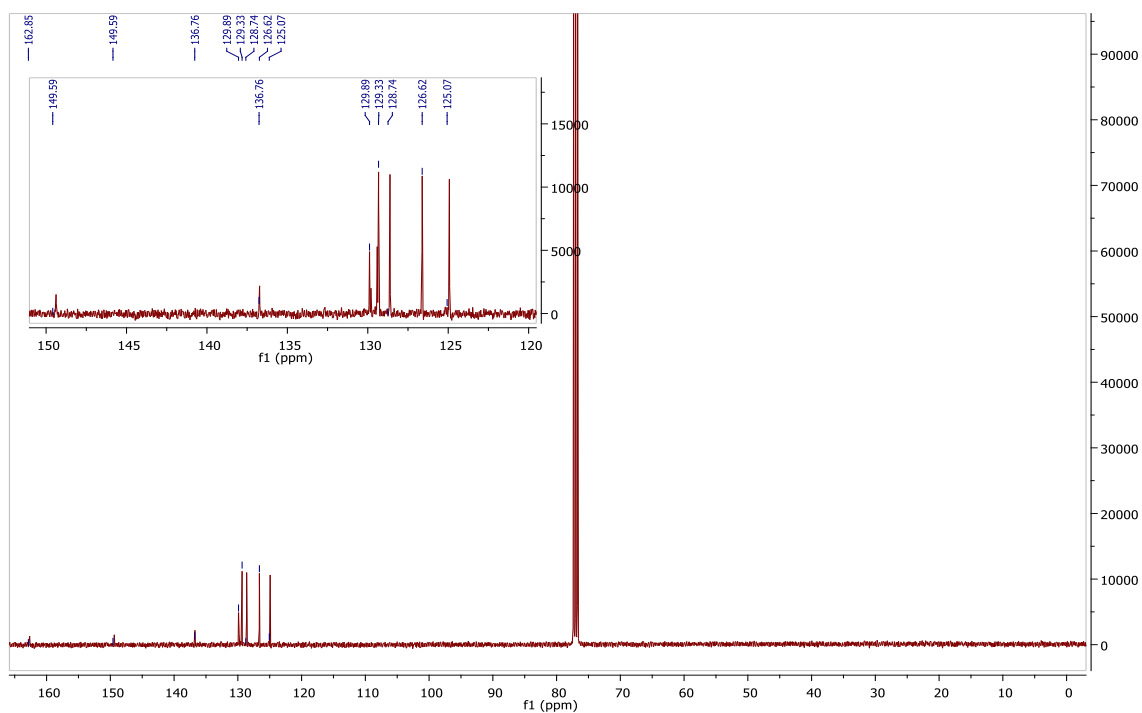


Figure A7.33 ^{13}C NMR 3-benzoyl-1-(phenylamino)thiourea (**52**).

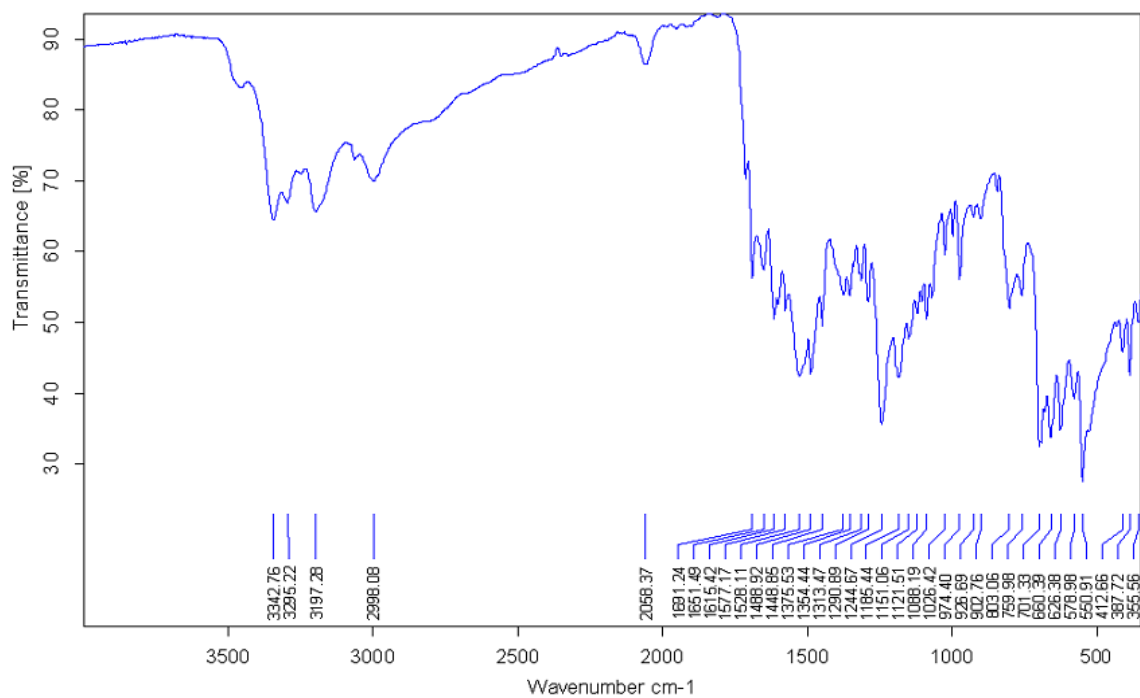


Figure A7.34 IR spectrum of 1-((benzamido)sulfanylenemethyl)urea (**53**).

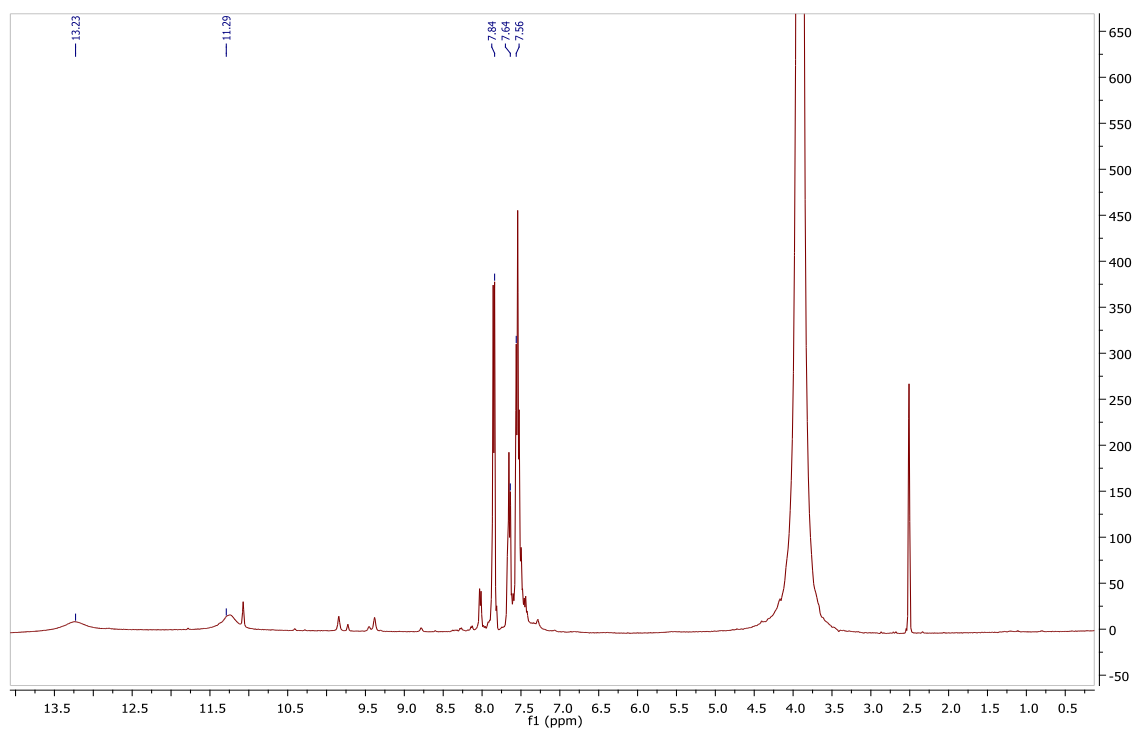


Figure A7.35 ^1H NMR spectrum of 1-((benzamido)sulfanylenemethyl)urea (**53**).

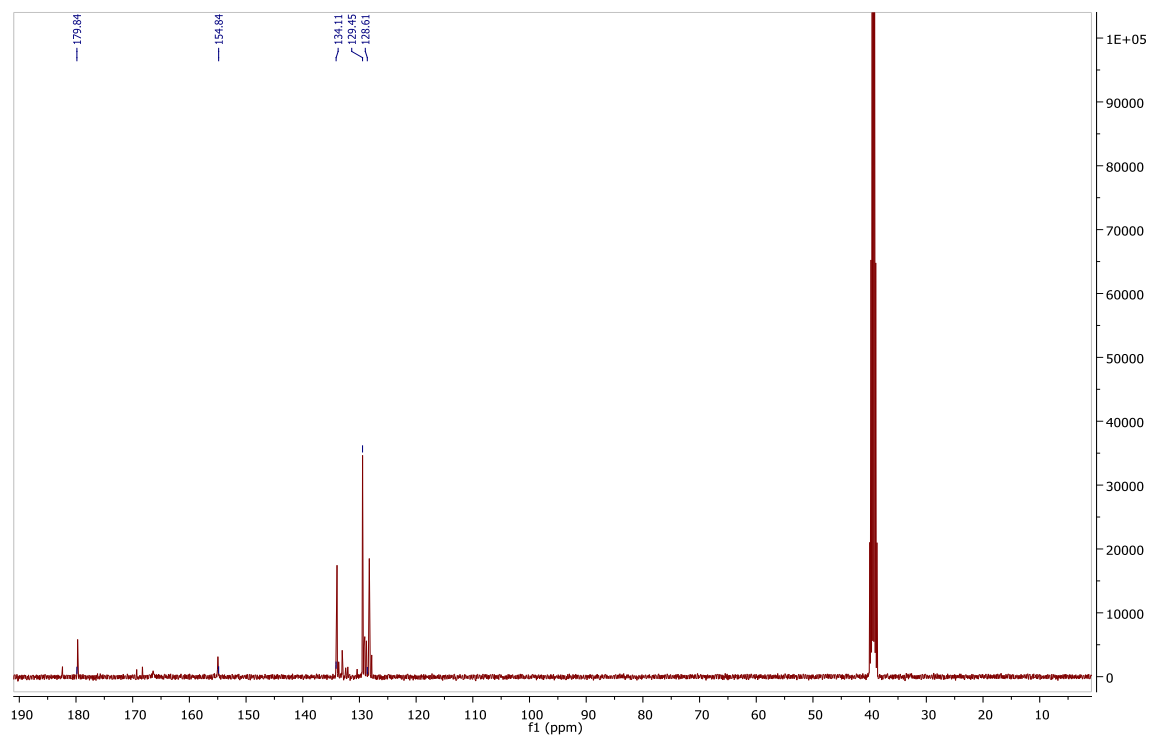


Figure A7.36 ^{13}C NMR spectrum of 1-((benzamido)sulfanylenemethyl)urea (**53**).

APPENDIX F

Gold and silver catalysed reactions of benzoyl isothiocyanate derivatives

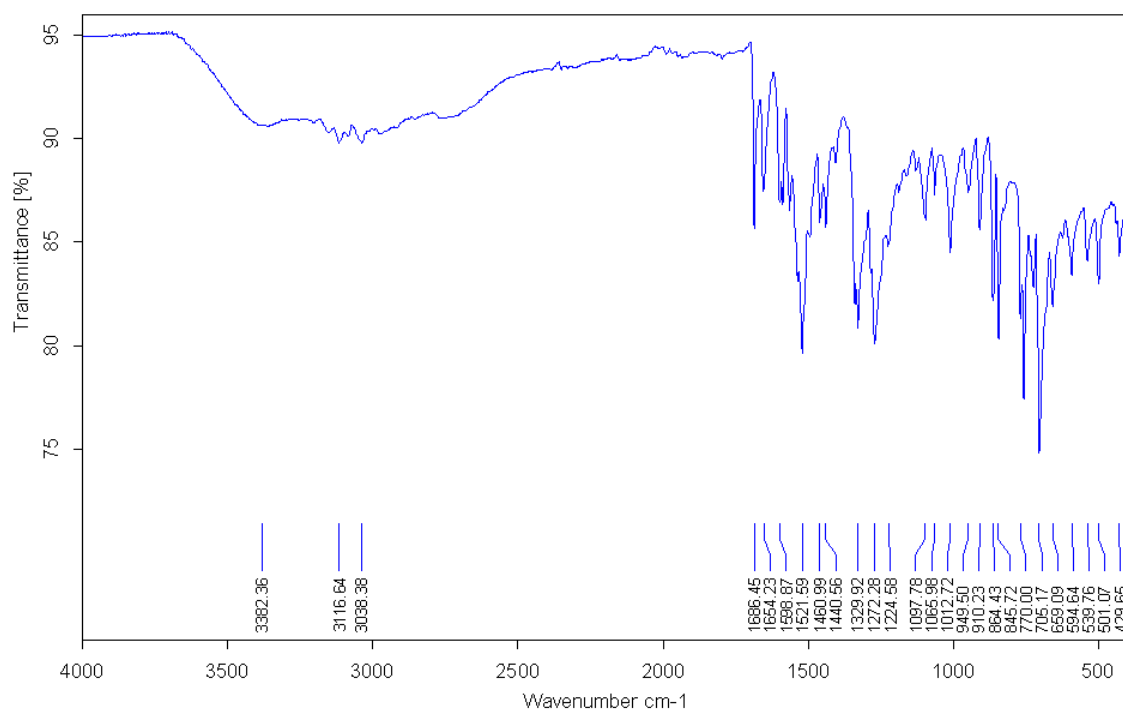


Figure A8.1 IR spectrum of *N*-(benzothiazol-2-yl)-4-nitrobenzamide (**55**).

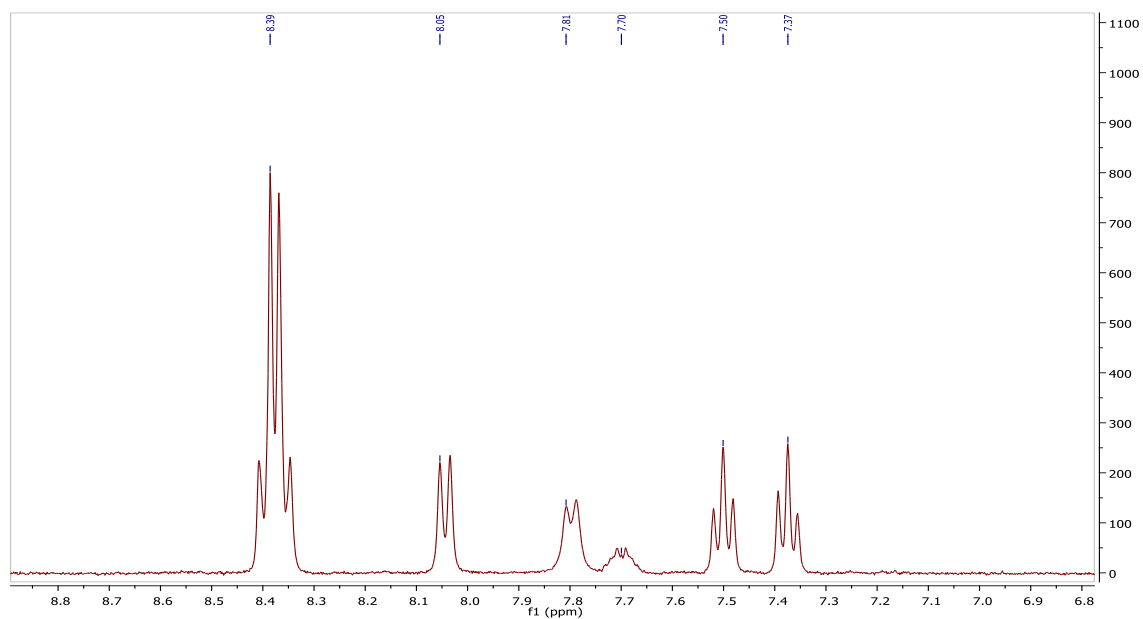


Figure A8.2 ¹H NMR spectrum of *N*-(benzothiazol-2-yl)-4-nitrobenzamide (**55**).

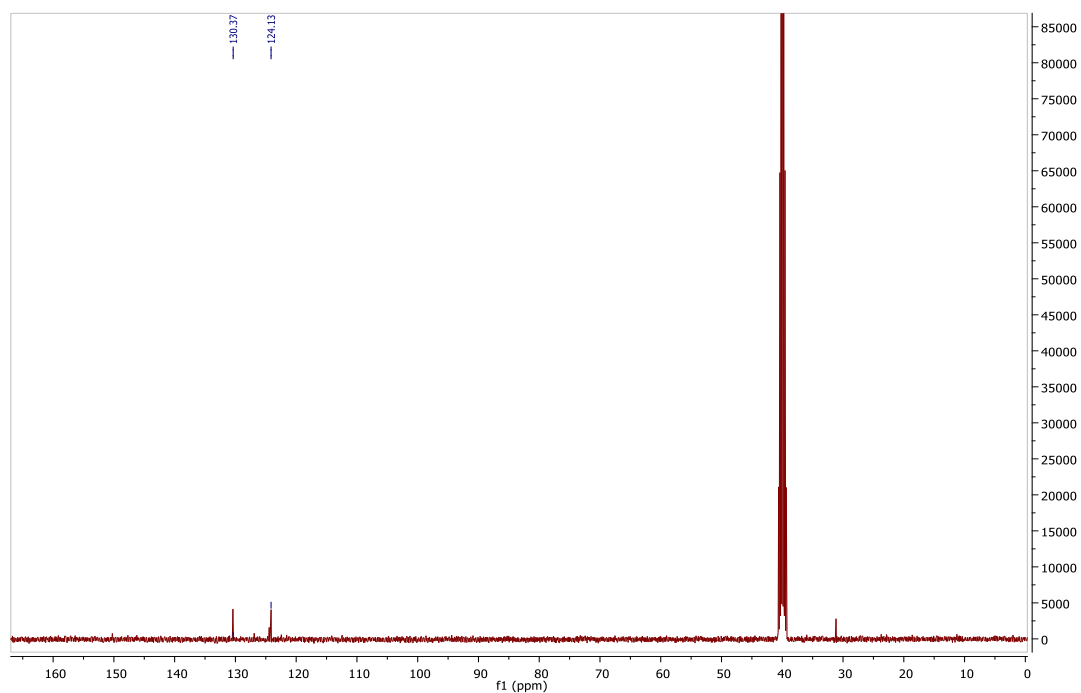


Figure A8.3 ^{13}C NMR spectrum of *N*-(benzothiazol-2-yl)-4-nitrobenzamide (**55**).

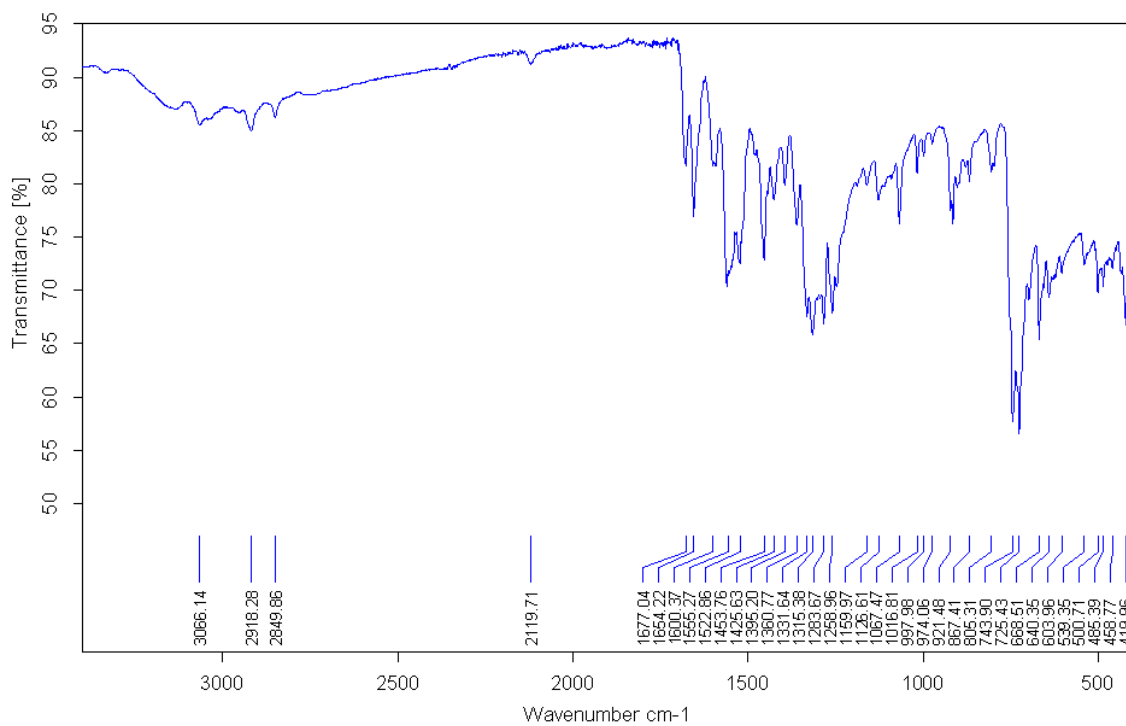


Figure A8.4 IR spectrum of *N*-(benzothiazol-2-yl)-3-bromobenzamide (**56**).

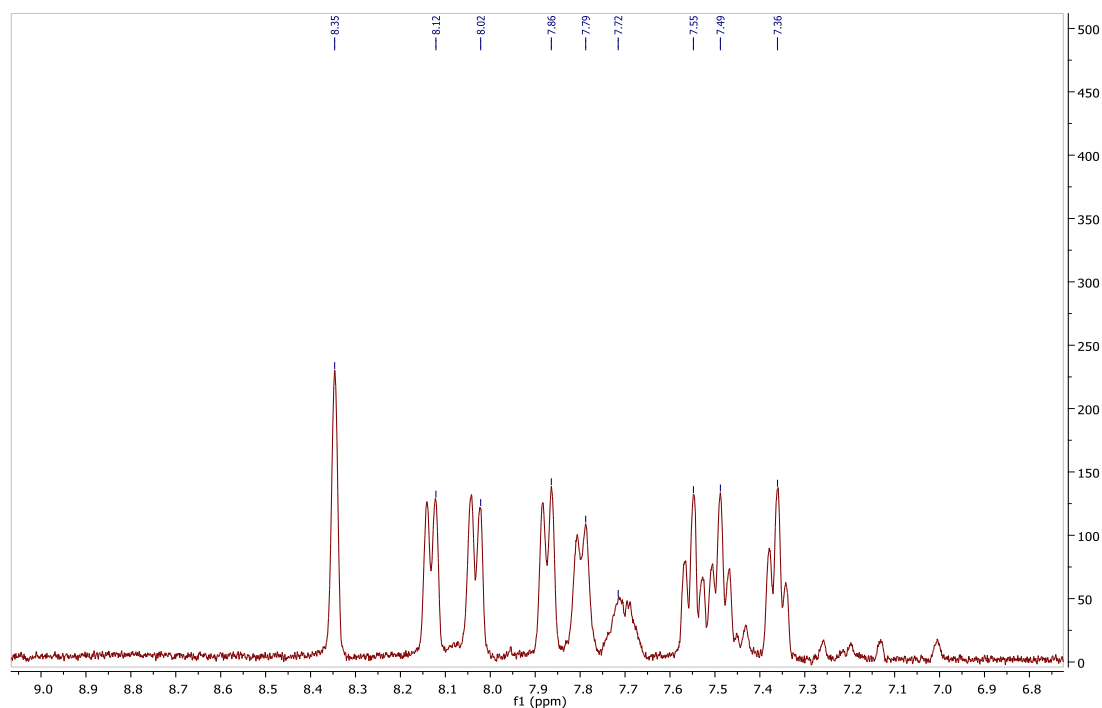


Figure A8.5 ^1H NMR spectrum of *N*-(benzothiazol-2-yl)-3-bromobenzamide (56).

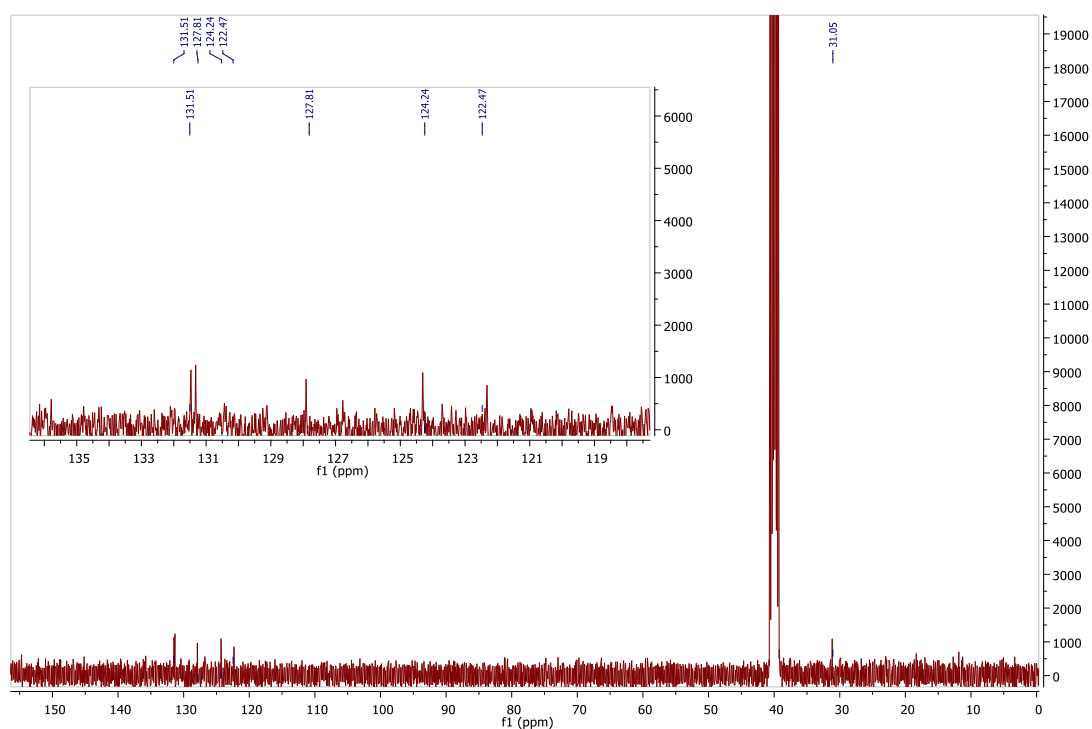


Figure A8.6 ^{13}C NMR spectrum of *N*-(benzothiazol-2-yl)-3-bromobenzamide (56).

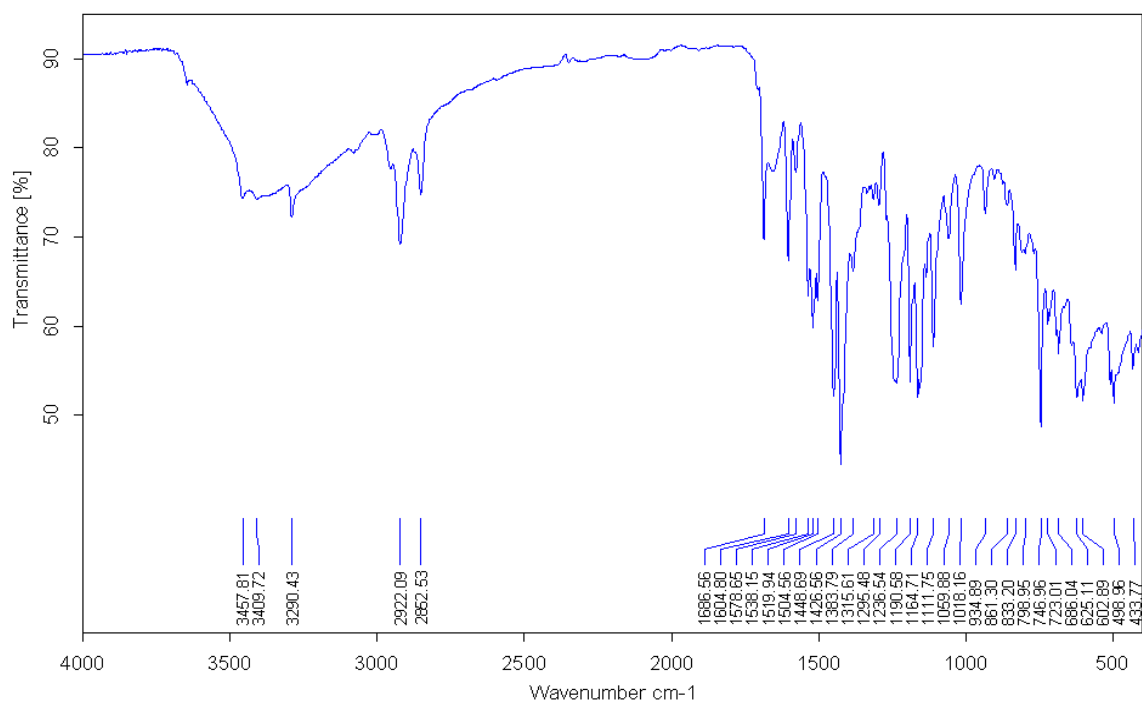


Figure A8.7 IR spectrum of *N*-(benzothiazol-2-yl)-3-methoxybenzamide (**57**).

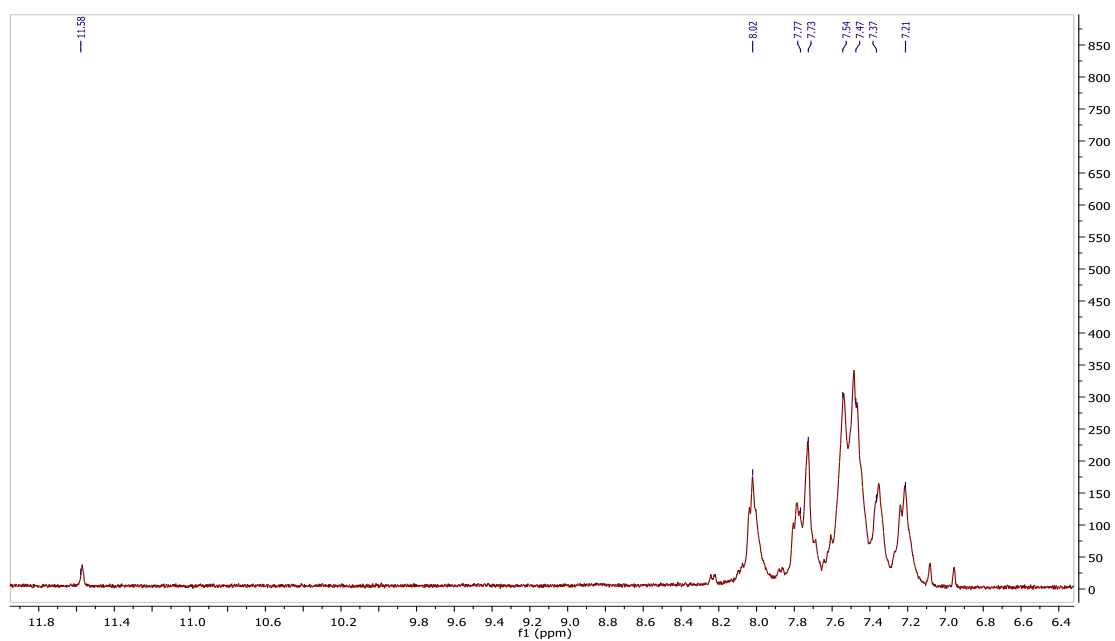


Figure A8.8 ¹H NMR spectrum of *N*-(benzothiazol-2-yl)-3-methoxybenzamide (**57**).

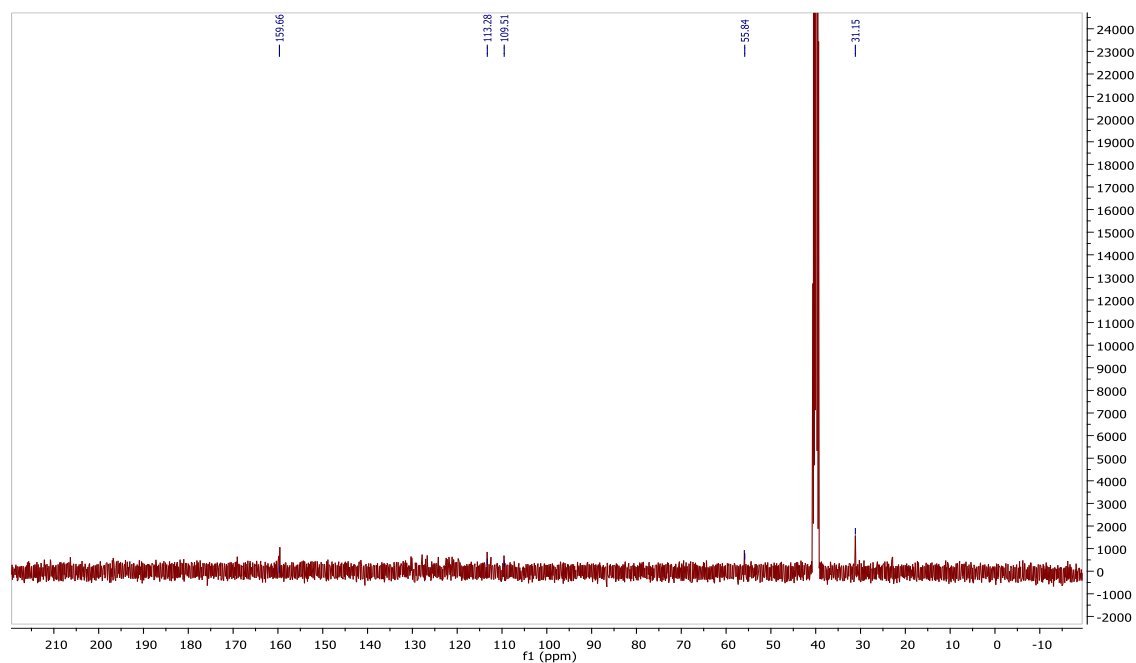


Figure A8.9 ^{13}C NMR spectrum of *N*-(benzothiazol-2-yl)-3-methoxybenzamide (57).

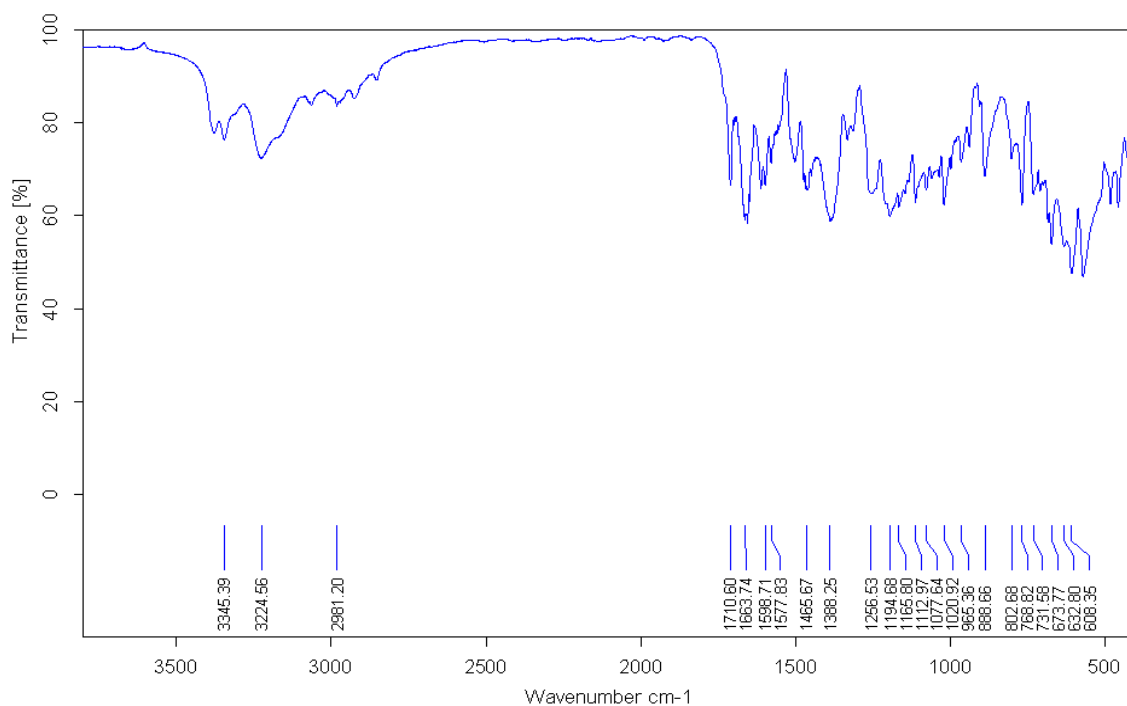


Figure A8.10 IR spectrum of 1-((benzamido)formyl)urea (59).

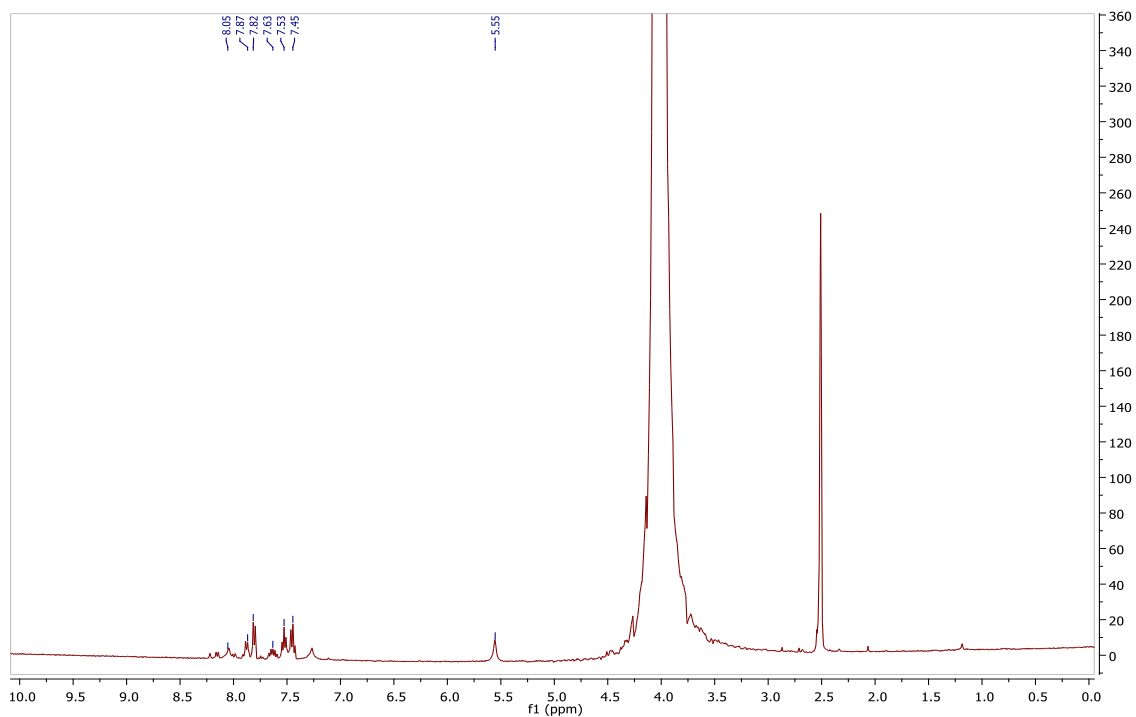


Figure A8.11 ^{13}C NMR spectrum of 1-((benzamido)formyl)urea (**59**).

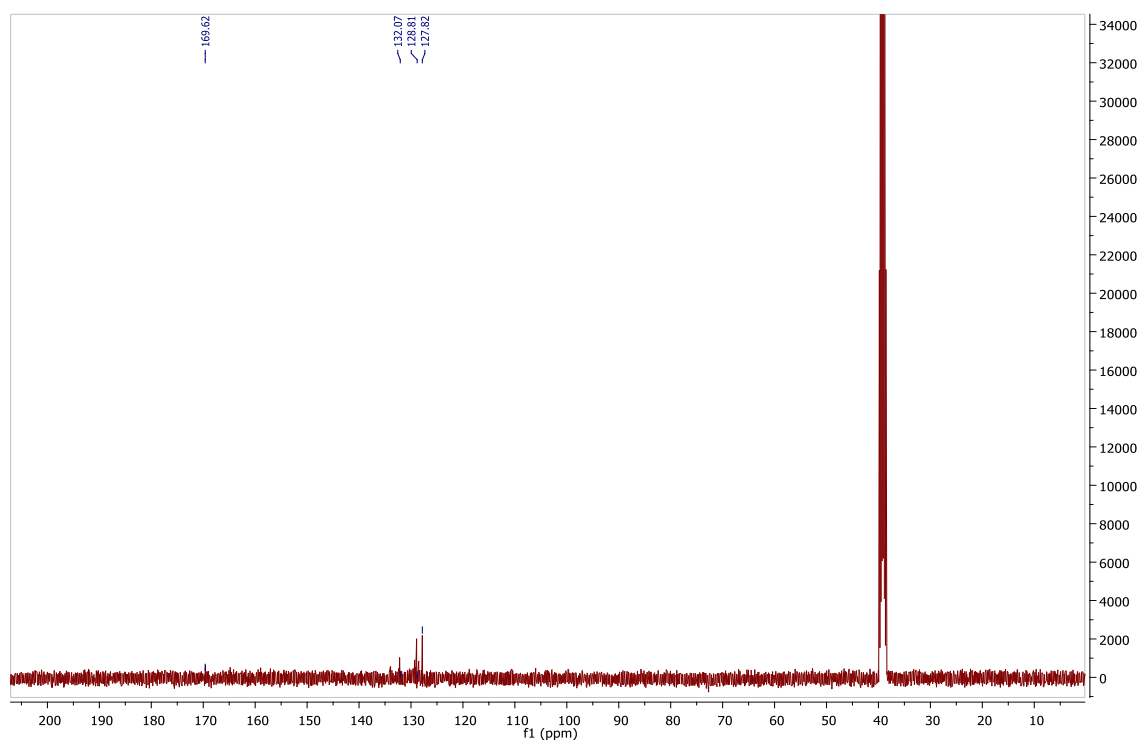


Figure A8.12 ^{13}C NMR spectrum of 1-((benzamido)formyl)urea (**59**).

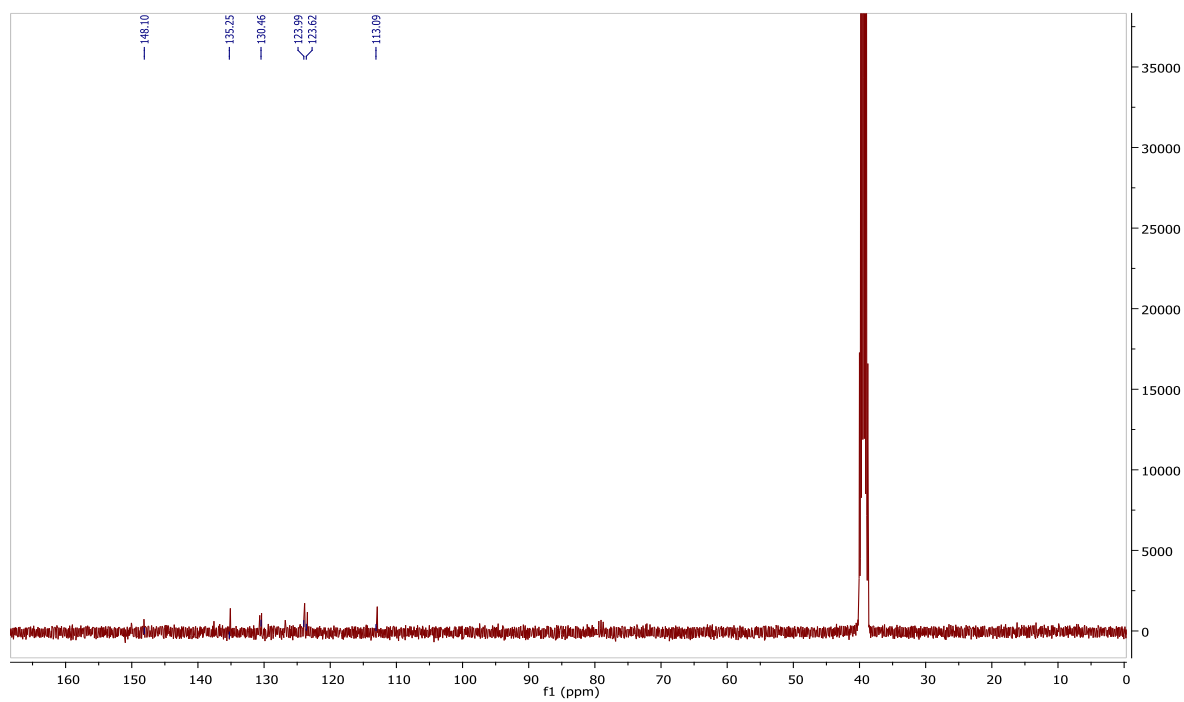


Figure A8.15 ^{13}C NMR spectrum of *N*-(2,3-dihydro-1*H*-benzimidazol-2-yl)-3-nitrobenzamide (**60**).